Theory for Molecular Tests of Fundamental Physics

THEORY FOR MOLECULAR TESTS OF FUNDAMENTAL PHYSICS

Kumulative Dissertation

zur Erlangung des akademischen Grades

Doktor der Naturwissenschaften
(Dr. rer. nat.)

dem Fachbereich Chemie der

Philipps-Universität Marburg
(Hochschulkennziffer:1180)

zur Begutachtung vorgelegt von

KONSTANTIN JOACHIM GAUL, M. SC.
aus Fulda

Marburg (Lahn) 2020

Eingereicht am	10.09.2020
Vom Fachbereich Chemie der Philipps-Universität Marburg als Dissertation angenommen am	18.11.2020
Tag der Disputation am	20.11.2020

Erstgutachter und Betreuer der Arbeit:	Prof. Dr. Robert Berger
Zweitgutachterin:	Prof. Dr. Anastasia Borschevsky
Weiteres Mitglied der Prüfungskommission:	Prof. Dr. Wolf-Christian Pilgrim

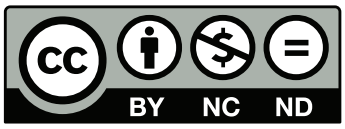

“There’s more stuff out there in the universe than we can see, that’s the point. We can see the stars and the galaxies and the things that shine, but for it all to hang together and not fly apart, there needs to be a lot more of it — to make gravity work, you see. But no one can detect it. So there are lots of different research projects trying to find out what it is, and this is one of them.”

Dr. Mary Malone
in Philip Pullman, *His Dark Materials: The Subtle Knife*, Ch. 4.

Preface

This dissertation is an accumulation of research which I conducted under supervision of Prof. Dr. Robert Berger at the Fachbereich Chemie of the Philipps-Universität Marburg between 2016 and 2020. The research projects resulted in eight manuscripts, six of them being already accepted or published in peer-reviewed scientific journals:[1]

8. K. Gaul, and R. Berger, *Complementary molecules for experimental disentanglement of sources of $\mathcal{P},\mathcal{T}$-violation from simple models*, *manuscript in preparation.*

7. K. Gaul, N. Gürlebeck, and R. Berger, *Enhancement of Lorentz invariance violation in iodine molecular clock transitions*, *manuscript in preparation.*

6. K. Gaul, M. G. Kozlov, T. A. Isaev, and R. Berger, *Parity nonconserving interactions of electrons in chiral molecules with cosmic fields*, Phys. Rev. A *accepted* **2020**;

5. K. Gaul, M. G. Kozlov, T. A. Isaev, and R. Berger, *Chiral molecules as sensitive probes for direct detection of $\mathcal{P}$-odd cosmic fields*, Phys. Rev. Lett. *accepted* **2020**;

4. K. Gaul, and R. Berger, *Toolbox approach for quasi-relativistic calculation of molecular properties for precision tests of fundamental physics*, J. Chem. Phys 152, 044101, **2020**.

3. K. Gaul, and R. Berger, *Ab initio study of parity and time-reversal violation in laser-coolable triatomic molecules*, Phys. Rev. A 101, 012508, **2020**.

2. K. Gaul, S. Marquardt, T. Isaev, and R. Berger, *Systematic study of relativistic and chemical enhancements of $\mathcal{P},\mathcal{T}$-odd effects in polar diatomic radicals*, Phys. Rev. A 99, 032509, **2019**.

1. N. Gürlebeck, L. Wörner, T. Schuldt, K. Döringshoff, K. Gaul, D. Gerardi, A. Grenzebach, N. Jha, E. Kovalchuk, A. Resch, T. Wendrich, R. Berger, S. Herrmann, U. Johann, M. Krutzik, A. Peters, E. M. Rasel, and C. Braxmaier, *BOOST: A satellite mission to test Lorentz invariance using high-performance optical frequency references*, Phys. Rev. D 97, 124051, **2018**.

The eight manuscripts and my personal contributions to them are discussed in Ch. 4 of this thesis.

With the finalization of this thesis a wonderful period of my life also comes to an end. I want to use the following space to thank all the persons without whom this thesis would not have been possible, or at least the time I spent for it would not have been a quarter as enjoyable as it has been.

Allen voran gilt mein Dank dem Betreuer dieser Arbeit, Prof. Robert Berger. Danke Robert, dass ich ein solch spannendes Thema in meiner Dissertation bearbeiten durfte, danke für die Freiheit, die du mir bei dessen Bearbeitung gelassen hast, und für die vielen lehrreichen Diskussionen. Darüber hinaus möchte ich mich für die Möglichkeiten, meine Forschung auf zahlreichen spannenden Konferenzen, Workshops und Sommerschulen vorzustellen und ein Teil vieler interessanter Kollaborationen mit internationalen Forschungsgruppen zu werden, bedanken. Vielen Dank für die letzten vier Jahre in denen ich so viel gelernt habe.

[1] A full list of my publications, including all presentations at conferences, seminars and summer schools that I gave during the work on this thesis, is provided in my CV in the Appendix.

I thank Prof. Anastasia Borschevsky very much for taking on the responsibility of second examiner and writing the second referee report of this thesis.

Ich bedanke mich auch bei Prof. Wolf-Christian Pilgrim, der sich die Zeit genommen hat meine Prüfungskommission zu vervollständigen.

An important part of this thesis would not have been possible without the fruitful collaboration with our colleagues in St. Petersburg, Misha Kozlov and Timur Isaev. I thank you a lot for raising my interest in dark matter and cosmic fields and all the helpful discussions. Furthermore, I want to thank the BOOST collaboration, and in particular, Norman Gürlebeck who trusted in our expertise and gave me the opportunity to contribute to a satellite mission with this thesis.

Dass die Arbeit an dieser Dissertation zu einer schönen Zeit wurde, verdanke ich vor allem der guten Atmosphäre und dem starken Zusammenhalt in unserer Arbeitsgruppe. Dazu haben allen voran die besten Kollegen, die man haben kann, beigetragen: Steffen Giesen, Anna Hansmann und Mira Diekmann. Ich danke euch für die vielen unterhaltsamen Stunden im Büro oder der Küche und natürlich die schönen Erlebnisse bei den zahlreichen Konferenzen. Danke auch Anna und Steffen, dass ihr mich bei der Verbesserung des Manuskripts dieser Arbeit unterstützt habt.

Hervorheben möchte ich auch unseren ehemaligen Kollegen Sebastian Marquardt, der mich bei meinem ersten Projekt in der AG Berger betreut hat und mit seinem Engagement entscheidend dazu beigetragen hat, mich für die Gruppe zu begeistern. Vielen Dank!

I would like to thank all other members of our group as well, for the nice working climate and the many interesting conversations. I thank you, Nityananda Sahu, Manjinder Kour and Kaushik Talukdar.

Schließlich möchte ich auch Ralf Tonner und seinen Doktoranden Fabian Pieck und Jan-Niclas Luy für die freundschaftliche Atmosphäre in der Marburger TC danken. Alles Gute in Regensburg!

Entscheidend für den reibungslosen Ablauf im Arbeitsalltag waren auch Anette und Reuti, die jeden Tag dafür arbeiten, die Infrastruktur aufrechtzuerhalten und Organisatorisches zu bewältigen. Insbesondere dir, Reuti, möchte ich für deine ständige Hilfsbereitschaft mich bei der Lösung kniffliger Hard- und Softwareprobleme zu unterstützen, danken.

Wenn es auch nicht in direktem Zusammenhang mit meiner Doktorarbeit stand, so war es doch eine gewinnbringende Erfahrung Mengyi Chen, Oliver Kreuz und Carsten Zülch in ihren Forschungspraktika zu betreuen. Ich möchte euch herzlich danken, dass ihr euch dafür entschieden habt, eine Vertiefung bei mir zu machen. An dieser Stelle möchte ich auch Prof. Florian Kraus für die fruchtbare Zusammenarbeit danken, durch die aus Mengyis Vertiefungspraktikum eine Veröffentlichung hervorgegangen ist.

Ich bin dankbar, dass ich Teil des Sonderforschungsbereichs (SFB) 1319 *Extreme light for sensing and driving molecular chirality* (ELCH) der Deutschen Forschungsgemeinschaft (DFG) sein konnte, der es mir ermöglicht hat, an spannenden Workshops, Retreats und einer Sommerschule teilzunehmen. Im Rahmen des SFB 1319 wurden auch drei der oben aufgeführten Publikationen gefördert.

Dass ich diese Arbeit schreiben konnte und die Zeit, in der sie entstanden ist, auch außerhalb der Universität eine schöne Zeit war, verdanke ich vor allem meiner Familie. Danke Mama, danke Papa für die sorglose Kindheit, die ich genießen konnte und die Möglichkeiten, die ihr mir für mein Leben gegeben habt. Danke auch an meine Geschwister Sebastian, Alexander und Katharina und ihre Familien, dass ihr die Familie zu einem Ort der Geborgenheit macht.

Danke Marianne, dass du mit mir dein Leben teilst und mich in meinen Lebensplänen unterstützt. Danke, dass wir gemeinsam in die Zukunft blicken. Und — nicht zuletzt — danke, dass du dich durch das Manuskript dieser Arbeit gekämpft hast und mich bei dessen Verbesserung unterstützt hast.

Contents

Abstract

Even today, fundamental difficulties remain in the understanding of our universe. Among those are inexplicable phenomena like the enormous excess of matter over anti-matter (baryon asymmetry) — connected to the question why is there matter at all — or dark matter (DM) and dark energy which are invoked to explain the structure and evolution of our universe, and problems like the unification of quantum theory with gravity. In order to take a step closer to resolving such issues, it is important to test the known laws of physics, summarized in the standard models of particle physics (SM) and cosmology (ΛCDM model), as accurately as possible. Direct experimental tests of the SM can be carried out with high energies at large colliders like the LHC at CERN, and direct tests of the ΛCDM model are usually performed at large observatories like LIGO.

In contrast, the theoretical foundations of chemistry are mostly well understood. Hence, molecules are theoretically and experimentally well controllable. Thus, measurements in standard-sized laboratories with ultra-high precision are possible, so that the less well understood laws of physics can be tested. Such low-energy experiments provide indirect tests of the standard models in the realm of chemistry by probing the fundamental symmetries of nature. Therewith, these tests are complementary to direct tests of the laws of physics in cosmology or high-energy physics.

In this cumulative thesis quantum chemical methods are developed and applied to design new experiments and improve existing experiments that employ molecules for tests of fundamental symmetries and, therewith, search for new physics beyond the standard models (BSM).

A simultaneous violation of parity and time-reversal symmetry ($\mathcal{P},\mathcal{T}$) is closely connected to baryon asymmetry. $\mathcal{P},\mathcal{T}$-violation appears in a larger amount in unifying BSM theories than in the SM itself. $\mathcal{P},\mathcal{T}$-violation on the elementary particle level is relativistically enhanced in heavy atoms and heavy-elemental molecules and results in *permanent* electric dipole moments (EDMs) of atoms and molecules which are non-vanishing in the limit of vanishing electric fields. In the first part of this thesis, $\mathcal{P},\mathcal{T}$-violations in diatomic and small polyatomic molecules are studied in order to find well-suited candidates for a first measurement of a permanent EDM. Within this study relativistic effects as well as effects due to the chemical environment of the heavy atom are systematically analyzed. Furthermore, the effects of various fundamental sources of $\mathcal{P},\mathcal{T}$-violation that contribute to the $\mathcal{P},\mathcal{T}$-odd EDM of a molecule are studied. It is discussed, how these sources can be disentangled from experiments that aim to measure the permanent EDMs of different molecules. Among this research one of the first calculations of $\mathcal{P},\mathcal{T}$-odd effects in polyatomic molecules is presented.

In the second part of this thesis, the applicability of chiral molecules as sensitive probes for $\mathcal{P}$-violating cosmic fields is demonstrated. $\mathcal{P}$-violating cosmic fields are predicted in several cold DM (CDM) models as well as in the standard model extension (SME) that allows for local Lorentz invariance violation (LLIV). LLIV appears in several theories that aim to unify quantum theory and gravity. It is shown that well-chosen chiral molecules containing heavy elements can improve present limits on $\mathcal{P}$-odd interactions of electrons with cosmic fields by at least two orders of magnitude. This renders chiral molecules particularly interesting for searches for BSM physics. In order to guide future searches for candidate molecules, challenges that may appear in the theoretical description or the design of experiments are discussed.

In the last part of this thesis, the possibilities to use a clock transition in the iodine molecule to limit LLIV are explored in cooperation with the BOOST collaboration. Quantum chemical studies of such effects in iodine are presented. These calculations are essential for an estimate of the expected sensitivity of the BOOST satellite mission, which employs the iodine molecular clock as probe for LLIV.

Kurzzusammenfassung

Auch heute gibt es noch grundlegende Schwierigkeiten im Verständnis unseres Universums. Dazu zählen unerklärliche Phänomene wie der gewaltige Überschuss von Materie zu Antimaterie (Baryonasymmetrie) — verknüpft mit der Frage warum es überhaupt Materie gibt — oder Dunkle Materie (DM) und Dunkle Energie, welche zur Erklärung der Struktur und Entwicklung unseres Universums dienen, und Probleme wie die Vereinbarkeit von Quantentheorie und Gravitation. Um der Lösung solcher Probleme einen Schritt näher zu kommen, ist es wichtig, die bekannten Gesetze der Physik, die in den Standardmodellen der Teilchenphysik (SM) und Kosmologie (ΛCDM Modell) zusammengefasst sind, so genau wie möglich zu überprüfen. Direkte experimentelle Tests des SM können mit hoher Energie an großen Teilchenbeschleunigern wie dem LHC am CERN durchgeführt werden und direkte Tests des ΛCDM Modells werden üblicherweise an großen Observatorien wie dem LIGO realisiert.

Im Gegensatz dazu sind die theoretischen Grundlagen der Chemie weitestgehend gut verstanden. Deshalb können Moleküle sowohl theoretisch als auch experimentell gut kontrolliert werden. Somit sind Messungen in normal großen Laboratorien mit sehr hoher Präzision möglich, die genutzt werden können, um weniger gut verstandene physikalische Gesetze zu testen. Solche Niedrigenergieexperimente bieten indirekte Tests der Standardmodelle im Bereich der Chemie, indem die fundamentalen Symmetrien der Natur untersucht werden. Damit sind diese Experimente komplementär zur direkten Überprüfung der Gesetze der Physik in der Kosmologie oder Hochenergiephysik.

In dieser kumulativen Dissertation werden quantenchemische Methoden entwickelt und angewendet, um neue Experimente zu entwickeln und bestehende Experimente zu verbessern, die mit Hilfe von Molekülen fundamentale Symmetrien testen und damit nach Physik jenseits der Standardmodelle [*beyond the standad models* (BSM)] suchen.

Die simultane Verletzung von Parität und Zeitumkehr ($\mathcal{P},\mathcal{T}$) ist eng mit der Baryonasymmetrie verknüpft. $\mathcal{P},\mathcal{T}$-Verletzung wird in vereinheitlichenden BSM-Theorien in einem größeren Umfang vorhergesagt als im SM selbst. $\mathcal{P},\mathcal{T}$-Verletzung auf der Ebene von Elementarteilchen wird in schweren Atomen und Molekülen mit schweren Elementen relativistisch verstärkt und führt zu *permanenten* elektrischen Dipolmomenten (EDMs) von Atomen und Molekülen, welche im Grenzfall von verschwindenden elektrischen Feldern nicht verschwinden. Im ersten Teil dieser Dissertation werden $\mathcal{P},\mathcal{T}$-Verletzungen in zweiatomigen und kleinen mehratomigen Molekülen untersucht, um geeignete Kandidaten für die erstmalige Messung eines permanenten EDMs zu identifizieren. Dabei werden relativistische Effekte sowie Effekte durch die chemische Umgebung des schweren Atoms in den Molekülen systematisch analysiert. Des Weiteren werden verschiedene fundamentale Quellen von $\mathcal{P},\mathcal{T}$-Verletzung, die zu einem $\mathcal{P},\mathcal{T}$-ungeraden EDM eines Moleküls beitragen können, untersucht. Es wird diskutiert, wie diese Quellen mit Experimenten, die eine Messung des permanenten EDMs von verschiedenen Molekülen anstreben, entkoppelt werden können. Innerhalb dieser Forschungsprojekte wird eine der ersten Berechnungen von $\mathcal{P},\mathcal{T}$-ungeraden Effekten in mehratomigen Molekülen präsentiert.

Im zweiten Teil dieser Dissertation wird erstmals die Anwendbarkeit von chiralen Molekülen als empfindliche Sonde für $\mathcal{P}$-verletzende kosmische Felder demonstriert. $\mathcal{P}$-verletzende kosmische Felder werden in verschiedenen Modellen für kalte DM (CDM) sowie in der Standardmodellerweiterung (SME), die eine lokale Lorentzinvarianzverletzung (LLIV) erlaubt, vorhergesagt. LLIV kommt in verschiedenen Theorien, die eine Vereinheitlichung von Quantentheorie und Gravitation anstreben, vor. Es wird gezeigt, dass günstig gewählte chirale Moleküle, die schwere Elemente enthalten, die bestehenden Schranken für $\mathcal{P}$-ungerade Wechselwirkungen von

Elektronen mit kosmischen Feldern um mindestens zwei Größenordnungen verbessern können. Dies macht chirale Moleküle für die Suche nach BSM-Physik besonders interessant. Um die zukünftige Suche nach geeigneten Molekülkandidaten zu leiten, werden die Herausforderungen, die sowohl in der theoretischen Beschreibung als auch im Design der Experimente auftauchen können, diskutiert.

Im letzten Teil dieser Dissertation werden in Zusammenarbeit mit der BOOST-Kollaboration die Möglichkeiten Uhrenübergänge im Iodmolekül zu nutzen, um LLIV einzuschränken, erforscht. Quantenchemische Berechnungen dieser LLIV-Effekte im Iodmolekül werden präsentiert. Diese Rechnungen sind unabdingbar für die Abschätzung der zu erwartenden Empfindlichkeit der BOOST-Satellitenmission, welche die Iodmoleküluhr als Sonde für LLIV nutzt.

1 Introduction. — Probing the laws of nature

> *“ The important thing is not to stop questioning; curiosity has its own reason for existing. One cannot help but be in awe when contemplating the mysteries of eternity, of life, of the marvelous structure of reality. It is enough if one tries merely to comprehend a little of the mystery every day. The important thing is not to stop questioning; never lose a holy curiosity. ”*
>
> Albert Einstein
>
> to William Miller, as quoted in *Life* magazine (2 May 1955).

Despite the successful prediction and explanation of most experimental observations, today's accepted laws of nature leave fundamental questions such as the origin of our universe unanswered. Furthermore, the history of physics shows that even if it is commonly accepted that a physical theory is complete, rigorous testing of the physical laws to high precision can reveal *new physics* and in long term enable developments of technologies not thought of. Such a revolution not only of physical theories, but also of physical thinking, for example, was initiated by the discovery of quantum mechanics, which did not only start a new era of physics, but as well changed our every-day life with technological development.

It is, thus, one of the most important tasks of science not only to explain our world with mathematical laws, but rather to push the experimental precision of tests of these laws to a maximum in order to assure that the laws of physics are universally valid. Hence, it is of uttermost importance to develop new techniques and experiments that allow such test on the border of what is explainable and what is not.

In this chapter the commonly accepted and experimentally validated laws of physics are adumbrated and a basic mathematical description is introduced. Their limitations and so far unexplained phenomena are discussed, with focus on those which are directly addressed by the developments of this thesis. The connection to symmetry properties of our universe and possible observables connected to a violation of these symmetries are highlighted.

1.1 What we know — The four forces and the standard models

The *state of the art* description of nature and its physical interpretation is formulated in the so called standard models of physics.

The Standard Model of particle physics (SM) comprises existing theories for microscopic matter and within those describes three of four known fundamental forces, namely the electromagnetic force and the so called weak and strong nuclear forces. The fourth force, gravity, is important for massive objects, and, thus, plays an essential role for the physics of the macroscopic world, in particular astrophysics and cosmology. Gravity is not included in the SM but described separately within

Table 1.1: The four forces of nature, mediating bosons, interaction strength with respect to the electromagnetic force and charge. For a similar table see, e.g., Ch. 2 of Ref. [1].

Force	Mediator	Strength	Charge
Strong	Gluon g	1×10^{3}	color
Electromagnetic	Photon γ	1	electric
Weak	$W^{\pm}$ & Z^{0}	1×10^{-11}	weak
Gravity	Graviton G	10×10^{-40}	mass

the General theory of Relativity (GR) which plays a major role in the so called standard model of cosmology called the Λ Cold Dark Matter (ΛCDM) model.

The four forces, their relative interaction strengths, mediators and their charge are summarized in Table 1.1.

1.1.1 The standard model of particle physics

The SM is topic of many text books. A good overview can be found, e.g., in Ref. [1] and a rigorous field theoretical introduction is given in Ref. [2].

In the SM electromagnetic and weak forces are described within the Standard Electro Weak Theory (SEWT), which unifies Quantum Electrodynamics (QED) with weak interactions. The strong forces are described within Quantum Chromodynamics (QCD). These theories are formulated as gauge theories, i.e., they are invariant under special local symmetries. Within these theories particles are described as quantized fields of harmonic oscillators (Quantum Field Theory (QFT)).

Besides quantum theory the most important concept on which these theories are based is the Special theory of Relativity (SR) which is build on the two postulates of relativity stated by Poincaré and Einstein [3, 4]:

1. Principle of relativity: The laws of physics do not depend on how one is moving. They are the same for a stationary observer as a constantly moving observer, and none of both can detect who is actually moving.

2. Principle of constant speed and direction of light: In vacuum light propagates at a finite speed c that *always* remains constant in a constant direction.

These two principles lead to a fundamental symmetry called Lorentz symmetry, which will be discussed in more detail in the next section.

The SM includes all experimentally observed elementary particles and describes their interactions within the above listed theories. An overview of all observed particles after mass generation in the Higgs mechanism (see paragraph 1.1.1.a) and interactions among these within the standard model is given in Figure 1.1.

In experiments discussed in this thesis observables correspond to energy values. The energy of a particle or many-particle system is characterized by its Hamiltonian H or Lagrangian L. For velocity independent potentials which are considered in this thesis, H and L can be written as

$$H = T + V \tag{1.1}$$

$$L = T - V, \tag{1.2}$$

where T is the kinetic energy and V is the potential energy. In the following interactions are represented as quantum mechanical Hamiltonian operators $\hat{H}$ with $H = \left\langle \psi \middle| \hat{H} \middle| \psi \right\rangle$ or Lagrangian densities $\mathcal{L}$ with $L = \int \mathrm{d}^3 r \mathcal{L}$, with the position coordinate $\vec{r} = (x, y, z)^\mathsf{T}$ in three-dimensional Euclidean space. In general the equations of motion for a particle are fully determined by its Lagrangian. All interactions in the SM can be described within QFT symbolically by so called *Feynman diagrams* as sketched in Figure 1.1. These are intuitive qualitative representations of the exact mathematical expressions for interactions and can be translated into the interaction Lagrangians, Hamiltonians or scattering amplitudes following the so called *Feynman rules*.

All properties that are discussed in this thesis can be elegantly written within Minkowski space, a four dimensional space that unifies the position space and time. In the following the Minkowski metric $\eta = \mathrm{diag}(1, -1, -1, -1)$ will be used. I use index tensor notation for a unified description of space and time via four dimensional quantities. For this purpose indices μ, ν, ρ, σ running from

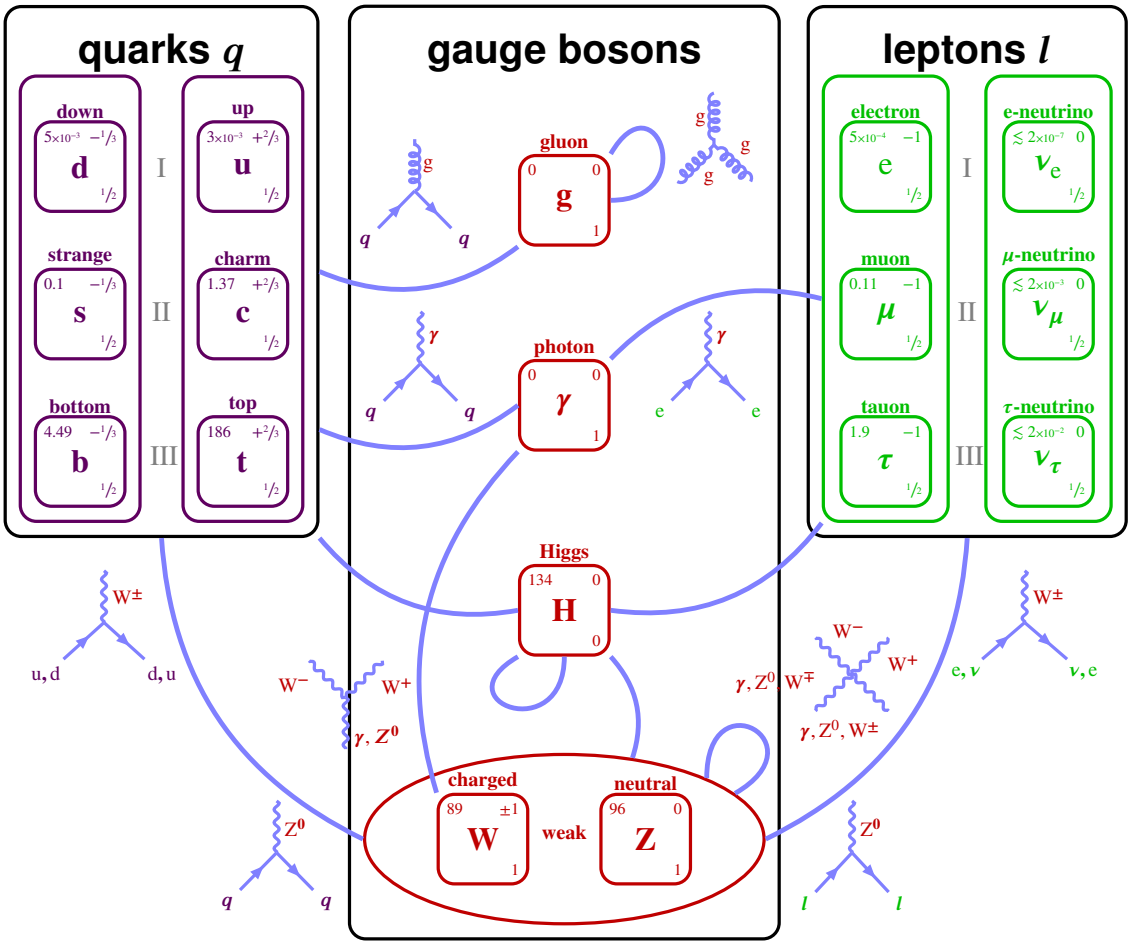

Figure 1.1: Summary of particles and their interactions in the standard model. Representative Feynman diagrams for different types of interactions within the standard model are shown. In Feynman diagrams time flows from left to right. Charged or electron-like leptons are denoted by e, positively charged or up-like quarks by u and negatively charged or down-like quarks by d. As in a periodic table for each elementary particle the mass is given in atomic mass units in the upper left corner. In the upper and lower right corners the electric charge and total spin are given, respectively. This idea is adapted from the *periodic table of elementary particles* in Ref. [5].

0 to 3 and i, j, k, l running from 1 to 3 are employed, where 0 represents time and 1 to 3 represent position space. For convenience Einstein's sum convention for repeated indices is used: $a_\mu a^\mu = a^\mu a_\mu = \sum_{\mu=0}^{3} a^\mu a_\mu$. Covariant vectors are defined as V_μ and contravariant vectors as $V^\mu = \eta^{\mu\nu} V_\nu$. The contravariant four-vector of spacetime coordinates is defined as $x^0 = ct$, $x^{(1-3)} = \vec{r}$ and the corresponding covariant derivative is $\partial_\mu = \frac{\partial}{\partial x^\mu}$.

In the following paragraphs I introduce the particles and their fundamental interactions within the framework of the SM step by step. Herein, focus is laid on electrons and interactions with electrons, as these are decisive for the structure of molecular systems.

1.1.1.a Gauge bosons

In the SM the mediating bosons are all *vector bosons*, i.e., they are spin 1 particles. Before mass generation due to the Higgs mechanism, there are twelve massless vector bosons: the eight gluons g_a (with $a = 1, 2, \ldots, 8$) and the electroweak bosons W_a (with $a = 1, 2, 3$) and B. All these vector bosons are represented as relativistic vector fields V^μ, i.e., the electroweak boson fields

(B^μ, W_a^μ) and the gluon fields (G_a^μ), where the index a runs over all three representations of W ($SU(2)$ group) or all eight color representations of G ($SU(3)$ group), respectively. They satisfy the Maxwell equations which appear in covariant form as:

$$\epsilon^{\mu\nu\rho\sigma}\partial_\rho F^a_{\mu\nu} = 0; \qquad \partial_\mu F^{\mu\nu}_a = j^\nu_a, \tag{1.3}$$

where $\epsilon^{\mu\nu\rho\sigma}$ is the Levi-Civita tensor of rank 4, and $F^{\mu\nu}_a = \partial^\mu V^\nu_a - \partial^\nu V^\mu_a + g_V f_{abc} V^\mu_b V^\nu_c$ is the field strength tensor of a contravariant vector field V^μ_a with its coupling constant g_V and the structure constant f_{abc} of the gauge group. The indices a, b, c run over all representations of the gauge group. The last term of $F^{\mu\nu}_a$ vanishes for an Abelian group such as $U(1)$ but is non-vanishing for non-Abelian groups such as $SU(2)$ and $SU(3)$. j^ν is the four-current containing the charge density $j^0 = c\rho$ and the current density $j^{1-3} = \vec{j}$ which are conserved $\partial_\mu j^\mu = 0$. Here, all interaction constants are contained in the definition of the densities ρ and $\vec{j}$. The B^μ field couples via the weak hypercharge Y ($U(1)$ group) and the W^μ_a fields couples only on left-handed fermions ($SU_\mathrm{L}(2)$). These equations of motions are determined by the kinetic energy Lagrangian density $\mathcal{L}_{\mathrm{kin},V} = -\frac{1}{4} F^a_{\mu\nu} F^{\mu\nu}_a$.

The Higgs boson, introduced independently by Higgs [6, 7], Englert and Brout [8] and Guralink *et.al.* [9] in 1964, is a *scalar boson*, i.e., it has spin 0 and is essential within the SM as it generates all masses by a mechanism of spontaneous symmetry breaking. It was discovered first in 2012 (see the two press releases [10, 11]). Within the SEWT by Glashow, Weinberg and Salam [12–14] the electroweak bosons B and W_i mix to the massive weak boson fields $Z^\mu = \cos\theta_\mathrm{W} W^\mu_3 - \sin\theta_\mathrm{W} B^\mu$, $W^\mu_\pm = \frac{1}{\sqrt{2}}(W^\mu_1 \mp \imath W^\mu_2)$ and the massless photon field $A^\mu = \sin\theta_\mathrm{W} W^\mu_3 + \cos\theta_\mathrm{W} B^\mu$ with the weak mixing angle or Weinberg angle θ_W by spontaneous symmetry breaking due to the Higgs mechanism (for details see, e.g., Chs. 11 and 13 in Ref. [15]).

The photon field still obeys the Maxwell equations and belongs to the $U(1)$ group, whereas the Lagrangian density of the massive spin 1 fields of the weak interaction (Z^μ and $W^\mu_\pm$) reads

$$\mathcal{L}_V = \mathcal{L}_{\mathrm{kin},V} - \underbrace{m_V^2 c^4 V^\mu V_\mu}_{\mathcal{L}_{\mathrm{mass},V}}, \tag{1.4}$$

where V can be $W_\pm$ or Z and the additional mass term is proportional to the squared particle mass m_V. This Lagrangian results in the so called Proca equations of motion (see Refs. [1, 2]).

The Higgs field ϕ_H itself is a massive scalar. A scalar field ϕ with mass m_ϕ has a Lagrangian density

$$\mathcal{L}_\phi = \frac{1}{2}(\partial_\mu \phi^\dagger)(\partial^\nu \phi) - \frac{1}{2} m_\phi^2 c^4 \phi^\dagger \phi\,, \tag{1.5}$$

and, thus, satisfies the Klein-Gordon equation [16, 17]:

$$(\hbar^2 \Box + m_\phi^2 c^4)\phi = 0, \tag{1.6}$$

where $\hbar = \frac{h}{2\pi}$ is the reduced Planck constant and $\Box = \partial_\mu \partial^\mu$ is the d'Alembertian.

The Higgs boson couples via electroweak bosons to charged leptons and quarks and generates the masses of them. For neutrinos it is not yet known whether the Higgs boson couples to them or not. In the following I will continue with the description of particles after mass generation in the Higgs mechanism, as presented in Figure 1.1. For details on mass generation of fermions see, e.g., Refs. [2, 15].

1.1.1.b Fermions and Interactions

Charged leptons and quarks are massive spin $^1/_2$ particles, i.e., fermions (f), and, thus, satisfy the Dirac equation [18, 19]:

$$\left(-\imath\hbar c\partial_\mu \boldsymbol{\gamma}^\mu + m_\mathrm{f} c^2\right)\psi_\mathrm{f} = 0\,. \tag{1.7}$$

Here ψ_f is a bispinor, i.e., $\psi_\mathrm{f} = \begin{pmatrix}\psi_\mathrm{f}^\mathrm{L}\\ \psi_\mathrm{f}^\mathrm{S}\end{pmatrix}$, with $\psi_\mathrm{f}^\mathrm{L}$ and $\psi_\mathrm{f}^\mathrm{S}$ being spinors commonly called the *large and small component*, which represent the positive (particle) and negative (anti-particle) energy states, respectively. The Dirac matrices $\boldsymbol{\gamma}^\mu$ are part of a set of 16 matrices $\boldsymbol{\Gamma}^{\mu\nu}$ that form a Clifford algebra. Their special symmetry implications and connections to different types of symmetries are discussed in the next sections. The Lagrangian density of a free fermion is

$$\mathcal{L}_\mathrm{f} = -\imath\hbar c\bar{\psi}_\mathrm{f}\partial_\mu\boldsymbol{\gamma}^\mu\psi_\mathrm{f} - m_\mathrm{f}c^2\bar{\psi}_\mathrm{f}\psi_\mathrm{f}\,, \tag{1.8}$$

where I have introduced the adjoint spinor $\bar{\psi}_\mathrm{f} = \psi_\mathrm{f}^\dagger\boldsymbol{\gamma}^0$ for which any bilinear $\bar{\psi}_\mathrm{f}\boldsymbol{\Gamma}^{\mu\nu}\psi_\mathrm{f}$ is covariant under Poincaré transformations. These covariant bilinears will be discussed in more detail in the next section.

In order to describe particle interactions the coupling to fields of the gauge bosons has to be considered. Within QFT interactions are typically described in the framework of perturbation theory. Most important for the description of systems consisting of electrons is the coupling to the photon field A^μ resulting in the electromagnetic interaction. The Dirac equation of an electron (e) that is moving in an external electromagnetic potential appears in leading order as

$$\left(-\imath\hbar c\partial_\mu\boldsymbol{\gamma}^\mu + eA_\mu\boldsymbol{\gamma}^\mu + m_\mathrm{e}c^2\right)\psi_\mathrm{e} = 0, \tag{1.9}$$

where the corresponding leading order interaction Lagrangian $\mathcal{L}_\mathrm{int} = -e\bar{\psi}_\mathrm{e}A_\mu\boldsymbol{\gamma}^\mu\psi_\mathrm{e}$, known as minimal coupling, is considered. Here, e is the elementary electric charge. Higher order multipole moments of the electron could couple through derivatives of the photon field. In next order electric and magnetic dipole moments can be considered, which then couple to the electromagnetic field tensor $F_{\mu\nu} = \partial_\mu A_\nu - \partial_\nu A_\mu$.

Electromagnetic interactions between fermions result in leading order in the fine structure constant in classical Coulomb interactions, if Coulomb gauge is used. The classical Coulomb interaction for two particles 1 and 2 results in the potential

$$V_\mathrm{C}(\vec{r}_1,\vec{r}_2) = \frac{q_1q_2}{4\pi\epsilon_0}\frac{\mathbf{1}_1\mathbf{1}_2}{|\vec{r}_1-\vec{r}_2|}\,, \tag{1.10}$$

where q_i is the electric charge, $\vec{r}_i$ the position in space of particle i, ϵ_0 is the electric constant, and $\mathbf{1}_i$ is the identity operator for particle i.

For the description of most bound-state many-particle systems such as atoms and molecules, the Coulomb approximation is usually sufficient. However, particularly for the accurate description of relativistic effects in light atoms and molecules, first order effects of the quantized fields of the electrons can become crucial. For this case, the so-called Breit potential can be employed for the electron-electron interactions [20]:

$$V_\mathrm{B}(\vec{r}_1,\vec{r}_2) = \frac{q_1q_2}{4\pi\epsilon_0}\left[\frac{\mathbf{1}_1\mathbf{1}_2}{|\vec{r}_1-\vec{r}_2|} - \frac{\vec{\boldsymbol{\alpha}}_1\cdot\vec{\boldsymbol{\alpha}}_2}{2|\vec{r}_1-\vec{r}_2|} + \frac{\left(\vec{\boldsymbol{\alpha}}_1\cdot\vec{r}_2\right)\left(\vec{\boldsymbol{\alpha}}_2\cdot\vec{r}_1\right)}{2|\vec{r}_1-\vec{r}_2|^3}\right]\,, \tag{1.11}$$

where the Dirac matrices $\vec{\boldsymbol{\alpha}}$ are part of the 16 matrices $\boldsymbol{\Gamma}^{\mu\nu}$, which is discussed in the next section. The Breit potential includes beside the classical Coulomb interactions (first term), the spin-other

orbit, spin-spin and orbit-orbit interactions of the two particles (second term, Gaunt term), and first order retardation effects (third term). Interactions of electrons mediated by weak bosons will be briefly discussed in the next chapter.

The above equations are valid for massive fermions only. Within the original SM formulations neutrinos remain massless and interact exclusively via weak interactions. The equations of motion for massless fermions are called Weyl equations and have the form

$$\sigma^{\mu}\partial_{\mu}\psi_{\nu,\mathrm{L}} = 0\,. \tag{1.12}$$

These equations are valid for left-handed neutrinos, which are described by the spinor fields $\psi_{\nu,\mathrm{L}}$. Here σ^{μ} are the Pauli spin matrices, which will be discussed in the next section. Within the SM only left-handed neutrinos (or right-handed anti-neutrinos) couple to any other form of matter. With the discovery of neutrino oscillations, and therewith, nonzero neutrino masses, an empirical neutrino mixing matrix was introduced (see also Review [21]) that can account for massive neutrinos. Such massive neutrinos are supposed to follow the so called Majorana equation, which is similar to the Dirac equation but introduces a charge conjugate spinor for the mass term.

1.1.1.c Composite particles

In the SM heavier particles are formed by interaction of fermions through the gauge bosons. There are baryons such as the nucleons (protons and neutrons), which are built up of three quarks, and mesons such as pions and kaons, which are built up of a quark and an antiquark. Together baryons and mesons form the group of hadrons which summarizes all particles formed by strong interactions.

Among the hadrons most important for the discussions in this thesis are the proton which is composed of two up and one down quark, and the neutron which is composed of two down and one up quark. The proton and neutron form the group of nucleons. Uncompensated strong forces within the proton and neutron lead to a Yukawa force and the formation of nuclei.

Larger structures, such as atoms and molecules, are predominantly formed by the electromagnetic interaction of leptons with nuclei.

Although very successful as an explanation of most observations of particle physics and being a very accurate theory, as can be seen by the prediction of 9 digits of the anomalous magnetic dipole moment [22, 23] of the electron, the SM does not describe SEWT and QCD in a unified theory, nor does it contain a description of gravity, and its borders are touched by many other observations, as will be topic of the next pages.

1.1.2 The standard model of cosmology

Cosmology describes the development of our universe from big bang to present and the structure of the cosmos. The ΛCDM model is the simplest model, which is in agreement with the most important cosmological observations (see the Review [24] and references therein for a detailed discussion of the ΛCDM model). It is capable to describe the accelerating expansion of the universe, the structure of the microwave background and the large-scale structure of the cosmos. Λ represents the cosmological constant associated with Dark Energy (DE). In this model the universe is assumed to be consistent of matter, Dark Matter (DM) and DE. The ΛCDM model depends only on six empirical parameters: the cosmological constant Λ, the ratio of baryonic matter to DM, the age of the universe, the scalar spectral index, the curvature fluctuation amplitude and the reionization optical depth (see Ref. [24]). Within ΛCDM GR is assumed to be the valid theory of gravitation on cosmological scales. GR describes gravitation as massless spin 2 field that follows

a non-linear equation of motion, the so called Einstein field equations [25, 26]:

$$R_{\mu\nu} - \frac{1}{2}\eta_{\mu\nu}R + \Lambda\eta_{\mu\nu} = \frac{8\pi G}{c^4}T_{\mu\nu}, \tag{1.13}$$

with the Ricci curvature tensor $R_{\mu\nu}$, the scalar curvature $R = \eta^{\mu\nu}R_{\mu\nu}$, Newton's gravitational constant G and the energy-momentum tensor of matter $T_{\mu\nu}$.

In ΛCDM, as indicated by the name, DM is assumed to be cold, i.e., it is only non-relativistically moving over the evolution of the universe. Despite enormous experimental success of the ΛCDM model (see, e.g., Refs. [27, 28]), so far there is no convincing explanation for the nature of DM and DE, as will be addressed in succeeding sections. Alternative models based on different theories of gravity such as MOdified Newtonian Dynamics (MOND) provide a competing mathematical description of cosmology (for more details see, e.g., Ref. [29]).

1.2 The symmetries of nature

In most natural sciences symmetry serves as an axiomatic principle and a guide for decisions. Symmetry manifests itself in nature on a macroscopic and microscopic level in many different flavors, ranging from perfect spheres to complex fractal structures. It is thus intuitive to expect symmetry playing a fundamental role in the laws of nature, mathematically accumulated in theoretical physics, as well. Indeed, the fundamental laws of physics are based on symmetry arguments: e.g., manifested in the Galilean invariance of Newton's laws of mechanics, or the gauge and Lorentz invariance of the Maxwell equations introduced in the preceding section [30].

With the development of quantum mechanics and special relativity, symmetry became even more fundamental and today is an important guide for the creation of theoretical models. In 1918 Emmy Noether published her famous formal mathematical connection between conservation laws in physics and symmetry [31, 32]. The implications of these connections for conserved quantities, and — most interesting for testing these axiomatically applied symmetry principles — the corresponding non-observable quantities are summarized for important physical laws in Table 1.2.

As can be seen in Table 1.2, in physics and chemistry three types of symmetries are relevant (see also Ref. [35]):

1. Continuous symmetries
    a) Space-time symmetries
2. Discrete symmetries
    a) Permutation symmetries
    b) $\mathcal{C}, \mathcal{P}, \mathcal{T}$-symmetries
3. Unitary symmetries
    a) Internal gauge symmetries.

Internal gauge symmetries are connected through Ward and Takahashi's analogue of Noethers theorem [33, 34] to conservation of quantum numbers (see Table 1.2, see also Ref. [39]).

Among the continuous symmetries, spacetime symmetries such as rotation and translation in space, translation in time, or joint spacetime transformations, such as Galileo, Lorentz or Poincaré transformations, play a prominent role in physics. Lorentz symmetry and transformation of spacetime were discovered by Lorentz in the late 19th century [40, 41]. It implies that the laws of nature

Table 1.2: Fundamental symmetries, connection to conservation laws of physics as defined by the Noether theorem [31, 32] for continuous symmetries and the Ward-Takashi identity [33, 34] for unitary symmetries and corresponding non-observable quantities (in parts adapted from Ref. [35]). For each symmetry the actual state of conservation is stated in the last column.

Symmetry	Conserved quantity	Non-observable	Conserved in nature
	Continuous symmetries		
translation in time	energy	absolute time	✓
translation in space	linear momentum	absolute spatial position	✓
rotation	angular momentum	absoulte spatial direction	✓
Lorentz symmetry	$\mathcal{CPT}$ [a]	absolute velocity	✓
	Discrete symmetries		
permutation symmetry	Bose-Einstein/Fermi-Dirac statistics	difference between identical particles	✓
inversion in space	parity ($\mathcal{P}$)	absolute left/right	✗
inversion in time	time-reversal ($\mathcal{T}$)	absolute direction of time	✗[b]
inversion of electric charge	charge conjugation ($\mathcal{C}$)	absolute sign of electric charge	✗
	Unitary symmetries		
$U(1)$ gauge invariance	electric charge Q	phase shifts between states of different Q	✓
$SU_{\mathrm{L}}(2)$ gauge invariance	weak charge Q_{W}	phase shifts between states of different Q_{W}	✓
$SU(3)$ gauge invariance	color charge Q_{c}	phase shifts between states of different Q_{c}	✓

[a] See Refs. [36–38].
[b] If Lorentz symmetry is conserved $\mathcal{CP}$-violation indicates that $\mathcal{T}$ must be broken due to the $\mathcal{CPT}$-theorem.

are invariant when going from one to another inertial system[1] and on its basis, SR was developed, mainly, by Einstein and Poincaré (see, e.g., Refs. [3, 4, 43–46]). For a comprehensive overview of the history of SR and further references, see, e.g., Ref. [42]. In contrast to the Lorentz group the Poincaré group additionally includes translations.

Discrete symmetry operations lead to a sign change of an object. Among such discrete operations permutations are important for systems that contain more than one indistinguishable particle. They manifest themselves within physics in Bose-Einstein and Fermi-Dirac statistics which

[1] The term inertial means that the systems are static or moving at *constant* velocity in present state. Thus Lorentz symmetry does not apply to accelerated objects. However, it shall be noted that all systems, whether accelerated in the past or not, are inertial systems, when their movement is uniform in the present. For details see, e.g., Ref. [42] or other books on relativity.

describe the permutation of bosons and fermions, respectively. Permutation symmetries are discussed in most books on quantum and statistical mechanics or molecular symmetry. E.g., for a comprehensive discussion of permutations of nuclei in molecules see Ref. [47]. In physics most important besides permutation symmetry are *parity* $\mathcal{P}$, which changes sign of all coordinates in position space, *charge conjugation* $\mathcal{C}$, which changes all signs of electric charges and *time-reversal* $\mathcal{T}$, which changes the sign of all momenta.

Among those discrete symmetries, I want to highlight in particular *parity* as it plays a major role not only in particle physics but also in molecular physics and chemistry. This symmetry operation inverts all signs in space:

$$\hat{\mathcal{P}} f(x, y, z) \hat{\mathcal{P}}^{-1} = f(-x, -y, -z) \tag{1.14}$$

Thus, the parity operation produces a *mirror image* of the initial object.

This is closely connected to the concept of *chirality* or *handedness* well-known in chemistry and physics. The parity operation turns a left-handed into a right-handed object. Elementary particles can be chiral as well if they have a non-zero spin and a linear momentum, i.e., they are moving. In case of a particle that moves with the speed of light, its chirality is equal to its *helicity* h (see Figure 1.2) determined by

$$h = \frac{\vec{s} \cdot \vec{p}}{|\vec{p}|}, \tag{1.15}$$

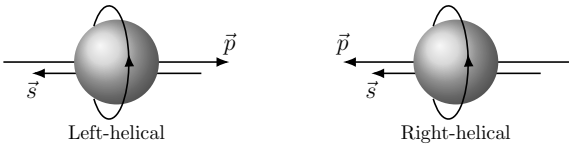

Figure 1.2: Helicity (or chirality for a massless particle) of a spinning particle with momentum $\vec{p}$. For the spin $\vec{s}$ pointing in opposite direction it is called left-helical (left-handed for a massless particle, left side) and for the spin directing in the same direction as the momentum the particle is called right-helical (right-handed for a massless particle, right side).

where $\vec{s}$ is the spin of the particle and $\vec{p}/|\vec{p}|$ is the direction of its momentum. For massive particles the helicity is not necessarily identical to its chirality as the observer can be chosen such that h changes sign in a relativistic theory.

In the early 1950s Schwinger [36], Pauli [38] and Lüders [37] proved, that in a Lorentz invariant quantum field theory, in which the principle of locality holds, the triple symmetry $\mathcal{CPT}$ is always conserved. This is well known as $\mathcal{CPT}$*-theorem*, and implies that it is impossible to design a Lorentz invariant quantum field theory in which $\mathcal{CPT}$ is broken. Introductions to $\mathcal{CPT}$ can be found in most text books on particle physics or quantum field theory, for example in Refs. [1, 2].

1.2.1 Dirac matrices as symmetry representations

In the previous section I introduced Dirac matrices $\mathbf{\Gamma}^{\mu\nu}$ in the mathematical formulation of the SM. These appeared as matrices that ensure Lorentz invariance of the Dirac equation. Thus, Dirac matrices are naturally a powerful tool for a quantitative discussion of implications of symmetry on the physics of fermionic systems.

The Dirac matrices build a Clifford algebra, whose irreducible representations are 4×4 matrices. To be more precise, the Dirac matrices form the basis of $SU(2) \times SU(2)$ and, thus, can be represented as Kronecker product of the basis matrices of $SU(2)$, that is the three Pauli spin matrices $\boldsymbol{\sigma}^i$ and the 2×2 identity matrix $\boldsymbol{\sigma}^0$:

$$\boldsymbol{\sigma}^0 = \begin{pmatrix} 1 & 0 \\ 0 & 1 \end{pmatrix}, \ \boldsymbol{\sigma}^1 = \begin{pmatrix} 0 & 1 \\ 1 & 0 \end{pmatrix}, \ \boldsymbol{\sigma}^2 = \begin{pmatrix} 0 & -\imath \\ \imath & 0 \end{pmatrix}, \ \boldsymbol{\sigma}^3 = \begin{pmatrix} 1 & 0 \\ 0 & -1 \end{pmatrix}, \tag{1.16a}$$

$$\mathbf{\Gamma}^{\mu\nu} = \boldsymbol{\sigma}^\mu \otimes \boldsymbol{\sigma}^\nu . \tag{1.16b}$$

The 16 Dirac matrices are commonly written as

$$\boldsymbol{\Gamma}^{0,0} = \boldsymbol{\sigma}^0 \otimes \boldsymbol{\sigma}^0 = \mathbf{1}_{4\times4} \tag{1.17a}$$
$$\boldsymbol{\Gamma}^{1,0} = \boldsymbol{\sigma}^1 \otimes \boldsymbol{\sigma}^0 = \imath\boldsymbol{\gamma}^0\boldsymbol{\gamma}^1\boldsymbol{\gamma}^2\boldsymbol{\gamma}^3 = \boldsymbol{\gamma}^5 \tag{1.17b}$$
$$\boldsymbol{\Gamma}^{2,0} = \boldsymbol{\sigma}^2 \otimes \boldsymbol{\sigma}^0 = -\imath\boldsymbol{\gamma}^0\boldsymbol{\gamma}^5 \tag{1.17c}$$
$$\boldsymbol{\Gamma}^{3,0} = \boldsymbol{\sigma}^3 \otimes \boldsymbol{\sigma}^0 = \boldsymbol{\gamma}^0 = \boldsymbol{\beta} \tag{1.17d}$$
$$\boldsymbol{\Gamma}^{0,i} = \boldsymbol{\sigma}^0 \otimes \boldsymbol{\sigma}^i = \boldsymbol{\gamma}^0\boldsymbol{\gamma}^5\boldsymbol{\gamma}^i = \boldsymbol{\Sigma}^i \tag{1.17e}$$
$$\boldsymbol{\Gamma}^{1,i} = \boldsymbol{\sigma}^1 \otimes \boldsymbol{\sigma}^i = \boldsymbol{\gamma}^0\boldsymbol{\gamma}^i = \boldsymbol{\alpha}^i \tag{1.17f}$$
$$\boldsymbol{\Gamma}^{2,i} = \boldsymbol{\sigma}^2 \otimes \boldsymbol{\sigma}^i = -\imath\boldsymbol{\gamma}^i \tag{1.17g}$$
$$\boldsymbol{\Gamma}^{3,i} = \boldsymbol{\sigma}^3 \otimes \boldsymbol{\sigma}^i = \boldsymbol{\gamma}^5\boldsymbol{\gamma}^i = \boldsymbol{\gamma}^0\boldsymbol{\Sigma}^i\,. \tag{1.17h}$$

The six matrices $-\imath\boldsymbol{\alpha}^i$ and $\boldsymbol{\Sigma}^i$ are the spinor representations of rotation and Lorentz boost transformations, respectively, and are the elements of the anti-symmetric tensor $\boldsymbol{\sigma}^{\mu\nu} = \frac{\imath}{2}[\boldsymbol{\gamma}^\mu, \boldsymbol{\gamma}^\nu]_-$. Corresponding finite Lorentz transformations can be found by their exponential representations. The discrete transformations of the homogeneous Lorentz group can be defined by the matrices $\hat{\mathcal{P}} = \boldsymbol{\gamma}^0$ (parity), $\hat{\mathcal{T}} = \boldsymbol{\gamma}^0\boldsymbol{\gamma}^5$ (time-reversal) and $\hat{\mathcal{C}} = \boldsymbol{\gamma}^5$ (charge conjugation).

Furthermore, the Dirac matrix $\boldsymbol{\gamma}^5$ connects two particles of opposite handedness and is, thus, often called chirality matrix. In combination with the identity matrix chiral projectors can be built:

$$\hat{P}_\mathrm{L} = \frac{\mathbf{1} - \boldsymbol{\gamma}^5}{2}, \qquad \hat{P}_\mathrm{R} = \frac{\mathbf{1} + \boldsymbol{\gamma}^5}{2}. \tag{1.18}$$

These generate the left and right handed-particles $\psi_\mathrm{L} = \hat{P}_\mathrm{L}\psi$, $\psi_\mathrm{R} = \hat{P}_\mathrm{R}\psi$.

All interaction Lagrangian densities of the elementary fermions can be constructed from the *bilinear covariants* $\bar{\psi}\boldsymbol{\Gamma}^{\mu\nu}\psi$. These fermionic densities can be classified according to their transformation under Lorentz symmetry:

$$\bar{\psi}\psi \quad \text{scalar (s)} \tag{1.19}$$
$$\bar{\psi}\boldsymbol{\gamma}^5\psi \quad \text{pseudoscalar (p)} \tag{1.20}$$
$$\bar{\psi}\boldsymbol{\gamma}^\mu\psi \quad \text{vector (v)} \tag{1.21}$$
$$\bar{\psi}\boldsymbol{\gamma}^5\boldsymbol{\gamma}^\mu\psi \quad \text{pseudovector (pv) or axial vector (a)} \tag{1.22}$$
$$\bar{\psi}\boldsymbol{\sigma}^{\mu\nu}\psi \quad \text{tensor (t)}\,. \tag{1.23}$$

Here, pseudo refers to a density that changes sign under parity transformation ($\mathcal{P}$-odd). Note that the pseudotensor bilinear covariant $\bar{\psi}\boldsymbol{\gamma}^5\boldsymbol{\sigma}^{\mu\nu}\psi$ can be represented as a linear combination of tensor covariants.

1.3 What we do not know — Beyond the standard models

Although today the SM is the most successful theory of physics [48, 49], there are frequent attempts to test its validity [49, 50]. Furthermore, the SM is considered to be not completely satisfactory, as among others it does not provide explanations for the origin of its 19 (26 when including neutrino oscillations) empirical parameters [51], DM and DE [52], nor does it contain a QFT formulation of gravity (for a discussion of the SM and its limitations see, e.g., Sec. 1.11 or Ch. 12 of Ref. [1] or Ref. [48]). The ΛCDM model appears to be not satisfactory as well. Today, there is no explanation for DE and all attempts to measure DM failed.

Unifying theories, i.e., theories that try to reformulate the SM and GR in a way that let the forces

converge to a unified force at high energy, aim to solve the above mentioned issues. Within the SM, SEWT and QCD appear as coexisting separate theories. Grand Unifying Theory (GUT) (see, e.g., Refs. [53, 54]), aim at a unification of SEWT and QCD, e.g., by introducing new symmetries as in SUperSYmmetry (SUSY) (see, e.g., Refs. [55, 56]). Theories that aim to unify the SM and GR are faced to the problem of formulating a theory of quantum gravity, i.e., reformulating the Einstein field equations as QFT. There are many approaches on how to achieve a theory of quantum gravity, among which the most famous are string theory and loop quantum gravity (see for an overview Ref. [57]).

A unification of all forces of nature could yield a Theory of Everything (ToE) and with this an explanation of the major unsolved questions of modern physics. In the following, a selection of the above mentioned problems which are of relevance for the present work is discussed in greater detail.

1.3.1 Unifying theories

One of the greatest unsolved problems of modern theoretical physics is the mathematical unification of the SM with GR. It is expected that such a unified theory is able to describe phenomena in the energy regime of $\sim 10^{19}$ GeV, the so called *Planck scale*, and, thus, can bring insight into the origin of our universe and the nature of black holes.

However, even an experimentally verified unification of QCD and SEWT within the SM (GUT) is still missing, although there are a number of promising approaches. Most notably are SUSY approaches, which introduce a symmetry that connects fermions to corresponding bosons and vice versa. SUSY is supposed to solve the so called hierarchy problem of the SM, i.e., the large difference between the strength of the weak interactions, represented by the mass of the Higgs boson of $\sim$ 125 GeV, and the mass scale that would be required under consideration of gravity (Planck scale). Moreover, SUSY allows convergence of the strong and electroweak forces at the so called GUT energy scale at 10^{16} GeV. For a detailed discussion of SUSY see, e.g., Ref. [57]. Although believed by many to be a symmetry of nature, predicted SUSY particles, which are supposed to be in reach of the Large Hadron Collider (LHC) at CERN, could not be detected in any experiment so far.

A number of promising theories have been developed in the past that aim to unify GR with quantum theory: the most noteworthy are loop quantum gravity and string theories. Loop quantum gravity attempts to quantize spacetime itself and to describe gravity not as force, but as fundamental property of spacetime (see Review [58]). String theories formulate quantum gravity by introduction of extra dimensions and with this multidimensional building blocks instead of point-like particles (see Ref. [57]).

Such unifying theories are assumed to describe the physical laws at the time of big bang, at which energies on the Planck scale were apparent and all forces are assumed to have been in balance. Nonetheless, today for none of these theories experimental evidences exist, and it is unknown if they are complete or lead to the correct physics [57, 59]. Direct experimental tests of these theories are very difficult to achieve because these theories become relevant at extremely high, inaccessible energies only. However, such unifying theories can be accompanied by Local Lorentz Invariance Violations (LLIVs) [60] or the breaking of other fundamental symmetries of the SM [61], and, thus, indirect tests are possible, as will be discussed in the next sections and following chapters.

1.3.2 Baryon assymetry

The prediction of antimatter implied by the so called Feynman-Stückelberg interpretation [62] of the Dirac equation [18] and its experimental discovery [63] were a great success of physics.

However, the existence of antimatter led to a oddity that lacks a convincing explanation: why is there so much matter in the universe, whereas antimatter exists only in tiny amounts not trivial to measure.

This inexplicable matter-antimatter asymmetry in our universe is commonly known as the baryon asymmetry problem describes. Neither the SM nor GR can explain this obvious dominance of matter. According to the known laws of physics the big bang must have produced equal amounts of matter and antimatter and these should have annihilated each other directly. Thus the origin of matter, i.e., baryongenesis is an unexplained problem of physics (see for review Ref. [64]).

One naive explanation for this asymmetry may be that we simply did not observe the missing antimatter yet. However, the fraction of antimatter in the universe is $< 10^{-6}$ [65] or $< 10^{-15}$ by arguments of supposed lifetimes of antimatter [66]. Even if there would be regions in the universe where antimatter may be accumulated, detectable γ-rays should be emitted due to the annihilation of matter with antimatter at the border of such regions. Experiments excluded such domains in our observable universe [67]. Alternatively, the separation between such antimatter-dominated regions must be as large as Mpc, and, thus, the presence of antimatter in the universe is not very likely [64].

Another solution is that the SM is not complete and that in the energy regime of the big bang matter and antimatter were produced at different rates resulting in the today observable universe. In 1967, Sakharov established three famous conditions (called *Sakharov conditions*) for baryongenesis, required to allow different rates for the production of matter and antimatter [68, 69]:

1. Baryon number (B) violation,
2. C- and CP-violation,
3. Deviation from thermal equilibrium.

The first condition is trivial, as the creation of matter ($B > 0$) from a vacuum ($B = 0$) would require $\Delta B \neq 0$ if there is not an equal amount of antimatter. If C- and CP-symmetry would be conserved during baryongenesis, each process that creates matter would be accompanied by a process that creates an equal amount of antimatter. Finally, in thermal equilibrium there would be no chance to arrive at a different state than one starts from.

Within the standard models all three conditions are fulfilled: C is maximally violated in weak interactions and also CP-violation appears due to the Cabibbo-Kobayashi-Maskawa (CKM) quark mixing matrix (see Section 1.4). The expansion of the universe requires the primordial plasma to have been out of equilibrium. Even baryon number is violated in the SEWT which, however, is not obvious but can be demonstrated (see, e.g., Ref. [70]).

However, the amount of CP-violation and deviation from equilibrium are by far too small to explain baryongenesis within the SM (see, e.g., Ref. [64]). Hence, it remains a mystery why there is matter at all.

1.3.3 Dark matter and dark energy

The idea of invisible matter in our universe is as old as science itself. With the development of Newton's theory of gravity a quantitative description became possible, and first quantitative proposals for invisible massive objects that influence the movement of visible astronomical bodies came up [71, 72].

In the early 20th century, interpretations of experimental observations led to the assumption that invisible matter makes up only the minority of all matter [73, 74]. In that time, the term of DM or rather in German *Dunkle Materie* was introduced by Zwicky [75]. In the meantime, within

cosmology high-precision measurements have been developed allowing for a deeper understanding of DM. These precision studies led to the assumption that in fact the majority of matter is not visible. Whereas DM is essential to explain the movement of planets and galaxies, the observed accelerated expansion of the universe requires uniformly distributed energy which is called Dark Energy (DE) (for review see Refs. [76, 77]). The assumed distribution of percentages of visible and invisible matter within the ΛCDM model as discussed in Ref. [24] is provided in Figure 1.3. Yet, the composition of DM remains open.

There is a large variety of candidates for DM that can range from super-massive objects such as Massive Astrophysical Compact Halo Objectss (MACHOs) or primordial black holes down to Beyond the Standard Models (BSM) elementary particles such as Weakly Interacting Massive Particles (WIMPs), axions and Axion Like Particles (ALPs), sterile neutrinos or dark photons. The wide mass range of these DM candidates is visualized in Figure 1.4.

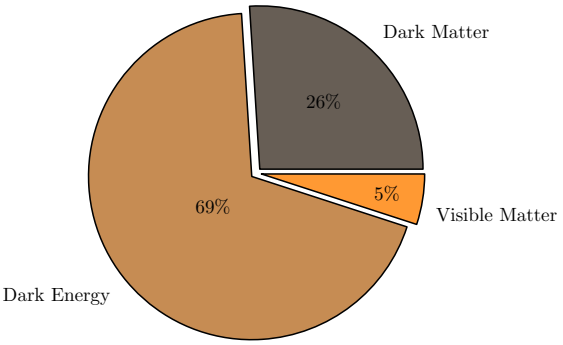

Figure 1.3: Schematic illustration of the fractions of visible matter, dark matter and dark energy on the total mass-energy density of the universe as predicted within the ΛCDM model from astronomical obersevations [24].

MACHOs are restricted by many experiments and can make up only up to 8 % of all DM [78, 79]. Other possible massive DM candidates are low-mass black holes, called primordial black holes, that originate from an early time before nucleosynthesis. Experiments restricted the possible mass range of primordial black holes to 10^{-11} to $10^{-14}\ M_\odot$, for all other masses they are excluded [80].

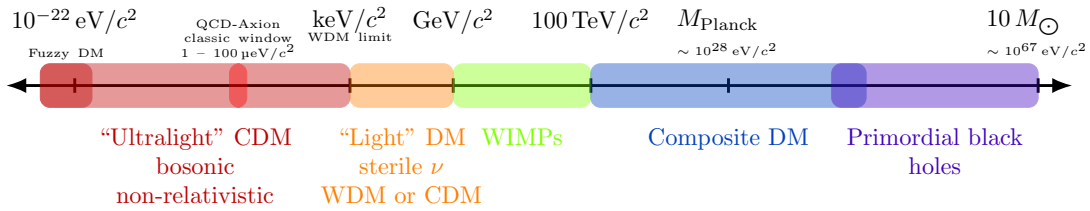

Figure 1.4: Overview over possible masses of dark matter objects (adapted from a comparable figure in Ref. [81]). Here, WDM means Warm DM. Note that the given mass ranges are general for the types of candidates but experiments have already excluded some of the masses shown above as discussed in the text.

WIMPs are supposed to be in a mass range of $10\,\mathrm{GeV}/c^2$ to $1\,\mathrm{TeV}/c^2$ and, e.g., could be some lighter SUSY particles [82]. As these large masses lead to a *freezing*, even at high temperatures, and, with this, generate an amount of DM that coincides with cosmological considerations, WIMPs are considered as one of the most promising candidates for DM. WIMPs can be searched by direct detection of scattering, high-energy collisions or detection of possible decay products. All these approaches are complementary and try to cover the large parameter space of WIMPs.

Like WIMPs, axions are hypothetical BSM particles. Axions were originally proposed as solution [83–85] to the strong $\mathcal{CP}$-problem posed by 't Hooft [86]. The strong $\mathcal{CP}$-problem raises the question, why there is no experimental evidence for strong $\mathcal{CP}$-violation, although a $\mathcal{CP}$-violating phase appears in QCD (here $G^{\mu\nu}$ is the gluon field strength tensor and $\tilde{G}_a^{\mu\nu} = \epsilon^{\mu\nu\rho\sigma} G^a_{\rho\sigma}$ is its dual):

$$\mathcal{L}^{\mathcal{P},\mathcal{T}}_{\mathrm{QCD}} = \theta \frac{g_s^2}{32\pi^2} \tilde{G}_a^{\mu\nu} G^a_{\mu\nu}, \tag{1.24}$$

where g_s is the strong coupling strength and θ is a free parameter for the amount of strong $\mathcal{CP}$-violation. In view of the baryon asymmetry problem this $\mathcal{CP}$-violating phase in the strong in-

teractions could give rise to leptongenesis in accordance with Sakharov's hypothesis. But, from experiments that search for the Electric Dipole Moment of the neutron (nEDM) [87] $\mathcal{CP}$-violation in strong interactions is excluded up to $\theta \lesssim 10^{-10}$.

The axion is a pseudoscalar boson that solves this issue by introducing an oscillation of θ over time. And as axions are supposed to interact with matter very weakly, it is a promising candidate for DM. Such a light pseudoscalar cosmic field obeys the Klein-Gordon equation and is non-relativistic, i.e., $\hbar\omega_\mathrm{a} \approx m_\mathrm{a}c^2$ with m_a being the axion mass. The oscillating axion field has the form

$$\phi_\mathrm{a}(\vec{r},t) = \phi_{\mathrm{a},0}\cos\left(\omega_\mathrm{a}t - \frac{\vec{r}\cdot\vec{p}_\mathrm{a}}{\hbar} + \varphi\right), \tag{1.25}$$

where, $\phi_{\mathrm{a},0}$ is the Cold Dark Matter (CDM) amplitude, $\vec{p}_\mathrm{a} = m_\mathrm{a}\vec{v}_\mathrm{a}$ is the linear momentum of the axion, which is proportional to its velocity $\vec{v}_\mathrm{a}$, and φ is a phase factor. As the relative velocity of the ALP field is suppressed by 10^{-3} with respect to the speed of light and CDM is supposed to be incoherent (see Refs. [88, 89] for details), for terrestrial experiments we can assume $\frac{\vec{r}\cdot\vec{p}_\mathrm{a}}{\hbar}$ to be constant and choose φ such that eq. (1.25) can be written as $\phi(\vec{r},t) = \phi_0\cos(\omega_\mathrm{a}t)$ (see also Ref. [90]).

However, the QCD axion as proposed originally by Wilczek and Weinberg [84, 85] was excluded by experiments already. More complex models for invisible axions like the Kim–Shifman–Vainshtein–Zakharov (KSVZ) and Dine–Fischler–Srednicki–Zhitnitsky (DFSZ) models are currently in discussion [91–94]. For review on axions and axion searches see, e.g., Ref. [95].

Beside ALPs and WIMPs, other bosonic DM is in discussion, such as dark photons or in general (pseudo)scalar and (pseudo)vector bosons [96–98]. These can be ultralight or massive.

Although promising in many regards, the concept of CDM also has its problems. Notable challenges are the cusps of halos in CDM simulations, which are not observed in rotation curves of galaxies [99], or the prediction of a large number of non-observed halos of CDM [100]. Several other challenges are discussed in Refs. [29, 101–103].

A solution to some of these problems is proposed by the concept of Fuzzy Cold Dark Matter (FCDM), which is supposed to be built up of ultra light particles with masses of about $10^{-22}\,\mathrm{eV}/c^2$ [104, 105].

Another solution to the problem of DM would be that the ΛCDM model is not complete or even wrong and that GR is not valid on cosmological scales. Hence, alternative theories of gravity, such as the MOND model [106, 107], provide possible solutions out of the dilemmas of the ΛCDM model (see, e.g., Refs. [108]).

1.4 Symmetry violation in and beyond the standard models

As mentioned above, even within the SM fundamental symmetries are violated to some extent. BSM theories are often developed by breaking symmetries that are conserved, at least to some extent, in the SM or GR, and therewith allow observation of effects which should not be visible according to the standard models. Hence, tests of such symmetry violations are good tests of the standard models of physics and BSM theories (see also Ref. [30]).

1.4.1 Violation of discrete symmetries

Until the beginning of the 20th century, discrete symmetries were commonly taken as naturally conserved. However, in the middle of the 19th century, i.e., even before first atomic models were known, Louis Pasteur discovered chirality of chemical substances and proposed a fundamental driving force that distinguishes between left and right and therewith violates parity [109]. About

100 years later, observations of paradox strange meson decays (also known as τ-θ puzzle) motivated Lee and Yang to question the conservation of parity in weak interactions as there was no experimental evidence for it. They proposed a number of experiments to test the violation of parity in weak decays [110]. Parity-violation, and, thus, a violation of discrete symmetries was observed for the first time in a realisation of one of these experiments by Wu *et al.* [111] in 1956. In this experiment the β-decay of oriented Co-nuclei was measured and it was discovered that parity is maximally violated in the weak interaction. This was a revolutionary result, meaning that nature is not ambidextrous but can distinguish between left and right.

The fall of parity in particle physics led to the assumption that what was intuitively meant by mirror image in nature is not a mirror image with respect to parity but to the combined symmetry of charge conjugation and parity $\mathcal{CP}$. I.e., the mirror image of a left-handed electron would not be a right-handed electron but a right-handed positron (see the discussion in Ref. [1]).

However, later it was emphasized by Barron that whereas $\mathcal{P}$ is connected to what can be understood as mirror symmetry (connected to chirality), $\mathcal{CP}$ leads to so called *false chirality* [112, 113]. Barron connects these phenomena also to molecular physics and highlights the similarity between *chirality* ($\mathcal{P}$-violation) and thermodynamics, and between *false chirality* ($\mathcal{CP}$-violation) and chemical catalysis [114]. He shows that whereas $\mathcal{P}$-violation can lead to energy differences, such as a change in thermodynamics of chemical reactions, $\mathcal{CP}$-violation can only lead to different rates, such as a catalyst in chemical reactions.

In 1964, Christenson *et al.* measured indications of a small amount of $\mathcal{CP}$-violation in Kaon decays [115], and, thus, $\mathcal{CP}$ was found not to be a symmetry of the weak interactions either. Kobayashi and Maskawa formulated a mixing of quarks of different generations in the weak interaction. Mathematically, this source of $\mathcal{CP}$-violation is incorporated in the SM via the CKM quark mixing matrix [116].

In the SM beside the CKM matrix, another term that theoretically allows $\mathcal{CP}$-violation in the strong sector appears, which was mentioned in the last section. This strong $\mathcal{CP}$-violation characterized by the parameter θ could not be observed in experiment so far, as was discussed above.

The discovery of neutrino oscillations gave evidence for $\mathcal{CP}$-violation in the lepton sector as well. In a similar way as the CKM quark mixing entered into the SM, a matrix of neutrino mixing can be formulated, which would introduce $\mathcal{CP}$-violation in the lepton-sector of the SM. For details see Review [21].

The evidence of $\mathcal{CP}$-violation indirectly suggests $\mathcal{T}$-violation due to the $\mathcal{CPT}$-theorem. Thus, a direct detection of $\mathcal{T}$-violation can be expected and is, therefore, searched for in various ways, as will be discussed in detail in the next chapter.

The search for $\mathcal{P}$- and $\mathcal{CP}$-violation, as discussed in the previous sections, is essential for a good understanding of the baryon asymmetry problem and may give evidence of proposed DM candidates. Furthermore, unifying theories, such as SUSY, predict an amount of $\mathcal{CP}$-violation that is larger than in the SM. Therefore, tests of $\mathcal{CP}$-violation are also direct tests of BSM physics (see next chapter).

1.4.2 Violation of Lorentz invariance

Whereas discrete symmetry violation appears in the SM, the SM and GR and, thus, ΛCDM are invariant under Lorentz symmetry.

In the context of theories that aim to unify gravity and quantum mechanics it was shown that spontaneous Lorentz symmetry breaking can occur [60]. Such a violation of LLIV can be described in so-called test theories, like the Robertson–Mansouri–Sexl framework (RMS) [117, 118] or the Standard Model Extension (SME) by Kostelecky and co-workers [119, 120]. In contrast to RMS, the SME is a *model-independent* toy theory based on the grounds of effective field theory that introduces a huge number of experimentally testable parameters in all sectors of the SM (a list

of the actual best limits is given in Ref. [121]) and is therefore preferred today. The different parameters can be tested in very different ways depending on how the actual interaction Lagrangian looks like. One type of experiment directly addresses length contractions or time dilatation. Such experiments lead to the discovery of SR and are conceptually easy to understand, which I therefore shortly explain.

Before the discovery of SR it was commonly assumed that a luminiferous aether is fixed in space and mediates all forces. Hence, it was expected that the laws of physics on a moving object like the earth depend on its actual position in spacetime as interactions are hooked to the aether. Therefore, it was assumed that a resulting *aether wind* would be measurable. In order to test this, Michelson developed in correspondence with Moreley [122, 123] an interferometer. In this interferometer a light beam is sent through a semi-permeable mirror and split by 90° into a beam orthogonal with respect to the aether wind, traveling a distance l_2, and one parallel to the aether wind, traveling a distance l_1 (see Figure 1.5). As the earth is moving with respect to the aether, a phase shift of $\Delta t = \frac{2}{c\gamma}(l_1/\gamma - l_2)$ in the arrival of the two light beams on the detector was expected, depending on the relative direction of the light beams to the motion of the earth. Here $\gamma = \sqrt{1 - \frac{v^2}{c^2}}$. However, all measurements yielded no phase shift, and, thus, negative results.

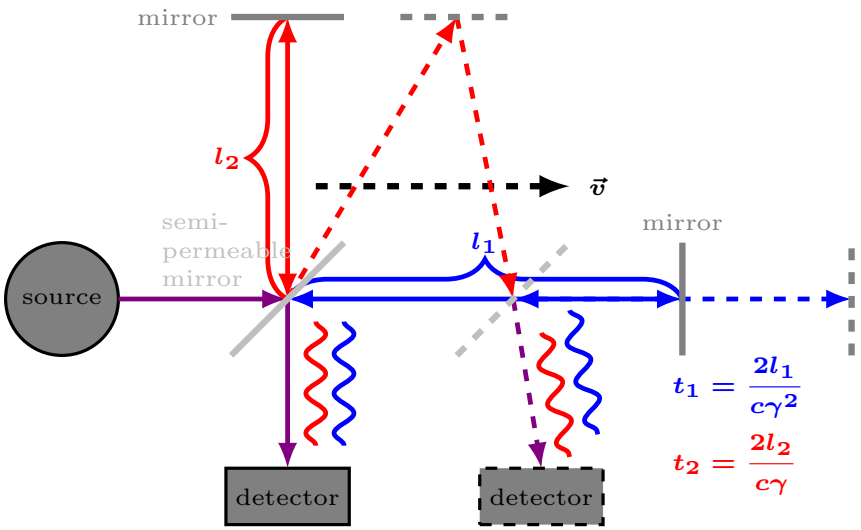

Figure 1.5: Measurement of the relative velocity of system with respect to a hypothetical aether as suggested by Michelson and Morley in the version of Kennedy and Thorndike ($l_1 \neq l_2$). As the observer is coupled to the absolute position in the aether, moving the experiment with velocity v relative to the aether would result in a phase shift of the incoming light travelling vertically with respect to the movement (red) and the light travelling in direction of the movement (blue). The dashed lines, mirrors and the dashed detector resemble the moved apparatus at a different time t due to velocity v. Thereby, the shown positions correspond to the different time steps at which the light beams arrive at the various positions. I.e., the first mirror which is passed by the light beam is less shifted than the second. Here $\gamma = \sqrt{1 - \frac{v^2}{c^2}}$.

Later, Lorentz and FitzGerald suggested that in direction of movement all lengths would contract with γ, which can explain the negative result [124, 125]. This contraction is considered as *Lorentz transformation* and γ is often called the *Lorentz factor*. It ensures that the laws of physics do not depend on how something moves. The Lorentz factor is $\gamma \sim 1$ for so-called non-relativistic objects with $v \ll c$. The Michelson–Moreley experiment was carried out with $l_1 = l_2$. Later a variant of the experiment with $l_1 \neq l_2$ known as Kennedy–Thorndike experiment confirmed the null result and gave evidence for time dilatation [126].

It should be noted that the measurement principle of the Kennedy–Thorndike experiment was used to detect gravitational waves [127] and, thus, served as test of GR as well. Variants of this

type of experiments are carried out to test LLIV with optical resonators (photon sector) and atomic or molecular clocks (nucleon and electron sectors) (see the Review and data collection [121][2] and all references therein). More details on the actual detection of LLIV with atoms and molecules will be discussed in the following chapter.

[2]This review and data collection gets frequently updated on https://arxiv.org/abs/0801.0287.

2 Low-energy precision tests of fundamental physics

In the last chapter major problems of fundamental physics and connections to violation of fundamental symmetries were discussed. Different approaches can be used to develop experiments that are capable of detecting such symmetry violations and to gain a deeper understanding of our universe. There are three major disciplines in physics that search for BSM physics: i) Cosmology and astronomy, ii) high-energy physics with large collider experiments and iii) low-energy physics employing bound state systems, such as nuclei, atoms or molecules, or even extended systems (e.g. solids). The different areas provide complementary tests of the laws of physics, as these tests are performed in very different energy regimes and on different time (and length) scales. In this thesis I focus on molecular physics searches for BSM physics. These have the charm to be executable in a standard size laboratory or on satellites under outer space conditions in contrast to experiments of high-energy physics.

BSM physics is expected to be dominant at very high-energy in the region of at least several TeV, as many proposed new particles are supposed to have very large masses. On earth such high-energies can only be achieved in collider experiments as those conducted at the LHC at CERN or the Tevatron at Fermilab, if at all. However, instead of generating such high-energies another possibility is to measure very precisely at low-energy, i.e., in an energy domain in which BSM physics is expected to be suppressed, and, thus, BSM effects are very tiny.

Achieving the precision that is needed to detect the tiny effects in such *low-energy precision tests* is possible only by exploiting the internal electronic and nuclear structure of atoms and molecules. Due to enormous internal field strengths that can occur, effects on the fundamental particle level can be enhanced by many orders of magnitude. However, these kinds of experiments are not only competitive with collider experiments, but also complementary in the sense that the fundamental forces are probed in different energy regimes, and, therewith, the overall validity of the physical laws can be tested.

2.1 Searches for discrete symmetry violation

In the following two sections the theoretical and experimental status of parity-nonconservation and $\mathcal{P},\mathcal{T}$-odd permanent Electric Dipole Moments (EDMs) in atoms and molecules will be summarized. Whereas searches for electroweak parity-violation in atoms and molecules are low-energy precision test of the SM itself, a nonzero measurement of a $\mathcal{P},\mathcal{T}$-odd permanent EDM with presently possible resolution would be a direct evidence for BSM physics.

2.1.1 Electroweak parity-nonconservation in atoms and molecules

As interactions in atoms and molecules are dominated by the electromagnetic interactions, the purely electromagnetic description of electronic movement in atoms and molecules is certainly an excellent approximation. However, due to its property of violating parity, the weak force can have an observable influence on the electronic structure of atoms and molecules, leading to new properties, such as optical activity of hydrogen molecules as noted by Zel'dovich [128] or to energy differences of enantiomers of chiral molecules as first discussed by Yamagata [129].

2.1.1.a Weak interactions in atoms and molecules

With the electroweak unification (see previous chapter) and the resulting prediction of a neutral weak vector boson Z^0 the theoretical foundation for the description of weak interactions in

atoms and molecules with stable particles was laid. Charged weak currents mediated by the $W^{\pm}$ bosons are important for β-decay reactions but play a minor role in bound systems like atoms or molecules. Rather, neutral current interactions mediated by the Z^0 boson are predominant. Feynman diagrams for neutral current interactions that can be expected in atoms or molecules are presented in Figure 2.1.

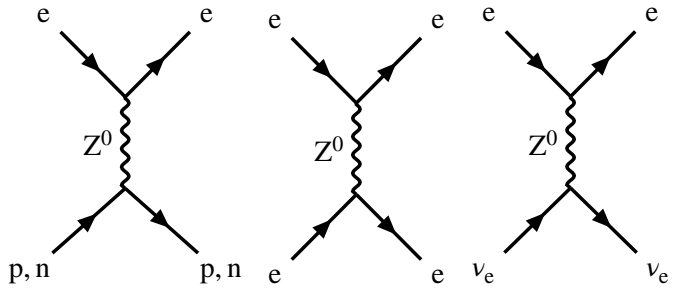

Figure 2.1: Feynman diagrams of electroweak neutral currents that can occur in an atom or a molecule. In the above diagrams time flows from left to right. Left: neutral weak scattering of electrons and nucleons (protons p and neutrons n). Center: neutral weak electron-electron scattering. Right: neutral weak electron-neutrino scattering. The first two interactions have photonic counterparts (in the first diagram only the interaction of the electron with the proton). As neutrino densities are very low, the process on the right is not probable to occur. In atoms and molecules the process on the left is by far the dominant one. See also Review [130].

Weak electron-electron interactions (central diagram in Figure 2.1) are expected to give a minor contribution to the total weak interaction in the molecule. Furthermore, the weak electron-neutrino coupling (right diagram in Figure 2.1) is improbable to occur as neutrino densities are very low [130].

The dominant weak process in a molecule corresponds to the left diagram in Figure 2.1. As the nucleons are not elementary particles, the interactions of electrons with nuclei have to be described via the interactions of electrons with quarks. However, the internal structure of the baryons within the nucleus can be described with effective parameters (for a detailed derivation and discussion see Ref. [130]). The interaction Lagrangian density for the weak electron-nucleon scattering in an atom with Z_A protons and N_A neutrons in nucleus A is in leading order:

$$\mathcal{L}_{\text{ew,atom}} = -\frac{G_\text{F}}{\sqrt{2}}\bar{\psi}_\text{e}\gamma_\mu\left(g_\text{v}^\text{e} - \gamma^5 g_\text{a}^\text{e}\right)\psi_\text{e}\sum_{i=1}^{Z_A+N_A}\left[\bar{\psi}_{\text{N}_i}\gamma^\mu\left(g_\text{v}^{\text{N}_i} - \gamma^5 g_\text{a}^{\text{N}_i}\right)\psi_{\text{N}_i}\right], \tag{2.1}$$

where $G_\text{F} = (\hbar c)^3\frac{\sqrt{2}}{8}\left(\frac{g_\text{Z}}{m_\text{Z}c^2}\right)^2 \approx 2.222\,49\times10^{-14}\,E_\text{h}\,{a_0}^3$ is Fermi's weak coupling constant which depends on the mass m_Z and interaction strength $g_\text{Z} = \frac{\sqrt{4\pi\alpha}}{\sin\theta_\text{W}\cos\theta_\text{W}}$ of the Z^0 boson with the fine structure constant being $\alpha = \frac{e^2}{4\pi\epsilon_0\hbar c} \approx \frac{1}{137}$. The Weinberg mixing angle is $\theta_\text{W} = \arccos\frac{m_\text{W}}{m_\text{Z}} \approx 0.492$, where m_W is the mass of the $W^{\pm}$ bosons. The vertex factors for vector and axial vector current interactions g_V and g_a are determined within SEWT for quarks and leptons by θ_W and are listed in Table 2.1. In case of nucleons, these vertex factors can be approximated as simple sum over contributing quark vertex factors, i.e., $g_{\text{v,a}}^\text{p} \approx 2g_{\text{v,a}}^\text{u} + g_{\text{v,a}}^\text{d}$ and $g_{\text{v,a}}^\text{p} \approx 2g_{\text{v,a}}^\text{d} + g_{\text{v,a}}^\text{u}$.

Table 2.1: Electroweak vertex factors of leptons and quarks (see Ref. [130]).

Fermion f	g_v^f	g_a^f
ν_e, ν_μ, ν_τ	$\frac{1}{2}$	$\frac{1}{2}$
e, μ, τ	$-\frac{1}{2} + 2\sin^2\theta_\text{W}$	$-\frac{1}{2}$
u, c, t	$\frac{1}{2} - \frac{4}{3}\sin^2\theta_\text{W}$	$\frac{1}{2}$
d, s, b	$-\frac{1}{2} + \frac{2}{3}\sin^2\theta_\text{W}$	$-\frac{1}{2}$

Whereas the vector-vector and axial vector-axial vector interactions yield a correction to the parity conserving potential, axial vector-vector and vector-axial vector

interactions contribute to a $\mathcal{P}$-odd potential, and, thus, can lead to new effects beyond the pure electromagnetic treatment of atoms and molecules.

In the limit of non-relativistically moving nuclei, the time-like component of the axial vector-vector nucleon-electron interaction and the spatial components of the vector-axial vector nucleon-electron interaction vanish. Hence, Lagrangian (2.1) yields two contributions to the energy.

One contribution can be interpreted as the weak nuclear charge density $Q_{\mathrm{W}}\rho_{\mathrm{nuc}}$ with the weak nuclear charge $Q_{\mathrm{W}} \approx \left(1 - 4\sin^2\theta_{\mathrm{W}}\right) Z - N$ interacting with the helical electrons $\bar{\psi}_{\mathrm{e}}\boldsymbol{\gamma}^0\boldsymbol{\gamma}^5\psi_{\mathrm{e}}$. This interaction results from the time-like component of the vector-axial vector nucleon-electron interaction and is nuclear spin-independent.

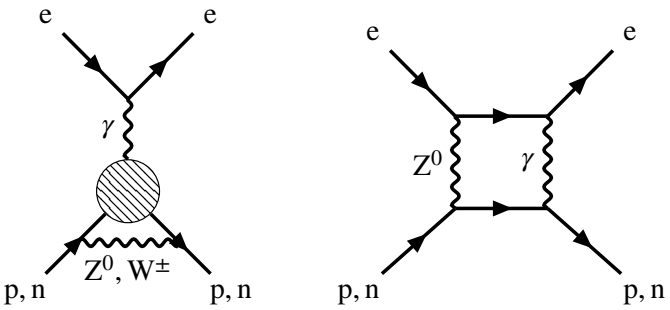

Figure 2.2: Feynman diagrams that contribute to nuclear spin-dependent parity violation in atoms and molecules. In the above diagrams time flows from left to right. Left: electroweak currents in the nucleus lead to the nuclear anapole moment, which interacts electromagnetically with an electron. Right: hyperfine-like electroweak electron-nucleon scattering. See also Review [131].

The second $\mathcal{P}$-odd contribution to the energy from Lagrangian (2.1) comes from the spatial components of the axial vector-vector nucleon-electron interaction and leads to a nuclear spin-dependent parity-violating effect proportional to $k_{\mathrm{av}}\vec{I}\rho_{\mathrm{nuc}}$, where k_{av} depends on the nuclear structure and $\vec{I}$ is the nuclear spin. Zel'dovich showed that within nuclei with spin $I \geq 1/2$ parity-violating electroweak currents lead to an additional nuclear moment $k_{\mathrm{A}}\vec{I}$, called the anapole moment [128, 132], where k_{A} depends on θ_{W} (see Figure 2.2 left). The anapole moment gives the second contribution to the nuclear spin-dependent parity-violating Hamiltonian. Furthermore, there is a third contribution to the nuclear spin-dependent parity-violating Hamiltonian from a hyperfine induced $\mathcal{P}$-odd interaction of strength k_{hfpv} proportional to Q_{W} (see Figure 2.2 right). All three nuclear moments $k_{\mathrm{av}}\vec{I}$, $k_{\mathrm{A}}\vec{I}$ and $k_{\mathrm{hfpv}}\vec{I}$ interact with the current density of the electrons $\bar{\psi}_{\mathrm{e}}\boldsymbol{\gamma}^i\psi_{\mathrm{e}}$.

The parameters Q_{W}, k_{av}, k_{A} and k_{hfpv} are determined by the nuclear structure and can be obtained from experiments or to limited accuracy from nuclear structure theory. The effective nuclear spin-dependent parity-violating parameters k_{av}, k_{A} and k_{hfpv} can be summarized in the interaction constant $k_{\mathcal{A}} = k_{\mathrm{av}} + k_{\mathrm{A}} + k_{\mathrm{hfpv}}$.

The leading order $\mathcal{P}$-odd molecular (or atomic) interaction Hamiltonian is:

$$\hat{H}_{\mathrm{ew}} = \frac{G_{\mathrm{F}}}{2\sqrt{2}} \sum_{i=1}^{N_{\mathrm{elec}}} \sum_{A=1}^{N_{\mathrm{nuc}}} \rho_{\mathrm{nuc},A}(\vec{r}_i) \left(Q_{\mathrm{W},A}\boldsymbol{\gamma}^5 + k_{\mathcal{A},A}\vec{\boldsymbol{\alpha}}_i \cdot \vec{I}_A \right). \tag{2.2}$$

Here, $\rho_{\mathrm{nuc},A}$ is the normalized nuclear charge density distribution of nucleus A in a molecule with N_{nuc} nuclei.

2.1.1.b Scaling laws and enhancement factors

Zel'dovich assumed that $\mathcal{P}$-odd effects in atoms are far to small to be measurable. However, in 1975 Bouchiat and Bouchiat [133] showed for the first time that electroweak $\mathcal{P}$-violation may be measurable in heavy atoms. For the case of hydrogen-like atoms, they calculated that the parity-violating energy splitting due to weak interactions scales steeply with nuclear charge number Z:

$$\delta E_{\mathrm{ew}} \sim \frac{G_{\mathrm{F}}\alpha}{2\sqrt{2}} Z^2 Q_{\mathrm{W}} R(Z,A) \approx -\frac{G_{\mathrm{F}}\alpha}{2\sqrt{2}} N Z^2 R(Z,A) \approx -\frac{G_{\mathrm{F}}\alpha}{2\sqrt{2}} Z^3 R(Z,A) \tag{2.3}$$

where A is the number of nucleons and N is the number neutrons in the nucleus of the atom, and $R(Z,A)$ is a relativistic enhancement factor that increases steeply with nuclear charge:

$$R(Z,A) = \frac{4}{\Gamma^2\left(2\gamma_{1/2}+1\right)} \left(2Z r_{\mathrm{nuc}}/a_0\right)^{2\gamma_{1/2}-2}. \tag{2.4}$$

Here, $\Gamma(x)$ is the gamma function, r_{nuc} is the mean nuclear charge radius that is in good approximation proportional to $A^{1/3}$, a_0 is the Bohr radius and

$$\gamma_j = \sqrt{\left(j+\frac{1}{2}\right)^2 - (\alpha Z)^2} \tag{2.5}$$

is the Lorentz factor for the electron in an atom, where $\alpha Z = \frac{v_{\mathrm{e}}}{c}$ with the velocity of the electron being $v_{\mathrm{e}} = \frac{e^2 Z}{4\pi\epsilon_0 \hbar}$. j is the total electronic angular momentum quantum number. The factor R is steeply increasing with nuclear charge Z ($R \approx 1$ for $Z = 1$, $R \approx 1.2$ for $Z = 20$ and $R \approx 8$ for $Z = 80$) leading, in combination with the Z^3 scaling, to a large increase of parity-violating matrix elements in heavy elemental atoms and molecules.

2.1.1.c Experimental tests of weak interactions in atoms and molecules

Due to their property of being parity-nonconserving, the above discussed effects of weak interactions can be observable in systems that appear to have close lying *states of opposite parity* and are particularly pronounced in those where these states are almost degenerate.

In *atomic systems* almost degenerate states of opposite parity are not easy to achieve and there are few systems that can be used for experiment. So far there have been measurements of parity-violation in atoms employing measurement of the optical rotation in an allowed M1 transition in bismuth [134, 135], and in the $^3\mathrm{P}_0 \rightarrow {}^3\mathrm{P}_1$ transition in lead [136], as well as by Stark interference experiments on the $6\mathrm{P}_{1/2} \rightarrow 6\mathrm{P}_{3/2}$ transition in thallium [137], the $6\mathrm{S}_{1/2} \rightarrow 7\mathrm{S}_{1/2}$ transition in cesium [138] and the $^1\mathrm{S}_0 \rightarrow {}^3\mathrm{D}_1$ transition in Yb [139] (see also Review [5] and references therein). Furthermore, there are ongoing but, by now, not successful experiments with Dy [140, 141]. Today, the most precise low-energy measurement of parity-violation was in Cs with a precision of 0.35 % [138] and the largest parity-violating energy shift was measured in Yb [139].

Whereas in atoms contributions induced by Q_{W} are dominant, these are suppressed in *open-shell diatomic* molecules, in which nuclear spin-dependent $\mathcal{P}$-violation dominate. This renders experiments with diatomic molecules particularly interesting for an observation of nuclear spin dependent $\mathcal{P}$-odd effects such as the anapole moment. Nuclear spin dependent parity-violating energy differences appear as splitting of Ω-doublets[1] [142, 143] of diatomic molecules. The effective spin-rotation interaction appears to be a $\mathcal{P}$-odd analogue of the hyperfine interaction and has

[1] Ω-doublets $|\pm\Omega\rangle$ are connected by parity and time reversal symmetry operations, such that $\mathcal{P}\,|\Omega\rangle\,\mathcal{P}^{-1} = |-\Omega\rangle$ and $\mathcal{T}\,|\Omega\rangle\,\mathcal{T}^{-1} = |-\Omega\rangle$.

the form (see for details Ref. [144]):

$$\hat{H}_{\mathrm{ew,sr}} = k_{\mathcal{A}} W_{\mathrm{a}} \vec{\lambda} \times \vec{S}' \cdot \vec{I}, \tag{2.6}$$

where $\vec{\lambda}$ is the unit vector pointing from the heavy to the light nucleus, $\vec{S}'$ is the effective dimensionless electron spin, $\vec{I}$ is the dimensionless nuclear spin and W_{a} is the effective electronic structure enhancement factor for nuclear spin-dependent parity-violating interactions. Many experiments have been proposed in the past for a wealth of molecular systems (see Reviews [144–147] and references therein as well as Refs. [148–150]). In 2018, in an experiment with ^{138}BaF ($I_{\mathrm{Ba}} = 0$) a resolution was demonstrated that is sufficient to resolve the nuclear-spin dependent $\mathcal{P}$-odd contribution from the Ba nucleus if the experiment was performed with ^{137}BaF [151].

Chiral molecules have a very small tunneling splitting for stereomutation, i.e., the interconversion of the two enantiomers. The two enantiomers are states of opposite parity and, thus, a chiral molecule has states of opposite parity that are as good as degenerate (see also Reviews [5, 130]). In contrast to atoms and diatomic molecules, in chiral molecules electroweak parity- violation leads to an energy splitting which can be measured as frequency differences (first discussed in the 1970s [152–157]), which can be done very accurately (see, e.g., Ref [158] or for the special case of $\mathcal{P}$-violation see Refs. [159, 160]).

First experimental attempts for measuring parity-violating energy splittings due to the weak charge were made in the 1970s with the chiral methane derivate CHBrClF via vibrational spectroscopy of the C–F stretching mode [161] and with vibrational spectroscopy of C=O stretching mode in camphor [162]. Understanding and improvement of the CHBrClF experiment was advanced by many experimental and theoretical studies [163–176]. In the group of Chardonnay, using ultrahigh-precision spectroscopy of the C–F stretching mode in CHBrClF, the currently best upper limit $\Delta\nu_{\mathrm{pv}}/\nu < 4 \times 10^{-13}$ of parity-violation in a chiral molecule was achieved [164, 171].

Other experiments that may be sensitive to the weak charge such as microwave spectroscopy [163], time-dependent optical activity measurements [157] or electronic spectroscopy [177–179] could not achieve a comparable sensitivity so far.

The nuclear spin-dependent electroweak interactions can lead to parity-violating shifts of absolute shielding or spin-spin coupling [180–192] in Nuclear Magnetic Resonance (NMR) spectra of chiral molecules. Recently, such NMR experiments regained attention due to new experimental setups [193].

Still, big challenges remain in finding suitable candidate molecules as discussed, e.g., in Reviews [5, 130, 194, 195]. Theory is challenged by many aspects: There is a need of accurate prediction of parity-violating energy splittings in electronic but also in vibrational and microwave spectra. In addition to an accurate description of the electronic wave function, the latter require the calculation of vibrational wave functions, which is very demanding when going beyond a one dimensional separable approximation. However, such non-separable anharmonic effects (multimode effects) can play an important role as was shown for CDBrClF in Refs. [196–198]. Electronic structure calculations of large heavy-elemental molecules are often restricted to Density Functional Theory (DFT) methods, which are not systematically improvable and error estimates are usually difficult to achieve. For smaller molecules relativistic electron correlation calculations at the level of coupled cluster theory can be used as a reference but are not available for many interesting larger heavy-elemental molecules.

2.1.2 Permanent electric dipole moments in atoms and diatomic molecules

One consequence of $\mathcal{P},\mathcal{T}$-violation would be the existence of an *permanent* EDM. As demonstrated in Figure 2.3, *permanent* EDMs simultaneously violate parity and time-reversal: the dipole moment $\vec{d}$ is a time-even polar vector, whereas the spin $\vec{s}$ is a time-odd axial vector.

Such a *permanent EDM* is not to be confused with what is commonly called a permanent EDM in chemistry and molecular physics, which appears in molecules such as water or ammonia. The latter EDMs are *induced* by an external electric field $\vec{\mathcal{E}}$ that polarizes the molecule, resulting in a dipole interaction $\vec{d} \cdot \vec{\mathcal{E}}$ that leads to a quadratic Stark shift. In the following, I refer to the $\mathcal{P},\mathcal{T}$-violating EDM as *permanent EDMs* as the resulting energetic splitting is non vanishing in the limit of a vanishing external field and leads to a linear Stark shift.

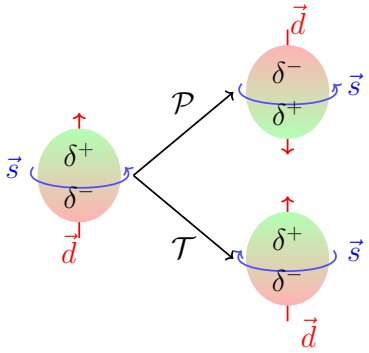

Figure 2.3: Simultaneous violation of time-reversal symmetry and parity of a permanent EDM of a fermion.

Purcell and Ramsey were the first to suggest experiments that test the existence of EDMs of nuclei and elementary particles, and with that, they proposed a serious test of violation of the discrete symmetries $\mathcal{P}$ and $\mathcal{T}$.

Salpeter discussed the effects of such hypothetical permanent EDMs in atoms [199] and its implications for experiments with positronium [200] and for the hydrogen spectrum and gave a mathematical formulation of such interactions.

Permanent EDMs are good tests of BSM physics such as SUSY as predictions from different theories can have very different orders of magnitude. So the Electric Dipole Moment of the electron (eEDM) is predicted to be on the order of about $10^{-40}\,e\,\mathrm{cm}$ in the SM, whereas the naivest SUSY models predict an eEDM of up to $10^{-24}\,e\,\mathrm{cm}$. This big difference can be understood from the fact that in the SM first contributing diagrams are of fourth order, whereas in SUSY models the first order diagrams can give a direct contribution (see Figure 2.4). For discussions of calculations of that kind see, e.g., Refs. [201–203].

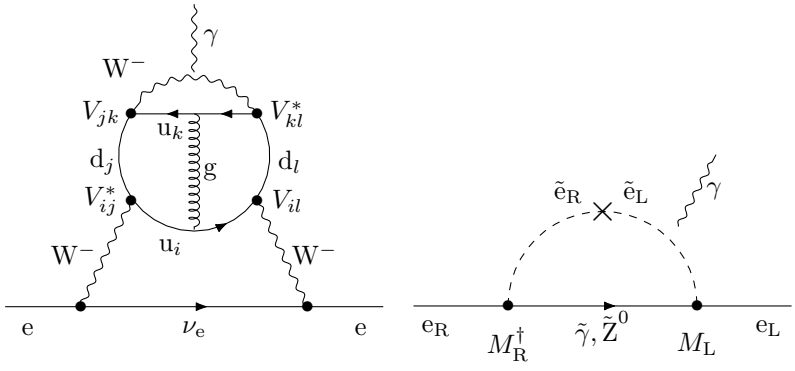

Figure 2.4: On the left, an example of a Feynman diagram of a quark four-loop contribution to the eEDM in the SM, induced by an EDM of the W boson, is shown. On the right, a SUSY one-loop contribution to the eEDM is shown. e_R and e_L are right-handed and left-handed electrons and $\tilde{e}$ are their supersymmetric partners (selectrons), $\tilde{\gamma}$ is the photino and $\tilde{Z}^0$ the supersymmetric partner of the neutral gauge boson of the weak interaction; u_i and d_i are up-like and down-like quarks of generation i, respectively, and ν_e is the electron neutrino. The cross denotes a mass intersection and the vertex factors V_{ij} are elements of the CKM mixing matrix. M_L and M_R are the unitary matrices which rotate left-handed and right-handed weak eigenstates within SUSY. In the diagrams time flows from left to right. For details see Refs. [201, 203].

2.1.2.a Sources of $\mathcal{P},\mathcal{T}$-violation

In atoms and molecules we are concerned with electrons and nucleons, i.e., protons and neutrons, which are composed of quark-gluon plasma. Possible $\mathcal{P},\mathcal{T}$-odd effects that can appear on the quark and electron level and resulting net $\mathcal{P},\mathcal{T}$-odd effects on subsequently lower-energy levels are given in Figure 2.5. EDMs appear as form factors in quantum field theory in the second

order coupling to the photon field via the electromagnetic field strength tensor $F_{\mu\nu}$ leading to the Lagrangian (see Ref. [199] and for the full $\mathcal{P},\mathcal{T}$-odd Lagrangian, e.g., Ref. [204]):

$$\mathcal{L}_{\text{EDM}}^{\mathcal{P},\mathcal{T}} = -\frac{d_\text{e}}{2}\bar{\psi}_\text{e}\imath\boldsymbol{\gamma}^5\boldsymbol{\sigma}_{\mu\nu}\psi_\text{e}F^{\mu\nu} - \frac{d_\text{q}}{2}\bar{\psi}_\text{q}\imath\boldsymbol{\gamma}^5\boldsymbol{\sigma}_{\mu\nu}\psi_\text{q}F^{\mu\nu} \tag{2.7}$$

when considering quarks q, which can be u or d, and electrons. Here d_e is the eEDM and d_q is a quark EDM.

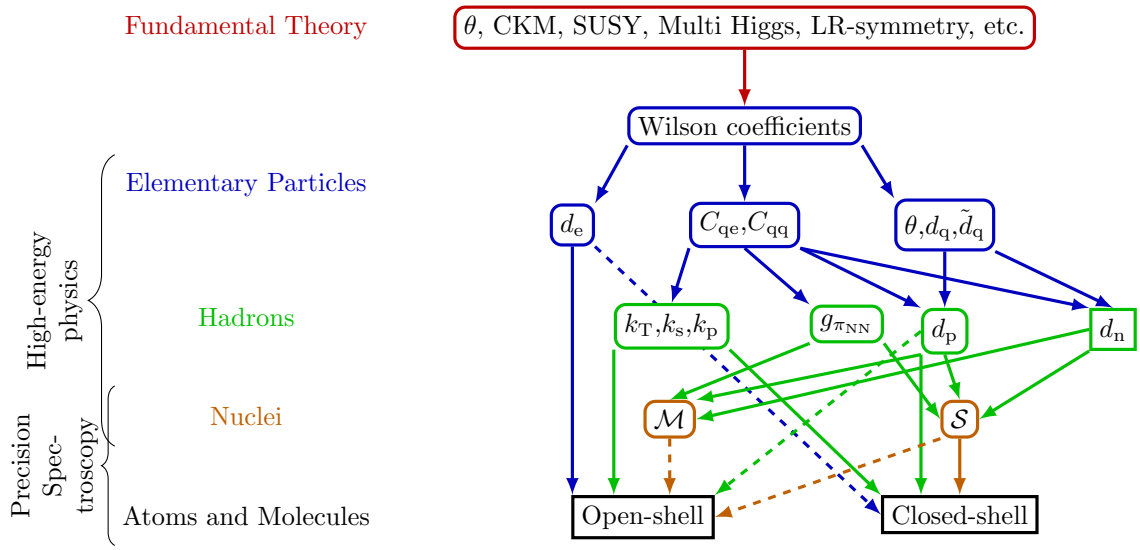

Figure 2.5: Overview of the sources of $\mathcal{P},\mathcal{T}$-violation on the fundamental particle level predicted in the SM and various BSM theories. Arrows on solid lines indicate main contributions and arrows on dashed lines less important contributions. Similar overviews considering parts of this overview can be found in Refs. [205–207]

In addition, $\mathcal{P},\mathcal{T}$-odd quark-quark currents and quark-electron currents can produce $\mathcal{P},\mathcal{T}$-odd moments of hadrons, nuclei, atoms and molecules. A full Lagrangian of $\mathcal{P},\mathcal{T}$-odd currents that can contribute to the permanent EDM of an atom or molecule reads (see Ref. [204]):

$$\begin{aligned}\mathcal{L}_{\text{current}}^{\mathcal{P},\mathcal{T}} = &-C_{\text{qe,sp}}\frac{G_\text{F}}{\sqrt{2}}\bar{\psi}_\text{e}\imath\boldsymbol{\gamma}^5\psi_\text{e}\bar{\psi}_\text{q}\psi_\text{q} - C_{\text{qe,ps}}\frac{G_\text{F}}{\sqrt{2}}\bar{\psi}_\text{e}\psi_\text{e}\bar{\psi}_\text{q}\imath\boldsymbol{\gamma}^5\psi_\text{q} - C_{\text{qe,pt}}\frac{G_\text{F}}{\sqrt{2}}\bar{\psi}_\text{e}\boldsymbol{\sigma}_{\mu\nu}\psi_\text{e}\bar{\psi}_\text{q}\boldsymbol{\sigma}^{\mu\nu}\imath\boldsymbol{\gamma}^5\psi_\text{q}\\ &- C_{\text{qq,sp}}\frac{G_\text{F}}{\sqrt{2}}\bar{\psi}_\text{q}\imath\boldsymbol{\gamma}^5\psi_\text{q}\bar{\psi}_\text{q}\psi_\text{q} - Q_{\text{qq,vp}}\bar{\psi}_\text{q}\vec{\partial}^\mu\boldsymbol{\gamma}^5\psi_\text{q}\bar{\psi}_\text{q}\boldsymbol{\gamma}_\mu\psi_\text{q}\\ &- Q_{\text{qe,vp}}\bar{\psi}_\text{e}\boldsymbol{\gamma}_\mu\psi_\text{e}\bar{\psi}_\text{q}\vec{\partial}^\mu\boldsymbol{\gamma}^5\psi_\text{q} - Q_{\text{qe,pv}}\bar{\psi}_\text{e}\vec{\partial}^\mu\boldsymbol{\gamma}^5\psi_\text{e}\bar{\psi}_\text{q}\boldsymbol{\gamma}_\mu\psi_\text{q},\end{aligned} \tag{2.8}$$

where $\vec{\partial}^\nu = \overleftarrow{\partial}^\nu - \vec{\partial}^\nu$. Furthermore, the QCD gluon field interaction of strength θ (eq. (1.24)) can induce $\mathcal{P},\mathcal{T}$-odd moments as well.

All the interaction terms appearing in the $\mathcal{P},\mathcal{T}$-odd interaction Lagrangian densities $\mathcal{L}_{\text{QCD}}^{\mathcal{P},\mathcal{T}}$ (eq. (1.24)), $\mathcal{L}_{\text{EDM}}^{\mathcal{P},\mathcal{T}}$ (eq. (2.7)) and $\mathcal{L}_{\text{current}}^{\mathcal{P},\mathcal{T}}$ (eq. (2.8)) can contribute to the EDM of an atom or molecule. Usually vector current interactions with strength $Q_{\text{qe,pv}}$, $Q_{\text{qe,vp}}$ and $Q_{\text{qq,vp}}$ are not considered as was noted in Ref. [204]. On the hadronic level quark-quark interactions (C_qq, Q_qq) and quark dipole moments d_q and strong $\mathcal{CP}$-violation (θ) contribute to the EDMs of the nEDM d_n and the Electric Dipole Moment of the proton (pEDM) d_p as well as to $\mathcal{P},\mathcal{T}$-odd pion-pion current interactions g_{π_NN}, which can be either isoscalar or isovector like. The quark-electron current interactions result in effective nucleon-electron current interaction parameters: i) scalar-pseudoscalar quark-electron currents $C_{\text{qe,sp}}$ contribute to k_s, ii) pseudoscalar-scalar quark-electron

currents $C_{\mathrm{qe,ps}}$ contribute to k_{p} and iii) pseudotensor-tensor currents $C_{\mathrm{qe,pt}}$ contribute to k_{T}.

On the nuclear structure level d_{n}, d_{p} and $g_{\pi_{\mathrm{NN}}}$ can produce net $\mathcal{P},\mathcal{T}$-odd nuclear moments; in leading order a Nuclear Electric Dipole Moment (NEDM) which is usually referred to as Schiff moment $\mathcal{S}$. Beyond dipoles, there can be the Nuclear Magnetic Quadrupole Moment (NMQM), the Nuclear Electric Octupole Moment (NEOM) and so forth.

Following Figure 2.5, the different possible sources of $\mathcal{P},\mathcal{T}$-violation we have to consider in an atom or molecule are an eEDM d_{e}, a pEDM d_{p}, interactions with net $\mathcal{P},\mathcal{T}$-odd moments of the nucleus, the Schiff moment $\mathcal{S}$, the NMQM $\mathcal{M}$ and higher nuclear moments, $\mathcal{P},\mathcal{T}$-odd Scalar-Pseudoscalar Nucleon-Electron Current (SPNEC) interactions k_{s}, Tensor-Pseudotensor Nucleon-Electron Current (TPNEC) interactions k_{T}, and Pseudoscalar-Scalar Nucleon-Electron Current (PSNEC) interactions k_{p}. The latter interaction is vanishing in the limit of non-relativistically moving nuclei (see Refs. [208, 209]).

The measurability of an atomic EDM was discussed by Schiff, who showed that even if a $\mathcal{P},\mathcal{T}$-odd EDM exists on the elementary particle or nuclear level, there cannot be a net EDM of an atom in the non-relativistic limit, which is known as Schiff's theorem [210]. However, Schiff showed that under consideration of relativistic effects a resulting net EDM of the atom would be possible. This showed that such $\mathcal{P},\mathcal{T}$-violation in atoms and molecules is a purely relativistic effect and indicated that the use of heavy elements as test systems can be advantageous.

2.1.2.b Searches for $\mathcal{P},\mathcal{T}$-violation with atoms and molecules

Whereas experiments with bare neutrons are important tools to search for the nEDM and $\mathcal{P},\mathcal{T}$-violation in the quark sector, such experiments are not possible with charged particles, such as electrons or protons, which would simply be accelerated to the oppositely charged wall. Therefore, experiments with atoms and molecules are indispensable for the study of the eEDM and other $\mathcal{P},\mathcal{T}$-violating parameters discussed above.

For an overview of early experiments on atomic EDMs I suggest Ch. 6.3 of Ref. [208] and Review [209] and references therein. An overview of the most recent results from most experiments can be found in Review [206]. The first limit on the eEDM of $d_{\mathrm{e}} < 2\times10^{-13}\,e\,\mathrm{cm}$ from the original experiment with hydrogen by Purcell and Ramsey [211] was set by Salpeter in his original discussion of the eEDM in atoms [199].

Following this, many experiments with other open-shell atoms such as Rb ($^2\mathrm{S}_{1/2}$), Cs ($^2\mathrm{S}_{1/2}$), Tl ($^2\mathrm{P}_{1/2}$), Fe^{3+} (in some $\mathrm{D}_{3/2}$-state) and Xe (metastable $6\mathrm{S}6\mathrm{P}^3\mathrm{P}_2$-state) [212–221] and closed-shell atoms such as Hg, Xe and Ra [222–226] were performed.[2]

With the achievement of better control of diatomic molecules by laser-cooling and other techniques (see Reviews [207, 227, 228]), molecules became the most interesting candidates for detection of $\mathcal{P},\mathcal{T}$-violation. Limits were placed with the closed-shell molecule TlF [229] and the open-shell molecules YbF ($\mathrm{X}^2\Sigma_{1/2}$), PbO ($\mathrm{A}_1{}^3\Sigma_{1/2}$), ThO ($\mathrm{H}^3\Delta_1$), HfF^+ ($\mathrm{H}^3\Delta_1$) [230–235]. Other running or planned experiments are performed with WC ($\mathrm{X}^3\Delta_1$), BaF ($\mathrm{X}^2\Sigma_{1/2}$) and RaF ($\mathrm{X}^2\Sigma_{1/2}$) [236–240].

An overview of actual best limits on atomic and molecular EDMs is given in Table 2.2.

After the proposal of laser-cooling of polyatomic molecules [241] and the subsequent experimental demonstration of it [242], the possibility of using polyatomic molecules to search for $\mathcal{P},\mathcal{T}$-violation arose [243]. This new field of research is addressed with developments of this thesis as well.

[2] In references such as Ref. [208] instead of open-shell and closed-shell the terms paramagnetic and diamagnetic are employed. However, as there can be closed-shell paramagnetic molecules, I use the more general terms open-shell and closed-shell, here. However, the determining factor is the actual spin state of the molecule.

In the search for $\mathcal{P},\mathcal{T}$-violation in atoms and molecules electronic structure theory has a primary role. Without theoretical prediction of effect sizes and spectroscopic parameters that show suitability for high-precision experiments the design of good experiments would hardly be possible. Furthermore, theory is indispensable for the interpretation of the experiments as only with knowledge of the electronic structure parameters W connection between frequency shifts in molecular experiments and the possible sources of $\mathcal{P},\mathcal{T}$-violation on the elementary particle level is possible as will be discussed in the next sections (see also discussions in Refs. [144, 146, 209]). An overview of the history of atomic structure calculations can be found in Ref. [209].

Table 2.2: Actual best limits on atomic d_{atom} and molecular EDMs d_{mol} (see also Refs. [206, 208]).

System	Reference	$d_{\text{atom,mol}}/e\,\text{cm}$
Open-shell atoms		
Xe 6S6P $^3P_2$	[214]	$0.7 \pm 1.4 \times 10^{-22}$
Fe^{3+} $D_{3/2}$	[217]	$4.2 \pm 6.0 \times 10^{-23}$
Rb $^2S_{1/2}$	[212]	$< 0.7 \times 10^{-18}$
Cs $^2S_{1/2}$	[218]	$-1.8 \pm 6.7 \times 10^{-24}$
Tl $^2P_{1/2}$	[221]	$-4.0 \pm 4.3 \times 10^{-25}$
Open-shell molecules[a]		
YbF $X^2\Sigma_{1/2}$	[231]	$1.8 \pm 5.2 \times 10^{-22}$
PbO $A_1{}^3\Sigma_{1/2}$	[232]	$0.7 \pm 4.2 \times 10^{-18}$
ThO $H^3\Delta_1$	[235]	$-2.1 \pm 2.8 \times 10^{-21}$
HfF^+ $H^3\Delta_1$	[234]	$1.4 \pm 14.7 \times 10^{-21}$
Closed-shell atoms		
Xe	[224]	$0.7 \pm 3.3 \times 10^{-27}$
Hg	[226]	$2.2 \pm 3.1 \times 10^{-30}$
Ra	[225]	$4 \pm 6 \times 10^{-24}$
Closed-shell molecules		
TlF	[229]	$-1.7 \pm 2.9 \times 10^{-23}$

[a] For open-shell molecules the molecular EDM is given as the frequency difference $\Delta\omega_+ - \Delta\omega_-$ and analysed directly in a single source model to set limits on d_e. I converted the original results into values for d_{mol} following eq. (2.11) with the external electric fields being $\mathcal{E}_{\text{YbF}} = 10\,\text{kV cm}^{-1}$, $\mathcal{E}_{\text{PbO}} = 100\,\text{V cm}^{-1}$, $\mathcal{E}_{\text{ThO}} = 80\,\text{V cm}^{-1}$, $\mathcal{E}_{\text{HfF}^+} = 24\,\text{V cm}^{-1}$ and their alignments being $\lambda_{z,\text{YbF}} = 0.558$, $\lambda_{z,\text{PbO}} = 1$, $\lambda_{z,\text{ThO}} = 1$, $\lambda_{z,\text{HfF}^+} = 1$ (see also the discussion in Ref. [244]).

Sanders pioneered calculations of enhancement of EDMs in heavy atoms. He calculated enhancing relativistic effects in the mixing of $s_{1/2}$ and $p_{1/2}$ orbitals [245–248] of the eEDM and found it to scale as [246]:

$$\left\langle s_{1/2} \left| \hat{H}_{\text{eEDM}} \right| p_{1/2} \right\rangle \sim \frac{\alpha^2 Z^3}{\gamma_{1/2}(\gamma_{1/2}^2 - 1)}, \tag{2.9}$$

which was affirmed by similar considerations in Refs. [249, 250]. From this relativistic enhancement it is obvious that $\mathcal{P},\mathcal{T}$-odd effects can be expected to be strongly pronounced in systems containing elements with large Z [251]. A summary of most scaling laws of $\mathcal{P},\mathcal{T}$-odd properties, derived analytically in the same hydrogen-like atom model, can be found in Ref. [208] and alongside some results in the Review [209]. In Appendix B I provide the scaling laws with respect to nuclear charge of $s_{1/2}$-$p_{1/2}$ matrix elements from such analytical considerations for all electronic structure parameters W that are discussed in this thesis.

Polar diatomic molecules appear to be excellent candidates for EDM measurements as they can have almost degenerate Ω doublet states (see also section before and Refs. [142, 143, 251, 252]).

In the beginning, the search for suitable molecular candidates was advanced by Labzovsky [142], Gorshkov *et. al* [253], Sushkov, Flambaum and Khriplovich [143, 254, 255] as well as by Kozlov and coworkers [256–264] mostly on a semi-empirical level of theory.

Due to the still negative results for $\mathcal{P},\mathcal{T}$-violation in low-energy systems, the search for suitable candidates for new EDM experiments is an active field. For this purpose modern relativistic quantum chemical methods are developed and employed [239, 265–298]. Although accuracy on the percent level is claimed for some calculations, so far no $\mathcal{P},\mathcal{T}$-odd effect has been measured and an accuracy of about 20% for the calculations is usually sufficient to set limits on parameters or to find suitable molecule candidates.

As has been discussed in the previous sections, interpretation of atomic and molecular EDM

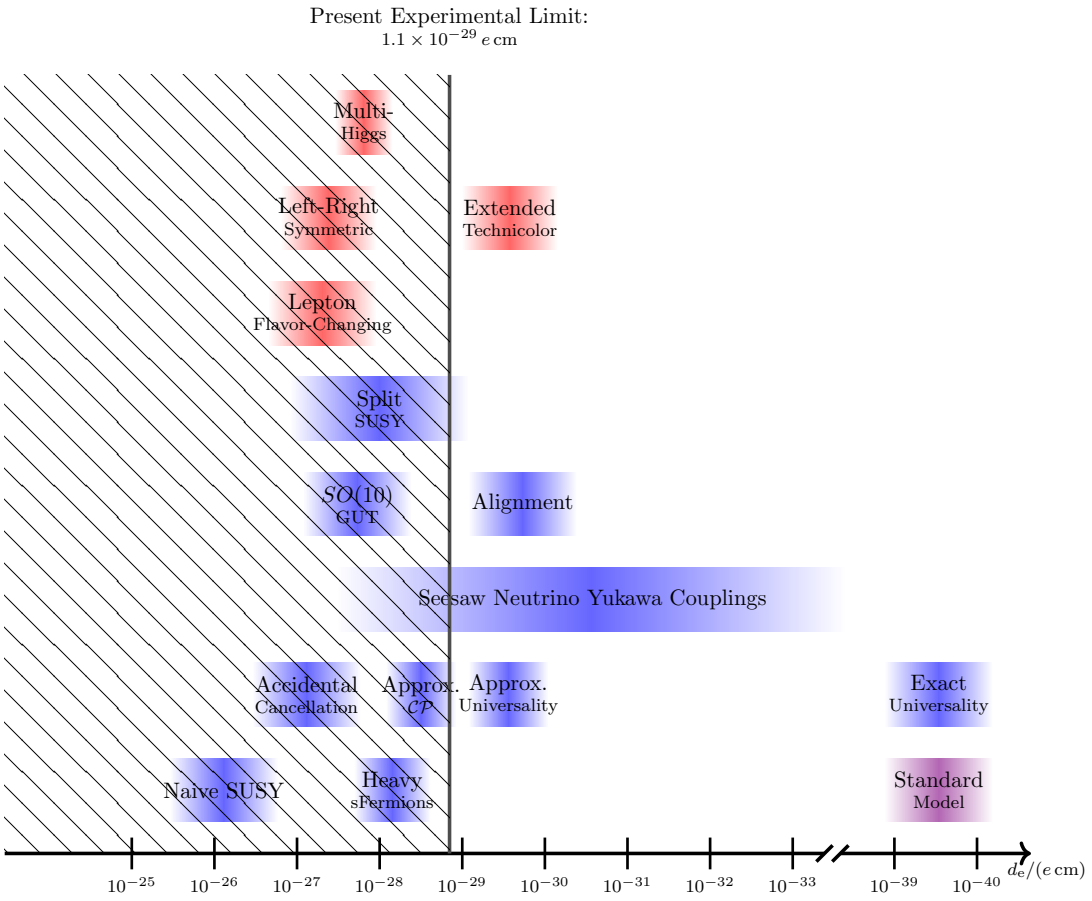

Figure 2.6: Overview of the predictions of an eEDM of the SM and various SM-extensions taken from Refs. [201–203]. Blue boxes belong to variants of SUSY and red to independent generic models. The present experimental limit was measured and extracted in Ref. [235] assuming d_e being the only source of $\mathcal{P},\mathcal{T}$-violation.

experiments is not trivial as many possible sources can contribute to an atomic EDM d_{atom} or molecular EDM d_{mol}. Obtained limits on parameters on the elementary particles are commonly derived in a single source model, i.e., only one fundamental $\mathcal{P},\mathcal{T}$-odd parameter is assumed to be existent. For example, within this approximation it is claimed that the ThO experiment sets a limit of $d_e < 1.1 \times 10^{-29}\, e\,\mathrm{cm}$ on the eEDM [235]. This limit would imply an exclusion of several BSM models or a restriction of their parameter space (see Figure 2.6).

Although it is common practice, there is no good reason to assume such a situation to be realistic and multivariate measurement models should be applied to obtain reasonable limits on parameters on the elementary particle level (see also discussions in Refs. [206, 244, 299, 300]). Here, it is important to note that nuclear spin dependent effects can contribute significantly in open-shell atoms and molecules if they consist of nuclei with non-zero spin, which is widely ignored. In fact, open-shell molecules are discussed in a two-dimensional parameter space in Refs. [206, 244, 299, 300]. In this regard, the field of EDM experiments is still highly unexplored. However, in recent studies possibilities to limit quark sector $\mathcal{P},\mathcal{T}$-violation from experiments with open-shell molecules with an NMQM [287, 292, 295] or by analyzing quark currents that contribute to k_s [301]. Even if a non-zero atomic or molecular EDM was measured, its interpretation and implications for BSM physics would require new experiments and in particular developments in the theoretical description of $\mathcal{P},\mathcal{T}$-odd effects in molecules, which I want to advance with this thesis.

2.1.2.c Effective $\mathcal{P},\mathcal{T}$-odd molecular Hamiltonian

The permanent EDM of a molecule $\vec{d}_{\text{mol}}$ is proportional to its total angular momentum $\vec{F}$: $\vec{d}_{\text{mol}} = d_{\text{mol}}\vec{F}$.

An EDM can be measured by exposure of the atom or molecule to an external electromagnetic field consistent of the electric field $\vec{\mathcal{E}}$ and magnetic field $\vec{\mathcal{B}}$ where the interaction Hamiltonian is $H_{\text{EDM}} = d_{\text{mol}}\vec{F}\cdot\vec{\mathcal{E}}$. By reversal of the electric field relative to the magnetic field a change in the Larmor frequency, i.e., an energy shift correlated with $\vec{\mathcal{E}}\cdot\vec{\mathcal{B}}$, can be measured.

In a polar diatomic or linear molecule with one heavy atom three Hund's coupling cases can be relevant [144]: (a) the spin-axis interaction dominates ($\vec{F} = \vec{I} + \vec{R} + (\Lambda + \Sigma)\vec{\lambda}$), (b) the spin-rotation interaction dominates ($\vec{F} = \vec{I} + \vec{R} + \vec{S} + \Lambda\vec{\lambda}$), and (c) the spin-orbit interaction dominates ($\vec{F} = \vec{I} + \vec{R} + \Omega\vec{\lambda}$). Here, $\vec{R}$ is the rotational angular momentum, $\Lambda = \vec{L}\cdot\vec{\lambda}$ and $\Sigma = \vec{L}\cdot\vec{\lambda}$ are the projections of the electronic orbital angular momentum $\vec{L}$ and the electron spin $\vec{S}$ on the molecular axis defined by the unit vector $\vec{\lambda}$ pointing from the heavy to the light nucleus. $\Omega = \vec{J}_{\text{e}}\cdot\vec{\lambda}$ is the projection of the total electronic angular momentum $\vec{J}_{\text{e}}$ on the molecular axis. The total angular momentum in case (a) can be written in terms of the total angular momentum of case (c), as $\vec{J}_{\text{e}} = \vec{L} + \vec{S}$ and, thus, $\Omega = \Lambda + \Sigma$. Case (b) can be related to case (c) by changing the quantization axis of the electron spin, which can be achieved by definition of an effective electron spin $\vec{S}'$ [144], which if $\Lambda = 0$, for case (b) $\vec{S}' = \vec{S}$. For cases (a) and (c) $\vec{S}' = \vec{J}_{\text{e}}$.

For low lying rotational states the total nuclear spin $\vec{I}$ is quantized on the molecular axis $\mathcal{I} = \vec{I}\cdot\vec{\lambda}$. Thus, the total angular momentum of the molecule can be written as $\vec{F} = (\Omega + \mathcal{I})\vec{\lambda} + \vec{R}$ for the above discussed coupling cases, where Ω is redefined as the projection of the effective electron spin $\vec{S}'$ on the molecular axis $\Omega = \vec{S}'\cdot\vec{\lambda}$ [144].

A permanent EDM of a linear molecule would now cause a relative shift of the spin precession frequency of

$$\Delta\omega_{\pm} = \frac{\left|\left\langle\vec{\mu}_{\text{mol}}\cdot\vec{\mathcal{B}}\right\rangle\right| \pm \left|\left\langle\vec{d}_{\text{mol}}\cdot\vec{\mathcal{E}}\right\rangle\right|}{\hbar}, \quad (2.10)$$

where $\vec{\mu}_{\text{mol}}$ is the molecular Magnetic Dipole Moment (MDM). The frequency shift $\Delta\omega_+$ corresponds to $\vec{\mathcal{E}} \uparrow\uparrow \vec{\mathcal{B}}$ and $\Delta\omega_-$ corresponds to $\vec{\mathcal{E}} \uparrow\downarrow \vec{\mathcal{B}}$. For an electric field along the z-axis the molecular (atomic) EDM is, thus, determined by

$$d_{\text{mol}} = \hbar\frac{\Delta\omega_+ - \Delta\omega_-}{2\mathcal{E}\lambda_z(\Omega + \mathcal{I})}, \quad (2.11)$$

where $\lambda_z = \left\langle\vec{\lambda}\cdot\vec{z}\right\rangle$ is a measure for the alignment of the molecular axis on the laboratory z-axis $\vec{z}$ and $\mathcal{E}$ is the magnitude of the applied external electric field. This setup is sketched for an open-shell molecule with an unpaired electron experiencing the effective internal electrical field of magnitude $\mathcal{E}_{\text{eff}}$ of the molecule in Figure 2.7.

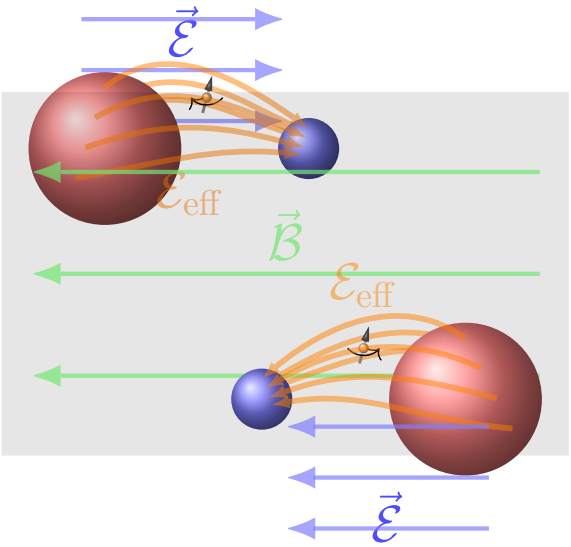

Figure 2.7: Schematic representation of the principle of permanent EDM measurements with polar diatomic open-shell molecules.

The full $\mathcal{P},\mathcal{T}$-odd effective spin-rotational Hamiltonian for an open-shell linear molecule with a nucleus A with nuclear spin quantum number larger than $1/2$ reads for Hund's coupling case (b)

with $\Lambda = 0$ and for cases (a) and (c) (for parts of H_{sr_A} see Refs. [144, 252])

$$H_{\mathrm{sr}_A}^{\mathcal{P},\mathcal{T}} = \Omega\left(W_{\mathrm{d}_A} d_\mathrm{e} + W_{\mathrm{s}_A} k_\mathrm{s}\right) + \underbrace{\vec{\lambda}^\mathsf{T} \cdot \mathbf{T}_A \cdot \vec{S}'}_{\Theta_A} W_{\mathcal{M}_A} \tilde{\mathcal{M}}_A + \text{higher moments...} \tag{2.12}$$

$$+ \mathcal{I}_A \left(W_{\mathrm{T}_A} k_\mathrm{T} + W_{\mathrm{p}_A} k_\mathrm{p} + W_{\mathrm{s}_A}^\mathrm{m} k_\mathrm{s} + W_{\mathcal{S}_A} \mathcal{S}_A + (W_{\mathrm{m}_A} + W_{\mathcal{S}_A} R_\mathrm{vol}) d_\mathrm{p} + W_{\mathrm{d}_A}^\mathrm{m} d_\mathrm{e}\right).$$

Here, $\mathbf{T}_A$ is a second-rank tensor with components $T_{A,ij} = I_{A,i} I_{A,j} + I_{A,j} I_{A,i} - \frac{2}{3}\delta_{ij} I_A (I_A + 1)$, where I_A is the total nuclear spin quantum number and $I_{A,j}$ are the components of $\vec{I}_A$ (for details see Ref. [144]), $\tilde{\mathcal{M}}_A = \frac{-1}{2I_A(2I_A-1)} \mathcal{M}_A$ with the NMQM $\mathcal{M}$ (see Ref. [144]). For a closed-shell molecule all terms that depend on the effective electronic spin $\vec{S}'$ (here all terms proportional to Ω and Θ) vanish. The constants W are electronic structure coupling constants enhancing $\mathcal{P},\mathcal{T}$-violating parameters in molecules, that need to be determined by electronic structure calculations. R_vol is a nuclear structure factor that enhances the pEDM and can be determined from nuclear structure calculations. Explicit forms of the $\mathcal{P},\mathcal{T}$-odd electronic structure coupling constants W are given in the appendix and can be found in Refs. [144, 208, 252] and references therein. Effects of higher order in α contributing to W_{d_A} and $W_{\mathrm{d}_A}^\mathrm{m}$ are discussed in Ref. [302] and in detail in Ref. [303].

Many modern EDM experiments employ Ramsey spectroscopy [211] in which coherent spin precession, i.e., a superposition of states with opposite sign, is measured. For this purpose an oscillating magnetic field tuned to almost the Larmor frequency with fixed duration τ is applied (for details see, e.g., [304] or [208, 305]). These two states produce a total precession phase of $\varphi \sim \Delta\Delta\omega\tau$, where $\Delta\Delta\omega \sim \Delta\omega_+ - \Delta\omega_-$, and, therefore, the measured phase shift is proportional to the EDM. Further technical aspects and different measurement principles of EDM experiments with diatomics are discussed elsewhere (e.g. Refs. [208, 233, 305]).

2.2 Searches for dark matter

As explained in the first chapter, the nature of DM is totally obscure, and, thus, there are completely different ways for searching for DM particles. In this work, I focus on CDM that causes fundamental symmetry violation. Other DM, in particular scalar DM, may also cause a variation of fundamental constants [306], which can be searched for with atoms and molecules as well (see Reviews [307–309] and references therein).

Parity violating effects can arise in interactions of electrons or nucleons with fermionic, weakly interacting DM, such as WIMPs. Such effects would be comparable to electron neutrino interactions described by the left diagram in Figure 2.1 and were estimated in Refs. [310–312]. Similar considerations are valid for dark neutrinos as long as they are left-handed.

Considering bosonic DM, most obviously pseudoscalar ALPs and pseudovector bosons can lead to $\mathcal{P}$-odd and $\mathcal{P},\mathcal{T}$-odd effects in atoms and molecules as was discussed among others in Refs. [90, 313–315].

The interaction of an electron with a pseudoscalar boson is described via the Lagrangian density [84, 85]

$$\mathcal{L}_\mathrm{p}^{\phi\mathrm{e}} = g_{\phi\bar{\mathrm{e}}\mathrm{e}} (\hbar c\, \partial_\mu \phi) \bar{\psi}_\mathrm{e} \boldsymbol{\gamma}^\mu \boldsymbol{\gamma}^5 \psi_\mathrm{e}\,, \tag{2.13}$$

and an equivalent Lagrangian density for interaction with nucleons can be formulated. Here, $g_{\phi\bar{\mathrm{e}}\mathrm{e}}$ is a coupling constant of dimension GeV^{-1}. The interaction of an electron with a pseudovector or

axial vector bosonic DM is described by the Lagrangian density

$$\mathcal{L}_{\mathrm{a}}^{b\mathrm{e}} = -b_{\mu}^{\mathrm{e}} \bar{\psi}_{\mathrm{e}} \boldsymbol{\gamma}^{\mu} \boldsymbol{\gamma}^{5} \psi_{\mathrm{e}}, \tag{2.14}$$

with the pseudovector field b_{μ}^{e} including the parameters for strength of interactions with electrons. This Lagrangian can be written analogously for the nucleons as well.

Molecular and atomic experiments mostly search for the parity-conserving axion wind effect [88, 89, 98, 316–320], i.e., the space-like components of (2.13) which can be interpreted as Zeeman-like effect of a pseudomagnetic field generated by the ALP field that interacts with the electronic or nuclear spin of an atom or molecule:[3]

$$H_{\mathrm{p},(1,2,3)}^{\phi\mathrm{e}} = g_{\phi\bar{\mathrm{e}}\mathrm{e}} (\vec{\nabla}\psi_{\phi}) \cdot \left\langle \psi_{\mathrm{e}} \middle| \vec{\boldsymbol{\Sigma}} \middle| \psi_{\mathrm{e}} \right\rangle \approx g_{\phi\bar{\mathrm{e}}\mathrm{e}} \hbar \omega_{\phi} \phi_0 \vec{v}_{\phi} \cdot \vec{S} \sin(\omega_{\phi} t) \tag{2.15}$$

$$H_{\mathrm{a},(1,2,3)}^{b\mathrm{e}} \approx \vec{b}^{\mathrm{e}} \cdot \vec{S} \sin(\omega_b t)\,. \tag{2.16}$$

These experiments are performed as spin interferometry with so called Superconducting QUantum Interference Devices (SQUIDs), which are highly sensitive to the slightest changes in the magnetic field, or with NMR, and, thus, can provide very strict limits on $g_{\phi\bar{\mathrm{e}}\mathrm{e}}$ and the spatial parts of b_{μ}^{e}. The present best limits from SQUID experiments are $\left|b_i^{\mathrm{e}}\right| < 10^{-30}\,\mathrm{GeV}$ and $\left|g_{\phi\bar{\mathrm{e}}\mathrm{e}}\right| < 10^{-7}\,\mathrm{GeV}^{-1}$ [320–322]. However, the time-like component b_0^{e} that mediates the interaction described by the Hamiltonian

$$\hat{H}_{\mathrm{a},0}^{b\mathrm{e}} = b_0^{\mathrm{e}} \sin(\omega_b t) \boldsymbol{\gamma}^{5} \tag{2.17}$$

remains inaccessible in such experiments. This parity-nonconserving interaction is accessible in atomic parity-violation experiments [90, 313]. Furthermore, in atomic parity-violation experiments a direct pseudoscalar coupling between the electrons and the pseudoscalar cosmic field can contribute (see, e.g., Ref. [313]):

$$\mathcal{L}_{\mathrm{dps}}^{\phi} = -\imath \tilde{g}_{\phi\bar{\mathrm{e}}\mathrm{e}} m_{\mathrm{e}} c^2 \phi \bar{\psi}_{\mathrm{e}} \boldsymbol{\gamma}^{5} \psi_{\mathrm{e}}\,. \tag{2.18}$$

This interaction can lead to parity-violating couplings when considering transition matrix elements relevant for atomic transition rates [90]. However, the direct pseudoscalar coupling does not contribute to parity-violating expectation values to which eq. (2.17) contributes, which are not measurable in atomic systems anyway. As discussed in Sec. 2.1.1 such $\mathcal{P}$-odd expectation values can be measured in chiral molecules, which will be explored in the context of DM in this thesis.

2.3 Searches for Lorentz invariance violation

In a recent review by Vargas a good overview of the relatively young research area of Lorentz invariance tests with atoms is given [323]. As discussed in the previous chapter, today the SME is the commonly used test theory for LLIVs. In good approximation only the QED sector of the SME has a direct impact on atomic or molecular structure. The QED sector of the SME can be tested with photons, atoms and charged sub-atomic particles, which has been done extensively [121, 324–327]. Molecular experiments are still exotic in this research area and not much is achieved in this respect so far.

Experiments with atoms and molecules are, first of all, sensitive to the electronic part of this sector. The SME is an effective field theory, adding perturbatively terms to the Lagrangians of the SM and GR that are contractions of field operators with tensors that define a fixed direction

[3] Note that I dropped the phase of the CDM field here as discussed in Sec. 1.3.3.

in spacetime, and with this introduce LLIV. The LLIV electronic Lagrangian density has the form [328]

$$\mathcal{L}_{\mathrm{e}}^{\mathrm{SME}} = \hbar c \bar{\psi}_{\mathrm{e}} \left[\tilde{c}_{\mu\nu} \boldsymbol{\gamma}^{\mu} + \tilde{d}_{\mu\nu} \boldsymbol{\gamma}_5 \boldsymbol{\gamma}^{\mu} + \tilde{e}_{\nu} + \tilde{f}_{\nu} \boldsymbol{\gamma}_5 + \frac{1}{2} \tilde{g}_{\lambda\mu\nu} \sigma^{\lambda\mu} \right] \frac{\imath}{2} \overleftrightarrow{\partial}^{\nu} \psi_{\mathrm{e}} - m_{\mathrm{e}} c^2 \bar{\psi}_{\mathrm{e}} \left[\tilde{a}_{\mu} \boldsymbol{\gamma}^{\mu} + \tilde{b}_{\mu} \boldsymbol{\gamma}_5 \boldsymbol{\gamma}^{\mu} + \frac{1}{2} \tilde{h}_{\mu\nu} \sigma^{\mu\nu} \right] \psi_{\mathrm{e}} \,. \quad (2.19)$$

The parameters of the electron-sector of the SME, which control the extent of LLIV are $\tilde{a}_{\mu}$ for even vector interactions, $\tilde{b}_{\mu}$ for even pseudovector interactions, $\tilde{c}_{\mu\nu}$ for odd vector interactions, $\tilde{d}_{\mu\nu}$ for odd pseudovector interactions, $\tilde{e}_{\mu}$ for odd scalar interactions, $\tilde{f}_{\mu}$ for odd pseudoscalar interactions, $\tilde{g}_{\mu\nu\lambda}$ for odd tensor interactions and $\tilde{h}_{\mu\nu}$ for the even tensor interactions. Here even and odd refer to the order in the four derivative ∂^{μ} and all parameters are chosen to be dimensionless.

Note that pseudovector interactions defined by $m_{\mathrm{e}} c^2 \tilde{b}_{\mu} = b_{\mu}^{\mathrm{e}}$ are identical to those that can be relevant for CDM discussed in the paragraph above. Thus, limits on LLIV characterized by $\tilde{b}_{\mu}$ can be drawn from the experiments that limit pseudovector CDM discussed in the previous paragraph.

Further experimental limits exist for $\tilde{c}_{\mu\nu}$ and some parts of the tensors $\tilde{d}_{\mu\nu}$, $\tilde{g}_{\mu\nu\lambda}$ and $\tilde{h}_{\mu\nu}$.[4] Atomic experiments with H [329], Ca^+ [330, 331], Yb^+ [332], Dy [333], comparison of Al^+ and Hg^+ (spectroscopy) [334], comparison of Hg and Cs (magnetometers) [335], Li^+ [336], Cs and Rb [337] set limits on different components and combinations of components of $\tilde{c}_{\mu\nu}$. Furthermore, also solids are used as probes for this LLIV parameter [338, 339]. E.g., present best limits on the diagonal elements $\tilde{c}_{11}$, $\tilde{c}_{22}$, $\tilde{c}_{33}$ are on the order of 10^{-15} [340].

In all these experiments the probed *low energy* valence electrons are assumed to be non-relativistic leading to an effective non-relativistic odd vector Hamiltonian of the form:

$$\hat{H}_{\mathrm{e,ov,nr}}^{\mathrm{SME}} \approx \sum_{i=1}^{N_{\mathrm{elec}}} \frac{1}{2m_{\mathrm{e}}} \hat{\vec{p}}_i^{\mathsf{T}} \cdot \tilde{\boldsymbol{c}} \cdot \hat{\vec{p}}_i, \quad (2.20)$$

where $\hat{\vec{p}}_i$ is the linear momentum operator of electron i and the sum runs over N_{elec} electrons.

Molecules can provide a powerful alternative to the aforementioned systems but so far are only considered by using the H_2 maser system [341]. A first study of the influence of LLIVs on chemical bonding and molecular spectra was carried out in Ref. [341]. Therein, it was shown that $D_{\infty h}$ symmetric molecules such as H_2 are sensitive to $\tilde{c}_{33}$ and $\tilde{c}_{11} = \tilde{c}_{22}$, when an alignment of the molecular axis along z is assumed. So far the potential of molecular precision spectroscopy to search for such LLIV remains to be exploited, which is one aspect of this thesis.

[4] In the non-minimal sector also for $\tilde{a}_{\mu}$ and $\tilde{f}_{\mu}$ experimental limits exist (see for details Ref. [121]).

3 Relativistic electronic structure theory

In this chapter I briefly highlight the essentials of electronic structure theory. As this is a wide field I focus on very few methods that are frequently used within this thesis and I only give a rather general description but do not discuss many technical details. For more technical aspects of the concepts and methods introduced in the following I suggest Refs. [342–346]. In the following I will discuss molecular electronic structure theory only, assuming that the Born-Oppenheimer approximation, i.e., a separation of nulcear and electronic motion, holds. Then the nuclei generate a fixed potential in which the electrons move. For details on the full molecular Hamiltonian and approximations to it I suggest Ref. [47].

3.1 Many-electron theory

The many-electron wave function Ψ can be written as an anti-symmetrized direct product of all N one-electron wave functions ψ_i:

$$\Psi = \hat{\mathcal{A}}\psi_1 \otimes \psi_2 \otimes \cdots \psi_N, \tag{3.1}$$

where the anti-symmetrization operator $\hat{\mathcal{A}}$ guarantees, that the wave-function obeys the Pauli principle, i.e., it is totally anti-symmetric regarding interchange of two electrons. An alternative to $\hat{\mathcal{A}}$ is to represent the one-electron functions ψ in second quantization with anhilation $\hat{a}$ and creation $\hat{a}^\dagger$ operators and let them act on the vacuum (see, e.g., Ch. 1 of Ref. [343]).

Whereas analytic solutions for one-particle problems exist, the quantum mechanical many-particle problem is not analytically solvable as the particles' movements are correlated.

A common numerical approach to solve this problem is to expand the vacuum space, in which the many-electron wave function is defined, in a finite set of one-electron wave functions ψ, called spin-orbitals. Due to the finiteness of this basis the solution is not exact anymore. However, the size of the basis may be adjusted to arrive at the target accuracy. Within this approximation the many-electron wave function Ψ may be defined as a linear combination of all possible arrangements Φ_i of N electrons in the space of M one-electron basis functions ψ:

$$\Psi = \sum_{I=1}^{\binom{M}{N}} C_I \Phi_I \,, \tag{3.2}$$

where the linear combination coefficients C_I are to be determined by the solution of the equations of motion, i.e., the Schrödinger or Dirac equations, respectively. This approach is also known as full Configuration Interaction (CI) because all possible *configurations* Φ_I of N electrons in the space of M orbitals are considered. In order to account for the anti-symmetry with respect to interchange of two electrons, all Φ can be represented as determinants of matrices of size $N \times N$, called Slater-Determinant (SD).

3.1.1 Mean-field approaches and broken symmetry

In this thesis the focus is on heavy-elemental systems in which relativistic effects dominate over electron correlation effects. Therefore, most calculations are performed on the mean-field level, i.e., only one SD of expansion (3.2) is taken into account. In order to determine the exact form of the SD Φ, it is necessary to find the wave function which describes each electron moving in the

mean field of all other electrons for a fixed occupation pattern of N electrons in M spin-orbtials. This mean-field approach is called Hartree–Fock (HF) approach [347, 348].[1]

Within HF the Hamiltonian operator $\hat{H}$ can be written as an effective one-electron operator, the so called Fock-operator $\hat{f}$. As the field of the electrons that one moving electron experiences depends on the ψ_i of all other electrons, the Fock operator is a function of the spin-orbitals ψ_i:

$$\hat{f}\left(\{\psi_i\}\right) = \hat{h} + \hat{J}\left(\{\psi_i\}\right) - \hat{K}\left(\{\psi_i\}\right) , \tag{3.3}$$

where $\hat{h}$ contains all one-electron operators and is independent of ψ, $\hat{J}$ is the direct Coulomb operator and $\hat{K}$ is the non-local exchange Coulomb operator. The spin-orbitals are required to be orthonormal: $\left\langle \psi_i \middle| \psi_j \right\rangle = \delta_{ij}$. A common approach to solve the resulting effective single-particle pseudo-eigenvalue equations

$$\hat{f}_i\left(\{\psi_i\}\right)\psi_i = \epsilon_i \psi_i \tag{3.4}$$

is to guess a set of trial orbitals $\{\tilde{\psi}_i\}$ and optimize until the field of the electrons ($\hat{J}$ and $\hat{K}$) does not change anymore (called Self-Consistent Field (SCF)). The orbitals can be expanded in a linear combination of N_{basis} known basis functions χ_μ, which is also known under the acronym Linear Combination of Atomic Orbitals (LCAO):

$$\psi_i = \sum_{\mu=1}^{N_{\text{basis}}} c_{\mu i}\chi_\mu \, . \tag{3.5}$$

The resulting generalized pseudo-eigenvalue equations appear in matrix form as

$$\boldsymbol{F}(\boldsymbol{D})\boldsymbol{C} = \boldsymbol{S}\boldsymbol{C}\boldsymbol{\epsilon}, \tag{3.6}$$

where $\boldsymbol{S}$ is the metric of the basis, calculated as the inner product or overlap matrix of the basis functions χ. $\boldsymbol{C}$ is the matrix of LCAO coefficients $c_{\mu i}$ and $\boldsymbol{F}$ is the Fock matrix in basis set (χ) representation. $\boldsymbol{\epsilon}$ is a diagonal matrix that contains the resulting eigenvalues of $\boldsymbol{F}$ which represent the energies of the spin-orbitals ψ_i. $\boldsymbol{F}$ is a Hermitian matrix and a function of the one-electron density matrix $\boldsymbol{D}$ which is calculated from the coefficient matrix $\boldsymbol{C}$:

$$\boldsymbol{D} = \boldsymbol{C}^\dagger \boldsymbol{n} \boldsymbol{C}, \tag{3.7}$$

where $\boldsymbol{n}$ is a diagonal matrix defining the occupation pattern of the spin-orbitals.

Within relativistic or quasi-relativistic theories, $\boldsymbol{D}$ and, thus, $\boldsymbol{F}$ are supposed to be invariant under time-reversal symmetry $\mathcal{T}$. In addition, a non-relativistic Hamiltonian is invariant under complex conjugation $\mathcal{K}$ and all spin rotations $\exp\left(-\imath\frac{\theta}{2}\boldsymbol{\sigma}^i\right)$, i.e., it commutes with $\hat{S}_z$ and $\hat{S}^2$. For the explicit form of $\boldsymbol{F}$ see text books on (relativistic) quantum chemistry, such as Refs. [342, 343, 349].

In order to describe static electron correlation effects, particularly spin-polarization, correlations within a mean-filed approach, without explicitly constructing other than the ground state SD, the symmetries of the non-relativistic $\boldsymbol{F}$ corresponding to the so called Restricted HF (RHF) solution, i.e., $\mathcal{T}$, $\mathcal{K}$, $\hat{S}_z$ and $\hat{S}^2$, can be considered as broken in order to find lower energy solutions, as was discussed by Čížek and Paldus and Fukutome in the late 1960s and 1970s [350–362] (see also the Review [363]). In comparison to RHF, according to the spin properties of $\boldsymbol{F}$, *spin unrestricted* methods are defined as Unrestricted HF (UHF) if $\hat{S}^2$ does not commute with $\boldsymbol{F}$, or Generalized HF (GHF) if $\hat{S}_z$ and $\hat{S}^2$ do not commute with $\boldsymbol{F}$.

[1] In relativistic calculations the acronym Dirac–Hartree–Fock (DHF) is commonly employed in order to differentiate from the usually employed Schrödinger-Hamiltonian that describes the non-relativistic limit.

Table 3.1: Classification of HF solutions by conserved symmetries as introduced by Stuber and Paldus [364]. It shall be noted that all UHF methods can be chosen with the spin aligned along any other axis as well. The acronym sp indicates if the method allows for spin-polarization or not. Here, $N \times N$ is the size of the density matrix $\boldsymbol{D}$.

Name	Conserved symmetries	Density matrix	sp
real RHF (rRHF)	$\left\{\hat{1}, \hat{S}^2, \hat{S}_z, \hat{\mathcal{T}}, \hat{\mathcal{K}}\right\}$	$\boldsymbol{D}^{(0)} \in \mathbb{R}^{N\times N} \wedge \boldsymbol{D}^{(i)} = \boldsymbol{0}$	✗
complex RHF (cRHF)	$\left\{\hat{1}, \hat{S}^2, \hat{S}_z, \hat{\mathcal{T}}\right\}$	$\boldsymbol{D}^{(0)} \in \mathbb{C}^{N\times N} \wedge \boldsymbol{D}^{(i)} = \boldsymbol{0}$	✗
paired UHF (pUHF)	$\left\{\hat{1}, \hat{S}_z, \hat{\mathcal{T}}\right\}$	$\boldsymbol{D}^{(0)} \in \mathbb{R}^{N\times N} \wedge \boldsymbol{D}^{(3)} \in \imath\mathbb{R}^{N\times N} \wedge \boldsymbol{D}^{(1,2)} = \boldsymbol{0}$	✗
real UHF (rUHF)	$\left\{\hat{1}, \hat{S}_z, \hat{\mathcal{K}}\right\}$	$\boldsymbol{D}^{(0)}, \boldsymbol{D}^{(3)} \in \mathbb{R}^{N\times N} \wedge \boldsymbol{D}^{(1,2)} = \boldsymbol{0}$	✓
complex UHF (cUHF)	$\left\{\hat{1}, \hat{S}_z\right\}$	$\boldsymbol{D}^{(0)}, \boldsymbol{D}^{(3)} \in \mathbb{C}^{N\times N} \wedge \boldsymbol{D}^{(1,2)} = \boldsymbol{0}$	✓
paired GHF (pGHF)	$\left\{\hat{1}, \hat{\mathcal{T}}\right\}$	$\boldsymbol{D}^{(0)} \in \mathbb{R}^{N\times N} \wedge \boldsymbol{D}^{(i)} \in \imath\mathbb{R}^{N\times N}$	✗
real GHF (rGHF)	$\left\{\hat{1}, \hat{\mathcal{K}}\right\}$	$\boldsymbol{D} \in \mathbb{R}^{N\times N}$	✓
complex GHF (cGHF)	$\left\{\hat{1}\right\}$	$\boldsymbol{D} \in \mathbb{C}^{N\times N}$	✓

Generally, the one-electron density matrix appears as complex matrix and can be written as

$$\boldsymbol{D} = \frac{1}{2}\sum_{\mu=1}^{4}(\boldsymbol{\sigma}^{\mu})^{*} \otimes \boldsymbol{D}^{(\mu)}, \tag{3.8}$$

where $\otimes$ denotes the Kronecker product and the four complex matrices $\boldsymbol{D}^{(\mu)}$ correspond to the number and spin densities, respectively. By introducing symmetries step-by-step $\boldsymbol{D}$ becomes more and more restricted. Stuber and Paldus classified all different broken symmetry HF solutions by the symmetry of $\boldsymbol{D}$ as given in Table 3.1 [364].

3.1.2 Density functional theory

It was shown by Hohenberg and Kohn in 1964, that it is not necessary to describe quantum systems by an abstract wave function, but the many-particle ground state energy can be written as unique functional of its observable density [365]. This Hohenberg-Kohn theorem motivated the development of Density Functional Theory (DFT) in which the energy of an N-electron system is treated as unique functional of the one-electron number density function:

$$\rho(\vec{r}) = N\mathfrak{R}\int\cdots\int \mathrm{d}^3r_2\cdots\mathrm{d}^3r_N\left(\Psi\left(\vec{r}_1,\ldots,\vec{r}_N\right)\right)^{\dagger}\Psi\left(\vec{r}_1,\ldots,\vec{r}_N\right). \tag{3.9}$$

For relativistic calculations an extension of the Hohenberg-Kohn theorem was formulated [366], that defined the ground state energy as unique functional of the four-current. I.e., in addition to the number density function ρ, the one-electron current density functions have to be considered:

$$\vec{j}(\vec{r}) = N\mathfrak{R}\int\cdots\int \mathrm{d}^3r_2\cdots\mathrm{d}^3r_N\left(\Psi\left(\vec{r}_1,\ldots,\vec{r}_N\right)\right)^{\dagger}\vec{\boldsymbol{\alpha}}_1 \otimes \mathbf{1}_2 \otimes\cdots\otimes \mathbf{1}_N\Psi\left(\vec{r}_1,\ldots,\vec{r}_N\right). \tag{3.10}$$

In all calculations in this thesis, only non-relativistic density functionals were employed which depend only on the one-electron number density function ρ. Spin-polarization was considered on the level of spin-up and spin-down number densities. In the spin-unpolarized case the total electronic energy is calculated as

$$E\left[\rho(\vec{r})\right] = T\left[\rho(\vec{r})\right] + V_{\mathrm{C}}\left[\rho(\vec{r})\right] + E_{\mathrm{XC}}\left[\rho(\vec{r})\right] . \tag{3.11}$$

Whereas the explicit form of the kinetic energy functional T and the classical Coulomb interaction V_{C} is known, no exact analytical form of the exchange-correlation functional $E_{\mathrm{XC}}\left[\rho(\vec{r})\right]$ is known. $E_{\mathrm{XC}}\left[\rho(\vec{r})\right]$ is approximately determined on different levels of complexity with various empirical models.

In practice, the kinetic energy functional and the classical Coulomb functional are often represented with orbitals, as in HF, which is named after its inventors Kohn-Sham (KS) DFT [367]. In practice, the only difference between HF and KS-DFT is the explicit form of $\boldsymbol{F}$, which in the framework of HF contains contributions originating from the non-local exchange operator $\hat{K}$, whereas in DFT the exact exchange energy is replaced by a usually local, often empirically determined exchange-correlation functional. Thus, KS-DFT allows an approximate calculation of electron correlation effects within the mean-field approach. Very common are also hybrid DFT approaches that combine DFT exchange-correlation functionals with some amount of HF exchange. Such functionals are termed *hybrid functionals*. For details on DFT see books [368–370].

3.2 Quasi-relativistic approximations

Most effort in relativistic mean field calculations that explicitly include all four components of the Dirac bi-spinor is required for the evaluation of two-electron integrals including the small component. This is the case, because for the description of the small component either a basis is needed that can span the space that is defined by $\frac{\vec{\sigma}\cdot\hat{\vec{p}}}{2m_{\mathrm{e}}c^2}\chi$ or the small component basis functions are directly calculated as $\frac{\vec{\sigma}\cdot\hat{\vec{p}}}{2m_{\mathrm{e}}c^2}\chi$.[2] Thus, for the description of the small component ~ 2.5 times as many basis functions as for the description of the large component would be needed [349]. Besides the computational costs, the explicit treatment of the small component can cause problems for variational approaches such as DHF, since the Dirac Hamiltonian is not bounded from below (see, e.g., Refs. [371, 372] for detailed discussions).

The above mentioned issues of the four-component methodology lead to an increasing interest in approximate quasi-relativistic approaches during the 1980s, treating only two components explicitly [373]. There are mainly two ways to avoid an explicit treatment of the small component (for an overview see Part IV of Ref. [349]). One is by unitary transformation, making the Dirac equation block diagonal, and the other is by description of the small component wave function via an approximate transformation of the large component wave function that allows to solve the equations for large component only. For the DHF equation of an electron moving in external fields described by a potential operator $\hat{\boldsymbol{V}}$ the exact relation between the large and small components of the four-component orbital i reads

$$\psi_i^{\mathrm{S}}(\vec{r}) = \underbrace{c\left(2m_{\mathrm{e}}c^2\mathbf{1}_{2\times2} - \hat{\boldsymbol{V}}^{\mathrm{SS}} + \epsilon\mathbf{1}_{2\times2}\right)^{-1}}_{=c\boldsymbol{\omega}} \underbrace{\left(\vec{\sigma}\cdot\hat{\vec{p}} + \hat{\boldsymbol{V}}^{\mathrm{SL}}\right)}_{\boldsymbol{\varpi}} \psi_i^{\mathrm{L}}(\vec{r}) . \tag{3.12}$$

Here ϵ_i is the energy of orbital i, $\hat{\vec{p}} = -\imath\hbar\vec{\nabla}$ is the one-electron linear momentum operator, $\hat{\boldsymbol{V}}^{\mathrm{SS}}$

[2] This is known under the acronym *kinetic balance*. Details can be read in Section 11.2 of Ref. [349].

is the small component-small component block of the effective one-electron potential operator appearing on the diagonal of the Hamiltonian, $\hat{\boldsymbol{V}}^{\mathrm{SL}}$ is the small component-large component block of a potential effective one-electron operator appearing on the off-diagonal of the Hamiltonian, as ,e.g., a vector potential or the effective one-electron Breit operator.

3.2.1 ZORA model potential approach

As $\hat{\boldsymbol{V}}^{\mathrm{SL}}$ is an effective one-electron operator, the modified momentum matrix $\boldsymbol{\varpi}$ can be decomposed into a linear combination of Pauli matrices (this notation is introduced in [K. Gaul and R. Berger, J. Chem. Phys. **152**, 044101 (2020)] as part of thesis):

$$\boldsymbol{\varpi} = \sum_{j=0}^{3} \sum_{k=0}^{1} \imath^k \boldsymbol{\sigma}^j \hat{\pi}^{j,k} \tag{3.13}$$

with the modified one-electron momentum operators $\hat{\vec{\pi}}^{j,k}$. Neglecting all off-diagonal potentials, $\boldsymbol{\varpi}$ simplifies in position space to

$$\boldsymbol{\varpi} \approx \vec{\boldsymbol{\sigma}} \cdot \hat{\vec{p}} = -\hbar\imath \vec{\boldsymbol{\sigma}} \cdot \vec{\nabla}, \tag{3.14}$$

so that $\hat{\vec{\pi}}^{(1,2,3),1} = -\hbar\vec{\nabla}$. For all $j = 0$ or $k = 0$ we have $\hat{\pi}_i^{j,k} = 0$. Most of the developments in this thesis were achieved within the Zeroth Order Regular Approximation (ZORA) [374, 375] in which $\boldsymbol{\omega}$ is approximated as

$$\omega^{\mathrm{ZORA}} = \left(2m_{\mathrm{e}}c^2 - \hat{V}^{\mathrm{SS}}\right)^{-1}, \tag{3.15}$$

where the SS potential is assumed to be determined by a scalar potential $\hat{\boldsymbol{V}}^{\mathrm{SS}} = \hat{V}^{\mathrm{SS}}\mathbf{1}_{2\times 2}$, and, thus, the ZORA-factor ω^{ZORA} is a scalar as well. A fundamental problem of the resulting ZORA Hamiltonian is that it is not gauge invariant, i.e., a shift in the potential energy V does not result in the same shift of the total energy:

$$V + \Delta E \nrightarrow E + \Delta E. \tag{3.16}$$

This problem obviously originates from the non-linear appearance of the potential in the ZORA factor. So far, there are two well-established ways to alleviate the problem: either by rescaling the ZORA energy, also known as electrostatic shift approximation [375], or by introducing a model potential $\tilde{V}(\vec{r})$ that does not depend on the SCF-orbitals but shows the correct behavior near the nucleus [376]. The latter method is employed in calculations of this thesis. The corresponding ZORA equations are

$$\left[\hat{V}(\vec{r}) + c^2 \vec{\boldsymbol{\sigma}} \cdot \hat{\vec{p}} \omega^{\mathrm{ZORA}} \vec{\boldsymbol{\sigma}} \cdot \hat{\vec{p}}\right] \psi_i^{\mathrm{ZORA}} = \epsilon_i \psi_i^{\mathrm{ZORA}}, \tag{3.17}$$

which are solved to receive the ZORA two-component spin-orbitals ψ_i^{ZORA} and the corresponding orbital energies ϵ_i.

Within the ZORA approach, approximate large and small component wave functions can be defined as

$$\psi_i^{\mathrm{L}}(\vec{r}) \approx \psi_i^{\mathrm{ZORA}}(\vec{r}) \tag{3.18}$$

$$\psi_i^{\mathrm{S}}(\vec{r}) \approx c\omega^{\mathrm{ZORA}}(\vec{r}) \vec{\boldsymbol{\sigma}} \cdot \hat{\vec{p}} \psi_i^{\mathrm{ZORA}}(\vec{r})\,. \tag{3.19}$$

In order to receive the full picture-change transformed ZORA wave function, the approximate

ψ_i^{L} and ψ_i^{S} above have to be renormalized by $\frac{1}{1+\sqrt{\int \mathrm{d}^3 r \left(\psi_i^{\mathrm{S}}(\vec{r})\right)^\dagger \psi_i^{\mathrm{S}}(\vec{r})}}$. The ZORA wave function is iteratively optimized within a GHF or Generalized KS (GKS) scheme. Relativistic properties can be calculated via the definitions given above. The development of a general approach to relativistic properties within this ZORA scheme is part of this thesis.

4 Cumulative Results

The aim of this thesis is to advance the field of low-energy precision tests of fundamental physics by contributing to the understanding of BSM effects in molecules and guiding future experiments. The search for BSM physics shall be brought forward in three major areas:

1. The first part is dedicated to the search for permanent EDMs and therewith molecular tests of $\mathcal{P},\mathcal{T}$-violation and BSM theories like SUSY. Here, focus is laid on the development of new theoretical methods that can be used to guide experiments that can give complementary information on the large $\mathcal{P},\mathcal{T}$-odd parameter space and to explore the advantages that polyatomic molecules may have.

2. In the second part new possibilities to widen our knowledge of the constituents of DM shall be explored by exploiting the advantages that chiral molecules have for the detection of $\mathcal{P}$-odd forces.

3. In the last part methods are developed to calculate effects of LLIV in molecular iodine. To know the size of these effects is indispensable for sensitivity estimates and interpretation of space based satellite experiments with a molecular iodine clock that aim to limit LLIV within the SME.

In this chapter the published and so far unpublished results of this thesis are presented. Each of the three following sections is dedicated to the developments in one of the above listed fields. For all project parts a short abstract and a paragraph in which I point out my personal contributions to the scientific outcome are provided. Reprints of published articles and those that are accepted for publication in a scientific journal can be found in Appendix F. So far unpublished content that is in preparation for publication in a scientific journal is presented in place in this chapter.

4.1 Systematic studies of sources of $\mathcal{P},\mathcal{T}$-violation in linear molecules

As pointed out in Sec. 2.1.2 there are many sources that can lead to permanent EDMs in molecules. Furthermore, beside relativistic enhancement and scaling with nuclear charge, little is known that allows to make qualitative predictions for $\mathcal{P},\mathcal{T}$-odd effects in molecular systems. With the theoretical demonstration of laser-coolability of polyatomic molecules [241] and its experimental realization [242] not only the number of molecular candidates for high-precision experiments grew but also the possibilities to tune effect-sizes of properties such as $\mathcal{P},\mathcal{T}$-violation by change of molecular structure. This thesis contributes to both: the first publication contributes to the understanding of effect-sizes by a systematic study of diatomic molecular candidates for $\mathcal{P},\mathcal{T}$-violation experiments and isoelectronic species across the periodic table of elements, and the second publication contributes to the new field of searches for $\mathcal{P},\mathcal{T}$-violation in polyatomic molecules.

In the third publication in this field, I expanded the possibilities to calculate relativistic one-electron properties within program packages for quasi-relativistic calculations that do not need to construct a four-component Hamiltonian. Whereas before for the study of any new effect a lot of tedious implementation work was needed, the developments of this thesis allow to compute user-defined operators within a single implementation. The newly developed method is applied to study various $\mathcal{P},\mathcal{T}$-odd effects in molecules that originate from different fundamental sources of $\mathcal{P},\mathcal{T}$-violation.

In the last part of this section results of a global analysis of the complete $\mathcal{P},\mathcal{T}$-odd parameter space of linear molecules and atoms within a simple atomic model are presented. With this I aim to

provide hints on how to design future experiments that search for permanent EDMs of molecules in order to maximally restrict all $\mathcal{P},\mathcal{T}$-odd parameters simultaneously.

4.1.1 Systematic study of relativistic and chemical enhancements of $\mathcal{P},\mathcal{T}$-odd effects in polar diatomic radicals

K. Gaul, S. Marquardt, T. Isaev, and R. Berger, Phys. Rev. A **99**, 032509 (2019).

Abstract.—*Polar diatomic molecules that have, or are expected to have a* $^2\Sigma_{1/2}$*-ground state are studied systematically with respect to simultaneous violation of parity* $\mathcal{P}$ *and time-reversal* $\mathcal{T}$ *with numerical methods and analytical models. Enhancements of* $\mathcal{P},\mathcal{T}$*-violating effects due to an electric dipole moment of the electron (eEDM) and* $\mathcal{P},\mathcal{T}$*-odd scalar-pseudoscalar nucleon-electron current interactions are analyzed by comparing trends within columns and rows of the periodic table of the elements. For this purpose electronic structure parameters are calculated numerically within a quasi-relativistic zeroth order regular approximation (ZORA) approach in the framework of complex generalized Hartree-Fock (cGHF) or Kohn-Sham (cGKS). Scaling relations known from analytic relativistic atomic structure theory are compared to these numerical results. Based on this analysis, problems of commonly used relativistic enhancement factors are discussed. Furthermore the ratio between both* $\mathcal{P},\mathcal{T}$*-odd electronic structure parameters mentioned above is analyzed for various groups of the periodic table. From this analysis an analytic measure for the disentanglement of the two* $\mathcal{P},\mathcal{T}$*-odd electronic structure parameters with multiple experiments in dependence of electronic structure enhancement factors is derived.*

Contributions.—This publication was inspired by a systematic study of nuclear spin-dependent parity violation effects in polar diatomic radicals [377]. As part of my master thesis [378] an implementation for the computation of eEDM enhancements was achieved [275, 378]. Therewith, preliminary results for eEDM enhancements and SPNEC interactions in all investigated molecules (Sec. IV A and parts of Sec. IV B of the article), except E120F and E121O, were obtained. SPNEC interactions were computed using an implementation by T. Isaev that was used also in Ref. [239]. Furthermore, a first non-conclusive analysis of the scaling of the studied $\mathcal{P},\mathcal{T}$-odd properties with nuclear charge (Sec. IV D of the article) was carried out.

As part of this doctoral thesis, I revised all results of my master thesis, added calculations of the compounds E120F and E121O, and, as suggested by R. Berger, computed the influence of the shape of the nucleus (Sec. IV A of the article). In addition, I studied various relativistic enhancement factors for the $\mathcal{P},\mathcal{T}$-odd properties (Sec. II B and IV B of the article), as suggested by S. Marquardt, who has analyzed relativistic enhancement of the hyperfine couplings. These are discussed in Sec. II B of the article. Furthermore, in collaboration with R. Berger I discussed the many-electron effects of $\mathcal{P},\mathcal{T}$-odd electronic structure enhancements (Sec. II C of the article) and I analyzed the ratio of the eEDM enhancement and SPNEC interactions (Sec. IV C of the article). Finally, with the analysis of this $\mathcal{P},\mathcal{T}$-odd ratio R. Berger and I developed a model for an optimal disentanglement of the two discussed $\mathcal{P},\mathcal{T}$-odd parameters (Sec. IV C of the article). The draft of the manuscript was written and all figures were produced by me and subsequently refined in collaboration with R. Berger. All coauthors discussed the results and contributed to the finalization of the manuscript.

4.1.2 *Ab initio* study of parity and time-reversal violation in laser-coolable triatomic molecules

K. Gaul and R. Berger, Phys. Rev. A **101**, 012508 (2020).

Abstract.—*Electronic structure enhancement factors of simultaneous parity and time-reversal violation ($\mathcal{P},\mathcal{T}$-violation) caused by an electric dipole moment of the electron (eEDM) and scalar-pseudoscalar nucleon-electron current (SPNEC) interactions are reported for various metal mono-hydroxides, several of which are considered laser–coolable and promising candidates for an eEDM measurement. Electronic structure enhancements are calculated ab initio within zeroth order regular approximation (ZORA) for CaOH, SrOH, BaOH, RaOH and YbOH. Scaling behavior with respect to nuclear charge numbers and the ratio of enhancement factors for both discussed sources of $\mathcal{P},\mathcal{T}$-violation are analyzed, which are crucial to obtain stringent bounds on parameters for new physics from experiments.*

Contributions.—I was inspired to study $\mathcal{P},\mathcal{T}$-violation in polyatomic molecules by our analysis of diatomic molecules and performed first calculations on my own initiative. The idea was revived by discussion with R. Berger and T. Isaev. R. Berger suggested a study of laser-coolable hydroxide molecules, including YbOH and RaOH which were proposed for a search of $\mathcal{P},\mathcal{T}$-violation in Refs. [277, 379].

I performed all calculations, produced all figures and analyzed the results. I wrote the draft of the manuscript and refined it subsequently in collaboration with R. Berger.

4.1.3 Toolbox approach for quasi-relativistic calculation of molecular properties for precision tests of fundamental physics

K. Gaul and R. Berger, J. Chem. Phys. **152**, 044101 (2020).

Abstract.—*A generally applicable approach for the calculation of relativistic properties described by one-electron operators within a two-component wave function approach is presented. The formalism is explicitly evaluated for the example of quasi-relativistic wave functions obtained within the zeroth order regular approximation (ZORA). The wide applicability of the scheme is demonstrated for the calculation of parity ($\mathcal{P}$) and time-reversal ($\mathcal{T}$) symmetry violating properties, which are important for searches of physics beyond the standard model of particle physics. The quality of the ZORA results is shown exemplarily for the molecules RaF and TlF by comparison to data from four-component calculations as far as available. Finally, the applicability of RaF in experiments that search for $\mathcal{P},\mathcal{T}$-violation not only in the electronic but also in quark sector is demonstrated.*

Contributions.—I had the idea for creating a program for arbitrary property calculation within ZORA that enables the calculation of arbitrary properties described by one-electron operators, including enhancement effects of all possible sources of $\mathcal{P},\mathcal{T}$-violation, within a single implementation within our ZORA program package. I derived all equations, implemented them and performed all calculations. I wrote the draft of the manuscript and refined it subsequently in collaboration with R. Berger.

4.1.4 Complementary molecules for an experimental disentanglement of sources of $\mathcal{CP}$-violation from simple models

K. Gaul and R. Berger, *manuscript in preparation*.

Abstract.—*Molecules are among the most promising candidates for a first detection of $\mathcal{P},\mathcal{T}$ violation beyond the Standard Model of particle physics. However, there are at least six fundamental sources of $\mathcal{P},\mathcal{T}$ violation that can contribute to a molecular EDM. In order to provide robust limits on this $\mathcal{P},\mathcal{T}$-odd parameter space, complementary molecules have to be found for future experiments. From perspective of electronic structure enhancement, a qualitative model is presented that can guide future experiments which aim to restrict the $\mathcal{P},\mathcal{T}$-odd parameter space with atoms or molecules. Simple qualitative atomic models are applied for the description of the electronic structure enhancement factors within a global model for $\mathcal{P},\mathcal{T}$-violation. Herein, we account for all possible sources of $\mathcal{P},\mathcal{T}$-violation at the same level, and no model-dependent approximations are assumed. Qualitative rules to identify well suited complementary molecular systems that can provide new information on the $\mathcal{P},\mathcal{T}$-odd parameter space are derived. And the special role that lighter molecules may have in future searches for $\mathcal{P},\mathcal{T}$-violation are highlighted.*

Contributions.—I was inspired to perform an optimization within the full $\mathcal{P},\mathcal{T}$-odd parameter space by our systematic study of the d_e-k_s parameter space in [K. Gaul et al., Phys. Rev. A **99**, 032509 (2019)]. I derived all equations, preformed all implementations and calculations and analyzed the results presented in the following.

Content

Measurement model.—The $\mathcal{P},\mathcal{T}$-odd spin-rotational Hamiltonian of a linear molecule is shown in eq. (2.12). Assuming nuclei to move non-relativistically k_p does not contribute and without further approximation at least six *different* experiments are required in order to set bounds on all parameters. This *minimal complete measurement model* can be described by a system of linear equations:

$$\hbar\vec{\omega} = \boldsymbol{W}\vec{x}_{\mathcal{P},\mathcal{T}}\,,$$

$$\boldsymbol{W} = \begin{pmatrix}
\Omega_1 W_{\mathrm{d},1}+\mathcal{I}_1 W^{\mathrm{m}}_{\mathrm{d},1} & \Omega_1 W_{\mathrm{s},1}+\mathcal{I}_1 W^{\mathrm{m}}_{\mathrm{s},1} & \mathcal{I}_1 W_{\mathrm{T},1} & \mathcal{I}_1 W_{\mathcal{S},1} & \Theta_1 W_{\mathcal{M},1} & \mathcal{I}_1(R_1 W_{\mathcal{S},1}+W_{\mathrm{m},1}) \\
\Omega_2 W_{\mathrm{d},2}+\mathcal{I}_2 W^{\mathrm{m}}_{\mathrm{d},2} & \Omega_2 W_{\mathrm{s},2}+\mathcal{I}_2 W^{\mathrm{m}}_{\mathrm{s},2} & \mathcal{I}_2 W_{\mathrm{T},2} & \mathcal{I}_2 W_{\mathcal{S},2} & \Theta_2 W_{\mathcal{M},2} & \mathcal{I}_2(R_2 W_{\mathcal{S},2}+W_{\mathrm{m},2}) \\
\Omega_3 W_{\mathrm{d},3}+\mathcal{I}_3 W^{\mathrm{m}}_{\mathrm{d},3} & \Omega_3 W_{\mathrm{s},3}+\mathcal{I}_3 W^{\mathrm{m}}_{\mathrm{s},3} & \mathcal{I}_3 W_{\mathrm{T},3} & \mathcal{I}_3 W_{\mathcal{S},3} & \Theta_3 W_{\mathcal{M},3} & \mathcal{I}_3(R_3 W_{\mathcal{S},3}+W_{\mathrm{m},3}) \\
\Omega_4 W_{\mathrm{d},4}+\mathcal{I}_4 W^{\mathrm{m}}_{\mathrm{d},4} & \Omega_4 W_{\mathrm{s},4}+\mathcal{I}_4 W^{\mathrm{m}}_{\mathrm{s},4} & \mathcal{I}_4 W_{\mathrm{T},4} & \mathcal{I}_4 W_{\mathcal{S},4} & \Theta_4 W_{\mathcal{M},4} & \mathcal{I}_4(R_4 W_{\mathcal{S},4}+W_{\mathrm{m},4}) \\
\Omega_5 W_{\mathrm{d},5}+\mathcal{I}_5 W^{\mathrm{m}}_{\mathrm{d},5} & \Omega_5 W_{\mathrm{s},5}+\mathcal{I}_5 W^{\mathrm{m}}_{\mathrm{s},5} & \mathcal{I}_5 W_{\mathrm{T},5} & \mathcal{I}_5 W_{\mathcal{S},5} & \Theta_5 W_{\mathcal{M},5} & \mathcal{I}_5(R_5 W_{\mathcal{S},5}+W_{\mathrm{m},5}) \\
\Omega_6 W_{\mathrm{d},6}+\mathcal{I}_6 W^{\mathrm{m}}_{\mathrm{d},6} & \Omega_6 W_{\mathrm{s},6}+\mathcal{I}_6 W^{\mathrm{m}}_{\mathrm{s},6} & \mathcal{I}_6 W_{\mathrm{T},6} & \mathcal{I}_6 W_{\mathcal{S},6} & \Theta_6 W_{\mathcal{M},6} & \mathcal{I}_6(R_6 W_{\mathcal{S},6}+W_{\mathrm{m},6})
\end{pmatrix}, \tag{4.1}$$

where $\vec{\omega} = (\Delta\Delta\omega_1, \ldots, \Delta\Delta\omega_6)$ is the vector of measured $\mathcal{P},\mathcal{T}$-odd frequency shifts for six different experiments, $\vec{x}_{\mathcal{P},\mathcal{T}} = (d_\mathrm{e}, k_\mathrm{s}, k_\mathrm{T}, \mathcal{S}, \tilde{\mathcal{M}}, d_\mathrm{p})$ is the vector of the six $\mathcal{P},\mathcal{T}$-odd parameters and $\boldsymbol{W}$ is the matrix of sensitivity coefficients determined by the electronic structure enhancement factors W_i and the spin quantum numbers Ω_i and $\mathcal{I}_i$ for each experiment i.

In the following, we are going to concentrate on electronic structure aspects and do not consider nuclear structure models for nuclear moments or volume effects, but treat nuclear structure constants as fundamental parameters. In order to construct a simple, easily applicable model we focus on only three important properties the molecule has: i) the electronic spin quantum number Ω, ii) the nuclear spin quantum number $\mathcal{I}$ of its heaviest nucleus and iii) the nuclear charge number Z of

its heaviest nucleus. In order to achieve this, we assume the finite nuclear size factor that enhances the pEDM

$$R_i = \left\langle \psi_\mathrm{p} \middle| r^2 \middle| \psi_\mathrm{p} \right\rangle \tag{4.2}$$

with the wave function of an unpaired proton in the nucleus ψ_p to be proportional to the mean squared nuclear radius $\left\langle r^2 \right\rangle$ which is approximately $(1.2\,\mathrm{fm}\,A^{1/3})^2$ with A being the mass number of the isotope.

Focusing on difference in the spin-rotational Hamiltonian we can discuss four classes of linear molecules with different sensitivity to the $\mathcal{P},\mathcal{T}$-odd parameter space:

I Open-shell molecules ($\Omega > 0$) with a closed-shell nucleus with $\mathcal{I} = 0$,

II Closed-shell molecules ($\Omega = 0$) with an open-shell nucleus with $\mathcal{I} = 1/2$,

III Open-shell molecules with an open-shell nucleus with $\mathcal{I} = 1/2$,

IV Open-shell molecules with an open-shell nucleus with $\mathcal{I} \geq 1$.

Class I molecules are sensitive to eEDM and SPNEC interactions only, class II and III molecules are sensitive to all parameters except the NMQM with different sensitivities to the eEDM and SPNEC interactions and class IV molecules are sensitive to the complete parameter space.

In total there are 46 possibilities to choose six molecules out of the four classes under consideration that at least one needs to be a class IV molecule and a maximum of two can be chosen from class I in order to prevent the system of equations to be undetermined.

Assuming Gaussian probability distributions for the measurements we receive ellipsoidal coverage regions of shape

$$\vec{x}_{\mathcal{P},\mathcal{T}}^{\,\mathsf{T}} \boldsymbol{U}_{\mathcal{P},\mathcal{T}}^{-1} \vec{x}_{\mathcal{P},\mathcal{T}} = P^N\,, \tag{4.3}$$

where $P = 2.45$ for an ellipsoidal region of 95 % probability. The covariance matrix $\boldsymbol{U}_{\mathcal{P},\mathcal{T}}$ can be obtained from the covariance matrix of the measured frequencies $\boldsymbol{U}_\omega$ via the matrix product $\boldsymbol{W}^{-1}\boldsymbol{U}_\omega \left(\boldsymbol{W}^{-1}\right)^\mathsf{T}$. When the measurements are assumed to be uncorrelated, $\boldsymbol{U}_\omega$ is a diagonal matrix containing the squared standard uncertainties of the experiments $u^2(\omega_i)$.

The quality of a set of N measurements for restriction of the total parameter space can be found by calculation of the volume of the ellipsoidal coverage region:[1]

$$V = P^{N/2} \frac{2\pi^{N/2}}{N\Gamma\left(N/2\right)} \det\left(\boldsymbol{U}_{\mathcal{P},\mathcal{T}}^{-1}\right)^{-1/2}\,, \tag{4.4}$$

where $\Gamma(x)$ is the gamma function. In case of $N = 6$ independent measurements the determinant of the inverse of the $\mathcal{P},\mathcal{T}$-odd covariance matrix is

$$\det\left(\boldsymbol{U}_{\mathcal{P},\mathcal{T}}^{-1}\right) = \det\left(\boldsymbol{W}^\mathsf{T}\boldsymbol{U}_\omega^{-1}\boldsymbol{W}\right) = \det\left(\boldsymbol{W}\right)^2 \prod_{i=1}^{6} \frac{1}{u(\omega_i)^2}\,, \tag{4.5}$$

and, thus, the volume is inversely proportional to the absolute value of the determinant of the sensitivity coefficient matrix:

$$V = P^6 \frac{\pi^3}{6} \frac{\prod_{i=1}^{6} \left|u(\omega_i)\right|}{\left|\det\left(\boldsymbol{W}\right)\right|}. \tag{4.6}$$

[1] For details on the volume of a N-dimensional ellipsoid see Appendix C.2.

For the case that there are more than six measurements, for equal standard uncertainties $u(\omega_i) = u_0$ the volume is proportional to $\frac{|u_0|^6}{\sqrt{\det(\boldsymbol{W}^\top \boldsymbol{W})}}$, and for unequal $u(\omega_i)$ we have to explicitly calculate $\frac{1}{\sqrt{\det(\boldsymbol{W}^\top \boldsymbol{U}_\omega^{-1} \boldsymbol{W})}}$.

Global minimization.—As we focus on the sensitivity of molecules to *new physics* in dependence on generic properties in the present approach, without defining specific molecules, it is reasonable to assume equal uncertainties for all experiments. By doing so the coverage volume is completely determined by $V \sim |\det(\boldsymbol{W})|^{-1}$. As outlined above, we assume that $\boldsymbol{W}$ is determined by Ω_i, $\mathcal{I}_i$ and the nuclear charge Z_i of each experiment i and not on any chemical or bonding parameter nor on any other nuclear structure parameter.

In order to find the optimal combination of molecules we need to minimize the volume with respect to these parameters:

$$\min_{\{\Omega_i, \mathcal{I}_i\} \in \left\{\frac{n}{2} | n \in \mathbb{N}_0\right\}, \{\{Z_i\} \in \mathbb{N}_0 : 20 \leq Z_i \leq 100\}} V\left(\left\{\Omega_i, \mathcal{I}_i, Z_i\right\}\right) . \tag{4.7}$$

For the global minimization we represent each class of molecules with minimal spin, i.e., we set $\Omega = 1/2$ for class I and $\mathcal{I} = 0$, $\Omega = 0$ and $\mathcal{I} = 1/2$ for class II, $\Omega = 1/2$ and $\mathcal{I} = 1/2$ for class III, $\Omega = 1/2$ and $\mathcal{I} = 1$ for class IV. At this point it has to be noted that different choices of nuclear or electronic spin may have an influence on the results of the optimization. Test calculations in which all nonzero spins were set to one deviated quantitatively from the results presented in the following. However, qualitatively they were in agreement with the present results.

We approximate all electronic structure enhancement factors W with analytic hydrogen-like atomic model calculations in dependence of Z_i. We always assume only one nucleus (the heavier one) of a molecule to be of interest for an experiment. The explicit expressions for W_d, W_d^m, W_s, W_s^m, W_S, $W_\mathcal{M}$ and W_T in dependence of Z, derived in Refs. [250, 254–256, 380, 381] (collected in Ref. [208]) are provided in Appendix B. Furthermore, an analytic Z-dependent expression for W_m is derived in Appendix B. The nuclear magnetic moment μ, that appears in W_d^m, W_s^m and W_m, was set in all calculations to $\mu = 1$. It shall be noted that μ can have different signs for diffrent atoms, which is not considered in the present study. This nuclear structure effect could have an important influence on the total coverage volume.

A minimization of V with respect to Z_i was performed for all 46 combinations of Ω_i and $\mathcal{I}_i$ described above (four different classes). Here, first, we used the restriction $20 \leq Z \leq 100$, as the employed atomic models give reasonable estimates for this region only (see [K. Gaul et al., Phys. Rev. A **99**, 032509 (2019)]), and, second, we used the restriction $20 \leq Z \leq 90$ as so far accessible linear molecules are limited to $Z \leq 90$ (Th as heaviest element).

The global minimization was performed with Mathematica 11 [382], employing different build-in optimization algorithms which are shown in Table C.1 in the appendix. The minimizations were performed within the domain of natural numbers and within the domain of real numbers. In the latter case real Z_i values obtained were rounded to the nearest integer for the calculation of the volume and its derivatives. In cases where different algorithms arrived at different results, the result with the smallest volume was employed.

The results were checked by calculation of the gradient and the Hessian in the domain of natural numbers and the result was accepted as minimum for $\left|\vec{\nabla}_Z V\right| / V(\vec{Z}_\mathrm{min}) < 0.5$ and if the smallest eigenvalue of the Hessian h_min satisfies $h_\mathrm{min}/V(\vec{Z}_\mathrm{min}) > -10^{-2}$ and $h_\mathrm{min}/h_\mathrm{max} > -10^{-1}$ and at least one other eigenvalue of the Hessian has $h_i/h_\mathrm{max} > 10^{-1}$. As a completely vanishing gradient could not be achieved, small negative eigenvalues of the Hessian were accepted. This limits the accuracy of the resulting volume to one significant figure.

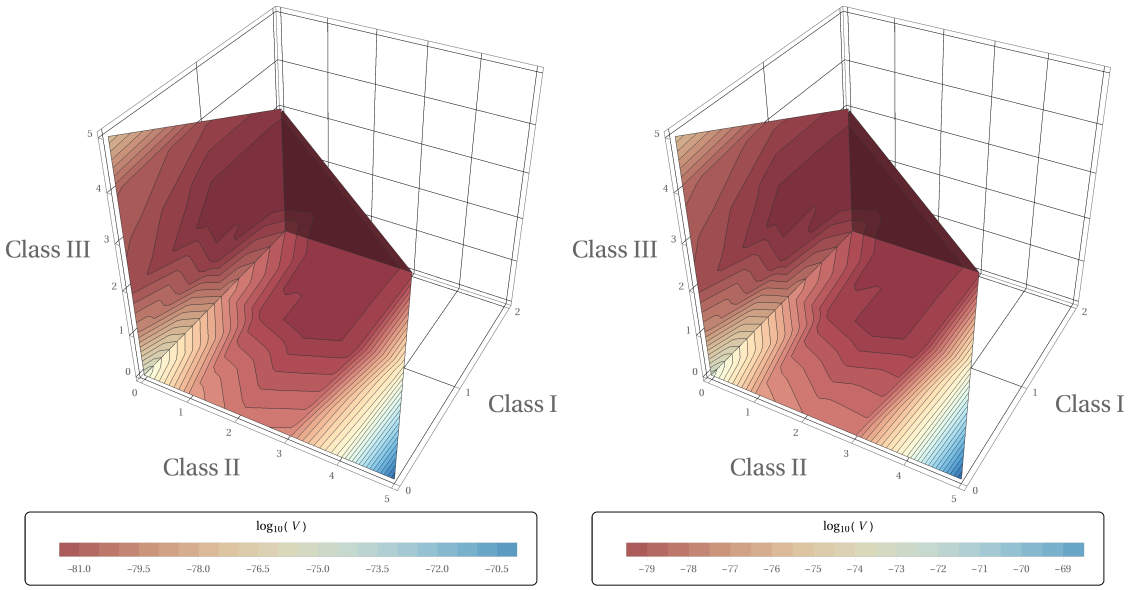

Figure 4.1: Results for a global minimization of the coverage volume in $\mathcal{P},\mathcal{T}$-odd parameter space with respect to nuclear charges of the heavy atoms in the molecules. The results are presented as a three-dimensional projection on the planes for different numbers of molecules from classes I to III defined above. The number of molecules of class IV is determined by the difference between the number of molecules from other classes and the number of total experiments (6). Results shown on the left were received for a minimization with restriction $20 \leq Z \leq 100$ and those on the right were received with restriction $20 \leq Z \leq 90$.

The detailed results of the minimization are shown in Appendix C.1 in Table C.2 and Table C.3. A visualization of the results is provided in Figure 4.1 in arbitrary units. Therein the size of the volume in $\mathcal{P},\mathcal{T}$-odd parameter space in dependence on the number of molecules from classes I to IV is shown.

We find the two minima of the optimizations for a setup of two class I, three class IV molecules and one class II ($20 \leq Z \leq 90$) or one class III ($20 \leq Z \leq 100$) molecule. Furthermore, both optimizations show no considerable difference in the size of the coverage volume for the best results (see Table C.2 and Table C.3). We ranked the results to the size of the coverage volume. In both optimizations, the places 30 to 46 yielded coverage volumes that are at least one order of magnitude worse than the best choices of molecules. However, the results show that the exact number of how many molecules are chosen from which class is not important, but from the best choices of molecules we may deduce following rules for a good choice of the number of molecules from each of the four classes:

1. The trivial requirements are: $N_{\mathrm{IV}} \geq 1$, $N_{\mathrm{I}} \leq 2$, $N_{\mathrm{I}} + N_{\mathrm{II}} + N_{\mathrm{III}} + N_{\mathrm{IV}} = 6$

2. At least three different classes (valid for places one to 29 for both optimizations)

3. $N_{\mathrm{IV}} \leq 3$ and $N_{\mathrm{II,III}} \leq 2$ (at least fulfilled for places one to 13 for both optimizations)

From these rules the most important is the second. From this restriction we can conclude that we need, as naively expected, molecular systems that have fundamentally different sensitivities to the different sources of $\mathcal{P},\mathcal{T}$-violation. This can best be achieved, when choosing molecules with fundamentally different spin-rotational Hamiltonians. Nonetheless, we see that it is less important how many molecules of each class are exactly used. However, the coverage volume can best be minimized if at least three molecules with fundamentally different spin-rotational Hamiltonians are chosen.

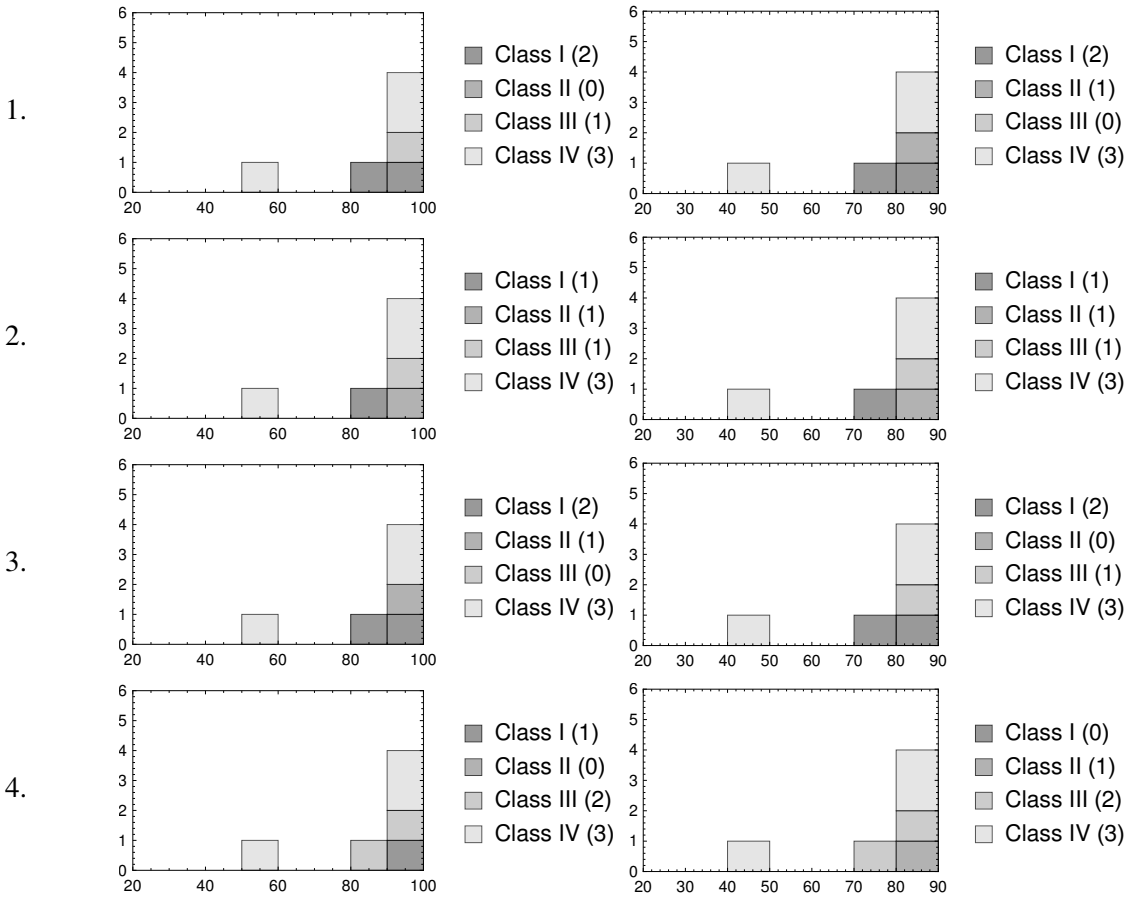

Figure 4.2: Optimum nuclear charge distributions for the global minimum for the four best different choices of molecules from the different classes for optimization in the regions of $20 \leq Z \leq 100$ (left) and $20 \leq Z \leq 90$ (right). The binning is chosen such that bins include all $x < Z \leq x + 10$ for $x = 30, 40, 50, \ldots, 100$. An exception is the first bin, which is chosen to include all $20 \leq Z \leq 30$.

Beside the classes of needed molecules we can also deduce the optimal distribution of nuclear charges. Exemplary, the distribution of nuclear charges separated for the different classes of the molecules is shown for the four best choices of molecules from the four classes in Figure 4.2 for both studied regions of Z. The distributions for all other cases can be found in Figure C.1 in Appendix C.1. Note that for the best 29 choices all distributions are qualitatively equivalent but show only slight deviations in absolute numbers of molecules corresponding to given bin of Z.

From all nuclear charge distributions of the optimization in the region $20 \leq Z \leq 90$ we can see that four out of six molecules have always $80 \leq Z \leq 90$ but that there is *always* at least one lighter molecule $Z \leq 50$ of class II, III or IV, which motivates the use of light molecules with $Z \leq 50$, of which isotopologues with $I \geq 1/2$ exist, such as CdF, for future searches of new physics. If the region of possible Z is extended to 100, there is still a distribution over different charge numbers, however, the nuclear charge number of the lightest molecule is then higher, lying in the region $Z \leq 60$. Furthermore, we see that if the number of molecules with a similar spin-rotation Hamiltonian increases, the Z of the molecules of same class are more and more equally distributed over the full range of Z and the number of lighter molecules increases. Our qualitative model shows that precision experiment on a lighter molecule can be of great value in future experiments that aim to restrict the $\mathcal{P}, \mathcal{T}$-odd parameter space.

In the present simple model we completely neglected the chemical influence on the electronic structure enhancement factor which can be pronounced, as we have shown in our previous work

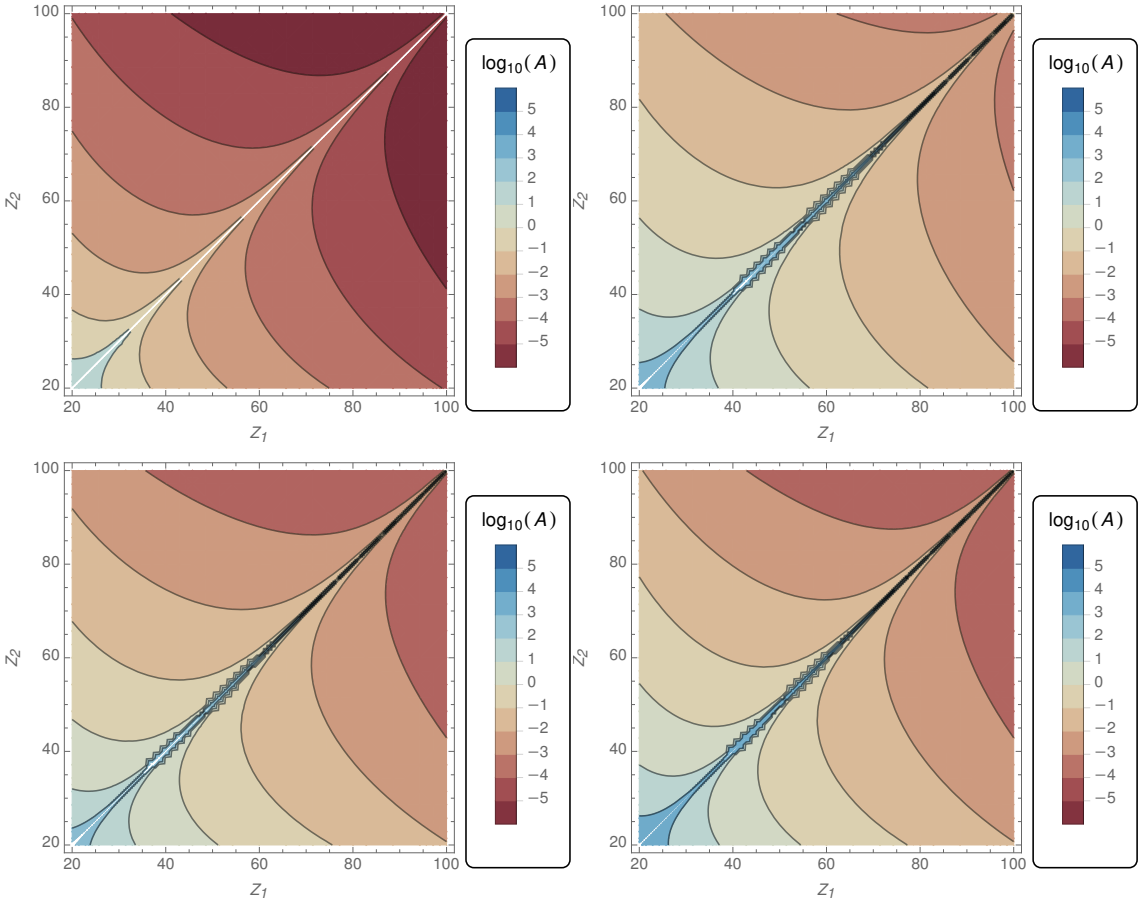

Figure 4.3: Influence of chemical enhancements on the size of an elliptical coverage region with area A in the parameter space of d_e and k_s. Comparison of the simple atomic model of the present paper (top left) with a model from ab initio calculations: $A \sim \frac{|u(\omega_1)u(\omega_2)|}{10^{b_{d,1}+b_{d,2}} \frac{Z_1^{a_{d,1}} Z_2^{a_{d,2}}}{\gamma_{1/2,1}^4 \gamma_{1/2,2}^4} \, 0.89 \cdot |1.0210^{Z_1} - 1.0210^{Z_2}| \times 10^{27} \, \frac{\mathrm{Hz}^2}{e\cdot\mathrm{cm}}}$ derived in [K. Gaul et al., Phys. Rev. A **99**, 032509 (2019)]. Different plots represent different choices of parameter sets a_d, b_d as derived in [K. Gaul et al., Phys. Rev. A **99**, 032509 (2019)] for different groups of molecules (both molecules containing a heavy element from group 2 of the periodic table (top right), one molecule containing a heavy element from group 2 and one from group 12 (bottom left), and both molecules containing a heavy element from group 12 (bottom right)). Experimental uncertainties were set to $u(\omega_1) = u(\omega_2) = 1\,\mathrm{Hz}$. All results are normalized by multiplication with $\sqrt{W_{d,1}(Z=100)W_{d,2}(Z=100)}\,\mathrm{Hz}^{-1}$, such that $[A] = 1$.

(see [K. Gaul et al., Phys. Rev. A **99**, 032509 (2019)]). Therein we studied the two dimensional parameter space of class I molecules extensively with accurate numerical methods.

In a comparison of the size of the coverage region in dependence of nuclear charges of two molecules in the d_e-k_s-parameter space (see Figure 4.3) the simple atomic model applied in this work is in qualitative agreement with our numerical study. However, absolute values deviate considerably, which highlights the importance of chemical enhancement. Nonetheless, it may not be too important for the present comparative study, as we are interested in guiding the development of future experiments in a qualitative manner and we have shown in [K. Gaul et al., Phys. Rev. A **99**, 032509 (2019)] that at least for the d_e-k_s parameter space no qualitative influence on the ratio of $\mathcal{P},\mathcal{T}$-odd properties which determines $\det(\boldsymbol{W})$ can be expected. However, this needs to be proven by numerical studies for the space of the other $\mathcal{P},\mathcal{T}$-odd parameters.

The neglect of the chemical environment as well as the neglect of nuclear sturcture can both have an important influence on the absolute value of the coverage volume in the $\mathcal{P},\mathcal{T}$-odd parameter space and could also influence the qualitative results. E.g., if two class II molecules would have

heavy nuclei of comparable nuclear charge $Z_1 \approx Z_2$ but nuclear magnetic moments of opposite charge $\mu_1 \sim -\mu_2$, in the present model they would result in a rather larger volume. But considering μ explicitly could make these two molecules complementary in the space of the parameters d_e, k_s and d_p as the enhancement factors W_d^m, W_s^m and W_m would have a different sign for the two molcules.

Conclusion.—Simple atomic model calculations were applied to determine the optimal choice of complementary molecules for a global minimization of the $\mathcal{P},\mathcal{T}$-odd parameter space from an electronic structure perspective. Our analysis is model-independent, however, $\mathcal{P},\mathcal{T}$-odd moments higher than NMQMs were neglected and nuclei were assumed to move non-relativistically. The choice of molecules in dependence of their spin properties and the nuclear charge of its heaviest atom was discussed. Our results show that it is most important to have experiments with complementary molecules, i.e., with fundamentally different sensitivity. Whereas heavy molecules are favorable for observing $\mathcal{P},\mathcal{T}$-odd effects, we found, most interestingly, that in all cases of chosen spin properties one molecule with nonzero nuclear spin has at best $Z \leq 50$ if the experiment with the heaviest molecule has $Z = 90$, although individual electronic structure enhancement factors for such light candidates are small. This motivates experiments with lighter molecules in which the heavier atom has a nonzero nuclear spin for detecting $\mathcal{P},\mathcal{T}$-odd fundamental parameters. With these findings we hope to help guiding direction of future experiments that search for fundamental $\mathcal{P},\mathcal{T}$-violation in molecules, and that our contribution can provide a new view on the topic, particularly on the role of light molecules.

4.2 Towards dark matter detection with chiral molecules

In Sec. 2.1.1 the special properties of chiral molecules and the advantages they can give in the search for $\mathcal{P}$-odd forces were discussed. In Secs. 2.2 and 2.3 it was highlighted that some proposed CDM particles like axions or dark photons can in principle induce $\mathcal{P}$-odd forces on electrons. In this section I summarize our collaboration with T. A. Isaev and M. G. Kozlov on possibilities to exploit the special qualities of chiral molecules for the detection of CDM and LLIV interactions in the electronic sector. The results are presented in a letter in which the principal idea and main results are discussed and full paper in which the details and derivations are given and methodological problems are discussed. Some further unpublished results that go beyond the two articles discussed in the following and strengthening their line of argument are provided in Appendix D.

4.2.1 Chiral molecules as sensitive probes for direct detection of $\mathcal{P}$-odd cosmic fields

K. Gaul, M. G. Kozlov, T. A. Isaev, and R. Berger, Phys. Rev. Lett. **accepted for publication** (2020).

Abstract.—*Potential advantages of chiral molecules for a sensitive search for parity violating cosmic fields are highlighted. Such fields are invoked in different models for cold dark matter or in the Lorentz-invariance violating standard model extensions and thus are signatures of physics beyond the standard model. The sensitivity of a twenty year old experiment with the molecule CHBrClF to pseudovector cosmic fields as characterized by the parameter* $\left|b_0^\mathrm{e}\right|$ *is estimated to be* $\mathcal{O}(10^{-12}\,\mathrm{GeV})$ *employing ab initio calculations. This allows to project the sensitivity of future experiments with favorable choices of chiral heavy-elemental molecular probes to be* $\mathcal{O}(10^{-17}\,\mathrm{GeV})$*, which will be an improvement of the present best limits by at least two orders of magnitude.*

Contributions.—The idea to study the expectation value of γ^5 in chiral molecules was initiated by M. G. Kozlov based on his analysis on the analytical scaling and a first numerical study by T. A. Isaev. This gave a first, but not fully conclusive analysis on how $\langle \gamma^5 \rangle$ may scale with nuclear charge in chiral molecules. From discussions with T. A. Isaev and M. G. Kozlov during a workshop at the Mainz Institute of Theoretical Physics (MITP), R. Berger and I developed the idea to study the influences of $\mathcal{P}$-odd cosmic fields in CHBrClF. I did all calculations and initial interpretations and derived initial limits on DM and LLIV parameters. I produced all figures and wrote the draft of the manuscript. The manuscript and interpretations therein were refined in collaboration with R. Berger, M. G. Kozlov and T. A. Isaev.

4.2.2 Parity nonconserving interactions of electrons in chiral molecules with cosmic fields

K. Gaul, M. G. Kozlov, T. A. Isaev, and R. Berger, Phys. Rev. A **accepted for publication** (2020).

Abstract.—*Parity ($\mathcal{P}$) violating pseudoscalar or pseudovector cosmic fields are invoked in different models for cold dark matter or in the standard model extension that allows for Lorentz invariance violation. A direct detection of the timelike-component of such fields requires a direct measurement of $\mathcal{P}$-odd potentials or their evolution over time. Herein, advantageous properties of chiral molecules, in which $\mathcal{P}$-odd potentials lead to resonance frequency differences between enantiomers, for direct detection of such $\mathcal{P}$-odd cosmic fields are demonstrated. Scaling behavior of electronic structure enhancements of such interactions with respect to nuclear charge number and the fine-structure constant is derived analytically. This allows a simple estimate of the effect sizes for arbitrary molecules. The analytical derivation is supported by quasi-relativistic numerical calculations in the molecules H_2X_2 and H_2XO with X = O, S, Se, Te, Po. Parity violating effects due to cosmic fields on the C–F stretching mode in CHBrClF are compared to electroweak parity violation and influences of non-separable anharmonic vibrational corrections are discussed. On this basis it was estimated in [K. Gaul et al., Phys. Rev. Lett.* ***accepted for publication*** *(2020)] from a twenty year old experiment with CHBrClF that bounds on Lorentz invariance violation as characterized by the parameter $\left|b_0^{\mathrm{e}}\right|$ can be pushed down to the order of 10^{-17} GeV in modern experiments with suitably selected molecular system, which will be an improvement of the current best limits by at least two orders of magnitude. This serves to highlight the particular opportunities that precision spectroscopy of chiral molecules provides in the search for new physics beyond the standard model.*

Contributions.—This work provides an analytical derivation and numerical proofs for scaling with nuclear charge of $\langle \gamma^5 \rangle$ in chiral molecules presented in [K. Gaul et al., Phys. Rev. Lett. **accepted for publication** (2020)] and a detailed discussion of the methodological challenges. This study was initiated by M. G. Kozlov who made all analytic derivations and by T. A. Isaev who did preliminary numerical calculations of scaling of $\langle \gamma^5 \rangle$ with nuclear charge. I did all numerical calculations presented in the paper, the analysis of the methodology, derived initial limits on dark matter and in collaboration with R. Berger interpreted the results. I produced all figures and wrote the most part of the manuscript draft. The manuscript and interpretations therein were subsequently refined in an iterative manner in collaboration with R. Berger, M. G. Kozlov and T. A. Isaev.

4.3 Local Lorentz invariance violation tests with molecular clocks

In the section before possibilities to limit LLIV with chiral molecules were presented. As explained in Sec. 2.3, atomic and molecular clock transitions can be sensitive to odd vector interactions of the SME (see eq. (2.19)). In this section I present our results from a collaboration with Norman Gürlebeck at the center of applied space technology and microgravity [*Zentrum für angewandte Raumfahrttechnologie und Mikrogravitation* (ZARM)] and the BOOST collaboration on the development of a new satellite based experiment with an iodine molecular clock.

4.3.1 BOOST: A satellite mission to test Lorentz invariance using high-performance optical frequency references

N. Gürlebeck, L. Wörner, T. Schuldt, K. Döringshoff, K. Gaul, D. Gerardi, A. Grenzebach, N. Jha, E. Kovalchuk, A. Resch, T. Wendrich, R. Berger, S. Herrmann, U. Johann, M. Krutzik, A. Peters, E. M. Rasel, and C. Braxmaier, Phys. Rev. D **97**, 124051 (2018).

Abstract.— *BOOST (BOOst Symmetry Test) is a proposed satellite mission to search for violations of Lorentz invariance by comparing two optical frequency references. One is based on a long-term stable optical resonator, and the other is based on a hyperfine transition in molecular iodine. This mission will allow us to determine several parameters of the standard model extension in the electron sector up to 2 orders of magnitude better than with the current best experiments. Here, we will give an overview of the mission, the science case, and the payload.*

Contributions.—The project was initiated by the BOOST collaboration under the lead of N. Gürlebeck, who also wrote the draft of the manuscript. I did calculations of enhancement factors of LLIV in clock transitions in iodine molecules (described in APPENDIX: SCIENCE SIGNAL in the article) and made all necessary implementations that were needed to enable calculations of such properties within a Complete Open-shell Configuration Interaction (COSCI) approach. These calculations were essential to arrive at the order of magnitude estimates of proposed sensitivity of the mission to specific LLIV parameters of the SME (Sec. B and Table II in the article). All authors discussed the results and contributed to the finalization of the manuscript.

4.3.2 Enhancement of Lorentz invariance violation in iodine molecular clock transitions

K. Gaul, N. Gürlebeck and R. Berger, *manuscript in preparation*.

Abstract.— *Within the BOOST (BOOst Symmetry Test) satellite mission a search for violations of Lorentz invariance by comparison of two optical frequency references is planned. One of the frequency references is based on a hyperfine transition in molecular iodine. In order to predict the sensitivity of this transition to Lorentz invariance violating parameters of the Standard Model Extension (SME), the electronic structure enhancement of these parameters has to be calculated. In this paper the electronic interaction Hamiltonian for Lorentz invariance violation in the proposed molecular clock transition of iodine is derived. With configuration interaction methods and empirical corrections the potential energy surfaces and properties corresponding to Lorentz invariance violation are studied. Vibrational corrections are calculated and results for vibronic Lorentz invariance violation effects on the iodine molecular clock transitions are compared to the H_2-maser.*

Contributions.—The idea for this project came up within the BOOST project under the lead of N. Gürlebeck (see above). N. Gürlebeck, R. Berger and I derived a molecular Hamiltonian

for LLIV in clock transitions in the iodine molecule. Subsequently, I implemented tools for calculating vibrational corrections of such properties and slightly modified the COSCI module of the program package DIRAC15. I performed all presented calculations. The results are presented below.

Content

Theory.—In the SME dropping Lorentz invariant terms the full relativistic electronic Hamiltonian corresponding to the Lagrangian (2.19) can be derived as shown in Ref. [328]. The Hamiltonian can be written in terms of LLIV operators that are of even or odd order in the four derivative:

$$\hat{H}_{\mathrm{LLIV,SME}} = \hat{\mathcal{O}} + \hat{\mathcal{E}}. \tag{4.8}$$

The full Hamiltonian with explicit expression for $\hat{\mathcal{O}}$ and $\hat{\mathcal{E}}$ can be found in Ref. [328]. When taking expectation values in the rest frame of a closed-shell molecule with an inversion center such as I_2, all $\mathcal{T}$-odd and $\mathcal{P}$-odd terms vanish and the Hamiltonian reads

$$\hat{H}_{\mathrm{LLIV,SME}} = \left(\tilde{c}_{ij} - \tilde{c}_{00}\eta_{ij}\right) c\boldsymbol{\alpha}^i \hat{p}^j \,. \tag{4.9}$$

The full Hamiltonian can be found in Ref. [328].

Kostelecký and Lane used a Foldy-Wouthuysen transformation to arrive at the Hamiltonian in the non-relativistic limit. Starting from the reduced form of the relativistic Hamiltonian (eq. (4.9)) and leaving out constant terms, which vanish when considering expectation values in a diatomic molecule, this non-relativistic Hamiltonian reads

$$\hat{H}_{\mathrm{LLIV,SME,nr}} = \left(\tilde{c}_{ij} + \frac{1}{2}\tilde{c}_{00}\delta_{ij}\right)\frac{\hat{p}^i\hat{p}^j}{m_\mathrm{e}} \tag{4.10}$$

with δ_{ij} being the Kronecker delta.

The Iodine Molecular Clock (IMC) transition takes place between the electronic states $X^1\Sigma_g^+(0_g^+)$ and $B^3\Pi_u(0_u^+)$. The molecular Hamiltonian in its non-relativistic and relativistic forms reads

$$\hat{H}^{\mathrm{nr}}_{\mathrm{LLIV,I_2}} = -\frac{1}{m_\mathrm{e}}\sum_{i=1}^{N_\mathrm{elec}} \hat{\vec{p}}_i \cdot \tilde{\boldsymbol{c}} \cdot \hat{\vec{p}}_i, \tag{4.11}$$

$$\hat{H}_{\mathrm{LLIV,I_2}} = -c\sum_{i=1}^{N_\mathrm{elec}} \vec{\boldsymbol{\alpha}}_i \cdot \tilde{\boldsymbol{c}} \cdot \hat{\vec{p}}_i. \tag{4.12}$$

Here, the sum runs over all N_elec electrons i, and $\tilde{\boldsymbol{c}}$ is a coefficient tensor of rank 2 consisting of the nine parameters $\tilde{c}_{ij} - \tilde{c}_{00}\eta_{ij} = \tilde{c}_{ij} + \frac{1}{2}\tilde{c}_{00}\delta_{ij}$.

We now use the analogy $i, j, k = 1, 2, 3 = x, y, z$. The iodine molecule has $D_{\infty h}$ symmetry. In a $D_{\infty h}$ symmetric molecule only the diagonal elements of $\tilde{\boldsymbol{c}}$ survive, i.e., those proportional to coefficients $\tilde{c}_{xx}$, $\tilde{c}_{yy}$ and $\tilde{c}_{zz}$. When the molecular axis is assumed to be along z, elements with indices xx and yy are equal in molecular iodine due to its axial symmetry.

The expectation value of the non-relativistic limit was evaluated only approximately using the full relativistic Dirac wave function in order to describe the excited state correctly. Thus the results of the non-relativistic operator contain an error stemming from an additional non-physical term $\left\langle \Psi_\mathrm{S} \middle| \hat{H}^{\mathrm{nr}}_{\mathrm{LLIV,I_2}} \middle| \Psi_\mathrm{S} \right\rangle \sim \mathcal{O}(\alpha^2)$, where Ψ_S is the lower or small component of the Dirac bi-spinor and α is the fine structure constant. The error for the correction of the transition is expected to be

small, since it is determined by the valence electrons which move much more slowly than c.

The LLIV energy shifts between the two electronic states are

$$\Delta_{kk}^{\mathrm{LLIV}} = -\tilde{c}_{kk}\left(\left\langle B0_u^+ \middle| c\sum_i \boldsymbol{\alpha}_i^k \hat{p}_i^k \middle| B0_u^+ \right\rangle - \left\langle X0_g^+ \middle| c\sum_i \boldsymbol{\alpha}_i^k \hat{p}_i^k \middle| X0_g^+ \right\rangle\right) \tag{4.13}$$

or when vibrational corrections are considered

$$\Delta_{kk}^{\mathrm{LLIV}} = -c_{kk}\left(\left\langle B0_u^+, v' \middle| c\sum_i \boldsymbol{\alpha}_i^k \hat{p}_i^k \middle| B0_u^+, v' \right\rangle - \left\langle X0_g^+, v \middle| c\sum_i \boldsymbol{\alpha}_i^k \hat{p}_i^k \middle| X0_g^+, v \right\rangle\right) \tag{4.14}$$

and similar equations hold in the corresponding non-relativistic limit ($\Delta_{kk}^{\mathrm{LLIV,nr}}$).

Methodology.—The iodine atom has a nuclear charge of $Z = 53$ and thus its electrons are expected to display pronounced relativistic effects and considerable spin-orbit coupling that leads to splitting of states. Therefore, the calculation of electronic wave functions in ground and excited states should be carried on a two- or four-component level including spin-orbit coupling. For calculations of four-component electronic wave functions we employed the program package DIRAC 15 [383] in this work. The four-component molecular orbitals were expanded in an atom-centered Gaussian basis set of triple-ζ quality optimized for relativistic calculations by Dyall [384, 385]. The ground state wave function was calculated in the Dirac-Hartree-Fock-Coulomb-Gaunt approximation and the two-electron integrals involving the small component only were estimated classically [386].

The electronically excited states of the iodine molecule were calculated within the COSCI approach [387] starting from an DHF average of configuration ground state. Here, we followed the work by de Jong *et al.* [388] who reported reasonable agreement with experimental data. The active space was chosen as ten electrons in twelve spinors. Thus, only the 5p-shell was considered in the electron-correlation calculations.

The excited state wave function was constructed by projecting the active part onto the inactive core wave function getting a density matrix $\tilde{\boldsymbol{D}}_{ij}$ for matrix elements between states i and j. In order to generate Born–Oppenheimer (BO) potential energy curves for the various electronic states, COSCI single point calculations were performed for a total of 52 interatomic distances in an interval between 2.45 Å and 5.00 Å.

The $\tilde{\boldsymbol{D}}_{ii}$ densities were used to calculate properties for an excited state i. The expectation value within a state i of a property, which is described by an operator $\hat{O}$, was computed from corresponding integrals of the atomic basis set, which are contained in a matrix $\boldsymbol{O}$, via $\left\langle i \middle| \hat{O} \middle| i \right\rangle = \mathrm{Tr}\left(\tilde{\boldsymbol{D}}_{ii}\boldsymbol{O}\right)$.

The COSCI approach accounts neither for core-valance electron-correlation effects nor for dynamic correlation. As a consequence, the resulting BO potential energy curves are much too shallow and the positions of the energy minima are not very accurate. This would hamper a detailed vibrational analysis in particular of the electronically excited states. As done in Ref. [388] for the iodine molecule, one can attempt to compute correction terms to the BO potentials by comparing to experimental data. For this purpose the method by Rydberg–Klein–Rees (RKR) [389–391] was implemented as proposed by Senn [392] and employed to calculate an experimental ground state potential $E_{\mathrm{gs,RKR}}(r)$. Details on RKR calculations are explained in appendix E.1.

The RKR-improved BO potentials were used to numerically solve the vibrational Schrödinger equation on an equidistant grid via the method of Discrete Variable Representation (DVR) [393] (see appendix E.2 for details).

The performance of the present approach in calculation of diatomic constants of I_2 can be found in appendix E.3.

Results.—Whereas in experiment the relevant vibrational states are the vibrational ground state ($v = 0$) of the electronic ground state and the 32nd vibrationally excited state ($v' = 32$) of the electronic excited state, in the present approximation the experimental wavenumber of this transition would correspond to a transition into the vibrational energy levels around $v' = 25$ and $v' = 26$ of the electronically excited state (for details see Appendix E.4). Thus, in the following results for both transitions, those into state $v' = 32$ and into state $v' = 25$, are presented. All results are summarized in Table 4.1.

Relativistic effects are relatively small, being on the order of $10\,\mathrm{m}E_\mathrm{h}$. However, the vibrational corrections have a remarkable influence on the result. This can be understood when we have a closer look at the potentials, vibrational wave functions and the property as functions of the bond length. This is shown for both properties in Figure 4.4.

Table 4.1: Differences between expectation values of relativistic LLIV properties $\Delta_{kk}^{\mathrm{LLIV}}$ and their approximated non-relativistic limits $\Delta_{kk}^{\mathrm{LLIV,nr}}$ in the electronic states $X0_g^+$ and $B0_u^+$ of iodine from a DHF–COSCI calculation. Values for a vertical approximation at the experimental ground state equilibrium bond distance 2.666 Å and with explicit consideration of the vibrational wave function for a transition from the $\left|X0_g^+, v=0\right\rangle$-state to the $\left|B0_u^+ v=0,25/32\right\rangle$-states.

$v_\mathrm{ex} \leftarrow v_\mathrm{gs}$	$\frac{\Delta_{xx}^{\mathrm{LLIV,nr}}}{\tilde{c}_{xx}E_\mathrm{h}}$	$\frac{\Delta_{xx}^{\mathrm{LLIV}}}{\tilde{c}_{xx}E_\mathrm{h}}$	$\frac{\Delta_{zz}^{\mathrm{LLIV,nr}}}{\tilde{c}_{zz}E_\mathrm{h}}$	$\frac{\Delta_{zz}^{\mathrm{LLIV}}}{\tilde{c}_{zz}E_\mathrm{h}}$
vertical	0.9079	0.8780	−2.5082	−2.4392
$0 \leftarrow 0$	1.0866	1.0481	−2.1518	−2.0969
$25 \leftarrow 0$	1.0542	1.0156	−2.1463	−2.0930
$32 \leftarrow 0$	1.0464	1.0077	−2.1434	−2.0906

The plots illustrate why the vertical excitation approach (solid vertical black lines) is not sufficient for a reasonable description of the properties: excited state properties steeply decrease in the region of the equilibrium internuclear distance of the ground state and vibrational averaging samples regions far off of the ground state equilibrium bond length. The differences between expectation values of the properties in various vibrational states are, however, comparatively small, because in the relevant region of the internuclear distances the properties only show a mild dependence on the bond length.

For reasons of comparison with the herein presented method we recalculated the results for LLIV in the system H_2–$H_2{}^+$, which was first determined by analytic calculations in Ref. [341]. As hydrogen has a nuclear charge of $Z = 1$ relativistic effects play a minor role and the difference between the relativistic and non-relativistic operators is below one per mil. The values of $\hat{H}_\mathrm{LLIV}$ for the transition from H_2–$H_2{}^+$ without vibrational correction received with COSCI (two electrons in two active orbitals) at bond length of $r(H_2) = 0.75$ Å and $r(H_2{}^+) = 1.05$ Å, respectively, are $\Delta_{xx} = -0.410\,E_\mathrm{h}$ and $\Delta_{zz} = -0.319\,E_\mathrm{h}$. This is in rough agreement with the results received by Müller *et al.* in Ref.[341] ($\Delta_{xx} = -0.382\,E_\mathrm{h}$ and $\Delta_{zz} = -0.340\,E_\mathrm{h}$).

In comparison to LLIV in the H_2 molecule, the electronic structure enhancement of LLIV effects in molecular iodine is larger by a factor of ~ 3 for the x/y-component and by a factor of ~ 6 for the z-component. Furthermore, there is a significant difference between the two factors and even the sign is opposite, whereas both properties are almost equal in the hydrogen maser transition. This shows that the IMC is more sensitive and measurements can be complementary to those with the H_2 system, which can be helpful for a disentanglement of the parameters.

Conclusion.—We calculated LLIV effects on the IMC transition at the DHF–COSCI level. Vibrational effects were included from RKR improved BO potentials. We could demonstrate that in the vibronic transition $B^3 0_u^+, v = 32 \leftarrow X^1 0_g^+, v = 0$ LLIV is considerably enhanced. By comparison to the H_2 maser we found an enhancement stronger by a factor of 3 for x/y-components and of 6 for the z-component of the $\tilde{\boldsymbol{c}}$-tensor of the SME. The methods presented herein can also be applied for future searches of even more favorable molecular clocks for the search of LLIV

characterized by the $\tilde{\boldsymbol{c}}$-tensor of the SME. Our calculations are an important ingredient to interpret upcoming measurements with the iodine molecular clock on satellites of the Gallileo system or in the BOOST satellite missions.

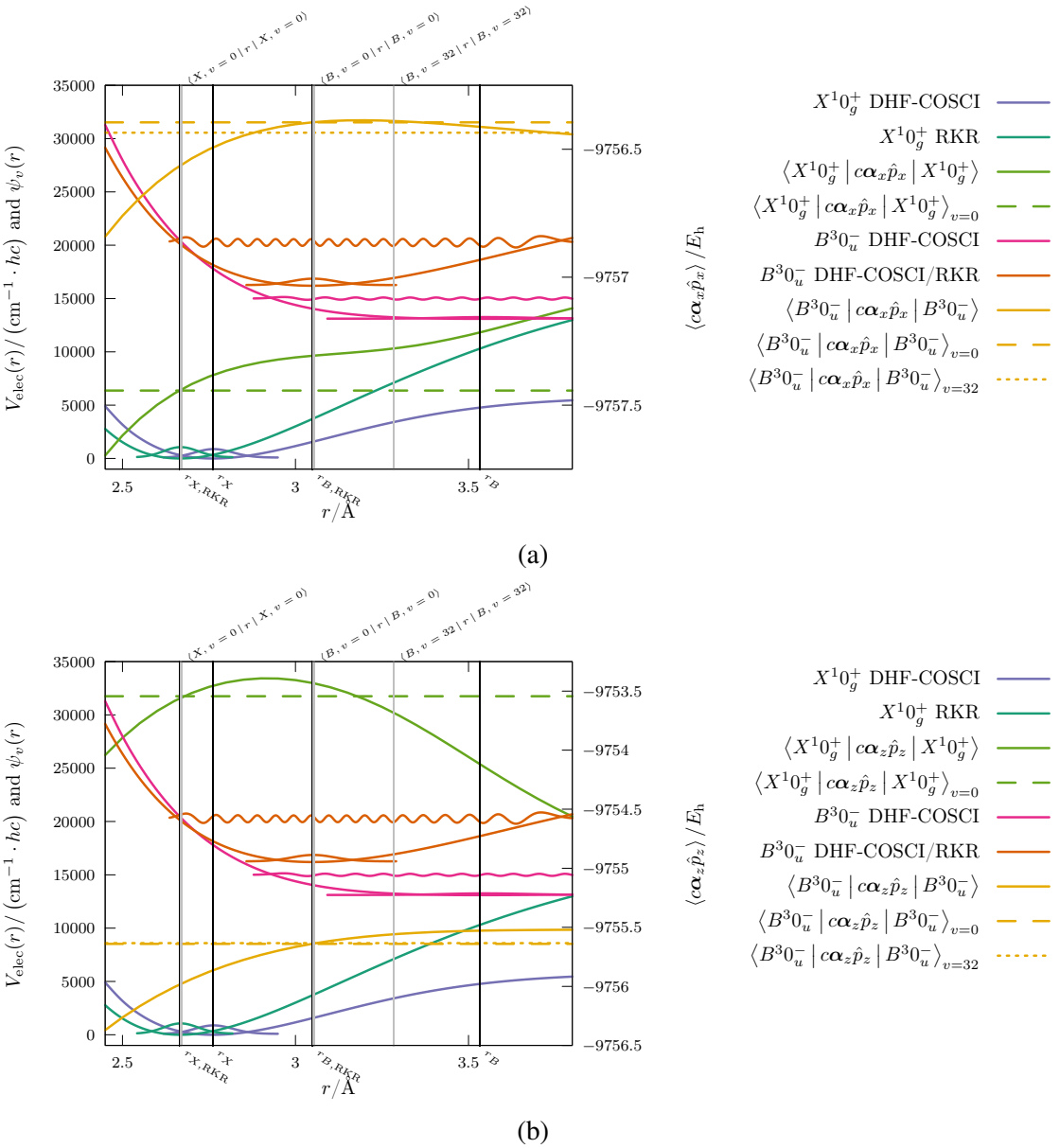

(a)

(b)

Figure 4.4: Potentials of the $X^1 0_g^+$ and $B^3 0_u^+$ states of the iodine molecule from a relativistic DHF–COSCI *ab initio* calculation, calculated via RKR from experimental data, and from RKR-improved DHF–COSCI calculations are shown. Vibrational wave-functions from a DVR calculation shown for $v = 0$ for the $X 0_g^+$ and $B 0_u^+$ states and for $v' = 32$ for the $B 0_u^+$ state. Bold black vertical lines indicate the equilibrium distances for RKR(-improved) calculations and the *ab initio* results for both excited states. Gray vertical lines show the expectation value for the bonding distance for vibrational states $v = 0$ and $v' = 32$ (the latter only for the B-state). The xx-component (a) and the zz-component (b) of the relativistic LLIV-Hamiltonian as a function of the bond distance for both electronic states and expectation values for distinct vibrational states (in dashed lines).

5 Conclusion

With this thesis contributions to three major areas of molecular tests of fundamental physics were made. $\mathcal{CP}$-violation or rather $\mathcal{P},\mathcal{T}$-violation which are connected to the baryon asymmetry of our universe and play an important role in unifying BSM theories. The understanding of the enhancement of $\mathcal{P},\mathcal{T}$-odd effect sizes in linear molecules was advanced. This is essential for the development of more sensitive experimental tests of $\mathcal{P},\mathcal{T}$-violation. The problem of CDM was addressed by demonstration of the applicability of high-precision experiments with chiral molecules to so far less well explored sectors of ultralight CDM. Finally, the search for LLIV, which is essential in many BSM theories that unify gravity and quantum mechanics, was brought forward by contributing to the development of a new satellite experiment using a molecular clock.

On the methodology side, within this thesis a new toolbox approach for the calculation of arbitrary relativistic properties described by one-electron operators was developed for approximate quasi-relativistic wave functions. This allows the customized evaluation of fundamental symmetry violating effects in large molecules in a two-component framework, which before required tedious implementation work for every single property.

$\mathcal{P},\mathcal{T}$-violation in linear molecules was studied systematically with respect to relativistic and chemical enhancements across the periodic table. Focus was laid on molecules that are supposed to have a $^2\Sigma_{1/2}$ ground state. Within these studies problems of commonly applied relativistic enhancement factors were identified and partially resolved and strong chemical enhancement of $\mathcal{P},\mathcal{T}$-odd effects was revealed.

Furthermore, it could be demonstrated that the chemical influence on the ratio of the $\mathcal{P},\mathcal{T}$-odd interaction constants W_d and W_s, which is important for the complementarity of two experiments that aim to limit the eEDM d_e and SPNEC interactions k_s, is very weak. The ratio rather increases exponentially with increasing nuclear charge. Thus, simple linear polyatomic molecules, such as metal hydroxides, yield essentially the same information on the $\mathcal{P},\mathcal{T}$-odd parameter space as diatomic metal fluorides with the same heavy element. These findings lead to a model for the size of the coverage area A in the d_e-k_s parameter space:

$$A \sim \frac{\left|u(\omega_1)u(\omega_2)\right|}{10^{b_{\mathrm{d},1}+b_{\mathrm{d},2}}\,\frac{Z_1^{a_{\mathrm{d},1}}\,Z_2^{a_{\mathrm{d},2}}}{\gamma_{1/2,1}^4\gamma_{1/2,2}^4}\;0.89\cdot\left|1.0210^{Z_1}-1.0210^{Z_2}\right|\times 10^{27}\;\frac{\mathrm{Hz}^2}{e\cdot\mathrm{cm}}}\,, \tag{5.1}$$

where b_d and a_d are empirical parameters without units for the groups of the periodic table and the indices 1 and 2 refer to two (different) molecules in two separate experiments with uncertainties $u(\omega)$. In this thesis the parameters b_d and a_d were obtained from ab initio calculations for diatomic molecules with heavy elements of groups 2, 3, 4, 12 and 13 of the periodic table.

Beyond these studies on the two dimensional parameter space of d_e-k_s, on a qualitative basis a minimization of the full six-dimensional $\mathcal{P},\mathcal{T}$-odd parameter space with respect to nuclear charge and the nuclear and electronic spin states of atoms and simple linear diatomic molecules was performed. In this study electronic structure enhancement factors were treated in simple analytical atomic models as a function of the nuclear charge of the heavy atom in the molecule. In doing so, effects due to nuclear structure and the chemical environment were neglected to simplify the description. For a simultaneous determination of all six $\mathcal{P},\mathcal{T}$-odd parameters experiments with at least six molecules or atoms are required. Within this simple model, it was found that for a good disentanglement of the $\mathcal{P},\mathcal{T}$-odd parameters at least three molecules with a fundamentally different spin-rotation Hamiltonian are needed. Most interestingly, the global optimization with

respect to nuclear charge indicated that molecules consisting of lighter elements can be of great value for an optimal design of complementary experiments, which motivates the use of such light molecules in upcoming EDM experiments.

Finally, in numerical studies of RaF large enhancement of all $\mathcal{P},\mathcal{T}$-violationing sources, .i.e., a large sensitivity to all sectors of the standard model could be identified. This renders the different isotopes of RaF interesting candidates for future searches of permanent EDMs with molecules from an electronic structure perspective.

In a collaboration with colleagues from St. Petersburg the influence of parity-nonconserving cosmic fields on the energetic landscape of chiral molecules was studied analytically and numerically. It could be verified that for a system containing two heavy main group elements with nuclear charge numbers Z_A and Z_B the following scaling relation holds in lowest order:

$$\left\langle \gamma^5 \right\rangle_{\mathrm{mol}} \sim c_1 \alpha^5 Z_A^2 Z_B^2 + c_2 \alpha^3 Z_A^2 + c_3 \alpha^3 Z_B^2 \,, \tag{5.2}$$

where the factor $\alpha^2 Z_B^2$ in the first term emerges from spin orbit coupling and the constants c_1, c_2 and c_3 depend on the electronic structure, where it can be assumed that $\left|c_{2,3}\right| \ll \left|c_1\right|$.

In addition, with ab initio calculations the sensitivity of a twenty year old experiment with the methane derivative CHBrClF to the pseudovector LLIV parameter b_0^{e} was calculated to be on the order of 10^{-12} GeV, which is as good as atomic parity violation experiments with Tl and Yb and only two orders of magnitude inferior to the present best limit from an experiment with Dy. This sensitivity was found to be improvable by at least five orders by experimental refinement (2 orders), well chosen heavy-elemental chiral molecules (2 orders) and choice of a different vibrational state for the experiment (1 order). With this the sensitivity of modern experiments with chiral molecules to the parameter b_0^{e} was estimated to be on the order of 10^{-17} GeV, which would be an improvement of current best limits on b_0^{e} by at least two orders of magnitude.

Furthermore, it could be demonstrated that *static* parity violation experiments with chiral molecules can be employed to study slowly oscillating pseudovector cosmic fields that correspond to CDM masses below $10^{-19}\,\mathrm{eV}/c^2$. This suggests the use of heavy elemental chiral molecules as sensors of pseudovector FCDM and the search for pseudovector LLIV interactions in molecules.

With detailed numerical calculations, possible methodological complications that may appear in an accurate description of vibrational energy splittings in chiral molecules were discussed. It was revealed that care has to be taken in the choice of the vibrational mode. In some cases multimode effects can play a decisive role and may even change the sign of the effects.

Finally, the calculation of LLIV effects in heavy elemental molecules was advanced. For molecular iodine, which is supposed to be the optical frequency reference in an upcoming satellite mission that was proposed by the BOOST collaboration, LLIV effects were calculated including vibrational corrections. These calculations were essential to estimate the sensitivity of the upcoming satellite experiment, which turned out to be able to improve actual limits on the LLIV parameters $\tilde{c}_{xx}$, $\tilde{c}_{yy}$ and $\tilde{c}_{zz}$ by two orders of magnitude. In comparison with LLIV effects in the H_2 maser system, it could be demonstrated that electronic enhancement in I_2 is a factor of six larger and parameters have a different relative sign.

The findings of this thesis show that in future searches for new candidate molecules for a first measurement of a permanent EDM more complex polyatomic molecules may bring advantages due to a fundamentally different spin-rotational Hamiltonian. Furthermore, the important role of closed shell molecules for the interpretation of $\mathcal{P},\mathcal{T}$-violation experiments was highlighted with this thesis, suggesting that more focus should be laid in future studies on the search for suitable closed shell molecules for $\mathcal{P},\mathcal{T}$-violation experiments. However, regarding nuclear-spin dependent $\mathcal{P},\mathcal{T}$-odd effects the lack of accurate predictions from nuclear structure theory makes

the understanding on the level of elementary particles, i.e., quarks and gluons, very difficult. To continue the research of this thesis, it would be important to systematically test the validity of discussed analytic models for $\mathcal{P},\mathcal{T}$-odd electronic structure enhancement as was done for W_d and W_s and to explore the influence of chemical surroundings of the heavy atoms. In this context it would be particularly important to validate and expand the presented analysis of the global $\mathcal{P},\mathcal{T}$-odd parameter space.

In the use of chiral molecules as probes for $\mathcal{P}$-violating cosmic fields, with this thesis, first important steps towards the understanding of such interactions were made and also possible computational difficulties were discussed. Searches for suitable candidates for a first observation of electroweak $\mathcal{P}$-violation in molecule have to be extended in order to identify molecules that are good candidates for cosmic field searches as well. With the ideas spread in this thesis, experiments would need to be refined in order to maximize sensitivity to such cosmic fields.

Within this thesis, first steps were made to explore tests of LLIV with molecular clocks. Yet, a deeper understanding of LLIV effect sizes in molecules is lacking. Therefore, to tie in with the work presented here, from a quantum chemical perspective more studies of different candidate molecules are needed to maximize the sensitivity of searches for LLIV with molecular clocks.

The results of this thesis highlight the potential that precision experiments with molecules have in the search for fundamental symmetry violations. Future precision experiments with molecules are among the most promising candidates to reveal new physics beyond the standard models of particle physics and cosmology.

A

$\mathcal{P},\mathcal{T}$-Odd Electronic Structure Constants

In the following the explicit representation of the electronic structure enhancement factors W that appear in eq. (2.12) are presented. W_{p_A} is not listed as it is supposed to be many orders of magnitude smaller than the other effects and vanishing for non-relativistically moving nuclei [208, 209]. Assuming the molecular axes to be aligned along the z-axis, the remaining electronic structure parameters are defined in the following (see, e.g., Refs. [144, 199, 208, 252, 302, 394]).

The electronic structure enhancement of the eEDM due to internal atomic or molecular electric fields is [199]:

$$W_{\mathrm{d},A} = \frac{\left\langle \Psi \left| \sum_{i=1}^{N_{\mathrm{elec}}} \gamma_i^0 \vec{\boldsymbol{\Sigma}}_i \cdot \left(\vec{\mathcal{E}}_{iA} + \sum_{j=1}^{N_{\mathrm{elec}}} \mathbf{1}_j \vec{\mathcal{E}}_{ij} \right) \right| \Psi \right\rangle}{\Omega}, \tag{A.1}$$

where the first term is a one-electron operator and the second term is a two-electron operator. $\vec{\mathcal{E}}_{iA}$ is the electric field due to the charge of nucleus A that electron i experiences and $\vec{\mathcal{E}}_{ij}$ is the electric field due to the charge of electron j that electron i experiences. By commutation of the Dirac Coulomb equation with a modified momentum operator it can be shown that this operator can be written in leading order as (see Ref. [303])

$$W_{\mathrm{d},A} = \frac{\left\langle \Psi \left| \sum_{i=1}^{N_{\mathrm{elec}}} (\mathbf{1}_i - \gamma_i^0) \vec{\boldsymbol{\Sigma}}_i \cdot \left(\vec{\mathcal{E}}_{iA} \right) \right| \Psi \right\rangle}{\Omega}. \tag{A.2}$$

This operator neglects all two-electron contributions, however, such many electron effects can be expected to be negligible in heavy-elemental compounds [303].Using a different modified momentum operator commutation properties of the Dirac Coulomb equation allow to rewrite operator (A.1) as the one-electron operator (for details see Refs. [302, 303]):

$$W_{\mathrm{d}} = \frac{\left\langle \Psi \left| \frac{2c}{e\hbar} \sum_{i=1}^{N_{\mathrm{elec}}} \imath \gamma_i^0 \gamma_i^5 \hat{\vec{p}}_i^2 \right| \Psi \right\rangle}{\Omega}. \tag{A.3}$$

In contrast to expression (A.2) operator (A.3) implicitly contains mean-field level two-electron contributions to the eEDM enhancement.

The electric field contribution is the leading order contribution to W_{d} in open-shell molecules but is zero in closed-shell molecules. In the latter, contributions stemming from internal magnetic fields to the electronic structure enhancement of the eEDM are dominant. These appear in leading order (see discussion in Ref. [303]) due to a magnetic field of the nuclei as given in Refs. [199, 255]:

$$W_{\mathrm{d,mag}}^{\mathrm{m}} = c \frac{k_{\mathrm{em}}}{k} \mu_A \times \left\langle \Psi \left| \sum_{i=1}^{N_{\mathrm{elec}}} \left[\imath \gamma_i^3 \frac{8\pi}{3} \delta(\vec{r}_i - \vec{r}_A) - \frac{3\imath \vec{\boldsymbol{\gamma}}_i \cdot (\vec{r}_i - \vec{r}_A)(z_i - z_A) - \imath \gamma_i^3 \left| \vec{r}_i - \vec{r}_A \right|^2}{\left| \vec{r}_i - \vec{r}_A \right|^5} \right] \right| \Psi \right\rangle, \tag{A.4}$$

with the nuclear magnetic moment μ_A, the constant k, which is 1 in SI units and c^{-1} in Gauss

units and the constant k_{em} being $\frac{\mu_0}{4\pi}$ in SI units with μ_0 being the magnetic constant (see Ref. [395] for other choices of k_{em} that correspond to different unit systems); or due to hyperfine induced electronic structure enhancement of the eEDM:

$$W_{\mathrm{d,hyp}}^{\mathrm{m}} = \sum_{j<a} \frac{\left| \left\langle \Psi_j \left| \frac{2c}{e\hbar} \sum_i^{N_{\mathrm{elec}}} \imath \gamma_i^0 \gamma_i^5 \hat{\vec{p}}_i^2 \right| \Psi_a \right\rangle \left\langle \Psi_a \left| c k_{\mathrm{em}} \mu_A \sum_{i=1}^{N_{\mathrm{elec}}} \frac{[(\vec{r}_i - \vec{r}_A)\times\vec{\alpha}_i]_z}{|\vec{r}_i - \vec{r}_A|^3} \right| \Psi_j \right\rangle \right|}{E_a - E_j}, \tag{A.5}$$

where the sums $\sum_{j<a}$ go over all electronic states with state j lying below state a and E_j are the energies of the corresponding electronic states. The total leading order magnetic contribution to the enhancement of the eEDM is $W_{\mathrm{d}}^{\mathrm{m}} = W_{\mathrm{d,mag}}^{\mathrm{m}} + W_{\mathrm{d,hyp}}^{\mathrm{m}}$.

Electronic structure enhancement of the NMQM is given by

$$W_{\mathcal{M}_A} = \frac{\left\langle \Psi \left| c e k_{\mathrm{em}} \frac{3}{2} \sum_{i=1}^{N_{\mathrm{elec}}} \frac{(z_i - z_A)(\vec{\alpha}\times(\vec{r}_i - \vec{r}_A))_z}{|\vec{r}_i - \vec{r}_A|^5} \right| \Psi \right\rangle}{\Omega}. \tag{A.6}$$

Electronic structure enhancement of nuclear Schiff moment and volume effect due to a pEDM is given by

$$W_{S,A} = \frac{2\pi}{3} \frac{\partial}{\partial z} \rho_{\mathrm{e}}(\vec{r}) \Big|_{\vec{r}=\vec{r}_A}, \tag{A.7}$$

where ρ_{e} is the electronic charge density distribution function. This Hamiltonian is a consequence of Schiff's theorem [210] and is the dipole contribution of an expansion of the electric potential of a finite nucleus (for details see Ref. [254]).

The electronic structure enhancement of the pEDM due to magnetic fields of moving electrons was originally derived in Ref. [252] and discussed in detail in Ref. [396]. The resulting simplified operator for a linear molecule or atom reads

$$W_{\mathrm{m}_A} = \left\langle \Psi \left| 4 \left(\frac{\mu_{\mathrm{N}}}{A_A} + \frac{\mu_A}{Z_A} \right) c \frac{k_{\mathrm{em}}}{k} \sum_{i=1}^{N_{\mathrm{elec}}} |\vec{r}_i - \vec{r}_A|^{-3} \left(\vec{\alpha}_i \times \hat{\vec{\ell}}_{iA} \right)_z \right| \Psi \right\rangle, \tag{A.8}$$

with the electronic orbital angular momentum operator with respect to nucleus A of electron i $\hbar\hat{\vec{\ell}}_{iA} = (\vec{r}_i - \vec{r}_A) \times \hat{\vec{p}}$, the nuclear magneton $\mu_{\mathrm{N}} = \frac{e\hbar}{2m_{\mathrm{p}}}$ with the mass of the proton m_{p}, the nuclear charge Z_A and mass number A_A of nucleus A. Here, it is assumed that the contributions stem from a single active valence proton in the nuclear shell (see Ref. [252]).

The electronic structure enhancement of SPNEC interactions is

$$W_{\mathrm{s}_A} = \frac{\left\langle \Psi \left| \frac{G_{\mathrm{F}}}{\sqrt{2}} \sum_{i=1}^{N_{\mathrm{elec}}} \imath \gamma_i^0 \gamma_i^5 \rho_{\mathrm{nuc},A}(\vec{r}_i) \right| \Psi \right\rangle}{\Omega}, \tag{A.9}$$

with the Fermi weak coupling constant $G_{\mathrm{F}} = 2.22249 \times 10^{-14} E_{\mathrm{h}} a_0^3$ and the normalized charge density distribution $\rho_{\mathrm{nuc},A}$ of nucleus A. This contribution is zero in closed-shell molecules in

which the corresponding hyperfine induced electronic structure enhancement dominates:

$$W_{\mathrm{s}}^{\mathrm{m}} = \sum_{j<a} \frac{\left| \left\langle \Psi_j \left| \frac{G_{\mathrm{F}}}{\sqrt{2}} \sum_{i=1}^{N_{\mathrm{elec}}} \imath \boldsymbol{\gamma}_i^0 \boldsymbol{\gamma}_i^5 \rho_{\mathrm{nuc},A}(\vec{r}_i) \right| \Psi_a \right\rangle \left\langle \Psi_a \left| c k_{\mathrm{em}} \mu_A \sum_{i=1}^{N_{\mathrm{elec}}} \frac{[(\vec{r}_i - \vec{r}_A) \times \vec{\boldsymbol{\alpha}}_i]_z}{|\vec{r}_i - \vec{r}_A|^3} \right| \Psi_j \right\rangle \right|}{E_a - E_j} . \quad \text{(A.10)}$$

Finally, the electronic structure enhancement of TPNEC interactions is

$$W_{\mathrm{T}_A} = \left\langle \Psi \left| \sqrt{2} G_{\mathrm{F}} \sum_{i=1}^{N_{\mathrm{elec}}} \imath \boldsymbol{\gamma}_i^3 \rho_{\mathrm{nuc},A}(\vec{r}_i) \right| \Psi \right\rangle . \quad \text{(A.11)}$$

B

Analytic expressions for electronic $\mathcal{P},\mathcal{T}$-odd enhancement factors

In the following I summarize atomic matrix elements of $\mathcal{P},\mathcal{T}$-odd operators as functions of the nuclear charge number Z in terms of relativistic enhancement factors introduced in Sec. 2.1.1. I discuss leading order matrix elements only. In most cases this corresponds to mixing of $s_{1/2}$ and $p_{1/2}$ orbitals and in some cases $p_{3/2}$ orbitals. The orbitals are always characterized by effective orbital quantum numbers ν, that contain all information on atomic orbitals and, when considering molecules, in addition, the ν contain information on linear combination coefficients of molecular orbitals. In the following all these ν are set to one in explicit calculations (Sec. 4.1.4).

A more detailed discussion of all matrix elements except that corresponding to the enhancement of the pEDM can be found in Ch. 8 of Ref. [208].

The radial part of the atomic wave functions employed to arrive at the enhancement factors is (see Ref. [208])

$$f_\kappa(r) = \frac{\kappa}{|\kappa| r\sqrt{Z a_0 \nu_\kappa^3}} \left((\kappa + \gamma_\kappa) J_{2\gamma_\kappa}\left(\sqrt{\frac{8Zr}{a_0}}\right) - \sqrt{\frac{2Zr}{a_0}} J_{2\gamma_\kappa - 1}\left(\sqrt{\frac{8Zr}{a_0}}\right)\right), \tag{B.1}$$

$$g_\kappa(r) = \frac{\kappa Z\alpha}{|\kappa| r\sqrt{Z a_0 \nu_\kappa^3}} J_{2\gamma_\kappa}\left(\sqrt{\frac{8Zr}{a_0}}\right), \tag{B.2}$$

where f and g are the radial functions of the large and small component wave functions, respectively. Here, κ is the relativistic angular momentum quantum number with values $\kappa = (-1)^{j+1/2-l}(j + 1/2)$ with the total electronic angular momentum quantum number $j = |\kappa| - 1/2 = s + l$ and the electronic orbital and spin angular momentum quantum numbers $s = -\frac{\kappa}{2|\kappa|}$ and $l = j - s$. J is the Bessel function of first kind. The full four component atomic wave function is

$$\psi_{\kappa,m}(r,\vartheta,\varphi) = \begin{pmatrix} f_\kappa(r)\Omega_{\kappa,m}(\vartheta,\varphi) \\ \imath g_\kappa(r)\Omega_{-\kappa,m}(\vartheta,\varphi) \end{pmatrix}, \tag{B.3}$$

with the angular wave function

$$\Omega_{\kappa,m}(\vartheta,\varphi) = \frac{1}{\sqrt{2l+1}} \begin{pmatrix} 2s\sqrt{l + \frac{1}{2} + 2sm} Y_{l,m-\frac{1}{2}}(\vartheta,\varphi) \\ \sqrt{l + \frac{1}{2} - 2sm} Y_{l,m+\frac{1}{2}}(\vartheta,\varphi) \end{pmatrix}, \tag{B.4}$$

with the spherical harmonics $Y_{l,m}$.

Following Ref. [208] closely, the electronic enhancement factors are presented in terms of units with $\hbar = 1$, $c = 1$, $4\pi\epsilon_0 = 1$ and length is given in units of cm: the Bohr radius is $a_0 = 5.29 \times 10^{-9}\,\mathrm{cm}$, the fine structure constant is $\alpha = e^2 \approx \frac{1}{137.036}$, the proton mass is $m_\mathrm{p} = 4.755\,11 \times 10^{13}\,\mathrm{cm}^{-1}$, the nuclear radius is $r_\mathrm{nuc} = 1.2 \times 10^{-13}\,\mathrm{cm}$, the Fermi constant is $G_\mathrm{F} = 1.027 \times 10^{-5}/m_\mathrm{p}^2$, the elementary charge is $e = \sqrt{\alpha}$, the electron mass is $m_\mathrm{e} = \frac{1}{\alpha a_0}$ and energy is given in units of Rydberg $\mathrm{Ry} = \frac{m_\mathrm{e}\alpha^2}{2}$.

The leading order electronic enhancement factor of the eEDM was derived in its full form in

Ref. [250]:

$$W_{\mathrm{d}}(Z) = \frac{4}{3}\frac{\alpha}{a_0^2}\frac{\alpha^2 Z^3}{(\nu_{\mathrm{p}_{1/2}}\nu_{\mathrm{s}_{1/2}})^{3/2}}\frac{3}{\gamma_{1/2}(4\gamma_{1/2}^2-1)}\,. \tag{B.5}$$

The magnetic contribution to it emerges from the second order contribution due to the nuclear hyperfine interaction (eq. (A.5)) and due to the magnetic field of the nuclei directly interacting with the electrons (eq. (A.4)). It was calculated in leading order as matrix element of $\mathrm{s}_{1/2}$ and $\mathrm{p}_{1/2}$ orbitals in Ref. [255] and the full analytic expression can be found in Ref. [208]:

$$W_{\mathrm{d}}^{\mathrm{m}}(Z) = -\frac{14}{3}\frac{e\mu}{m_{\mathrm{p}}a_0^3}\frac{\alpha Z^2}{(\nu_{\mathrm{p}_{1/2}}\nu_{\mathrm{s}_{1/2}})^{3/2}}(R(Z,A)-1)\,. \tag{B.6}$$

The matrix elements of the SPNEC interaction were discussed in Refs. [256, 380]:

$$W_{\mathrm{s}}(Z) = \frac{G_{\mathrm{F}}m_{\mathrm{e}}^2\alpha\,\mathrm{Ry}}{\sqrt{2}\pi}\frac{\alpha Z^3}{(\nu_{\mathrm{p}_{1/2}}\nu_{\mathrm{s}_{1/2}})^{3/2}}R(Z,A)\gamma_{1/2}\,. \tag{B.7}$$

A refined relativistic enhancement factor was calculated in Ref. [381]:

$$W_{\mathrm{s}}(Z) = \frac{G_{\mathrm{F}}m_{\mathrm{e}}^2\alpha\,\mathrm{Ry}}{\sqrt{2}\pi}\frac{\alpha Z^3}{(\nu_{\mathrm{p}_{1/2}}\nu_{\mathrm{s}_{1/2}})^{3/2}}R(Z,A)\frac{\gamma_{1/2}+1}{2}f_0(Z)\,, \tag{B.8}$$

with $f_0(Z) = (1-0.56\alpha^2Z^2)/(1-0.283\alpha^2Z^2)^2$.

The second order contribution that is induced due to hyperfine coupling of magnetic nuclei (eq. (A.10)) was derived in Ref. [208] to be in leading order:

$$W_{\mathrm{s}}^{\mathrm{m}}(Z) = -\frac{8}{3}\frac{G_{\mathrm{F}}m_{\mathrm{e}}^2\alpha\,\mathrm{Ry}}{\sqrt{2}\pi}\frac{\alpha\mu}{m_{\mathrm{p}}r_{\mathrm{nuc}}A^{1/3}}\frac{\alpha Z^3}{(\nu_{\mathrm{p}_{1/2}}\nu_{\mathrm{s}_{1/2}})^{3/2}}R(Z,A)\,. \tag{B.9}$$

Matrix elements of the TPNEC interaction were discussed in Ref. [255] and the full analytic calculation was presented in Ref. [208]:

$$W_{\mathrm{T}}(Z) = -\frac{4G_{\mathrm{F}}m_{\mathrm{e}}^2\alpha\,\mathrm{Ry}}{\sqrt{2}\pi}\frac{\alpha Z^2}{(\nu_{\mathrm{p}_{1/2}}\nu_{\mathrm{s}_{1/2}})^{3/2}}R(Z,A)\frac{(2+\gamma_{1/2})}{3}\,. \tag{B.10}$$

The interactions of atomic electrons with the $\mathcal{P},\mathcal{T}$-odd nuclear moments, namely the Schiff moment and the NMQM, were derived in Ref. [254] and read in leading order

$$W_{\mathcal{S}}(Z) = \frac{e}{a_0^4}\frac{Z^2}{(\nu_{\mathrm{p}_{1/2}}\nu_{\mathrm{s}_{1/2}})^{3/2}}R(Z,A)\frac{3\gamma_{1/2}}{2\gamma_{1/2}+1}\,, \tag{B.11}$$

and

$$W_{\mathcal{M}}(Z) = -\frac{4}{3}\frac{m_{\mathrm{e}}\alpha\,\mathrm{Ry}}{m_{\mathrm{p}}ea_0}\frac{\alpha Z^2}{(\nu_{\mathrm{p}_{3/2}}\nu_{\mathrm{s}_{1/2}})^{3/2}} \times\frac{720\Gamma\left(\gamma_{1/2}+\gamma_{3/2}-2\right)}{\Gamma\left(3+\gamma_{1/2}-\gamma_{3/2}\right)\Gamma\left(3-\gamma_{1/2}+\gamma_{3/2}\right)\Gamma\left(3+\gamma_{1/2}+\gamma_{3/2}\right)}\,. \tag{B.12}$$

It shall be noted that the $\mathrm{s}_{1/2}$-$\mathrm{p}_{1/2}$ matrix element vanishes for $W_{\mathcal{M}}$.

To my knowledge there is no analytic expression for the enhancement of the pEDM due to

magnetic electrons. The operator appears in spherical coordinates as

$$\hat{H}_{\mathrm{m}} \sim \frac{1}{r^3}\vec{\boldsymbol{\alpha}} \times \hat{\vec{\ell}}\,, \tag{B.13}$$

where $\alpha \times \hat{\ell}$ is a pure angular operator. As the $s_{1/2}$-$p_{1/2}$ matrix elements are vanishing I calculated the $s_{1/2}$-$p_{3/2}$ matrix element of W_{m}, where I used the same atomic wave functions as presented in Ref. [208] shown above:

$$\vec{W}_{\mathrm{m}}(Z) \approx 2\Re \iiint \mathrm{d}r\mathrm{d}\vartheta\mathrm{d}\varphi\, r^2 \sin\vartheta \psi^{\dagger}_{0,1/2} \frac{1}{r^3}\vec{\boldsymbol{\alpha}} \times \hat{\vec{\ell}} \psi_{-2,3/2} = \int \mathrm{d}r\, r^{-1} f_{-2}(r) g_{-1}(r) \begin{pmatrix} \frac{2}{\sqrt{6}} \\ \imath\frac{2}{\sqrt{6}} \\ 0 \end{pmatrix}. \tag{B.14}$$

For the chosen wave function when taking the expectation value the only non-vanishing component is the x component. The radial integral results in an enhancement factor that is proportional to

$$\frac{15}{16\gamma_{1/2}^2 - 1} \frac{\sin\left(\pi(\gamma_{3/2} - \gamma_{1/2})\right)}{\alpha\pi}\,, \tag{B.15}$$

where the sine approaches zero for $Z \to 0$. The sine was expanded in a series in $\alpha^2 Z^2 = 1 - \gamma_{1/2}^2$ around zero and gives $-\frac{\pi}{4}\alpha^2 Z^2$ in leading order. Dividing by $-\frac{\pi}{4}\alpha^2 Z^2$ yields a relativistic enhancement factor that approaches one for $Z \to 0$. The series converges in second order very well to $\sin\left(\pi(\gamma_{3/2} - \gamma_{1/2})\right)$ and reads

$$-\frac{\pi}{4}\alpha^2 Z^2 \left(1 + \frac{7}{16}(1 - \gamma_{1/2}^2) + \frac{93 - 4\pi^2}{384}(1 - \gamma_{1/2}^2)^2\right). \tag{B.16}$$

Finally, we arrive at the electronic enhancement factor:

$$W_{\mathrm{m}}(Z) = 2\left(\frac{1}{A} + \frac{\mu\alpha}{2Zm_{\mathrm{p}}}\right) \frac{\alpha m_{\mathrm{e}}}{2\sqrt{6}a_0^3 e\,\mathrm{Ry}} \frac{\alpha Z^2}{(\nu_{\mathrm{s}_{1/2}}\nu_{\mathrm{p}_{3/2}})^{3/2}} \times \frac{15\left(1 + \frac{7}{16}(1 - \gamma_{1/2}^2) + \frac{93-4\pi^2}{384}(1 - \gamma_{1/2}^2)^2\right)}{16\gamma_{1/2}^2 - 1}. \tag{B.17}$$

C

Supplementary information for *Complementary molecules for an experimental disentanglement of sources of $\mathcal{CP}$-violation from simple models*

C.1 Supplementary figures and tables

Table C.1: Used Mathematica 11 algorithms and options for a global minimization of the volume in the $\mathcal{P},\mathcal{T}$-odd parameter space with respect to nuclear charges Z_i. For all applied options not listed default values were employed.

Index[c]	Method	Tolerance[a]	Search points[a]
1	Simulated Annealing	1×10^{-5}	75
2	Simulated Annealing	1×10^{-8}	100
3	Simulated Annealing	1×10^{-10}	75
4	Differential Evolution	1×10^{-5}	75
5	Differential Evolution	1×10^{-8}	100
6	Differential Evolution	1×10^{-10}	75
7	Nelder-Mead	1×10^{-10}	-
8	Automatic[b]	-	-

[a] Tolerance is the threshold at which a point is accepted or withdrawn and search points is the number of initially generated points. Several other values for these two options have been tested for selected sets of molecular classes and the herein covered range was found to be most stable.

[b] The standard Mathematica algorithm with default options.

[c] The algorithms were evaluated in this order. And the result was accepted as minimum if the resulting volume in the $\mathcal{P},\mathcal{T}$-odd parameter space was smaller than that found by the previous algorithm.

Figure C.1: Optimum nuclear charge distributions for the global minimum for the fifth to least best different choices of molecules from the different classes for optimization in the regions of $20 \leq Z \leq 100$ (left) and $20 \leq Z \leq 90$ (right). The binning is chosen such that bins include all $x < Z \leq x + 10$ for $x = 30, 40, 50, \ldots, 100$. An exception is the first bin, which is chosen to include all $20 \leq Z \leq 30$.

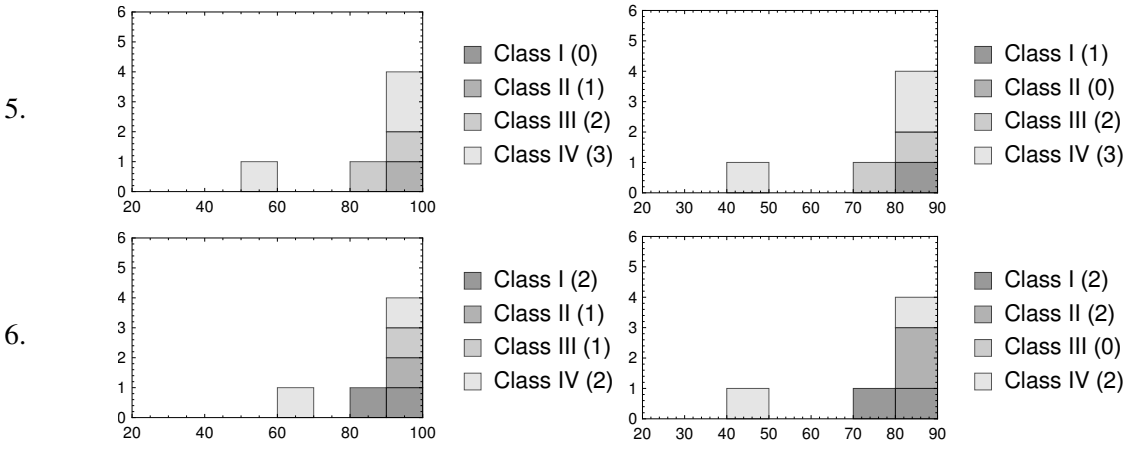

7.

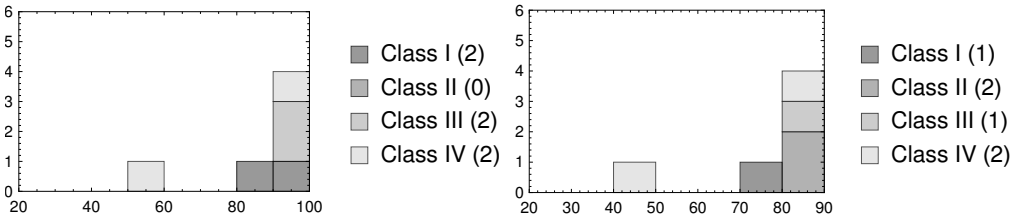

8.

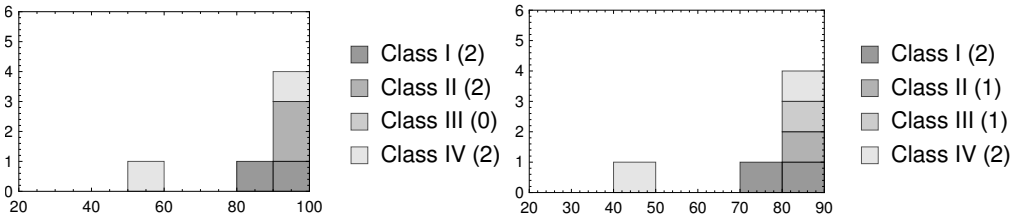

9.

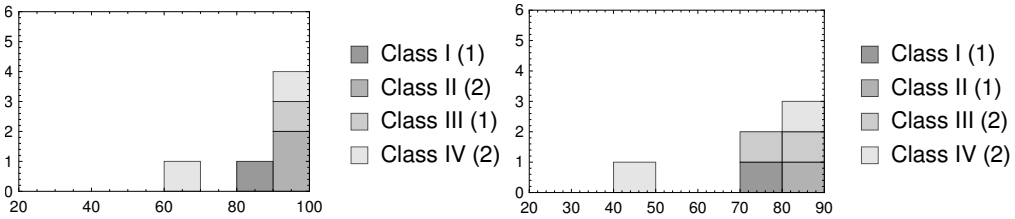

10.

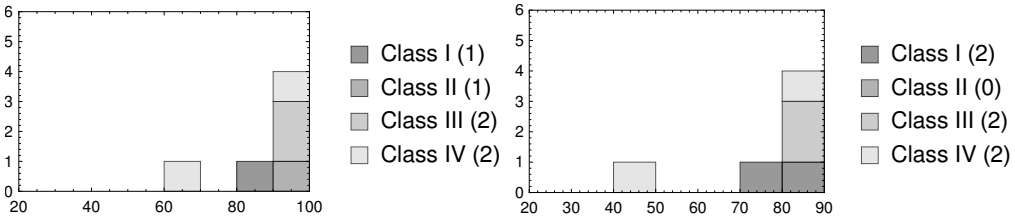

11.

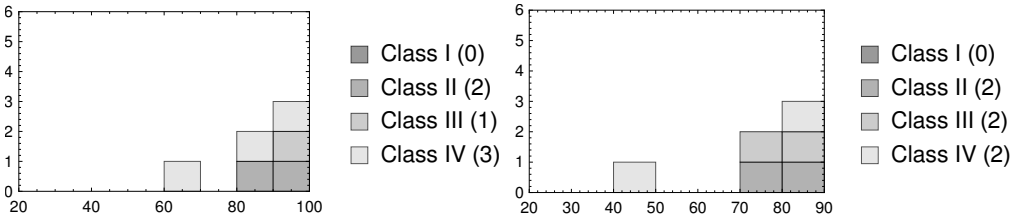

12.

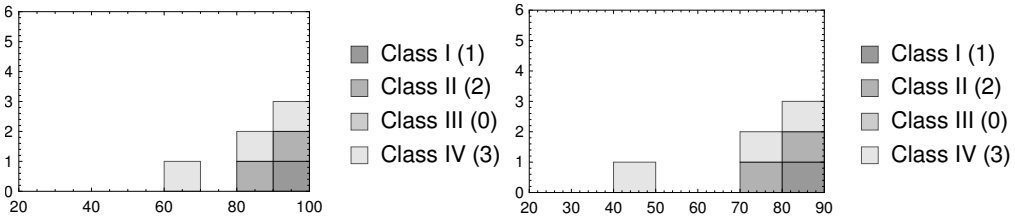

13.

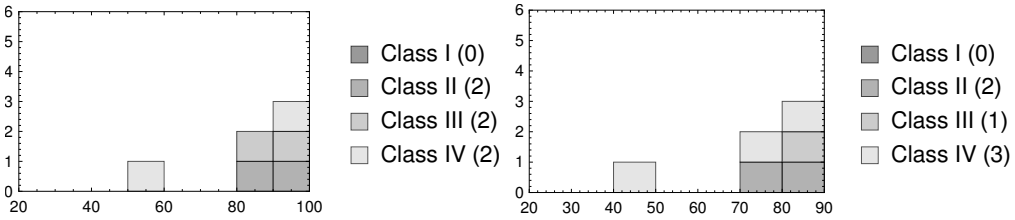

14.

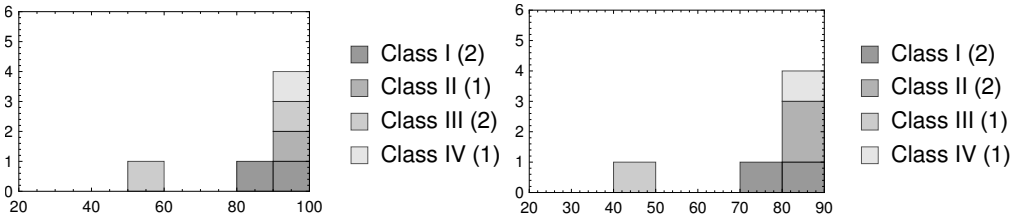

15.

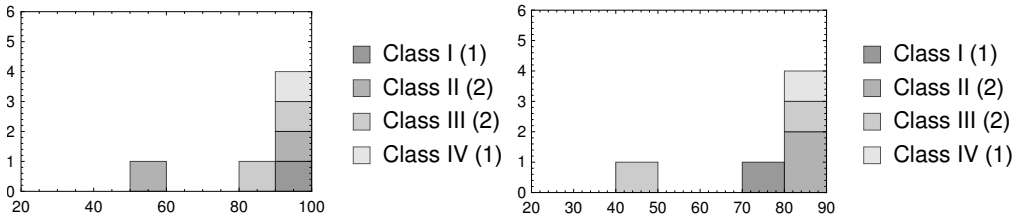

16.

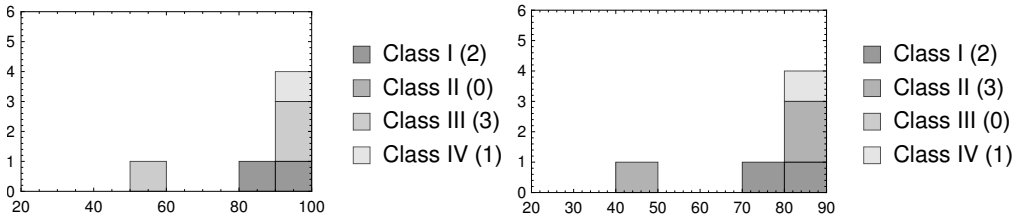

17.

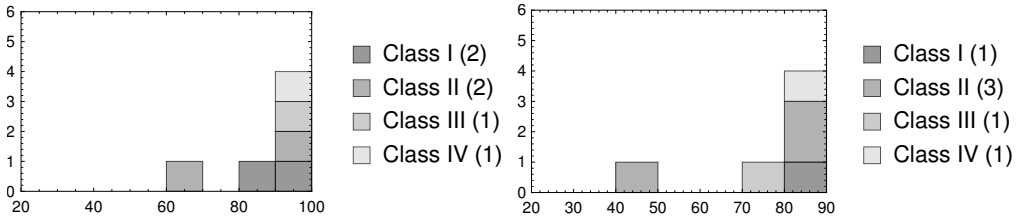

18.

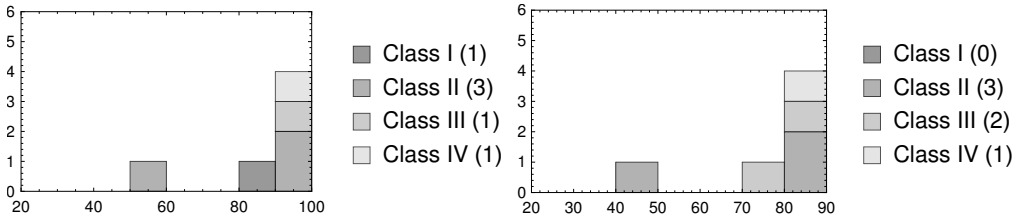

19.

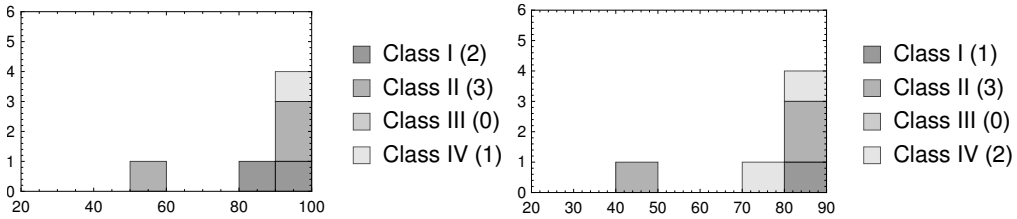

20.

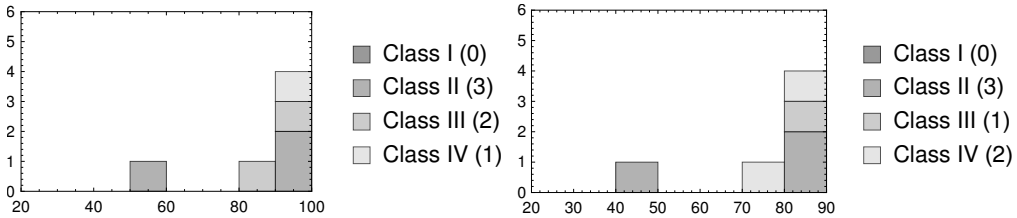

21.

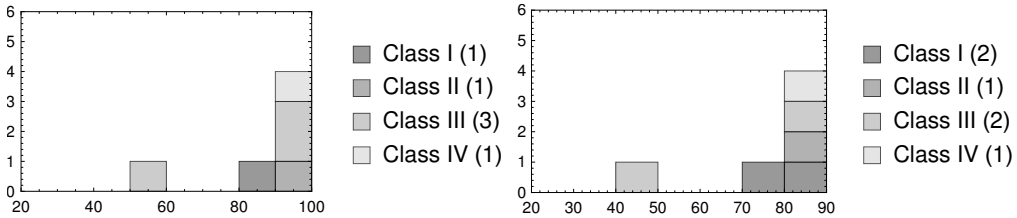

22.

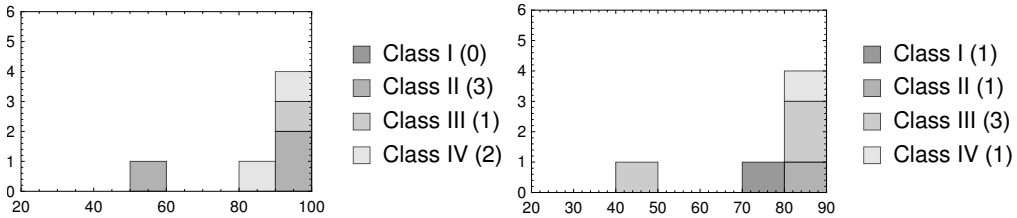

23.

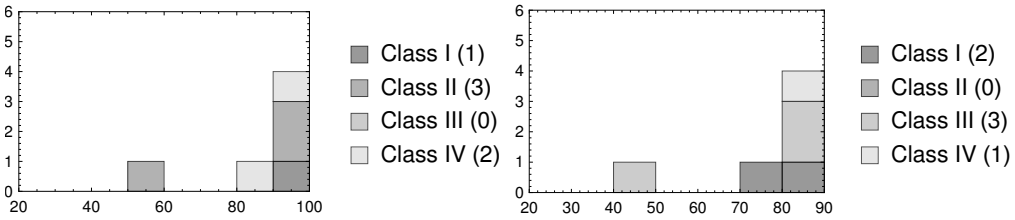

24.

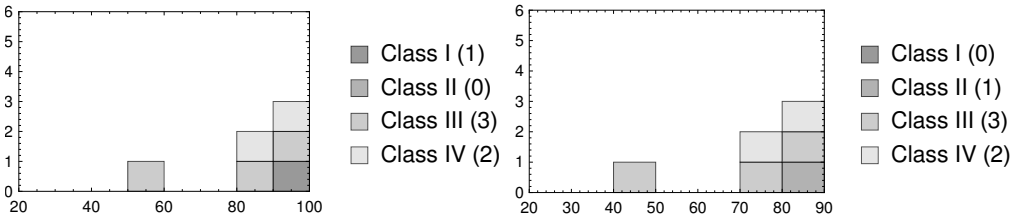

25.

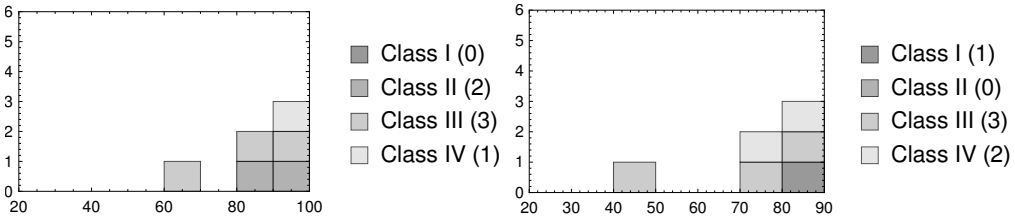

26.

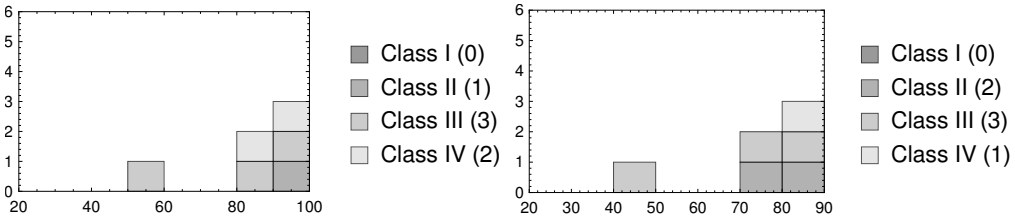

27.

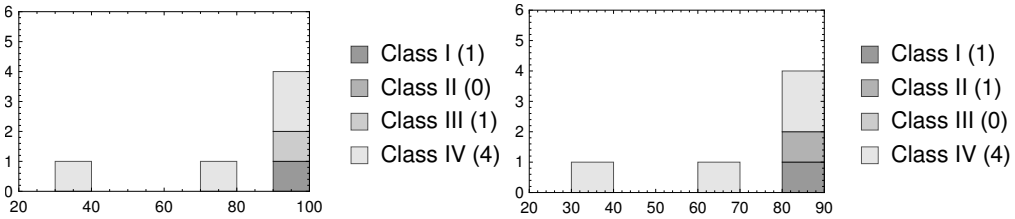

28.

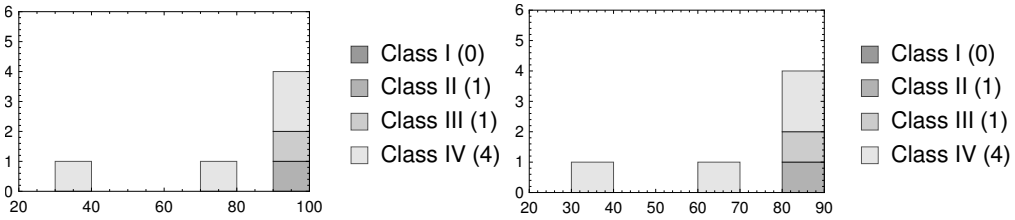

29.

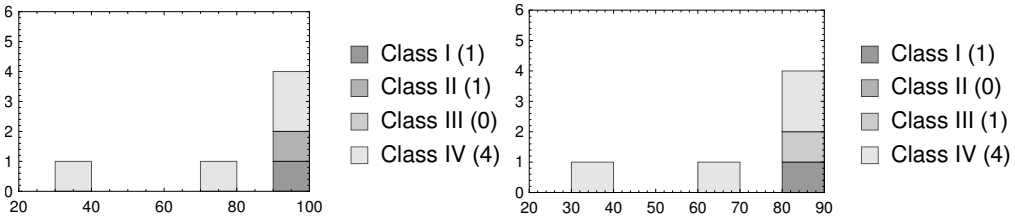

30.

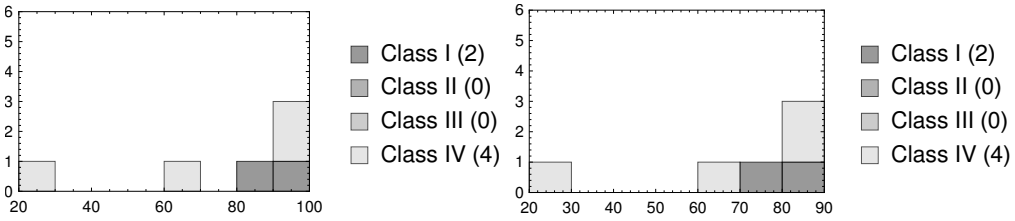

31.

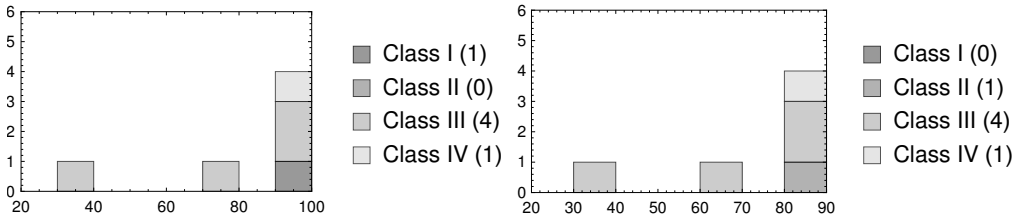

32.

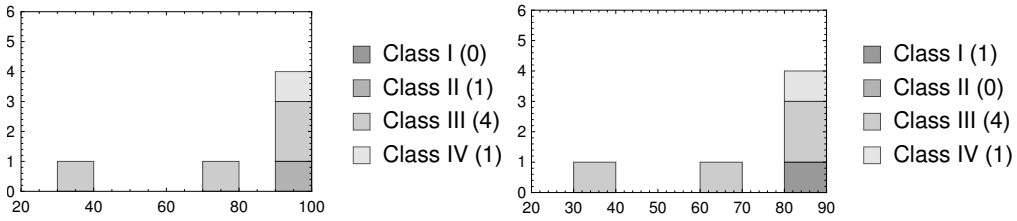

33.

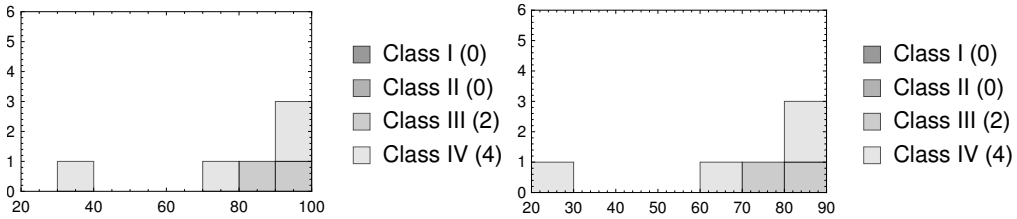

34.

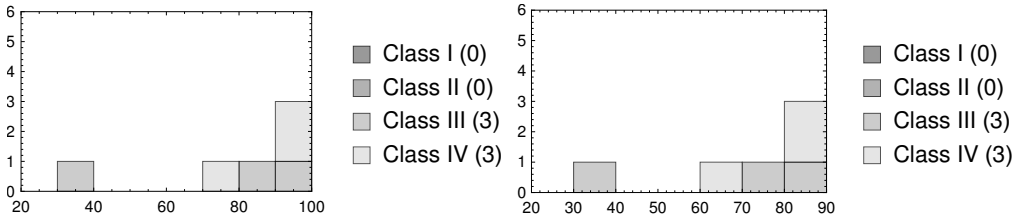

35.

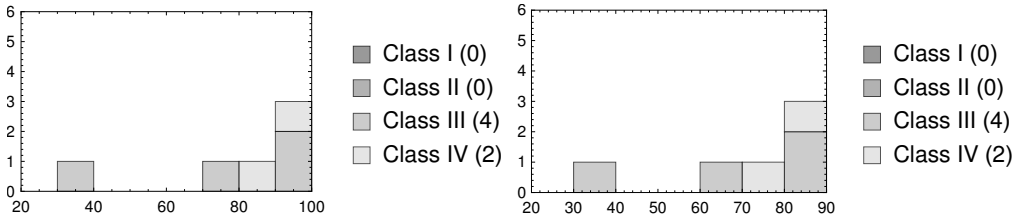

36.

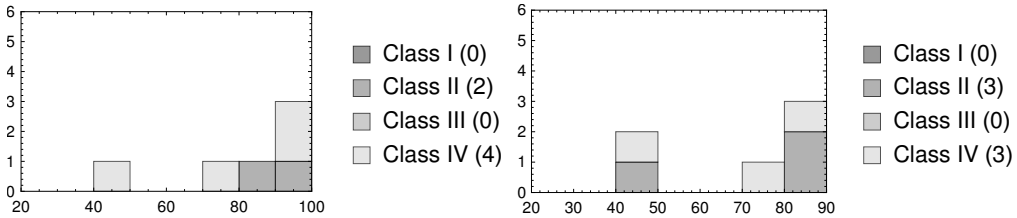

37.

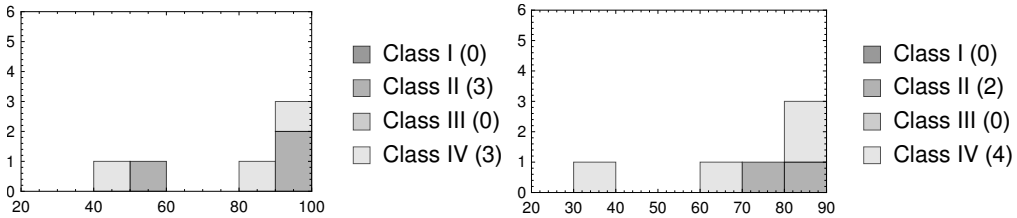

38.

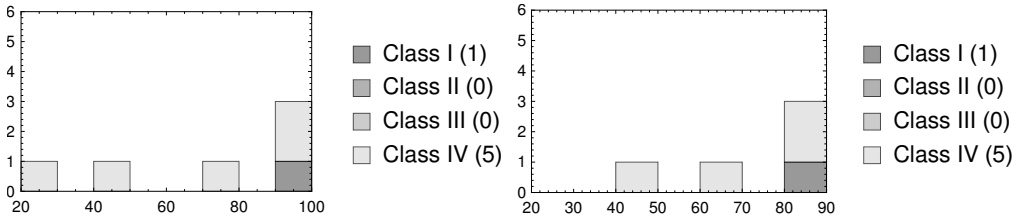

39.

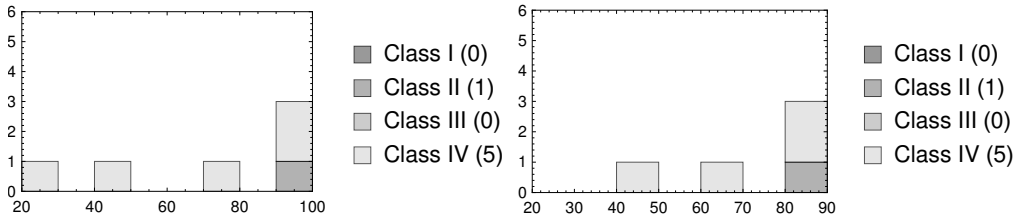

40.

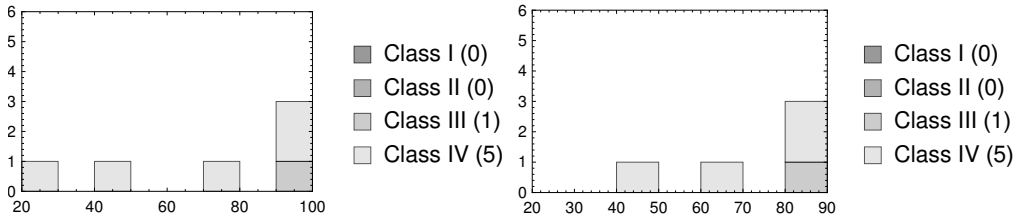

41.

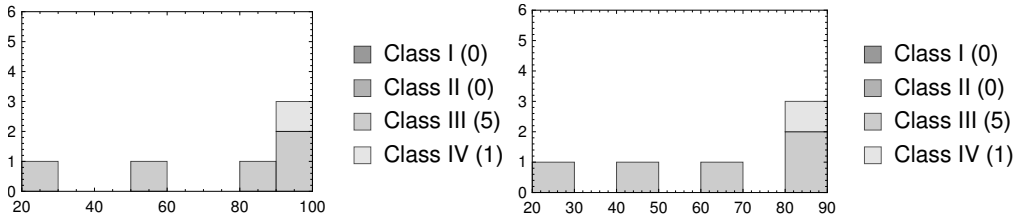

42.

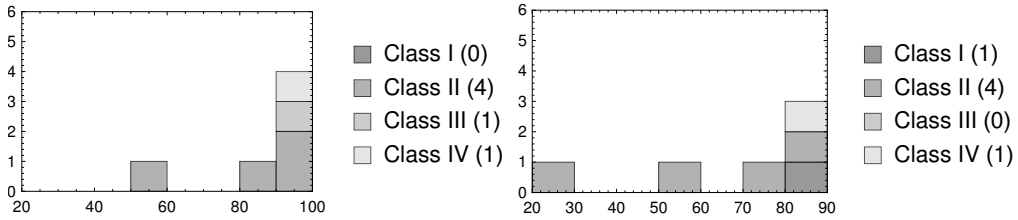

43.

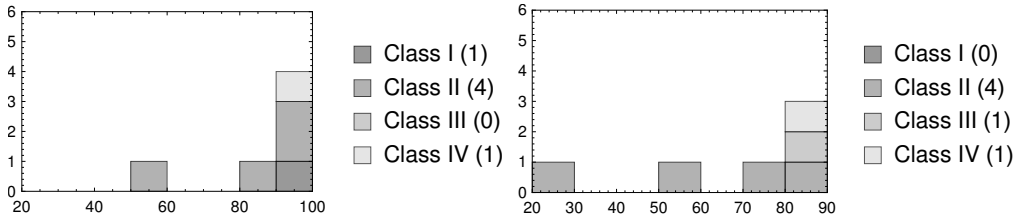

44.

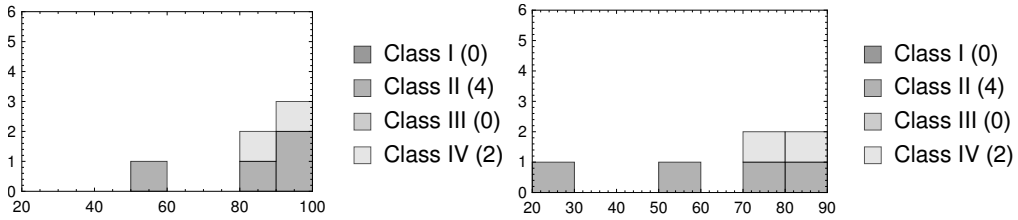

45.

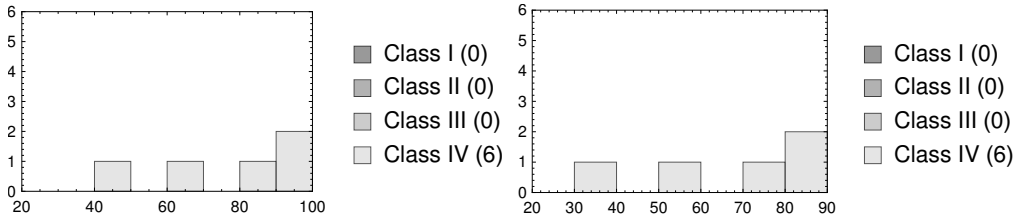

46.

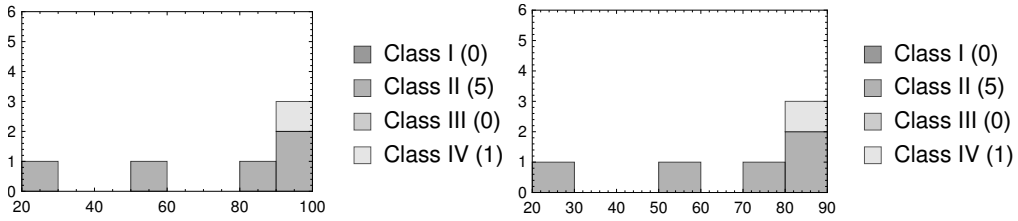

Table C.2: Results of a global minimization of the volume in the $\mathcal{P},\mathcal{T}$-odd parameter space with respect to nuclear charges Z_i for different classes of molecules (I to IV) in the range of $20 \leq Z_i \leq 100$. For each combination of molecules of each class the minimal volume is presented alongside the relative gradient and the minimal (h_{min}) and maximal (h_{max}) eigenvalues of the Hessian relative to the absolute minimal volume. Results are given in order of increasing volume. The number of shown figures is given for comparability and does not represent the accuracy of the optimization.

Place	N_{I}	N_{II}	N_{III}	N_{IV}	$V_{\text{min}} \times 10^{80}$/arb.u.	$\frac{\lvert\bar{\nabla}_Z V_{\text{min}}\rvert}{V_{\text{min}}}$	$\frac{h_{\text{min}}}{V_{\text{min}}}$	$\frac{h_{\text{max}}}{V_{\text{min}}}$	Algorithm Index[a]
1	2	0	1	3	7.7×10^{-2}	2.7×10^{-1}	-1.2×10^{-3}	8.4×10^{-2}	1,ℝ
2	1	1	1	3	8.0×10^{-2}	2.6×10^{-1}	-2.6×10^{-3}	7.9×10^{-2}	4,ℝ
3	2	1	0	3	8.0×10^{-2}	2.7×10^{-1}	-7.9×10^{-4}	8.3×10^{-2}	1,ℝ
4	1	0	2	3	1.4×10^{-1}	2.8×10^{-1}	-3.6×10^{-3}	8.9×10^{-2}	1,ℝ
5	0	1	2	3	1.5×10^{-1}	2.8×10^{-1}	-1.5×10^{-4}	8.9×10^{-2}	4,ℝ
6	2	1	1	2	1.5×10^{-1}	2.9×10^{-1}	-9.1×10^{-4}	9.4×10^{-2}	4,ℝ
7	2	0	2	2	1.5×10^{-1}	2.8×10^{-1}	-10.0×10^{-4}	9.1×10^{-2}	7,ℝ
8	2	2	0	2	1.6×10^{-1}	2.7×10^{-1}	-7.5×10^{-4}	8.5×10^{-2}	7,ℝ
9	1	2	1	2	1.6×10^{-1}	2.7×10^{-1}	-3.5×10^{-3}	8.4×10^{-2}	7,ℕ
10	1	1	2	2	1.6×10^{-1}	2.7×10^{-1}	-4.8×10^{-3}	8.3×10^{-2}	4,ℝ
11	0	2	1	3	1.7×10^{-1}	2.6×10^{-1}	-3.8×10^{-3}	7.4×10^{-2}	4,ℝ
12	1	2	0	3	1.7×10^{-1}	2.6×10^{-1}	-3.7×10^{-3}	7.4×10^{-2}	4,ℝ
13	0	2	2	2	1.7×10^{-1}	2.7×10^{-1}	-1.1×10^{-3}	7.8×10^{-2}	7,ℝ
14	2	1	2	1	3.0×10^{-1}	2.7×10^{-1}	-2.0×10^{-3}	8.6×10^{-2}	4,ℝ
15	1	2	2	1	3.1×10^{-1}	2.7×10^{-1}	-2.1×10^{-3}	7.7×10^{-2}	4,ℝ
16	2	0	3	1	3.1×10^{-1}	2.7×10^{-1}	-2.1×10^{-3}	8.3×10^{-2}	7,ℝ
17	2	2	1	1	3.1×10^{-1}	2.8×10^{-1}	-2.0×10^{-3}	8.7×10^{-2}	4,ℝ
18	1	3	1	1	3.2×10^{-1}	2.6×10^{-1}	-2.0×10^{-3}	7.8×10^{-2}	1,ℝ
19	2	3	0	1	3.2×10^{-1}	2.6×10^{-1}	-2.0×10^{-3}	7.8×10^{-2}	7,ℝ
20	0	3	2	1	3.2×10^{-1}	2.6×10^{-1}	-2.0×10^{-3}	7.8×10^{-2}	4,ℝ
21	1	1	3	1	3.2×10^{-1}	2.6×10^{-1}	-2.3×10^{-3}	7.9×10^{-2}	7,ℝ
22	0	3	1	2	3.2×10^{-1}	2.6×10^{-1}	-3.3×10^{-3}	7.8×10^{-2}	4,ℝ
23	1	3	0	2	3.2×10^{-1}	2.6×10^{-1}	-3.3×10^{-3}	7.8×10^{-2}	4,ℝ
24	1	0	3	2	3.3×10^{-1}	2.7×10^{-1}	-5.1×10^{-3}	7.7×10^{-2}	7,ℝ
25	0	2	3	1	3.3×10^{-1}	2.6×10^{-1}	-2.4×10^{-3}	7.5×10^{-2}	1,ℝ
26	0	1	3	2	3.4×10^{-1}	2.6×10^{-1}	-3.0×10^{-3}	7.5×10^{-2}	4,ℝ
27	1	0	1	4	3.5×10^{-1}	3.0×10^{-1}	-2.3×10^{-3}	1.1×10^{-1}	1,ℝ
28	0	1	1	4	3.7×10^{-1}	2.9×10^{-1}	-3.0×10^{-3}	1.1×10^{-1}	4,ℝ
29	1	1	0	4	3.7×10^{-1}	2.9×10^{-1}	-3.1×10^{-3}	1.1×10^{-1}	4,ℝ
30	2	0	0	4	1.2	2.9×10^{-1}	-7.6×10^{-4}	1.0×10^{-1}	1,ℝ
31	1	0	4	1	1.4	3.0×10^{-1}	-2.3×10^{-3}	1.1×10^{-1}	7,ℝ
32	0	1	4	1	1.5	2.9×10^{-1}	-2.1×10^{-3}	1.1×10^{-1}	4,ℝ
33	0	0	2	4	2.0	3.1×10^{-1}	-1.0×10^{-3}	1.1×10^{-1}	1,ℝ
34	0	0	3	3	3.2	3.0×10^{-1}	-2.7×10^{-5}	1.1×10^{-1}	4,ℝ
35	0	0	4	2	6.5	3.1×10^{-1}	-9.3×10^{-4}	1.2×10^{-1}	7,ℝ
36	0	2	0	4	8.0	3.4×10^{-1}	-3.1×10^{-4}	1.4×10^{-1}	1,ℝ
37	0	3	0	3	1.7×10^{1}	2.5×10^{-1}	2.9×10^{-4}	7.3×10^{-2}	7,ℝ
38	1	0	0	5	3.0×10^{1}	3.2×10^{-1}	-1.9×10^{-3}	1.3×10^{-1}	7,ℝ
39	0	1	0	5	5.3×10^{1}	3.2×10^{-1}	-5.7×10^{-4}	1.3×10^{-1}	1,ℝ
40	0	0	1	5	7.3×10^{1}	3.2×10^{-1}	-1.4×10^{-3}	1.3×10^{-1}	1,ℝ
41	0	0	5	1	1.3×10^{3}	3.6×10^{-1}	-2.1×10^{-3}	1.7×10^{-1}	7,ℝ
42	0	4	1	1	5.1×10^{3}	3.8×10^{-1}	-2.3×10^{-3}	1.9×10^{-1}	4,ℝ
43	1	4	0	1	5.1×10^{3}	3.8×10^{-1}	-2.3×10^{-3}	1.9×10^{-1}	7,ℝ
44	0	4	0	2	2.3×10^{4}	4.0×10^{-1}	-10.0×10^{-4}	2.0×10^{-1}	7,ℝ
45	0	0	0	6	7.8×10^{4}	4.4×10^{-1}	3.5×10^{-3}	2.7×10^{-1}	7,ℝ
46	0	5	0	1	4.1×10^{9}	3.6×10^{-1}	-2.0×10^{-3}	1.8×10^{-1}	4,ℝ

[a] Index of the used minimization algorithm given in Table C.1. ℕ means optimization with Z_i being limited to the domain of natural numbers and ℝ means optimization with Z_i being limited to the domain of real numbers.

Table C.3: Results of a global minimization of the volume in the $\mathcal{P},\mathcal{T}$-odd parameter space with respect to nuclear charges Z_i for different classes of molecules (I to IV) in the range of $20 \leq Z_i \leq 90$. For each combination of molecules of each class the minimal volume is presented alongside the relative gradient and the minimal ($h_{\min}$) and maximal ($h_{\max}$) eigenvalues of the Hessian relative to the absolute minimal volume. Results are given in order of increasing volume. The number of shown figures is given for comparability and does not represent the accuracy of the optimization.

Place	N_{I}	N_{II}	N_{III}	N_{IV}	$V_{\min} \times 10^{80}$/arb.u.	$\frac{\lvert\vec{\nabla}_Z V_{\min}\rvert}{V_{\min}}$	$\frac{h_{\min}}{V_{\min}}$	$\frac{h_{\max}}{V_{\min}}$	Algorithm Index[a]
1	2	1	0	3	4.2	2.6×10^{-1}	5.6×10^{-6}	7.7×10^{-2}	1,ℝ
2	1	1	1	3	4.2	2.5×10^{-1}	-2.7×10^{-3}	7.3×10^{-2}	4,ℝ
3	2	0	1	3	4.3	2.6×10^{-1}	-6.6×10^{-5}	7.7×10^{-2}	7,ℝ
4	0	1	2	3	7.7	2.7×10^{-1}	5.1×10^{-4}	8.5×10^{-2}	4,ℝ
5	1	0	2	3	7.8	2.7×10^{-1}	-1.4×10^{-3}	8.4×10^{-2}	7,ℝ
6	2	2	0	2	8.4	2.7×10^{-1}	1.0×10^{-5}	8.3×10^{-2}	7,ℝ
7	1	2	1	2	8.4	2.6×10^{-1}	-2.2×10^{-3}	8.1×10^{-2}	7,ℝ
8	2	1	1	2	8.5	2.7×10^{-1}	3.2×10^{-6}	8.2×10^{-2}	7,ℝ
9	1	1	2	2	8.5	2.5×10^{-1}	-4.7×10^{-3}	7.3×10^{-2}	4,ℝ
10	2	0	2	2	8.6	2.7×10^{-1}	-4.5×10^{-5}	8.2×10^{-2}	7,ℝ
11	0	2	2	2	8.9	2.6×10^{-1}	-3.1×10^{-4}	7.7×10^{-2}	7,ℝ
12	1	2	0	3	8.9	2.5×10^{-1}	-2.4×10^{-3}	7.0×10^{-2}	1,ℝ
13	0	2	1	3	8.9	2.5×10^{-1}	-2.4×10^{-3}	7.0×10^{-2}	4,ℝ
14	2	2	1	1	1.7×10^{1}	2.6×10^{-1}	-4.8×10^{-4}	7.6×10^{-2}	7,ℝ
15	1	2	2	1	1.7×10^{1}	2.5×10^{-1}	-2.7×10^{-3}	7.5×10^{-2}	4,ℝ
16	2	3	0	1	1.7×10^{1}	2.5×10^{-1}	-4.8×10^{-4}	7.6×10^{-2}	7,ℝ
17	1	3	1	1	1.7×10^{1}	2.5×10^{-1}	-4.8×10^{-4}	7.6×10^{-2}	7,ℝ
18	0	3	2	1	1.7×10^{1}	2.5×10^{-1}	-4.8×10^{-4}	7.6×10^{-2}	4,ℝ
19	1	3	0	2	1.7×10^{1}	2.5×10^{-1}	-6.3×10^{-4}	7.6×10^{-2}	7,ℝ
20	0	3	1	2	1.7×10^{1}	2.5×10^{-1}	-6.3×10^{-4}	7.6×10^{-2}	7,ℝ
21	2	1	2	1	1.7×10^{1}	2.5×10^{-1}	-4.8×10^{-4}	7.6×10^{-2}	7,ℝ
22	1	1	3	1	1.7×10^{1}	2.5×10^{-1}	-2.5×10^{-3}	7.4×10^{-2}	1,ℝ
23	2	0	3	1	1.7×10^{1}	2.6×10^{-1}	-4.9×10^{-4}	7.6×10^{-2}	7,ℝ
24	0	1	3	2	1.7×10^{1}	2.6×10^{-1}	-1.3×10^{-3}	7.9×10^{-2}	7,ℝ
25	1	0	3	2	1.8×10^{1}	2.6×10^{-1}	-3.0×10^{-3}	7.7×10^{-2}	7,ℝ
26	0	2	3	1	1.8×10^{1}	2.5×10^{-1}	-2.1×10^{-3}	7.0×10^{-2}	7,ℝ
27	1	1	0	4	2.0×10^{1}	2.8×10^{-1}	-1.2×10^{-3}	1.0×10^{-1}	4,ℝ
28	0	1	1	4	2.0×10^{1}	2.8×10^{-1}	-9.7×10^{-4}	1.0×10^{-1}	1,ℝ
29	1	0	1	4	2.1×10^{1}	2.9×10^{-1}	-6.9×10^{-4}	1.1×10^{-1}	7,ℝ
30	2	0	0	4	6.1×10^{1}	2.9×10^{-1}	8.5×10^{-5}	10.0×10^{-2}	7,ℝ
31	0	1	4	1	8.2×10^{1}	2.8×10^{-1}	-5.0×10^{-4}	1.0×10^{-1}	7,ℝ
32	1	0	4	1	8.3×10^{1}	2.8×10^{-1}	-6.7×10^{-4}	1.0×10^{-1}	7,ℝ
33	0	0	2	4	1.1×10^{2}	2.9×10^{-1}	-2.0×10^{-6}	1.1×10^{-1}	4,ℝ
34	0	0	3	3	1.7×10^{2}	2.9×10^{-1}	1.3×10^{-3}	1.0×10^{-1}	4,ℝ
35	0	0	4	2	3.9×10^{2}	3.0×10^{-1}	1.5×10^{-4}	1.1×10^{-1}	7,ℝ
36	0	3	0	3	5.5×10^{2}	2.5×10^{-1}	4.9×10^{-4}	7.6×10^{-2}	1,ℝ
37	0	2	0	4	6.3×10^{2}	3.3×10^{-1}	2.3×10^{-4}	1.4×10^{-1}	1,ℝ
38	1	0	0	5	1.5×10^{3}	3.1×10^{-1}	-3.7×10^{-4}	1.3×10^{-1}	7,ℝ
39	0	1	0	5	2.5×10^{3}	3.1×10^{-1}	-2.1×10^{-4}	1.3×10^{-1}	1,ℝ
40	0	0	1	5	3.8×10^{3}	3.1×10^{-1}	2.4×10^{-4}	1.3×10^{-1}	1,ℝ
41	0	0	5	1	5.7×10^{4}	3.2×10^{-1}	-5.1×10^{-4}	1.4×10^{-1}	1,ℝ
42	1	4	0	1	5.1×10^{5}	2.2×10^{-1}	-4.7×10^{-4}	6.0×10^{-2}	7,ℝ
43	0	4	1	1	5.1×10^{5}	2.2×10^{-1}	-4.7×10^{-4}	6.0×10^{-2}	4,ℝ
44	0	4	0	2	1.6×10^{6}	2.4×10^{-1}	4.3×10^{-4}	6.4×10^{-2}	4,ℝ
45	0	0	0	6	6.4×10^{6}	4.5×10^{-1}	4.0×10^{-3}	2.8×10^{-1}	7,ℝ
46	0	5	0	1	2.3×10^{11}	3.6×10^{-1}	-4.7×10^{-4}	1.8×10^{-1}	1,ℝ

[a] Index of the used minimization algorithm given in Table C.1. ℕ means optimization with Z_i being limited to the domain of natural numbers and ℝ means optimization with Z_i being limited to the domain of real numbers.

C.2 Volume of a N-dimensional ellipsoid

A N-dimensional ellipsoid can be described by N half-axes a_i. In Euclidean space its volume is

$$V = \frac{2\pi^{N/2}}{N\Gamma(N/2)} \prod_{i=1}^{N} a_i, \tag{C.1}$$

which reduces to the volume of a N-ball if all half-axes are equal. In general an ellipsoid centered at $\vec{x}_0$ can be represented as quadric:

$$\left(\vec{x} - \vec{x}_0\right)^{\mathsf{T}} \boldsymbol{A} \left(\vec{x} - \vec{x}_0\right) = b, \tag{C.2}$$

where the eigenvectors of $\boldsymbol{A}$ are the principal axes of the ellipsoid and the eigenvalues of $b^{-1}\boldsymbol{A}$ are the inverse, squared half-axes of the ellipsoid. Thus, the equivalence

$$V = \frac{2\pi^{N/2}}{N\Gamma(N/2)} \prod_{i=1}^{N} a_i \qquad \Leftrightarrow \qquad V = \frac{2\pi^{N/2}}{N\Gamma(N/2)} \left(\det(\boldsymbol{a})\right)^{-1/2}, \tag{C.3}$$

with

$$b^{-1}\boldsymbol{A}\boldsymbol{U} = \boldsymbol{a}\boldsymbol{U}; \qquad \boldsymbol{U}^{\dagger}\boldsymbol{U} = \mathbf{1}, \tag{C.4}$$

holds. Here, $\boldsymbol{U}$ is the matrix of eigenvectors of $\boldsymbol{A}$. As a unitary transformation does not change the determinant of a matrix, the volume can be written as

$$V = b^{1/2} \frac{2\pi^{N/2}}{N\Gamma(N/2)} \left(\det(\boldsymbol{A})\right)^{-1/2}. \tag{C.5}$$

D

Multimode-effects on parity violating vibrational energy shifts in CHBrClF

In the article [K. Gaul et al., Phys. Rev. A **accepted for publication** (2020)] the influence of non-separable vibrational corrections was discussed. In the following I present the quantitative influence of these multimode effects on the vibrational energy shifts, based on cubic force constants calculated by Sascha Brück in his diploma thesis with the program package Molpro [397]. The results are shown in Figure D.1

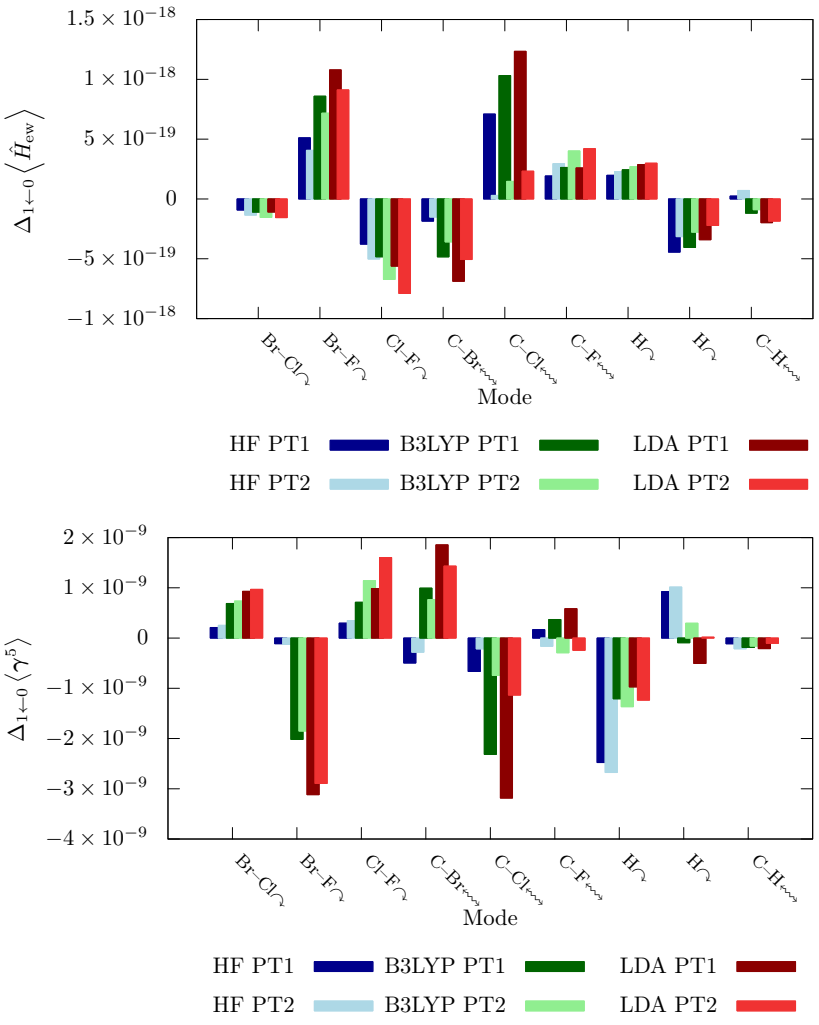

Figure D.1: Influence of non-separable anharmonic vibrational effects on the vibrational splittings between the vibrational ground state and first excited vibrational state $\Delta_{1\leftarrow 0}$ of the properties $\langle \gamma^5 \rangle$ and $\langle \hat{H}_{ew} \rangle$ in (*S*)-CHBrClF. Cubic force constants were calculated at the level of CCSD(T)/cc-pVDZ with an effective core potential at Br with two dimensional polynomials within Molpro in the diploma thesis of Sascha Brück [397]. Gradients with respect to the normal modes of the properties $\langle \gamma^5 \rangle$ and $\langle \hat{H}_{ew} \rangle$ were calculated as described in [K. Gaul et al., Phys. Rev. A **accepted for publication** (2020)] at levels of ZORA-cGHF and ZORA-GKS with the LDA and B3LYP functionals. Here, PT1 and PT2 refer to one-dimensional and two-dimensional vibrational perturbation theory of second order, respectively (see [K. Gaul et al., Phys. Rev. A **accepted for publication** (2020)]). The symbol ↷ refers to bending modes and the symbol ⇜⇝ refers to stretching modes.

These figures show a dramatical dependence of the expectation value of γ^5 on the multimode

effects that even leads to a change in the sign of the effect for the C–F stretching mode. However, low-frequency bending modes seem to be stable regarding these non-separable anharmonic effects, whereas stretching modes are more influenced. This shows that considerations from the gradients made in [K. Gaul et al., Phys. Rev. A **accepted for publication** (2020)] are justified.

E

Supplementary information for *Enhancement of Lorentz invariance violation in iodine molecular clock transitions*

E.1 Details on RKR calculations

Here, the RKR–potential was produced by calculation of the turning points for 30100 vibrational numbers ranging from $v = 0$ to $v = 150$ with an increment of $\delta v = 0.01$ from experimental data from NIST data base [398–400]. A correction potential was then computed as $E_{\mathrm{gs,RKR}}(r) - E_{\mathrm{gs,COSCI}}(r)$ and added to the various potentials computed on the COSCI level.

E.2 Calculation of vibrational corrections via DVR

For the DVR [393] calculation the empirically improved BO potentials of the electronic ground and excited states were interpolated to $N_{\mathrm{grid}} = 2005$ grid points between $r_0 = 2.250$ Å and 4.254 Å with an increment of $\delta = 0.001$ Å. The resulting vibrational eigenvalues which were obtained in the DVR framework for the ground state potential for $v < 94$ differ less than 1% from the eigenvalues obtained in the RKR calculation.

In order to also correct calculated molecular properties, these were evaluated at various bond lengths and fitted subsequently to a polynomial of the type

$$f(r) = \sum_{k=0}^{N} a_k r^k. \tag{E.1}$$

Here, r corresponds to the bond length of the iodine molecule. The polynomial expansion was truncated at the order $N = 5$. Thus, the expectation value of a given molecular property in the vibrational state v was obtained as

$$\langle v \mid f \mid v \rangle = \sum_{k=0}^{N} a_k \left\langle v \middle| r^k \middle| v \right\rangle, \tag{E.2}$$

and, hence, was calculated from the vibrational moments. The latter were estimated from the vibrational eigenstates in the DVR via

$$\left\langle v \middle| r^k \middle| v \right\rangle = \sum_{j=1}^{N_{\mathrm{grid}}} \left|\psi_v(j\delta + r_0)\right|^2 \left(j\delta + r_0\right)^k. \tag{E.3}$$

Here, ψ_v is the value of the DVR representation of the vibrational wave function for state v at the given grid point j and δ is the grid spacing.

E.3 Quality of the methods

With the methods described in the theory paragraph of section 4.3.2 the Born-Oppenheimer potential was calculated and empirically improved for the $X^1 0_g^+$ and the $B 0_g^+$ states of the iodine molecule. Subsequently the vibrational Schrödinger equation was solved numerically within the

DVR framework. The resulting diatomic constants from the COSCI calculation and the RKR–improved potentials are those derived from experiment in Table E.1.

Table E.1: Comparison of diatomic constants received from potentials from DHF–COSCI calculations and from RKR–improved DHF–COSCI potentials (DHF–COSCI/RKR) analyzed via the DVR spectrum (DHF–COSCI/RKR/DVR) to those derived from experimental data as reported in the National Institute of Standards and Technology (NIST) data base. Equilibrium distances r_{eq}, adiabatic electronic excitation wavenumbers $\tilde{T}_e$, harmonic vibrational wave numbers $\tilde{\omega}_e$, first anharmonicity constants $\tilde{\omega}_e x_e$ and dissociation limits $\tilde{D}_e$.

Constant	$X0_g^+$-state	$B0_u^+$-state
DHF–COSCI		
r_{eq}/Å	2.761	3.533
$\tilde{T}_e$/cm^{-1}		13 096
$\tilde{\omega}_e$/cm^{-1}(fit)[a]	181.6(2)	28.0(17)
$\tilde{\omega}_e$/cm^{-1}(MO)[b]	185.5	33.5
$\tilde{\omega}_e x_e$/cm^{-1}(fit)[a]	1.09(2)	0.71(19)
$\tilde{\omega}_e x_e$/cm^{-1}(MO)[b]	1.4	0.18
$\tilde{D}_e$/cm^{-1}(BS)[c]	5963	1548 [d]
$\tilde{D}_e$/cm^{-1}(fit)[e]	7563(2)	276(15)
DHF–COSCI/RKR/DVR		
r_{eq}/Å	2.666	3.049
$\tilde{T}_e$/cm^{-1}		16 199
$\tilde{\omega}_e$/cm^{-1}(fit)[a]	214.827(1)	133.467(4)
$\tilde{\omega}_e$/cm^{-1}(MO)[b]	214.8	134.0
$\tilde{\omega}_e x_e$/cm^{-1}(fit)[a]	0.614 61(9)	0.2168(5)
$\tilde{\omega}_e x_e$/cm^{-1}(MO)[b]	0.619	0.303
$\tilde{D}_e$/cm^{-1}(BS)[c]	18 733	14 873
$\tilde{D}_e$/cm^{-1}(fit)[e]	18 772.32(1)	20 541.32(3)
exp.		
r_{eq}/Å	2.666	3.024
$\tilde{T}_e$/cm^{-1}		15 769
$\tilde{\omega}_e$/cm^{-1}	214.50	125.69
$\tilde{\omega}_e x_e$/cm^{-1}	0.614	0.764
$\tilde{D}_e$/cm^{-1}	18 733	5169

[a] Constants calculated via a polynomial fit up to order $\left(v+\frac{1}{2}\right)^4$.

[b] Constants calculated in the Morse oscillator (MO) approximation with dissociation energy from c.

[c] Dissociation energy received from Birge-Sponer (BS) extrapolation of the energy spectrum added by the energy eigenvalue of the vibrational ground state.

[d] Dissociation energy estimated as difference of the vibrational ground state energy and the energy of state $v = 33$ added by the energy eigenvalue of the vibrational ground state.

[e] Dissociation energy calculated from fitted harmonic and anharmonic constants via $D_e = \frac{\tilde{\omega}_e^2}{4\tilde{\omega}_e x_e}$.

For the RKR-improved excited state potential we observe a significant improvement of the equilibrium distance (deviation before $\sim$ 17 % and after $<$ 1 %), the adiabatic electronic excitation wavenumber (deviation before $\sim$ 17 % and after $\sim$ 3 %) and the harmonic wavenumber (deviation before $\sim$ 27 % and after $\sim$ 7 %). These RKR-improved diatomic constants are in good agreement and the experimental ones can be seen. However, the anharmonicity wavenumber and dissociation limit of the electronically excited state potential are not well described in the present approach (deviations of $\sim$ 60 % for the anharmonicity wavenumber and $>$ 180 % for the dissociation limit), which is not an issue as wave functions of considered vibrational states are sufficiently decayed much before the dissociation limit.

E.4 Choice of vibrational states

In the experiment relevant vibrational states are the vibrational ground state ($v = 0$) of the electronic ground state and the 32nd vibrationally excited state ($v' = 32$) of the electronic excited state. In our calculations the $B0_u^+, v' = 32 \leftarrow X0_g^+, v = 0$ transition has a wavenumber of 20 215 cm^{-1} (4056 cm^{-1} with respect to the vibrational ground state in the B-state) whereas experimentally the $B0_u^+, v' = 32 \leftarrow X0_g^+, v = 0$ transition has a wavenumber of 19 108 cm^{-1} (3277 cm^{-1} with respect to the vibrational ground state in the B-

state) (determined by a RKR calculation with experimental data [398–400]). This difference is mainly caused by a dissociation limit computed to be too high in the electronic excited state. In the present approximation this wavenumber would correspond to a transition into the vibrational energy levels around $v' = 25$ and $v' = 26$.

However, in the naive picture of a vertical transition from the vibrational and electronic ground state into the electronic excited state, for the RKR–improved COSCI calculation the transition is at an energy of 19 942 cm^{-1} and in a RKR calculation from experimental data at 18 381 cm^{-1}. These deviations from the transition into the 32nd excited vibrational state may be explained by neglected rotational and hyperfine effects [401], which are present in experiments with IMCs. Thus, one can naively expect the vibrational corrections in our approach to be somewhere between those from the 25th and those from the 32nd vibrational level of the electronic excited state.

F Publication Reprints

On the following pages the publications discussed in Ch. 4 are reprinted in the same order as discussed in Ch. 4:

1. Reproduced from [K. Gaul et al., Phys. Rev. A **99**, 032509 (2019)]. Copyright (2019) by The American Physical Society.

2. Reproduced from [K. Gaul and R. Berger, Phys. Rev. A **101**, 012508 (2020)]. Copyright (2020) by The American Physical Society.

3. Reproduced from [K. Gaul and R. Berger, J. Chem. Phys. **152**, 044101 (2020)], with the permission of AIP Publishing.

4. Accepted manuscript of [K. Gaul et al., Phys. Rev. Lett. **accepted for publication** (2020)]. Rights to publish by The American Physical Society under Creative Commons Attribution 4.0 International license (CC BY 4.0).

5. Accepted manuscript of [K. Gaul et al., Phys. Rev. A **accepted for publication** (2020)]. Copyright (2020) by The American Physical Society.

6. Reproduced from [N. Gürlebeck et al., Phys. Rev. D **97**, 124051 (2018)]. Copyright (2018) by The American Physical Society.

Systematic study of relativistic and chemical enhancements of $\mathcal{P}, \mathcal{T}$-odd effects in polar diatomic radicals

Konstantin Gaul,[1,*] Sebastian Marquardt,[1] Timur Isaev,[2] and Robert Berger[1,†]

[1]*Fachbereich Chemie, Philipps-Universität Marburg, Hans-Meerwein-Straße 4, 35032 Marburg, Germany*

[2]*NRC "Kurchatov Institute" - Petersburg Nuclear Physics Institute by B.P. Konstantinov, Orlova Roscha. 1, 188300 Gatchina, Russia*

(Received 19 June 2018; published 21 March 2019)

Polar diatomic molecules that have, or are expected to have, a $^2\Sigma_{1/2}$-ground state are studied systematically with respect to simultaneous violation of parity $\mathcal{P}$ and time-reversal $\mathcal{T}$ with numerical methods and analytical models. Enhancements of $\mathcal{P}, \mathcal{T}$-violating effects due to an electric dipole moment of the electron (eEDM) and $\mathcal{P}, \mathcal{T}$-odd scalar-pseudoscalar nucleon-electron current interactions are analyzed by comparing trends within columns and rows of the periodic table of the elements. For this purpose electronic structure parameters are calculated numerically within a quasirelativistic zeroth order regular approximation (ZORA) approach in the framework of complex generalized Hartree-Fock (cGHF) or Kohn-Sham (cGKS). Scaling relations known from analytic relativistic atomic structure theory are compared to these numerical results. Based on this analysis, problems of commonly used relativistic enhancement factors are discussed. Furthermore, the ratio between both $\mathcal{P}, \mathcal{T}$-odd electronic structure parameters mentioned above is analyzed for various groups of the periodic table. From this analysis an analytic measure for the disentanglement of the two $\mathcal{P}, \mathcal{T}$-odd electronic structure parameters with multiple experiments in dependence of electronic structure enhancement factors is derived.

DOI: 10.1103/PhysRevA.99.032509

I. INTRODUCTION

Simultaneous violation of space ($\mathcal{P}$) and time ($\mathcal{T}$) parity in the charged lepton sector is considered to be a strong indicator for physics beyond the standard model of particle physics [1]. Exploiting enhancement effects in bound systems, such as atoms or molecules, low-energy experiments actually provide the best limits on $\mathcal{P}, \mathcal{T}$ violation in this sector and thus are among the most useful tools to exclude new physical theories and to test the standard model [2,3].

Understanding these atomic and molecular enhancement effects in detail is essential for the development of experiments sensitive to $\mathcal{P}, \mathcal{T}$ violation.

A permanent atomic or molecular electric dipole moment (EDM) that causes a linear Stark shift in the limit of zero external fields would violate $\mathcal{P}, \mathcal{T}$ [3]. Mainly four sources of a permanent EDM are commonly considered for molecules: permanent electric dipole moments of the nuclei, $\mathcal{P}, \mathcal{T}$-odd nucleon-nucleon current interactions, a permanent electric dipole moment of the electron (eEDM), and $\mathcal{P}, \mathcal{T}$-odd nucleon-electron current interactions (see, e.g., [4]). Of these sources the latter two have the most important contribution in paramagnetic systems [4]. Furthermore, in open-shell molecules nucleon-electron interactions are expected to be dominated by scalar-pseudoscalar interactions that are nuclear spin independent.

Since the formulation of an eEDM interaction Hamiltonian for atoms by Salpeter in the year 1958 [5], there have been many studies on eEDM enhancement in atoms and molecules. Sandars worked out analytical relations of atomic eEDM interactions in the 1960s [6–9], which were confirmed also by others [10,11]. Sandars calculated that the enhancement of the eEDM in atoms scales with $\alpha^2 Z^3$, where α is the fine-structure constant and Z is the nuclear charge number. Enhancements of scalar-pseudoscalar nucleon-electron current interactions in atoms scale as αZ^3 [12]. Since then, a number of numerical studies was conducted, but most of the previous investigations focused on the description of $\mathcal{P}, \mathcal{T}$-odd effects in individual or few molecular candidates.

Some attempts were made to obtain a deeper understanding of enhancement of $\mathcal{P}, \mathcal{T}$-odd effects in molecules beyond established Z-dependent scaling laws: In Ref. [13], for instance, the influence of the nuclear charge number of the electronegative partner on eEDM enhancements in mercury monohalides was studied. Furthermore, effects of the polarization of the molecule by the electronegative partner on the eEDM enhancement are discussed. In Ref. [13] it was concluded that the nuclear charge of the lighter halogen atom influences the eEDM enhancement less than its electronegativity.

Recently Sunaga *et al.* studied large eEDM enhancement effects in hydrides within orbital interaction theory and remarked an influence of the energy difference between the interacting valence orbitals of the electronegative atom and the unoccupied $p_{1/2}$ orbital of the heavy atom [14]. Both of the mentioned studies confirmed that large contributions of s- and p-type atomic orbitals in the singly occupied molecular orbital increase $\mathcal{P}, \mathcal{T}$-odd effects, as predicted in Ref. [12]. A similar result was obtained by Ravaine *et al.* in 2005 [15], who showed that the covalent character of HI^+ causes a stronger s-p mixing and therefore a larger enhancement of the eEDM than in ionically bound HBr^+.

---

*Parts of this work were reported in preliminary form in the M.Sc. thesis of Konstantin Gaul.

†robert.berger@uni-marburg.de

The majority of previous studies on $\mathcal{P},\mathcal{T}$-violating effects in molecules were performed within a four-component (relativistic) framework. Our recently developed two-component (quasirelativistic) approach for the calculation of $\mathcal{P},\mathcal{T}$-odd effects [16] allows for routine calculations of a large number of molecules on an *ab initio* level. In this paper we study diatomic radicals systematically across the periodic table, which are known to have a $^2\Sigma_{1/2}$-ground state, or for which at least a $^2\Sigma_{1/2}$-ground state is naively expected from simple chemical bonding concepts. In combination with analytic scaling relations, we calculate the Z-dependent and Z-independent electronic structure effects in different groups of the periodic table. Furthermore, we gauge the "chemical" influences on the $\mathcal{P},\mathcal{T}$-odd enhancement particularly using an analysis of isolobal diatomic molecules, i.e., changes in the enhancement throughout the columns of the periodic table.

Herewith, we provide a consistent overview of $\mathcal{P},\mathcal{T}$-odd effects in a large number of diatomic molecules, which may serve as a suitable starting point for further research with higher-level electronic structure methods, where needed. By analyzing general trends of the ratio between molecular enhancement factors of the eEDM and nucleon-electron current interactions, we draw conclusions on their possible disentanglement in experiments with polar diatomic radicals that feature a $^2\Sigma_{1/2}$-ground state.

II. THEORY

In this section we shortly introduce the employed Hamiltonians used for calculations of $\mathcal{P},\mathcal{T}$-odd effects in diatomic molecules in order to clarify their limitations. Additionally, we give an overview of relativistic enhancement effects in the herein studied properties, which are important for the following discussions. Finally, we present neglected many-electron and magnetic effects that may significantly influence the performed studies of $\mathcal{P},\mathcal{T}$-odd effects in molecules without heavy elements.

A. $\mathcal{P},\mathcal{T}$-odd spin-rotational Hamiltonian

We present herein electronic structure calculations for polar diatomic molecules that are expected to have a $^2\Sigma_{1/2}$-ground state. For these systems an effective spin-rotational Hamiltonian can be derived that in particular describes a transition of Hund's coupling case (c) to case (b) [17–19]. This corresponds to cases where the rotational constant is much smaller than the spin-doubling constant but much larger than the Ω-doubling constant (for details see Ref. [20]). The $\mathcal{P},\mathcal{T}$-odd part of this effective spin-rotational Hamiltonian reads (see, e.g., Refs. [20,21])

$$H_{\mathrm{sr}} = (k_{\mathrm{s}}W_{\mathrm{s}} + d_{\mathrm{e}}W_{\mathrm{d}})\Omega = W_{\mathrm{d}}(k_{\mathrm{s}}W_{\mathrm{s}}/W_{\mathrm{d}} + d_{\mathrm{e}})\Omega, \tag{1}$$

where $\Omega = \vec{J}_{\mathrm{e}}\cdot\vec{\lambda}$ is the projection of the reduced total electronic angular momentum $\vec{J}_{\mathrm{e}}$ on the molecular axis, defined by the unit vector $\vec{\lambda}$ pointing from the heavy to the light nucleus. k_{s} is the $\mathcal{P},\mathcal{T}$-odd scalar-pseudoscalar nucleon-electron current interaction constant and d_{e} is the eEDM. The $\mathcal{P},\mathcal{T}$-odd electronic structure parameters are defined by

$$W_{\mathrm{s}} = \frac{\langle\Psi\,|\,\hat{H}_{\mathrm{s}}\,|\,\Psi\rangle}{k_{\mathrm{s}}\Omega}, \tag{2a}$$

$$W_{\mathrm{d}} = \frac{\langle\Psi\,|\,\hat{H}_{\mathrm{d}}\,|\,\Psi\rangle}{d_{\mathrm{e}}\Omega}, \tag{2b}$$

where Ψ is the electronic wave function and the molecular $\mathcal{P},\mathcal{T}$-odd Hamiltonians are [3,5]

$$\hat{H}_{\mathrm{s}} = \imath k_{\mathrm{s}}\frac{G_{\mathrm{F}}}{\sqrt{2}}\sum_{i=1}^{N_{\mathrm{elec}}}\sum_{A=1}^{N_{\mathrm{nuc}}}\rho_A(\vec{r}_i)Z_A\boldsymbol{\gamma}^0\boldsymbol{\gamma}^5, \tag{3}$$

$$\hat{H}_{\mathrm{d}} = -d_{\mathrm{e}}\sum_{i=1}^{N_{\mathrm{elec}}}(\boldsymbol{\gamma}^0 - \mathbf{1}_{2\times2})\vec{\boldsymbol{\Sigma}}\cdot\vec{\mathcal{E}}(\vec{r}_i). \tag{4}$$

In this equation $\hat{H}_{\mathrm{d}}$ refers to $\hat{H}_{\mathrm{d,I}}$, obtained according to stratagem I by commuting the unperturbed Dirac-Coulomb Hamiltonian with a modified momentum operator as reported in Ref. [22]. In the following the index I is only used, when we compare to other forms of the Hamiltonian. If no additional index (I, II, or other) is used we refer always to $\hat{H}_{\mathrm{d,I}}$. Here the sums run over all N_{elec} electrons and all N_{nuc} nuclei, ρ_A is the normalized nuclear density distribution of nucleus A with charge number Z_A, $\vec{r}_i$ is the position vector of electron i, $\vec{\mathcal{E}}$ is the internal electrical field, $G_{\mathrm{F}} = 2.22249\times10^{-14}\ E_{\mathrm{h}}a_0^3$ is Fermi's weak coupling constant, $\imath = \sqrt{-1}$ is the imaginary unit, and the Dirac matrices in standard notation are defined as ($k = 1, 2, 3$)

$$\begin{aligned}\boldsymbol{\gamma}^0 &= \begin{pmatrix}\mathbf{1}_{2\times2} & \mathbf{0}_{2\times2}\\ \mathbf{0}_{2\times2} & -\mathbf{1}_{2\times2}\end{pmatrix}, \quad \boldsymbol{\gamma}^k = \begin{pmatrix}\mathbf{0}_{2\times2} & \boldsymbol{\sigma}^k\\ -\boldsymbol{\sigma}^k & \mathbf{0}_{2\times2}\end{pmatrix},\\ \boldsymbol{\gamma}^5 &= \begin{pmatrix}\mathbf{0}_{2\times2} & \mathbf{1}_{2\times2}\\ \mathbf{1}_{2\times2} & \mathbf{0}_{2\times2}\end{pmatrix}, \quad \boldsymbol{\Sigma}^k = \begin{pmatrix}\boldsymbol{\sigma}^k & \mathbf{0}_{2\times2}\\ \mathbf{0}_{2\times2} & \boldsymbol{\sigma}^k\end{pmatrix},\end{aligned} \tag{5}$$

with the vector of the Pauli spin matrices $\vec{\boldsymbol{\sigma}}$. For better readability we have dropped all electron indices on Dirac and Pauli matrices as these are in the present discussion only referred to as the electron with index i.

In this work the electronic structure parameters were calculated, using the corresponding quasirelativistic Hamiltonians within the zeroth order regular approximation (ZORA) [16,23,24]

$$\hat{H}_{\mathrm{s}}^{\mathrm{ZORA}} = \imath\sum_{i=1}^{N_{\mathrm{elec}}}\sum_{A=1}^{N_{\mathrm{nuc}}}Z_A[\rho_A(\vec{r}_i)\tilde{\omega}_{\mathrm{s}}(\vec{r}_i), \vec{\boldsymbol{\sigma}}\cdot\hat{\vec{p}}_i]_-, \tag{6}$$

$$\hat{H}_{\mathrm{d}}^{\mathrm{ZORA}} = \sum_{i=1}^{N_{\mathrm{elec}}}(\vec{\boldsymbol{\sigma}}\cdot\hat{\vec{p}}_i)\tilde{\omega}_{\mathrm{d}}(\vec{r}_i)\vec{\boldsymbol{\sigma}}\cdot\vec{\mathcal{E}}(\vec{r}_i)(\vec{\boldsymbol{\sigma}}\cdot\hat{\vec{p}}_i), \tag{7}$$

where $\hat{\vec{p}}$ is the linear momentum operator, $[A,B]_- = AB - BA$ is the commutator, and the modified ZORA factors are defined as

$$\tilde{\omega}_{\mathrm{s}}(\vec{r}_i) = \frac{G_{\mathrm{F}}k_{\mathrm{s}}c}{\sqrt{2}[2m_{\mathrm{e}}c^2 - \tilde{V}(\vec{r}_i)]}, \tag{8}$$

$$\tilde{\omega}_{\mathrm{d}}(\vec{r}_i) = \frac{2d_{\mathrm{e}}c^2}{[2m_{\mathrm{e}}c^2 - \tilde{V}(\vec{r}_i)]^2}\ , \tag{9}$$

with the model potential $\tilde{V}$ introduced by van Wüllen [25], which is used to alleviate the gauge dependence of ZORA. Here c is the speed of light in vacuum and m_e is the mass of the electron. The internal electrical field can be approximated as the field of the nuclei [16,22]:

$$\vec{\mathcal{E}}(\vec{r}_i) \approx \sum_{A=1}^{N_{\rm nuc}} k_{\rm es} Z_A e \frac{\vec{r}_i - \vec{r}_A}{|\vec{r}_i - \vec{r}_A|^3}, \tag{10}$$

with e being the elementary charge and the constant $k_{\rm es}$ being $(4\pi\epsilon_0)^{-1}$ in SI units with the electric constant ϵ_0.

For heavy elements, however, finite size effects of the nucleus can play a crucial role for the description of the internal electric field. The internal electrical field generated by a Gaussian shaped nucleus is described by

$$\vec{\mathcal{E}}(\vec{r}_i) \approx \sum_{A=1}^{N_{\rm nuc}} \frac{k_{\rm es} Z_A e}{|\vec{r}_i - \vec{r}_A|^2} \left[\frac{\mathrm{erf}(\sqrt{\zeta_A}|\vec{r}_i - \vec{r}_A|)}{|\vec{r}_i - \vec{r}_A|} - 2\left(\frac{\zeta_A}{\pi}\right)^{1/2} \exp(-\zeta_A |\vec{r}_i - \vec{r}_A|^2) \right] (\vec{r}_i - \vec{r}_A), \tag{11}$$

where $\zeta_A = \frac{3}{2r_{{\rm nuc},A}^2}$ and the root mean square radius $r_{{\rm nuc},A}$ of nucleus A was used as suggested by Visscher and Dyall [26].

An alternative expression for the eEDM interaction Hamiltonian, including two-electron interactions implicitly, denoted as stratagem II in Ref. [22], can be derived [27]:

$$\hat{H}_{\rm d,II} = \frac{2\imath c d_e}{\hbar e} \sum_{i=1}^{N_{\rm elec}} \boldsymbol{\gamma}^0 \boldsymbol{\gamma}^5 \hat{\vec{p}}_i^2. \tag{12}$$

In this form of the eEDM-Hamiltonian effects due to the finite size of the nuclei are considered implicitly, if the wave function of electrons moving in the potential of a finite nucleus is employed. The corresponding ZORA-Hamiltonian is given by [16]

$$\hat{H}_{\rm d,II}^{\rm ZORA} = \sum_{i=1}^{N_{\rm elec}} \left[\imath \hat{\vec{p}}_i^2 \omega_{\rm d,II}(\vec{r}_i)(\vec{\sigma}\cdot\hat{\vec{p}}_i) - \imath(\vec{\sigma}\cdot\hat{\vec{p}}_i)\omega_{\rm d,II}(\vec{r}_i)\hat{\vec{p}}_i^2 \right], \tag{13}$$

where the modified ZORA factor is defined as

$$\omega_{\rm d,II}(\vec{r}_i) = \frac{2 d_e c^2}{2e\hbar m_e c^2 - e\hbar\tilde{V}(\vec{r}_i)}. \tag{14}$$

Furthermore, the total angular momentum projection was calculated explicitly by

$$\Omega = \left(\langle \Psi_{\rm ZORA} | \sum_i \hat{\vec{\ell}}_i | \Psi_{\rm ZORA} \rangle + \frac{1}{2} \langle \Psi_{\rm ZORA} | \sum_i \vec{\sigma}_i | \Psi_{\rm ZORA} \rangle \right) \cdot \vec{\lambda}, \tag{15}$$

where $\hat{\vec{\ell}}_i$ is the reduced orbital angular momentum operator for electron i and $\Psi_{\rm ZORA}$ is the ZORA multielectron wave function.

B. Scaling relations of $\mathcal{P},\mathcal{T}$-odd properties

Within the relativistic Fermi-Segrè model for electronic wave functions [28] the matrix elements of the $\mathcal{P},\mathcal{T}$-odd operators can be obtained analytically for atomic systems [12,29]. The results for the $\mathcal{P},\mathcal{T}$-odd nucleon-electron current interactions can be expressed in terms of a relativistic enhancement factor

$$R(Z,A) = \frac{4}{\Gamma^2(2\gamma+1)} (2Z r_{\rm nuc}/a_0)^{2\gamma-2}, \tag{16}$$

where $\Gamma(z)$ is the gamma function, Z and A are the nuclear charge and mass numbers, respectively, $r_{\rm nuc} \approx 1.2\ \mathrm{fm}\, A^{1/3}$ is the nuclear radius, a_0 is the Bohr radius, and

$$\gamma = \sqrt{\left(j+\frac{1}{2}\right)^2 - (\alpha Z)^2}, \tag{17}$$

with the fine structure constant $\alpha \approx \frac{1}{137}$ and the total electronic angular momentum quantum number j.

In terms of the relativistic enhancement the parameters of the $\mathcal{P},\mathcal{T}$-odd spin-rotational Hamiltonian can now be estimated to behave as (see Ref. [12] for $W_{\rm s}$ and Refs. [11,30] for $W_{\rm d}$)

$$W_{\rm s} \approx -\frac{G_{\rm F}}{2\pi\sqrt{2}a_0^3} \underbrace{R(Z,A)\gamma}_{R_{\rm s}(Z,A)} Z^3 \alpha \varkappa, \tag{18}$$

$$W_{\rm d} \approx -\frac{4E_{\rm h}}{3e\,a_0} \underbrace{\frac{3}{\gamma(4\gamma^2-1)}}_{R_{\rm d,CS}(Z)} Z^3 \alpha^2 \varkappa, \tag{19}$$

where $\varkappa$ is a constant that depends on the effective electronic structure of the system under study. In relation (19) the label CS indicates that the factor was derived by Sandars [7] from a method by Casimir.

We note in passing that the relativistic enhancement factor of the eEDM induced permanent atomic EDM $R_{\rm d,CS}(Z)$ is the same as the one for hyperfine interactions published first by Racah in 1931 [31]: $R_{\rm d,CS}(Z) = R_{\rm hf,R}(Z)$. The denominator in relation (19) has two roots: one at $Z = \frac{\sqrt{j^2+j}}{\alpha}$ and one at $Z = \frac{\frac{1}{2}+j}{\alpha}$. Thus the relativistic enhancement factor causes problems not only for $Z > 137$ but diverges at $Z = \frac{\sqrt{3}}{2\alpha} \approx 118.65$ for ${}^2\Sigma_{1/2}$ states (see Fig. 1). This was also found by Dinh *et al.* in a study of hyperfine interactions in super heavy atoms [32]. These findings imply that relation (19) is of limited use to estimate $W_{\rm d}$ for elements with $Z > 100$.

An alternative relativistic enhancement factor for hyperfine interactions was found empirically by Fermi and Segrè [28,33], who interpolated numerically calculated data by Racah and Breit [31,34]:

$$R_{\rm hf,FS}(Z) = \frac{1}{\gamma^4}, \tag{20}$$

where the label FS was introduced referring to Fermi and Segrè. $R_{\rm hf,FS}(Z)$ has no singularities for $Z < 137$, and therefore no severe problems in the description of elements up to $Z \leqslant 118$ are expected. Furthermore, Eq. (20) can also be applied to estimate the eEDM enhancement, because the atomic

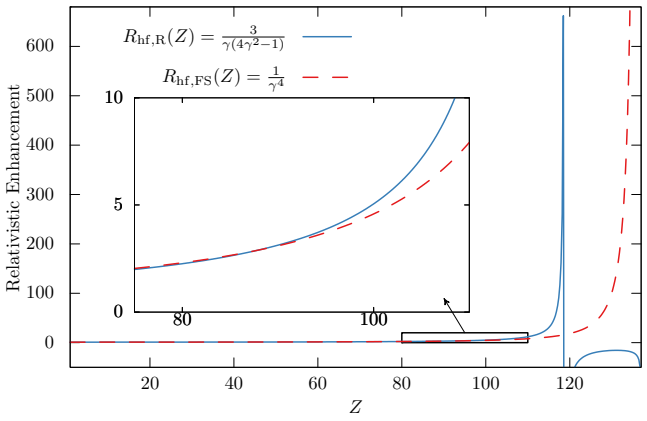

FIG. 1. Comparison of relativistic enhancement factors for eEDM induced permanent EDMs of atoms. Factor by Sandars derived analytically with Casimirs method (CS) and empirical factor for hyperfine interaction found by Fermi and Segrè (FS). Plots are shown for the case of $j = \frac{1}{2}$ as in $^2\Sigma_{1/2}$ states.

integrals relevant for the hyperfine structure and eEDM enhancement do not differ significantly within the Fermi-Segrè model and result in similar enhancement factors differing only by a factor of αZ (see also above and [7]):

$$R_{\mathrm{hf}}(Z) \sim \int dr\, r^{-2} g_0(r) f_0(r), \tag{21a}$$

$$R_{\mathrm{d}}(Z) \sim \int dr\, r^{-2} f_1(r) f_0(r), \tag{21b}$$

where g_ℓ and f_ℓ are the upper and lower component of the Dirac bispinor for a specific orbital angular quantum number ℓ, respectively. As $g_0(r)\alpha Z \approx f_1(r) +$ corrections, for hydrogenlike atoms, the integrals in Eqs. (21a) and (21b) are in a first approximation identical up to a factor of αZ. Thus the empirical factor (20) can be employed for our purposes (see also Fig. 1).

An improved relativistic enhancement factor for the $\mathcal{P},\mathcal{T}$-odd nucleon-electron current interaction parameter W_{s} was calculated with an analytical atomic model in [35]

$$W_{\mathrm{s}} \approx -\frac{G_{\mathrm{F}}}{2\pi\sqrt{2}a_0^3} Z^3 \alpha R(Z,A) f(Z) \frac{\gamma+1}{2} \varkappa, \tag{22}$$

with the Z-dependent function

$$f(Z) = \frac{1 - 0.56\alpha^2 Z^2}{(1 - 0.283\alpha^2 Z^2)^2}, \tag{23}$$

which results from a polynomial expansion of the atomic wave functions (see the Appendix of Ref. [35] for details).[1]

In Refs. [23,35] the eEDM enhancement parameter W_{d} was estimated from W_{s} by use of a relativistic enhancement factor for the ratio $W_{\mathrm{d}}/W_{\mathrm{s}}$ derived from Eqs. (22) and (19):

$$\tilde{R}_{\mathrm{CS}}(Z,A) = \frac{6}{\gamma(4\gamma^2-1)(\gamma+1) f(Z) R(Z,A)}. \tag{24}$$

In combination with summarized conversion factors and constant prefactors of W_{s} and W_{d}:

$$c_{\mathrm{conv}} = \frac{8\sqrt{2}\pi\alpha}{3\frac{G_{\mathrm{F}} e}{E_{\mathrm{h}} a_0^2}}, \tag{25}$$

an estimate for W_{d} is received from W_{s} via

$$W_{\mathrm{d}} \approx c_{\mathrm{conv}} \tilde{R}_{\mathrm{CS}}(Z,A) W_{\mathrm{s}}. \tag{26}$$

When relation (20) is used instead of (19), one obtains an alternative relativistic enhancement factor, which is expected to be more accurate for atoms with a high Z:

$$\tilde{R}_{\mathrm{FS}}(Z,A) = \frac{2}{\gamma^4(\gamma+1) R(Z,A) f(Z)}. \tag{27}$$

For comparison, instead of the improved relativistic factor for W_{s} [Eq. 22] relation (18) can be used to receive relativistic enhancement factors:

$$\tilde{\tilde{R}}_{\mathrm{CS}}(Z,A) = \frac{3}{\gamma^2(4\gamma^2-1) R(Z,A)}, \tag{28a}$$

$$\tilde{\tilde{R}}_{\mathrm{FS}}(Z,A) = \frac{1}{\gamma^5 R(Z,A)}. \tag{28b}$$

In the following discussion we will show that Eqs. (20) and (27) indeed agree much better with numerical calculations for $Z > 100$ than Eqs. (19) and (24), while there is no appreciable difference for molecules with lighter atoms.

C. Neglected many-electron effects in light molecules

In the approximation of the nuclear internal field [Eq. (10)] all $\mathcal{P},\mathcal{T}$-odd operators shown in Sec. II A are one-electron operators. Their expectation values scale with the nuclear charge number as Z^3. Thus these contributions are dominant in high-Z molecules. However, in light molecules many-electron effects with lower Z dependence stemming from the Hartree-Fock picture or the Breit interaction can have an important contribution to the enhancement factors, which we want to outline here for completeness, as our results reported for light molecules may be affected by this.

In the following we focus first on additional contributions in the Dirac-Hartree-Fock (DHF) picture that arise from the ZORA transformation. The DHF equation without magnetic fields and with perturbations (4) and (3) reads

$$\begin{pmatrix} \hat{V}_0(\vec{r})\mathbf{1}_{2\times2} - \hat{\mathbf{K}}_{\phi\phi} - \epsilon_i \mathbf{1}_{2\times2} & c\vec{\sigma}\cdot\hat{\vec{p}} - \hat{\mathbf{K}}_{\phi\chi} + \imath k_{\mathrm{s}} \frac{G_{\mathrm{F}}}{\sqrt{2}} \rho_{\mathrm{nuc}}(\vec{r})\mathbf{1}_{2\times2} \\ c\vec{\sigma}\cdot\hat{\vec{p}} - \hat{\mathbf{K}}_{\chi\phi} - \imath k_{\mathrm{s}} \frac{G_{\mathrm{F}}}{\sqrt{2}} \rho_{\mathrm{nuc}}(\vec{r})\mathbf{1}_{2\times2} & [\hat{V}_0(\vec{r}) - 2m_{\mathrm{e}}c^2]\mathbf{1}_{2\times2} - \hat{\mathbf{K}}_{\chi\chi} - \epsilon_i \mathbf{1}_{2\times2} + 2d_{\mathrm{e}}\vec{\sigma}\cdot\vec{\mathcal{E}}(\vec{r}) \end{pmatrix} \begin{pmatrix} \phi_i \\ \chi_i \end{pmatrix} = \begin{pmatrix} 0 \\ 0 \end{pmatrix}, \tag{29}$$

[1]The explicit numerical factors in $f(Z)$ were printed partially wrong in Ref. [35], which was mentioned in Ref. [23].

where ϕ_i and χ_i are the upper and lower components of the Dirac bispinor of orbital i, respectively, and ϵ_i is its orbital energy. The nuclear charge density is summarized as $\rho_{\text{nuc}}(\vec{r}) = \sum_{A=1}^{N_{\text{nuc}}} Z_A \rho_A(\vec{r})$ and $\hat{V}_0(\vec{r}) = \hat{V}_{\text{ext}}(\vec{r}) + \hat{V}_{\text{nuc}}(\vec{r}) + \hat{J}_{\phi\phi}(\vec{r}) + \hat{J}_{\chi\chi}(\vec{r})$ is the potential energy operator appearing on the diagonal, where $\hat{V}_{\text{ext}}$ and $\hat{V}_{\text{nuc}}$ are the external and nuclear potential energy operators, respectively. $\hat{J}_{\phi\phi}$ and $\hat{J}_{\chi\chi}$ are the direct parts and $\hat{\mathbf{K}}_{\phi\phi}$, $\hat{\mathbf{K}}_{\phi\chi}$, $\hat{\mathbf{K}}_{\chi\phi}$, $\hat{\mathbf{K}}_{\chi\chi}$ are the exchange parts that emerge from the two-electron Coulomb operator in DHF theory.

Whereas the direct Dirac-Coulomb contributions $\hat{J}_{\phi\phi}$ and $\hat{J}_{\chi\chi}$ are local and appear on the diagonal, the exchange contributions are nonlocal and nondiagonal

$$\hat{\mathbf{K}} = \begin{pmatrix} \hat{\mathbf{K}}_{\phi\phi} & \hat{\mathbf{K}}_{\phi\chi} \\ \hat{\mathbf{K}}_{\chi\phi} & \hat{\mathbf{K}}_{\chi\chi} \end{pmatrix}. \tag{30}$$

Thus when deriving an approximate relation between ϕ and χ, as when transforming into the ZORA picture, the exchange terms can result in additional contributions to the $\mathcal{P},\mathcal{T}$-odd enhancement.

We start our discussion with the scalar-pseudoscalar nucleon-electron current interaction Hamiltonian. The effective one-electron ZORA-Hamiltonian with this nucleon-electron current perturbation appears as

$$\begin{aligned} &\hat{h}_0^{\text{ZORA-HF}} + \hat{h}_{\text{s}}^{\text{ZORA-HF}} \\ &= \left(\vec{\boldsymbol{\sigma}} \cdot \hat{\vec{p}} - \frac{1}{c}\hat{\mathbf{K}}_{\phi\chi} + \imath k_{\text{s}} \frac{G_{\text{F}}}{c\sqrt{2}} \rho_{\text{nuc}} \mathbf{1}_{2\times 2}\right)\omega \\ &\quad \times \left(\vec{\boldsymbol{\sigma}} \cdot \hat{\vec{p}} - \frac{1}{c}\hat{\mathbf{K}}_{\chi\phi} - \imath k_{\text{s}} \frac{G_{\text{F}}}{c\sqrt{2}} \rho_{\text{nuc}} \mathbf{1}_{2\times 2}\right), \end{aligned} \tag{31}$$

where $\hat{h}_0^{\text{ZORA-HF}} = (\vec{\boldsymbol{\sigma}} \cdot \hat{\vec{p}} - \frac{1}{c}\hat{\mathbf{K}}_{\phi\chi})\omega(\vec{\boldsymbol{\sigma}} \cdot \hat{\vec{p}} - \frac{1}{c}\hat{\mathbf{K}}_{\chi\phi})$ is the unperturbed ZORA-Hamiltonian in the HF approximation and $\omega = \frac{c^2}{2m_{\text{e}}c^2 - \tilde{V}}$ is the ZORA factor with the model potential $\tilde{V}$. This results in additional correction terms to (6) stemming from the many-electron mean-field picture (only terms to first order in G_{F} are shown):

$$\Delta\hat{h}_{\text{s}}^{\text{ZORA-HF}} = \frac{1}{c}\rho_{\text{nuc}}\tilde{\omega}_{\text{s}}\hat{\mathbf{K}}_{\chi\phi} - \frac{1}{c}\hat{\mathbf{K}}_{\phi\chi}\tilde{\omega}_{\text{s}}\rho_{\text{nuc}}. \tag{32}$$

$\tilde{\omega}_{\text{s}}$ and the exchange operators $\hat{\mathbf{K}}_{\phi\chi}, \hat{\mathbf{K}}_{\chi\phi}$ are $O(\alpha)$, that is of order α, and therefore these correction terms are $O(\alpha^3)$, whereas the Hamiltonian defined in Eq. (3) is of first order in α.

We now focus on the eEDM interaction Hamiltonian. The ZORA transformation of the DHF operator using our method from [16] yields

$$\hat{h}_{\text{d}}^{\text{ZORA-HF}} = \left(\vec{\boldsymbol{\sigma}} \cdot \hat{\vec{p}} - \frac{1}{c}\hat{\mathbf{K}}_{\phi\chi}\right)(\tilde{\omega}_{\text{d}}\vec{\boldsymbol{\sigma}} \cdot \vec{\mathcal{E}})\left(\vec{\boldsymbol{\sigma}} \cdot \hat{\vec{p}} - \frac{1}{c}\hat{\mathbf{K}}_{\chi\phi}\right). \tag{33}$$

Thus many-electron mean-field correction terms to (7) are received as

$$\begin{aligned} \Delta\hat{h}_{\text{d}}^{\text{ZORA-HF}} = &-\frac{1}{c}\hat{\mathbf{K}}_{\phi\chi}\tilde{\omega}_{\text{d}}\vec{\boldsymbol{\sigma}} \cdot \vec{\mathcal{E}}\vec{\boldsymbol{\sigma}} \cdot \hat{\vec{p}} - \frac{1}{c}\vec{\boldsymbol{\sigma}} \cdot \hat{\vec{p}}\tilde{\omega}_{\text{d}}\vec{\boldsymbol{\sigma}} \cdot \vec{\mathcal{E}}\hat{\mathbf{K}}_{\chi\phi} \\ &+ \frac{1}{c^2}\hat{\mathbf{K}}_{\phi\chi}\tilde{\omega}_{\text{d}}\vec{\boldsymbol{\sigma}} \cdot \vec{\mathcal{E}}\hat{\mathbf{K}}_{\chi\phi}. \end{aligned} \tag{34}$$

The terms are sorted by their order in α. The first two terms are $O(\alpha^4)$ and the last term is $O(\alpha^6)$ and thus is suppressed. The first two terms are suppressed by a factor α^2 in comparison to the operator of Eq. (7). This is why the correction terms of Eqs. (32) and (34) have been neglected in the present study even when HF is used. For light elements, however, such terms can become more important, as has been shown, e.g., in Ref. [36].

In a density functional theory (DFT) picture none of the above terms $\Delta\hat{h}_{\text{d}}^{\text{ZORA-HF}}$, $\Delta\hat{h}_{\text{s}}^{\text{ZORA-HF}}$ arises if conventional nonrelativistic density functionals are used. Thus we would expect a larger deviation of HF-ZORA from DHF calculations than of Kohn-Sham (KS)-ZORA from Dirac-Kohn-Sham (DKS) calculations. However, if hybrid functionals are used as in our present paper, Fock exchange is considered explicitly and inclusion of the correction terms mentioned above may become necessary for light elements.

If the above discussed exchange terms become important, terms of comparatively low order in α, which have been neglected so far, may become important as well. These include the two-electron part of the internal electrical field

$$-\sum_{i<j}^{N_{\text{elec}}} k_{\text{es}} e\left(\boldsymbol{\gamma}_i^0 - \mathbf{1}_{2\times 2i}\right)\vec{\boldsymbol{\Sigma}}_i \cdot \frac{\vec{r}_i - \vec{r}_j}{|\vec{r}_i - \vec{r}_j|^3}\mathbf{1}_{2\times 2j}. \tag{35}$$

However, if the alternative effective one-electron form of the operator [Eq. (12)] is used, the two-electron contributions from the electric field can be included implicitly within a mean-field approach [27]. Our previous calculations [16] have shown that these effects are negligible. In our present study the effects for light molecules are below 5% and for super heavy elements below 1%, as can be seen in Sec. IV A, and are thus not important for the present discussion.

Another term of comparatively low order in α is the Breit contribution to the interaction with an eEDM, which was discussed in Ref. [22].

Additional corrections appear from the ZORA transformation, when the Breit interaction is considered, which appears as well on the off-diagonal elements of the Hamiltonian (see, e.g., [36]). These Breit interaction corrections appear for $\hat{H}_{\text{s}}$ as well.

For a more accurate calculation of the eEDM enhancement other magnetic terms $O(\alpha^2)$, which were neglected in the deviation in our previous paper [16], can play an important role as well and should be considered (see, e.g., [22]).

Beside the magnetic contributions, which stem from the interaction of the eEDM with the internal magnetic field [5], second order terms arising from hyperfine corrections to the wave function have to be considered. As the operators $\hat{H}_{\text{d,I}}$ and $\hat{H}_{\text{d,II}}$ arise from a transformation of the Dirac-Coulomb Hamiltonian, magnetic terms emerging from this transformation would have to be considered as well (for a detailed discussion see, e.g., [22]).

Furthermore, additional magnetic contributions arise from the ZORA transformation due to the vector potential appearing on the off-diagonal elements of the Hamiltonian matrix.

Regarding many-body effects of the operator itself, things would become more complicated in a DFT picture, where only one-electron operators are well defined. Whereas the direct contribution could be calculated analogously to HF, a

correction term to the exchange-correlation potential would appear and special exchange-correlation energy functionals would have to be designed. In case of hybrid DFT, additionally Fock exchange contributions would have to be computed. Herein, however, an inclusion of such correction terms is not attempted.

In our present calculations all these many-electron operators are neglected. In principle, this could cause a deviation from comparable four-component calculations, which becomes in relative terms more pronounced in light molecules than in high-Z molecules and is expected to originate mainly from the terms (32) and (34). But these are still expected to be small.

This concludes our general discussion of many-electron effects in light molecules and we will present in the following the computational details of our numerical studies.

III. COMPUTATIONAL DETAILS

Quasirelativistic two-component calculations are performed within ZORA at the level of complex generalized Hartree-Fock (cGHF) or Kohn-Sham (cGKS) with a modified version [16,37–40] of the quantum chemistry program package Turbomole [41]. In order to calculate the $\mathcal{P},\mathcal{T}$-odd properties, the program was extended with the corresponding ZORA Hamiltonians (see [16] for details on the implementation).

For Kohn-Sham (KS)-density functional theory (DFT) calculations the hybrid Becke three parameter exchange functional and Lee, Yang, and Parr correlation functional (B3LYP) [42–45] was employed. In comparison to relativistic coupled cluster calculations this functional performed well for the description of $\mathcal{P},\mathcal{T}$-odd effects in diatomic radicals in our previous work, which motivates the present choice [16].

For all calculations a basis set of 37 s, 34 p, 14 d, and 9 f uncontracted Gaussian functions with the exponential coefficients α_i composed as an even-tempered series by $\alpha_i = ab^{N-i}; i = 1,\ldots,N$, with $b = 2$ for s and p function and with $b = (5/2)^{1/25} \times 10^{2/5} \approx 2.6$ for d and f functions was used for the electropositive atom (for details see the Supplemental Material [46]).[2] This basis set has proven successful in calculations of nuclear-spin dependent $\mathcal{P}$-violating interactions and $\mathcal{P},\mathcal{T}$-odd effects induced by an eEDM in heavy polar diatomic molecules [16,23,39,47]. The N, F, and O atoms were represented with a decontracted atomic natural orbital (ANO) basis set of triple-ζ quality [48] and for H the s,p subset of a decontracted correlation-consistent basis of quadruple-ζ quality [49] was used.

The ZORA-model potential $\tilde{V}(\vec{r})$ was employed with additional damping [50] as proposed by van Wüllen [25].

The model potential of O g, the element with highest Z of all known elements [51], was renormalized to the nuclear charge number of E120 and E121. These renormalized model potentials were employed in all calculations of molecules containing E120 and E121, respectively.

For calculations of two-component wave functions and properties a finite nucleus was used, described by a normalized spherical Gaussian nuclear density distribution $\rho_A(\vec{r}) = \frac{\zeta_A^{3/2}}{\pi^{3/2}} e^{-\zeta_A|\vec{r}-\vec{r}_A|^2}$. The mass numbers A were chosen as nearest integer to the standard relative atomic mass, i.e., ^{11}B, ^{24}Mg, ^{27}Al, ^{40}Ca, ^{45}Sc, ^{48}Ti, ^{65}Zn, ^{70}Ga, ^{88}Sr, ^{90}Y, ^{91}Zr, ^{112}Cd, ^{115}In, ^{137}Ba, ^{139}La, ^{140}Ce, ^{173}Yb, ^{175}Lu, ^{178}Hf, ^{201}Hg, ^{204}Tl, ^{226}Ra, ^{227}Ac, ^{232}Th, ^{259}No, ^{260}Lr, ^{261}Rf, ^{284}Cn; for E120 (unbinilium, Ubn, eka-actinium) and E121 (unbiunium, Ubu, eka-radium) the mass number was calculated by $2.5Z$, resulting in 300 and 303, respectively.

The nuclear equilibrium distances were obtained at the levels of GHF-ZORA and GKS-ZORA/B3LYP, respectively. As convergence criteria an energy change of less than $10^{-5}\ E_h$ was used. For DFT calculations of analytic energy gradients with respect to the displacement of the nuclei the nuclei were approximated as point charges. The equilibrium distances obtained are given in the Results section.

IV. RESULTS AND DISCUSSION

A. Numerical calculation of $\mathcal{P},\mathcal{T}$-violating properties

In this section the study of quite a number of diatomic molecules with $^2\Sigma_{1/2}$-ground state or for which at least a $^2\Sigma_{1/2}$-ground state can be expected, is presented. The set of molecules includes group 2 monofluorides (Mg–E120)F, group 3 mono-oxides (Sc–E121)O, group 4 mononitrides (Ti–Rf)N, group 12 monohydrides (Zn–Cn)H, group 13 monooxides (B–Tl)O, and the mononitrides (Ce–Th)N, monofluorides (Yb–No)F, and mono-oxides (Lu–Lr)O of some f-block groups, respectively.

The numerically calculated values of symmetry violating properties are presented for the listed molecules together with deviations between the methods cGHF and cGKS/B3LYP in Table I. The calculated equilibrium bond length r_e and numerical values of the reduced total electronic angular momentum projection quantum number Ω are shown as well.

The equilibrium bond lengths and values of Ω determined with GHF and GKS are typically in reasonable agreement. Large deviations in the bond length of about 0.1 a_0 are observed for LaO, YbF, and group 13 oxides excluding BO, indicating a more complicated electronic structure. Nearly all values of Ω are approximately equal to $\pm\frac{1}{2}$. Furthermore, in nearly all cases the reduced orbital angular momentum projection was $\Lambda \approx 0$ and thus there appears no significant contamination by Π states. Exceptions are CnH and RfN as well as TiN, which show large electron correlation effects (as gauged by the difference GHF-GKS) and seem to have a complicated electronic structure that requires more advanced electronic structure methods for a reliable description.

In the case of CnH the angular momentum projection quantum number was $\Omega = 0.5$, but some admixture of higher angular momentum states was found ($\Lambda \approx 0.14$). However, in the case of RfN and TiN $\Lambda \approx 0$ is valid and there was no significant admixture of Π contributions.

Especially in the case of RfN the methods employed herein are not able to give reliable results, indicated by enormous

[2]For the calculation of row 8 compounds the basis set was augmented with more diffuse functions and a set of g functions. However, these showed no remarkable influence on $\mathcal{P},\mathcal{T}$-odd properties and thus the results for the same basis set as for the other elements are presented.

TABLE I. Diatomic constants and $\mathcal{P},\mathcal{T}$-violating properties of diatomic molecules calculated *ab initio* within a quasirelativistic two-component ZORA approach at the cGHF and cGKS/B3LYP level. Dev. refers to the relative deviation $|\frac{W_{\mathrm{cGHF}}-W_{\mathrm{cGKS}}}{W_{\mathrm{cGHF}}}|$ between cGHF and cGKS results.

		r_e/a_0		Ω[a]		$W_s \frac{1}{h\,\mathrm{Hz}}$			$W_d \frac{e\,\mathrm{cm}}{10^{24}\,h\,\mathrm{Hz}}$		
Molecule	Z	cGHF	cGKS	cGHF	cGKS	cGHF	cGKS	Dev.	cGHF	cGKS	Dev.
group 2 fluorides											
MgF	12	3:28	3:33	0.500	0.500	-5.93×10^{1}	-6.48×10^{1}	9%	-4.66×10^{-2}	-5.22×10^{-2}	12%
CaF	20	3.74	3.68	0.500	0.500	-2.19×10^{2}	-2.09×10^{2}	5%	-1.47×10^{-1}	-1.40×10^{-1}	4%
SrF	38	3.98	3.94	−0.500	0.500	-2.01×10^{3}	-1.94×10^{3}	4%	−1.05	−1.01	3%
BaF	56	4.16	4.11	0.500	0.500	-8.67×10^{3}	-7.58×10^{3}	13%	−3.32	−2.90	12%
RaF	88	4.30	4.26	−0.500	−0.500	-1.52×10^{5}	-1.36×10^{5}	10%	-2.80×10^{1}	-2.51×10^{1}	10%
E120F	120	4.37	4.36	0.500	0.499	-3.98×10^{6}	-3.45×10^{6}	13%	-3.49×10^{2}	-3.02×10^{2}	14%
group 3 oxides											
ScO	21	3.15	3.14	0.500	0.500	-3.65×10^{2}	-2.83×10^{2}	22%	-2.42×10^{-1}	-1.87×10^{-1}	23%
YO	39	3.37	3.39	0.500	0.500	-3.04×10^{3}	-2.54×10^{3}	17%	−1.58	−1.32	17%
LaO	57	3.60	3.46	0.500	0.500	-1.30×10^{4}	-1.01×10^{4}	22%	−4.82	−3.76	22%
AcO	89	3.64	3.67	0.500	−0.500	-2.42×10^{5}	-1.94×10^{5}	20%	-4.34×10^{1}	-3.49×10^{1}	20%
E121O	121	3.82	3.87	−0.500	0.500	-7.41×10^{6}	-4.94×10^{6}	33%	-6.36×10^{2}	-4.24×10^{2}	33%
group 4 nitrides											
TiN	22	2.94	2.94	0.358	0.358	-6.80×10^{2}	-3.18×10^{2}	53%	-4.37×10^{-1}	-2.06×10^{-1}	53%
ZrN	40	3.11	3.19	0.492	0.492	-3.96×10^{3}	-2.68×10^{3}	32%	−2.00	−1.37	32%
HfN	72	3.30	3.26	0.500	0.500	-1.09×10^{5}	-5.79×10^{4}	47%	-2.93×10^{1}	-1.58×10^{1}	46%
RfN[b]	104	3.55	3.48	(−0.500)	(−0.500)	(2.04×10^{6})	(1.60×10^{5})	92%	(2.51×10^{2})	(1.70×10^{1})	93%
f-block nitrides											
CeN	58	3.29	3.26	0.500	0.500	-1.65×10^{4}	-1.18×10^{4}	28%	−5.94	−4.32	27%
ThN	90	3.41	3.44	0.500	0.500	-3.50×10^{5}	-2.64×10^{5}	25%	-6.10×10^{1}	-4.62×10^{1}	24%
f-block uorides											
YbF	70	3.90	3.76	0.500	0.489	-4.12×10^{4}	-3.46×10^{4}	16%	-1.16×10^{1}	−9.69	16%
NoF	102	3.96	3.92	0.500	−0.500	-7.37×10^{5}	-7.38×10^{5}	0%	-9.65×10^{1}	-9.65×10^{1}	0%
f-block oxides											
LuO	71	3.41	3.39	0.500	0.500	-6.57×10^{4}	-5.59×10^{4}	15%	-1.81×10^{1}	-1.55×10^{1}	15%
LrO	103	3.51	3.53	−0.500	−0.500	-1.22×10^{6}	-9.38×10^{5}	23%	-1.56×10^{2}	-1.21×10^{2}	23%
group 12 hydrides											
ZnH	30	3.05	3.04	−0.500	−0.500	-2.03×10^{3}	-1.94×10^{3}	4%	−1.14	−1.09	4%
CdH	48	3.36	3.38	0.500	0.500	-1.51×10^{4}	-1.32×10^{4}	12%	−6.35	−5.59	12%
HgH	80	3.30	3.33	0.500	0.500	-3.77×10^{5}	-2.63×10^{5}	30%	-7.98×10^{1}	-5.60×10^{1}	30%
CnH	112	3.04	3.13	0.500	−0.500	-8.51×10^{6}	-5.26×10^{6}	38%	-8.69×10^{2}	-5.38×10^{2}	38%
group 13 oxides											
BO	5	2.23	2.27	−0.500	−0.500	8.88	9.31	5%	9.42×10^{-3}	1.05×10^{-2}	12%
AlO	13	3.17	3.07	0.500	0.500	-5.59×10^{1}	-1.17×10^{2}	109%	-2.12×10^{-2}	-7.91×10^{-2}	272%
GaO	31	3.37	3.24	0.500	0.500	-1.45×10^{3}	-2.15×10^{3}	48%	-7.72×10^{-1}	−1.17	51%
InO	49	3.79	3.67	−0.500	−0.500	-9.25×10^{3}	-1.09×10^{4}	18%	−3.75	−4.45	19%
TlO	81	4.09	3.86	0.500	0.500	-2.35×10^{5}	-1.63×10^{5}	30%	-4.92×10^{1}	-3.42×10^{1}	31%

[a]The absolute sign of Ω is arbitrary. However, relative to the sign of the effective electric field $W_d\Omega$ it is always such that $\mathrm{sgn}(W_d) = -1$. Exceptions from this (RfN and BO) are discussed in the text.
[b]No reliable results could be obtained for RfN.

differences (by an order of magnitude in the case of the $\mathcal{P},\mathcal{T}$-odd parameters) between DFT and HF calculations, not only for properties but also for the ordering and pairing of molecular spin orbitals. The values given for RfN are only included for completeness, but are not to be considered as estimates of the expected effect sizes. Therefore, results for RfN are omitted in the plots presented below.

In Table II deviations between results obtained with the Hamiltonian in Eq. (7) and those computed with the Hamiltonian of Eq. (13) are shown for all molecules that are content of our paper (except RfN). This table shows that deviations between stratagem I and II are only in molecules containing super heavy elements noteworthy but remain always below 10% and thus are not important for the present discussion.

Furthermore, calculations with an internal electric field stemming from explicitly Gaussian shaped nuclei are compared to results of calculations with an internal electric field that stems from a pointlike nucleus in Table II.

TABLE II. Differences of $\mathcal{P},\mathcal{T}$-odd eEDM enhancement in diatomic molecules in a $^2\Sigma_{1/2}$-ground state between different forms of the interaction operator calculated *ab initio* within a quasirelativistic two-component ZORA approach at the cGHF and cGKS/B3LYP level. Relative difference $\Delta_{\mathrm{I/II}} = |\frac{W_{\mathrm{d,I}} - W_{\mathrm{d,II}}}{W_{\mathrm{d,II}}}|$ between strategem I [Eq. (7)] and II [Eq. (13)] and $\Delta_{\mathrm{IG/II}} = |\frac{W_{\mathrm{d,I,Gauß}} - W_{\mathrm{d,II}}}{W_{\mathrm{d,II}}}|$ between strategem I with internal electric field of a Gaussian shaped nucleus [Eq. (11)] and II [Eq. (13)].

		$W_{\mathrm{d}}^{\mathrm{cGHF}}\ \frac{e\,\mathrm{cm}}{10^{24}\,h\,\mathrm{Hz}}$					$W_{\mathrm{d}}^{\mathrm{cGKS}}\ \frac{e\,\mathrm{cm}}{10^{24}\,h\,\mathrm{Hz}}$				
Molecule	Z	$W_{\mathrm{d,I}}$	$W_{\mathrm{d,I,Gauß}}$	$W_{\mathrm{d,II}}$	$\Delta_{\mathrm{I/II}}$	$\Delta_{\mathrm{IG/II}}$	$W_{\mathrm{d,I}}$	$W_{\mathrm{d,I,Gauß}}$	$W_{\mathrm{d,II}}$	$\Delta_{\mathrm{I/II}}$	$\Delta_{\mathrm{IG/II}}$
				group 2 fluorides							
MgF	12	-4.66×10^{-2}	-4.69×10^{-2}	-4.56×10^{-2}	2%	3%	-5.22×10^{-2}	-5.26×10^{-2}	-5.12×10^{-2}	2%	3%
CaF	20	-1.47×10^{-1}	-1.48×10^{-1}	-1.44×10^{-1}	2%	2%	-1.40×10^{-1}	-1.41×10^{-1}	-1.38×10^{-1}	2%	2%
SrF	38	-1.05	-1.06	-1.04	1%	2%	-1.01	-1.02	-1.00	1%	2%
BaF	56	-3.32	-3.33	-3.28	1%	1%	-2.90	-2.91	-2.87	1%	1%
RaF	88	-2.80×10^{1}	-2.76×10^{1}	-2.73×10^{1}	3%	1%	-2.51×10^{1}	-2.47×10^{1}	-2.44×10^{1}	3%	1%
E120F	120	-3.49×10^{2}	-3.23×10^{2}	-3.20×10^{2}	8%	1%	-3.02×10^{2}	-2.79×10^{2}	-2.76×10^{2}	8%	1%
				group 3 oxides							
ScO	21	-2.42×10^{-1}	-2.44×10^{-1}	-2.38×10^{-1}	2%	2%	-1.87×10^{-1}	-1.89×10^{-1}	-1.84×10^{-1}	2%	2%
YO	39	-1.58	-1.59	-1.56	1%	2%	-1.32	-1.32	-1.30	1%	2%
LaO	57	-4.82	-4.83	-4.76	1%	1%	-3.76	-3.76	-3.71	1%	1%
AcO	89	-4.34×10^{1}	-4.27×10^{1}	-4.22×10^{1}	3%	1%	-3.49×10^{1}	-3.43×10^{1}	-3.39×10^{1}	3%	1%
E121O	121	-6.36×10^{2}	-5.86×10^{2}	-5.80×10^{2}	9%	1%	-4.24×10^{2}	-3.90×10^{2}	-3.87×10^{2}	9%	1%
				group 4 nitrides							
TiN	22	-4.37×10^{-1}	-4.40×10^{-1}	-4.30×10^{-1}	1%	2%	-2.06×10^{-1}	-2.08×10^{-1}	-2.03×10^{-1}	2%	2%
ZrN	40	-2.00	-2.01	-1.98	1%	2%	-1.37	-1.37	-1.35	1%	2%
HfN	72	-2.93×10^{1}	-2.92×10^{1}	-2.89×10^{1}	2%	1%	-1.58×10^{1}	-1.58×10^{1}	-1.56×10^{1}	2%	1%
				f-block nitrirides							
CeN	58	-5.94	-5.95	-5.87	1%	1%	-4.32	-4.33	-4.27	1%	1%
ThN	90	-6.10×10^{1}	-5.98×10^{1}	-5.92×10^{1}	3%	1%	-4.62×10^{1}	-4.53×10^{1}	-4.49×10^{1}	3%	1%
				f-block uorides							
YbF	70	-1.16×10^{1}	-1.15×10^{1}	-1.14×10^{1}	2%	1%	-9.69	-9.65	-9.55	1%	1%
NoF	102	-9.65×10^{1}	-9.32×10^{1}	-9.23×10^{1}	4%	1%	-9.65×10^{1}	-9.32×10^{1}	-9.22×10^{1}	4%	1%
				f-block oxides							
LuO	71	-1.81×10^{1}	-1.81×10^{1}	-1.79×10^{1}	2%	1%	-1.55×10^{1}	-1.54×10^{1}	-1.52×10^{1}	2%	1%
LrO	103	-1.56×10^{2}	-1.50×10^{2}	-1.49×10^{2}	5%	1%	-1.21×10^{2}	-1.16×10^{2}	-1.15×10^{2}	5%	1%
				group 12 hydrides							
ZnH	30	-1.14	-1.15	-1.13	1%	1%	-1.09	-1.10	-1.09	1%	1%
CdH	48	-6.35	-6.38	-6.30	1%	1%	-5.59	-5.61	-5.55	1%	1%
HgH	80	-7.98×10^{1}	-7.90×10^{1}	-7.83×10^{1}	2%	1%	-5.60×10^{1}	-5.54×10^{1}	-5.49×10^{1}	2%	1%
CnH	112	-8.69×10^{2}	-8.20×10^{2}	-8.13×10^{2}	6%	1%	-5.38×10^{2}	-5.08×10^{2}	-5.04×10^{2}	6%	1%
				group 13 oxides							
BO	5	9.42×10^{-3}	9.50×10^{-3}	9.19×10^{-3}	2%	3%	1.05×10^{-2}	1.06×10^{-2}	1.02×10^{-2}	3%	4%
AlO	13	-2.12×10^{-2}	-2.14×10^{-2}	-2.11×10^{-2}	1%	2%	-7.91×10^{-2}	-7.97×10^{-2}	-7.77×10^{-2}	2%	3%
GaO	31	-7.72×10^{-1}	-7.77×10^{-1}	-7.68×10^{-1}	1%	1%	-1.17	-1.18	-1.16	1%	1%
InO	49	-3.75	-3.76	-3.72	1%	1%	-4.45	-4.46	-4.41	1%	1%
TlO	81	-4.92×10^{1}	-4.87×10^{1}	-4.82×10^{1}	2%	1%	-3.42×10^{1}	-3.38×10^{1}	-3.35×10^{1}	2%	1%

A comparison with enhancement factors calculated with the internal electric field of a Gaussian nucleus shows that deviations between stratagem I and stratagem II in heavy nuclei stem solely from the finite size of the nucleus, which is implicitly included in the Hamiltonian of stratagem II. As expected, two-electron effects are larger than 1% for light elements only.

Returning again to the results obtained with the Hamiltonian of Eq. (7), we can observe large deviations between GHF and GKS values of W_{d} and W_{s} for some of the group 13 oxides (especially AlO and GaO). These indicate that there are electron correlation effects which cannot accurately be described by the present approaches. In these compounds also large spin-polarization effects could be observed. Especially for AlO more sophisticated electronic structure methods should be applied, if higher accuracy is desired. Nonetheless, for the present discussion of overall trends the description within the cGHF/cGKS scheme appears to suffice.

Generally the agreement between the HF and DFT descriptions is within 20% to 30%. Yet, in cases where d orbitals play an important role, such as group 4 nitrides or group 12 hydrides, additional electron correlation considered via the

DFT method has a pronounced impact on the value of the $\mathcal{P},\mathcal{T}$-odd properties. In case of mercury monofluoride these effects where already discussed in Ref. [16].

The two parameters W_d and W_s behave analogously with respect to inclusion of additional electron correlation effects when going along the periodic table.

The largest enhancement of $\mathcal{P},\mathcal{T}$-odd effects can be found in compounds of the seventh and eighth row of the periodic table, i.e., RaF, AcO, ThN, NoF, LrO, (RfN), CnH, E120F, and E121O. But also some compounds of the sixth row show enhancement of a similar of magnitude, namely HfN, HgH, TlO, YbF, and LuO. It shall be noted that even the exotic molecule CnH may be a candidate for future experiments, since ongoing research aims to achieve very long lived isotopes for the super heavy element Cn [52–54].

The investigation of $\mathcal{P},\mathcal{T}$-violation in group 13 oxides shows problems for the methods employed herein, as mentioned above. As comparatively large enhancement effects were calculated for TlO, a study of this molecule with more sophisticated electronic structure methods could be interesting in order to obtain an accurate description of its electronic structure. Little is known about TlO from the experimental side, however, so that significant further research would be necessary to take advantage of such enhancement effects.

B. Estimation of $\mathcal{P},\mathcal{T}$-violating properties from atomic scaling relations

In order to gain deeper insight into the scaling behavior of the above discussed properties the numerical results can be compared to analytical and empirical atomic models. Using the relations presented in the theory section [Eqs. (24) and (27)] within the quasirelativistic GHF/GKS-ZORA approach the parameter W_d is estimated from W_s and compared to the results of the numerical calculations.

Results for estimations of W_d from W_s for both the analytically derived expression by Sandars and the empirical factor found by Fermi and Segrè are shown in Table III, where again the labels FS and CS are used for properties calculated with the corresponding factors $\tilde{R}_{CS}$ and $\tilde{R}_{FS}$.

Relative deviations of the estimated $\mathcal{P},\mathcal{T}$-odd property W_d from the numerical calculations are typically below 10% for molecules with $Z < 100$. For light molecules of the first (BO) or second row (MgF, AlO) the deviations are much larger. In this region the atomic models do not work well. For these cases with light elements both the analytically derived CS equation and the empirical FS relation yield much too low (BO, AlO) or too high (MgF) values of W_d. It has to be pointed out that the case of BO is somewhat special, since boron is even lighter than oxygen and the "heavy" atom of this molecule is actually oxygen. By this also the sign of the $\mathcal{P},\mathcal{T}$-odd properties W_d and W_s is reversed and a different behavior than for all other group 13 compounds is expected.

In the region of super heavy elements ($Z > 100$) the abruptly rising analytically derived relativistic enhancement factor of the eEDM (reaching infinity at $Z \sim 118.65$) causes a large overestimation of W_d resulting in deviations of $\geqslant$35% for NoF ($Z = 102$) and LrO ($Z = 103$) and 146% for CnH ($Z = 112$) between the estimate and the numerical value. Here the empirical factor performs much better and a much lower increase in the deviation from the numerical calculations can be observed. However, even in the case of the empirically obtained relativistic enhancement factor the $\mathcal{P},\mathcal{T}$-odd enhancement in super heavy element compounds is strongly overestimated (deviations $\gg$10%) with these simple atomic models. This may be explained with the influence of the pole at $Z > 137$ of the used relativistic enhancement factors.

For the two studied compounds with $Z > 118$ the analytically derived factor is not applicable anymore, which results in deviations far beyond 500%, whereas the estimates obtained with the empirical factor deviate still less than 100% from numerical calculations. Nonetheless, the influence of the pole at $Z = 137$ of the relativistic enhancement factors for eEDM induced permanent molecular EDMs and scalar-pseudoscalar nucleon-electron current interactions causes deviations >10%.

C. Ratio of $\mathcal{P},\mathcal{T}$-violating properties

Various $\mathcal{P},\mathcal{T}$-odd parameters contribute to a permanent EDM in a molecule. In order to set limits on more than one parameter, experiments with different sensitivity to the $\mathcal{P},\mathcal{T}$-odd parameters have to be compared (for a detailed discussion see Refs. [55] or [56]).

In the following we numerically determine the trends of the ratio of $\mathcal{P},\mathcal{T}$-odd enhancement parameters in the periodic table and analyze how the sensitivity of an experiment to the herein discussed $\mathcal{P},\mathcal{T}$-odd effects d_e and k_s is influenced by the choice of the molecule.

As pointed out in Sec. II B, Dzuba *et al.* proposed an analytical model [Eq. (24)] for determination of the ratio W_d/W_s in atoms and diatomic molecules [35]. In their paper, however, its applicability was not generally tested for diatomic molecules, but only for the example of YbF. In the following we compare the analytical model of Ref. [35], with the improved version (27) and compare them to our numerical calculations.

The ratio W_d/W_s of the various open-shell diatomic molecules is studied, for which both the analytically derived and the empirically derived relativistic enhancement factors presented in Sec. II are compared. In Fig. 2 the ratio W_d/W_s calculated with the four different relativistic enhancement factors $\tilde{R}$ [Eqs. (24)–(28b)] is compared to all numerical results for the value of W_d/W_s. The empirically derived relativistic enhancement factor for W_d included in Eqs. (27) and (28b) is in much better agreement with the numerical results for $Z > 90$ as was also seen in the last section in the comparison of estimates of W_d with numerical values. Furthermore, values calculated with the improved relativistic enhancement factor for W_s [Eq. (22)] are in better agreement with numerical values also for $Z \ll 90$.

However, all the ratios derived from the analytical models show a wrong behavior in the region of $Z < 30$ and $Z > 90$ in comparison to the numerical results. This causes large deviations for the estimates discussed in the last section.

A logarithmic plot of the numerical results (see Fig. 3) shows an exponential behavior of the ratio of $\mathcal{P},\mathcal{T}$-odd properties W_d/W_s, which can be interpolated by a linear fit model

TABLE III. eEDM enhancement parmeter W_d of diatomic molecules estimated from numerically calculated $\mathcal{P},\mathcal{T}$-odd interaction parameter W_s via an analytical and an empirical relation from atomic considerations and comparison to numerical results. $\Delta_{CS/FS} = |\frac{W_d - W_{d,CS/FS}}{W_d}|$ refers to the relative deviation of estimates with respect to numerical calculations.

		cGHF				cGKS			
Molecule	Z	$W_{d,CS}\,\frac{e\,cm}{10^{24}\times h\,Hz}$	Δ_{CS}	$W_{d,FS}\,\frac{e\,cm}{10^{24}\times h\,Hz}$	Δ_{FS}	$W_{d,CS}\,\frac{e\,cm}{10^{24}\times h\,Hz}$	Δ_{CS}	$W_{d,FS}\,\frac{e\,cm}{10^{24}\times h\,Hz}$	Δ_{FS}
				group 2 fluorides					
MgF	12	-4.2×10^{-2}	11%	-4.2×10^{-2}	11%	-4.5×10^{-2}	13%	-4.5×10^{-2}	13%
CaF	20	-1.4×10^{-1}	3%	-1.4×10^{-1}	2%	-1.4×10^{-1}	3%	-1.4×10^{-1}	3%
SrF	38	-1.0	1%	-1.0	0%	-10.0×10^{-1}	2%	-1.0	0%
BaF	56	-3.2	3%	-3.3	0%	-2.8	3%	-2.9	0%
RaF	88	-3.0×10^{1}	8%	-3.0×10^{1}	8%	-2.7×10^{1}	8%	-2.7×10^{1}	8%
E120F	120	-3.1×10^{3}	981%	-6.1×10^{2}	75%	-2.7×10^{3}	983%	-5.3×10^{2}	76%
				group 3 oxides					
ScO	21	-2.4×10^{-1}	2%	-2.4×10^{-1}	2%	-1.8×10^{-1}	2%	-1.8×10^{-1}	2%
YO	39	-1.5	3%	-1.6	1%	-1.3	3%	-1.3	1%
LaO	57	-4.7	2%	-4.8	1%	-3.7	2%	-3.8	1%
AcO	89	-4.8×10^{1}	9%	-4.7×10^{1}	9%	-3.8×10^{1}	9%	-3.8×10^{1}	9%
E121O	121	-3.1×10^{3}	582%	-1.2×10^{3}	84%	-2.0×10^{3}	582%	-7.8×10^{2}	84%
				group 4 nitrides					
TiN	22	-4.4×10^{-1}	0%	-4.4×10^{-1}	0%	-2.0×10^{-1}	1%	-2.0×10^{-1}	1%
ZrN	40	-2.0	2%	-2.0	0%	-1.3	2%	-1.4	1%
HfN	72	-2.9×10^{1}	1%	-3.0×10^{1}	3%	-1.6×10^{1}	1%	-1.6×10^{1}	1%
RfN[a]	104	(3.7×10^{2})	47%	(3.1×10^{2})	23%	(2.9×10^{1})	70%	(2.4×10^{1})	43%
				f-block nitrides					
CeN	58	-5.9	1%	-6.0	2%	-4.2	2%	-4.3	0%
ThN	90	-6.8×10^{1}	11%	-6.7×10^{1}	10%	-5.1×10^{1}	11%	-5.1×10^{1}	10%
				f-block uorides					
YbF	70	-1.2×10^{1}	0%	-1.2×10^{1}	3%	-9.7	0%	-10.0	3%
NoF	102	-1.3×10^{2}	35%	-1.1×10^{2}	19%	-1.3×10^{2}	36%	-1.1×10^{2}	19%
				f-block oxides					
LuO	71	-1.8×10^{1}	0%	-1.9×10^{1}	2%	-1.5×10^{1}	1%	-1.6×10^{1}	2%
LrO	103	-2.2×10^{2}	39%	-1.9×10^{2}	20%	-1.7×10^{2}	39%	-1.4×10^{2}	20%
				group 12 hydrides					
ZnH	30	-1.2	3%	-1.2	4%	-1.1	3%	-1.1	4%
CdH	48	-6.5	3%	-6.7	5%	-5.7	2%	-5.8	4%
HgH	80	-8.7×10^{1}	9%	-8.8×10^{1}	11%	-6.0×10^{1}	8%	-6.2×10^{1}	10%
CnH	112	-2.1×10^{3}	146%	-1.2×10^{3}	41%	-1.3×10^{3}	146%	-7.6×10^{2}	40%
				group 13 oxides					
BO	5	6.5×10^{-3}	31%	6.5×10^{-3}	31%	6.8×10^{-3}	36%	6.8×10^{-3}	36%
AlO	13	-3.9×10^{-2}	83%	-3.9×10^{-2}	83%	-8.1×10^{-2}	3%	-8.1×10^{-2}	3%
GaO	31	-8.3×10^{-1}	8%	-8.4×10^{-1}	9%	-1.2	5%	-1.2	6%
InO	49	-3.9	5%	-4.0	7%	-4.6	4%	-4.7	6%
TlO	81	-5.3×10^{1}	8%	-5.4×10^{1}	9%	-3.7×10^{1}	8%	-3.8×10^{1}	10%

[a] No reliable results could be obtained for RfN.

with

$$\log_{10}\left\{\left|\frac{W_d}{W_s}\right|\times10^{-21}\,e\,cm\right\} = qZ + p. \tag{36}$$

In this plot Fig. 3 also results in calculations reported by Fleig for the two molecules HfF^+ and ThO, where a $^3\Delta$ state is of relevance for experiments, are included [57]. It can be inferred that the ratio W_d/W_s is rather insensitive to the chemical environment of the heavy nucleus, but is essentially determined by the exponential Z dependence determined in Fig. 3.

In order to disentangle the $\mathcal{P},\mathcal{T}$-odd parameters k_s and d_e, at least two experiments with molecules 1 and 2 are needed. The measurement model then is a 2×2-matrix problem described by the system of equations

$$h\begin{pmatrix}\nu_1\\ \nu_2\end{pmatrix} = \Omega\underbrace{\begin{pmatrix}W_{d,1} & W_{s,1}\\ W_{d,2} & W_{s,2}\end{pmatrix}}_{\mathbf{C}}\begin{pmatrix}d_e\\ k_s\end{pmatrix}, \tag{37}$$

where $\mathbf{C}$ is the matrix of sensitivity coefficients. We follow now Ref. [58] in order to describe the uncertainties and

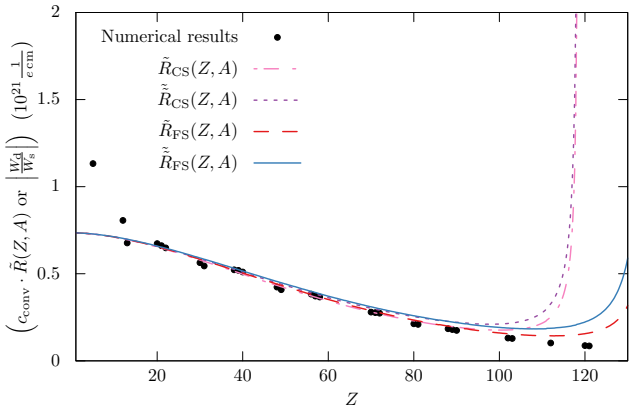

FIG. 2. Comparison of combined relativistic enhancement factors and conversion factors for the ratio between $\mathcal{P},\mathcal{T}$-odd eEDM and nucleon-electron current interactions $W_{\mathrm{d}}/W_{\mathrm{s}}$. The relativistic factors $\tilde{R}$ derived from the analytically derived factor (CS) and the empirical factor (FS) are shown, as well as their analogs derived from an old relativistic enhancement factor for W_{s} $\tilde{\tilde{R}}$. Plots are shown for the case of $j=\frac{1}{2}$ as in ${}^2\Sigma_{1/2}$ states. Mass numbers A were assumed as the natural mass number corresponding to the next integer value of Z. Numerical values shown are from cGKS calculations.

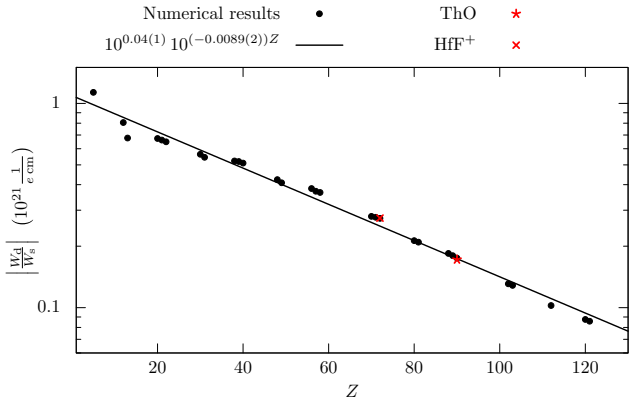

FIG. 3. Fit of the Z dependence of the ratio between $\mathcal{P},\mathcal{T}$-odd eEDM and scalar-pseudoscalar nucleon-electron current interactions $W_{\mathrm{d}}/W_{\mathrm{s}}$. The values of $W_{\mathrm{d}}/W_{\mathrm{s}}$ for HfF^+ and ThO were calculated by Fleig in a four-component configuration interaction framework in Ref. [57] and are shown for comparison but are not included in the fit. All other numerical values correspond to results from cGKS calculations.

coverage regions determined by two experiments. The covariance matrix $\mathbf{U}_{\mathcal{P},\mathcal{T}}$ of k_{s} and d_{e} can be obtained from the covariances of the measured frequencies $\mathbf{U}_{\nu}$ via the matrix product $\mathbf{C}^{-1}\mathbf{U}_{\nu}(\mathbf{C}^{-1})^T$. Assuming the measurements are uncorrelated, $\mathbf{U}_{\nu}$ is a diagonal matrix with the squared standard uncertainties of the measurements $u^2(\nu_1)$ and $u^2(\nu_2)$ on the diagonal. Thus the covariance matrix $\mathbf{U}_{\mathcal{P},\mathcal{T}}$ has the form

$$\mathbf{U}_{\mathcal{P},\mathcal{T}}=h^2\begin{pmatrix}\frac{u^2(\nu_1)}{\left(\frac{W_{\mathrm{d},1}}{W_{\mathrm{s},1}}-\frac{W_{\mathrm{d},2}}{W_{\mathrm{s},2}}\right)^2W_{\mathrm{s},1}^2}+\frac{u^2(\nu_2)}{\left(\frac{W_{\mathrm{d},1}}{W_{\mathrm{s},1}}-\frac{W_{\mathrm{d},2}}{W_{\mathrm{s},2}}\right)^2W_{\mathrm{s},2}^2} & -\frac{u^2(\nu_1)}{\frac{W_{\mathrm{d},2}}{W_{\mathrm{s},2}}\left(\frac{W_{\mathrm{s},1}}{W_{\mathrm{d},1}}-\frac{W_{\mathrm{s},2}}{W_{\mathrm{d},2}}\right)^2W_{\mathrm{d},1}^2}-\frac{u^2(\nu_2)}{\frac{W_{\mathrm{d},1}}{W_{\mathrm{s},1}}\left(\frac{W_{\mathrm{s},1}}{W_{\mathrm{d},1}}-\frac{W_{\mathrm{s},2}}{W_{\mathrm{d},2}}\right)^2W_{\mathrm{d},2}^2}\\ -\frac{u^2(\nu_1)}{\frac{W_{\mathrm{d},2}}{W_{\mathrm{s},2}}\left(\frac{W_{\mathrm{s},1}}{W_{\mathrm{d},1}}-\frac{W_{\mathrm{s},2}}{W_{\mathrm{d},2}}\right)^2W_{\mathrm{d},1}^2}-\frac{u^2(\nu_2)}{\frac{W_{\mathrm{d},1}}{W_{\mathrm{s},1}}\left(\frac{W_{\mathrm{s},1}}{W_{\mathrm{d},1}}-\frac{W_{\mathrm{s},2}}{W_{\mathrm{d},2}}\right)^2W_{\mathrm{d},2}^2} & \frac{u^2(\nu_1)}{\left(\frac{W_{\mathrm{s},1}}{W_{\mathrm{d},1}}-\frac{W_{\mathrm{s},2}}{W_{\mathrm{d},2}}\right)^2W_{\mathrm{d},1}^2}+\frac{u^2(\nu_2)}{\left(\frac{W_{\mathrm{s},1}}{W_{\mathrm{d},1}}-\frac{W_{\mathrm{s},2}}{W_{\mathrm{d},2}}\right)^2W_{\mathrm{d},2}^2}\end{pmatrix},\tag{38}$$

where we have expressed the sensitivity factors in terms of the $\mathcal{P},\mathcal{T}$-odd ratios. In order to set tight bounds on both of the $\mathcal{P},\mathcal{T}$-odd parameters the coverage region in the parameter space of k_{s} and d_{e} has to become small. We consider now the commonly applied case of an ellipsoidal coverage region. The $\mathcal{P},\mathcal{T}$-odd parameters are characterized by a bivariate Gaussian probability distribution function with $\binom{d_{\mathrm{e}}}{k_{\mathrm{s}}}$ and $\mathbf{U}_{\mathcal{P},\mathcal{T}}$. The ellipse centered at $\binom{d_{\mathrm{e}}}{k_{\mathrm{s}}}=\vec{0}$ is described by

$$\underbrace{\begin{pmatrix}x_{\mathrm{d}}\\x_{\mathrm{s}}\end{pmatrix}^T\mathbf{U}_{\mathcal{P},\mathcal{T}}^{-1}\begin{pmatrix}x_{\mathrm{d}}\\x_{\mathrm{s}}\end{pmatrix}}_{f_{\mathrm{e}}(x_{\mathrm{d}},x_{\mathrm{s}})}=k_p^2,\tag{39}$$

where $k_p=2.45$ for an elliptical region of 95% probability and x_{d} and x_{s} are the coordinates in the parameter space in direction of d_{e} and k_{s}, respectively. Calculation of the inverse and the products yields an ellipse centered at $\binom{d_{\mathrm{e}}}{k_{\mathrm{s}}}=\vec{0}$ described by

$$f_{\mathrm{e}}(x_{\mathrm{d}},x_{\mathrm{s}})=\left(\frac{W_{\mathrm{d},1}^2}{u^2(\nu_1)}+\frac{W_{\mathrm{d},2}^2}{u^2(\nu_2)}\right)x_{\mathrm{d}}^2+2\left(\frac{W_{\mathrm{d},1}^2}{u^2(\nu_1)}\frac{W_{\mathrm{s},1}}{W_{\mathrm{d},1}}+\frac{W_{\mathrm{d},2}^2}{u^2(\nu_2)}\frac{W_{\mathrm{s},2}}{W_{\mathrm{d},2}}\right)x_{\mathrm{d}}x_{\mathrm{s}}+\left[\frac{W_{\mathrm{d},1}^2}{u^2(\nu_1)}\left(\frac{W_{\mathrm{s},1}}{W_{\mathrm{d},1}}\right)^2+\frac{W_{\mathrm{d},2}^2}{u^2(\nu_2)}\left(\frac{W_{\mathrm{s},2}}{W_{\mathrm{d},2}}\right)^2\right]x_{\mathrm{s}}^2.\tag{40}$$

The area of the ellipse can be readily evaluated via

$$A_{\mathrm{ellipse}}=\frac{2h^2k_p^2\pi}{\sqrt{\frac{\partial^2f_{\mathrm{e}}(x_{\mathrm{d}},x_{\mathrm{s}})}{\partial x_{\mathrm{s}}^2}\frac{\partial^2f_{\mathrm{e}}(x_{\mathrm{d}},x_{\mathrm{s}})}{\partial x_{\mathrm{d}}^2}-\left(\frac{\partial^2f_{\mathrm{e}}(x_{\mathrm{d}},x_{\mathrm{s}})}{\partial x_{\mathrm{d}}\partial x_{\mathrm{s}}}\right)^2}}.\tag{41}$$

Thus the ellipse has an area of

$$A_{\mathrm{ellipse}}=\frac{h^2k_p^2\pi\,|u(\nu_1)u(\nu_2)|}{|W_{\mathrm{d},1}W_{\mathrm{d},2}|\left|\frac{W_{\mathrm{s},1}}{W_{\mathrm{d},1}}-\frac{W_{\mathrm{s},2}}{W_{\mathrm{d},2}}\right|}.\tag{42}$$

In order to disentangle d_{e} and k_{s} in two experiments (1 and 2) and set tight limits, assuming equal uncertainties for experiments 1 and 2 the expression

$$|W_{\mathrm{d},1}W_{\mathrm{d},2}|\,0.91(2)|1.0207(5)^{Z_1}-1.0207(5)^{Z_2}|\times10^{-21}\,e\,\mathrm{cm}.\tag{43}$$

has to become large. The enhancement of the eEDM in both experiments, which is determined by $W_{\mathrm{d},1}W_{\mathrm{d},2}$ is strongly

dependent on the chemical environment, as will be discussed in the following sections. However, assuming at this point a scaling behavior of $W_{\mathrm{d},1}$ as in Eqs. (19) and (20) for atomic systems, the area of the coverage region is inversely proportional to

$$\frac{(Z_1 Z_2)^3}{\gamma_1^4 \gamma_2^4}\, 0.91(2)|1.0207(5)^{Z_1} - 1.0207(5)^{Z_2}| \times 10^{-21}\, \frac{1}{e\,\mathrm{cm}}. \tag{44}$$

Thus, in order to set tight limits on both $\mathcal{P},\mathcal{T}$-odd parameters, experiments with molecules that have a high nuclear charge and at the same time differ considerably in the nuclear charge Z of the electropositive atom are required. For example, when assuming equal uncertainties $u(\nu_i)$, a comparison of experiments with YbF and RaF or ThO would provide tighter bounds than a comparison of a BaF experiment with a ThO experiment but also than a comparison of experiments with RaF and ThO. However, the possibilities are limited for paramagnetic molecules because enhancement effects of the individual properties still increase steeply with increasing Z, which is the dominating effect. Alternatively experiments with diamagnetic atoms and molecules can further tighten bounds on d_e and k_s, as they show different dependencies on the nuclear charge (see, e.g., Refs. [55,59]).

This scheme can also be expanded for experiments that aim to set accurate limits on more than the herein discussed parameters. However, for this purpose first the respective enhancement factors have to be calculated for a systematic set of molecules. Furthermore, it should be noted that the present picture is not complete because of other sources of permanent EDMs that were not accounted for, namely $\mathcal{P},\mathcal{T}$-odd tensor and pseudoscalar-scalar electron-nucleon current interactions, as well as $\mathcal{P},\mathcal{T}$-odd nuclear dipole moments, which lead to the nuclear Schiff moment and nuclear magnetic quadrupole interactions (see for an overview, e.g., [3]).

D. Periodic trends of $\mathcal{P},\mathcal{T}$-violating properties

The analytical scaling relations presented in Eqs. (22), (19), and (20) can also be used to determine the numerical Z scaling within a group of compounds with electropositive atoms of the same column of the periodic table. For this purpose the property is divided by its relativistic enhancement factor and plotted on a logarithmic scale on both axes, as has been done for the nuclear spin-dependent $\mathcal{P}$-violating interaction parameter in Refs. [39,47,60]:

$$\log_{10}\left\{\frac{|W_\mathrm{s}|}{R(Z,A)f(Z)^{\frac{\gamma+1}{2}}} \times \frac{1}{h\mathrm{Hz}}\right\} = b_\mathrm{s} + \log_{10}\{Z^{a_\mathrm{s}}\}, \tag{45}$$

$$\log_{10}\left\{|W_\mathrm{d}|\gamma(4\gamma^2-1) \times 10^{-24}\frac{e\,\mathrm{cm}}{h\mathrm{Hz}}\right\} = b_{\mathrm{d,CS}} + \log_{10}\{Z^{a_{\mathrm{d,CS}}}\}, \tag{46}$$

$$\log_{10}\left\{|W_\mathrm{d}|\gamma^4 \times 10^{-24}\frac{e\,\mathrm{cm}}{h\mathrm{Hz}}\right\} = b_{\mathrm{d,FS}} + \log_{10}\{Z^{a_{\mathrm{d,FS}}}\}. \tag{47}$$

From Eqs. (18) and (19) the exponents of Z can be expected to be approximately three. For both parameters the Z scaling is studied herein not only within columns, but also for isolobal diatomics within rows of the periodic table.

The resulting Z-scaling parameters a and Z-independent factors 10^b will be discussed in the following for both, GHF and GKS results.

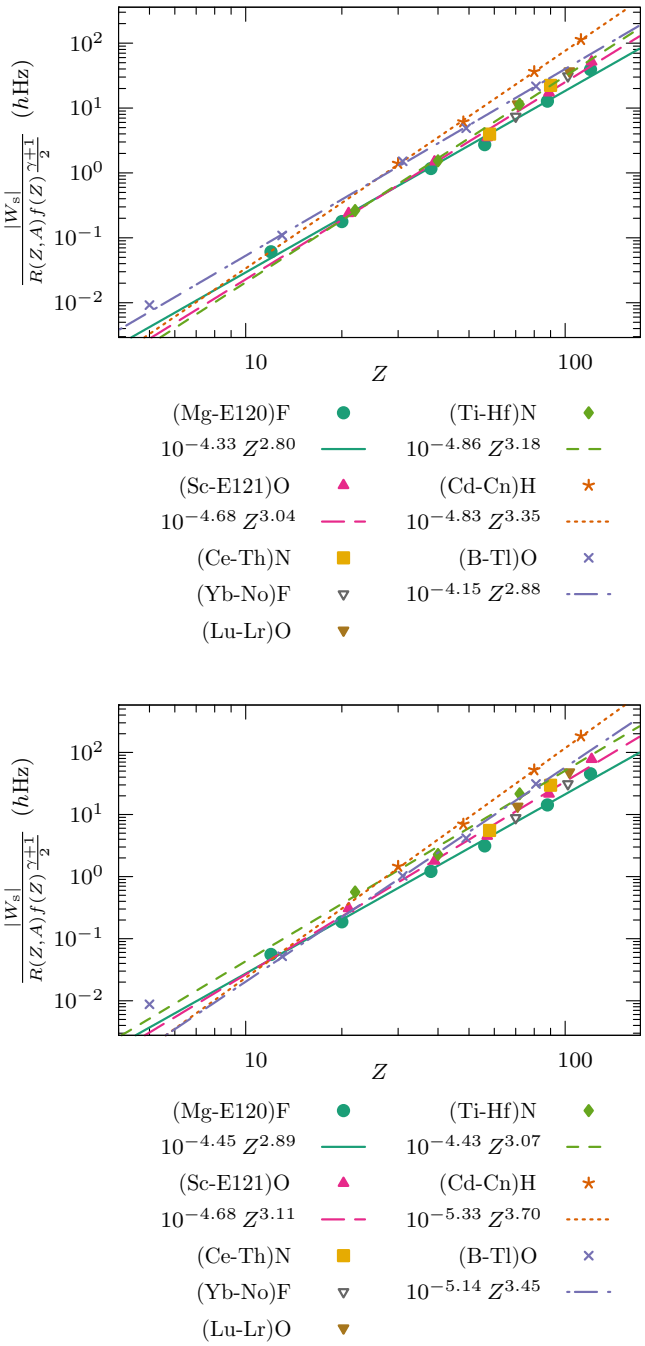

FIG. 4. Scaling of $\log_{10}\{\frac{|W_\mathrm{s}|}{R(Z,A)f(Z)^{\frac{\gamma+1}{2}}} \times \frac{1}{h\mathrm{Hz}}\}$ with $\log_{10}\{Z\}$ for group 2 fluorides (Mg-E120)F, group 3 oxides (Sc-E121)O, group 4 nitrides (Ti-Hf)N, group 12 hydrides (Zn-Cn)H, and group 13 oxides (B-Tl)O at the level of GKS-ZORA/B3LYP (top) and GHF-ZORA (bottom). Corresponding functional expressions of the fits are plotted in each panel as a solid line, long-dashed line, short-dashed line, dotted line, and dash-dotted line, respectively. Plot of the f-block groups (Ce-Th)N, (Yb-No)F, and (Lu-Lr)O without fit. Boron was not included in the fit of group 13 oxides (see text).

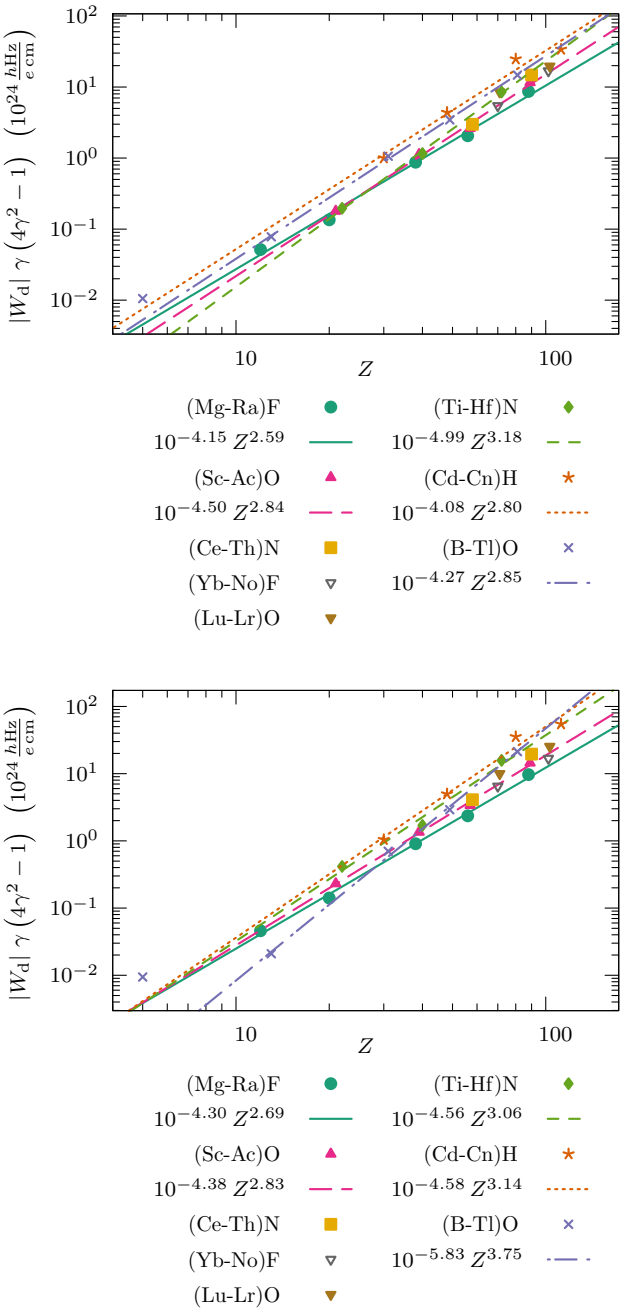

FIG. 5. Scaling of $\log_{10}\{|W_d|\gamma(4\gamma^2-1)\times 10^{-24}\,\frac{e\,\mathrm{cm}}{\hbar\mathrm{Hz}}\}$ with $\log_{10}\{Z\}$ for group 2 fluorides (Mg-Ra)F, group 3 oxides (Sc-Ac)O, group 4 nitrides (Ti-Hf)N, group 12 hydrides (Zn-Cn)H, and group 13 oxides (B-Tl)O at the level of GKS-ZORA/B3LYP (top) and GHF-ZORA (bottom). Corresponding functional expressions of the fits are plotted in each panel as a solid line, long-dashed line, short-dashed line, dotted line, and dash-dotted line, respectively. Plot of the f-block groups (Ce-Th)N, (Yb-No)F, and (Lu-Lr)O without fit. Boron was not included in the fit of group 13 oxides (see text).

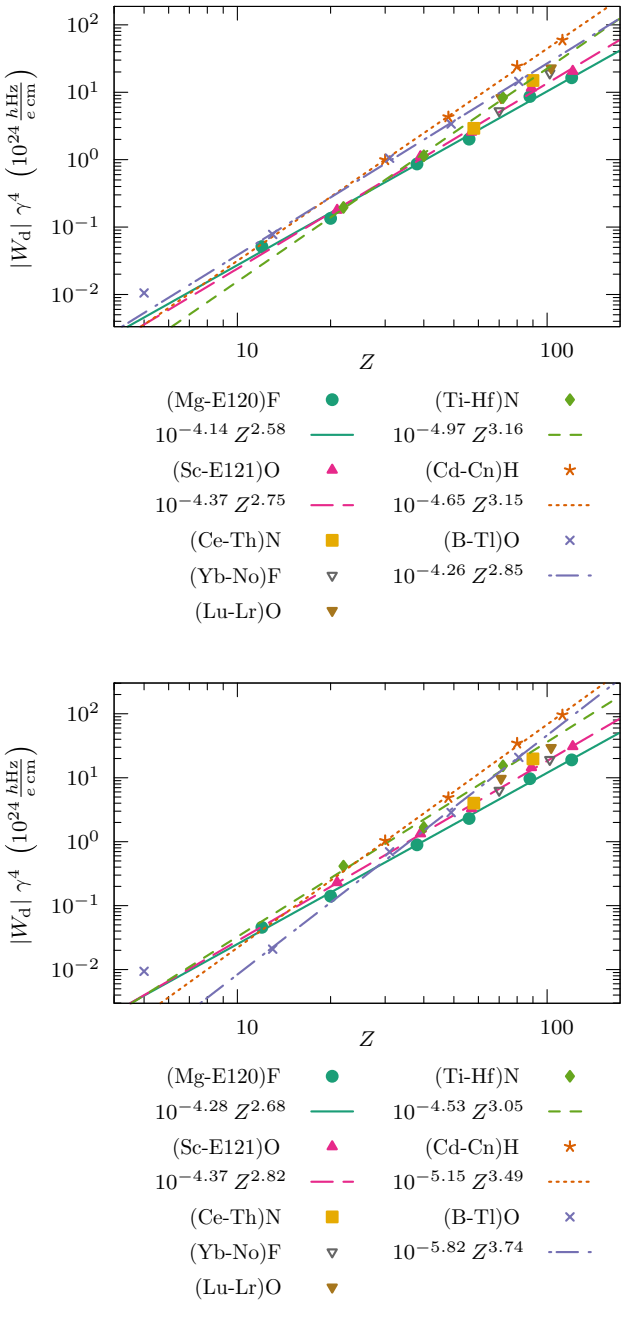

FIG. 6. Scaling of $\log_{10}\{|W_d|\gamma^4\times 10^{-24}\,\frac{e\,\mathrm{cm}}{\hbar\mathrm{Hz}}\}$ with $\log_{10}\{Z\}$ for group 2 fluorides (Mg-E120)F, group 3 oxides (Sc-E121)O, group 4 nitrides (Ti-Hf)N, group 12 hydrides (Zn-Cn)H, and group 13 oxides (B-Tl)O at the level of GKS-ZORA/B3LYP (top) and GHF-ZORA (bottom). Corresponding functional expressions of the fits are plotted in each panel as a solid line, long-dashed line, short-dashed line, dotted line, and dash-dotted line, respectively. Plot of the f-block groups (Ce-Th)N, (Yb-No)F, and (Lu-Lr)O without fit. Boron was not included in the fit of group 13 oxides (see text).

1. Z scaling within groups of the periodic table

In the following the scaling within the groups of the periodic table is studied. The graphical representation of the Z scaling of W_s and W_d can be found in Figs. 4–6. In case of group 13 oxides, boron was not included in the linear fit, because it has a very different character (see discussion above).

Comparing the two different relativistic enhancement factors for eEDM interactions, which were employed in this study, we see for most of the groups of molecules no

TABLE IV. Z-scaling a and Z-independent factors b of $\frac{|W_s|}{R(Z,A)f(Z)\frac{\gamma+1}{2}}$ and $|W_d|\gamma^4$ (empirical relativistic enhancement factor) for group 2 fluorides (Mg-Ra)F, group 3 oxides (Sc-Ac)O, group 4 nitrides (Ti-Hf)N, group 12 hydrides (Zn-Cn)H, and group 13 oxides (Al-Tl)O at the level of GHF-ZORA and GKS-ZORA/B3LYP. Standard uncertainties of the fit are given in parentheses with respect to the last or two last significant digits.

	a_s		b_s		$a_{d,FS}$		$b_{d,FS}$	
Group	GHF	GKS	GHF	GKS	GHF	GKS	GHF	GKS
(Mg-E120)F	2.89(10)	2.80(12)	−4.45(17)	−4.33(19)	2.68(6)	2.58(8)	−4.28(10)	−4.14(14)
(Sc-E121)O	3.11(17)	3.04(13)	−4.7(3)	−4.7(2)	2.82(7)	2.75(11)	−4.37(12)	−4.37(19)
(Ti-Hf)N	3.1(4)	3.18(13)	−4.4(7)	−4.9(2)	3.0(4)	3.16(12)	−4.5(7)	−5.0(2)
(Cd-Cn)H	3.70(9)	3.35(5)	−5.33(17)	−4.83(10)	3.49(9)	3.15(9)	−5.15(18)	−4.65(16)
(Al-Tl)O	3.45(11)	2.88(6)	−5.14(17)	−4.15(10)	3.74(12)	2.85(6)	−5.82(19)	−4.26(9)

appreciable differences between the analytically derived and the empirical factor. Yet, in case of group 12 hydrides it is important to use the empirical scaling factor. Cn has a nuclear charge of $Z = 112$, which is close to the singularity of the analytically derived factor. This results in a strong overestimation of the relativistic enhancement and thus a strong underestimation of the plotted value, which explains the large deviations from a power relationship for group 12 hydrides in Fig. 5. Furthermore, with the analytically derived enhancement factor no meaningful plot that includes the row 8 compounds E120F and E121O is possible. Therefore, in the following we will use the results obtained with the empirical enhancement factor for our discussions.

The Z-scaling parameters a and the Z-independent prefactors 10^b are summarized in Table IV. It should be noted that the inclusion of the values of the row 8 compounds into the fit causes no notable changes in the Z scaling in case of the eEDM and $\mathcal{P},\mathcal{T}$-odd nucleon-electron current enhancement.

For all parameters the agreement between GHF and GKS calculations is excellent for group 2 fluorides, group 3 oxides, and group 4 nitrides, whereas DFT predicts a considerably different behavior for group 12 hydrides and group 13 oxides. As could be seen in [16] the DFT approach performs much better in the case of group 12 compounds than GHF due to pronounced electron correlation effects and therefore can be taken as more reliable. In the previous sections large electron correlation effects in group 13 compounds, which lead to large differences between GHF an GKS, were already discussed.

The scaling of $\mathcal{P},\mathcal{T}$-odd interactions seems to follow the same laws as that of nuclear spin-dependent $\mathcal{P}$-violating interactions studied in [39,60]. The Z scaling increases up to group 12 hydrides, when going along the periods of the periodic table. This maximum effect of $\mathcal{P},\mathcal{T}$-violation enhancement in group 12 compounds seen here is similar to the maximum of relativistic and quantum electrodynamic effects in group 11 compounds [61,62]. At the same time the Z-independent factor 10^b is smallest for these compounds. This damping is, however, only dominant in the region of small Z, which coincides with the findings in [39,60] for $\mathcal{P}$-odd interactions.

In [60] the large Z-scaling of group 4 and group 12 compounds compared to group 2 or 3 compounds was attributed mainly to the filling of the d shells, which causes an increment of the effective nuclear charge because the shielding of the nuclear charge by d orbitals is less efficient than by s or p orbitals. Furthermore, therein it was argued that the lower electronegativity of nitrogen compared to oxygen (group 4 shows larger scaling than group 3, although isoelectronic) causes the large effects in group 4 nitrides. A comparison of the molecules with f-block elements next to group 3, that is CeN and ThN, shows a similar behavior as for group 3 or group 2 compounds. Thus the filling of the f shell has a considerable effect on the size of $\mathcal{P},\mathcal{T}$-violating effects as well, which causes group 4 nitrides to be behave differently than group 3 oxides, whereas CeN and ThN are more similar to group 3 oxides.

Relating the Z scaling of the fits to the expected Z scaling [see Eqs. (18) and (19)], yields a quantitative Z-dependent factor for the effects of the molecular electronic structure on $\mathcal{P},\mathcal{T}$ violation. Referring to the GKS result we get an additional scaling factor of $\sim Z^{-0.2}$ for W_s and $\sim Z^{-0.4}$ for W_d for group 2 fluorides, thus there is some damping of $\mathcal{P},\mathcal{T}$-violating effects due to the electronic structure. This can be observed for group 3 oxides regarding eEDM enhancement as well ($Z^{-0.2}$ for W_d), but for W_s, in contrast, there is no additional Z-dependent damping.

A similar damping can be observed for group 13 oxides on the GKS level, whereas GHF predicts a considerable Z-dependent enhancement instead. The group 4 and 12 compounds show an additional Z-dependent enhancement of $\mathcal{P},\mathcal{T}$-odd effects: $\sim Z^{0.1}$ for W_s and W_d in group 4, $\sim Z^{0.4}$ for W_s, and $\sim Z^{0.2}$ for W_d in group 12. Thus we see a strong enhancement due to Z-dependent electronic structure effects in group 12 hydrides, which does not originate from relativistic enhancement factors obtained from atomic considerations based on Eqs. (18) and (19).

The Z-independent electronic structure factors 10^b show a behavior inverse to that of Z^a and are largest for group 2 fluorides and group 13 oxides in the DFT case, whereas the factors for group 12 hydrides and group 4 nitrides are almost an order of magnitude smaller. Yet, in GHF calculations the Z-independent effects are on the same order for group 13 oxides as for group 12 hydrides.

Now we can return to the discussion of disentanglement of d_e and k_s in the two-dimensional parameter space (Sec. IV C). With the chemical group specific effective Z dependence of the eEDM enhancement factors for paramagnetic molecules, Eq. (42) for the area in the parameter space of d_e and k_s covered by experiments with two different molecules 1 and 2

can be rewritten as

$$A_{\text{ellipse}} = \frac{k_p^2 \pi}{0.91(2) \times 10^{27}\,\frac{\text{Hz}^2}{e\,\text{cm}}} \times \frac{|u(v_1)u(v_2)|}{10^{b_{\text{d},1}+b_{\text{d},2}}\,\frac{Z_1^{a_{\text{d},1}} Z_2^{a_{\text{d},2}}}{\gamma_1^4 \gamma_2^4}\,|1.0207(5)^{Z_1} - 1.0207(5)^{Z_2}|}. \tag{48}$$

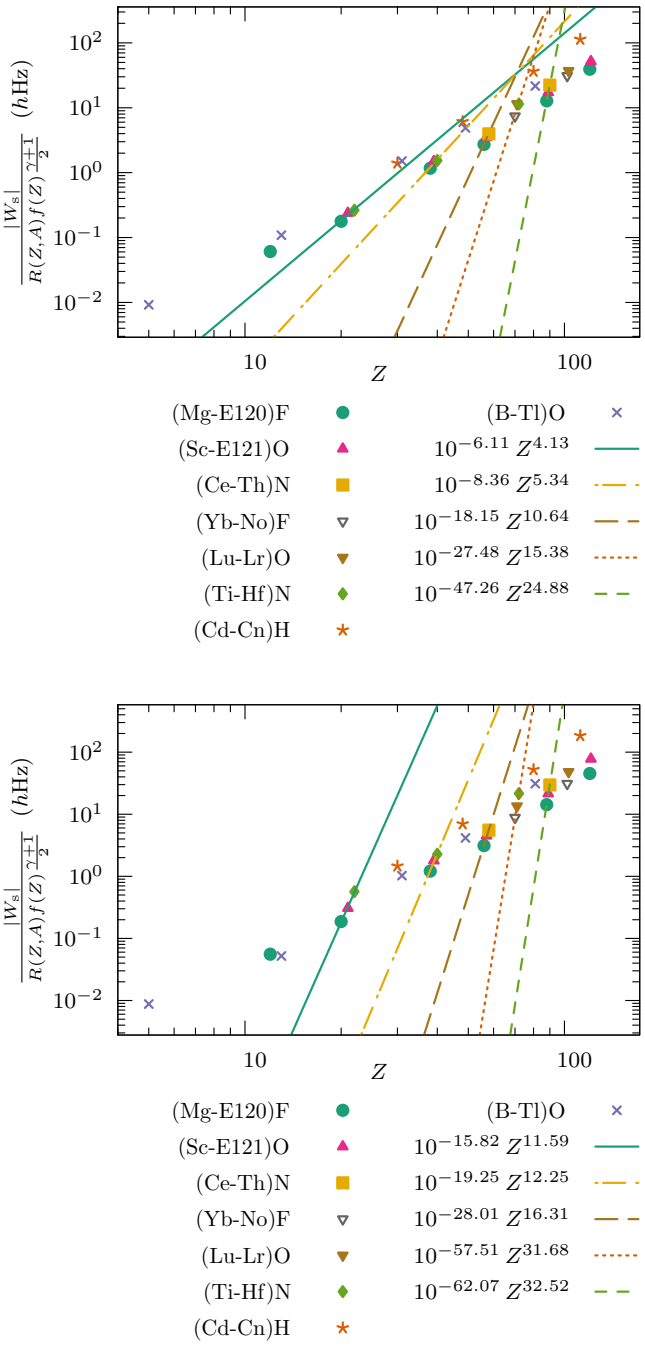

FIG. 7. Scaling of $\log_{10}\{\frac{|W_s|}{R(Z,A)f(Z)^{\frac{\gamma+1}{2}}} \times \frac{1}{h\text{Hz}}\}$ with $\log_{10}\{Z\}$ for row 4 (Ca-Ti; solid line), row 5 (Sr-Zr; dash-dotted line), row 6 (Ba-Ce; long-dashed line, Yb-Hf; dotted line), and row 7 (Ra-Th; short-dashed line) at the level of GKS-ZORA/B3LYP (top) and GHF-ZORA (bottom).

Here the factor 10^{27} and the units result from Eq. (47), wherein W_d is in units of $10^{24}\,\frac{h\text{Hz}}{e\,\text{cm}}$.

What remains to be analyzed in future works is the detailed influence of molecular orbitals on $\mathcal{P}, \mathcal{T}$-violating effects that causes the observed enhancement effects.

2. *Z scaling of isolobal molecules*

Now we focus on the Z scaling for isolobal diatomic molecules within the rows of the periodic table. When

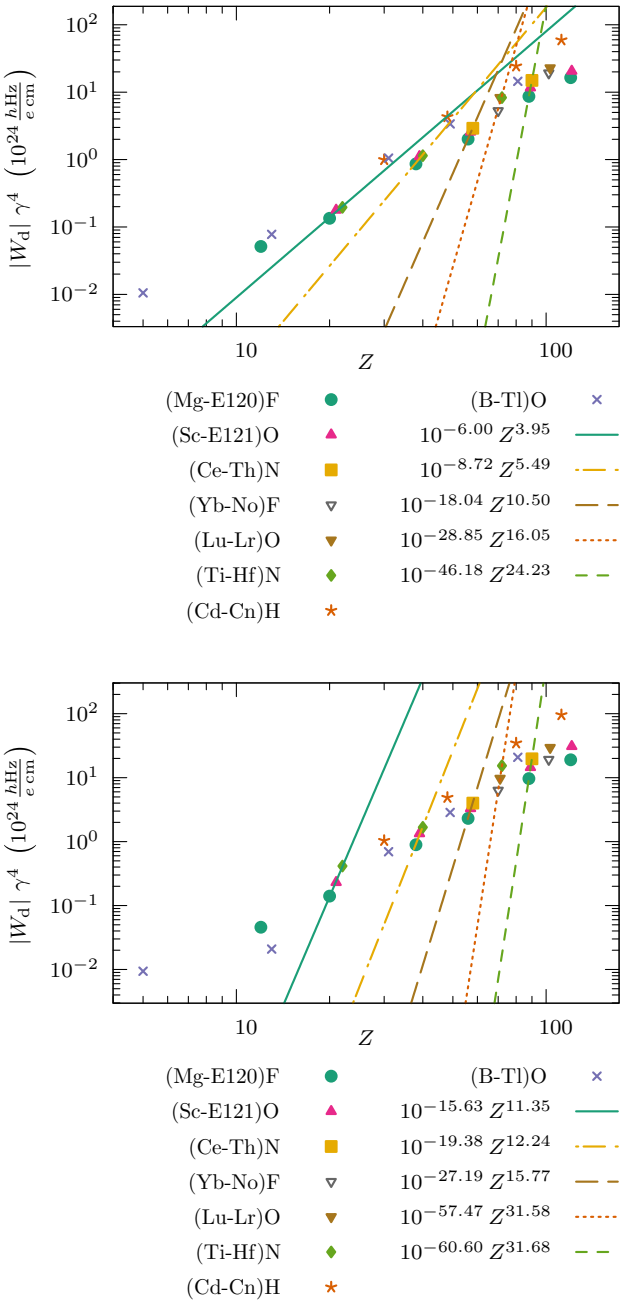

FIG. 8. Scaling of $\log_{10}\{|W_d|\gamma^4 \times 10^{-24}\,\frac{e\,\text{cm}}{h\text{Hz}}\}$ with $\log_{10}\{Z\}$ for row 4 (Ca-Ti; solid line), row 5 (Sr-Zr; dash-dotted line), row 6 (Ba-Ce; long-dashed line, Yb-Hf; dotted line), and row 7 (Ra-Th; short-dashed line) at the level of GKS-ZORA/B3LYP (top) and GHF-ZORA (bottom).

TABLE V. Z-scaling a and Z-independent factors b of $\frac{|W_s|}{R(Z,A)f(Z)^{\frac{\gamma+1}{2}}}$ and $|W_d|\gamma^4$ for isolobal diatomic molecules in row 4 (Ca-Ti), row 5 (Sr-Zr), row 6 (Ba-Ce; Yb-Hf), and row 7 (Ra-Th) at the level of GHF/GKS-ZORA. Standard uncertainties of the fit are given in parentheses with respect to the last or two last significant digits.

	a_s		b_s		$a_{d,FS}$		$b_{d,FS}$	
Row	GHF	GKS	GHF	GKS	GHF	GKS	GHF	GKS
4 (Ca-Ti)	11.6(8)	4.1(11)	−15.8(11)	−6.1(14)	11.3(7)	3.9(11)	−15.6(9)	−6.0(15)
5 (Sr-Zr)	12.2(16)	5(2)	−19(3)	−8(4)	12.2(19)	5(3)	−19(3)	−9(4)
6 (Ba-Ce)	16(3)	11(2)	−28(5)	−18(4)	16(3)	10.5(19)	−27(5)	−18(3)
6 (Yb-Hf)	31.7(11)	15(9)	−58(2)	−27(17)	31.6(7)	16(9)	−57.5(14)	−29(17)
7 (Ra-Th)	33(2)	24.9(10)	−62(4)	−47(2)	32(2)	24.2(12)	−61(5)	−46(2)

discussing eEDM enhancement we concentrate on the results obtained with the empirical relativistic enhancement factor in the following. For comparison, results obtained from the analytically derived relativistic enhancement factor are provided in the Supplemental Material [46]. The corresponding plots can be found in Fig. 7 for W_s and Fig. 8 for W_d and the resulting scaling and damping parameters are listed in Table V.

Trends, similar to those reported in [47] for the $\mathcal{P}$-odd nuclear spin-dependent interaction can also be observed for the $\mathcal{P},\mathcal{T}$-odd properties. However, we can see a large discrepancy ($\gtrsim$20% for parameter a and b) between results obtained from GHF and GKS calculations. Deviations for a and b of more than 50% between the GHF and GKS results in the fourth and fifth row probably stem from electron correlation effects, which lead to a considerable reduction (of 30% to 50%) of the enhancement effects in group 4 compounds. Fits of the DFT results have large errors that lead to qualitative differences. Especially for row 6 compounds with a filled f shell (violet line in Figs. 7 and 8) a large fit error (>40%) can be observed, since HfN does not fold into the power-law model. The results of GHF fit much better into this model and show that the scaling behavior of post-f-block compounds of row 6 is approximately similar to that of row 7 compounds without a filled f shell. Comparing compounds with a filled d shell (group 12 and 13), we see that the slope becomes negative. This again indicates a maximum of enhancement of $\mathcal{P},\mathcal{T}$-odd effects in group 12 as discussed before.

The investigations show that the chemical environment of the heavy atom can have a much more important effect on the Z-dependent enhancement than the physical nature of the atom. This can result in effects scaling as $\sim 10^b Z^{30}$ for row 7 compounds. Thus a more complex chemical environment may allow for better tuning of the size of $\mathcal{P},\mathcal{T}$-odd enhancement effects. Hence we may speculate that polyatomic molecules might be capable to give larger enhancement effects due to the electronic structure surrounding the heavy atom.

V. CONCLUSION

In this paper we calculated $\mathcal{P},\mathcal{T}$-odd properties due to eEDM and nucleon-electron current interactions in polar open-shell diatomic molecules. We determined periodic trends of $\mathcal{P},\mathcal{T}$ violation by comparison to atomic scaling relations and showed that the trends are very similar to those of nuclear spin-dependent $\mathcal{P}$-violating interactions. Furthermore, this comparison revealed problems of frequently used scaling relation for eEDM enhancement in the regime of heavy elements with $Z > 100$. We showed that an alternative relativistic enhancement factor found empirically by Fermi and Segrè resolves the problems for $Z < 137$ partially. Group 12 hydrides and group 4 nitrides were identified to show a very steep Z scaling and therefore interesting Z-dependent electronic structure effects, enhancing $\mathcal{P},\mathcal{T}$ violation in these compounds, were identified. Furthermore, a study of the ratio between $\mathcal{P},\mathcal{T}$-odd properties W_d/W_s, showed that electronic structure effects and the chemical environment have a very small influence on the ratio. The ratio is mainly determined by an exponential dependence on the nuclear charge Z. Thus for experiments aiming to differentiate between d_e and k_s, the use of molecules with a relatively large difference in nuclear charge Z would be favorable. The analysis of the scaling of isolobal systems and the study of the ratio W_d/W_s showed the limitations of polar diatomic molecules and point towards possible advantages in the use of more complex systems, such as polyatomic molecules. The latter will be focus of future research in our laboratory.

ACKNOWLEDGMENTS

Financial support by the State Initiative for the Development of Scientific and Economic Excellence (LOEWE) in the LOEWE-Focus ELCH and computer time provided by the Center for Scientific Computing (CSC) Frankfurt are gratefully acknowledged. T.I. is grateful to RFBR Grant N 16-02-01064 for partial support. S.M. gratefully acknowledges support from Fonds der Chemischen Industrie. We thank Yuri Oganessian for inspiring discussions on super heavy elements.

[1] D. J. Gross, Proc. Natl. Acad. Sci. USA **93**, 14256 (1996).
[2] N. Fortson, P. Sandars, and S. Barr, Phys. Today **56**, 33 (2003).
[3] I. B. Khriplovich and S. K. Lamoreaux, *CP Violation without Strangeness* (Springer, Berlin, 1997).

[4] J. S. M. Ginges and V. V. Flambaum, Phys. Rep. **397**, 63 (2004).
[5] E. Salpeter, Phys. Rev. **112**, 1642 (1958).
[6] P. Sandars, Phys. Lett. **14**, 194 (1965).
[7] P. G. H. Sandars, Phys. Lett. **22**, 290 (1966).
[8] P. G. H. Sandars, J. Phys. B **1**, 511 (1968).
[9] P. G. H. Sandars, J. Phys. B **1**, 499 (1968).
[10] V. K. Ignatovich, Sov. Phys. JETP **29**, 1084 (1969).
[11] V. V. Flambaum, Yad. Fiz. **24**, 383 (1976) [Sov. J. Nucl. Phys. **24**, 199 (1976)].
[12] I. B. Khriplovich, *Parity Nonconservation in Atomic Phenomena* (Gordon and Breach, Philadelphia, PA, 1991).
[13] V. S. Prasannaa, A. C. Vutha, M. Abe, and B. P. Das, Phys. Rev. Lett. **114**, 183001 (2015).
[14] A. Sunaga, M. Abe, M. Hada, and B. P. Das, Phys. Rev. A **95**, 012502 (2017).
[15] B. Ravaine, S. G. Porsev, and A. Derevianko, Phys. Rev. Lett. **94**, 013001 (2005).
[16] K. Gaul and R. Berger, J. Chem. Phys. **147**, 014109 (2017).
[17] F. Hund, Z. Phys. **40**, 742 (1927).
[18] F. Hund, Z. Phys. **42**, 93 (1927).
[19] F. Hund, Z. Phys. **43**, 805 (1927).
[20] M. G. Kozlov and L. N. Labzowsky, J. Phys. B **28**, 1933 (1995).
[21] Y. Y. Dmitriev, Y. G. Khait, M. G. Kozlov, L. N. Labzowsky, A. O. Mitrushenkov, A. V. Shtoff, and A. V. Titov, Phys. Lett. A **167**, 280 (1992).
[22] E. Lindroth, B. W. Lynn, and P. G. H. Sandars, J. Phys. B **22**, 559 (1989).
[23] T. A. Isaev and R. Berger, arXiv:1302.5682.
[24] A. D. Kudashov, A. N. Petrov, L. V. Skripnikov, N. S. Mosyagin, T. A. Isaev, R. Berger, and A. V. Titov, Phys. Rev. A **90**, 052513 (2014).
[25] C. van Wüllen, J. Chem. Phys. **109**, 392 (1998).
[26] L. Visscher and K. G. Dyall, At. Data Nucl. Data Tables **67**, 207 (1997).
[27] A. Mårtensson-Pendrill and P. Öster, Phys. Scr. **36**, 444 (1987).
[28] E. Fermi and E. Segrè, Z. Phys. **82**, 729 (1933).
[29] M. A. Bouchiat and C. Bouchiat, J. Phys. (Paris) **35**, 899 (1974).
[30] O. P. Sushkov and V. V. Flambaum, Sov. Phys. JETP **48**, 608 (1978).
[31] G. Racah, Z. Phys. **71**, 431 (1931).
[32] T. H. Dinh, V. A. Dzuba, and V. V. Flambaum, Phys. Rev. A **80**, 044502 (2009).
[33] E. Fermi and E. Segrè, Mem. Accad. d'Italia **4**, 131 (1933).
[34] G. Breit, Phys. Rev. **38**, 463 (1931).
[35] V. A. Dzuba, V. V. Flambaum, and C. Harabati, Phys. Rev. A **84**, 052108 (2011).
[36] R. Berger, J. Chem. Phys. **129**, 154105 (2008).
[37] R. Berger and C. van Wüllen, J. Chem. Phys. **122**, 134316 (2005).
[38] R. Berger, N. Langermann, and C. van Wüllen, Phys. Rev. A **71**, 042105 (2005).
[39] T. A. Isaev and R. Berger, Phys. Rev. A **86**, 062515 (2012).
[40] S. Nahrwold and R. Berger, J. Chem. Phys. **130**, 214101 (2009).
[41] R. Ahlrichs, M. Bär, M. Häser, H. Horn, and C. Kölmel, Chem. Phys. Lett. **162**, 165 (1989).
[42] P. J. Stephens, F. J. Devlin, C. F. Chabalowski, and M. J. Frisch, J. Phys. Chem. **98**, 11623 (1994).
[43] S. H. Vosko, L. Wilk, and M. Nuisar, Can. J. Phys. **58**, 1200 (1980).
[44] A. D. Becke, Phys. Rev. A **38**, 3098 (1988).
[45] C. Lee, W. Yang, and R. G. Parr, Phys. Rev. B **37**, 785 (1988).
[46] See Supplemental Material at http://link.aps.org/supplemental/10.1103/PhysRevA.99.032509 for details on the used basis sets and further plots of trends derived with the analytical relativistic enhancement factor by Sandars.
[47] T. A. Isaev and R. Berger, J. Mol. Spectrosc. **300**, 26 (2014).
[48] B. O. Roos, R. Lindh, P. k. Malmqvist, V. Veryazov, and P. O. Widmark, J. Phys. Chem. A **108**, 2851 (2004).
[49] T. H. Dunning, Jr., J. Chem. Phys. **90**, 1007 (1989).
[50] W. Liu, C. van Wüllen, F. Wang, and L. Li, J. Chem. Phys. **116**, 3626 (2002).
[51] Y. T. Oganessian, V. K. Utyonkov, Y. V. Lobanov, F. S. Abdullin, A. N. Polyakov, R. N. Sagaidak, I. V. Shirokovsky, Y. S. Tsyganov, A. A. Voinov, G. G. Gulbekian, S. L. Bogomolov, B. N. Gikal, A. N. Mezentsev, S. Iliev, V. G. Subbotin, A. M. Sukhov, K. Subotic, V. I. Zagrebaev, G. K. Vostokin, M. G. Itkis, K. J. Moody, J. B. Patin, D. A. Shaughnessy, M. A. Stoyer, N. J. Stoyer, P. A. Wilk, J. M. Kenneally, J. H. Landrum, J. F. Wild, and R. W. Lougheed, Phys. Rev. C **74**, 044602 (2006).
[52] Y. Oganessian, A. Yeremin, G. Gulbekian, S. Bogomolov, V. Chepigin, B. Gikal, V. Gorshkov, M. Itkis, A. Kabachenko, V. Kutner, A. Lavrentev, O. Malyshev, A. Popeko, J. Roháč, R. Sagaidak, S. Hofmann, G. Münzenberg, M. Veselsky, S. Saro, N. Iwasa, and K. Morita, Eur. Phys. J. A **5**, 63 (1999).
[53] Y. Oganessian, J. Phys.: Conf. Ser. **312**, 082003 (2011).
[54] V. K. Utyonkov, N. T. Brewer, Y. T. Oganessian, K. P. Rykaczewski, F. S. Abdullin, S. N. Dmitriev, R. K. Grzywacz, M. G. Itkis, K. Miernik, A. N. Polyakov, J. B. Roberto, R. N. Sagaidak, I. V. Shirokovsky, M. V. Shumeiko, Y. S. Tsyganov, A. A. Voinov, V. G. Subbotin, A. M. Sukhov, A. V. Karpov, A. G. Popeko, A. V. Sabel'nikov, A. I. Svirikhin, G. K. Vostokin, J. H. Hamilton, N. D. Kovrizhnykh, L. Schlattauer, M. A. Stoyer, Z. Gan, W. X. Huang, and L. Ma, Phys. Rev. C **97**, 014320 (2018).
[55] M. Jung, J. High Energy Phys. 05 (2013) 168.
[56] T. Chupp and M. Ramsey-Musolf, Phys. Rev. C **91**, 035502 (2015).
[57] T. Fleig, Phys. Rev. A **96**, 040502 (2017).
[58] JCGM 102:2011, Evaluation of measurement data—Supplement 2 to the Guide to the expression of uncertainty in measurement—Extension to any number of output quantities, Standard (Joint Committee for Guides in Metrology, Paris, FR, 2011).
[59] T. Fleig and M. Jung, J. High Energy Phys. 07 (2018) 12.
[60] A. Borschevsky, M. Ilias, V. A. Dzuba, V. V. Flambaum, and P. Schwerdtfeger, Phys. Rev. A **88**, 022125 (2013).
[61] P. Pyykkö and J. P. Desclaux, Acc. Chem. Res. **12**, 276 (1979).
[62] C. Thierfelder and P. Schwerdtfeger, Phys. Rev. A **82**, 062503 (2010).

Supplemental Material for "Systematic study of relativistic and chemical enhancements of $\mathcal{P},\mathcal{T}$-odd effects in polar diatomic radicals"

Konstantin Gaul,[1] Sebastian Marquardt,[1] Timur Isaev,[2] and Robert Berger[1]

[1] *Fachbereich Chemie, Philipps-Universität Marburg, Hans-Meerwein-Straße 4, 35032 Marburg, Germany*

[2] *Petersburg Nuclear Physics Institute, Orlova Roscha. 1, 188300 Gatchina, Russia*

(Dated: January 27, 2019)

I. BASIS SETS

Table I. Basis set parameters for GHF/GKS-ZORA calculations. Even-tempered basis sets of uncontracted Gaussians are given in the form $N_{\mathrm{bas}}\ell$: (α_{max}; α_{min}), where N_{bas} is the number of Gaussians, ℓ is the symbol for the angular momentum quantum numbers and α_{max} and α_{min} are the largest and smallest exponent coefficients, respectively, given in units of a_0^{-2} with a_0 being the Bohr radius.

Basis for all 'heavy' centers		N ANO basis		
		s	p	d
37s:	(2000000000; 0.0291)	74761.715	126.66657	2.7500000
34p:	(500000000; 0.0582)	11123.654	29.837389	0.9625000
14d:	(13300.758; 0.0521)	2512.6857	9.394038	0.3368750
9f:	(751.8368350; 0.3546)	703.77729	3.405104	0.1179060
		225.47879	1.350000	
		79.61581	0.5576960	
		30.237283	0.2324490	
		12.263622	0.0942640	
		5.265086	0.0329920	
		2.333471		
		0.901856		
		0.358336		
		0.141093		
		0.049383		
H Dunning basis		F/O ANO basis		
s	p	s	p	d
82.640	2.2920000	103109.46	245.33029	5.000000
12.410	0.8380000	15281.007	56.919005	1.750000
2.8240	0.2920000	3441.5392	17.604568	0.612500
0.7977		967.09483	6.2749950	0.214375
0.2581		314.03534	2.4470300	
0.08989		113.44230	0.9950600	
		44.644727	0.4039730	
		18.942874	0.1548100	
		8.5327430	0.0541840	
		3.9194010		
		1.5681570		
		0.6232900		
		0.2408610		
		0.0843010		

II. SUPPORTING FIGURES

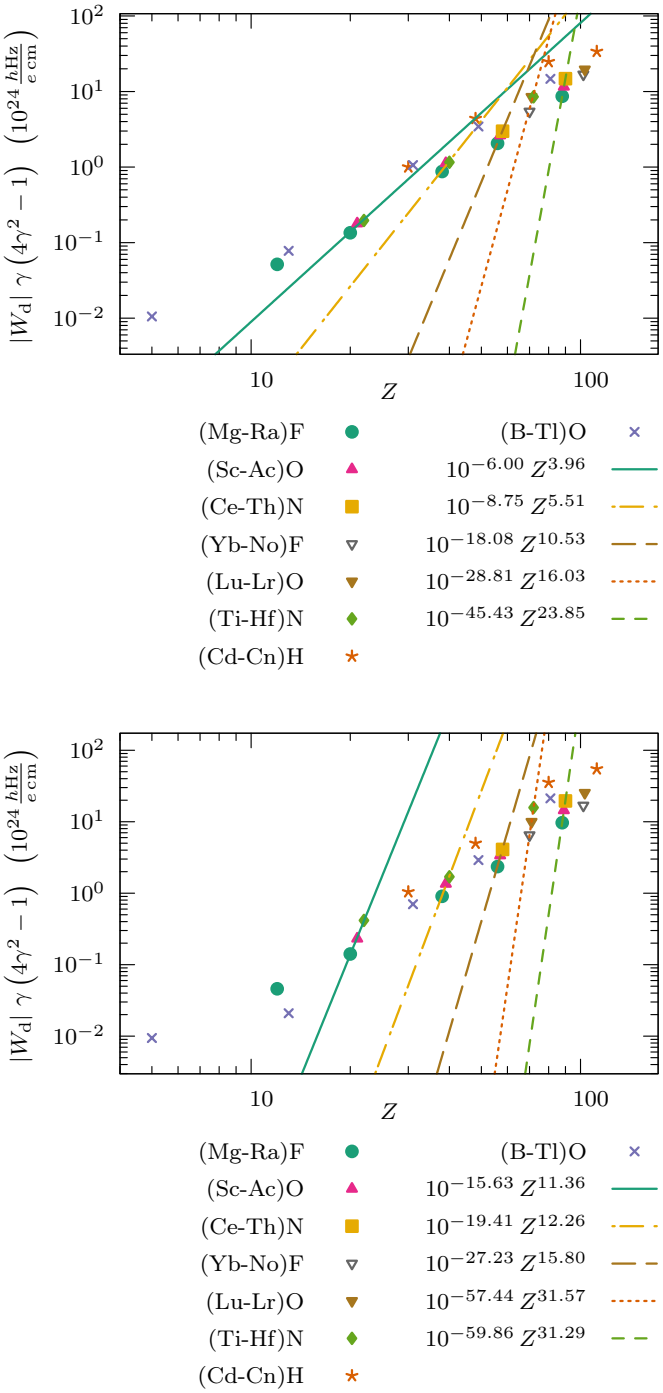

Figure 1. Scaling of $\log_{10}\left\{|W_\mathrm{d}|\gamma\left(4\gamma^2-1\right)\right\}$ with $\log_{10}\{Z\}$ for row 4 (Ca-Ti: solid line), row 5 (Sr-Zr: dash-dotted line), row 6 (Ba-Ce: long-dashed line, Yb-Hf: dotted line), and row 7 (Ra-Th: short-dashed line) at the level of GKS-ZORA/B3LYP (top) and GHF-ZORA (bottom).

Ab initio study of parity and time-reversal violation in laser-coolable triatomic molecules

Konstantin Gaul and Robert Berger*
Fachbereich Chemie, Philipps-Universität Marburg, Hans-Meerwein-Straße 4, 35032 Marburg, Germany

(Received 4 July 2019; published 13 January 2020)

Electronic structure enhancement factors of simultaneous parity and time-reversal violation ($\mathcal{P},\mathcal{T}$ violation) caused by an electric dipole moment of the electron (eEDM) and scalar-pseudoscalar nucleon-electron current (SPNEC) interactions are reported for various metal monohydroxides, several of which are considered laser-coolable and promising candidates for an eEDM measurement. Electronic structure enhancements are calculated *ab initio* within zeroth-order regular approximation (ZORA) for CaOH, SrOH, BaOH, RaOH, and YbOH. Scaling behavior with respect to nuclear charge numbers and the ratio of enhancement factors for both discussed sources of $\mathcal{P},\mathcal{T}$ violation are analyzed, which are crucial to obtaining stringent bounds on parameters for new physics from experiments.

DOI: 10.1103/PhysRevA.101.012508

I. INTRODUCTION

High-precision spectroscopy of diatomic molecules serves as a powerful tool for probing high-energy scales of new physics beyond the standard model of particle physics [1]. Signatures of new physics are expected for instance from simultaneous parity $\mathcal{P}$ and time-reversal $\mathcal{T}$ violation [2]. Such a violation of fundamental symmetries can in principle result in a permanent electric dipole moment of a molecule in a vanishing electric field. With cold polar heavy molecules such as ThO, currently the strictest limits are set on $\mathcal{P},\mathcal{T}$-violating effects due to the electric dipole moment of the electron (eEDM) [3,4]. This is due to electronic structure effects in polar heavy diatomic molecules, which strongly enhance $\mathcal{P},\mathcal{T}$-odd effects such as an eEDM d_e or scalar-pseudoscalar nucleon-electron current (SPNEC) interactions [5]. References [6–8] highlighted the particular situation of $\mathcal{P},\mathcal{T}$-odd effects in the diatomic system RaF, which was earlier identified to have the advantage of being also a molecular candidate for laser cooling [9]. Based on simple theoretical concepts [10] (for a review see [11]) it was subsequently concluded that not only diatomic, but also polyatomic molecules can be cooled with lasers. This renders such molecules promising laboratories for the study of fundamental symmetry violations. A number of molecular candidates were proposed [10] which included the particular example of CaOH. The first successful experiment of laser cooling of a polyatomic molecule was subsequently realized with SrOH [12]. Isaev *et al.* [13] suggested laser cooling of RaOH and its use to search for new physics. They presented also the first calculation of SPNEC interactions enhancement in a polyatomic molecule.

Kozyryev *et al.* elucidated that laser-coolable polyatomic molecules, and in particular YbOH, can have advantages over diatomic molecules in experimental setups and may improve sensitivity of eEDM experiments [14]. And it was pointed out in Ref. [15] that diatomic molecules are limited in the sensitivity of a simultaneous determination of d_e as well as the coupling constant of SPNEC interactions k_s when one analyzes the scaling behavior of the enhancement factors with respect to the charge of the heavy nucleus.

To provide these enhancement factors for upcoming experiments on triatomic molecules, we present in this paper predictions of W_d and W_s, the electronic structure enhancement factors of an eEDM and SPNEC interactions, respectively, in the laser-coolable polyatomic molecules CaOH, SrOH, RaOH, and YbOH, as well as for BaOH, which is isoelectronic to BaF, a promising candidate for the first detection of molecular parity violation [16]. We compare herein also the ratio W_d/W_s to those obtained for diatomic molecules in order to gauge the advantage of polyatomic over diatomic molecules with respect to electronic structure enhancement effects.

II. THEORY

A. $\mathcal{P},\mathcal{T}$-odd spin-rotational Hamiltonian of a linear molecule

The metal hydroxides (MOH) studied herein are linear molecules and expected to have a $^2\Sigma_{1/2}$ ground state. Thus the effective $\mathcal{P},\mathcal{T}$-odd spin-rotational Hamiltonian (see review [17]) when neglecting contributions of the light nuclei and nuclear spin-dependent effects is the same as for diatomic molecules studied in Ref. [15], namely,

$$H_{sr} = (k_s W_s + d_e W_d)\Omega, \tag{1}$$

where $\Omega = \vec{J}_e \cdot \vec{\lambda}$ is the projection of the reduced total electronic angular momentum $\vec{J}_e$ on the molecular axis, defined by the unit vector $\vec{\lambda}$ pointing from the heavy nucleus to the OH group. k_s is the $\mathcal{P},\mathcal{T}$-odd scalar-pseudoscalar nucleon-electron current interaction constant and d_e is the eEDM. The complete $\mathcal{P},\mathcal{T}$-odd spin-rotational operator, including nuclear spin-dependent terms, we discuss elsewhere [18]. The $\mathcal{P},\mathcal{T}$-odd electronic structure parameters are defined by

$$W_s = \frac{\langle\Psi|\hat{H}_s|\Psi\rangle}{k_s\Omega} \quad \text{and} \quad W_d = \frac{\langle\Psi|\hat{H}_d|\Psi\rangle}{d_e\Omega}, \tag{2}$$

*Corresponding author: robert.berger@uni-marburg.de

where Ψ is the electronic wave function. The molecular $\mathcal{P},\mathcal{T}$-odd Hamiltonians [2,19,20]

$$\hat{H}_{\mathrm{s}} = \imath k_{\mathrm{s}} \frac{G_{\mathrm{F}}}{\sqrt{2}} \sum_{i=1}^{N_{\mathrm{elec}}} \sum_{A=1}^{N_{\mathrm{nuc}}} \rho_A(\vec{r}_i) Z_A \boldsymbol{\gamma}^0 \boldsymbol{\gamma}^5, \tag{3}$$

$$\hat{H}_{\mathrm{d}} = \frac{2\imath c d_{\mathrm{e}}}{\hbar e} \sum_{i=1}^{N_{\mathrm{elec}}} \boldsymbol{\gamma}^0 \boldsymbol{\gamma}^5 \hat{\vec{p}}_i^2 \tag{4}$$

were implemented and evaluated in a quasirelativistic framework within the zeroth-order regular approximation (ZORA) [15,21]:

$$\hat{H}_{\mathrm{s}}^{\mathrm{ZORA}} = \imath \sum_{i=1}^{N_{\mathrm{elec}}} \sum_{A=1}^{N_{\mathrm{nuc}}} Z_A [\rho_A(\vec{r}_i)\tilde{\omega}_{\mathrm{s}}(\vec{r}_i), \vec{\boldsymbol{\sigma}} \cdot \hat{\vec{p}}_i]_-, \tag{5}$$

$$\hat{H}_{\mathrm{d}}^{\mathrm{ZORA}} = \imath \sum_{i=1}^{N_{\mathrm{elec}}} \hat{\vec{p}}_i^2 \tilde{\omega}_{\mathrm{d}}(\vec{r}_i)(\vec{\boldsymbol{\sigma}} \cdot \hat{\vec{p}}_i) - (\vec{\boldsymbol{\sigma}} \cdot \hat{\vec{p}}_i)\tilde{\omega}_{\mathrm{d}}(\vec{r}_i)\hat{\vec{p}}_i^2. \tag{6}$$

Here ρ_A is the normalized nuclear charge density distribution of nucleus A with charge number Z_A, $\vec{r}_i$ is the position vector of electron i, $G_{\mathrm{F}} = 2.22249 \times 10^{-14}\ E_{\mathrm{h}} a_0^3$ is Fermi's weak coupling constant, $\imath = \sqrt{-1}$ is the imaginary unit, $\hat{\vec{p}}$ is the linear momentum operator, $\vec{\boldsymbol{\sigma}}$ is the vector of the Pauli spin matrices, $[A, B]_- = AB - BA$ is the commutator, and the modified ZORA factors are defined as

$$\tilde{\omega}_{\mathrm{s}}(\vec{r}_i) = \frac{G_{\mathrm{F}} k_{\mathrm{s}} c}{\sqrt{2}(2m_{\mathrm{e}}c^2 - \tilde{V}(\vec{r}_i))}, \tag{7}$$

$$\tilde{\omega}_{\mathrm{d}}(\vec{r}_i) = \frac{2d_{\mathrm{e}}c^2}{2e\hbar m_{\mathrm{e}}c^2 - e\hbar\tilde{V}(\vec{r}_i)}, \tag{8}$$

with the model potential $\tilde{V}$ introduced by van Wüllen [22], which is used to alleviate the gauge dependence of ZORA. Here c is the speed of light in vacuum, $\hbar = \frac{h}{2\pi}$ is the reduced Planck constant, and m_{e} is the mass of the electron.

B. Calculation of hyperfine coupling constants within cGHF and cGKS

Hyperfine coupling constants were evaluated starting from the relativistic electronic hyperfine operator of nucleus A:

$$\hat{H}_{\mathrm{hf}} = \sum_i \vec{\boldsymbol{\alpha}} \cdot \vec{\mu}_A \times \frac{(\vec{r}_i - \vec{r}_A)}{|\vec{r}_i - \vec{r}_A|^3}, \tag{9}$$

with the nuclear magnetic moment $\vec{\mu}_A$. The effective spin-rotation Hamiltonian of hyperfine couplings appears as

$$\hat{H}_{\mathrm{sr,hf}} = \vec{I}_A \cdot \mathbf{A} \cdot \vec{S}, \tag{10}$$

where $\mathbf{A}$ is the hyperfine tensor, and $\vec{I}_A$ and $\vec{S}$ are the effective nuclear and electron spin, respectively. In a linear molecule with the molecular axis being aligned on the z axis we have

$$\hat{H}_{\mathrm{sr,hf}} = I_{z,A} S_z A_{\parallel} + (I_{x,A} S_x + I_{y,A} S_y) A_{\perp}. \tag{11}$$

In our complex generalized Hartree-Fock/complex generalized Kohn-Sham (cGHF/cGKS) approach, which accounts for spin polarization, the molecular orbitals are not necessarily obtained as Kramers pairs. The zz component of the hyperfine tensor is thus calculated by

$$A_{zz} = -\frac{\mu_A}{2cm_{\mathrm{p}} I_A S_z} \left\langle \sum_i \frac{[(\vec{r}_i - \vec{r}_A) \times \vec{\boldsymbol{\alpha}}]_z}{|\vec{r}_i - \vec{r}_A|^3} \right\rangle. \tag{12}$$

Here μ_A is the nuclear magnetic moment in units of μ_{N}, I_A is the nuclear spin quantum number and $\langle \hat{O} \rangle$ is the expectation value of operator $\hat{O}$ computed for the cGHF or cGKS determinant. Therefore, the $A_{\parallel}$ component was calculated from A_{zz} [Eq. (12)] by alignment of the molecular axis and the electronic spin on the z axis, whereas the $A_{\perp}$ component was received from the A_{zz} for the wave function with the molecular axis aligned on the x axis but the electronic spin aligned on the z axis.

III. COMPUTATIONAL DETAILS

The quasirelativistic two-component calculations reported herein are performed within ZORA at the level of complex generalized Hartree-Fock (cGHF) or Kohn-Sham (cGKS) with a modified version [23–26] of the quantum chemistry program package TURBOMOLE [27]. For details on our implementation of $\mathcal{P},\mathcal{T}$-odd properties within this ZORA framework see Refs. [15,21,28]. For Kohn-Sham (KS) density functional theory (DFT) calculations, the hybrid Becke three-parameter exchange functional and Lee, Yang, and Parr correlation functional (B3LYP) [29–32] were employed.

For all calculations a basis set of $37s$, $34p$, $14d$, and $9f$ uncontracted Gaussian functions with the exponential coefficients α_i composed as an even-tempered series as $\alpha_i = ab^{N-i}$; $i = 1, \ldots, N$, with $b = 2$ for s and p functions and with $b = (5/2)^{1/25} \times 10^{2/5} \approx 2.6$ for d and f functions was used for the electropositive atom. The largest exponent coefficients of the s, p, d and f subsets are $2 \times 10^9\ a_0^{-2}$, $5 \times 10^8\ a_0^{-2}$, 13300.758 a_0^{-2} and 751.8368350 a_0^{-2}, respectively. The O atoms were represented with a decontracted s, p, d substratum of the atomic natural orbital (ANO) basis set of triple-ζ quality for F [33] and for H the s, p subsets of a decontracted correlation-consistent basis of quadruple-ζ quality [34] was used.

The ZORA-model potential $\tilde{V}(\vec{r})$ was employed with additional damping [35] as proposed by van Wüllen [22]. For two-component wave functions and properties a finite nucleus was used, described by a normalized spherical Gaussian nuclear density distribution $\rho_A(\vec{r}) = \rho_0\, e^{-\frac{3}{2\zeta_A}\vec{r}^2}$. The rms radius ζ_A of nucleus A was used as suggested by Visscher and Dyall [36], where the mass numbers A are ^{43}Ca, ^{87}Sr, ^{137}Ba, ^{173}Yb, ^{223}Ra.

The nuclear equilibrium distances were obtained at the levels of GHF-ZORA and GKS-ZORA/B3LYP, respectively. For calculations of energy gradients at the DFT level the nucleus was approximated as a point charge. The molecular structure parameters obtained are summarized in Table I.

IV. RESULTS

Our results for W_{d} and W_{s} are presented together with angular momentum quantum numbers Ω in Table II. All Ω values are close to the expected value $1/2$. Minor numerical deviations from $1/2$ are due to an imperfect alignment of the total electronic spin and angular momentum on the molecular

TABLE I. Molecular structure parameters calculated within a quasirelativistic ZORA approach at the cGHF and cGKS/B3LYP levels for metal hydroxide radicals MOH with M = Ca, Sr, Ba, Ra, Yb.

	$r(M\text{-O})$ (Å)		r(O-H) (Å)		$\sphericalangle(M\text{-O-H})$ (deg)	
M	cGHF	cGKS	cGHF	cGKS	cGHF	cGKS
Ca	2.006	1.972	0.932	0.954	179.91	179.70
Sr	2.134	2.110	0.933	0.955	179.99	179.93
Ba	2.239	2.207	0.935	0.956	179.93	179.95
Ra	2.315	2.289	0.935	0.956	179.93	179.93
Yb	2.083	2.002	0.933	0.953	179.92	179.92

axis, which cannot always be enforced within the cGHF or cGKS approach.

Values calculated for W_d and W_s on the DFT level for group 2 hydroxides differ only slightly from those obtained with GHF, which is in agreement with previous studies of $\mathcal{P},\mathcal{T}$ violation in group 2 compounds [15]. The larger deviation for YbOH hints that electron correlation effects are more important for this f-block compound. However, previous comparisons of our method with four-component coupled-cluster calculations for corresponding metal fluoride molecules show that the accuracy of the present approach can be estimated to be on the order of about 20% (see Ref. [21]), which is fully sufficient for the present purpose.

We find that compared to $\mathcal{P},\mathcal{T}$-odd enhancement in metal fluorides, calculated in Ref. [15], the values for the corresponding hydroxides are slightly larger in magnitude, but all in all differences are very small, below 5%. Considering possible improvements of the experimental setup with polyatomic molecules as described in Ref. [14], experiments with laser-coolable RaOH or YbOH as promising candidates for an improvement of current limits on the eEDM consequently would benefit mainly from full polarization of the molecule and the existence of internal co-magnetometer states, but not from improved electronic enhancement factors. The potential of the latter in polyatomic molecules is thus yet to be explored.

The proposed eEDM measurements in polyatomic molecules are planned to be performed in the first vibrational excited state [14] of the electronic ground state. However, vibrational corrections to the $\mathcal{P},\mathcal{T}$-odd properties presented herein are expected to be on the order of <10% and, thus, are below the predicted precision of our calculations. Furthermore, the first vibrational excited states in MOH compounds are the degenerate H-O bending modes v_2, which do not affect the M-O bonding much. For example, a rough estimate of vibrational corrections in the first vibrational state of YbOH was calculated from the potential energy surface (PES) within ZORA-cGHF (see Fig. 1). In leading order, vibrational corrections to the isotropic part of W_d for the H-O

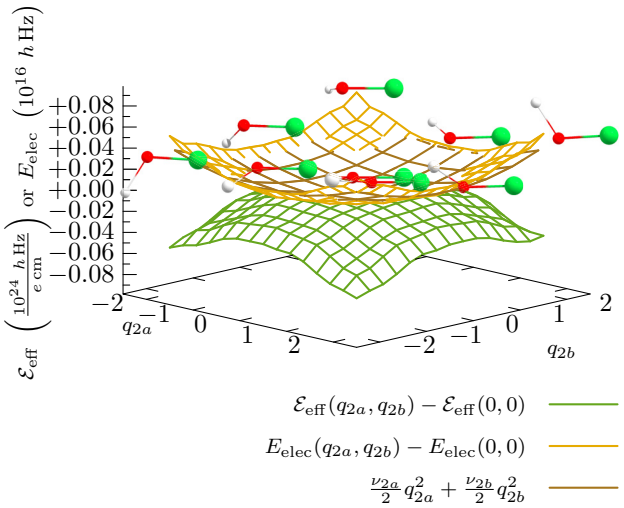

FIG. 1. Potential energy surface (PES) of YbOH in the space of the Yb-O-H bending mode q_{2a} and q_{2b} (lowest lying vibrational modes) with respect to the energy of the equilibrium structure at $q_{2a}=0$, $q_{2b}=0$: $E_\mathrm{elec}(q_{2a},q_{2b})-E_\mathrm{elec}(0,0)$ (yellow [light gray] plane), compared to the pure harmonic PES of YbOH (brown [dark gray] plane). The harmonic PES is determined from the harmonic vibrational wave number $\tilde{\nu}_{2a}=321$ cm^{-1} and $\tilde{\nu}_{2b}=347$ cm^{-1} corresponding to q_{2a} and q_{2b}, respectively. The degeneracy of the harmonic wave numbers is thus slightly lifted due to numerical reasons. The change of the effective internal electrical field that enhances the eEDM $\mathcal{E}_\mathrm{eff}=\Omega W_\mathrm{d}$ at the equilibrium structure is shown in dependency of q_{2a} and q_{2b} as well (green [medium gray] plane). All data were obtained at the level of ZORA-cGHF with a large even-tempered basis set. The equilibrium structure and displaced structures of YbOH for q_{2a}, $q_{2b}=-2.2, 0, 2.2$ are shown. Elements are represented as Yb (big, green [medium gray]), O (medium, red [dark gray]), and H (small, light grey).

TABLE II. Projection of the reduced total electronic angular momentum on the molecular axis and $\mathcal{P},\mathcal{T}$-violating properties of hydroxide radicals calculated *ab initio* within a quasirelativistic two-component ZORA approach at the cGHF and cGKS/B3LYP level. Dev. refers to the relative deviation between cGHF and cGKS results.

		Ω[a]		W_s (h Hz)			W_d ($10^{24}\,\frac{h\,\mathrm{Hz}}{e\,\mathrm{cm}}$)		
Molecule	Z	cGHF	cGKS	cGHF	cGKS	Dev.	cGHF	cGKS	Dev.
CaOH	20	−0.494	−0.499	-2.18×10^{2}	-2.14×10^{2}	2%	-1.44×10^{-1}	-1.41×10^{-1}	2%
SrOH	38	−0.500	−0.500	-2.00×10^{3}	-1.97×10^{3}	1%	−1.04	−1.03	1%
BaOH	56	0.483	0.483	-8.79×10^{3}	-7.91×10^{3}	10%	−3.32	−2.98	10%
RaOH	88	0.494	0.471	-1.53×10^{5}	-1.41×10^{5}	8%	-2.75×10^{1}	-2.53×10^{1}	8%
YbOH	70	−0.500	−0.495	-4.12×10^{4}	-3.08×10^{4}	25%	-1.14×10^{1}	−8.54	25%

[a]The absolute sign of Ω is arbitrary. However, relative to the sign of the effective electric field $W_\mathrm{d}\Omega$ it is always such that $\mathrm{sgn}(W_\mathrm{d})=-1$.

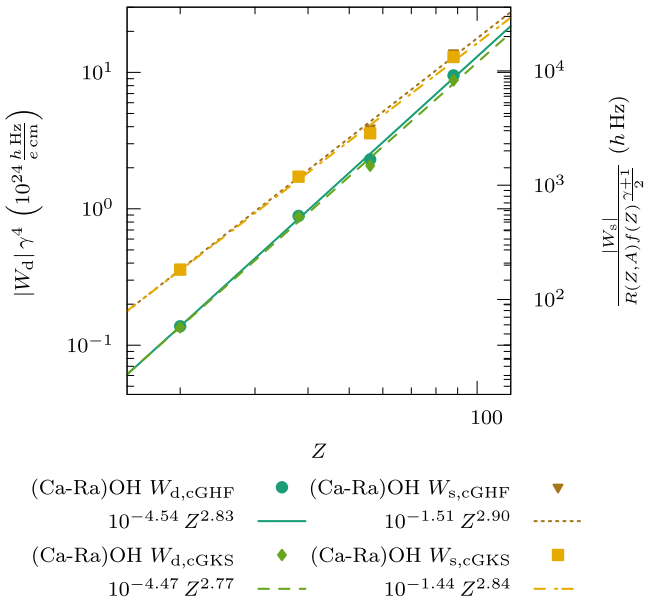

FIG. 2. Scaling of $\log_{10}\{|W_d|\gamma^4 \times 10^{-24}\,\frac{e\,\mathrm{cm}}{h\,\mathrm{Hz}}\}$ and $\log_{10}\{\frac{|W_s|}{R(Z,A)f(Z)^{\frac{\gamma+1}{2}}} \times \frac{1}{h\mathrm{Hz}}\}$ with $\log_{10}\{Z\}$ for group 2 hydroxides (Ca-Ra)OH at the level of GKS-ZORA/B3LYP and GHF-ZORA.

bending modes can be determined from

$$\langle\Psi, v_2 = 1|\hat{H}_d|\Psi, v_2 = 1\rangle \sim \frac{3}{8}\left(\frac{\partial^2\langle\Psi|\hat{H}_d|\Psi\rangle}{\partial q_{2a}^2} + \frac{\partial^2\langle\Psi|\hat{H}_d|\Psi\rangle}{\partial q_{2b}^2}\right), \quad (13)$$

where q_{2a} and q_{2b} are the dimensionless reduced normal coordinates of the degenerate O-H bending modes. The derivatives were evaluated numerically from the points of the PES. Our calculation predicts vibrational corrections on eEDM enhancement of $9 \times 10^{21}\,\frac{h\,\mathrm{Hz}}{e\,\mathrm{cm}}$, which is much less than 1% of W_d of YbOH and therefore far below the predicted accuracy of the present calculations. This is negligible as long as no eEDM has been measured. If one were led to use vibrational levels in higher lying electronic states as measurement states, computational methods for the description of electronically excited states would have to be used instead.

For further insight the scaling with nuclear charge Z is studied. For this purpose nonpolynomial relativistic enhancement is separated as described in Ref. [15] using relativistic enhancement factors known from atomic considerations [37–39]: $R_s = R(Z,A)f(Z)^{\frac{\gamma+1}{2}}$ and $R_d = \frac{1}{\gamma^4}$ with $f(Z) = \frac{1-0.56\alpha^2Z^2}{(1-0.283\alpha^2Z^2)^2}$ and $R(Z,A) = \frac{4}{\Gamma^2(2\gamma+1)}(2Zr_{nuc}/a_0)^{2\gamma-2}$. Here $\gamma = [(j+1/2)^2 - (\alpha Z)^2]^{1/2}$, j is the total electronic angular momentum quantum number, α is the fine structure constant, a_0 is the Bohr radius and $r_{nuc} \approx 1.2\ \mathrm{fm}\,A^{1/3}$. A double logarithmic plot for reduced cGHF and cGKS results as a function of Z together with a linear fit is presented in Fig. 2. The Z dependence for W_s (cGKS) of $Z^{2.83}$ is similar to that reported for group 2 fluorides in Ref. [15] for W_s (cGKS) of $Z^{2.79}$, whereas W_d scales steeper for MOH ($Z^{2.77}$) than for group 2 fluorides (Ref. [15]: $Z^{2.57}$).

In measurements of permanent molecular EDMs, various possible sources can be discussed and thus for robust bounds on $\mathcal{P},\mathcal{T}$-odd parameters, as the eEDM or k_s, complementary experiments have to be found, which are performed on systems with different electronic enhancement of the parameters. As discussed in detail in Ref. [15] the ratio W_d/W_s of two different experiments determines if the experiments are complementary or redundant for a parallel determination of k_s and d_e. In Table III the ratios W_d/W_s are compared to those of corresponding fluorides determined in Ref. [15].

TABLE III. $\mathcal{P},\mathcal{T}$-odd ratios W_d/W_s of hydroxide radicals MOH calculated within a quasirelativistic two-component ZORA approach at the cGKS/B3LYP level in comparison to ratios of corresponding fluoride radicals MF calculated in Ref. [15].

	$W_d/W_s\ (\frac{10^{20}}{e\,\mathrm{cm}})$	
M	MOH	MF
Ca	6.60	6.62
Sr	5.22	5.17
Ba	3.77	3.78
Ra	1.79	1.79
Yb	2.77	2.76

The values show that the metal hydroxides fit perfectly in the model developed in Ref. [15]. Hence there is in terms of electronic enhancement factors no immediate advantage of using a metal hydroxide instead of a fluoride. With respect to the coverage region in the parameter space of k_s and d_e, however, an experiment with MOH would be able to reduce the size of the coverage region due to the expected smaller systematic experimental uncertainties because of the presence of comagnetometer states. Experiments with the corresponding MF compounds could become redundant as essentially the same information regarding k_s and d_e is obtained.

As hyperfine coupling constants are sensitive to the behavior of s and p orbitals close to the nucleus, as well, and are directly measurable, we provide the parallel $A_\parallel$ and perpendicular components $A_\perp$ of the hyperfine coupling tensor calculated at the level of cGKS- and cGHF-ZORA in Table IV. $A_\parallel$ and $A_\perp$ can help to roughly estimate the error of the predicted $\mathcal{P},\mathcal{T}$-odd enhancement factors with respect to experiment, once microwave spectra of the proposed metal hydroxides containing high-spin isotopes of metal atoms are measured.

V. CONCLUSION

In this paper we reported the calculation of enhancements of an electric dipole moment of the electron in simple polyatomic molecules. Our calculations show that there is no considerable difference for enhancement factors between fluorides and hydroxides. This is also true for the ratio W_d/W_s. Thus, from a perspective of electronic enhancement factors there is no advantage in the use of MOH alongside MF in experiments as both experiments yield the same information on the parameter space of d_e and k_s. In order to see distinct differences from diatomic molecules it may be necessary to study more complex and nonlinear polyatomic molecules. However, together with the experimental benefits of polyatomic molecules described in Ref. [14] the herein studied molecules are promising candidates for an improvement of current limits on $\mathcal{P},\mathcal{T}$-violating effects.

TABLE IV. Hyperfine coupling constants calculated within a quasirelativistic ZORA approach at the cGHF and cGKS/B3LYP level for radical metal hydroxides MOH with $M = {}^{43}$Ca, ^{87}Sr, ^{137}Ba, ^{223}Ra, ^{173}Yb. Nuclear spins and nuclear magnetic moments are taken from Refs. [42,43].

			$A_\parallel$ (MHz)		$A_\perp$ (MHz)	
M	I_M	μ_M (μ_N)	cGHF	cGKS	cGHF	cGKS
^{43}Ca	$^7/_2$	−1.317 27	-3.6×10^2	-4.4×10^2	-3.4×10^2	-4.3×10^2
^{87}Sr	$^9/_2$	−1.092 83	-4.5×10^2	-5.8×10^2	-4.3×10^2	-5.6×10^2
^{137}Ba	$^3/_2$	0.937 365	1.9×10^3	2.3×10^3	1.8×10^3	2.3×10^3
^{223}Ra	$^3/_2$	0.2703	1.8×10^3	2.1×10^3	1.7×10^3	2.0×10^3
^{173}Yb	$^5/_2$	−0.67989	-1.6×10^3	-1.3×10^3	-1.6×10^3	–[a]

[a]The $^2\Sigma_{1/2}$ state of YbOH with total electronic spin aligned on the z axis and the molecular axis aligned on the x axis could not be converged within cGKS.

Note added. Recently, two other studies on $\mathcal{P},\mathcal{T}$-odd effects in YbOH and BaOH [40] and YbOH [41] were published. In Ref. [40] the results of our present paper are discussed and good agreement (relative deviations smaller than 7%) of the cGHF values has been found in comparison to their values obtained on the coupled-cluster level. As Dirac-Hartree-Fock results in Ref. [40] were obtained on the paired GHF level only, their values show larger discrepancy with coupled-cluster results due to the lack of spin-polarization effects. The coupled-cluster results for the effective electric field $\mathcal{E}_{\text{eff}}$ presented in Ref. [41] for linear structures of YbOH are also in good agreement (relative deviation less than 1%) with values at the level of cGHF.

ACKNOWLEDGMENTS

We thank Timur Isaev for inspiring discussions. Computer time provided by the Center for Scientific Computing (CSC) Frankfurt is gratefully acknowledged.

[1] D. DeMille, Phys. Today **68**(12), 34 (2015).
[2] I. B. Khriplovich and S. K. Lamoreaux, *CP Violation without Strangeness* (Springer, Berlin, 1997).
[3] J. Baron, W. C. Campbell, D. DeMille, J. M. Doyle, G. Gabrielse, Y. V. Gurevich, P. W. Hess, N. R. Hutzler, E. Kirilov, I. Kozyryev, B. R. O'Leary, C. D. Panda, M. F. Parsons, E. S. Petrik, B. Spaun, A. C. Vutha, and A. D. West, Science **343**, 269 (2014).
[4] V. Andreev, D. G. Ang, D. DeMille, J. M. Doyle, G. Gabrielse, J. Haefner, N. R. Hutzler, Z. Lasner, C. Meisenhelder, B. R. O'Leary, C. D. Panda, A. D. West, E. P. West, X. Wu, and A.C.M.E. Collaboration, Nature **562**, 355 (2018).
[5] J. S. M. Ginges and V. V. Flambaum, Phys. Rep. **397**, 63 (2004).
[6] T. A. Isaev and R. Berger, arXiv:1302.5682.
[7] A. D. Kudashov, A. N. Petrov, L. V. Skripnikov, N. S. Mosyagin, T. A. Isaev, R. Berger, and A. V. Titov, Phys. Rev. A **90**, 052513 (2014).
[8] S. Sasmal, H. Pathak, M. K. Nayak, N. Vaval, and S. Pal, Phys. Rev. A **93**, 062506 (2016).
[9] T. A. Isaev, S. Hoekstra, and R. Berger, Phys. Rev. A **82**, 052521 (2010).
[10] T. A. Isaev and R. Berger, Phys. Rev. Lett. **116**, 063006 (2016).
[11] T. A. Isaev and R. Berger, CHIMIA Int. J. Chem. **72**, 375 (2018).
[12] I. Kozyryev, L. Baum, K. Matsuda, B. L. Augenbraun, L. Anderegg, A. P. Sedlack, and J. M. Doyle, Phys. Rev. Lett. **118**, 173201 (2017).
[13] T. A. Isaev, A. V. Zaitsevskii, and E. Eliav, J. Phys. B **50**, 225101 (2017).
[14] I. Kozyryev and N. R. Hutzler, Phys. Rev. Lett. **119**, 133002 (2017).
[15] K. Gaul, S. Marquardt, T. Isaev, and R. Berger, Phys. Rev. A **99**, 032509 (2019).
[16] E. Altuntaş, J. Ammon, S. B. Cahn, and D. DeMille, Phys. Rev. Lett. **120**, 142501 (2018).
[17] M. G. Kozlov and L. N. Labzowsky, J. Phys. B **28**, 1933 (1995).
[18] K. Gaul and R. Berger, arXiv:1907.10432 [J. Chem. Phys. (to be published)].
[19] E. Salpeter, Phys. Rev. **112**, 1642 (1958).
[20] A. Mårtensson-Pendrill and P. Öster, Phys. Scr. **36**, 444 (1987).
[21] K. Gaul and R. Berger, J. Chem. Phys. **147**, 014109 (2017).
[22] C. van Wüllen, J. Chem. Phys. **109**, 392 (1998).
[23] R. Berger, N. Langermann, and C. van Wüllen, Phys. Rev. A **71**, 042105 (2005).
[24] R. Berger and C. van Wüllen, J. Chem. Phys. **122**, 134316 (2005).
[25] S. Nahrwold and R. Berger, J. Chem. Phys. **130**, 214101 (2009).
[26] C. van Wüllen, Z. Phys. Chem. **224**, 413 (2010).
[27] R. Ahlrichs, M. Bär, M. Häser, H. Horn, and C. Kölmel, Chem. Phys. Lett. **162**, 165 (1989).
[28] T. A. Isaev and R. Berger, Phys. Rev. A **86**, 062515 (2012).
[29] P. J. Stephens, F. J. Devlin, C. F. Chabalowski, and M. J. Frisch, J. Phys. Chem. **98**, 11623 (1994).
[30] S. H. Vosko, L. Wilk, and M. Nuisar, Can. J. Phys. **58**, 1200 (1980).
[31] A. D. Becke, Phys. Rev. A **38**, 3098 (1988).

[32] C. Lee, W. Yang, and R. G. Parr, Phys. Rev. B **37**, 785 (1988).
[33] B. O. Roos, R. Lindh, P. k. Malmqvist, V. Veryazov, and P. O. Widmark, J. Phys. Chem. A **108**, 2851 (2004).
[34] T. H. Dunning, Jr., J. Chem. Phys. **90**, 1007 (1989).
[35] W. Liu, C. van Wüllen, F. Wang, and L. Li, J. Chem. Phys. **116**, 3626 (2002).
[36] L. Visscher and K. G. Dyall, At. Data Nucl. Data Tables **67**, 207 (1997).
[37] V. A. Dzuba, V. V. Flambaum, and C. Harabati, Phys. Rev. A **84**, 052108 (2011).
[38] E. Fermi and E. Segrè, Mem. Acad. Ital. **4**, 131 (1933).
[39] E. Fermi and E. Segrè, Z. Phys. **82**, 729 (1933).
[40] M. Denis, P. A. B. Haase, R. G. E. Timmermans, E. Eliav, N. R. Hutzler, and A. Borschevsky, Phys. Rev. A **99**, 042512 (2019).
[41] V. S. Prasannaa, N. Shitara, A. Sakurai, M. Abe, and B. P. Das, Phys. Rev. A **99**, 062502 (2019).
[42] I. Mills, T. Cvitas, K. Homann, N. Kallay, and K. Kuchitsu, *Quantities, Units and Symbols in Physical Chemistry* (Blackwell Science, Oxford, 1988).
[43] K. M. Lynch, S. G. Wilkins, J. Billowes, C. L. Binnersley, M. L. Bissell, K. Chrysalidis, T. E. Cocolios, T. Goodacre, R. P. de Groote, G. J. Farooq-Smith, D. V. Fedorov, V. N. Fedosseev, K. T. Flanagan, S. Franchoo, R. F. Garcia Ruiz, W. Gins, R. Heinke, Á. Koszorús, B. A. Marsh, P. L. Molkanov *et al.*, Phys. Rev. C **97**, 024309 (2018).

The Journal of Chemical Physics ARTICLE scitation.org/journal/jcp

Toolbox approach for quasi-relativistic calculation of molecular properties for precision tests of fundamental physics

Cite as: J. Chem. Phys. 152, 044101 (2020); doi: 10.1063/1.5121483
Submitted: 25 July 2019 • Accepted: 14 October 2019 •
Published Online: 22 January 2020

Konstantin Gaul and Robert Berger[a)]

AFFILIATIONS

Fachbereich Chemie, Philipps-Universität Marburg, Hans-Meerwein-Straße 4, 35032 Marburg, Germany

[a)]Electronic mail: robert.berger@uni-marburg.de

ABSTRACT

A generally applicable approach for the calculation of relativistic properties described by one-electron operators within a two-component wave function approach is presented. The formalism is explicitly evaluated for the example of quasirelativistic wave functions obtained within the zeroth order regular approximation (ZORA). The wide applicability of the scheme is demonstrated for the calculation of parity ($\mathcal{P}$) and time-reversal ($\mathcal{T}$) symmetry violating properties, which are important for searches of physics beyond the standard model of particle physics. The quality of the ZORA results is shown exemplarily for the molecules RaF and TlF by comparison with data from four-component calculations as far as available. Finally, the applicability of RaF in experiments that search for $\mathcal{P},\mathcal{T}$-violation not only in the electronic but also in the quark sector is demonstrated.

I. INTRODUCTION

In order to explore the boundaries of the standard model of particle physics and of general relativity, a wealth of experiments was proposed in the last decades (see, e.g., Ref. 1), aiming for the detection of new physics. Molecular systems have gained meanwhile increasing importance for this research direction, which has recently been reviewed, for instance, in Ref. 2. Modern experiments take advantage of the rich but also highly complex vibronic internal structure of molecules, which is why theory plays a crucial role in the design and interpretation of established and future experiments.

From this search for new physics emerges also a large number of new properties of interest, of which many violate symmetries that are either conserved or only very weakly broken in established physics (see, e.g., Ref. 3). Several of the proposed phenomena are considered to be favorably enhanced in heavy-elemental molecules due to relativistic effects and therefore demand on the theory side a corresponding description of the electronic wave function, including spin-orbit coupling.

An accurate treatment of spin-orbit coupling in heavy elements requires at least a two-component wave function, which is nowadays available in many quantum chemistry software packages. However, naturally relativistic properties typically are described in a four-component framework. Therefore, all operators have to be transformed from four-component to two-component pictures in order to be consistent with quasirelativistic wave function formulations. As most programs do not include direct support for four-component treatments, this requires derivation of analytical expressions of two-component operators and commonly also a new, often tedious and error-prone implementation for every property.

In this paper, we develop a general formalism for flexible calculation of arbitrary relativistic properties described by one-electron operators within a two-component framework. We introduce our formalism in terms of two-component, one-electron density functions, and we provide a general formulation of corresponding properties for the case of zeroth order regular approximation (ZORA) wave functions. Our generally applicable scheme is demonstrated on the example of different sources of simultaneous parity ($\mathcal{P}$) and time-reversal ($\mathcal{T}$) symmetry violation in the diatomic molecules RaF and TlF, which are promising candidates for the first measurement of $\mathcal{P},\mathcal{T}$-violation beyond the Standard Model.[4–7] In future applications, the concepts and implementation derived in the following can also be used to study conventional nuclear magnetic

resonance (NMR) shielding constants and parity violating shifts in chiral molecules[8,9] and a wealth of further properties.

II. THEORY

A. Relativistic one-particle wave functions and operators

Relativistic electronic one-particle wave functions have a bispinor structure, which can be decomposed as

$$\psi = \begin{pmatrix} \psi^{\mathrm{L}} \\ \psi^{\mathrm{S}} \end{pmatrix} = \begin{pmatrix} \psi^{\mathrm{L}}_{\alpha} \\ \psi^{\mathrm{L}}_{\beta} \\ \psi^{\mathrm{S}}_{\alpha} \\ \psi^{\mathrm{S}}_{\beta} \end{pmatrix}. \tag{1}$$

Here, ψ^{L} and ψ^{S} are the spinors of the large or upper component and the small or lower component of the Dirac one-particle wave function ψ, respectively, and ψ_α and ψ_β are the spin orbitals with electron spin up and down, respectively. A similar structure is also found for one-particle operators in four component theory. Operators can be decomposed in a 2 × 2-block structure as

$$\hat{\mathbf{O}} = \begin{pmatrix} \hat{\mathbf{O}}^{\mathrm{LL}}_{2\times2} & \hat{\mathbf{O}}^{\mathrm{LS}}_{2\times2} \\ \hat{\mathbf{O}}^{\mathrm{SL}}_{2\times2} & \hat{\mathbf{O}}^{\mathrm{SS}}_{2\times2} \end{pmatrix}. \tag{2}$$

Thus, we can deduce four kinds of one-particle densities, which appear as contribution to all expectation values of custom one-electron operators in one-particle, four-component theory. These are contributions from large component-large component (LL), large component-small component (LS), small component-large component (SL), and small component-small component (SS) matrix elements. This formulation allows a decomposition of expectation values of four-component, one-electron operators in a sum of modified relativistic one-electron density functions $\Omega^{IJ}(\vec{r}) = \left(\psi^{I}(\vec{r})\right)^{\dagger}\hat{\mathbf{O}}^{IJ}_{2\times2}\psi^{J}(\vec{r})$, where IJ can be LL, LS, SL, or SS,

$$\left\langle\hat{\mathbf{O}}\right\rangle = \int \mathrm{d}\vec{r}\left[\Omega^{\mathrm{LL}}(\vec{r}) + \Omega^{\mathrm{SL}}(\vec{r}) + \Omega^{\mathrm{LS}}(\vec{r}) + \Omega^{\mathrm{SS}}(\vec{r})\right]. \tag{3}$$

In the following, all Ω^{IJ} are reformulated in terms of two-component density functions exploiting Lorentz symmetry properties of relativistic operators. Finally, this reformulation will allow a generally applicable procedure for the computation of Ω^{IJ} within an approximate two-component theory.

B. Lorentz group and relativistic density functions

The explicit representation of four-component, one-electron operators can be reduced to a linear combination of a special unitary basis of matrices in a four-dimensional space that corresponds to the Lorentz group $SU(2) \times SU(2)$, which represents the 2 × 2-block structure of the Dirac equation. This basis is formed by the 16 (or rather 32, allowing an imaginary phase of $\imath^k$ with the imaginary unit $\imath = \sqrt{-1}$ and $k \in \mathbb{N}_0$) Dirac matrices that are well known from quantum field theory,

$$\mathbf{\Gamma}^{i,j,k} = \imath^k\boldsymbol{\sigma}^i \otimes \boldsymbol{\sigma}^j;\ i,j = 0,1,2,3\ \wedge\ k \in \mathbb{N}_0, \tag{4}$$

where $\boldsymbol{\sigma}^i$ for i = 1, 2, 3 are the Pauli spin matrices and $\boldsymbol{\sigma}^0 = 1_{2\times2}$ is the two-dimensional identity matrix, which build the basis of $SU(2)$, and ⊗ is the Kronecker product.

The usual notation for theses matrices is

$$\mathbf{\Gamma}^{0,0,k} = \imath^k\boldsymbol{\sigma}^0 \otimes \boldsymbol{\sigma}^0 = \imath^k\mathbf{1}_{4\times4}, \tag{5a}$$

$$\mathbf{\Gamma}^{1,0,k} = \imath^k\boldsymbol{\sigma}^1 \otimes \boldsymbol{\sigma}^0 = \imath^k\boldsymbol{\gamma}^5, \tag{5b}$$

$$\mathbf{\Gamma}^{2,0,k} = \imath^{k-1}\imath\boldsymbol{\sigma}^2 \otimes \boldsymbol{\sigma}^0 = \imath^{k-1}\boldsymbol{\gamma}^0\boldsymbol{\gamma}^5, \tag{5c}$$

$$\mathbf{\Gamma}^{3,0,k} = \imath^k\boldsymbol{\sigma}^3 \otimes \boldsymbol{\sigma}^0 = \imath^k\boldsymbol{\gamma}^0 = \imath^k\boldsymbol{\beta}, \tag{5d}$$

$$\vec{\mathbf{\Gamma}}^{0,(1,2,3),k} = \imath^k\boldsymbol{\sigma}^0 \otimes \vec{\boldsymbol{\sigma}} = \imath^k\vec{\boldsymbol{\Sigma}}, \tag{5e}$$

$$\vec{\mathbf{\Gamma}}^{1,(1,2,3),k} = \imath^k\boldsymbol{\sigma}^1 \otimes \vec{\boldsymbol{\sigma}} = \imath^k\boldsymbol{\gamma}^0\vec{\boldsymbol{\gamma}} = \imath^k\vec{\boldsymbol{\alpha}}, \tag{5f}$$

$$\vec{\mathbf{\Gamma}}^{2,(1,2,3),k} = \imath^{k-1}\imath\boldsymbol{\sigma}^2 \otimes \vec{\boldsymbol{\sigma}} = \imath^{k-1}\vec{\boldsymbol{\gamma}}, \tag{5g}$$

$$\vec{\mathbf{\Gamma}}^{3,(1,2,3),k} = \imath^k\boldsymbol{\sigma}^3 \otimes \vec{\boldsymbol{\sigma}} = \imath^k\boldsymbol{\gamma}^0\vec{\boldsymbol{\Sigma}}. \tag{5h}$$

Employing this structure and switching to a specific reference frame in which time independence is assumed, we can define 32 Dirac one-electron density functions of electron 1 which are build as

$$\Gamma^{i,j,k}(\vec{r}_1,\vec{r}_1') = \hat{\mathcal{D}}\Big[\left(\Psi(\vec{R})\right)^{\dagger}\vec{\mathbf{\Gamma}}^{i,j,k}_1 \otimes \mathbf{\Gamma}^{0,0,0}_2 \otimes \cdots \otimes \mathbf{\Gamma}^{0,0,0}_{N_{\mathrm{elec}}}\Psi(\vec{R}')\Big]. \tag{6}$$

We have introduced in this equation the many-particle wave function Ψ, which depends on the set $\vec{R} = \{\vec{r}_1,\ldots,\vec{r}_N\}$ of N_{elec} spatial coordinates, with $\vec{r}_i$ for each electron i, and the one-electron density projection operator

$$\hat{\mathcal{D}} = N_{\mathrm{elec}}\mathfrak{Re}\int\cdots\int_{\vec{r}_i=\vec{r}_i';\ i=2,\ldots,N} \mathrm{d}\vec{r}_2\cdots\mathrm{d}\vec{r}_N, \tag{7}$$

which integrates out all coordinates, except one spatial coordinate $\vec{r}_1$. Coordinates with a prime are introduced to formally allow a discrimination between the left and right function that contributes to the density function, in order to enable the definition of operators acting on the left or right function, respectively.

Employing the 2 × 2-block structure of the one-particle Dirac equation, we can decompose the Dirac one-electron density functions further by introducing four kinds of two-component densities for each of the four four-component densities $\rho^{IJ,j,k}$. For $I = J = \mathrm{L}$ the two-component density functions can be classified as (i) number density functions $\rho^{IJ,0,2k}$, (ii) number current density functions $\rho^{IJ,0,2k+1}$, (iii) spin density functions $\vec{\rho}^{IJ,(1,2,3),2k}$, and (iv) spin current density functions $\vec{\rho}^{IJ,(1,2,3),2k+1}$. Thus, there are in total 4 × 4 = 16 two-component, one-electron density functions, which can be combined linearly to give the 32 Dirac one-electron density functions,

$$\Gamma^{0,j,k}(\vec{r},\vec{r}') = \rho^{\mathrm{LL},j,k}(\vec{r},\vec{r}') + \rho^{\mathrm{SS},j,k}(\vec{r},\vec{r}'), \tag{8a}$$

$$\Gamma^{1,j,k}(\vec{r},\vec{r}') = \rho^{\mathrm{LS},j,k}(\vec{r},\vec{r}') + \rho^{\mathrm{SL},j,k}(\vec{r},\vec{r}'), \tag{8b}$$

$$\Gamma^{2,j,k}(\vec{r},\vec{r}') = \rho^{\mathrm{LS},j,k-1}(\vec{r},\vec{r}') - \rho^{\mathrm{SL},j,k-1}(\vec{r},\vec{r}'), \tag{8c}$$

$$\Gamma^{3,j,k}(\vec{r},\vec{r}') = \rho^{\mathrm{LL},j,k}(\vec{r},\vec{r}') - \rho^{\mathrm{SS},j,k}(\vec{r},\vec{r}'). \tag{8d}$$

We introduce the spin tensor function in correspondence to the four Pauli matrices with a complex phase,

$$\boldsymbol{\varsigma}(j,k) = \imath^k \boldsymbol{\sigma}^j. \tag{9}$$

Using this spin tensor function, the two-component, one-electron density functions of electron 1 are build with the spinors of the Dirac one-particle wave function containing either only the large component for the first electron Ψ^{L} or only the small component for the first electron Ψ^{S} as

$$\rho^{IJ,j,k}(\vec{r}_1,\vec{r}_1') = \hat{\mathcal{D}}\Big[\left(\Psi^I(\vec{R})\right)^\dagger \boldsymbol{\varsigma}_1(j,k) \otimes \boldsymbol{\sigma}_2^0 \otimes \cdots \otimes \boldsymbol{\sigma}_{N_{\mathrm{elec}}}^0 \Psi^J(\vec{R}')\Big]. \tag{10}$$

C. Quasirelativistic approximation and ZORA

In order to be able to calculate these relativistic density functions in two-component theories, we need to approximate the small component wave function. The exact transformation of the large-component, one-particle wave function into the small-component, one-particle wave function is given by

$$\psi^{\mathrm{S}}(\vec{r}) = \underbrace{c\left(2m_{\mathrm{e}}c^2\mathbf{1}_{2\times2} - \hat{\mathbf{V}}_{\mathrm{diag}}^{\mathrm{SS}} + \epsilon\mathbf{1}_{2\times2}\right)^{-1}}_{=c\boldsymbol{\omega}} \underbrace{\left(\vec{\boldsymbol{\sigma}}\cdot\hat{\vec{p}} + \hat{\mathbf{V}}_{\mathrm{off}}^{\mathrm{SL}}\right)}_{\bar{\boldsymbol{\omega}}} \psi^{\mathrm{L}}(\vec{r}). \tag{11}$$

Here, ϵ is the electronic energy of the single particle state; $\hat{\vec{p}} = -\imath\hbar\vec{\nabla}$ is the one-electron linear momentum operator in position space, with $\hbar = \frac{h}{2\pi}$ being the reduced Planck's constant; $\hat{\mathbf{V}}_{\mathrm{diag}}^{\mathrm{SS}}$ is the SS-block of the potential effective one-electron operator appearing on the diagonal of the Hamiltonian; $\hat{\mathbf{V}}_{\mathrm{off}}^{\mathrm{SL}}$ is the SL-block of a potential effective one-electron operator appearing on the off-diagonal of the Hamiltonian, as, e.g., a vector potential or the Breit operator, both as effective one-electron operators; m_{e} is the electron mass; and c is the speed of light in vacuum.

For a two-component method, we can replace ψ^{L} approximately by the wave function optimized within this specific method and use the corresponding approximate transformation matrix $\boldsymbol{\omega}$ to construct an approximate ψ^{S}.

As $\hat{\mathbf{V}}_{\mathrm{off}}^{\mathrm{SL}}$ is an effective one-electron operator, the modified momentum matrix $\bar{\boldsymbol{\omega}}$ can be decomposed into a linear combination of spin tensor functions as

$$\bar{\boldsymbol{\omega}} = \sum_{j=0}^{3}\sum_{k=0}^{1} \boldsymbol{\varsigma}(j,k)\hat{\pi}^{j,k}, \tag{12}$$

with the modified one-electron momentum operators $\hat{\pi}^{j,k}$. Neglecting all off-diagonal potentials, $\bar{\boldsymbol{\omega}}$ simplifies to

$$\bar{\boldsymbol{\omega}} \approx \vec{\boldsymbol{\sigma}}\cdot\hat{\vec{p}} = -\hbar\imath\vec{\boldsymbol{\sigma}}\cdot\vec{\nabla}, \tag{13}$$

so that $\hat{\vec{\pi}}^{(1,2,3),1} = -\hbar\vec{\nabla}$. For all $j = 0$ or $k = 0$, we have $\hat{\pi}_i^{j,k} = 0$.

In the present paper, we implemented the scheme within zeroth order regular approximation (ZORA) without potentials appearing on the off-diagonal,

$$\psi^{\mathrm{L}}(\vec{r}) \approx \psi^{\mathrm{ZORA}}(\vec{r}), \tag{14}$$

$$\psi^{\mathrm{S}}(\vec{r}) \approx \underbrace{\frac{c}{2m_{\mathrm{e}}c^2 - \tilde{V}(\vec{r})}}_{=c\omega^{\mathrm{ZORA}}(\vec{r})} \vec{\boldsymbol{\sigma}}\cdot\hat{\vec{p}}\psi_i^{\mathrm{ZORA}}(\vec{r}), \tag{15}$$

where we assume an unperturbed scalar transformation factor ω, which depends only on a model-potential $\tilde{V}$ as introduced by van Wüllen.[10] The model-potential is an effective one-electron operator that does not depend on the molecular wave function and is designed to alleviate the gauge variance of ZORA. All perturbations to the diagonal potential $\hat{\mathbf{V}}_{\mathrm{diag}}$ are neglected in $\tilde{V}$. We emphasize that our scheme can be used similarly for the computation of expectation values, when a corresponding infinite order regular approximation (IORA) approach is applied to determine the unperturbed wave functions.

Corrections stemming from the presence of vector potentials appear as additional terms and can be included afterward by calculation of matrix elements of the corresponding operators, which is straightforward in the present approach.

In the mean-field approximation, the ZORA N_{elec}-electron wave function is represented as N_{elec} Slater determinant of one-electron wave functions ψ_i^{ZORA}, which are composed of N_{basis} real spatial basis functions χ_μ and complex two component coefficients $\vec{C}_{i\mu}$,

$$\Psi^{\mathrm{ZORA}} = |\psi_1^{\mathrm{ZORA}}\cdots\psi_N^{\mathrm{ZORA}}|, \tag{16}$$

with

$$\psi_i^{\mathrm{ZORA}} = \sum_{\mu=1}^{N_{\mathrm{basis}}} \vec{C}_{i\mu}\chi_\mu, \tag{17}$$

where

$$\vec{C}_{i\mu} = \begin{pmatrix} C_{i\mu}^{\alpha} \\ C_{i\mu}^{\beta} \end{pmatrix}. \tag{18}$$

Only the coefficients depend on the spin component so that spin can in this form easily be integrated out. Furthermore, in this approach, we can define for each molecular orbital (MO) i a MO-density function $\rho_i^{IJ,j,k}$. The total ZORA-density function is a sum of all N_{orb} MO-density functions weighted by their occupation number n_i, which is 0 for unoccupied orbitals or 1 for occupied orbitals,

$$\rho^{IJ,j,k}(\vec{r},\vec{r}') = \sum_{i=1}^{N_{\mathrm{orb}}} n_i\rho_i^{IJ,j,k}(\vec{r},\vec{r}'). \tag{19}$$

Within ZORA, the one-electron MO-density functions $\rho_i^{IJ,j,k}$ are evaluated explicitly as

$$\rho_i^{\mathrm{LL},j,k}(\vec{r},\vec{r}') = \sum_{\mu\nu}^{N_{\mathrm{basis}}} \underbrace{\mathfrak{Re}\left\{\vec{C}_{i\mu}^\dagger\vec{\boldsymbol{\varsigma}}(j,k)\vec{C}_{i\nu}\right\}}_{\mathcal{D}_{i\mu\nu}^{j,k,(0,0)}} \cdot \underbrace{\left(\chi_\mu\chi_\nu'\right)}_{\mathcal{I}_{\mu\nu}^{(0,0)}}, \tag{20a}$$

$$\rho_i^{\mathrm{LS},j,k}(\vec{r},\vec{r}') = \sum_{\mu\nu}^{N_{\mathrm{basis}}}\sum_{l=1}^{3} \underbrace{\mathfrak{Re}\left\{\vec{C}_{i\mu}^\dagger\boldsymbol{\varsigma}(j,k)\left(-\imath\boldsymbol{\sigma}^l\vec{C}_{i\nu}\right)\right\}}_{\mathcal{D}_{i\mu\nu}^{j,k,(0,l)}} \cdot \underbrace{\left(\hbar c\chi_\mu\omega'(\vec{\partial}_\nu')_l\right)}_{\mathcal{I}_{\mu\nu}^{(0,l)}}, \tag{20b}$$

$$\rho_i^{\mathrm{SL},j,k}(\vec{r},\vec{r}') = \sum_{\mu\nu}^{N_{\mathrm{basis}}} \sum_{l=1}^{3} \underbrace{\mathfrak{Re}\left\{\left(\vec{C}_{i\mu}^{\dagger}\imath\boldsymbol{\sigma}^{l}\right)\boldsymbol{\varsigma}(j,k)\vec{C}_{i\nu}\right\}}_{\mathcal{D}_{i\mu\nu}^{j,k,(l,0)}} \cdot \underbrace{\left(\hbar c(\vec{\partial}_{\mu})_{l}\omega\chi_{\nu}'\right)}_{\mathcal{I}_{\mu\nu}^{(l,0)}}, \tag{20c}$$

$$\rho_i^{\mathrm{SS},j,k}(\vec{r},\vec{r}') = \sum_{\mu\nu}^{N_{\mathrm{basis}}} \sum_{l=1}^{3} \sum_{m=1}^{3} \underbrace{\mathfrak{Re}\left\{\left(\vec{C}_{i\mu}^{\dagger}\imath\boldsymbol{\sigma}^{l}\right)\boldsymbol{\varsigma}(j,k)\left(-\imath\boldsymbol{\sigma}^{m}\vec{C}_{i\nu}\right)\right\}}_{\mathcal{D}_{i\mu\nu}^{j,k,(l,m)}} \cdot \underbrace{\left(\hbar^2 c^2(\vec{\partial}_{\mu})_{l}\omega\omega'(\vec{\partial}_{\nu}')_{m}\right)}_{\mathcal{I}_{\mu\nu}^{(l,m)}}. \tag{20d}$$

Here, we used the short-hand notations: $\chi_\mu(\vec{r}) = \chi_\mu$, $\chi_\mu(\vec{r}') = \chi_\mu'$, $\nabla\chi_\mu = \vec{\partial}_\mu$, $\nabla'\chi_\mu' = \vec{\partial}_\mu'$, $\omega^{\mathrm{ZORA}}(\vec{r}) = \omega$, and $\omega^{\mathrm{ZORA}}(\vec{r}') = \omega'$. Generalization of Eqs. (20a)–(20d) in terms of $\mathcal{D}$, $\mathcal{I}$ gives

$$\rho_i^{IJ,j,k}(\vec{r},\vec{r}') = \sum_{\mu\nu}^{N_{\mathrm{basis}}} \sum_{l\in M(I)} \sum_{m\in M(J)} \mathcal{D}_{i\mu\nu}^{j,k,(l,m)} \mathcal{I}_{\mu\nu}^{(l,m)}(\vec{r},\vec{r}'), \tag{21}$$

where $M(I) = \begin{cases} \{1,2,3\}, & \text{if } I = \mathrm{S} \\ \{0\}, & \text{if } I = \mathrm{L} \end{cases}$ is a mapping between spin indices l, m of $\boldsymbol{\mathcal{D}}_i^{j,k,(l,m)}$ and $\boldsymbol{\mathcal{I}}^{(l,m)}$ and the relativistic type of the two-component density function I, J and

$$\mathcal{D}_{i\mu\nu}^{j,k,(l,m)} = \mathfrak{Re}\left\{\left(\vec{C}_{i\mu}\right)^{\dagger}\boldsymbol{\varsigma}(l,1-\delta_{l0})\boldsymbol{\varsigma}(j,k)\boldsymbol{\varsigma}(m,3-3\delta_{m0})\vec{C}_{i\nu}\right\}, \tag{22}$$

$$\mathcal{I}_{\mu\nu}^{(l,m)}(\vec{r},\vec{r}') = (\hbar c)^{2-\delta_{l0}-\delta_{m0}} \partial_{\mu}^{(l)} \omega^{1-\delta_{l0}} \omega'^{1-\delta_{m0}} \partial_{\nu}'^{(m)}, \tag{23}$$

with $\partial_\mu^{(i)} = \begin{cases} \frac{\partial\chi_\mu}{\partial(\vec{r})_i}, & \text{if } i = 1,2,3 \\ \chi_\mu, & \text{if } i = 0 \end{cases}$ and analogously with prime.

Here, the density matrices $\boldsymbol{\mathcal{D}}^{j,k,(l,m)} = \sum_{i=1}^{N_{\mathrm{occ}}} \boldsymbol{\mathcal{D}}_i^{j,k,(l,m)}$ can be constructed from the four (eight when separating real and imaginary parts) two-component density matrices $\mathbf{D}^{(k)}$, which are defined in terms of Pauli matrices as

$$D_{\mu\nu}^{(k)} = \sum_{i=1}^{N_{\mathrm{occ}}} \underbrace{\vec{C}_{i\mu}^{\dagger}\boldsymbol{\sigma}^{k}\vec{C}_{i\nu}}_{D_{i\mu\nu}^{(k)}}. \tag{24}$$

The explicit expressions for $\boldsymbol{\mathcal{D}}^{j,k,(k,l)}$ in terms of $\mathbf{D}^{(k)}$ can be evaluated following Eq. (22) and using commutator relations of Pauli matrices.

D. Generic tensor function formulation of molecular properties

With the two-component formulation of relativistic density functions introduced in Sec. II C, we can formulate a generic one-electron tensor function which can directly be connected to an arbitrary molecular property described by one-electron operators. For this purpose, we introduce, besides the relativistic $\Gamma^{i,j,k}$ or quasirelativistic one-electron density function $\rho^{IJ,j,k}$, a general differential tensor operator $\hat{\boldsymbol{\partial}}(\vec{r}' \vee \vec{r})$, which acts on $\vec{r}'$ or $\vec{r}$. Within this flexible formulation, we do not use turnover rule, which can complicate calculations as pointed out in Ref. 11. Furthermore, a general tensor operator $\hat{\mathbf{t}}(\vec{r})$ and a general scalar operator $\hat{s}$ are defined. All these operators may be defined arbitrarily. In Sec. V, some explicit realizations for these operators will be discussed. A generic one-electron tensor function can now be written as

$$\boldsymbol{\Omega}^{i,j,k}(\vec{r}) = \hat{s}\hat{\mathbf{t}} \circ \hat{\boldsymbol{\partial}}(\vec{r}' \vee \vec{r}) \circ \Gamma^{i,j,k}(\vec{r},\vec{r}')\Big|_{\vec{r}'=\vec{r}}, \tag{25}$$

or for two-component density functions as

$$\boldsymbol{\Omega}^{IJ,j,k}(\vec{r}) = \hat{s}\hat{\mathbf{t}} \circ \hat{\boldsymbol{\partial}}(\vec{r}' \vee \vec{r}) \circ \rho^{IJ,j,k}(\vec{r},\vec{r}')\Big|_{\vec{r}'=\vec{r}}, \tag{26}$$

where $\circ = \otimes, \cdot, \times$, with $\otimes$ being the outer product, $\cdot$ being the inner product, and $\times$ being the cross product. The latter is defined only within $\mathbb{R}^3$. Here, j can be 0 or (1, 2, 3). In the latter case, $\Gamma^{i,j,k}$ is a three-dimensional vector. This formulation allows the flexible construction of one-electron operators that can correspond to molecular properties. The expectation value is received by integration over space,

$$\left\langle \hat{\mathbf{O}}(\boldsymbol{\Gamma}^{i,j,k}, \hat{s}, \hat{\mathbf{t}}, \hat{\boldsymbol{\partial}}) \right\rangle = \int \mathrm{d}^3\vec{r}\, \boldsymbol{\Omega}^{i,j,k}(\vec{r}). \tag{27}$$

With explicit expressions for quasirelativistic ZORA density functions given in Eqs. (21)–(23) and the definitions of the relativistic density functions in Eq. (8), the working equation for the computation of the expectation value of an arbitrary relativistic one-electron operator within ZORA is

$$\left\langle \hat{\mathbf{O}}(\boldsymbol{\Gamma}^{i,j,k}, \hat{s}, \hat{\mathbf{t}}, \hat{\boldsymbol{\partial}}) \right\rangle = \sum_{IJ\in\mathcal{M}(i)} \sum_{n}^{N_{\mathrm{occ}}} \sum_{\mu\nu}^{N_{\mathrm{basis}}} \sum_{l\in M(I)} \sum_{m\in M(J)} \mathcal{D}_{n\mu\nu}^{j,k,(l,m)} \circ \int_{\vec{r}'=\vec{r}} \mathrm{d}^3\vec{r}\left[\hat{s}(\vec{r})\hat{\mathbf{t}}(\vec{r}) \circ \hat{\boldsymbol{\partial}}(\vec{r}' \vee \vec{r})\mathcal{I}_{\mu\nu}^{(l,m)}(\vec{r},\vec{r}')\right]. \tag{28}$$

Here, $\mathcal{M}(i)$ maps the index i of the Dirac density function to a sum of two-component density functions with appropriate sign following Eq. (8).

The above expressions are valid for properties within first order perturbation theory only. In the case of second order properties, the corresponding density functions have to be constructed with perturbed density matrices $\tilde{\mathbf{D}}^{(k)}$ or rather transition density matrices. These can be received via common algorithms by solving the coupled perturbed Hartree-Fock (CPHF) or Kohn-Sham (CPKS) equations. For uncoupled problems, the above density functions can be used in a simple sum-over-states (SoS) framework. For this purpose, instead of the MO-coefficients of only occupied orbitals, also the MO-coefficients of unoccupied orbitals have to be considered, weighted by the orbital energy differences.

III. IMPLEMENTATION

The above formalism was implemented within a two-component ZORA version[12] of the quantum chemistry program package Turbomole.[13] The derivative operator $\hat{\boldsymbol{\partial}}(\vec{r}' \vee \vec{r})$ was limited to first and second derivatives. The tensor operator can always be reduced to any sum of tensor products of the electronic position vector with respect to some arbitrary origin $\vec{r} - \vec{r}_{\mathrm{O}}$ or with respect to the center of a nucleus A: $\vec{r} - \vec{r}_A$. Equation (28) is rewritten in terms of two-component density matrices $\mathbf{D}^{(k)}$ as

$$\left\langle \hat{\mathbf{O}}(\mathbf{\Gamma}^{i,j,k}, \hat{s}, \hat{\mathbf{t}}, \hat{\boldsymbol{\partial}}) \right\rangle = \sum_{IJ \in \mathcal{M}(i)} \sum_{n}^{N_{\text{occ}}} \sum_{\mu\nu}^{N_{\text{basis}}} \sum_{m=0}^{3} \mathfrak{Re}\left\{ \imath^{l} D_{n\mu\nu}^{(m)} \right\} \circ \underbrace{\int \mathrm{d}^3\vec{r} \left[\hat{s}(\vec{r}) \hat{\mathbf{t}}(\vec{r}) \circ \hat{\boldsymbol{\partial}}(\vec{r}' \vee \vec{r}) \tilde{\mathcal{I}}_{\mu\nu}^{IJ,j,k,(m,l)}(\vec{r}, \vec{r}') \right]_{\vec{r}'=\vec{r}}}_{O_{\text{AO},\mu\nu}^{IJ,j,k,(m,l)}}. \tag{29}$$

Within the above-mentioned restrictions for the derivative operator, a Fortran code was automatically generated for the evaluation of the integrand of Eq. (29) (term in square brackets) with the computer algebra system Mathematica.[14]

The code was generated for the derivative operators $\vec{\nabla}\otimes$, $\vec{\nabla}\cdot$, $\vec{\nabla}\times$, $\vec{\nabla}\otimes\vec{\nabla}\cdot$, $\vec{\nabla}\cdot\vec{\nabla}\otimes$, $\vec{\nabla}\otimes\vec{\nabla}\times$, and $\vec{\nabla}\times\vec{\nabla}\times$. For computation of maximally second derivatives, at most third derivatives of basis functions are required due to the appearance of first derivatives of matrix elements containing the small component. Furthermore, up to second derivatives of the model potential are needed with respect to $\vec{r}$. These were implemented following Ref. 10. In the case of second derivatives, third derivatives of density functionals with respect to the model density are required. These were approximated by central finite differences of analytical second derivatives of the density functional.

Within our implementation, integrals are evaluated by default on a grid using standard numerical integration methods, established for density functional theory (DFT) calculations. Integrals that do not contain the ZORA-factor ω can typically be evaluated analytically. In the present implementation, however, only a few analytical integrals are available.

We added also a SoS module for the calculation of second order properties within an uncoupled DFT approach. The SoS calculation is carried out with transition density functions that are evaluated analogously to Eqs. (20a)–(20d) as densities between occupied and unoccupied orbitals i, a,

$$\tilde{\rho}_{ia}^{\text{LL},j,k}(\vec{r}, \vec{r}') = \sum_{\mu\nu}^{N_{\text{basis}}} \left\{ \vec{C}_{i\mu}^{\dagger} \boldsymbol{\varsigma}(j,k) \vec{C}_{a\nu} \right\} \cdot \left(\chi_\mu \chi_\nu' \right), \tag{30}$$

and so on. The second order SoS expression is

$$\sum_{i=1}^{N_{\text{occ}}} \sum_{a=1+N_{\text{occ}}}^{N_{\text{orb}}} \frac{\left\langle \psi_i \middle| \hat{\mathbf{O}}_1 \middle| \psi_a \right\rangle \left\langle \psi_a \middle| \hat{\mathbf{O}}_2 \middle| \psi_i \right\rangle}{(\epsilon_i - \epsilon_a)} + \text{cc}, \tag{31}$$

where ϵ are the orbital energies, i are indices of occupied orbitals, and a are indices of unoccupied orbitals. The integrals $\left\langle \psi_i \middle| \hat{\mathbf{O}} \middle| \psi_a \right\rangle$ are evaluated via the corresponding generic transition one-electron tensor functions as

$$\left\langle \psi_i \middle| \hat{\mathbf{O}} \middle| \psi_a \right\rangle = \int \mathrm{d}^3\vec{r}\, \tilde{\mathbf{\Omega}}_{ia}^{j,k}(\vec{r}), \tag{32}$$

with

$$\tilde{\mathbf{\Omega}}_{ia}^{IJ,j,k}(\vec{r}) = \hat{s}\hat{\mathbf{t}} \circ \hat{\boldsymbol{\partial}}(\vec{r}' \vee \vec{r}) \tilde{\rho}_{ia}^{IJ,j,k}(\vec{r}, \vec{r}')\Big|_{\vec{r}'=\vec{r}}. \tag{33}$$

The contraction of AO-matrix elements with LCAO-coefficients is implemented via density matrices as described in Sec. II D or matrix multiplications of the type $(\mathbf{C}_{\text{occ}}^{(\xi)})^{\dagger} \mathbf{O}_{\text{AO}}^{IJ,j,k,(m,l)} \mathbf{C}_{\text{unocc}}^{(\xi)}$, where ξ can be α or β and $\mathbf{C}_{\text{occ}}^{(\xi)}$ and $\mathbf{C}_{\text{unocc}}^{(\xi)}$ are the α- and β-spin blocks of the block of occupied and unoccupied orbitals in the coefficient matrix, respectively. Here, for component (m, l) of the matrix of integrals in AO-basis $\mathbf{O}_{\text{AO}}^{IJ,j,k,(m,l)}$, the sum of matrix multiplications with α- and β-coefficient matrices, which correspond to $\boldsymbol{\varsigma}(m, l)$, is formed.

In order to account for renormalization effects, which are in the ZORA approach, particularly relevant for the description of the energetically lowest lying orbitals with main contributions close to the nucleus, we implemented the possibility of renormalization of the ZORA wave function by redefinition of the coefficient matrices

$$\tilde{\vec{C}}_{i\mu} = \frac{\vec{C}_{i\mu}}{\sqrt{1 + \int \mathrm{d}^3\vec{r}\, \rho_i^{\text{SS},0,0}(\vec{r})}}. \tag{34}$$

This renormalization can be evaluated directly within the general implementation of one-electron operators presented above.

IV. COMPUTATIONAL DETAILS

Quasirelativistic two-component calculations are performed within ZORA at the level of complex generalized Hartree–Fock (cGHF) or Kohn–Sham (cGKS) with a modified version[12] of the quantum chemistry program package Turbomole.[13]

For Kohn–Sham (KS)-DFT calculations, the hybrid Becke three parameter exchange functional and Lee, Yang, and Parr correlation functional (B3LYP)[15–18] was employed. In comparison with the relativistic coupled cluster (CC) calculations, this functional performed well for the description of $\mathcal{P},\mathcal{T}$-odd effects in diatomic radicals in our previous work, which motivates the present choice.[19–21]

For all calculations, a basis set of 37 s, 34 p, 14 d, and 9 f uncontracted Gaussian functions with the exponential coefficients α_i composed as an even-tempered series by $\alpha_i = a \cdot b^{N-i}$; $i = 1, \ldots, N$, with $b = 2$ for s- and p-function and with $b = (5/2)^{1/25} \times 10^{2/5} \approx 2.6$ for d- and f-functions was used for Tl and Ra. The largest exponent coefficients of the s, p, d, and f subsets are $2 \times 10^9\ a_0^{-2}$, $5 \times 10^8\ a_0^{-2}$, 13 300.758 a_0^{-2}, and 751.836 835 0 a_0^{-2}, respectively. This basis set has proven successful in the calculations of nuclear-spin dependent $\mathcal{P}$-violating interactions and $\mathcal{P},\mathcal{T}$-odd effects induced by an electric dipole moment of the electron (eEDM) in heavy polar diatomic molecules.[6,19–23] In Refs. 6, 22, and 23, however, a slightly larger basis set was used on radium with two more diffuse s functions and one additional diffuse f function from this even-tempered series, but resulting relative changes in the properties reported in the present paper would remain below 1%. The F atom was represented with the s, p, d subset of a decontracted atomic natural orbital (ANO) basis set of triple-ζ quality.[24]

The ZORA-model potential $\tilde{V}(\vec{r})$ as proposed by van Wüllen[10] was employed with additional damping.[25]

For calculations of two-component wave functions and properties, a finite nucleus was used, described by a normalized spherical Gaussian nuclear density distribution $\rho_{\text{nuc},A}(\vec{r}) = \frac{\zeta_A^{3/2}}{\pi^{3/2}} \mathrm{e}^{-\zeta_A |\vec{r} - \vec{r}_A|^2}$, where $\zeta_A = \frac{3}{2r_{\text{nuc},A}^2}$ and the root-mean-square radius $r_{\text{nuc},A}$ of nucleus A was used as suggested by Visscher and Dyall.[26] The mass numbers A were chosen to correspond to the isotopes ^{205}Tl and ^{223}Ra.

Nuclear equilibrium distances were obtained at the levels of GHF-ZORA and GKS-ZORA/B3LYP, respectively. As convergence criteria, an energy change of less than 10^{-5} E_h was used. For DFT calculations of analytic energy gradients with respect to the displacement of the nuclei, the nuclei were approximated as point charges. The equilibrium distances obtained are for ^{205}TlF 2.08 Å (cGHF) and 2.12 Å (cGKS) and for ^{223}RaF 2.28 Å (cGHF) and 2.26 Å (cGKS).

All properties were computed with and without renormalization of the wave function according to (34).

V. RESULTS AND DISCUSSION

A. Enhancement of various sources of $\mathcal{P},\mathcal{T}$-violation in paramagnetic RaF and diamagnetic TlF

Measurement of a permanent electric dipole moment in vanishing electric field would indicate a simultaneous violation of parity $\mathcal{P}$ and time-reversal $\mathcal{T}$ symmetry (see, e.g., Ref. 3). Molecular systems provide currently the strictest experimental limits on permanent electric dipole moments.[27,28]

There are many possible $\mathcal{P},\mathcal{T}$-violating sources that can lead to a permanent electric dipole moment in a molecule depending on the nuclear and electronic spin states of the molecule.[3,29] For paramagnetic molecules such as RaF, pronounced sensitivity is expected for a potential permanent electric dipole moment of the electron (eEDM) d_e and from $\mathcal{P},\mathcal{T}$-odd scalar-pseudoscalar nucleon-electron current (SPNEC) interactions k_S.[30]

However, in the case of a nonzero nuclear spin, additional contributions from interactions of the electron cloud with a potential permanent electric dipole moment of the proton (pEDM) d_p, interactions with a net electric dipole moment of the nucleus, called Schiff moment $\mathcal{S}$, tensor-pseudotensor nucleon-electron current (TPNEC) interactions k_T, and pseudoscalar-scalar nucleon-electron current (PSNEC) interactions k_p can occur. The latter, PSNEC, vanishes in the limit of infinitely large mass of the nucleus, which appears to be a reasonable approximation for heavy-elemental molecules, as $m_e \ll m_{nuc}$.[3]

Nuclear spin-dependent contributions are the dominating sources for $\mathcal{P},\mathcal{T}$-violation in diamagnetic molecules such as TlF, where interactions with an eEDM or due to SPNECs appear only as indirect interactions via hyperfine induced coupling, because of vanishing total effective electron spin.

In paramagnetic molecules that contain nuclei with spin quantum number I larger than 1/2, also interactions with higher $\mathcal{P},\mathcal{T}$-odd nuclear moments, such as nuclear magnetic quadrupole moments (NMQM), could contribute to a permanent molecular EDM.

The full $\mathcal{P},\mathcal{T}$-odd effective spin-rotational Hamiltonian for a paramagnetic diatomic molecule for nucleus A with nuclear spin quantum number larger than 1/2 reads as (for parts of $\hat{H}_{\mathrm{sr}_A}$, see Refs. 29 and 4)

$$\begin{aligned}\hat{H}_{\mathrm{sr}_A} = &\underbrace{\vec{\lambda}\cdot\hat{\vec{S}}}_{\Omega}\left(W_{\mathrm{d}_A} d_e + W_{\mathrm{s}_A} k_s\right)\\ &+ \underbrace{\vec{\lambda}^T\cdot\hat{\mathbf{T}}_A\cdot\hat{\vec{S}}}_{\Theta_A} W_{\mathcal{M}_A}\tilde{\mathcal{M}}_A + \text{higher moments}\ldots\\ &+ \underbrace{\vec{\lambda}\cdot\hat{\vec{I}}_A}_{\mathcal{I}_A}\left(W_{\mathrm{T}_A} k_T + W_{\mathrm{p}_A} k_p + W^{\mathrm{m}}_{\mathrm{s}_A} k_s + W_{\mathcal{S}_A}\mathcal{S}_A\right.\\ &\left.+ \left(W_{\mathrm{m}_A} + W_{\mathcal{S}_A} R_{\mathrm{vol}}\right) d_p + W^{\mathrm{m}}_{\mathrm{d}_A} d_e\right). \end{aligned} \tag{35}$$

Here, $\vec{\lambda}$ is the unit vector pointing from the heavy to the light nucleus, $\hat{\vec{S}}$ is the effective reduced electron spin of the molecule, $\hat{\vec{I}}_A$ is the effective reduced nuclear spin of nucleus A, $\hat{\mathbf{T}}_A$ is a second-rank tensor that can be constructed from the components of $\hat{\vec{I}}_A$ (for details, see Ref. 29), $\tilde{\mathcal{M}}_A = \frac{-1}{2I_A(2I_A-1)}\mathcal{M}_A$ with the NMQM $\mathcal{M}$ (see Ref. 29), Ω is the projection of the effective reduced electron spin on the molecular axis, and $\mathcal{I}_A$ is the projection of $\hat{\vec{I}}_A$ on the molecular axis. For a diamagnetic molecule, all terms that depend on the effective electronic spin $\vec{S}$ (here, all proportional to Ω and Θ) vanish. The constants W are electronic structure coupling constants enhancing $\mathcal{P},\mathcal{T}$-violating parameters in molecules, which need to be determined by electronic structure calculations. R_{vol} is a nuclear structure factor that enhances the pEDM and can be determined from nuclear structure calculations.

In the following, we will focus on the electronic structure enhancement factors W in RaF and TlF. Thereby, we will not calculate W_{p_A} which is supposed to be many orders of magnitude smaller than the other effects.[3,30] Furthermore, we do not include in our discussion nuclear-spin dependent effects $W^{\mathrm{m}}_{\mathrm{s}_A}$ and $W^{\mathrm{m}}_{\mathrm{d}_A}$ that are induced by hyperfine coupling and thus are second-order molecular properties that can be obtained from a linear response treatment. Assuming the molecular axes to be aligned along the z axis, the remaining electronic structure parameters are defined in the following (see, e.g., Refs. 3, 4, 29, 31, and 32):

(i) electronic structure enhancement of the eEDM,

$$W_{\mathrm{d}} = \frac{\left\langle\Psi\left|\frac{2c}{e\hbar}\imath\boldsymbol{\gamma}^0\boldsymbol{\gamma}^5\hat{\vec{p}}^2\right|\Psi\right\rangle}{\Omega}, \tag{36}$$

with e being the elementary charge and $\hbar = \frac{h}{2\pi}$ being the reduced Planck's constants;

(ii) electronic structure enhancement of the NMQM,

$$W_{\mathcal{M}_A} = \frac{\left\langle\Psi\left|cek_{\mathrm{em}}\frac{3}{2}\frac{(z-z_A)(\vec{\boldsymbol{\alpha}}\times(\vec{r}-\vec{r}_A))_z}{|\vec{r}-\vec{r}_A|^5}\right|\Psi\right\rangle}{\Omega}, \tag{37}$$

with the constant k_{em} being $\frac{\mu_0}{4\pi}$ in SI units, with μ_0 being the magnetic constant (see Ref. 33 for other choices of k_{em} that correspond to different unit systems);

(iii) electronic structure enhancement of nuclear Schiff moment and volume effect due to a pEDM,

$$W_{\mathcal{S},A} = \frac{2\pi}{3}\frac{\partial}{\partial z}\Gamma^{0,0,0}(\vec{r},\vec{r})\Big|_{\vec{r}=\vec{r}_A}, \tag{38}$$

in calculations of $W_{\mathcal{S},A}$, the value was calculated at eight points at a distance of 1.7×10^{-25} a_0 around the nucleus (cubic arrangement) and averaged; this Hamiltonian is a consequence of Schiff's theorem[34] and is the dipole contribution of an expansion of the electric potential of a finite nucleus (for details, see Ref. 35);

(iv) electronic structure enhancement of the pEDM due to magnetic fields of moving electrons,

$$W_{\mathrm{m}_A} = \left\langle\Psi\left|4\left(\frac{\mu_{\mathrm{N}}}{A_A}+\frac{\mu_A}{Z_A}\right)c\frac{k_{\mathrm{em}}}{k}|\vec{r}-\vec{r}_A|^{-3}\left(\vec{\boldsymbol{\alpha}}\times\hat{\vec{\ell}}_A\right)_z\right|\Psi\right\rangle, \tag{39}$$

TABLE I. Representation of various $\mathcal{P},\mathcal{T}$-odd properties in the formalism of general tensor functions.

Property	Prefactor	$\hat{s}$	$\hat{\mathrm{t}}\circ$	$\hat{\boldsymbol{\partial}}\circ$	$\mathbf{\Gamma}^{i,j,k}$
W_d	$-\frac{2c\hbar}{e\Omega}$	...	...	$\vec{\nabla}\cdot\vec{\nabla}\otimes$	$\mathbf{\Gamma}^{2,0,2}$
$W_\mathcal{M}$	$\frac{3}{2\Omega}cek_\mathrm{em}$	$\frac{z-z_A}{\lvert\vec{r}-\vec{r}_A\rvert^5}$	$-(\vec{r}-\vec{r}_A)\times$	...	$\vec{\mathbf{\Gamma}}^{1,(1,2,3),0}$
$W_\mathcal{S}$	$\frac{2\pi}{3}$	$\delta(\vec{r}_A-\vec{r})$	...	$\vec{\nabla}\otimes$	$\mathbf{\Gamma}^{0,0,0}$
W_m	$4\left(\frac{\mu_\mathrm{N}}{A_A}+\frac{\mu_A}{Z_A}\right)c\frac{k_\mathrm{em}}{k}$	$\lvert\vec{r}-\vec{r}_A\rvert^{-3}$	$(\vec{r}-\vec{r}_A)\times$	$\vec{\nabla}\times$	$\vec{\mathbf{\Gamma}}^{1,(1,2,3),1}$
W_s	$\frac{G_\mathrm{F}}{\sqrt{2}\Omega}$	$\rho_\mathrm{nuc}(\vec{r})$	...	...	$\mathbf{\Gamma}^{2,0,2}$
W_T	$\sqrt{2}G_\mathrm{F}$	$\rho_\mathrm{nuc}(\vec{r})$	...	...	$\mathbf{\Gamma}^{2,3,2}$

with constant k, which is 1 in SI units and c^{-1} in Gauss units, the orbital angular momentum operator with respect to nucleus A $\hbar\hat{\vec{\ell}}_A=(\vec{r}-\vec{r}_A)\times\hat{\vec{p}}$, the nuclear magneton $\mu_\mathrm{N}=\frac{e\hbar}{2m_\mathrm{p}}$ with the mass of the proton m_p, the nuclear magnetic moment μ_A, the nuclear charge Z_A, and mass number A_A of nucleus A. Here, we assume that the contributions stem from a single active valence proton in the nuclear shell (see Ref. 4);

(v) electronic structure enhancement of SPNEC interactions,

$$W_{\mathrm{s}_A}=\frac{\left\langle\Psi\middle|\frac{G_\mathrm{F}}{\sqrt{2}}\imath\gamma^0\gamma^5\rho_{\mathrm{nuc},A}\middle|\Psi\right\rangle}{\Omega}, \tag{40}$$

with the Fermi weak coupling constant $G_\mathrm{F}=2.222\,49\times10^{-14}E_\mathrm{h}a_0^3$;

(vi) electronic structure enhancement of TPNEC interactions,

$$W_{\mathrm{T}_A}=\left\langle\Psi\middle|\sqrt{2}G_\mathrm{F}\imath\gamma^3\rho_{\mathrm{nuc},A}\middle|\Psi\right\rangle. \tag{41}$$

With the method presented in Secs. II and III, all these properties can be directly evaluated as illustrated in Table I. We choose as exemplary molecular systems RaF and TlF, which were well studied before and are considered promising candidates for experiments that aim at a measurement of $\mathcal{P},\mathcal{T}$-odd properties.[4,6,32,36–38]

We neglect any magnetic or many-electron effects on the above-presented properties that may arise from the ZORA transformation as these are expected to be low for heavy elements. For some of the properties, such effects were discussed elsewhere (see, e.g., Refs. 20 and 39).

1. Diamagnetic molecules: TlF

In this section, we discuss the results for TlF that were obtained from property calculations with an implementation of the approach described in Sec. III. Results of our calculations on the level of cGHF- and cGKS-B3LYP-ZORA are compared with results from literature in Table II.

We see an excellent agreement (deviations ≲5%) between cGHF-ZORA and DHF results reported by Quiney *et. al.* for all calculated properties.[32] Furthermore, renormalization of the wave function does not play an important role for the nuclear spin-dependent properties and is always below 1%. This is to be expected as all major contributions stem from the valence molecular orbitals at the position of the nucleus. This shows that ZORA is appropriate for the quantitative description of relativistic effects due to nuclear-spin dependent $\mathcal{P},\mathcal{T}$-odd interactions in a heavy molecule, which reinforces related previous findings for nuclear-spin independent and nuclear-spin dependent $\mathcal{P}$-odd interactions in molecules.[8,22,23,40–43] Correlation effects were estimated on the DFT level with the B3LYP hybrid density functional. This functional, however, seems to overshoot electron correlation effects leading to values being too low in magnitude with deviations of up to 23% in comparison with GRECP/RCC-SD calculations.[44]

2. Paramagnetic molecules: RaF

We report results on electronic structure enhancement factors of nuclear spin-dependent and nuclear spin-independent $\mathcal{P},\mathcal{T}$-effects in ^{223}RaF in Table III and compare with all available literature data.

Also for nuclear-spin independent properties and the nuclear- and electron-spin dependent NMQM, most important contributions stem from valence molecular orbitals and thus effects of renormalization are negligible. The reasonable agreement between cGHF/cGKS-ZORA and four component coupled cluster calculations[36,37] for W_d and W_s was discussed elsewhere.[19,20,36] Our present values for W_d and W_s differ in the last reported digit from the results in Refs. 19 and 20 as we consider herein a different isotope of Ra.

TABLE II. Nuclear spin-dependent, electron spin-independent $\mathcal{P},\mathcal{T}$-odd electronic structure parameters of the diamagnetic molecule ^{205}TlF evaluated at the level of cGHF- and cGKS-ZORA with a large even tempered basis set with (wr) and without renormalization (wor) of the density according to Eq. (34). Comparison with literature values determined with different computational method. The value $\mu(^{205}\mathrm{Tl})=1.638\,213\,5\,\mu_\mathrm{N}$ was used for the nuclear magnetic moment of ^{205}Tl.[47]

Method	W_T/h Hz	$W_\mathrm{m}/\frac{10^{18}\,h\,\mathrm{Hz}}{e\,\mathrm{cm}}$	$W_\mathcal{S}/a_0^4$
cGHF-ZORA-wor	4697	−4.74	8443
cGHF-ZORA-wr	4690	−4.72	8428
cGKS-ZORA-B3LYP-wr	3375	−3.10	5720
DHF[a] (Ref. 32)	4632	−4.78	8747
GRECP-RCC-SD[b] (Ref. 44)	...	−4.04	7635
DF[c] (Ref. 38)	...	−5.46	7738

[a]Dirac–Hartree–Fock calculation without electron correlation.
[b]Generalized relativistic effective core potential, two-step approach with restricted active space SCF electron-correlation calculation at the level of single and double excitations.
[c]Dirac-Fock calculation without electron correlation.

TABLE III. Electron and nuclear spin-dependent $\mathcal{P},\mathcal{T}$-odd electronic structure parameters of the paramagnetic molecule ^{223}RaF evaluated at the level of cGHF- and cGKS-ZORA with a large even tempered basis set with (wr) and without renormalization (wor) of the density according to Eq. (34). Comparison with the available literature values determined with different computational methods. The value $\mu(^{223}\text{Ra}) \simeq 0.27\ \mu_N$ was used for the nuclear magnetic moment of ^{223}Ra.[47,48] In all our calculations, $\Omega = 0.500$.

Method	W_T/hHz	$W_m/\frac{10^{18}\ h\,\text{Hz}}{e\,\text{cm}}$	W_S/a_0^4	W_s/h kHz	$W_d/\frac{10^{24}\ h\,\text{Hz}}{e\,\text{cm}}$	$W_{\mathcal{M}}/\frac{10^{33}\ h\,\text{Hz}}{c\,e\,\text{cm}^2}$
cGHF-ZORA-wor	−1810	0.66	−4235	−152	−27.2	−1.17
cGHF-ZORA-wr	−1809	0.66	−4229	−152	−27.2	−1.17
cGKS-ZORA-B3LYP-wr	−1617	0.58	−3686	−138	−24.6	−1.03
FS-RCCSD + Δ_{basis} + Δ_{triples}[a] (Ref. 36)	...	...	−4260	−139	−25.6	...
DF-CCSD[b] (Ref. 37)	...	...	...	−141	−25.4	...

[a]Relativistic two-component Fock-space coupled-cluster approach with single and double excitations (CCSD) with basis set corrections from CCSD calculations with normal and large sized basis sets and triple excitation corrections from CCSD calculations with and without perturbative triples.
[b]Dirac-Fock calculation with electron-correlation effects on the level of coupled cluster with single and double excitations.

Our calculations of W_S are with deviations of 8% (cGHF) in good agreement with GRECP-FSCC calculations (Ref. 36). As observed in previous studies,[19,20] DFT tends to give results too low in absolute value. However, the value of W_S still agrees reasonably (deviation is 12%) with the coupled cluster calculations. From this, we expect a similar precision of cGHF- and cGKS-ZORA calculations of W_T and W_m.

Our calculations show that nuclear-spin dependent $\mathcal{P},\mathcal{T}$-odd enhancement factors in RaF are by about a factor of 1/2–1/8 smaller in magnitude compared with TlF. The ratios of $\frac{W_T}{W_S}$ and $\frac{W_m}{W_S}$ are considerably different for TlF and RaF. Thus, data from the measurements of RaF would complement data from TlF measurements as different regions in the parameter space of the $\mathcal{P},\mathcal{T}$-odd parameters k_T, d_p, and $\mathcal{S}$ are covered.

In Table III, we present values for $W_{\mathcal{M}}$, as well. In comparison with predictions of NMQM enhancement made for other molecules,[45] the values for RaF are very large (as large as predicted for YbF or ThO). Furthermore, the ^{223}Ra nucleus is known to have an octupole deformation, which is expected to enhance NMQM effects significantly on the nuclear structure level.[46] This makes ^{223}RaF a promising candidate for setting strict limits on NMQM induced permanent electric dipole moments.

VI. CONCLUSION

We outlined a generally applicable approach to the evaluation of arbitrary relativistic properties within an approximate quasirelativistic wave function. Automated code generation via a computer algebra system was applied to obtain a pilot implementation within a modified version of a quantum chemical program for ZORA wave functions. Within the approach presented herein, relativistic first and second order properties ranging from commonly available molecular properties, such as NMR-shielding constants, to less common discrete symmetry violating properties are accessible in a single implementation. The flexibility of this property toolbox approach was demonstrated by computation of a number of $\mathcal{P},\mathcal{T}$-odd effects that are important for fundamental physics research with diatomic molecules.

Within this study, large enhancements of the nuclear magnetic quadrupole moment and nuclear spin-dependent as well as nuclear spin-independent sources of $\mathcal{P},\mathcal{T}$-violation in RaF were determined. This shows that ^{223}RaF is a well suited system for setting strict limits on $\mathcal{CP}$-violation in essentially all sectors of particle physics.

ACKNOWLEDGMENTS

Computer time provided by the Center for Scientific Computing (CSC), Frankfurt, and financial support by the Deutsche Forschungsgemeinschaft via Sonderforschungsbereich Grant No. 1319 (ELCH) "Extreme Light for Sensing and Driving Molecular Chirality" are gratefully acknowledged.

REFERENCES

[1] D. DeMille, J. M. Doyle, and A. O. Sushkov, "Probing the frontiers of particle physics with tabletop-scale experiments," Science **357**, 990–994 (2017).
[2] M. S. Safronova, D. Budker, D. DeMille, D. F. J. Kimball, A. Derevianko, and C. W. Clark, "Search for new physics with atoms and molecules," Rev. Mod. Phys. **90**, 025008 (2018).
[3] I. B. Khriplovich and S. K. Lamoreaux, *CP Violation without Strangeness* (Springer, Berlin, 1997).
[4] E. A. Hinds and P. G. H. Sandars, "Electric dipole hyperfine structure of TlF," Phys. Rev. A **21**, 471–479 (1980).
[5] L. R. Hunter, S. K. Peck, A. S. Greenspon, S. S. Alam, and D. DeMille, "Prospects for laser cooling TlF," Phys. Rev. A **85**, 012511 (2012).
[6] T. A. Isaev and R. Berger, "Lasercooled radium monofluoride: A molecular all-in-one probe for new physics," e-print arXiv:1302.5682 [physics.chem-ph] (2013).
[7] E. B. Norrgard, E. R. Edwards, D. J. McCarron, M. H. Steinecker, D. DeMille, S. S. Alam, S. K. Peck, N. S. Wadia, and L. R. Hunter, "Hyperfine structure of the $B^3\Pi_1$ state and predictions of optical cycling behavior in the $X \rightarrow B$ transition of TlF," Phys. Rev. A **95**, 062506 (2017).
[8] S. Nahrwold and R. Berger, "Zeroth order regular approximation approach to parity violating nuclear magnetic resonance shielding tensors," J. Chem. Phys. **130**, 214101 (2009).
[9] S. Nahrwold, R. Berger, and P. Schwerdtfeger, "Parity violation in nuclear magnetic resonance frequencies of chiral tetrahedral tungsten complexes NWXYZ (X, Y, Z = H, F, Cl, Br or I)," J. Chem. Phys. **140**, 024305 (2014).
[10] C. van Wüllen, "Molecular density functional calculations in the regular relativistic approximation: Method, application to coinage metal diatomics, hydrides, fluorides and chlorides, and comparison with first-order relativistic calculations," J. Chem. Phys. **109**, 392–399 (1998).
[11] W. Kutzelnigg, "Origin and meaning of the fermi contact interaction," Theor. Chim. Acta **73**, 173–200 (1988).

[12]C. van Wüllen, "A quasirelativistic two-component density functional and Hartree-Fock program," Z. Phys. Chem **224**, 413–426 (2010).
[13]R. Ahlrichs, M. Bär, M. Häser, H. Horn, and C. Kölmel, "Electronic structure calculations on workstation computers: The program system turbomole," Chem. Phys. Lett. **162**, 165–169 (1989).
[14]Wolfram Research, Inc., Mathematica 10.4, 2016.
[15]P. J. Stephens, F. J. Devlin, C. F. Chabalowski, and M. J. Frisch, "*Ab initio* calculation of vibrational absorption and circular dichroism spectra using density functional force fields," J. Phys. Chem. **98**, 11623–11627 (1994).
[16]S. H. Vosko, L. Wilk, and M. Nuisar, "Accurate spin-dependent electron liquid correlation energies for local spin density calculations: A critical analysis," Can. J. Phys. **58**, 1200–1211 (1980).
[17]A. D. Becke, "Density-functional exchange-energy approximation with correct asymptotic-behavior," Phys. Rev. A **38**, 3098–3100 (1988).
[18]C. Lee, W. Yang, and R. G. Parr, "Development of the Colle-Salvetti correlation-energy formula into a functional of the electron-density," Phys. Rev. B **37**, 785–789 (1988).
[19]K. Gaul and R. Berger, "Zeroth order regular approximation approach to electric dipole moment interactions of the electron," J. Chem. Phys. **147**, 014109 (2017).
[20]K. Gaul, S. Marquardt, T. Isaev, and R. Berger, "Systematic study of relativistic and chemical enhancements of $\mathcal{P},\mathcal{T}$-odd effects in polar diatomic radicals," Phys. Rev. A **99**, 032509 (2019); e-print arXiv:1805.05494 [physics.chem-ph].
[21]K. Gaul and R. Berger, "*Ab initio* study of parity and time-reversal violation in laser-coolable triatomic molecules," Phys Rev. A **101**, 012508 (2020).
[22]T. A. Isaev and R. Berger, "Electron correlation and nuclear charge dependence of parity-violating properties in open-shell diatomic molecules," Phys. Rev. A **86**, 062515 (2012).
[23]T. A. Isaev and R. Berger, "Periodic trends in parity-violating hyperfine coupling constants of open-shell diatomic molecules," J. Mol. Spectrosc. **300**, 26–30 (2014).
[24]B. O. Roos, R. Lindh, P. k. Malmqvist, V. Veryazov, and P. O. Widmark, "Main group atoms and dimers studied with a new relativistic ANO basis set," J. Phys. Chem. A **108**, 2851–2858 (2004).
[25]W. Liu, C. van Wüllen, F. Wang, and L. Li, "Spectroscopic constants of MH and M_2 (M = Tl, E113, Bi, E115): Direct comparisons of four- and two-component approaches in the framework of relativistic density functional theory," J. Chem. Phys. **116**, 3626–3634 (2002).
[26]L. Visscher and K. G. Dyall, "Dirac-Fock atomic electronic structure calculations using different nuclear charge distributions," At. Data Nucl. Data Tables **67**, 207–224 (1997).
[27]D. DeMille, "Diatomic molecules, a window onto fundamental physics," Phys. Today **68**(12), 34–40 (2015).
[28]V. Andreev, D. G. Ang, D. DeMille, J. M. Doyle, G. Gabrielse, J. Haefner, N. R. Hutzler, Z. Lasner, C. Meisenhelder, B. R. O'Leary, C. D. Panda, A. D. West, E. P. West, X. Wu, and ACME Collaboration, "Improved limit on the electric dipole moment of the electron," Nature **562**, 355–360 (2018).
[29]M. G. Kozlov and L. N. Labzowsky, "Parity violation effects in diatomics," J. Phys. B: At., Mol. Opt. Phys. **28**, 1933–1961 (1995).
[30]J. S. M. Ginges and V. V. Flambaum, "Violations of fundamental symmetries in atoms and tests of unification theories of elementary particles," Phys. Rep. **397**, 63–154 (2004).
[31]A. Mårtensson-Pendrill and P. Öster, "Calculations of atomic electric dipole moments," Phys. Scr. **36**, 444–452 (1987).
[32]H. M. Quiney, J. K. Laerdahl, K. Fægri, and T. Saue, "*Ab initio* Dirac-Hartree-Fock calculations of chemical properties and PT-odd effects in thallium fluoride," Phys. Rev. A **57**, 920–944 (1998).
[33]E. R. Cohen, T. Cvitas, J. G. Frey, B. Holmström, K. Kuchitsu, R. Marquardt, I. Mills, F. Pavese, M. Quack, J. Stohner, H. L. Strauss, M. Takami, and A. J. Thor, in *Quantities, Units and Symbols in Physical Chemistry*, 3rd ed. (IUPAC & RSC Publishing, Cambridge, 2008).
[34]L. I. Schiff, "Measurability of nuclear electric dipole moments," Phys. Rev. **132**, 2194–2200 (1963).
[35]O. P. Sushkov, V. V. Flambaum, and I. B. Khriplovich, "Possibility of investigating P- and T-odd nuclear forces in atomic and molecular experiments," Sov. Phys. JETP **60**, 873–883 (1984).
[36]A. D. Kudashov, A. N. Petrov, L. V. Skripnikov, N. S. Mosyagin, T. A. Isaev, R. Berger, and A. V. Titov, "*Ab initio* study of radium monofluoride (RaF) as a candidate to search for parity- and time-and-parity violation effects," Phys. Rev. A **90**, 052513 (2014).
[37]S. Sasmal, H. Pathak, M. K. Nayak, N. Vaval, and S. Pal, "Relativistic coupled-cluster study of RaF as a candidate for the parity- and time-reversal-violating interaction," Phys. Rev. A **93**, 062506 (2016).
[38]F. A. Parpia, "Electric-dipole hyperfine matrix elements of the ground state of the TlF molecule in the Dirac–Fock approximation," J. Phys. B: At., Mol. Opt. Phys. **30**, 3983 (1997).
[39]E. Lindroth, B. W. Lynn, and P. G. H. Sandars, "Order α^2 theory of the atomic electric dipole moment due to an electric dipole moment of the electron," J. Phys. B: At., Mol. Opt. Phys. **22**, 559–576 (1989).
[40]R. Berger, N. Langermann, and C. van Wüllen, "Zeroth order regular approximation approach to molecular parity violation," Phys. Rev. A **71**, 042105 (2005).
[41]R. Berger and C. van Wüllen, "Density functional calculations of molecular parity violating effects within the zeroth order regular approximation," J. Chem. Phys. **122**, 134316 (2005).
[42]R. Berger and J. L. Stuber, "Electroweak interactions in chiral molecules: Two-component density functional theory study of vibrational frequency shifts in polyhalomethanes," Mol. Phys. **105**, 41–49 (2007).
[43]T. A. Isaev, S. Hoekstra, and R. Berger, "Laser-cooled RaF as a promising candidate to measure molecular parity violation," Phys. Rev. A **82**, 052521 (2010).
[44]A. N. Petrov, N. S. Mosyagin, T. A. Isaev, A. V. Titov, V. F. Ezhov, E. Eliav, and U. Kaldor, "Calculation of *P, T*-odd effects in ^{205}TlF including electron correlation," Phys. Rev. Lett. **88**, 073001 (2002).
[45]V. V. Flambaum, D. DeMille, and M. G. Kozlov, "Time-reversal symmetry violation in molecules induced by nuclear magnetic quadrupole moments," Phys. Rev. Lett. **113**, 103003 (2014).
[46]V. Flambaum, "Spin hedgehog and collective magnetic quadrupole moments induced by parity and time invariance violating interaction," Phys. Lett. B **320**, 211–215 (1994).
[47]I. Mills, T. Cvitas, K. Homann, N. Kallay, and K. Kuchitsu, Quan., Units and Symb. in Phys. Chem., 13–165 (1988).
[48]K. M. Lynch, S. G. Wilkins, J. Billowes, C. L. Binnersley, M. L. Bissell, K. Chrysalidis, T. E. Cocolios, T. Goodacre, R. P. de Groote, G. J. Farooq-Smith, D. V. Fedorov, V. N. Fedosseev, K. T. Flanagan, S. Franchoo, R. F. Garcia Ruiz, W. Gins, R. Heinke, A. Koszorús, B. A. Marsh, P. L. Molkanov, P. Naubereit, G. Neyens, C. M. Ricketts, S. Rothe, C. Seiffert, M. D. Seliverstov, H. H. Stroke, D. Studer, A. R. Vernon, K. D. A. Wendt, and X. F. Yang, Phys. Rev. C **97**, 024309 (2018).

Chiral molecules as sensitive probes for direct detection of $\mathcal{P}$-odd cosmic fields

Konstantin Gaul,[1] Mikhail G. Kozlov,[2,3] Timur A. Isaev,[2] and Robert Berger[1]

[1] *Fachbereich Chemie, Philipps-Universität Marburg, Hans-Meerwein-Straße 4, 35032 Marburg, Germany*

[2] *Petersburg Nuclear Physics Institute of NRC "Kurchatov Institute", Gatchina 188300, Russia*

[3] *St. Petersburg Electrotechnical University "LETI", Prof. Popov Str. 5, 197376 St. Petersburg*

(Dated: August 13, 2020)

Potential advantages of chiral molecules for a sensitive search for parity violating cosmic fields are highlighted. Such fields are invoked in different models for cold dark matter or in the Lorentz-invariance violating standard model extensions and thus are signatures of physics beyond the standard model. The sensitivity of a twenty year old experiment with the molecule CHBrClF to pseudovector cosmic fields as characterized by the parameter $|b_0^e|$ is estimated to be $\mathcal{O}(10^{-12}\,\mathrm{GeV})$ employing ab initio calculations. This allows to project the sensitivity of future experiments with favorable choices of chiral heavy-elemental molecular probes to be $\mathcal{O}(10^{-17}\,\mathrm{GeV})$, which will be an improvement of the present best limits by at least two orders of magnitude.

Introduction.—The nature of dark matter (DM), the existence of which is invoked to explain the cosmological motion of visible matter, is considered to be one of the biggest unsolved problems of modern physics (see e.g. Ref. [1]). Among the various DM theories, the cold DM (CDM) variant appears to provide a simple explanation for a wealth of astrophysical observations [2]. Up to now, however, the constituents of CDM are unknown and can range from macroscopic objects such as black holes to new particles like weakly interacting massive particles (WIMPs), axions, sterile neutrinos or dark photons (see e.g. Refs. [3–5]).

The model of CDM has also several shortcomings [6–11]. In order to overcome some of these, so-called fuzzy CDM models, which assume CDM to consist of ultra light particles with masses of $m_\phi \sim 1 \times 10^{-22}\,\mathrm{eV}/c^2$, were proposed [12, 13].

CDM candidates are different types of weakly interacting particles (an overview can be found e.g. in Ref. [14]). Among those, we focus in the following on pseudoscalar and pseudovector particles as they are a source of direct parity ($\mathcal{P}$) violation. Other DM candidates that are potential sources for $\mathcal{P}$-odd interactions with a hypothetical neutrino background [15] are discussed elsewhere [16, 17].

Pseudoscalar cosmic fields behave as axion fields, which were originally proposed [18–20] as a solution to the so-called strong $\mathcal{CP}$-problem [21], i.e. the apparently missing violation under combined charge conjugation $\mathcal{C}$ and $\mathcal{P}$ in quantum chromodynamics (QCD) although there is a free parameter in QCD that can account for such a violation. The window to search for such particles can be restricted to a defined parameter space, like for the QCD axion (see e.g. [22]) which has to solve the strong $\mathcal{CP}$-problem, or can be large as for axionic particles that are not bound to solve the strong $\mathcal{CP}$-problem. The latter are often referred to as axion-like particles (ALPs). *Pseudovector* cosmic fields are important for models such as dark photons [23, 24] and also appear as sources of local Lorentz invariance violation in the Standard Model Extension (SME) [25].

In the last decade many proposals for new experiments and improved bounds on pseudoscalar CDM appeared, some of which employ atomic spectroscopy (see e.g. [26–31]). Among the latter, direct measurement of $\mathcal{P}$-violation with modern atomic precision spectroscopy [29, 32] provided strict limits on static $\mathcal{P}$-odd cosmic fields, where effects of these cosmic fields adds to $\mathcal{P}$-violating effects stemming from electroweak electron-nucleus interactions mediated by the Z^0 boson.

It is well known that such $\mathcal{P}$-odd effects are strongly enhanced in chiral molecules, as the chiral arrangement of the nuclei leads to helicity in the electron cloud (see e.g. Refs. [33, 34]). Such $\mathcal{P}$-odd effects can be measured as energy difference between enantiomers of chiral molecules or as resonance frequency differences between the two non-identical mirror-image molecules [35, 36]. As frequency shifts can be measured very accurately, this appears to be a particularly promising tool to search for $\mathcal{P}$-odd cosmic fields (for recent reviews on molecular $\mathcal{P}$-violation see [33, 34, 37–41]). In the following we show advantages of the use of chiral molecules to search for $\mathcal{P}$-odd cosmic fields. We estimate the sensitivity on cosmic $\mathcal{P}$-violation of a twenty year old experiment [42] with the chiral methane derivative CHBrClF [43, 44] and discuss the prospects of modern experiments with chiral molecules.

Theory.—We write the *pseudoscalar* cosmic field as $\phi(t) = \phi_0 \cos(\omega_\phi t)$ (see e.g. Ref. [32]), which is supposed to behave non-relativistically $\hbar\omega_\phi \approx m_\phi c^2$. The interaction of electrons ψ_e with such pseudoscalar cosmic fields $\phi(t)$ can be described by the following Lagrangian density (see e.g. [19, 20])

$$\mathcal{L}_\mathrm{ps}^\phi = g_{\phi\bar{\mathrm{e}}\mathrm{e}}(\hbar c\,\partial_\mu\phi)\bar{\psi}_\mathrm{e}\boldsymbol{\gamma}^\mu\boldsymbol{\gamma}^5\psi_\mathrm{e}\,, \tag{1}$$

where $g_{\phi\bar{\mathrm{e}}\mathrm{e}}$ is a coupling constant of dimension GeV^{-1}. Here the 4×4 Dirac matrices are defined as

$$\boldsymbol{\gamma}^0 = \begin{pmatrix} \mathbf{1}_{2\times2} & \mathbf{0}_{2\times2} \\ \mathbf{0}_{2\times2} & -\mathbf{1}_{2\times2} \end{pmatrix}, \qquad \boldsymbol{\gamma}^k = \begin{pmatrix} \mathbf{0}_{2\times2} & \boldsymbol{\sigma}^k \\ -\boldsymbol{\sigma}^k & \mathbf{0}_{2\times2} \end{pmatrix}, \tag{2}$$

where $\boldsymbol{\sigma}^k$ are the Pauli spin matrices with upper indices $k = 1, 2, 3$. The index μ runs as $\mu = 0, 1, 2, 3$. We define

$\boldsymbol{\gamma}^5 = \imath\boldsymbol{\gamma}^0\boldsymbol{\gamma}^1\boldsymbol{\gamma}^2\boldsymbol{\gamma}^3$ with $\imath = \sqrt{-1}$ being the imaginary unit. $\partial_\mu = \frac{\partial}{\partial x^\mu}$ is the first derivative with respect to the four-vector $x^\mu = (ct, x, y, z)$ and we use Einstein's sum convention here for convenience. The time-derivative of the pseudoscalar field leads to the $\mathcal{P}$-odd one-electron Hamiltonian

$$\hat{h}_{\mathrm{ps}} = g_{\phi\bar{\mathrm{e}}\mathrm{e}}\sqrt{2(hc)^3\rho_{\mathrm{CDM}}}\sin(\omega_\phi t)\boldsymbol{\gamma}^5, \tag{3}$$

where $\rho_{\mathrm{CDM}} \approx \frac{(\hbar\omega_\phi\phi_0)^2}{2(hc)^3}$ is the CDM energy density, for which we assume all ALPs to comprise all of the CDM with a uniform density: $(hc)^3\rho_{\mathrm{CDM}} = (hc)^3\ 0.4\,\mathrm{GeV\,cm^{-3}} = 7.6\times10^{-4}\,\mathrm{eV}^4$ (see Ref. [45]).

Electronic interactions with *pseudovector* cosmic fields can be described by the Lagrangian density

$$\mathcal{L}^b_{\mathrm{pv}} = -b^{\mathrm{e}}_\mu\bar{\psi}_{\mathrm{e}}\boldsymbol{\gamma}^\mu\boldsymbol{\gamma}^5\psi_{\mathrm{e}}, \tag{4}$$

which appears e.g. in the SME (for details see Refs. [25, 46]). The $\mathcal{P}$ non-conserving one-electron interaction Hamiltonian for the temporal component $\mu = 0$ is

$$\hat{h}_{\mathrm{pv}} = b^{\mathrm{e}}_0(t)\boldsymbol{\gamma}^5, \tag{5}$$

where the field can be static $b^{\mathrm{e}}_0(t) = b^{\mathrm{e}}_0$ or dynamic $b^{\mathrm{e}}_0(t) = b^{\mathrm{e}}_0\sin(\omega_b t)$. Here b^{e}_0 is the interaction strength of the timelike-component of the field with the electrons.

The operators corresponding to electronic interactions with $\mathcal{P}$-odd cosmic fields shown above are proportional to $\boldsymbol{\gamma}^5$. The electronic expectation value of $\langle\boldsymbol{\gamma}^5\rangle$ can be expanded in orders of the fine structure constant α giving in leading order:

$$\langle\boldsymbol{\gamma}^5\rangle \approx \alpha\left\langle\vec{\boldsymbol{\sigma}}\cdot\hat{\vec{p}}\right\rangle, \tag{6}$$

where $\hat{\vec{p}}$ is the electronic linear momentum operator. As $\vec{\boldsymbol{\sigma}}\cdot\hat{\vec{p}}$ is an imaginary, electron-spin dependent operator, this expectation value vanishes in the strict electrostatic limit, but it can become non-zero when spin-orbit coupling $\hat{H}_{\mathrm{so}}$ is accounted for, similarly to the situation for $\mathcal{P}$-violation in chiral molecules due to weak neutral currents [47, 48]. Furthermore, it is obvious from eq. (6) that $\langle\boldsymbol{\gamma}^5\rangle$ depends on the helicity of the electron cloud. Thus, $\langle\boldsymbol{\gamma}^5\rangle$ can be non-zero in a chiral molecule, in which the electrons move in a $\mathcal{P}$-noninvariant potential caused by the chiral arrangement of the nuclei, whereas in a non-chiral molecule or in an atom $\langle\boldsymbol{\gamma}^5\rangle$ vanishes in the absence of additional $\mathcal{P}$-odd forces.

It can be shown from perturbation theory that for systems containing two heavy main group elements with nuclear charge numbers Z_A and Z_B the following scaling relation holds in lowest order:

$$\langle\boldsymbol{\gamma}^5\rangle_{\mathrm{mol}} \sim c_1\alpha^5 Z_A^2 Z_B^2 + c_2\alpha^3 Z_A^2 + c_3\alpha^3 Z_B^2, \tag{7}$$

Here the factor $\alpha^2 Z_B^2$ in the first term emerges from spin-orbit coupling. The constants c_1, c_2 and c_3 are dependent on the electronic structure and we can expect that $|c_{2,3}| \ll |c_1|$. A detailed derivation together with evidence from numerical studies of several chiral molecules will be provided in a separate publication [49]. From this it can be deduced that contributions at the nuclear center dominate the electronic expectation value of $\boldsymbol{\gamma}^5$ and let it behave similarly to nuclear-spin independent electroweak electron-nucleon current interactions described by the one-electron Hamiltonian

$$\hat{h}_{\mathrm{ew}} = \frac{G_{\mathrm{F}}}{2\sqrt{2}}\sum_{A=1}^{N_{\mathrm{nuc}}} Q_{\mathrm{W},A}\rho_A(\vec{r})\boldsymbol{\gamma}^5 \tag{8}$$

with G_{F} being Fermi's constant, $Q_{\mathrm{W},A}$ being the weak nuclear charge of nucleus A with nuclear density distribution $\rho_A(\vec{r})$ and the sum running over all N_{nuc} nuclei. In a previous study the electronic expectation value of $\boldsymbol{\gamma}^5$ was discussed as possible total molecular chirality measure [50], but we refer to the critical discussion in Ref. [51] on the utility of pseudoscalar functions as chirality measures.

Thus, molecular experiments that aim to test $\mathcal{P}$-violation due to weak interactions can also be used for searches of $\mathcal{P}$-violating cosmic fields with a comparable sensitivity.

Results and Discussion.—In the following we estimate the expected sensitivity of experiments with chiral molecules to $\mathcal{P}$-odd cosmic fields as characterized by the b^{e}_0 parameter from an experiment with CHBrClF reported by Daussy *et. al.*[42]. In this experiment the C–F stretching fundamental vibration (ν_4) in enantioenriched samples of CHBrClF was studied by high-resolution infrared spectroscopy. We are interested in the $\mathcal{P}$-violating splittings of the vibrational resonance frequency induced by cosmic fields interacting through $\langle\boldsymbol{\gamma}^5\rangle$.

Our calculations for CHBrClF, which are described in more detail in a separate publication [49], were carried out following Ref. [52], which utilized the separable anharmonic adiabatic approximation framework as described in Ref. [53]. Parity-violating molecular properties were computed on the level of two-component zeroth order regular approximation complex generalized Kohn-Sham (ZORA-cGKS) (see Refs. [54–56]) employing the exchange correlation functional B3LYP[57–60]. We reuse electronic densities and Kohn-Sham orbitals as well as vibrational wave functions determined in Ref. [52]. With these, electronic expectation values of $\boldsymbol{\gamma}^5 = \sum_i \boldsymbol{\gamma}^5_i$, with index i running over all electrons in the system, and of the nuclear-spin independent electroweak electron-nucleon current interaction term induced by $\hat{H}_{\mathrm{ew}} = \sum_i \hat{h}_{\mathrm{ew}}(i)$ were calculated with our ZORA property toolbox approach outlined in Ref. [56]. Vibrational corrections of the properties were computed as described in Ref. [52].

The (negative) result of the experimental test for a $\mathcal{P}$-violating frequency shift reported in Ref. [42] is $|\Delta\nu| = 9.4 \pm 5.1 \pm 12.7\,\mathrm{Hz}$, where $\pm5.1\,\mathrm{Hz}$ is the statistical uncertainty and $\pm12.7\,\mathrm{Hz}$ the systematic error.

The expectation values of $\boldsymbol{\gamma}^5$ for the ground and first excited vibrational states along the C-F stretching mode

of (*S*)-CHBrClF are computed to be

$$\left\langle v_4 = 0 \,\middle|\, \boldsymbol{\gamma}^5 \,\middle|\, v_4 = 0 \right\rangle = -8.28 \times 10^{-9}\,, \tag{9}$$

$$\left\langle v_4 = 1 \,\middle|\, \boldsymbol{\gamma}^5 \,\middle|\, v_4 = 1 \right\rangle = -7.91 \times 10^{-9}\,. \tag{10}$$

This leads to an estimate for the splitting between the two enantiomers of CHBrClF due to the perturbation with $\boldsymbol{\gamma}^5$ for the transition between the vibrational ground and first excited states of v_4 of

$$\Delta_{(R,S)} \left\langle \boldsymbol{\gamma}^5 \right\rangle = 2 \left(\left\langle v_4 = 1 \,\middle|\, \boldsymbol{\gamma}^5 \,\middle|\, v_4 = 1 \right\rangle - \left\langle v_4 = 0 \,\middle|\, \boldsymbol{\gamma}^5 \,\middle|\, v_4 = 0 \right\rangle \right) \approx 7.4 \times 10^{-10}. \tag{11}$$

We define the dimensionless reduced normal coordinate q_r, which describes the collective motion of the nuclei in vibrational mode r. As we discuss in more detail in Ref. [49] non-separable anharmonic effects can play a prominent role for the C–F stretching mode in CHBrClF as effects characterized by the first and second derivatives with respect to q_4 can be expected to be of the same order as those characterized by first derivatives with respect to $q_{r\neq 4}$. This can best be seen from a plot of $\left\langle \boldsymbol{\gamma}^5 \right\rangle$ on one-dimensional cuts along all modes (see Figure 1). Therein the weak dependence of $\left\langle \boldsymbol{\gamma}^5 \right\rangle$ on q_4 in comparison to the pronounced dependence on other modes stands out. Therefore, we can expect that multimode effects have the potential to change even the sign of the predicted value of $\Delta_{(R,S)} \left\langle \boldsymbol{\gamma}^5 \right\rangle$ and, thus, it is not possible to provide a robust theoretical value for $\left\langle \boldsymbol{\gamma}^5 \right\rangle$ for the C–F stretching mode, but we give rather the order of magnitude, which is $\Delta_{(R,S)} \left\langle \boldsymbol{\gamma}^5 \right\rangle \sim \mathcal{O}(10^{-10})$. The sensitivity of this experiment to b_0^{e} is found to be of the order

$$|b_0^{\mathrm{e}}| \lesssim \left| \frac{12.7\,\mathrm{Hz}}{\mathcal{O}(10^{-10})} h \right| \sim \mathcal{O}(10^{-12}\,\mathrm{GeV})\,. \tag{12}$$

This sensitivity based on the twenty year old experiment on CHBrClF is about two orders of magnitude inferior to the best limit from modern atomic experiments of $7 \times 10^{-15}\,\mathrm{GeV}$ so far [29]. An improvement in theory, most importantly by consideration of multi-mode effects [49, 61] and additionally by calculations with more sophisticated electronic structure methods, would allow to place a robust limit as we have highlighted in Ref. [49].

The sensitivity of the molecular experiment is supposed to be improvable by two orders of magnitude or better by a different experimental setup as discussed in Refs. [62–64], with Ref. 62 reporting also a slightly improved sensitivity of $|\Delta\nu| < 8\,\mathrm{Hz}$ that was realized experimentally therein. The scaling behavior in eq. (7) suggests that further sensitivity improvements are possible by selecting heavy-elemental chiral molecules. Electroweak $\mathcal{P}$-odd effects, which scale like $N_A Z_A^2 Z_B^2$ with N_A being the number of neutrons of nucleus A, were estimated to give vibrational splittings that can become three orders of magnitude larger in well-chosen heavy-elemental molecules, such as CHAtFI or methyltrioxorhenium derivatives, when compared to CHBrClF [52, 63]. Due to the missing N_A scaling, an enhancement by two orders of magnitude can thus be anticipated for $\Delta_{(R,S)} \left\langle \boldsymbol{\gamma}^5 \right\rangle$. Furthermore, as indicated in Figure 1 and highlighted in Ref. [49], the sensitivity is improvable by an order of magnitude by choice of a different vibrational transition. In case of CHBrClF, for instance, we may expect that the sensitivity of vibrational transitions involving the Br–F deformation mode or the lower-frequency H-deformation mode could be larger by an order of magnitude in comparison to the C–F stretching mode (for a detailed discussion see Ref. [49]).

Thus we can estimate that in future $\mathcal{P}$-violation experiments with chiral molecules the sensitivity of the 1999 experiment can be improved by at least five orders of magnitude down to $10^{-17}\,\mathrm{GeV}$, i.e. an improvement of the actual best limit by at least two orders of magnitude. This renders experiments with suitably chosen chiral molecules sensitive probes for physics beyond the Standard Model.

To exploit its full potential, however, a measurement of cosmic $\mathcal{P}$-violation on the background of the larger electroweak frequency splittings would become necessary, which makes additional demands on accuracy of the accompanying computational approaches or calls for experimental schemes to disentangle these two contributions for instance by measuring isotope-dependent electroweak frequency splittings.

The experiment discussed above is sensitive to *oscillating* $\mathcal{P}$-odd interactions of electrons as well. We can exploit the fact that the experiment was performed over a time span of ten days with a well defined set of measurements on each day. In the following we estimate expected sensitivities for this kind of experiments to oscillating pseudoscalar and pseudovector cosmic fields. As CHBrClF is not an optimal choice, we do not aim to determine the best possible limit from the actual experiment but rather highlight the applicability of such a type of experiment for the direct detection of oscillating pseudovector cosmic fields.

The measured frequency shift due to electronic interactions with ALP fields is proportional to

$$g_{\phi\bar{\mathrm{e}}\mathrm{e}} \sqrt{2(hc)^3 \rho_{\mathrm{CDM}}} \sim 4 \times 10^{-20}\,\mathrm{GeV}^2 g_{\phi\bar{\mathrm{e}}\mathrm{e}}\,. \tag{13}$$

For *pseudoscalar* cosmic fields, measurements of the time-derivative of the ALP field as well as the spatial-derivatives are sensitive to the same parameter $g_{\phi\bar{\mathrm{e}}\mathrm{e}}$. Thus, it would require static bounds on the order of $10^{-30}\,\mathrm{GeV}$ (i.e. a precision of $10^{-17}\,\mathrm{Hz}$ in the CHBrClF experiment) to be competitive with spin precession experiments that set limits of $|g_{\phi\bar{\mathrm{e}}\mathrm{e}}| < 10^{-7}\mathrm{GeV}^{-1}$ (see Refs. [31, 65]). This appears not to be achievable with experiments available today that follow this approach for chiral molecules.

Chiral molecules, however, are directly sensitive to the timelike-component of oscillating *pseudovector* cosmic fields, which is not favorably accessible in spin precession experiments. In the following we discuss briefly the expected sensitivity on b_0^{e} of oscillating fields that can

in principle be obtained from available experiments with chiral molecules.

To obtain a rough estimate for the sensitivity to b_0^e in dependence of ω_b due to the sinusoidal behavior of $b_0^e(t)$ we assume that the sensitivity is decreasing for larger frequencies with $\sin(\omega_b t_{\rm tot}) \approx \omega_b t_{\rm tot}$. Furthermore we can expect that the experimental uncertainty increases with resulting shorter interrogation times for larger ω_b as $\sim \sqrt{\omega_b t_{\rm tot}}$ and we expect the experiment not to be sensitive to frequencies with $\omega_b t_{\rm tot} > n_{\rm tot}$, where $n_{\rm tot}$ is the total number of individual measurements. As CDM is supposed to be incoherent for small frequencies $\omega_b < 2\pi/t_{\rm tot}$ we can expect that b_0^e converges to the static limit. The experiment in Ref. [42] was performed on 10 separate days with a total of 580 individual measurements. When assuming a continuous measurement campaign on each day of 58 subsequent measurements we have $t_{\rm tot} \approx 1\,\mathrm{d}$ and $n_{\rm tot} \approx 58$. In total we arrive at the sensitivities

$$b_0^e \lesssim \begin{cases} 10^{-12}\,\mathrm{GeV}, & \text{if } \frac{\omega_b}{2\pi} \leq 1.2\,\mu\mathrm{Hz} \\ (\omega_b t_{\rm tot})^{3/2} 10^{-12}\,\mathrm{GeV}, & \text{if } 1.2\,\mu\mathrm{Hz} < \frac{\omega_b}{2\pi} \leq 0.7\,\mathrm{mHz} \\ \infty, & \text{if } \frac{\omega_b}{2\pi} > 0.7\,\mathrm{mHz} \end{cases} . \tag{14}$$

The expected sensitivities on b_0^e in CHBrClF and future experiments in dependence on the pseudovector CDM oscillation frequency ω_b is shown in Figure 2. It shall be noted that the region of ω_b to which the experiment is sensitive may be smaller or even extended depending on the actual timing of the measurements. However, robust bounds require an extended theoretical description and a rigorous statistical analysis of the actual data sets as was also discussed in Refs. [66–68].

Conclusion.—We have shown in this letter that $\mathcal{P}$-odd interactions of electrons with cosmic fields are strongly pronounced in chiral molecules. We could demonstrate that chiral molecules are suitable systems to tighten bounds on $\mathcal{P}$-odd electronic interactions of static pseudovector cosmic fields that emerge e.g. from the SME. By performing quasi-relativistic calculations of expectation values of $\mathcal{P}$-odd cosmic field interactions in CHBrClF including vibrational corrections, we demonstrated that the C–F stretching mode is not a good choice to place robust limits on $\mathcal{P}$-odd cosmic fields as the effects are comparatively small and also difficult to predict due to pronounced multimode contributions. However, we estimated the sensitivity of this mode to the parameter b_0^e to be on the order of 10^{-12} GeV in a 20 year old experiment. This sensitivity is inferior by two orders of magnitude to the actual best direct measurements drawn from modern atomic $\mathcal{P}$-violation experiments. We estimate the achievable sensitivity to $\mathcal{P}$-odd cosmic fields with modern high-resolution molecular spectroscopy on suitably chosen chiral molecules to be on the order of 10^{-17} GeV for static cosmic fields (see Figure 2). This would be an improvement of the current best limit on b_0^e by two orders of magnitude. Furthermore, we discussed possibilities of direct detection of ultra light DM by studying oscillating parity violating potentials in chiral molecules. We have shown that without design of a fundamentally new experimental concept limits on electronic interactions of ultra light oscillating pseudovector particles b_0^e with frequencies of around $\omega_b \lesssim 10\,\mu$Hz could be pushed to about 10^{-17} GeV or better with modern experiments with chiral molecules. This corresponds to a direct detection of CDM masses below $10^{-19}\,\mathrm{eV}/c^2$ and thus can be interesting for fuzzy CDM searches.

ACKNOWLEDGMENTS

The authors are grateful to the Mainz Institute for Theoretical Physics (MITP) for its hospitality and its partial support during the completion of this work. The Marburg team gratefully acknowledges computer time provided by the center for scientific computing (CSC) Frankfurt and financial support by the Deutsche Forschungsgemeinschaft (DFG, German Research Foundation) – Projektnummer 328961117 – SFB 1319 ELCH. The work of M.G.K. and T.A.I. was supported by the Russian Science Foundation (RSF) grant No. 18-12-00227. The authors thank Benoît Darquié for his comments on the manuscript. R.B. acknowledges discussions with Nils Huntemann on tests of Lorentz symmetry.

[1] G. Bertone, D. Hooper, and J. Silk, Phys. Rep. **405**, 279 (2005).
[2] M. Davis, G. Efstathiou, C. S. Frenk, and S. D. M. White, Astrophys. J. **292**, 371 (1985).
[3] S. Dodelson and L. M. Widrow, Phys. Rev. Lett. **72**, 17 (1994).
[4] H.-C. Cheng, J. L. Feng, and K. T. Matchev, Phys. Rev. Lett. **89**, 211301 (2002).
[5] P. Arias, D. Cadamuro, M. Goodsell, J. Jaeckel, J. Redondo, and A. Ringwald, J. Cosmol. Astropart. Phys. **2012**, 013 (2012).
[6] G. Gentile, P. Salucci, U. Klein, D. Vergani, and P. Kalberla, Mon. Notices Royal Astron. Soc. **351**, 903 (2004), http://oup.prod.sis.lan/mnras/article-pdf/351/3/903/3595222/351-3-903.pdf.
[7] A. Klypin, A. V. Kravtsov, O. Valenzuela, and F. Prada, Astrophys. J. **522**, 82 (1999).
[8] M. S. Pawlowski, B. Famaey, H. Jerjen, D. Merritt, P. Kroupa, J. Dabringhausen, F. Lghausen, D. A. Forbes, G. Hensler, F. Hammer, M. Puech, S. Fouquet, H. Flores, and Y. Yang, Mon. Notices Royal Astron. Soc. **442**, 2362 (2014), http://oup.prod.sis.lan/mnras/article-pdf/442/3/2362/3481343/stu1005.pdf.
[9] J. Kormendy, N. Drory, R. Bender, and M. E. Cornell, Astrophys. J. **723**, 54 (2010).
[10] S. Sachdeva and K. Saha, Astrophys. J. **820**, L4 (2016).

[11] Kroupa, P., Famaey, B., de Boer, K. S., Dabringhausen, J., Pawlowski, M. S., Boily, C. M., Jerjen, H., Forbes, D., Hensler, G., and Metz, M., Astron. Astrophys. **523**, A32 (2010).
[12] W. Hu, R. Barkana, and A. Gruzinov, Phys. Rev. Lett. **85**, 1158 (2000).
[13] Lee, Jae-Weon, EPJ Web Conf. **168**, 06005 (2018).
[14] P. W. Graham, D. E. Kaplan, J. Mardon, S. Rajendran, and W. A. Terrano, Phys. Rev. D **93**, 075029 (2016).
[15] L. Stodolsky, Phys. Rev. Lett. **34**, 110 (1975); Erratum: Phys. Rev. Lett. **34**, 508 (1975).
[16] P. Bargueño and I. Gonzalo, Origins Life Evol. B. **36**, 171 (2006).
[17] P. Bargueño, A. Dobado, and I. Gonzalo, EPL (Europhysics Letters) **82**, 13002 (2008).
[18] R. D. Peccei and H. R. Quinn, Phys. Rev. Lett. **38**, 1440 (1977).
[19] F. Wilczek, Phys. Rev. Lett. **40**, 279 (1978).
[20] S. Weinberg, Phys. Rev. Lett. **40**, 223 (1978).
[21] G. 't Hooft, Phys. Rev. Lett. **37**, 8 (1976).
[22] G. G. di Cortona, E. Hardy, J. P. Vega, and G. Villadoro, J. High Energy Phys. **2016**, 34 (2016).
[23] H. An, M. Pospelov, J. Pradler, and A. Ritz, Physics Letters B **747**, 331 (2015).
[24] R. Catena, K. Fridell, and V. Zema, J. Cosmol. Astropart. Phys. **2018**, 018 (2018).
[25] D. Colladay and V. A. Kostelecký, Phys. Rev. D **58**, 116002 (1998).
[26] P. W. Graham and S. Rajendran, Phys. Rev. D **84**, 055013 (2011).
[27] P. W. Graham and S. Rajendran, Phys. Rev. D **88**, 035023 (2013).
[28] P. Sikivie, Phys. Rev. Lett. **113**, 201301 (2014).
[29] B. M. Roberts, Y. V. Stadnik, V. A. Dzuba, V. V. Flambaum, N. Leefer, and D. Budker, Phys. Rev. Lett. **113**, 081601 (2014).
[30] Y. V. Stadnik and V. V. Flambaum, Phys. Rev. D **89**, 043522 (2014).
[31] P. W. Graham, D. E. Kaplan, J. Mardon, S. Rajendran, W. A. Terrano, L. Trahms, and T. Wilkason, Phys. Rev. D **97**, 055006 (2018).
[32] B. M. Roberts, Y. V. Stadnik, V. A. Dzuba, V. V. Flambaum, N. Leefer, and D. Budker, Phys. Rev. D **90**, 096005 (2014).
[33] R. Berger, in *Relativistic Electronic Structure Theory, Part: 2, Applications*, edited by P. Schwerdtfeger (Elsevier, Netherlands, 2004) Chap. 4, pp. 188–288.
[34] R. Berger and J. Stohner, WIREs Comput. Mol. Sci. **9**, e1396 (2019), https://onlinelibrary.wiley.com/doi/pdf/10.1002/wcms.1396.
[35] M. Quack, Chem. Phys. Lett. **132**, 147 (1986).
[36] V. S. Letokhov, Phys. Lett. A **53**, 275 (1975).
[37] P. Schwerdtfeger, "The search for parity violation in chiral molecules," in *Computational Spectroscopy: Methods, Experiments and Applications*, edited by J. Grunenberg (Wiley, Netherlands, 2010) Chap. 7, pp. 201–221.
[38] M. Quack, J. Stohner, and M. Willeke, Annu. Rev. Phys. Chem. **59**, 741 (2008).
[39] M. Quack and J. Stohner, Chimia **59**, 530 (2005).
[40] J. Crassous, C. Chardonnet, T. Saue, and P. Schwerdtfeger, Org. Biomol. Chem. **3**, 2218 (2005).
[41] M. Quack, Angew. Chem. Int. Ed. **41**, 4618 (2002).
[42] C. Daussy, T. Marrel, A. Amy-Klein, C. T. Nguyen, C. J. Bordé, and C. Chardonnet, Phys. Rev. Lett. **83**, 1554 (1999).
[43] O. N. Kompanets, A. R. Kukudzhanov, V. S. Letokhov, and L. L. Gervits, Opt. Commun. **19**, 414 (1976).
[44] A. Bauder, A. Beil, D. Luckhaus, F. Müller, and M. Quack, J. Chem. Phys. **106**, 7558 (1997).
[45] J. Vergados and Y. Semertzidis, Nucl. Phys. B **915**, 10 (2017).
[46] V. A. Kosteleck and C. D. Lane, J. Math. Phys. **40**, 6245 (1999), https://doi.org/10.1063/1.533090.
[47] B. Y. Zel'dovich, D. B. Saakyan, and I. I. Sobel'man, JETP Lett. **25**, 94 (1977).
[48] R. A. Harris and L. Stodolski, Phys. Lett. B **78**, 313 (1978).
[49] K. Gaul, M. Kozlov, T. A. Isaev, and R. Berger, arXiv **physics.chem-ph**, 2005.03938 (2020), arXiv:2005.03938 [physics.chem-ph].
[50] M. Senami and K. Ito, Phys. Rev. A **99**, 012509 (2019).
[51] E. Ruch, Acc. Chem. Res. **5**, 49 (1972).
[52] R. Berger and J. L. Stuber, Mol. Phys. **105**, 41 (2007).
[53] M. Quack and J. Stohner, Z. Phys. Chem. **214**, 675 (2000).
[54] C. van Wüllen, Z. Phys. Chem **224**, 413 (2010).
[55] R. Berger, N. Langermann, and C. van Wüllen, Phys. Rev. A **71**, 042105 (2005).
[56] K. Gaul and R. Berger, J. Chem. Phys. **152**, 044101 (2020), arXiv:1907.10432 [physics.chem-ph].
[57] P. J. Stephens, F. J. Devlin, C. F. Chabalowski, and M. J. Frisch, J. Phys. Chem. **98**, 11623 (1994).
[58] S. H. Vosko, L. Wilk, and M. Nuisar, Can. J. Phys. **58**, 1200 (1980).
[59] A. D. Becke, J. Chem. Phys. **98**, 1372 (1993).
[60] A. D. Becke, J. Chem. Phys. **98**, 5648 (1993).
[61] M. Quack and J. Stohner, J. Chem. Phys. **119**, 11228 (2003).
[62] M. Ziskind, C. Daussy, T. Marrel, and C. Chardonnet, Eur. Phys. J. D **20**, 219 (2002).
[63] B. Darquie, C. Stoeffler, A. Shelkovnikov, C. Daussy, A. Amy-Klein, C. Chardonnet, S. Zrig, L. Guy, J. Crassous, P. Soulard, P. Asselin, T. R. Huet, P. Schwerdtfeger, R. Bast, and T. Saue, Chirality **22**, 870 (2010).
[64] A. Cournol, M. Manceau, M. Pierens, L. Lecordier, D. B. A. Tran, R. Santagata, B. Argence, A. Goncharov, O. Lopez, M. Abgrall, Y. L. Coq, R. L. Targat, H. A. Martinez, W. K. Lee, D. Xu, P. E. Pottie, R. J. Hendricks, T. E. Wall, J. M. Bieniewska, B. E. Sauer, M. R. Tarbutt, A. Amy-Klein, S. K. Tokunaga, and B. Darquié, Quantum Electronics **49**, 288 (2019).
[65] I. M. Bloch, Y. Hochberg, E. Kuflik, and T. Volansky, J. High Energy Phys. **2020**, 167 (2020), arXiv:arXiv:1907.03767 [hep-ph].
[66] E. G. Adelberger and W. A. Terrano, Phys. Rev. Lett. **123**, 169001 (2019).
[67] T. Wu, J. W. Blanchard, G. P. Centers, N. L. Figueroa, A. Garcon, P. W. Graham, D. F. J. Kimball, S. Rajendran, Y. V. Stadnik, A. O. Sushkov, A. Wickenbrock, and D. Budker, Phys. Rev. Lett. **123**, 169002 (2019).
[68] G. P. Centers, J. W. Blanchard, J. Conrad, N. L. Figueroa, A. Garcon, A. V. Gramolin, D. F. J. Kimball, M. Lawson, B. Pelssers, J. A. Smiga, Y. Stadnik, A. O. Sushkov, A. Wickenbrock, D. Budker, and A. Derevianko, "Stochastic amplitude fluctuations of bosonic dark matter and revised constraints on linear couplings," (2019), arXiv:1905.13650 [astro-ph.CO].

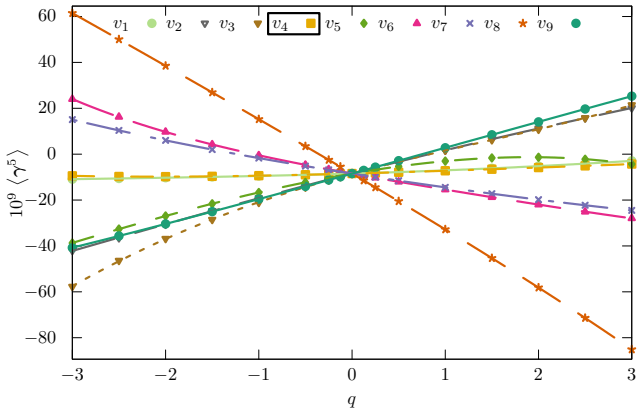

Figure 1. Dependence of the expectation value of $\boldsymbol{\gamma}^5$ on the dimensionless reduced normal coordinates q of the nine different modes in $(S)-$CHBrClF computed at the level of ZORA-cGKS with the B3LYP functional and polynomial fits to $\langle \boldsymbol{\gamma}^5 \rangle$ to fourth order (lines). The C–F stretching mode ν_4 was studied in the experiment in Ref. [42].

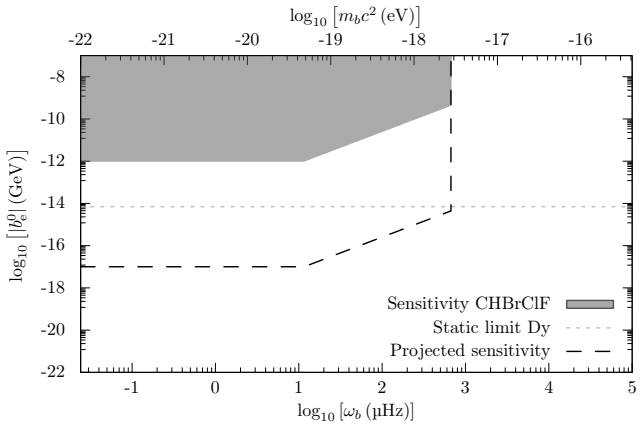

Figure 2. Sensitivity on electron couplings with the timelike-component of pseudovector cosmic fields b_0^e in dependence of the CDM pseudovector oscillation frequency ω_b from a twenty year old experiment with CHBrClF[42] (gray area) compared to the actual best static limit on b_0^e from the Dy experiment (see Ref. [29], dashed light gray line). The projected sensitivity (dashed black line) indicated for modern experiments with chiral molecules assumes an improvement in sensitivity of 5 orders of magnitude compared to the CHBrClF experiment of 1999 (see text).

Parity nonconserving interactions of electrons in chiral molecules with cosmic fields

Konstantin Gaul,[1] Mikhail G. Kozlov,[2,3] Timur A. Isaev,[2] and Robert Berger[1]

[1] *Fachbereich Chemie, Philipps-Universität Marburg, Hans-Meerwein-Straße 4, 35032 Marburg, Germany*

[2] *Petersburg Nuclear Physics Institute of NRC "Kurchatov Institute", Gatchina 188300, Russia*

[3] *St. Petersburg Electrotechnical University "LETI", Prof. Popov Str. 5, 197376 St. Petersburg*

(Dated: August 13, 2020)

Parity ($\mathcal{P}$) violating pseudoscalar or pseudovector cosmic fields are invoked in different models for cold dark matter or in the standard model extension that allows for Lorentz invariance violation. A direct detection of the timelike-component of such fields requires a direct measurement of $\mathcal{P}$-odd potentials or their evolution over time. Herein, advantageous properties of chiral molecules, in which $\mathcal{P}$-odd potentials lead to resonance frequency differences between enantiomers, for direct detection of such $\mathcal{P}$-odd cosmic fields are demonstrated. Scaling behavior of electronic structure enhancements of such interactions with respect to nuclear charge number and the fine-structure constant is derived analytically. This allows a simple estimate of the effect sizes for arbitrary molecules. The analytical derivation is supported by quasi-relativistic numerical calculations in the molecules H_2X_2 and H_2XO with X = O, S, Se, Te, Po. Parity violating effects due to cosmic fields on the C–F stretching mode in CHBrClF are compared to electroweak parity violation and influences of non-separable anharmonic vibrational corrections are discussed. On this basis it was estimated in [Gaul *et. al.*,arXiv:2005.02429[hep-h]] from a twenty year old experiment with CHBrClF that bounds on Lorentz invariance violation as characterized by the parameter $|b_0^e|$ can be pushed down to the order of 10^{-17} GeV in modern experiments with suitably selected molecular system, which will be an improvement of the current best limits by at least two orders of magnitude. This serves to highlight the particular opportunities that precision spectroscopy of chiral molecules provides in the search for new physics beyond the standard model.

I. INTRODUCTION

In our recent work [1] the virtues and prospects of chiral molecules as direct sensors for pseudovector and pseudoscalar cosmic fields were demonstrated. In the present paper we derive scaling laws for interactions of electrons with these fields, presented in Ref. [1] and provide support from numerical calculations. Furthermore, the methods applied for derivation of limits on cosmic field interactions from experiments with chiral molecules are presented in a more detailed manner and accompanied by comparison to other computational methods.

One of the biggest puzzles of modern physics is the nature and composition of dark matter (DM) (see e.g. [2]). Many different models for DM exist, considering objects that range from macroscopic to microscopic and from being hot (ultra-relativistic) to cold (non-relativistic). Among these DM theories cold DM (CDM) theory serves to provide a simple explanation for many cosmological observations [3]. However, the constituents of CDM are unknown and can in principle fall in the range from macroscopic objects such as black holes to new fundamental particles like weakly interacting massive particles (WIMPs), axions, sterile neutrinos or dark photons (see e.g. Refs. [4–6]).

Despite its merits, the model of CDM has several drawbacks [7–12]. Notable challenges are the cusps of halos in CDM simulations, which are not observed in rotation curves of galaxies [7], or the prediction of a large number of non-observed halos of CDM [8]. A possible solution of some of these, such as the large number of absent halos or cusps of halos is provided by fuzzy CDM models [13]. Fuzzy CDM is supposed to consist of ultra light particles with masses of $m_\phi \sim 1 \times 10^{-22}\,\mathrm{eV}/c^2$ [13, 14]. This model makes searches for ultralight CDM oscillating with frequencies on the order of 1 µHz particularly interesting.

CDM can consist of various types of weakly interacting particles (an overview can be found e.g. in Ref. [15]). Among those pseudoscalar and pseudovector fields are of special interest as they are a source of parity ($\mathcal{P}$) violation.

Pseudoscalar CDM particles behave like axions, which were originally proposed [16–18] to solve the strong $\mathcal{CP}$-problem of quantum chromodynamics (QCD) [19]. The search for CDM particles can be restricted to a comparatively small parameter space assessable to the QCD axion (see e.g. [20]) or can involve a wide range for axionic particles that are not bound to solve the strong $\mathcal{CP}$-problem. The latter are often referred to as axion-like particles (ALPs). *Pseudovector* fields are important for models such as dark photons [21, 22] and also appear as sources of local Lorentz invariance violation in the Standard Model Extension (SME) by Kostelecký and coworkers [23].

In the last decade many new proposals for new experiments and improved bounds on pseudoscalar CDM appeared, employing atomic spectroscopy (see e.g. [24–29]). Among those, strict limits on static $\mathcal{P}$-odd fields were set from direct detection of $\mathcal{P}$-violation with modern atomic precision spectroscopy [27, 30]. In these experiments the dominating effect for $\mathcal{P}$-violation stems from the electroweak Z^0-mediated electron-nuclear interaction.

Such $\mathcal{P}$-odd effects are strongly enhanced in chiral

molecules as well (for recent reviews on molecular $\mathcal{P}$-violation see [31–37]). The chiral arrangement of the nuclei in the molecule leads to helicity of the electron cloud (see e.g. Ref. [36]). Additional $\mathcal{P}$-odd effects can then be measured as energy difference between enantiomers of chiral molecules or as resonance frequency differences between the two non-identical mirror-image molecules [38–40]. As frequency shifts can be measured very accurately (see e.g. Ref [41] or for the special case of $\mathcal{P}$-violation see Refs. [42, 43]), this appears to be a particularly promising tool to search for $\mathcal{P}$-odd cosmic fields.

In the following we analyse in detail the effects that emerge from $\mathcal{P}$-odd cosmic fields in chiral molecules. We derive scaling laws with respect to nuclear charge and the fine structure constant and compare to what is known from $\mathcal{P}$-violation due to electroweak interactions. From our analysis we demonstrate advantages of the use of chiral molecules to search for $\mathcal{P}$-odd cosmic fields. We perform quasi-relativistic calculations at different levels of theory and estimate the effect sizes in the vibrational spectra of the chiral methane derivate CHBrClF [44, 45]. Thereby, the computational difficulties are highlighted. From a twenty year old experiment with this molecule [46] we estimated the sensitivity on cosmic $\mathcal{P}$-violation [1] and discuss the scope for improvement on these limits in modern experiments with chiral molecules and by improvement of present theoretical methods.

II. THEORY

A. Parity non-conserving interactions of electrons with cosmic fields

$\mathcal{P}$-odd interactions of electrons with pseudoscalar and pseudovector cosmic fields were discussed in detail in Ref. [30]. A light pseudoscalar cosmic field obeys the Klein-Gordon equation. Assuming it to be non-relativistic, i.e. $\hbar\omega_\phi \approx m_\phi c^2$ with m_ϕ being the CDM particle mass and c being the speed of light in vacuum, we can write

$$\phi(\vec{r},t) = \phi_0 \cos\left(\omega_\phi t - \frac{\vec{r}\cdot\vec{p}_\phi}{\hbar} + \varphi\right), \tag{1}$$

where $\hbar = \frac{h}{2\pi}$ is the reduced Planck's constant, ϕ_0 is the CDM amplitude, $\vec{p}_\phi = m_\phi \vec{v}_\phi$ is the momentum of the CDM particle, which is proportional to its velocity $\vec{v}_\phi$ and φ is a phase factor. CDM is supposed to be incoherent and the relative velocity of the ALP field is suppressed by 10^{-3} with respect to the speed of light (see Refs. [24, 25] for details). Thus, for terrestrial experiments we can assume $\frac{\vec{r}\cdot\vec{p}_\phi}{\hbar}$ to be constant and choose φ such that eq. (1) can be written as $\phi(\vec{r},t) = \phi_0\cos(\omega_\phi t)$ (see also Ref. [30]).

The interaction of the electronic field ψ_e with such pseudoscalar fields ϕ can be described by (see e.g. [17, 18])

$$\mathcal{L}^\phi_\mathrm{ps} = g_{\phi\bar{\mathrm{e}}\mathrm{e}}(\hbar c\,\partial_\mu\phi)\bar{\psi}_\mathrm{e}\boldsymbol{\gamma}^\mu\boldsymbol{\gamma}^5\psi_\mathrm{e}\,, \tag{2}$$

where $g_{\phi\bar{\mathrm{e}}\mathrm{e}}$ is a coupling constant of dimension GeV^{-1}. Herein the Dirac matrices are defined as

$$\boldsymbol{\gamma}^0 = \begin{pmatrix}\mathbf{1}_{2\times2} & \mathbf{0}_{2\times2}\\ \mathbf{0}_{2\times2} & -\mathbf{1}_{2\times2}\end{pmatrix}, \qquad \boldsymbol{\gamma}^k = \begin{pmatrix}\mathbf{0}_{2\times2} & \boldsymbol{\sigma}^k\\ -\boldsymbol{\sigma}^k & \mathbf{0}_{2\times2}\end{pmatrix}, \tag{3}$$

where $\boldsymbol{\sigma}^k$ are the Pauli spin matrices, $k = 1,2,3$ and $\mu = 0,1,2,3$. $\boldsymbol{\gamma}^5 = \imath\boldsymbol{\gamma}^0\boldsymbol{\gamma}^1\boldsymbol{\gamma}^2\boldsymbol{\gamma}^3$, where $\imath = \sqrt{-1}$ is the imaginary unit, $\partial_\mu = \frac{\partial}{\partial x^\mu}$ is the first derivative with respect to the four-vector $x^\mu = (ct,x,y,z)$ and Einstein's sum convention is used. Additionally a direct pseudoscalar coupling between the electrons and the pseudoscalar cosmic field can be considered (see e.g. Ref. [27]):

$$\mathcal{L}^\phi_\mathrm{dps} = -\imath\tilde{g}_{\phi\bar{\mathrm{e}}\mathrm{e}} m_\mathrm{e} c^2 \phi\bar{\psi}_\mathrm{e}\boldsymbol{\gamma}^5\psi_\mathrm{e}\,, \tag{4}$$

where $\tilde{g}_{\phi\bar{\mathrm{e}}\mathrm{e}}$ is a dimensionless coupling constant and m_e is the mass of the electron. Whereas this interaction can lead to $\mathcal{P}$-violating couplings when considering transition matrix elements of atomic or molecular excitations [30], it does not contribute to $\mathcal{P}$-violating expectation values, which give dominant contributions to frequency differences in spectra of chiral molecules. Thus these interactions are not discussed any further in the following.

The time-derivative of the pseudoscalar field leads to the $\mathcal{P}$-odd single-electron Hamiltonian

$$\hat{h}_\mathrm{ps} = g_{\phi\bar{\mathrm{e}}\mathrm{e}}\sqrt{2(hc)^3\rho_\mathrm{CDM}}\sin(\omega_\phi t)\boldsymbol{\gamma}^5, \tag{5}$$

where $\rho_\mathrm{CDM} \approx \frac{(\hbar\omega_\phi\phi_0)^2}{2(hc)^3}$ is the CDM energy density, for which we assume all ALPs to comprise all of the CDM with a uniform density: $(hc)^3\rho_\mathrm{CDM} = (hc)^3 0.4\,\mathrm{GeV\,cm^{-3}} = 7.6\times10^{-4}\,\mathrm{eV}^4$ (see Ref. [47]). We use lowercase letters ($\hat{h}$) for single-electron operators and uppercase letters ($\hat{H}$) for multi-electron operators. These are in the case of $\hat{H}_\mathrm{ps}$ (as well as $\hat{H}_\mathrm{pv}$, $\hat{H}_\mathrm{ew}$ given below) simple sums over all electrons of the system, e.g. $\hat{H}_\mathrm{ps} = \sum_i \hat{h}_\mathrm{ps}(i)$

Electronic interactions with pseudovector cosmic fields can be described by the Lagrangian

$$\mathcal{L}^b_\mathrm{pv} = -b_\mu\bar{\psi}_\mathrm{e}\boldsymbol{\gamma}^\mu\boldsymbol{\gamma}^5\psi_\mathrm{e}, \tag{6}$$

which appears e.g. in the SME (for details see Refs. [23, 48]).

The parity non-conserving interaction Hamiltonian for the temporal component is

$$\hat{h}_\mathrm{pv} = b_0(t)\boldsymbol{\gamma}^5, \tag{7}$$

where the field can be static $b_0(t) = b_0^\mathrm{e}$ or dynamic $b_0^\mathrm{e}(t) = b_0^\mathrm{e}\sin(\omega_b t)$. Here b_0^e is the interaction strength of the timelike-component of the pseudovector field with the electrons.

In spectra of chiral molecules the interactions discussed above lead to shifts (static fields) or oscillations (dynamic fields) of frequency shifts due to the nuclear spin-independent electroweak interactions, the main contribution to which is in closed-shell molecules expected to arise

from the electron-nuclei weak neutral-current interaction Hamiltonian (see e.g. [31, 32]):

$$\hat{h}_{\mathrm{ew}} = \frac{G_{\mathrm{F}}}{2\sqrt{2}} \sum_{A=1}^{N_{\mathrm{nuc}}} Q_{\mathrm{W},A} \rho_A(\vec{r}) \boldsymbol{\gamma}^5 \,, \tag{8}$$

where $G_{\mathrm{F}} = 2.222\,49 \times 10^{-14}\, E_{\mathrm{h}}\, {a_0}^3$ is Fermi's weak coupling constant, $Q_{\mathrm{W},A}$ and ρ_A are the weak charge and normalized charge density of nucleus A, respectively. The total number of nuclei is N_{nuc}. Contributions from $\mathcal{P}$-odd nuclear-spin dependent terms when combined with $\mathcal{P}$-even hyperfine coupling [49, 50] are estimated to give only minor contributions in closed-shell molecules. Similar considerations hold for the contribution from neutral-current interaction terms between electrons.

It shall be noted that in chiral molecules weakly interacting dark matter candidates, such as WIMPs, or cosmic neutrinos can also lead to shifts or oscillations of the $\mathcal{P}$-odd potential as was discussed by Bargueño *et.al.* [51–53]. These interactions as well as those of electrons with pseudoscalar and pseudovector fields discussed above are proportional to $\langle \boldsymbol{\gamma}^5 \rangle$. In the following we will discuss in general the chiral operator $\boldsymbol{\gamma}^5$, which leads to parity non-conservation and compare to known properties of operator eq. (8).

B. Molecular expectation value of $\boldsymbol{\gamma}^5$

The time-independent Dirac-Coulomb equation for the electronic system of the molecule reads

$$\hat{H}_{\mathrm{DC}} \Psi_I = E_I \Psi_I, \tag{9}$$

with Ψ_I and E_I being the Ith eigenfunction and eigenvalue of the Dirac-Coulomb Hamiltonian being given by

$$\begin{aligned} \hat{H}_{\mathrm{DC}} = \sum_i^{N_{\mathrm{elec}}} \Bigg[& c\boldsymbol{\gamma}^0 \vec{\boldsymbol{\gamma}} \cdot \hat{\vec{p}}_i + \left(\boldsymbol{\gamma}^0 - \mathbf{1}\right) m_{\mathrm{e}} c^2 \\ & + V_{\mathrm{nuc}}(\vec{r}_i) + \frac{1}{2} \sum_{j \neq i}^{N_{\mathrm{elec}}} k_{\mathrm{es}} \frac{e^2}{|\vec{r}_i - \vec{r}_j|} \Bigg] \,, \end{aligned} \tag{10}$$

where we shifted the energy levels by $-m_{\mathrm{e}}c^2$ to bring the upper part of the spectrum into correspondence with the non-relativistic limit of the energy levels. Here e is the elementary electric charge, k_{es} is in SI units $\frac{1}{4\pi\epsilon_0}$ with ϵ_0 being the electric constant and V_{nuc} being the potential the nuclei in the molecule produce.

In the Dirac–Hartree–Fock–Coulomb (DHFC) approach, the multi-electron states Ψ_I are approximated by a Slater determinant build from an orthonormal set of single-electron bi-spinors ψ_i with orbital energy ϵ_i. From the lower equation of the resulting single-electron Dirac equations expressions for the lower components χ_i of the Dirac bi-spinors

$$\psi_i(\vec{r}) = \begin{pmatrix} \varphi_i(\vec{r}) \\ \chi_i(\vec{r}) \end{pmatrix} \tag{11}$$

can be found via

$$\chi_i(\vec{r}) = c \left(2m_{\mathrm{e}}c^2 - \hat{V} + \varepsilon_i\right)^{-1} \vec{\boldsymbol{\sigma}} \cdot \hat{\vec{p}} \varphi_i(\vec{r}), \tag{12}$$

where we have omitted all multi-electron effects for the sake of simplifying the discussion below.

For the remaining part of this section we will use atomic units, in which $\hbar$, $|e|$ and m_{e} have the numerical value of 1. Then, the term in parentheses in eq. (12) can be expanded in orders of the fine structure constant $\alpha = c^{-1}$ as

$$c \left(2c^2 - \hat{V} + \varepsilon_i\right)^{-1} = \frac{\alpha}{2} \sum_{k=0}^{\infty} \left[\frac{\alpha}{2}\left(\hat{V} - \varepsilon_i\right)\right]^k . \tag{13}$$

Truncation after first order yields the Pauli approximation:

$$\chi_i(\vec{r}) = \left[\frac{\alpha}{2} + \frac{\alpha^3}{4}\left(\hat{V} - \varepsilon_i\right)\right] \vec{\boldsymbol{\sigma}} \cdot \hat{\vec{p}} \varphi_i(\vec{r}). \tag{14}$$

In a molecule, the expectation value of $\boldsymbol{\gamma}^5$ for a single Slater determinant is determined by a summation over contributions from all occupied molecular orbitals i:

$$\left\langle \psi_i \middle| \boldsymbol{\gamma}^5 \middle| \psi_i \right\rangle = \left\langle \varphi_i \middle| \chi_i \right\rangle + \left\langle \chi_i \middle| \varphi_i \right\rangle . \tag{15}$$

Insertion of the first term of the expansion eq. (14) in eq. (15) gives the first order contribution to $\boldsymbol{\gamma}^5$:

$$\left\langle \psi_i \middle| \boldsymbol{\gamma}^5 \middle| \psi_i \right\rangle \approx \alpha \left\langle \varphi_i \middle| \vec{\boldsymbol{\sigma}} \cdot \hat{\vec{p}} \middle| \varphi_i \right\rangle . \tag{16}$$

This obviously vanishes if the overall electron density of the molecule is non-helical, but can, in the static case and when remaining in first order with respect to $\mathcal{P}$-odd operators, only be non-zero for a chiral molecule, in which the electron density can have non-vanishing helicity.

In order to determine scaling laws with respect to the nuclear charge number Z and the fine-structure constant α, eq. (15) itself is not immediately useful. This is why we follow Ref. [27] and write the operator $\boldsymbol{\gamma}^5$ for electron i as a commutator:

$$\boldsymbol{\gamma}_i^5 = \frac{\imath}{c} \left[\hat{H}_{\mathrm{DC}}, \vec{\boldsymbol{\Sigma}}_i \cdot \vec{r}_i\right]_- + 2 \begin{pmatrix} \mathbf{0} & \hat{\mathbf{k}}_i \\ \hat{\mathbf{k}}_i & \mathbf{0} \end{pmatrix}, \tag{17}$$

$$\hat{\mathbf{k}}_i = -(\mathbf{1}_i + \vec{\boldsymbol{\sigma}}_i \cdot \hat{\vec{l}}_i) \,, \qquad \vec{\boldsymbol{\Sigma}}_i = \begin{pmatrix} \vec{\boldsymbol{\sigma}}_i & \mathbf{0} \\ \mathbf{0} & \vec{\boldsymbol{\sigma}}_i \end{pmatrix} . \tag{18}$$

Eigenvalues of the operator $\hat{\mathbf{K}} = \sum_i \hat{\mathbf{k}}_i$ in atomic systems correspond to the relativistic quantum numbers $\varkappa = (\ell - j)(2j+1)$, where ℓ and j are the orbital and total angular momentum quantum numbers, respectively.

As long as we are interested in expectation values of the operator $\boldsymbol{\gamma}^5$ on the molecular DHFC-orbitals ψ_i, the commutator part in eq. (17) turns to zero. DHFC molecular orbital matrix elements of the second term in eq. (17) have the form

$$\left\langle \psi_i \middle| \boldsymbol{\gamma}^5 \middle| \psi_i \right\rangle = 2 \left\langle \varphi_i \middle| \hat{\mathbf{k}} \middle| \chi_i \right\rangle + 2 \left\langle \chi_i \middle| \hat{\mathbf{k}} \middle| \varphi_i \right\rangle . \tag{19}$$

The non-relativistic limit of $\langle \boldsymbol{\gamma}^5 \rangle$ vanishes as can be shown by insertion of the first term of the expansion eq. (14) in eq. (19):

$$\langle \psi_i \,|\, \boldsymbol{\gamma}^5 \,|\, \psi_i \rangle \approx \alpha \left\langle \varphi_i \,\middle|\, \left\{ \hat{\mathbf{k}}, \vec{\boldsymbol{\sigma}} \cdot \hat{\vec{p}} \right\}_+ \,\middle|\, \varphi_i \right\rangle = 0 \,, \tag{20}$$

where we use the fact that operator $\hat{\mathbf{k}}$ anti-commutes with $\vec{\boldsymbol{\sigma}} \cdot \hat{\vec{p}}$:

$$\left\{ \hat{\mathbf{k}}, \vec{\boldsymbol{\sigma}} \cdot \hat{\vec{p}} \right\}_+ = 0 \,. \tag{21}$$

The terms of order α^3 give:

$$\langle \psi_i \,|\, \boldsymbol{\gamma}^5 \,|\, \psi_i \rangle \approx \frac{\alpha^3}{2} \left\langle \varphi_i \,\middle|\, (\vec{\boldsymbol{\sigma}} \cdot \hat{\vec{p}}) \hat{V} \hat{\mathbf{k}} + \hat{\mathbf{k}} \hat{V} (\vec{\boldsymbol{\sigma}} \cdot \hat{\vec{p}}) \,\middle|\, \varphi_i \right\rangle \,, \tag{22}$$

where the terms containing orbital energies ε_i reduce to the anti-commutator eq. (21). Eq. (22) can be rewritten as:

$$\begin{aligned} \langle \psi_i \,|\, \boldsymbol{\gamma}^5 \,|\, \psi_i \rangle &\approx \frac{\alpha^3}{2} \left\langle \varphi_i \,\middle|\, \left[\vec{\boldsymbol{\sigma}} \cdot \hat{\vec{p}}, \hat{V}(\vec{r}) \right]_- \hat{\mathbf{k}} + \hat{V}(\vec{r}) \left\{ \hat{\mathbf{k}}, \vec{\boldsymbol{\sigma}} \cdot \hat{\vec{p}} \right\}_+ + \left[\hat{\mathbf{k}}, \hat{V}(\vec{r}) \right]_- \vec{\boldsymbol{\sigma}} \cdot \hat{\vec{p}} \,\middle|\, \varphi_i \right\rangle \\ &= \frac{\alpha^3}{2} \left\langle \varphi_i \,\middle|\, \left[\vec{\boldsymbol{\sigma}} \cdot \hat{\vec{p}}, \hat{V}(\vec{r}) \right]_- \hat{\mathbf{k}} + \left[\hat{\mathbf{k}}, \hat{V}(\vec{r}) \right]_- \vec{\boldsymbol{\sigma}} \cdot \hat{\vec{p}} \,\middle|\, \varphi_i \right\rangle , \end{aligned} \tag{23}$$

where we once again used eq. (21). In general, the molecular potential energy operator $\hat{V}$ does not commute with both operators $\hat{\mathbf{k}}$ and $(\vec{\boldsymbol{\sigma}} \cdot \hat{\vec{p}})$. However, its spherically symmetric part $\hat{V}_\mathrm{s}(|\vec{r}|)$ commutes with the operator $\hat{\mathbf{k}}$. Therefore, for the spherically symmetric potential the last term in eq. (23) turns to zero. Let us separate the contribution of $\hat{V}_\mathrm{s}(|\vec{r}|)$:

$$\langle \psi_i \,|\, \boldsymbol{\gamma}^5 \,|\, \psi_i \rangle = \langle \psi_i \,|\, \boldsymbol{\gamma}^5 \,|\, \psi_i \rangle_\mathrm{s} + \langle \psi_i \,|\, \boldsymbol{\gamma}^5 \,|\, \psi_i \rangle_\mathrm{a} \,, \tag{24}$$

$$\langle \psi_i \,|\, \boldsymbol{\gamma}^5 \,|\, \psi_i \rangle_\mathrm{s} = \frac{\alpha^3}{2} \left\langle \varphi_i \,\middle|\, -\imath (\vec{\boldsymbol{\sigma}} \cdot \vec{r}) \frac{\hat{V}_\mathrm{s}'(|\vec{r}|)}{|\vec{r}|} \hat{\mathbf{k}} \,\middle|\, \varphi_i \right\rangle \tag{25}$$

and consider the term eq. (25) in more detail. Note that $\hat{V}_\mathrm{s}'(|\vec{r}|)/|\vec{r}|$ commutes with both operators $\vec{\boldsymbol{\sigma}} \cdot \vec{r}$ and $\hat{\mathbf{k}}$. By analogy with eq. (21) we can assume that $\left\{ \vec{\boldsymbol{\sigma}} \cdot \vec{r}, \hat{\mathbf{k}} \right\}_+ = 0$. Thus, we can write:

$$\imath (\vec{\boldsymbol{\sigma}} \cdot \vec{r}) \hat{\mathbf{k}} = \frac{\imath}{2} \left[\vec{\boldsymbol{\sigma}} \cdot \vec{r}, \hat{\mathbf{k}} \right]_- \,, \tag{26}$$

which proves that the operator in eq. (25) is hermitian, and allows to rewrite this expression as:

$$\langle \psi_i \,|\, \boldsymbol{\gamma}^5 \,|\, \psi_i \rangle_\mathrm{s} = \frac{\alpha^3}{4} \langle \varphi_i \,|\, \vec{\boldsymbol{\sigma}} \cdot \vec{v}_{\mathcal{T},\mathrm{s}} \,|\, \varphi_i \rangle \,, \tag{27}$$

$$\vec{v}_{\mathcal{T},\mathrm{s}} = \frac{\hat{V}_\mathrm{s}'(|\vec{r}|)}{|\vec{r}|} \left(|\vec{r}|^2 \hat{\vec{p}} - \vec{r} (\hat{\vec{p}} \cdot \vec{r}) \right) \,. \tag{28}$$

We see that expectation value eq. (27) has the form of a scalar product of the spin with an electronic orbital $\mathcal{T}$-odd vector $\vec{v}_{\mathcal{T},\mathrm{s}}$. Molecular matrix elements of $\vec{\boldsymbol{\sigma}} \cdot \vec{v}_\mathcal{T}$ turn to zero in the non-relativistic approximation for two reasons: (i) for a singlet state an expectation value of the spin is zero; (ii) matrix elements of orbital $\mathcal{T}$-odd vectors are imaginary, so their expectation values are zero. In order to get a non-zero expectation value of such operators one needs to include spin-orbit interactions $\hat{H}_\mathrm{so}$, which mix singlet and triplet molecular states and have imaginary matrix elements. Therefore, the energy shift $\delta E_{\boldsymbol{\gamma}^5,\mathrm{s}}$ of the molecular (ground) singlet state due to the interaction $\vec{\boldsymbol{\sigma}} \cdot \vec{v}_{\mathcal{T},\mathrm{s}}$ appears in double perturbation theory as:

$$\delta E_{\boldsymbol{\gamma}^5,\mathrm{s}} \sim \frac{\alpha^3}{2} \frac{2\mathrm{Re} \left\{ \langle \Psi_\mathrm{s} \,|\, \vec{\boldsymbol{\sigma}} \cdot \vec{v}_{\mathcal{T},\mathrm{s}} \,|\, \Psi_\mathrm{t} \rangle \left\langle \Psi_\mathrm{t} \,\middle|\, \hat{H}_\mathrm{so} \,\middle|\, \Psi_\mathrm{s} \right\rangle \right\}}{E_\mathrm{s} - E_\mathrm{t}} \,, \tag{29}$$

where E_s, E_t and Ψ_s, Ψ_t are the non-relativistic singlet and triplet energies and wave functions, respectively.

Eq. (29) allows to estimate the scaling law for $\delta E_{\boldsymbol{\gamma}^5,\mathrm{s}}$ with the nuclear charge Z and the fine structure constant α. The matrix element of the spin-orbit interaction $\left\langle \psi_\mathrm{t} \,\middle|\, \hat{H}_\mathrm{so} \,\middle|\, \psi_\mathrm{s} \right\rangle$ scales as $\alpha^2 Z^2$. The Z scaling of the matrix element of the operator $\vec{v}_{\mathcal{T},\mathrm{s}}$ depends on the distances where the integral is accumulated. Taking into account that this operator appears in third order in α, we can assume that the integral is accumulated at short distances near the nucleus, where relativistic corrections are larger. At such distances the potential of the nucleus is practically unscreened, $\hat{V}_\mathrm{s} \sim Z/r$. Furthermore, at these distances the electron moves Z times faster, so $\hat{\vec{p}} \sim Z$. Therefore, we can assume that $\int v_{\mathcal{T},\mathrm{s}} d^3 r \sim Z^2$. Then the overall scaling is:

$$\delta E_{\boldsymbol{\gamma}^5,\mathrm{s}} \sim \alpha^5 Z^4 \,. \tag{30}$$

The last expression does not take into account "the single center theorem" [54, 55], which implies that electron helicity in molecules is suppressed in the vicinity of a single heavy nucleus and one has to take two matrix

elements of expression eq. (29) at two different heavy centers. Therefore, the final scaling should be:

$$\delta E_{\boldsymbol{\gamma}^5,\mathrm{s}} \sim \alpha^5 Z_A^2 Z_B^2 \,, \tag{31}$$

where A and B are typically taken as the two heaviest atoms in the molecule.

Now let us analyze the second term in eq. (24). In this case both terms from eq. (23) can contribute. For the first term we can use the same arguments as above, but the asymmetric part of the molecular potential at short distances is much weaker, so this term will add small corrections to eq. (31). Thus, we will focus on the second term, which was zero for the symmetric potential.

We assume again that the matrix element is accumulated at short distances, where the molecular potential can be expanded in spherical harmonics [56]. The second term of this expansion can be written as $(\vec{a}\cdot\vec{r})\hat{V}_\mathrm{a}(|\vec{r}|)$, where $\vec{a}$ is some constant polar vector. In this approximation we get:

$$\Big[\hat{\mathbf{k}}, \hat{V}(|\vec{r}|)\Big]_- = -\imath(\vec{\boldsymbol{\sigma}}\cdot(\vec{r}\times\vec{a}))\hat{V}_\mathrm{a}(|\vec{r}|)\,. \tag{32}$$

Substituting this into the second term in eq. (23) we find that:

$$\begin{aligned}&\left\langle\psi_i\,\middle|\,\boldsymbol{\gamma}^5\,\middle|\,\psi_i\right\rangle_\mathrm{a}\\ &\quad\approx \frac{\alpha^3}{2}\left\langle\varphi_i\,\middle|\,-\imath(\vec{\boldsymbol{\sigma}}\cdot\vec{r}\times\vec{a})\hat{V}_\mathrm{a}(|\vec{r}|)(\vec{\boldsymbol{\sigma}}\cdot\hat{\vec{p}})\,\middle|\,\varphi_i\right\rangle.\end{aligned} \tag{33}$$

Simplifying this further and neglecting the term, which is similar to eq. (28), we get:

$$\left\langle\psi_i\,\middle|\,\boldsymbol{\gamma}^5\,\middle|\,\psi_i\right\rangle_\mathrm{a} \approx \frac{\alpha^3}{2}\left\langle\varphi_i\,\middle|\,\vec{a}\cdot\vec{v}_\mathrm{a}\,\middle|\,\varphi_i\right\rangle, \tag{34}$$

$$\vec{v}_\mathrm{a} = 2\hat{V}_\mathrm{a}(|\vec{r}|)\,\vec{r}\times\vec{\nabla}\,. \tag{35}$$

The orbital pseudovector $\vec{v}_\mathrm{a}$ is $\mathcal{T}$-even. The expected scaling with α is given by eq. (34). Scaling with Z for operators eq. (28) and eq. (35) should be similar, so we assume:

$$\delta E_{\boldsymbol{\gamma}^5,\mathrm{a}} \sim \alpha^3 Z^2\,. \tag{36}$$

Combining the two terms in eq. (24) together suggests an estimate for a molecule with two heavy atoms A and B:

$$\delta E_{\boldsymbol{\gamma}^5} \approx c_1\alpha^5 Z_A^2 Z_B^2 + c_2\alpha^3 Z_A^2 + c_3\alpha^3 Z_B^2\,. \tag{37}$$

The first term is formed on both heavy centers, while the other two terms are formed independently in the vicinity of each heavy nucleus. The chiral structure of the molecule is weakly felt locally [54, 56], so we can expect that $|c_{2,3}| \ll |c_1|$.

In the following we discuss the implications in molecular systems of the equation derived above for $\langle\boldsymbol{\gamma}^5\rangle$ and compare to results from numerical computations. Hereby, we focus on scaling with respect to the nuclear charge number and the fine structure constant. Furthermore, we compare to energy shifts due to nuclear spin-independent electroweak neutral-current interactions.

III. COMPUTATIONAL DETAILS

Quasi-relativistic two-component calculations of H_2X_2 and H_2XO with X = O, S, Se, Te, Po and CHBrClF are performed within the zeroth order regular approximation (ZORA) at the level of complex generalized Hartree–Fock (cGHF) or Kohn–Sham (cGKS) with a modified version [57–63] of the quantum chemistry program package Turbomole [64].

For calculations of H_2X_2 and H_2XO compounds a basis set of 25 s, 25 p, 14 d and 11 f uncontracted Gaussian functions with the exponential coefficients α_i composed as an even-tempered series by $\alpha_i = a\cdot b^{N-i}$; $i = 1,\ldots,N$ with $a = 0.02\,a_0{}^{-2}$, $b = (5/2\times10^{10})^{1/25} \approx 2.606$ and $N = 26$ was used for X = O, S, Se, Te, Po. The largest exponent coefficients of the s, p, d and f subsets are $5\times10^8\ a_0^{-2}$, $1.91890027\times10^8\ a_0^{-2}$, $13300.758\ a_0^{-2}$ and $751.8368350\ a_0^{-2}$, respectively. A similar but slightly smaller basis set (three f functions less) has proven successful in calculations of $\mathcal{P}$-violating energy shifts in H_2Po_2 [58, 65]. The H atom was represented with the s,p-subset of a decontracted correlation-consistent basis of quadruple-ζ quality [66].

Structure parameters of H_2X_2 were chosen as in Refs. [58, 65]. For H_2XO compounds the equilibrium bond-length of the O–X bond, for X = S, Se, Te, Po was obtained by full structure optimization at the level of ZORA-cGHF. As convergence criteria an energy change of less than $10^{-5}\ E_\mathrm{h}$ was used. Bond angles H–O–X and bond distances H–O of H_2XO were assumed to be equal to H_2O_2 and bond angles H–X–O and distances H–X were assumed to be equal to H_2X_2. Employed structure parameters are summarized in Table I.

Structure parameters, harmonic vibrational wave numbers and normal coordinates, of CHBrClF, as well as electronic densities and vibrational wave functions along the C–F stretching mode were employed as described in Ref. [67]. Electronic densities along other normal coordinates were calculated on the level of ZORA-cGHF and ZORA-cGKS with the same basis set employed in Ref. [67]. Properties were calculated on the levels of ZORA-cGHF and ZORA-cGKS. Used density functionals are the local density approximation (LDA)[68–70] and the Lee, Yang and Parr correlation functional (LYP)[71] with a generalized gradient exchange functional by Becke (BLYP) [72] or the hybrid Becke three parameter exchange functional (B3LYP)[69, 73–75].

The ZORA-model potential $\tilde{V}(\vec{r})$ as proposed by van Wüllen [76] was employed with additional damping [77].

For calculations of two-component wave functions and properties a finite nucleus was used, described by a normalized spherical Gaussian nuclear density distribution $\rho_{\mathrm{nuc},A}(\vec{r}) = \frac{\zeta_A^{3/2}}{\pi^{3/2}}\mathrm{e}^{-\zeta_A|\vec{r}-\vec{r}_A|^2}$, where $\zeta_A = \frac{3}{2r^2_{\mathrm{nuc},A}}$ and the root mean square radius $r_{\mathrm{nuc},A}$ of nucleus A was used as suggested by Visscher and Dyall [78]. The mass numbers A were chosen to correspond to the isotopes ^{1}H, ^{12}C, ^{16}O, ^{19}F, ^{32}S, ^{35}Cl, ^{79}Br, ^{80}Se, ^{130}Te, ^{209}Po. The weak

nuclear charges $Q_{\mathrm{W},A}$ of the various isotopes with charge number Z_A and neutron number N_A were included as $Q_{\mathrm{W},A} \approx (1 - 4\sin^2\theta_{\mathrm{W}})Z_A - N_A$, where we have used $\sin^2\theta_{\mathrm{W}} = 0.2319$ as the numerical value of the Weinberg parameter.

All relativistic expectation values of $\boldsymbol{\gamma}^5$ and $\hat{H}_{\mathrm{ew}}$ were calculated with our ZORA property toolbox approach described in Ref. [63].

IV. RESULTS

A. Scaling laws for $\langle\boldsymbol{\gamma}^5\rangle$ in molecules

In order to confirm results of section II B we performed quasi-relativistic numerical calculations at the level of ZORA of (P)-enantiomers of H_2X_2 compounds with an dihedral angle of 45°, varying X = O, S, Se, Te, Po. These compounds are established as a common test system for electroweak $\mathcal{P}$-violation and its scaling behavior with respect to nuclear charge [58–60, 65, 79–81]. In the above scaling law a factor of $\alpha^2 Z_B^2$ emerges from spin-orbit coupling. This factor is in good approximation equal to α^2 in main group element containing molecules with only one heavy center (see e.g. Refs. [54]). Therefore, for a variation of one heavy X atom while holding the other one fixed as oxygen atom (H_2XO) we would expect roughly a scaling of $\sim \alpha^3 Z_A^2$ (corresponding to the second term in eq. (37)) as the spin-orbit coupling contribution (corresponding to the first term in eq. (37)) is suppressed by a factor of α^2.

The numerical results are summarized in Table II and Table III. Figure 1 shows a double logarithmic plot and a linear fit for the determination of the Z-scaling law in ZORA-cGHF calculations. From numerical calculations of H_2X_2 compounds we find a Z-scaling with $Z^{4.4}$, which agrees well with the analytical prediction. Furthermore for H_2XO compounds we find a scaling of $Z^{2.1}$, which is in perfect agreement with the expectations above and shows the missing spin-orbit coupling contribution as the nuclear charge of oxygen is close to 1.

In order to test the predicted α-dependence the speed of light was varied in the quasi-relativistic calculations of wave functions and properties for H_2PoO and H_2Po_2. The results show the expected scaling of $\alpha^{5.4} \approx \alpha^5$ for H_2Po_2 and a scaling of $\alpha^{3.6}$ for H_2PoO showing the weak influence of spin-orbit coupling in compounds with only one heavy nucleus. The results are in perfect agreement with the analytical analysis.

B. Comparison to electroweak electron-nucleon interactions

Similar considerations, as detailed in the previous section, are known to hold also for parity non-conserving nuclear spin-independent electroweak interactions described by Hamiltonian eq. (8) in chiral molecules. The main difference of this Hamiltonian to the ones discussed in the theory section is that $\hat{H}_{\mathrm{ew}}$ evaluates the expectation value of $\boldsymbol{\gamma}^5$ at positions inside the nuclei only. To further compare $\hat{H}_{\mathrm{ew}}$ with $\boldsymbol{\gamma}^5$ we evaluated the dependence of the expectation value of both operators on the dihedral angle in H_2X_2 for X = O and Po, and found similar behavior (see Figure 3 and for the explicit data see the Supplement). It shall be noted, that the sign of $\hat{H}_{\mathrm{ew}}$ is inverted in comparison to $\boldsymbol{\gamma}^5$ as $\hat{H}_{\mathrm{ew}}$ contains in addition the weak charge for which $Q_{\mathrm{W}} \approx -N < 0$.

In a recent work [82], similar calculations on $\boldsymbol{\gamma}^5$ in H_2X_2 compounds were performed and similar results were obtained. However, unfortunately, in Ref. [82] insufficient basis sets for oxygen were employed resulting in qualitatively wrong results for the dihedral angle dependence in H_2O_2.

The similar dependence on the molecular structure together with the steep scaling with nuclear charge indicates that contributions at the nuclear centers dominate also the expectation value of $\boldsymbol{\gamma}^5$ and, thus, imply that molecular experiments that aim to test $\mathcal{P}$-violation due to weak interactions can also be used for searches of $\mathcal{P}$-odd cosmic fields with a comparable sensitivity. This aspect will be discussed in the following in detail.

C. Limits on cosmic fields from experiments with chiral molecules

1. *Test system and choice of methods*

The expected sensitivity of experiments with chiral molecules to $\mathcal{P}$-odd cosmic fields characterized by b_0^{e} is estimated from an experiment with CHBrClF performed by Daussy *et. al.* [46], in which a hyperfine component of the $40_{7,34} \leftarrow 40_{8,33}$ transition ($J'_{K'_a,K'_c} \leftarrow J''_{K''_a,K''_c}$) of the C–F stretching fundamental in enantiomerically enriched samples of the mirror images R-CHBrClF and S-CHBrClF was studied.

Our interest is in a possible splitting of the vibrational resonance frequency between enantiomers that is caused by cosmic fields interacting through $\langle\boldsymbol{\gamma}^5\rangle$. For this purpose frequency shifts in the vibrational spectrum due to electronic interactions via $\boldsymbol{\gamma}^5$ have to be evaluated. This test system, CHBrClF, was excessively studied by theory [67, 83–90] and experiment [44–46, 91, 92] and is supposed to be reasonably well understood with respect to electroweak $\mathcal{P}$-violation.

However, the influence from non-separable anharmonic effects (multimode effects) on electroweak $\mathcal{P}$-violation in CHBrClF is largely unexplored. Quack and Stohner studied the deuterated isotopomer CDBrClF [93] with respect to multimode contributions in a four-dimensional, anharmonically treated subspace involving the C–F stretch, C–D stretch and the two C–D bending modes to find an increase of the $\mathcal{P}$-odd frequency splitting in the C–F stretch fundamental ν_4 by almost a factor of two — depending on the specific model, they obtained

up to 75 % relative deviation with respect to the separable anharmonic adiabatic approximation. Although not directly comparable due to the different isotope, this at least suggests that pronounced multimode effects can also exist for $\langle \boldsymbol{\gamma}^5 \rangle$.

We have reported major findings and implications for future experiments in a separate letter [1], but provide herein more details on the computational challenges and subsequent analysis.

We estimate the influence of multimode effects within a perturbative treatment by calculation of derivatives of the property of interest with respect to all normal coordinates. One-dimensional and two-dimensional vibrational corrections to a property O for a single dimensionless reduced normal coordinate q_r are in leading order given by [94]:

$$O_{q_r}^{\mathrm{1D}} \approx \frac{1}{2}\left(v_r + \frac{1}{2}\right)\left(\frac{\partial^2 O_0}{\partial q_r^2} - \frac{\phi_{rrr}}{\tilde{\nu}_r}\frac{\partial O_0}{\partial q_r}\right), \tag{38}$$

$$O_{q_r}^{\mathrm{2D}} \approx -\frac{1}{2}\left(v_r + \frac{1}{2}\right)\sum_{s\neq r}\frac{\phi_{rrs}}{\tilde{\nu}_s}\frac{\partial O_0}{\partial q_s}, \tag{39}$$

where ϕ_{rst} are the cubic force constants and $\tilde{\nu}_r$ are the harmonic vibrational wave numbers.

Properties are evaluated along the dimensionless reduced normal coordinate q_r and fitted to a polynomial of degree 4:

$$\left\langle \psi_{\mathrm{e}} \middle| \hat{H}_{\mathrm{ew}} \middle| \psi_{\mathrm{e}} \right\rangle_r \approx \sum_{k=0}^{4} c_{\mathrm{ew},r,k} q_r^k, \tag{40}$$

$$\left\langle \psi_{\mathrm{e}} \middle| \boldsymbol{\gamma}^5 \middle| \psi_{\mathrm{e}} \right\rangle_r \approx \sum_{k=0}^{4} c_{\boldsymbol{\gamma}^5,r,k} q_i^k. \tag{41}$$

In Figure 4 the dependence of $\langle \boldsymbol{\gamma}^5 \rangle$ and $\left\langle \hat{H}_{\mathrm{ew}} \right\rangle$ on the normal coordinates for the different methods in the region $q_r = -3, \ldots, 3$ (for the explicit data see the Supplement). Within this region the probability density of the first two vibrational states in the mode q_4 is sufficiently decayed (see Fig. 1 of Ref. [67]), as can also be expected by considering classical turning points of a harmonic approximation to the parity-conserving potential, which are located at $|q_4| = 1$ for the ground vibrational state of a harmonic oscillator and at $|q_4| = \sqrt{3}$ in the first vibrationally excited state. The resulting fit parameters $c_{\boldsymbol{\gamma}^5,r,k}$ alongside the explicit values for the one-dimensional cuts through the hypersurface for all normal coordinates q_r are reported in the Supplement.

The derivatives of the properties with respect to the normal coordinate q_r are given by

$$\frac{\partial \left\langle \psi_{\mathrm{e}} \middle| \boldsymbol{\gamma}^5 \middle| \psi_{\mathrm{e}} \right\rangle_r}{\partial q_r} = c_{\boldsymbol{\gamma}^5,r,1}, \tag{42}$$

$$\frac{\partial^2 \left\langle \psi_{\mathrm{e}} \middle| \boldsymbol{\gamma}^5 \middle| \psi_{\mathrm{e}} \right\rangle_r}{\partial q_r^2} = 2c_{\boldsymbol{\gamma}^5,r,2}, \tag{43}$$

and analogously for $\hat{H}_{\mathrm{ew}}$. Resulting first and second derivatives from the fit in Figure 4 are listed in Table V and Table VI. From these we see that the C–F stretching mode has a weak influence on $\langle \boldsymbol{\gamma}^5 \rangle$ in comparison to the other modes and, thus, is not an optimal choice for an experiment. In particular along the deformation normal coordinates q_9 (Br–Cl), q_8 (Br–F), q_3 (H) and q_2 (H) the first derivatives of $\langle \boldsymbol{\gamma}^5 \rangle$ are considerably larger in magnitude than for q_4. The second derivatives with respect to the C-F stretching coordinate are smaller in absolute value than those first derivatives mentioned, by about an order of magnitude (see Table V and Table VI). We may assume that anharmonic constants can be roughly of the order $\phi_{rrr} \sim \mathcal{O}(0.1\tilde{\nu}_r)$ and $\phi_{rrs} \sim \mathcal{O}(0.01\tilde{\nu}_s)$ or even larger (see e.g. Ref. [95, 96] for some cubic force constants in CDBrClF). In total, two-dimensional effects on the C–F stretching mode for $\langle \boldsymbol{\gamma}^5 \rangle$ can be on the same order as one-dimensional vibrational effects. Thus not only the effect of $\mathcal{P}$-odd interactions on the C-F stretching mode is very weak, but also the theoretical description is limited by the need of an excellent description of all modes, which is exceedingly difficult.

It is important to note, that the use of a different vibrational mode (such as Br-F (ν_8) or H (ν_3) deformation) in CHBrClF can result in vibrational frequency splittings that are larger by about an order of magnitude and may reduce error bars considerably. This has to be analyzed in more detail, however, using anharmonic vibrational force fields.

Due to the resulting large error bars for vibrational corrections for the C–F stretching mode we do not provide a final value for the enhancement of b_0^{e} in the C–F stretching but rather give an order of magnitude estimate.

For this purpose, within the separable anharmonic adiabatic approximation as described in Ref. [84], where we follow for this specific application Ref. [67] closely, the vibrationally averaged expectation value for the C–F stretching mode is evaluated from a series expansion in the vibrational moments $\langle v \,|\, q^k \,|\, v \rangle$, where v represents the vibrational quantum number of the vth vibrational state. The vibrational wave functions and corresponding moments were received in Ref. [67] from a discrete variable representation on an equidistant grid. The moments were reported in the supplementary material to Ref. [67] and are reused for calculating interactions of CHBrClF with cosmic fields.

In order to estimate electron correlation effects, for the C–F stretching mode the vibrationally averaged expectation values where evaluated at the DFT and HF level, the former with different flavors of density functionals. The results of these methods are compared in Table IV.

In previous studies on electroweak $\mathcal{P}$-violating vibrational frequency splittings in CHBrClF with density functional approaches [67, 89] much reduced variations between the methods were found for the C–F stretching fundamental as can be expected by the nearly parallel curves shown in Figure 5. In Ref. [67] we have observed a spread of about 20 % from the mean value for the four

methods used also in the present work. The variation amongst the various density functionals (B3LYP, BLYP and LDA) was below 5 %. In Ref. [89] it was found that B3LYP, BLYP and LDA estimates deviate by 6 % or less from the values predicted on the second order many-body perturbation theory level (MP2), with the latter method giving also absolute values at the equilibrium structure that agree well with the corresponding CCSD(T) estimates. Hartree–Fock based predictions, in contrast, displayed larger deviations from those of the mentioned density functional calculations. Similar trends are observed in the present work (see Table IV), but with more pronounced variations for the structure dependence of $\langle \boldsymbol{\gamma}^5 \rangle$ as compared to $\left\langle \hat{H}_{\rm ew} \right\rangle$: Vibrational splittings vary by about 50 % from the mean value of all four methods, with variations amongst the density functionals being on the order of 25 % or less from their mean. Assuming again that the density functionals outperform the Hartree–Fock approach for this property and give again similar results as MP2, we are lead to a rough error estimate of about 30 % for the density functionals. Of the different functionals, we give herein tentative preference to the B3LYP results as i) the absolute values at the equilibrium structures for electroweak $\mathcal{P}$-violation were for B3LYP closer to the MP2 and CCSD(T) values [89, 90], ii) the atomic contributions studied in Refs. [89, 90], which are differently weighted by $\langle \boldsymbol{\gamma}^5 \rangle$ as compared to $\left\langle \hat{H}_{\rm ew} \right\rangle$, were found to be more consistent with MP2 and CCSD(T) values and iii) the vibrational splitting on the B3LYP level is smaller than for the other functionals, which results in more conservative sensitivity estimates.

2. *Sensitivity to static cosmic fields*

The expectation values of $\boldsymbol{\gamma}^5$ and splittings between enantiomers are given in Table IV. As discussed above, we expect multimode effects of the same size as single-mode effects and at the present stage are not able to set upper bounds on $b_0^{\rm e}$ from the CHBrClF experiment. In Ref. [1] we rather estimated the sensitivity of this experiment. Assuming B3LYP to give the best performance (see discussion above) $\Delta_{(R,S)} \langle \boldsymbol{\gamma}^5 \rangle$ is on the order of 10^{-10} ($\mathcal{O}(10^{-10})$).

The sensitivity of the CHBrClF experiment, performed by Daussy et al. in 1999 [46], to $b_0^{\rm e}$ was in Ref. [1] estimated from the experimental upper bound of the $\mathcal{P}$-odd frequency splitting in the C-F stretching fundamental $|\Delta\nu| = 12.7\,\mathrm{Hz}$[46] as:

$$|b_0^{\rm e}| \lesssim \left| \frac{12.7\,\mathrm{Hz}}{\mathcal{O}(10^{-10})} h \right| \sim \mathcal{O}(10^{-12}\,\mathrm{GeV})\,. \qquad (44)$$

In comparison to the actual best direct limits on $b_0^{\rm e}$ from modern atomic experiments, that are $2 \times 10^{-14}\,\mathrm{GeV}$ from Cs and $7 \times 10^{-15}\,\mathrm{GeV}$ from Dy [30], the 1999 CHBrClF experiment is less sensitive by about two orders of magnitude [1]. However, it is as sensitive as atomic experiments with Tl and Yb ($|b_0^{\rm e}| < 2 \times 10^{-12}\,\mathrm{GeV}$, see Ref. [30]).

As emphasized in the discussion of multimode effects the sensitivity of future experiments can be increased by an order of magnitude, when choosing favorable vibrational transitions. As we pointed out in Ref. [1], it was emphasized in Refs. [92, 97, 98] that the sensitivity of the experiment discussed above is improvable by at least two orders of magnitude by experimental refinement. A choice of a more favorable molecule is expected to lead to further enhancement by two orders of magnitude. Thus it was estimated in Ref. [1] that in future $\mathcal{P}$-violation experiments with chiral molecules the limits from the 1999 experiment can be improved down to $10^{-17}\,\mathrm{GeV}$, i.e. an improvement of the actual best limit by at least two orders of magnitude. This makes experiments with chiral molecules highly powerful tools to search for Lorentz invariance violation beyond the Standard Model of particle physics.

The accuracy of the estimate for cosmic field effects in CHBrClF, which was in this work indirectly inferred by comparison to previous studies on electroweak $\mathcal{P}$-violation, can in principle be benchmarked by future explicit calculations with systematically improvable electron correlation methods and the presently neglected multi-mode contributions can be accounted for by explicit calculation of anharmonicity constants. As the main purpose of the present studies was to explore the general potential of chiral molecules to act as sensitive probes for new physics, more accurate theoretical estimates specifically for CHBrClF do not seem to be pressing until new experiments with higher accuracy are performed. Given the pronounced scaling with nuclear charge that was shown analytically and confirmed numerically in this paper, the main focus will likely be shifted to accurate estimates for chiral compounds with heavier elements. Furthermore, our study showed that care has to be taken by choice of the vibrational mode, which on the one hand can directly influence the sensitivity by an order of magnitude and on the other hand can be crucial for accurate theoretical predictions, which are essential to provide limits on cosmic fields from experiments.

V. CONCLUSION AND OUTLOOK

In this paper we have shown that interactions of electrons with the timelike-component of pseudovector cosmic fields are strongly pronounced in chiral molecules. Due to the $\mathcal{P}$-odd contributions of the nuclear potential, that electrons experience in a chiral molecule, these interactions lead to $\mathcal{P}$-odd resonance frequency splittings between enantiomers, similar to those from electroweak $\mathcal{P}$-violating interactions. We could show analytically and numerically that these interactions are strongly enhanced in heavy element containing molecules and are dominated from contributions that stem from the region near the

nucleus. It was demonstrated that $\mathcal{P}$-odd interactions of electrons with cosmic fields behave similarly to interactions due to an electroweak coupling of electrons and nucleons in chiral molecules. Thus, knowledge from electroweak quantum chemistry can be employed to find promising candidate molecules to limit $\mathcal{P}$-odd electronic coupling to cosmic fields. However, care has to be taken as our calculations revealed a stronger dependence of γ^5 on molecular structure.

We calculated matrix elements of $\mathcal{P}$-odd cosmic field interactions in CHBrClF with quasi-relativistic ab initio methods, including vibrational corrections, and compared the results of different DFT functionals. Our calculations of $\mathcal{P}$-odd effects along the different normal coordinates of CHBrClF revealed an important role of non-separable anharmonic effects and showed that the C–F stretching mode in particular is from this perspective not ideally suited for a measurement of $\mathcal{P}$-violation due to cosmic fields. Effects on some other modes are expected to be larger by an order of magnitude. These findings underline the importance to select not only a favorable molecule, but also to carefully choose the vibrational transition. However, from our calculations the sensitivity of a 20 year old experiment with CHBrClF to $|b_0^e|$ was estimated to be $\mathcal{O}(10^{-12}\,\mathrm{GeV})$. This sensitivity is inferior by two orders to the actual best direct measurements drawn from modern atomic $\mathcal{P}$-violation experiments, but was considered to be improvable to the order of $\mathcal{O}(10^{-17}\,\mathrm{GeV})$ or better for static pseudovector fields, which would be an improvement of the actually best limit on b_0^e by at least two orders of magnitude. This demonstrates the specific virtue that studies on chiral molecules provides in the search for new physics beyond the standard model.

ACKNOWLEDGMENTS

The authors are grateful to the Mainz Institute for Theoretical Physics (MITP) for its hospitality and its partial support during the completion of this work. The Marburg team gratefully acknowledges computer time provided by the center for scientific computing (CSC) Frankfurt and financial support by the Deutsche Forschungsgemeinschaft (DFG, German Research Foundation) – Projektnummer 328961117 – SFB 1319 ELCH. The work of M.G.K. and T.A.I. was supported by the Russian Science Foundation (RSF) grant No. 19-12-00157.

[1] K. Gaul, M. G. Kozlov, T. A. Isaev, and R. Berger, arXiv **hep-ph**, 2005.02429 (2020), arXiv:2005.02429 [hep-ph].
[2] G. Bertone, D. Hooper, and J. Silk, Phys. Rep. **405**, 279 (2005).
[3] M. Davis, G. Efstathiou, C. S. Frenk, and S. D. M. White, Astrophys. J. **292**, 371 (1985).
[4] S. Dodelson and L. M. Widrow, Phys. Rev. Lett. **72**, 17 (1994).
[5] H.-C. Cheng, J. L. Feng, and K. T. Matchev, Phys. Rev. Lett. **89**, 211301 (2002).
[6] P. Arias, D. Cadamuro, M. Goodsell, J. Jaeckel, J. Redondo, and A. Ringwald, J. Cosmol. Astropart. Phys. **2012**, 013 (2012).
[7] G. Gentile, P. Salucci, U. Klein, D. Vergani, and P. Kalberla, Mon. Notices Royal Astron. Soc. **351**, 903 (2004), http://oup.prod.sis.lan/mnras/article-pdf/351/3/903/3595222/351-3-903.pdf.
[8] A. Klypin, A. V. Kravtsov, O. Valenzuela, and F. Prada, Astrophys. J. **522**, 82 (1999).
[9] M. S. Pawlowski, B. Famaey, H. Jerjen, D. Merritt, P. Kroupa, J. Dabringhausen, F. Lghausen, D. A. Forbes, G. Hensler, F. Hammer, M. Puech, S. Fouquet, H. Flores, and Y. Yang, Mon. Notices Royal Astron. Soc. **442**, 2362 (2014), http://oup.prod.sis.lan/mnras/article-pdf/442/3/2362/3481343/stu1005.pdf.
[10] J. Kormendy, N. Drory, R. Bender, and M. E. Cornell, Astrophys. J. **723**, 54 (2010).
[11] S. Sachdeva and K. Saha, Astrophys. J. **820**, L4 (2016).
[12] Kroupa, P., Famaey, B., de Boer, K. S., Dabringhausen, J., Pawlowski, M. S., Boily, C. M., Jerjen, H., Forbes, D., Hensler, G., and Metz, M., Astron. Astrophys. **523**, A32 (2010).
[13] W. Hu, R. Barkana, and A. Gruzinov, Phys. Rev. Lett. **85**, 1158 (2000).
[14] Lee, Jae-Weon, EPJ Web Conf. **168**, 06005 (2018).
[15] P. W. Graham, D. E. Kaplan, J. Mardon, S. Rajendran, and W. A. Terrano, Phys. Rev. D **93**, 075029 (2016).
[16] R. D. Peccei and H. R. Quinn, Phys. Rev. Lett. **38**, 1440 (1977).
[17] F. Wilczek, Phys. Rev. Lett. **40**, 279 (1978).
[18] S. Weinberg, Phys. Rev. Lett. **40**, 223 (1978).
[19] G. 't Hooft, Phys. Rev. Lett. **37**, 8 (1976).
[20] G. G. di Cortona, E. Hardy, J. P. Vega, and G. Villadoro, J. High Energy Phys. **2016**, 34 (2016).
[21] H. An, M. Pospelov, J. Pradler, and A. Ritz, Physics Letters B **747**, 331 (2015).
[22] R. Catena, K. Fridell, and V. Zema, J. Cosmol. Astropart. Phys. **2018**, 018 (2018).
[23] D. Colladay and V. A. Kostelecký, Phys. Rev. D **58**, 116002 (1998).
[24] P. W. Graham and S. Rajendran, Phys. Rev. D **84**, 055013 (2011).
[25] P. W. Graham and S. Rajendran, Phys. Rev. D **88**, 035023 (2013).
[26] P. Sikivie, Phys. Rev. Lett. **113**, 201301 (2014).
[27] B. M. Roberts, Y. V. Stadnik, V. A. Dzuba, V. V. Flambaum, N. Leefer, and D. Budker, Phys. Rev. Lett. **113**, 081601 (2014).
[28] Y. V. Stadnik and V. V. Flambaum, Phys. Rev. D **89**, 043522 (2014).
[29] P. W. Graham, D. E. Kaplan, J. Mardon, S. Rajendran, W. A. Terrano, L. Trahms, and T. Wilkason, Phys. Rev. D **97**, 055006 (2018).
[30] B. M. Roberts, Y. V. Stadnik, V. A. Dzuba, V. V. Flam-

baum, N. Leefer, and D. Budker, Phys. Rev. D **90**, 096005 (2014).
[31] R. Berger and J. Stohner, WIREs Comput. Mol. Sci. **9**, e1396 (2019), https://onlinelibrary.wiley.com/doi/pdf/10.1002/wcms.1396.
[32] P. Schwerdtfeger, "The search for parity violation in chiral molecules," in *Computational Spectroscopy: Methods, Experiments and Applications*, edited by J. Grunenberg (Wiley, Netherlands, 2010) Chap. 7, pp. 201–221.
[33] M. Quack, J. Stohner, and M. Willeke, Annu. Rev. Phys. Chem. **59**, 741 (2008).
[34] M. Quack and J. Stohner, Chimia **59**, 530 (2005).
[35] J. Crassous, C. Chardonnet, T. Saue, and P. Schwerdtfeger, Org. Biomol. Chem. **3**, 2218 (2005).
[36] R. Berger, in *Relativistic Electronic Structure Theory, Part: 2, Applications*, edited by P. Schwerdtfeger (Elsevier, Netherlands, 2004) Chap. 4, pp. 188–288.
[37] M. Quack, Angew. Chem. Int. Ed. **41**, 4618 (2002).
[38] M. Quack, Chem. Phys. Lett. **132**, 147 (1986).
[39] É. Gajzágó and G. Marx, Atomki Közl. Suppl. **16/2**, 177 (1974).
[40] V. S. Letokhov, Phys. Lett. A **53**, 275 (1975).
[41] T. Udem, R. Holzwarth, and T. W. Hänsch, Nature **416**, 233 (2002).
[42] M. A. Bouchiat and C. Bouchiat, Eur. Phys. J. D **15**, 5 (2001).
[43] M.-A. Bouchiat, Phys. Rev. Lett. **98**, 043003 (2007).
[44] O. N. Kompanets, A. R. Kukudzhanov, V. S. Letokhov, and L. L. Gervits, Opt. Commun. **19**, 414 (1976).
[45] A. Bauder, A. Beil, D. Luckhaus, F. Müller, and M. Quack, J. Chem. Phys. **106**, 7558 (1997).
[46] C. Daussy, T. Marrel, A. Amy-Klein, C. T. Nguyen, C. J. Bordé, and C. Chardonnet, Phys. Rev. Lett. **83**, 1554 (1999).
[47] J. Vergados and Y. Semertzidis, Nucl. Phys. B **915**, 10 (2017).
[48] V. A. Kosteleck and C. D. Lane, J. Math. Phys. **40**, 6245 (1999), https://doi.org/10.1063/1.533090.
[49] V. G. Gorshkov, M. G. Kozlov, and L. N. Labzowsky, Sov. Phys. JETP **55**, 1042 (1982).
[50] Hobi, Fabian and Berger, Robert and Stohner, Juergen, Mol. Phys. **111**, 2345 (2013).
[51] P. Bargueño and I. Gonzalo, Origins Life Evol. B. **36**, 171 (2006).
[52] P. Bargueño and R. Pérez de Tudela, Origins Life Evol. B. **37**, 253 (2007).
[53] P. Bargueño, A. Dobado, and I. Gonzalo, EPL (Europhysics Letters) **82**, 13002 (2008).
[54] R. A. Hegstrom, D. W. Rein, and P. G. H. Sandars, J. Chem. Phys. **73**, 2329 (1980).
[55] M. G. Kozlov and V. I. Kopp, Vestn. Leningrad. Univ. , Fiz. Khim. **16**, 120 (1982).
[56] B. Y. Zel'dovich, D. B. Saakyan, and I. I. Sobel'man, JETP Lett. **25**, 94 (1977).
[57] C. van Wüllen, Z. Phys. Chem **224**, 413 (2010).
[58] R. Berger, N. Langermann, and C. van Wüllen, Phys. Rev. A **71**, 042105 (2005).
[59] R. Berger and C. van Wüllen, J. Chem. Phys. **122**, 134316 (2005).
[60] S. Nahrwold and R. Berger, J. Chem. Phys. **130**, 214101 (2009).
[61] T. A. Isaev and R. Berger, Phys. Rev. A **86**, 062515 (2012).
[62] K. Gaul and R. Berger, J. Chem. Phys. **147**, 014109 (2017).
[63] K. Gaul and R. Berger, J. Chem. Phys. **152**, 044101 (2020), arXiv:1907.10432 [physics.chem-ph].
[64] R. Ahlrichs, M. Bär, M. Häser, H. Horn, and C. Kölmel, Chem. Phys. Lett. **162**, 165 (1989).
[65] J. K. Laerdahl and P. Schwerdtfeger, Phys. Rev. A **60**, 4439 (1999).
[66] T. H. Dunning, Jr., J. Chem. Phys. **90**, 1007 (1989).
[67] R. Berger and J. L. Stuber, Mol. Phys. **105**, 41 (2007).
[68] W. Kohn and L. J. Sham, Phys. Rev. **140**, 1133 (1965).
[69] S. H. Vosko, L. Wilk, and M. Nuisar, Can. J. Phys. **58**, 1200 (1980).
[70] P. A. M. Dirac, Proc. Cambridge Phil. Soc. **26**, 376 (1930).
[71] C. Lee, W. Yang, and R. G. Parr, Phys. Rev. B **37**, 785 (1988).
[72] A. D. Becke, Phys. Rev. A **38**, 3098 (1988).
[73] P. J. Stephens, F. J. Devlin, C. F. Chabalowski, and M. J. Frisch, J. Phys. Chem. **98**, 11623 (1994).
[74] A. D. Becke, J. Chem. Phys. **98**, 1372 (1993).
[75] A. D. Becke, J. Chem. Phys. **98**, 5648 (1993).
[76] C. van Wüllen, J. Chem. Phys. **109**, 392 (1998).
[77] W. Liu, C. van Wüllen, F. Wang, and L. Li, J. Chem. Phys. **116**, 3626 (2002).
[78] L. Visscher and K. G. Dyall, At. Data Nucl. Data Tables **67**, 207 (1997).
[79] L. Wiesenfeld, Mol. Phys. **64**, 739 (1988).
[80] J. N. P. van Stralen, L. Visscher, C. V. Larsen, and H. J. A. Jensen, Chem. Phys. **331**, 81 (2005).
[81] A. Shee, L. Visscher, and T. Saue, J. Chem. Phys. **145** (2016), 10.1063/1.4966643.
[82] M. Senami and K. Ito, Phys. Rev. A **99**, 012509 (2019).
[83] M. Quack and J. Stohner, Phys. Rev. Lett. **84**, 3807 (2000).
[84] M. Quack and J. Stohner, Z. Phys. Chem. **214**, 675 (2000).
[85] J. K. Laerdahl, P. Schwerdtfeger, and H. M. Quiney, Phys. Rev. Lett **84**, 3811 (2000).
[86] R. G. Viglione, R. Zanasi, P. Lazzeretti, and A. Ligabue, Phys. Rev. A **62**, 052516 (2000).
[87] M. Quack and J. Stohner, Chirality **13**, 745 (2001).
[88] P. Schwerdtfeger, J. K. Laerdahl, and C. Chardonnet, Phys. Rev. A **65**, 042508 (2002).
[89] P. Schwerdtfeger, T. Saue, J. N. P. van Stralen, and L. Visscher, Phys. Rev. A **71**, 012103 (2005).
[90] C. Thierfelder, G. Rauhut, and P. Schwerdtfeger, Phys. Rev. A **81**, 032513 (2010).
[91] T. Marrel, M. Ziskind, C. Daussy, and C. Chardonnet, J. Mol. Struct. **599**, 195 (2001).
[92] M. Ziskind, C. Daussy, T. Marrel, and C. Chardonnet, Eur. Phys. J. D **20**, 219 (2002).
[93] M. Quack and J. Stohner, J. Chem. Phys. **119**, 11228 (2003).
[94] A. D. Buckingham and W. Urland, Chem. Rev. **75**, 113 (1975), https://doi.org/10.1021/cr60293a005.
[95] A. Beil, D. Luckhaus, and M. Quack, Ber. Bunsenges. Phys. Chem. **100**, 1853 (1996).
[96] A. Beil, D. Luckhaus, M. Quack, and J. Stohner, Ber. Bunsenges. Phys. Chem. **101**, 311 (1997), https://onlinelibrary.wiley.com/doi/pdf/10.1002/bbpc.19971010303.
[97] B. Darquie, C. Stoeffler, A. Shelkovnikov, C. Daussy, A. Amy-Klein, C. Chardonnet, S. Zrig, L. Guy, J. Crassous, P. Soulard, P. Asselin, T. R. Huet, P. Schwerdtfeger,

R. Bast, and T. Saue, Chirality **22**, 870 (2010).
[98] A. Cournol, M. Manceau, M. Pierens, L. Lecordier, D. B. A. Tran, R. Santagata, B. Argence, A. Goncharov, O. Lopez, M. Abgrall, Y. L. Coq, R. L. Targat, H. A. Martinez, W. K. Lee, D. Xu, P. E. Pottie, R. J. Hendricks, T. E. Wall, J. M. Bieniewska, B. E. Sauer, M. R. Tarbutt, A. Amy-Klein, S. K. Tokunaga, and B. Darquié, Quantum Electronics **49**, 288 (2019).

Table I. Molecular structure parameters for compounds of type H_2X_2 and H_2XO with X = O, S, Se, Te, Po employed in all calculations. Parameters for H_2X_2, where taken from Refs. [58, 65]. O–X bond length determined by full structure optimization of H_2XO compounds at the level of ZORA-cGHF.

X	$r(X-X)$/Å	$r(X-O)$/Å	$r(X-H)$/Å	$\sphericalangle(X-X-H)/^\circ$
O	1.490	1.490	0.970	100
S	2.055	1.627	1.352	92
Se	2.480	1.768	1.450	92
Te	2.840	1.933	1.640	92
Po	2.910	2.057	1.740	92

Table II. Electronic expectation value of $\boldsymbol{\gamma}^5$ for (P)-enantiomers of compounds of type H_2XO and H_2X_2 at a dihedral angle of 45° calculated at the level of ZORA-cGHF.

Z_X	$\langle\boldsymbol{\gamma}_5\rangle$	
	H_2XO	H_2X_2
8	7.02×10^{-9}	7.02×10^{-9}
16	1.81×10^{-8}	7.23×10^{-8}
34	9.66×10^{-8}	2.87×10^{-6}
52	2.67×10^{-7}	1.95×10^{-5}
84	8.69×10^{-7}	2.11×10^{-4}

Table III. Electronic expectation value of $\boldsymbol{\gamma}^5$ for (P)-enantiomers of H_2PoO and H_2Po_2 at a dihedral angle of 45° calculated at the level of ZORA-cGHF for different values of the fine structure constant α including α_0 which is $\frac{1}{c}$ in atomic units.

α	$\langle\boldsymbol{\gamma}_5\rangle$	
	H_2PoO	H_2Po_2
$\frac{1}{90}$	3.20×10^{-6}	1.38×10^{-3}
α_0	8.69×10^{-7}	2.11×10^{-4}
$\frac{1}{300}$	3.42×10^{-8}	2.10×10^{-6}
$\frac{1}{400}$	1.23×10^{-9}	4.60×10^{-7}
$\frac{1}{1000}$	6.65×10^{-10}	4.33×10^{-9}

Table IV. Molecular expectation value of $\boldsymbol{\gamma}^5$ in (S)-CHBrClF for the vibrational ground state and vibrational first excited state along the q_4 normal coordinate (C-F-stretching mode) at the level of ZORA-cGHF (HF) and ZORA-cGKS with LDA, BLYP and B3LYP functionals within the separable anharmonic adiabatic approximation.

Method	$\langle\boldsymbol{\gamma}_5\rangle$		
	$v=0$, (S)	$v_4=1$, (S)	$v_4=1 \leftarrow v=0$, $\Delta_{(R,S)}$
HF	-1.89×10^{-9}	-1.71×10^{-9}	3.61×10^{-10}
B3LYP	-8.28×10^{-9}	-7.91×10^{-9}	7.40×10^{-10}
BLYP	-8.27×10^{-9}	-7.82×10^{-9}	9.02×10^{-10}
LDA	-1.21×10^{-8}	-1.15×10^{-8}	1.18×10^{-9}

Table V. One dimensional first and second derivatives of the molecular expectation value of $\boldsymbol{\gamma}^5$ with respect to the reduced normal coordinate q_r in (S)-CHBrClF at the level of ZORA-cGHF (HF) and ZORA-cGKS with LDA, BLYP and B3LYP functionals.

r	$10^9\,\frac{\partial\langle\boldsymbol{\gamma}^5\rangle}{\partial q_r}$			$10^9\,\frac{\partial^2\langle\boldsymbol{\gamma}^5\rangle}{\partial q_r^2}$		
	LDA	B3LYP	HF	LDA	B3LYP	HF
9	14.67	11.21	5.63	0.24	0.14	−0.20
8	−34.05	−23.96	−3.61	−1.39	−0.62	0.29
7	−8.71	−6.35	−1.07	1.03	0.74	0.48
6	−9.13	−7.32	−0.39	2.41	0.95	−1.05
5	8.75	6.96	2.26	−4.05	−2.79	−0.73
4	2.21	1.10	−0.31	0.28	0.30	0.46
3	15.65	11.01	4.90	−1.90	−2.39	−4.94
2	7.89	10.47	13.57	−1.37	−0.67	1.22
1	1.42	1.21	0.65	0.46	0.38	0.17

Table VI. One dimensional first and second derivatives of the molecular expectation value of $\hat{H}_{\mathrm{ew}}$ with respect to the reduced normal coordinate q_r in (S)-CHBrClF at the level of ZORA-cGHF (HF) and ZORA-cGKS with LDA, BLYP and B3LYP functionals.

r	$10^{18}\,\frac{\partial\langle\hat{H}_{\mathrm{ew}}\rangle}{\partial q_r}$ (E_{h})			$10^{18}\,\frac{\partial^2\langle\hat{H}_{\mathrm{ew}}\rangle}{\partial q_r^2}$ (E_{h})		
	LDA	B3LYP	HF	LDA	B3LYP	HF
9	−2.10	−1.90	−1.42	0.01	−0.01	−0.03
8	11.47	9.43	6.27	0.52	0.38	0.13
7	6.97	6.29	5.11	−0.37	−0.29	−0.20
6	3.37	2.45	1.24	−0.90	−0.62	−0.19
5	−2.24	−1.72	−1.39	1.87	1.61	1.05
4	1.97	2.06	1.92	−0.27	−0.30	−0.39
3	−6.68	−5.95	−5.04	0.56	0.47	0.38
2	−6.01	−6.58	−6.88	−0.41	−0.51	−0.57
1	0.50	0.37	0.07	−0.09	−0.01	0.09

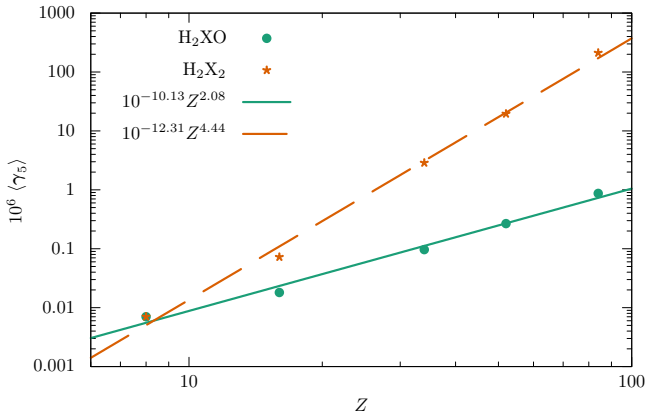

Figure 1. Dependence of the expectation value of $\boldsymbol{\gamma}^5$ on the nuclear charge Z for the (P)-enantiomers of H_2X_2 and H_2XO with X = O, S, Se, Te, Po at an dihedral angle of 45° calculated at the ZORA-cGHF level.

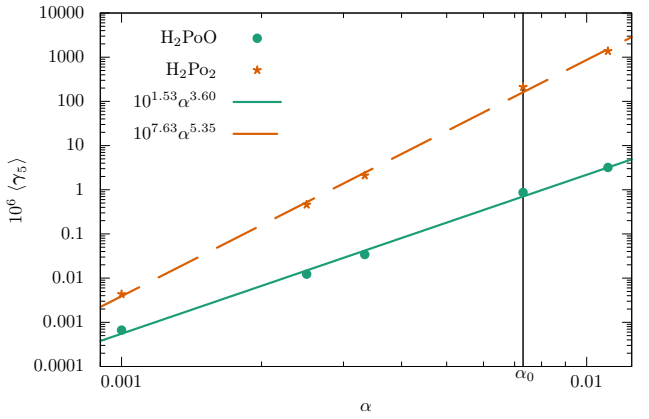

Figure 2. Dependence of the expectation value of $\boldsymbol{\gamma}^5$ on the fine structure constant α for the (P)-enantiomers of H_2Po_2 and H_2PoO at an dihedral angle of 45° calculated at the ZORA-cGHF level.

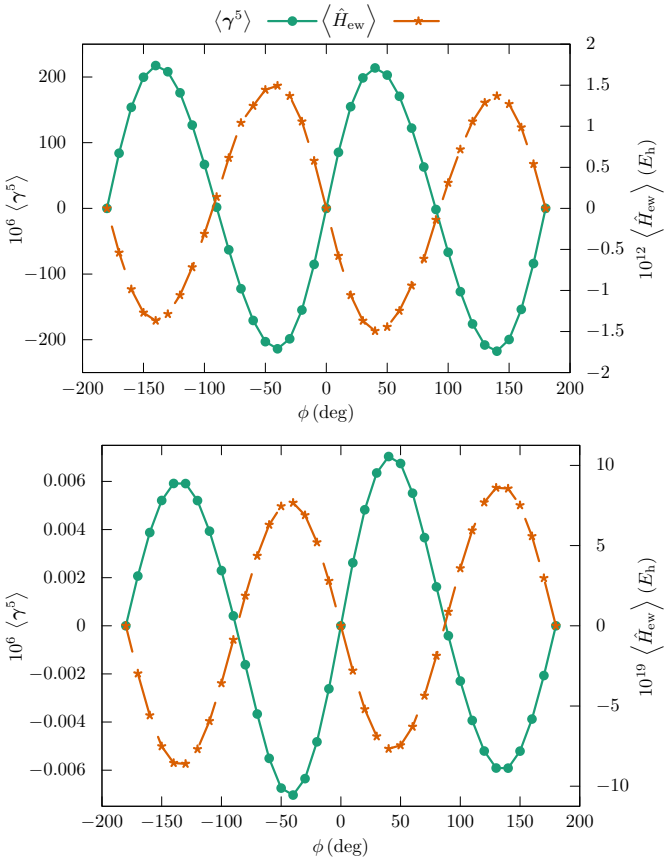

Figure 3. Dependence of the expectation value of $\boldsymbol{\gamma}^5$ in comparison to the expectation value of $\hat{H}_{\mathrm{ew}}$ on the dihedral angle ϕ in H_2Po_2 (top) and H_2O_2 (bottom) calculated at the ZORA-cGHF level. The results on $\hat{H}_{\mathrm{ew}}$ slightly differ from those of Ref. [58] due to the use of a different basis set. Straight lines connecting the computed points are drawn to guide the eye.

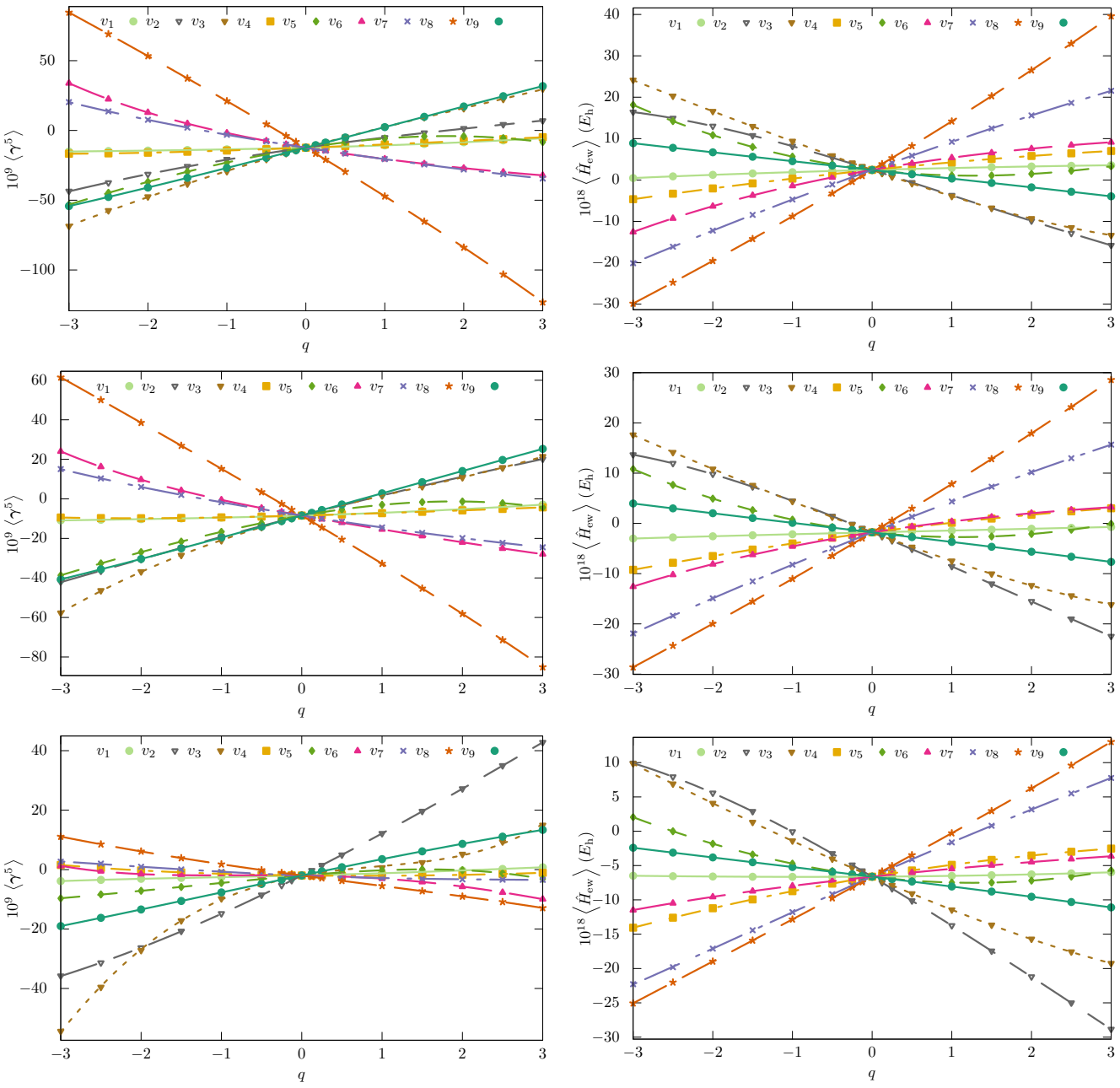

Figure 4. Dependence of the expectation value of $\boldsymbol{\gamma}^5$ (left) and $\hat{H}_{\mathrm{ew}}$ (right) on the nine normal coordinates in (*S*)–CHBrClF computed at the ZORA-cGKS and ZORA-cGHF level of theory. Data points are fitted to polynomials of fourth order (lines). (a) $\langle \boldsymbol{\gamma}^5 \rangle$, ZORA-cGKS, LDA; (b) $\left\langle \hat{H}_{\mathrm{ew}} \right\rangle$, ZORA-cGKS, LDA; (c) Figure as of Ref. [1] with values corresponding to $\langle \boldsymbol{\gamma}^5 \rangle$, ZORA-cGKS, B3LYP; (d) $\left\langle \hat{H}_{\mathrm{ew}} \right\rangle$, ZORA-cGKS, B3LYP; (e) $\langle \boldsymbol{\gamma}^5 \rangle$, ZORA-cGHF and (f) $\left\langle \hat{H}_{\mathrm{ew}} \right\rangle$, ZORA-cGHF. Results for $\hat{H}_{\mathrm{ew}}$ in the C–F stretching mode (v_4) are a recalculation of those presented in Ref. [67] and are thus identical to those.

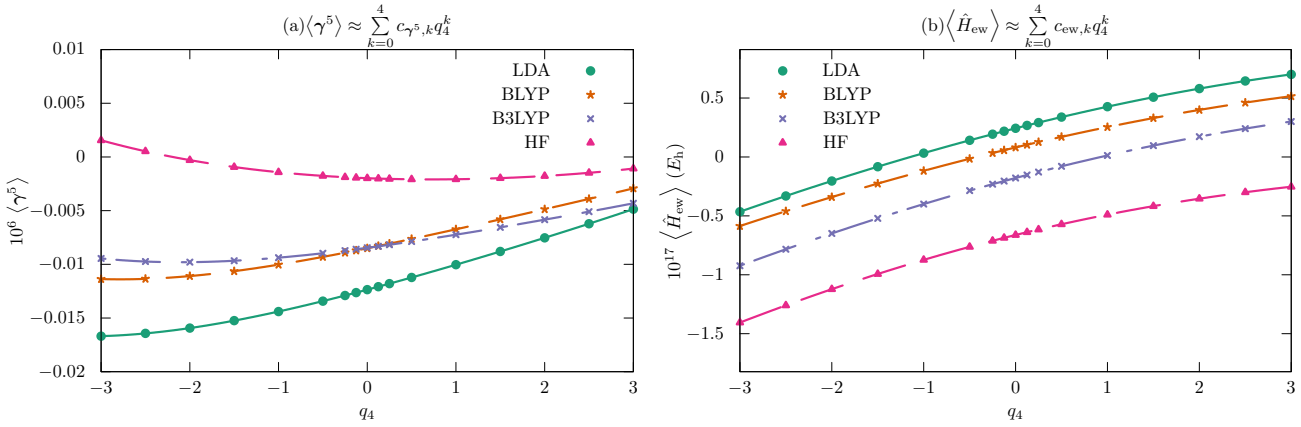

Figure 5. Dependence of the expectation value of (a) $\boldsymbol{\gamma}^5$ and (b) $\hat{H}_{\mathrm{ew}}$ on the C-F stretching normal coordinate q_4 in $(S)-$CHBrClF computed at the level of ZORA-cGHF and ZORA-cGKS with different exchange-correlation functionals (points) and polynomial fits to the $\left\langle \hat{H}_{\mathrm{ew}} \right\rangle$ and $\langle \boldsymbol{\gamma}^5 \rangle$ to fourth order (lines). The results for $\hat{H}_{\mathrm{ew}}$ are a recalculation of those presented in Ref. [67] and are thus identical to those.

Supplemantary Material to *Parity nonconserving interactions of electrons in chiral molecules with cosmic fields*

Konstantin Gaul,[1] Mikhail G. Kozlov,[2,3] Timur A. Isaev,[2] and Robert Berger[1]

[1] *Fachbereich Chemie, Philipps-Universität Marburg, Hans-Meerwein-Straße 4, 35032 Marburg, Germany*
[2] *Petersburg Nuclear Physics Institute of NRC "Kurchatov Institute", Gatchina 188300, Russia*
[3] *St. Petersburg Electrotechnical University "LETI", Prof. Popov Str. 5, 197376 St. Petersburg*

(Dated: May 8, 2020)

In the following, we list numerical data that is plotted in different figures of the paper *Parity nonconserving interactions of electrons in chiral molecules with cosmic fields*.

Data for the dihedral angle dependence of $\left\langle \hat{H}_{\rm ew} \right\rangle$ in H_2Po_2 and H_2O_2 differ slightly from those presented in Ref. [1] due to the choice of a different basis set.

The one-dimensional cut through the multi-dimensional parity violating potential energy surface of $\left\langle \hat{H}_{\rm ew} \right\rangle$ along the dimensionless reduced normal coordinate (q_4) corresponding to the C–F stretching mode for the (S)-enantiomer of CHBrClF is a recalculation of that in Ref. [2]. Parameters for the polynomial fit of this one-dimensional cut can be found in Ref. [2].

---

[1] R. Berger, N. Langermann, and C. van Wüllen, Phys. Rev. A **71**, 042105 (2005).
[2] R. Berger and J. L. Stuber, Mol. Phys. **105**, 41 (2007).

Table I. Dihedral angle ϕ dependence of $\langle \boldsymbol{\gamma}^5 \rangle$ and $\left\langle \hat{H}_{\mathrm{ew}} \right\rangle$ for the compounds H_2Po_2 and H_2O_2. Negative values of ϕ correspond to the (M)-enantiomer, positive values of ϕ correspond to the (P)-enantiomer. Due to the use of a different basis set the values differ slightly from those in Ref. [1].

	H_2O_2		H_2Po_2	
$\phi/^\circ$	$\langle \boldsymbol{\gamma}^5 \rangle \times 10^9$	$\left\langle \hat{H}_{\mathrm{ew}} \right\rangle \times 10^{19}/E_{\mathrm{h}}$	$\langle \boldsymbol{\gamma}^5 \rangle \times 10^4$	$\left\langle \hat{H}_{\mathrm{ew}} \right\rangle \times 10^{12}/E_{\mathrm{h}}$
−180	(0.000003)	(0.00000005)	(0.0000001)	(0.0000007)
−170	2.07	−2.97	0.84	−0.54
−160	3.88	−5.58	1.54	−0.99
−150	5.21	−7.51	2.00	−1.27
−140	5.92	−8.55	2.17	−1.37
−130	5.91	−8.60	2.08	−1.29
−120	5.20	−7.69	1.76	−1.06
−110	3.93	−5.94	1.27	−0.72
−100	2.29	−3.58	0.67	−0.31
−90	0.41	−0.87	0.02	0.14
−80	−1.62	1.87	−0.63	0.61
−70	−3.66	4.36	−1.22	0.94
−60	−5.51	6.30	−1.71	1.25
−50	−6.75	7.45	−2.03	1.44
−40	−7.04	7.67	−2.14	1.49
−30	−6.35	6.89	−1.99	1.37
−20	−4.82	5.20	−1.55	1.06
−10	−2.62	2.80	−0.85	0.58
0	(0.0000005)	(-0.00000005)	(0.0000002)	(-0.0000004)
10	2.62	−2.80	0.85	−0.58
20	4.82	−5.20	1.55	−1.06
30	6.35	−6.89	1.99	−1.37
40	7.04	−7.67	2.14	−1.49
50	6.75	−7.45	2.03	−1.44
60	5.51	−6.30	1.71	−1.25
70	3.66	−4.36	1.22	−1.04
80	1.62	−1.87	0.63	−0.61
90	0.41	0.87	0.02	−0.14
100	−2.29	3.58	−0.67	0.31
110	−3.93	5.94	−1.27	0.72
120	−5.20	7.69	−1.76	1.06
130	−5.91	8.60	−2.08	1.29
140	−5.92	8.55	−2.17	1.37
150	−5.21	7.51	−2.00	1.27
160	−3.88	5.58	−1.54	0.99
170	−2.07	2.97	−0.84	0.54
180	(0.00001)	(0.000002)	(0.00000003)	(-0.000002)

Table II. One dimensional cut through the parity violating potential of $\left\langle \hat{H}_{\mathrm{ew}} \right\rangle$ and of $\langle \boldsymbol{\gamma}^5 \rangle$ along the dimensionless reduced normal coordinate (q_1) corresponding to the C–H stretching mode for the (S)-enantiomer of CHBrClF.

q_1	$\langle \boldsymbol{\gamma}^5 \rangle \times 10^9$			$\left\langle \hat{H}_{\mathrm{ew}} \right\rangle \times 10^{17}/E_{\mathrm{h}}$		
	HF	B3LYP	LDA	HF	B3LYP	LDA
−3.000	−3.873	−10.908	−15.102	−0.649	−0.302	0.047
−2.500	−3.478	−10.598	−14.799	−0.655	−0.278	0.087
−2.000	−3.102	−10.261	−14.434	−0.660	−0.256	0.124
−1.500	−2.810	−9.899	−14.019	−0.663	−0.236	0.158
−1.000	−2.556	−9.496	−13.551	−0.665	−0.216	0.189
−0.500	−2.278	−9.027	−13.007	−0.665	−0.197	0.217
−0.250	−2.156	−8.760	−12.698	−0.664	−0.188	0.231
−0.125	−2.065	−8.617	−12.532	−0.663	−0.183	0.237
0.000	−1.978	−8.461	−12.360	−0.662	−0.179	0.243
0.125	−1.914	−8.312	−12.178	−0.661	−0.174	0.249
0.250	−1.828	−8.149	−11.989	−0.660	−0.169	0.255
0.500	−1.634	−7.804	−11.586	−0.657	−0.160	0.267
1.000	−1.221	−7.037	−10.680	−0.650	−0.142	0.289
1.500	−0.778	−6.174	−9.638	−0.641	−0.124	0.309
2.000	−0.301	−5.217	−8.454	−0.629	−0.107	0.327
2.500	0.206	−4.145	−7.112	−0.615	−0.089	0.343
3.000	0.776	−2.917	−5.577	−0.598	−0.072	0.357

Table III. One dimensional cut through the parity violating potential of $\left\langle \hat{H}_{\mathrm{ew}} \right\rangle$ and of $\langle \boldsymbol{\gamma}^5 \rangle$ along the dimensionless reduced normal coordinate (q_2) corresponding to a H deformation mode for the (S)-enantiomer of CHBrClF.

q_2	$\langle \boldsymbol{\gamma}^5 \rangle \times 10^9$			$\left\langle \hat{H}_{\mathrm{ew}} \right\rangle \times 10^{17}/E_{\mathrm{h}}$		
	HF	B3LYP	LDA	HF	B3LYP	LDA
−3.000	−35.802	−42.051	−43.518	0.992	1.367	1.641
−2.500	−31.382	−36.544	−37.496	0.793	1.194	1.492
−2.000	−26.313	−30.629	−31.421	0.557	0.980	1.301
−1.500	−20.746	−24.723	−25.765	0.288	0.729	1.073
−1.000	−14.824	−19.057	−20.746	−0.007	0.448	0.817
−0.500	−8.563	−13.666	−16.333	−0.325	0.144	0.538
−0.250	−5.329	−11.050	−14.303	−0.492	−0.016	0.392
−0.125	−3.661	−9.755	−13.322	−0.577	−0.097	0.318
0.000	−1.978	−8.461	−12.360	−0.662	−0.179	0.243
0.125	−0.305	−7.186	−11.413	−0.749	−0.261	0.168
0.250	1.423	−5.908	−10.480	−0.836	−0.345	0.092
0.500	4.916	−3.365	−8.651	−1.013	−0.513	−0.061
1.000	12.146	1.668	−5.117	−1.375	−0.856	−0.371
1.500	19.614	6.573	−1.754	−1.745	−1.204	−0.681
2.000	27.204	11.266	1.375	−2.121	−1.553	−0.988
2.500	34.980	15.732	4.254	−2.501	−1.902	−1.288
3.000	42.788	20.095	6.976	−2.885	−2.248	−1.580

Table IV. One dimensional cut through the parity violating potential of $\left\langle \hat{H}_{\mathrm{ew}} \right\rangle$ and of $\langle \boldsymbol{\gamma}^5 \rangle$ along the dimensionless reduced normal coordinate (q_3) corresponding to a H deformation mode for the (S)-enantiomer of CHBrClF.

q_3	$\langle \boldsymbol{\gamma}^5 \rangle \times 10^9$			$\left\langle \hat{H}_{\mathrm{ew}} \right\rangle \times 10^{17}/E_{\mathrm{h}}$		
	HF	B3LYP	LDA	HF	B3LYP	LDA
−3.000	−54.412	−57.731	−68.613	0.983	1.761	2.414
−2.500	−39.591	−46.409	−57.416	0.690	1.414	2.028
−2.000	−27.193	−36.853	−47.533	0.407	1.082	1.658
−1.500	−17.211	−28.536	−38.322	0.131	0.758	1.295
−1.000	−9.790	−21.118	−29.410	−0.140	0.439	0.938
−0.500	−4.832	−14.443	−20.713	−0.405	0.126	0.586
−0.250	−3.205	−11.370	−16.481	−0.535	−0.027	0.413
−0.125	−2.536	−9.898	−14.405	−0.599	−0.103	0.328
0.000	−1.978	−8.461	−12.360	−0.662	−0.179	0.243
0.125	−1.522	−7.079	−10.347	−0.725	−0.253	0.160
0.250	−1.123	−5.730	−8.372	−0.787	−0.327	0.077
0.500	−0.479	−3.145	−4.536	−0.910	−0.472	−0.086
1.000	0.651	1.661	2.662	−1.146	−0.748	−0.395
1.500	2.333	6.191	9.324	−1.367	−1.004	−0.678
2.000	5.156	10.761	15.741	−1.571	−1.235	−0.931
2.500	9.361	15.724	22.370	−1.757	−1.440	−1.151
3.000	14.944	21.425	29.706	−1.925	−1.617	−1.337

Table V. One dimensional cut through the parity violating potential of $\left\langle \hat{H}_{\mathrm{ew}} \right\rangle$ and of $\langle \boldsymbol{\gamma}^5 \rangle$ along the dimensionless reduced normal coordinate (q_4) corresponding to the C–F stretching mode for the (S)-enantiomer of CHBrClF. Recalculated values of $\left\langle \hat{H}_{\mathrm{ew}} \right\rangle$ are indentical to those in Ref. [2].

q_4	$\langle \boldsymbol{\gamma}^5 \rangle \times 10^9$				$\left\langle \hat{H}_{\mathrm{ew}} \right\rangle \times 10^{17}/E_{\mathrm{h}}$			
	HF	B3LYP	BLYP	LDA	HF	B3LYP	BLYP	LDA
−3.00	1.552	−9.451	−11.373	−16.689	−1.405	−0.923	−0.586	−0.465
−2.50	0.529	−9.736	−11.351	−16.430	−1.260	−0.783	−0.460	−0.331
−2.00	−0.294	−9.796	−11.092	−15.935	−1.122	−0.649	−0.340	−0.204
−1.50	−0.937	−9.667	−10.639	−15.245	−0.993	−0.521	−0.226	−0.083
−1.00	−1.420	−9.381	−10.033	−14.398	−0.873	−0.400	−0.118	0.032
−0.50	−1.762	−8.970	−9.310	−13.426	−0.763	−0.286	−0.015	0.141
−0.25	−1.885	−8.726	−8.915	−12.903	−0.711	−0.231	0.033	0.193
−0.125	−1.935	−8.596	−8.710	−12.634	−0.687	−0.205	0.057	0.218
0.00	−1.978	−8.461	−8.502	−12.360	−0.662	−0.179	0.081	0.243
0.125	−2.014	−8.321	−8.290	−12.082	−0.639	−0.153	0.104	0.268
0.25	−2.042	−8.177	−8.075	−11.799	−0.616	−0.128	0.126	0.292
0.50	−2.079	−7.877	−7.637	−11.223	−0.571	−0.079	0.170	0.339
1.00	−2.075	−7.237	−6.735	−10.034	−0.490	0.012	0.254	0.427
1.50	−1.972	−6.556	−5.811	−8.803	−0.417	0.096	0.330	0.507
2.00	−1.772	−5.842	−4.870	−7.533	−0.354	0.172	0.399	0.580
2.50	−1.476	−5.096	−3.910	−6.220	−0.299	0.240	0.461	0.645
3.00	−1.085	−4.317	−2.925	−4.858	−0.253	0.301	0.516	0.701

Table VI. One dimensional cut through the parity violating potential of $\left\langle \hat{H}_{\mathrm{ew}} \right\rangle$ and of $\langle \boldsymbol{\gamma}^5 \rangle$ along the dimensionless reduced normal coordinate (q_5) corresponding to the C–Cl stretching mode for the (S)-enantiomer of CHBrClF.

q_5	$\langle \boldsymbol{\gamma}^5 \rangle \times 10^9$			$\left\langle \hat{H}_{\mathrm{ew}} \right\rangle \times 10^{17}/E_{\mathrm{h}}$		
	HF	B3LYP	LDA	HF	B3LYP	LDA
−3.000	−9.682	−38.716	−53.160	0.205	1.082	1.815
−2.500	−8.372	−32.636	−44.684	−0.001	0.766	1.422
−2.000	−7.138	−26.939	−36.818	−0.182	0.494	1.084
−1.500	−5.857	−21.622	−29.579	−0.339	0.264	0.798
−1.000	−4.516	−16.718	−23.025	−0.472	0.075	0.564
−0.500	−3.209	−12.301	−17.247	−0.580	−0.072	0.379
−0.250	−2.593	−10.305	−14.685	−0.624	−0.130	0.305
−0.125	−2.283	−9.365	−13.491	−0.644	−0.156	0.273
0.000	−1.978	−8.461	−12.360	−0.662	−0.179	0.243
0.125	−1.716	−7.613	−11.291	−0.679	−0.199	0.217
0.250	−1.441	−6.805	−10.288	−0.694	−0.217	0.193
0.500	−0.947	−5.332	−8.486	−0.718	−0.245	0.154
1.000	−0.220	−3.018	−5.758	−0.747	−0.272	0.110
1.500	0.073	−1.652	−4.282	−0.748	−0.260	0.108
2.000	−0.219	−1.349	−4.175	−0.720	−0.211	0.147
2.500	−1.246	−2.219	−5.515	−0.661	−0.126	0.223
3.000	−3.154	−4.351	−8.360	−0.571	−0.007	0.332

Table VII. One dimensional cut through the parity violating potential of $\left\langle \hat{H}_{\mathrm{ew}} \right\rangle$ and of $\langle \boldsymbol{\gamma}^5 \rangle$ along the dimensionless reduced normal coordinate (q_6) corresponding to the C–Br stretching mode for the (S)-enantiomer of CHBrClF.

q_6	$\langle \boldsymbol{\gamma}^5 \rangle \times 10^9$			$\left\langle \hat{H}_{\mathrm{ew}} \right\rangle \times 10^{17}/E_{\mathrm{h}}$		
	HF	B3LYP	LDA	HF	B3LYP	LDA
−3.000	1.256	23.994	33.867	−1.149	−1.258	−1.256
−2.500	−0.534	16.251	22.471	−1.048	−1.022	−0.928
−2.000	−1.492	9.723	12.893	−0.956	−0.811	−0.634
−1.500	−1.907	4.200	4.879	−0.873	−0.624	−0.373
−1.000	−1.976	−0.537	−1.832	−0.796	−0.457	−0.141
−0.500	−1.929	−4.696	−7.498	−0.726	−0.309	0.063
−0.250	−1.937	−6.620	−10.015	−0.694	−0.242	0.156
−0.125	−1.964	−7.552	−11.207	−0.678	−0.210	0.201
0.000	−1.978	−8.461	−12.360	−0.662	−0.179	0.243
0.125	−2.043	−9.369	−13.474	−0.647	−0.148	0.285
0.250	−2.106	−10.257	−14.555	−0.632	−0.119	0.325
0.500	−2.307	−12.004	−16.622	−0.603	−0.063	0.401
1.000	−3.010	−15.413	−20.439	−0.548	0.038	0.538
1.500	−4.161	−18.746	−23.902	−0.496	0.126	0.656
2.000	−5.744	−21.996	−27.038	−0.449	0.202	0.757
2.500	−7.684	−25.100	−29.813	−0.405	0.267	0.842
3.000	−9.935	−27.951	−32.142	−0.364	0.322	0.912

Table VIII. One dimensional cut through the parity violating potential of $\left\langle \hat{H}_{\mathrm{ew}} \right\rangle$ and of $\langle \boldsymbol{\gamma}^5 \rangle$ along the dimensionless reduced normal coordinate (q_7) corresponding to the Cl–F deformation mode for the (S)-enantiomer of CHBrClF.

q_7	$\langle \boldsymbol{\gamma}^5 \rangle \times 10^9$			$\left\langle \hat{H}_{\mathrm{ew}} \right\rangle \times 10^{17}/E_{\mathrm{h}}$		
	HF	B3LYP	LDA	HF	B3LYP	LDA
−3.000	2.661	15.056	20.305	−2.229	−2.190	−2.012
−2.500	1.995	10.349	13.674	−1.981	−1.837	−1.613
−2.000	0.942	6.017	7.618	−1.710	−1.492	−1.223
−1.500	0.042	2.010	2.055	−1.443	−1.153	−0.843
−1.000	−0.766	−1.715	−3.087	−1.179	−0.821	−0.472
−0.500	−1.440	−5.196	−7.874	−0.918	−0.496	−0.110
−0.250	−1.728	−6.856	−10.151	−0.790	−0.337	0.068
−0.125	−1.869	−7.668	−11.264	−0.726	−0.257	0.156
0.000	−1.978	−8.461	−12.360	−0.662	−0.179	0.243
0.125	−2.122	−9.256	−13.439	−0.599	−0.100	0.330
0.250	−2.236	−10.033	−14.503	−0.536	−0.022	0.416
0.500	−2.449	−11.554	−16.587	−0.410	0.132	0.587
1.000	−2.817	−14.473	−20.588	−0.163	0.435	0.921
1.500	−3.096	−17.233	−24.381	0.080	0.731	1.245
2.000	−3.298	−19.834	−27.967	0.318	1.018	1.560
2.500	−3.412	−22.267	−31.339	0.550	1.297	1.863
3.000	−3.459	−24.515	−34.475	0.776	1.567	2.155

Table IX. One dimensional cut through the parity violating potential of $\left\langle \hat{H}_{\mathrm{ew}} \right\rangle$ and of $\langle \boldsymbol{\gamma}^5 \rangle$ along the dimensionless reduced normal coordinate (q_8) corresponding to the Br–F deformation mode for the (S)-enantiomer of CHBrClF.

q_8	$\langle \boldsymbol{\gamma}^5 \rangle \times 10^9$			$\left\langle \hat{H}_{\mathrm{ew}} \right\rangle \times 10^{17}/E_{\mathrm{h}}$		
	HF	B3LYP	LDA	HF	B3LYP	LDA
−3.000	11.097	61.469	84.571	−2.506	−2.862	−2.985
−2.500	8.517	50.044	69.095	−2.202	−2.433	−2.475
−2.000	6.114	38.520	53.341	−1.897	−1.997	−1.954
−1.500	3.883	26.912	37.325	−1.591	−1.554	−1.422
−1.000	1.796	15.222	21.049	−1.284	−1.104	−0.879
−0.500	−0.150	3.437	4.497	−0.974	−0.645	−0.324
−0.250	−1.092	−2.498	−3.891	−0.819	−0.413	−0.042
−0.125	−1.535	−5.478	−8.114	−0.740	−0.296	0.100
0.000	−1.978	−8.461	−12.360	−0.662	−0.179	0.243
0.125	−2.432	−11.467	−16.626	−0.584	−0.060	0.387
0.250	−2.881	−14.476	−20.915	−0.505	0.058	0.532
0.500	−3.772	−20.529	−29.564	−0.347	0.298	0.824
1.000	−5.495	−32.794	−47.170	−0.028	0.784	1.418
1.500	−7.232	−45.318	−65.246	0.296	1.282	2.028
2.000	−9.034	−58.164	−83.867	0.625	1.793	2.654
2.500	−10.888	−71.404	−103.117	0.960	2.318	3.297
3.000	−12.911	−85.116	−123.090	1.303	2.858	3.960

Table X. One dimensional cut through the parity violating potential of $\left\langle \hat{H}_{\mathrm{ew}} \right\rangle$ and of $\langle \boldsymbol{\gamma}^5 \rangle$ along the dimensionless reduced normal coordinate (q_9) corresponding to the Br–Cl deformation mode for the (S)-enantiomer of CHBrClF.

q_9	$\langle \boldsymbol{\gamma}^5 \rangle \times 10^9$			$\left\langle \hat{H}_{\mathrm{ew}} \right\rangle \times 10^{17}/E_{\mathrm{h}}$		
	HF	B3LYP	LDA	HF	B3LYP	LDA
−3.000	−19.015	−40.759	−54.207	−0.241	0.396	0.888
−2.500	−16.245	−35.655	−47.676	−0.312	0.299	0.778
−2.000	−13.423	−30.408	−40.917	−0.382	0.202	0.669
−1.500	−10.565	−25.044	−33.971	−0.452	0.106	0.561
−1.000	−7.691	−19.586	−26.872	−0.522	0.011	0.454
−0.500	−4.826	−14.053	−19.659	−0.592	−0.084	0.348
−0.250	−3.409	−11.266	−16.018	−0.627	−0.131	0.296
−0.125	−2.701	−9.868	−14.191	−0.645	−0.155	0.270
0.000	−1.978	−8.461	−12.360	−0.662	−0.179	0.243
0.125	−1.296	−7.065	−10.524	−0.680	−0.202	0.217
0.250	−0.589	−5.660	−8.685	−0.698	−0.226	0.191
0.500	0.807	−2.846	−5.002	−0.733	−0.274	0.139
1.000	3.521	2.794	2.386	−0.806	−0.369	0.034
1.500	6.136	8.438	9.785	−0.879	−0.466	−0.072
2.000	8.652	14.071	17.175	−0.954	−0.564	−0.178
2.500	11.087	19.690	24.541	−1.031	−0.664	−0.285
3.000	13.350	25.282	31.771	−1.110	−0.766	−0.395

Table XI. Resulting parameters of the polynomial fit to the one dimensional cut through the parity violating potential due to $\langle \boldsymbol{\gamma}^5 \rangle$ along the dimensionless reduced normal coordinate (q_1) corresponding to the C–H stretching mode for the (S)-enantiomer of CHBrClF. The standard uncertainties resulting from the fit procedure are given in parenthesis in units of the last preceeding one or two digits.

k	$c_{\boldsymbol{\gamma}^5,k} \times 10^9$			$c_{\mathrm{ew},k} \times 10^{18}/E_{\mathrm{h}}$		
	HF	B3LYP	LDA	HF	B3LYP	LDA
0	−1.982(5)	−8.461(3)	−12.354(3)	−6.622 09(12)	−1.785 54(7)	2.433 19(6)
1	0.646(5)	1.210(3)	1.419(3)	0.071 84(12)	0.366 23(7)	0.497 68(6)
2	0.087(4)	0.188(2)	0.231(2)	0.046 17(9)	−0.005 22(5)	−0.043 81(4)
3	0.0144(8)	0.0133(5)	0.0188(4)	0.001 357(19)	0.001 893(11)	0.002 094(9)
4	−0.0044(5)	−0.0018(3)	−0.0009(2)	−0.000 372(11)	−0.000 432(6)	−0.000 284(5)

Table XII. Resulting parameters of the polynomial fit to the one dimensional cut through the parity violating potential due to $\langle \boldsymbol{\gamma}^5 \rangle$ along the dimensionless reduced normal coordinate (q_2) corresponding to the H deformation mode for the (S)-enantiomer of CHBrClF. The standard uncertainties resulting from the fit procedure are given in parenthesis in units of the last preceeding one or two digits.

k	$c_{\boldsymbol{\gamma}^5,k} \times 10^9$			$c_{\mathrm{ew},k} \times 10^{18}/E_{\mathrm{h}}$		
	HF	B3LYP	LDA	HF	B3LYP	LDA
0	−1.976(16)	−8.43(3)	−12.32(5)	−6.6219(16)	−1.7850(10)	2.4338(11)
1	13.573(16)	10.47(4)	7.89(5)	−6.8816(17)	−6.5817(10)	−6.0084(11)
2	0.612(12)	−0.33(2)	−0.68(3)	−0.2864(12)	−0.2541(8)	−0.2030(8)
3	−0.052(2)	−0.010(5)	0.062(7)	0.0467(2)	0.062 13(16)	0.071 36(17)
4	−0.0006(14)	0.005(3)	0.002(4)	−0.003 28(14)	−0.004 12(9)	−0.003 72(10)

Table XIII. Resulting parameters of the polynomial fit to the one dimensional cut through the parity violating potential due to $\langle \boldsymbol{\gamma}^5 \rangle$ along the dimensionless reduced normal coordinate (q_3) corresponding to the H deformation mode for the (S)-enantiomer of CHBrClF. The standard uncertainties resulting from the fit procedure are given in parenthesis in units of the last preceeding one or two digits.

k	$c_{\boldsymbol{\gamma}^5,k} \times 10^9$			$c_{\mathrm{ew},k} \times 10^{18}/E_\mathrm{h}$		
	HF	B3LYP	LDA	HF	B3LYP	LDA
0	−2.05(14)	−8.50(5)	−12.39(10)	−6.621(5)	−1.785(9)	2.433(11)
1	4.90(14)	11.01(5)	15.65(10)	−5.036(5)	−5.945(9)	−6.680(11)
2	−2.47(10)	−1.19(3)	−0.95(7)	0.190(3)	0.235(6)	0.278(8)
3	0.75(2)	0.238(7)	0.072(15)	0.0214(7)	0.0359(13)	0.0487(17)
4	0.057(12)	0.014(4)	0.019(9)	0.0024(4)	0.0048(8)	0.0056(9)

Table XIV. Resulting parameters of the polynomial fit to the one dimensional cut through the parity violating potential due to $\langle \boldsymbol{\gamma}^5 \rangle$ along the dimensionless reduced normal coordinate (q_4) corresponding to the C–F stretching mode for the (S)-enantiomer of CHBrClF. For corresponding fit parameters of $\left\langle \hat{H}_\mathrm{ew} \right\rangle$ see the supplement of Ref. [2]. The standard uncertainties resulting from the fit procedure are given in parenthesis in units of the last preceeding one or two digits.

k	$c_{\boldsymbol{\gamma}^5,k} \times 10^9$			
	HF	B3LYP	BLYP	LDA
0	−1.9758(3)	−8.4609(8)	−8.4991(8)	−12.3571(7)
1	−0.3133(3)	1.0967(8)	1.6758(8)	2.2055(7)
2	0.2289(2)	0.1488(6)	0.1145(6)	0.1408(5)
3	−0.014 03(4)	−0.026 84(12)	−0.029 90(12)	−0.026 09(10)
4	0.001 87(5)	0.002 94(7)	0.003 97(7)	0.003 94(6)

Table XV. Resulting parameters of the polynomial fit to the one dimensional cut through the parity violating potential due to $\langle \boldsymbol{\gamma}^5 \rangle$ along the dimensionless reduced normal coordinate (q_5) corresponding to the C–Cl stretching mode for the (S)-enantiomer of CHBrClF. The standard uncertainties resulting from the fit procedure are given in parenthesis in units of the last preceeding one or two digits.

k	$c_{\boldsymbol{\gamma}^5,k} \times 10^9$			$c_{\mathrm{ew},k} \times 10^{18}/E_\mathrm{h}$		
	HF	B3LYP	LDA	HF	B3LYP	LDA
0	−1.990(9)	−8.467(9)	−12.361(10)	−6.6223(6)	−1.7856(13)	2.4332(11)
1	2.262(9)	6.960(9)	8.746(11)	−1.3870(6)	−1.7214(13)	−2.2413(12)
2	−0.365(6)	−1.393(7)	−2.026(8)	0.5257(5)	0.8027(10)	0.9370(9)
3	−0.1313(13)	−0.1378(14)	−0.1432(16)	0.010 53(9)	−0.0104(2)	−0.025 41(17)
4	−0.0141(7)	−0.0065(8)	−0.0021(9)	0.000 72(5)	−0.000 80(11)	−0.001 66(10)

Table XVI. Resulting parameters of the polynomial fit to the one dimensional cut through the parity violating potential due to $\langle \boldsymbol{\gamma}^5 \rangle$ along the dimensionless reduced normal coordinate (q_6) corresponding to the C–Br stretching mode for the (S)-enantiomer of CHBrClF. The standard uncertainties resulting from the fit procedure are given in parenthesis in units of the last preceeding one or two digits.

k	$c_{\boldsymbol{\gamma}^5,k} \times 10^9$			$c_{\mathrm{ew},k} \times 10^{18}/E_\mathrm{h}$		
	HF	B3LYP	LDA	HF	B3LYP	LDA
0	−1.992(10)	−8.470(10)	−12.363(12)	−6.6221(2)	−1.7855(2)	2.433 18(18)
1	−0.386(10)	−7.319(10)	−9.132(13)	1.2360(2)	2.4533(2)	3.367 77(19)
2	−0.524(8)	0.473(7)	1.205(9)	−0.097 17(15)	−0.309 38(16)	−0.448 57(14)
3	−0.1653(16)	−0.1497(15)	−0.2089(19)	0.007 99(3)	0.019 88(3)	0.027 30(2)
4	0.0293(9)	0.0276(9)	0.0295(11)	−0.000 858(17)	−0.001 350(19)	−0.001 481(16)

Table XVII. Resulting parameters of the polynomial fit to the one dimensional cut through the parity violating potential due to $\langle \boldsymbol{\gamma}^5 \rangle$ along the dimensionless reduced normal coordinate (q_7) corresponding to the Cl–F deformation mode for the (S)-enantiomer of CHBrClF. The standard uncertainties resulting from the fit procedure are given in parenthesis in units of the last preceeding one or two digits.

k	$c_{\boldsymbol{\gamma}^5,k} \times 10^9$			$c_{\mathrm{ew},k} \times 10^{18}/E_\mathrm{h}$		
	HF	B3LYP	LDA	HF	B3LYP	LDA
0	−2.01(2)	−8.4670(10)	−12.3597(9)	−6.616(10)	−1.785 58(10)	2.433 13(13)
1	−1.07(2)	−6.3547(10)	−8.7064(10)	5.107(10)	6.285 21(10)	6.966 44(13)
2	0.238(15)	0.3690(7)	0.5143(7)	−0.101(7)	−0.143 52(8)	−0.184 91(9)
3	0.004(3)	−0.026 79(15)	−0.047 16(14)	−0.0102(15)	−0.002 693(16)	−0.002 471(19)
4	−0.0064(18)	0.005 15(8)	0.007 98(8)	0.0031(9)	−0.000 465(9)	−0.000 679(11)

Table XVIII. Resulting parameters of the polynomial fit to the one dimensional cut through the parity violating potential due to $\langle \boldsymbol{\gamma}^5 \rangle$ along the dimensionless reduced normal coordinate (q_8) corresponding to the Br–F deformation mode for the (S)-enantiomer of CHBrClF. The standard uncertainties resulting from the fit procedure are given in parenthesis in units of the last preceeding one or two digits.

k	$c_{\boldsymbol{\gamma}^5,k} \times 10^9$			$c_{\mathrm{ew},k} \times 10^{18}/E_\mathrm{h}$		
	HF	B3LYP	LDA	HF	B3LYP	LDA
0	−1.991(3)	−8.4668(14)	−12.3594(13)	−6.6223(2)	−1.785 58(8)	2.433 15(17)
1	−3.607(3)	−23.9595(15)	−34.0517(14)	6.2705(3)	9.427 43(9)	11.474 90(18)
2	0.145(2)	−0.3118(11)	−0.6932(10)	0.0645(2)	0.187 96(6)	0.262 09(13)
3	−0.0438(4)	−0.0525(2)	−0.0622(2)	0.008 59(4)	0.011 728(13)	0.011 03(2)
4	−0.0027(2)	−0.006 79(12)	−0.008 16(12)	0.000 30(2)	0.000 867(7)	0.001 026(15)

Table XIX. Resulting parameters of the polynomial fit to the one dimensional cut through the parity violating potential due to $\langle \boldsymbol{\gamma}^5 \rangle$ along the dimensionless reduced normal coordinate (q_9) corresponding to the Br–Cl deformation mode for the (S)-enantiomer of CHBrClF. The standard uncertainties resulting from the fit procedure are given in parenthesis in units of the last preceeding one or two digits.

k	$c_{\boldsymbol{\gamma}^5,k} \times 10^9$			$c_{\mathrm{ew},k} \times 10^{18}/E_\mathrm{h}$		
	HF	B3LYP	LDA	HF	B3LYP	LDA
0	−1.989(3)	−8.4665(7)	−12.361(3)	−6.622 21(13)	−1.785 57(10)	2.433 03(11)
1	5.626(3)	11.2115(7)	14.674(3)	−1.417 17(13)	−1.896 17(11)	−2.096 90(11)
2	−0.101(2)	0.0695(5)	0.120(2)	−0.014 21(9)	−0.005 04(8)	0.006 51(8)
3	−0.0258(4)	−0.022 75(10)	−0.0379(5)	−0.003 510(19)	−0.004 501(16)	−0.004 706(16)
4	0.0008(2)	0.001 27(6)	0.0008(3)	−0.000 057(11)	−0.000 220(9)	−0.000 331(9)

BOOST: A satellite mission to test Lorentz invariance using high-performance optical frequency references

Norman Gürlebeck,[1,2,*] Lisa Wörner,[1,2] Thilo Schuldt,[2] Klaus Döringshoff,[3] Konstantin Gaul,[4] Domenico Gerardi,[5] Arne Grenzebach,[1,2] Nandan Jha,[6] Evgeny Kovalchuk,[3] Andreas Resch,[2] Thijs Wendrich,[6] Robert Berger,[4] Sven Herrmann,[1] Ulrich Johann,[5] Markus Krutzik,[3] Achim Peters,[3] Ernst M. Rasel,[6] and Claus Braxmaier[1,2]

[1]*ZARM, University of Bremen, Am Fallturm 2, 28359 Bremen, Germany*
[2]*DLR Institute for Space Systems, Robert-Hooke-Strasse 7, 28359 Bremen, Germany*
[3]*Humboldt University Berlin, Institute of Physics, Newtonstrasse 15, 12489 Berlin, Germany*
[4]*Philipps-University Marburg, Hans-Meerwein-Strasse 4, 35032 Marburg, Germany*
[5]*Airbus Defence and Space GmbH, 88039 Friedrichshafen, Germany*
[6]*Leibniz University Hannover, Institute for Quantumoptics, Welfengarten 1, 30167 Hannover, Germany*

(Received 15 December 2017; published 20 June 2018)

BOOST (BOOst Symmetry Test) is a proposed satellite mission to search for violations of Lorentz invariance by comparing two optical frequency references. One is based on a long-term stable optical resonator, and the other is based on a hyperfine transition in molecular iodine. This mission will allow us to determine several parameters of the standard model extension in the electron sector up to 2 orders of magnitude better than with the current best experiments. Here, we will give an overview of the mission, the science case, and the payload.

DOI: 10.1103/PhysRevD.97.124051

I. INTRODUCTION

General relativity and quantum theory are experimentally justified theories describing nature. One of the biggest challenges of contemporary theoretical physics is to formulate a theory capable of unifying both; see, e.g., Ref. [1] and references therein. Such a theory of quantum gravity could additionally explain phenomena at the Planck scale. Among others, such a theory is expected to resolve the singularity residing in a black hole and provide insights into the very early history of our Universe. Despite enormous efforts, a commonly accepted theory has not yet been found, although some candidates like loop quantum gravity, string theory, discrete approaches such as causal dynamical triangulations, and noncommutative geometry have been suggested; see, e.g., Refs. [2,3] and references therein. However, there is no experimental evidence of the quantum properties of spacetime yet, presumably due to the inaccessibility of the energy scale at which they become relevant. Thus, highly accurate experiments must be performed to detect the minuscule remnants of these effects in our currently available regimes.

Such alternative theories usually violate some of the fundamental assumptions of our current physical theories like the Lorentz invariance, which is a basic building block of special relativity, where it holds globally. In general relativity, it is still satisfied locally. A detection of a violation of Lorentz invariance (LIV) or the determination of tighter upper bounds on such violations aids the future development of new theoretical frameworks.

To not be limited to specific alternative theories, test theories, which quantify and catalog LIVs, most notably the standard model extension (SME) [4–6] but also the Robertson-Mansouri-Sexl (RMS) theory [7–10], were developed. Whereas the first describes general Lorentz violations for each particle, the second deforms Lorentz transformations introducing, e.g., a frame dependence in the speed of light. The latter approach is kinematic; i.e., it describes the LIV, but it does not provide alternative field equations from which these effects ensue.

The satellite mission BOOST (Boost Symmetry Test) plans to measure these LIVs with unprecedented sensitivity by comparing two highly stable frequency references aboard the satellite. One laser is stabilized to a length standard given by an optical resonator, and the other is stabilized to a hyperfine transition in molecular iodine [11]. Both frequency standards will be compared over the course of the satellite orbits. Since the changes of the frequencies of those two references are affected differently by possible LIVs in these test theories, a beat measurement provides estimates on the parameters involved; see Sec. II A.

Within BOOST, several key technologies are used and developed further so that they can be transferred to fit future developments and space-based missions. The ultrastable, highly precise frequency references developed for BOOST provide new and valuable options for probing the gravitational field of the Earth. For example, the Gravity Recovery and Climate Experiment-Follow On mission

*norman.guerlebeck@zarm.uni-bremen.de

(GRACE-FO) determines the gravity-induced change in the distance between two satellites using a laser ranging instrument as a technology demonstration; see Ref. [12]. Here, the laser source is frequency stabilized using an optical resonator developed by Jet Propulsion Laboratory (JPL) and Ball Aerospace, Inc., USA; see Ref. [13]. Similar concepts are considered for European Space Agency's (ESA) Next Generation Gravity Mission (NGGM). Another example is the gravitational wave detector Laser Interferometer Space Antenna (LISA), for which an optical resonator is the baseline laser frequency prestabilization [14].

Global navigation satellite systems (GNSSs) such as GPS or Galileo require high-performance clocks onboard as the main payload. Their timing signals are used for position determination on Earth. Thus, the frequency stability of these clocks is one limiting factor for the accuracy of the positioning. Whereas current GNSSs use microwave clock technology like Cs or Rb clocks as well as H-maser, future systems can benefit from optical frequency references like the iodine reference developed for BOOST.

Currently, different efforts are underway for developing optical frequency references for space. Laser frequency stabilization to an optical resonator is investigated, e.g., within the ESA projects Optical Stabilizing Reference Cavity with the NGGM as application, see Ref. [15], as well as a clock laser for a strontium lattice clock and high-stability laser, again with an application for the NGGM; see Ref. [16]. Further space developments are carried out by SODERN (France) [17] and by JPL/Ball Aerospace with respect to the flight model development for GRACE-FO; see Refs. [13,18]. The optical resonator for BOOST is based on the German Aerospace Agency (DLR) developments toward a long-term stable optical resonator setup on elegant breadboard (EBB) level and frequency stabilization to molecular iodine on the EBB and engineering model level; see Refs. [19,20] and [11,21], respectively. Within the JOKARUS project led by the Humboldt University Berlin, an iodine-based system is currently integrated for a payload on a sounding rocket with a tentative launch in 2018; see Ref. [22]. Note that the iodine frequency reference fulfills the frequency stability requirements for LISA and the NGGM [11,21].

Aside from the novel techniques in the field of highly stable frequency references, advanced laser technologies will be developed for the project. Currently, only specific wavelengths are accessible using space-qualified sources. With the planned diode lasers, the accessible range of wavelengths is broadened, while the lasers' budgets are reduced at the same time. Such lasers could be envisaged for a multitude of future missions as well as in Earth-bound laboratories. They are also developed in the scope of the atom interferometry sounding rocket mission MAIUS [23].

The paper is organized as follows. In Sec. II, we introduce the mission including the science case and the driving requirements. Section III gives an overview of the payload and provides instrument budgets. In Sec. IV, the payload subsystems are described, and the corresponding error sources are discussed together with the respective error mitigation strategies.

II. MISSION OVERVIEW

The satellite mission BOOST searches for LIVs, in particular, regarding the dynamics of electrons and photons. It is currently considered by the DLR in the scope of the national large mission program. It is based on previous studies of the satellite mission proposals STAR, BOOST, and mSTAR; see Refs. [24–27], respectively. The tentative schedule foresees a launch in 2025.

Subsequently, we describe the science case and the derived mission requirements.

A. Science case

There are different test theories available to describe possible LIVs. We describe here the expected results of BOOST in the RMS framework and the SME. A detailed calculation will be given elsewhere.

1. Robertson-Mansouri-Sexl test theory

In the RMS theory, a distortion of the Lorentz transformation between the preferred frame Σ_{PF}, in which the speed of light c_0 is assumed to be isotropic, and the experiment's rest frame Σ_{S}, which moves with the velocity $\vec{v}$ relative to Σ_{PF}, is introduced. The deviation from the ordinary Lorentz transformations depends to leading order in $\frac{\vec{v}}{c_0}$ on the three parameters α, β, and γ [7–10]. They measure a deviation from the time dilation; longitudinal length contraction, i.e., in the direction of $\vec{v}$; and transversal length contraction as they are predicted by special relativity, in which $\alpha = -\beta = -\frac{1}{2}, \gamma = 0$. This leads to a speed of light c that depends on the relative velocity $\vec{v}$ and orientation θ of the light path with respect to the preferred frame,

$$\frac{c(\theta,\vec{v})}{c_0} = 1 + (\beta - \alpha - 1)\frac{\vec{v}^2}{c_0^2} + \left(\frac{1}{2} - \beta + \gamma\right)\frac{\vec{v}^2}{c_0^2}\sin^2\theta + O\left(\left|\frac{\vec{v}}{c}\right|^3\right), \tag{1}$$

where we already assumed that $\vec{v}$ is small compared to the speed of light. Note that this is the two-way speed of light; i.e., the light travels from an observer A to a mirror B and back to A. Thus, a convention on how to synchronize clocks as for a one-way measurement is not necessary.

Combinations of the RMS parameters are measured by the three classical experiments (see Refs. [28–30]):

(1) The Michelson Morley experiment measures $\alpha_{\mathrm{MM}} = \frac{1}{2} - \beta + \gamma$ using the variation of the orientation θ.
(2) The Kennedy-Thorndike experiment measures $\alpha_{\mathrm{KT}} = \beta - \alpha - 1$ using the variation of the relative velocity $\vec{v}$.

TABLE I. Current constraints for the experimental determination of the RMS coefficients.

Parameter	Current best constraint	Reference
α_{KT}	$(4.8 \pm 3.7) \times 10^{-8}$	[31]
α_{MM}	$(4 \pm 8) \times 10^{-12}$	[32][a]
α_{IS}	$(-0.38 \pm 1.06) \times 10^{-8}$	[33]

[a]Recently, Ref. [34] gave the most precise constraints on orientation-dependent relative frequency changes $\Delta\nu/\nu$ to $9.2 \pm 10.7 10^{-19}$, 1 order of magnitude better than in Ref. [32]. Although in Ref. [34] the experiment was not evaluated in the RMS framework, this implies also approximately an order of magnitude of improvement in α_{MM} since the experiment was carried out at the same location.

(3) The Ives-Stillwell experiment measures the time dilation and hence $\alpha_{IS} = \alpha + \frac{1}{2}$ directly.

The most stringent constraints are given in Table I.

Subsequently, we apply the RMS framework to the experiment planned with BOOST consisting of an optical resonator and an iodine clock. The dependence of both on the potential variation of the speed of light (1) will be evaluated, and the science signal will be identified.

The resonance frequency $\nu_{OR}(\Sigma_S)$ of the optical resonator depends on its rest frame Σ_S and the value of the speed of light in that frame. The frequency of the laser stabilized on a hyperfine transition of the iodine molecule ν_{I_2}, on the other hand, is determined to leading order by the nonrelativistic Hamiltonian and thus is on this level of approximation independent of the speed of light and $\vec{v}$. In fact, at higher orders of approximation, a dependence appears via the fine structure constant, which is, however, suppressed compared to the frequency variations in the optical resonator. It serves as an absolute reference in this context. Thus, a beat measurement between the two yields

$$\frac{\delta\nu_{RMS}}{\nu_{OR}(\Sigma_{PF})} = \frac{\nu_{OR}(\Sigma_S) - \frac{1}{2}\nu_{I_2}}{\nu_{OR}(\Sigma_{PF})} = \frac{c(\theta,\vec{v})}{c_0} - \frac{\nu_{I_2}}{2\nu_{OR}(\Sigma_{PF})}, \quad (2)$$

where the latter term is a constant offset, which we will not measure. The frequency $\nu_{OR}(\Sigma_{PF})$ is the frequency of a hypothetical optical resonator at rest in Σ_{PF}, which is used solely for scaling purposes. Note that the factor $1/2$ in front of the ν_{I_2} is due to the fact that in the planned experiment the resonance frequency of the optical resonator is compared with a laser that is first frequency doubled and then stabilized on the hyperfine transition of the iodine as described below, cf. Fig. 1. Together with Eq. (1), this beat signal varies with $\vec{v}$ over one orbit and allows to determine α_{KT}. In fact, at the frequencies detectable with BOOST, $\vec{v}$ varies only due to the change in the satellite's velocity, i.e., due to the changes of the direction of its velocity. The Michelson-Morley coefficient α_{MM} will be obtained simultaneously. However, the sensitivity of BOOST will not suffice to improve on the best-known

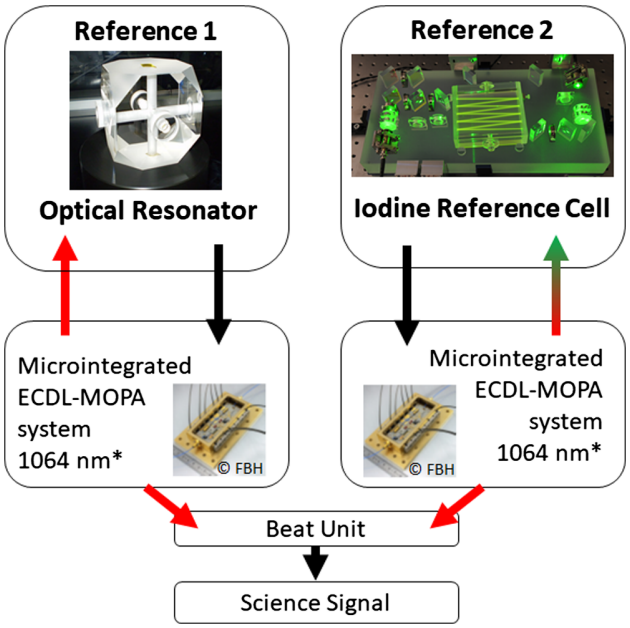

FIG. 1. Schematic overview of the measurement principle. An optical resonator and an iodine spectroscopy unit are employed to stabilize their respective lasers developed by the FBH. The resulting stabilized frequencies are then compared in the beat measurement. The time variation of the beat signal yields the science signal. (*cf. Ref. [22].)

constraints for that parameter, cf. Table I, and we will omit its discussion here for brevity. Nonetheless, α_{MM} will be considered in the data analysis of the mission.

One drawback of the RMS theory is that it requires a preferred frame. Although this can be chosen in principle arbitrarily, it is usually taken to be the rest frame of the cosmic microwave background, where the radiation is to a high degree isotropic. Nonetheless, future observations with different physical settings might suggest another preferred frame. Even though the results obtained for one frame can be easily transformed into any other frame, this can also involve a loss of sensitivity. Here, we will choose an orbit, which is sensitive to any possible direction of the preferred frame. Moreover, the RMS theory does not describe new field equations, say, for the dynamics of photons.

2. Standard model extension

Both issues of the RMS theory, the need for a preferred frame and the lack of new field equations, are overcome by the SME, which is nowadays the test theory of choice; see Refs. [4–6]. It extends the action of the standard model with terms violating the Lorentz invariance, thereby describing modifications of the dynamics of all particles. To achieve comparability of the results of different experiments, the measurements are always referred to a natural Sun-centered celestial equatorial frame (SCF) (X^1, X^2, X^3, T); see, e.g., Refs. [35,36]. The X^3 axis is aligned with Earth's axis of rotation, and X^1 points to the vernal equinox on the celestial

sphere. The axis X^2 is chosen such that this frame is right handed. The center of the Sun is chosen as the spatial origin of the SCF, and the origin of the time axis is chosen as the vernal equinox in the year 2000.

The frequency of the optical resonator depends on the dynamics of the photons and also on the electron sector of the SME, which, e.g., describes the modification of the length of the optical resonator. It was argued in Ref. [37] that the latter effect is suppressed compared to the former. Thus, the optical resonator is essentially sensitive to the photon sector of the SME, which is summarized in the modified Maxwell equations, cf. Ref. [35],

$$\frac{\partial}{\partial x^{\mu_2}} F^{\mu_2}_{\mu_1} + (k_F)_{\mu_1\mu_2\mu_3\mu_4} \eta^{\mu_2\mu_5} \frac{\partial}{\partial x^{\mu_5}} F^{\mu_3\mu_4} = 0, \tag{3}$$

where F is the Faraday tensor, η is the Minkowski metric with the signature $(+,-,-,-)$, and the μ_i are Lorentz indices running from 0 to 3. They are raised and lowered with the Minkowski metric. The x^{μ_i} are the spacetime coordinates, where x^0 and x^1, x^2, x^3 denote the timelike and spacelike ones, respectively. Note that we used the Einstein summation convention. Whereas the first term in Eq. (3) is the ordinary source-free Maxwell equation, the second term is the modification of the SME parametrized by the k_F tensor, which will be measured by BOOST. We neglected already terms proportional to the vector k_{AF}, i.e., those modifications depending explicitly on the 4-potential A_μ as well, following Ref. [35].

On the other hand, the iodine frequency reference is sensitive to the electron sector governed by the standard Hamiltonian with the Lorentz invariance–violating correction, which reads in the nonrelativistic limit, cf. Ref. [38],

$$\begin{aligned}\delta H = c^2 &\left[-b_j + m_e d_{j0} - \frac{1}{2}\epsilon_{jkl}(m_e g_{kl0} - H_{kl})\right]\sigma^j \\ &- \left[c_{jk} + \frac{1}{2}c_{00}\delta_{jk}\right]\frac{p_j p_k}{m_e} \\ &+ \left(\frac{1}{2}\left[b_l + \frac{1}{2}m_e\epsilon_{lmn}g_{mn0}\right]\delta_{jk} + \left[m_e(d_{0j} + d_{j0})\right.\right. \\ &\left.\left. - \frac{1}{2}\left(b_j + m_e d_{j0} + \frac{1}{2}\epsilon_{jmn}(m_e g_{mn0} + H_{mn})\right)\right]\delta_{kl} \right. \\ &\left. - m_e\epsilon_{jlm}(g_{m0k} + g_{mk0})\right)\frac{p_j p_k}{m_e^2}\sigma^l, \end{aligned} \tag{4}$$

where m_e is the electron mass; c is the speed of light; and $\frac{\hbar}{2}\sigma^j$ and p_j are the spin and momentum operator of the electron, respectively. ϵ_{ijk} is the totally antisymmetric Levi-Civita symbol, and δ_{jk} is the Kronecker symbol. The lowercase latin indices j, k, l, m, and n run over the three spatial directions 1, 2, and 3, whereas the index 0 refers to the timelike one. Analogously to the Einstein summation convention, we sum over repeated latin indices in formula (4). The Lorentz tensors b_{μ_1}, $c_{\mu_1\mu_2}$, $d_{\mu_1\mu_2}$, $H_{\mu_1\mu_2}$, and $g_{\mu_1\mu_2\mu_3}$ parametrize the LIV in the electron sector of the SME. Note that we neglected here already terms odd in the electron's momentum, which vanish in the molecule's rest frame, and constant terms, which do not contribute to a shift in the transition frequency.

A detailed treatment of the iodine frequency reference in the formalism of the standard model extension, which will be presented elsewhere, shows that only the terms proportional to the diagonal terms of $c^{\mathrm{L}}_{\mu\nu}$ in the laboratory frame contribute to the overall shift of the frequency. This is due to the symmetries of the iodine molecule and the fact that all orientations of the iodine molecule contribute to the spectral line. The other terms either vanish or they yield a broadening of the line, which is not yet detectable. The transformation of these parameters $c^{\mathrm{L}}_{\mu\mu}$ to the tensor components $c^{\mathrm{SCF}}_{\mu\nu}$ in the Sun-centered frame will, however, also introduce off-diagonal terms again.

The combination of the expressions of the photon and the electron sector yields, following the formalism of Ref. [36], the beat signal of the form

$$\begin{aligned}\frac{\delta\nu_{\mathrm{SME}}}{\nu} = \sum_{i=1}^{3}\sum_{j=-3}^{3} &[S_{ij}\sin(i\omega_{\mathrm{S}}T + j\Omega_{\oplus}T) \\ &+ C_{ij}\cos(i\omega_{\mathrm{S}}T + j\Omega_{\oplus}T)], \end{aligned} \tag{5}$$

where ω_{S} is the frequency corresponding to one satellite orbit and $\Omega_{\oplus}$ to one revolution of the Earth around the Sun and T is the time in the SCF. The coefficients S_{ij} and C_{ij} depend on the coefficients of the LIV, the orbit, and the orientation of the optical resonator as well as the modification of the transition energies in the iodine molecules. Although we derive these coefficients explicitly elsewhere, we give in the Appendix two of them for illustration purposes. Note that $S_{1\pm3} = C_{1\pm3} = S_{3\pm3} = C_{3\pm3} = C_{30} = 0$. This implies that there are in general 33 fitting parameters to such a science signal or equivalently peaks in the power spectral density of the relative frequency. However, they will not all be independent, and not all will be observable; i.e., they are already constrained by previous experiments below our noise limit, cf. Ref. [39].[1] Thus, comparing the S_{ij} and C_{ij} with the expected stability of the used references gives the estimates for the experimental outcome as will be discussed in the next section.

B. Science and mission requirements

The science requirements that follow from the previous section are summarized subsequently. Of course, the requirements on the orbit and the instrument are not

[1]Note that some of these known constraints are also based on theoretical arguments like in the case of astrophysical birefringence, whereas BOOST would measure them directly. Nonetheless, we omit such constraints in the discussion below for brevity, cf. Table II, and present them elsewhere.

entirely independent. Taking Eqs. (2) and (5) into account, it is obvious that the variations take place at frequencies near the orbital frequency. Thus, the references have to perform well at this timescale.

Generally, an orbit with a low altitude is preferable for several reasons. First, the satellite's speed is higher for lower altitudes. This gives, together with the change of the direction of the velocity of the satellite over one orbit, higher velocity variations, which will be beneficial for both test theories. Second, since during one complete orbit one estimate of the different constraints of the test theories can be generated, the statistics is improved with a lower altitude, implying more orbits per day if a similar relative frequency stability is assumed at orbit time. Both effects are also the main reasons why this experiment is more sensitive to LIVs if carried out on a satellite rather than on the ground: for a low-Earth orbit, this amounts to an improvement by roughly 2 orders of magnitude if the same experiment is carried out for the same period in the laboratory or aboard a satellite.

Moreover, shorter orbital periods entail a less restrictive requirement on the stability of the frequency references, which is especially important for the optical resonator. If the altitude becomes too low, however, the atmospheric drag will either shorten the lifetime of the mission or increase its complexity by the need to reposition the spacecraft. Thus, a low-Earth orbit below the inner van Allen belt (1000 km), where the sensitivity varies only by a few percent with the altitude, is preferable.

To be able to resolve the different frequencies in Eq. (5) in a Fourier analysis of the science data, the mission should be in science mode for at least one year. Assuming a duty cycle of about 50%, a mission lifetime of two years is required. To allow an appropriate data analysis later, like in Ref. [32], for example, the satellite should operate ten full orbits in science mode without disturbances. Nonetheless, we will assume here a continuous science mode of the satellite for one year in the science case evaluation consistently with the level of approximations done subsequently.

We want the experiment to be sensitive to all possible directions of the preferred frame in the RMS theory. In the SME, this is equivalent to requiring being sensitive to all spatial components of the tensors measuring Lorentz violation like $c_{\mu\nu}$. This leads to an orbit in which the orbital plane sweeps out the entire space in the course of one year, which is guaranteed with a Sun-synchronous orbit. This reduces also eclipses for the satellite and relaxes the requirements on the thermal control system and power management of the satellite.

The analysis of different orbit options indicated that a 6 a.m. dawn-dusk Sun-synchronous orbit at 650 km altitude is a good compromise satisfying the aforementioned constraints, guaranteeing the necessary sensitivity level for the science signal, and the need to reduce the impact by drag effects. Moreover, the remaining eclipse time is reduced even further, and with this choice, the satellite can deorbit freely in 25 years as required for the space debris mitigation. The ground visibility is acceptable, too.

TABLE II. Expected constraints on LIV by the proposed mission BOOST after one year of observation.

Constraints[a]
$\lvert c_{10}^{\mathrm{SCF}} + c_{01}^{\mathrm{SCF}}\rvert \leq 3 \times 10^{-13}$
$\lvert c_{30}^{\mathrm{SCF}} + c_{03}^{\mathrm{SCF}}\rvert \leq 3 \times 10^{-13}$
$\lvert c_{12}^{\mathrm{SCF}} + c_{21}^{\mathrm{SCF}}\rvert \leq 4 \times 10^{-17}$
$\lvert c_{13}^{\mathrm{SCF}} + c_{31}^{\mathrm{SCF}}\rvert \leq 2 \times 10^{-17}$
$\lvert c_{23}^{\mathrm{SCF}} + c_{32}^{\mathrm{SCF}}\rvert \leq 3 \times 10^{-17}$
$\lvert c_{11}^{\mathrm{SCF}} + c_{22}^{\mathrm{SCF}} - 2c_{33}^{\mathrm{SCF}}\rvert \leq 4 \times 10^{-17}$
$\lvert \alpha_{\mathrm{KT}}\rvert \leq 7.5 \times 10^{-10}$[b]

[a]Note that the precision of the constraints of the SME parameters is limited, e.g., by the precision of the estimates of the expectation value of the perturbation of the Hamiltonian in Eq. (4).

[b]The value for α_{KT} is referring to the rest frame of the cosmic microwave background as the preferred frame. Preferred frames in directions orthogonal to this one yield analogous results, provided they move at the same speed with respect to us, which is just a scaling for comparability.

The orientation of the optical resonator should be chosen such that the orientations of the optical paths change over one orbit, which enhances the time variability of the science signal in the SME evaluation. Hence, one optical path should be pointing in the direction of the relative velocity of the satellite with respect to the Earth and the other one should be parallel to its relative acceleration, i.e., nadir pointing. Assuming that the optical resonator is mounted rigidly to the spacecraft, this implies an attitude for the satellite in which the angles between the satellite axes and the optical paths are fixed.[2] Note that this is not required for measuring the Kennedy-Thorndike coefficient in the RMS theory.

With this orbit, the scientific output can be predicted, cf. Table II as follows. Requiring a relative frequency stability of the references of 1×10^{-15} at orbit time and assuming white noise in the relevant frequency regime, an expected power spectral density (PSD) can be derived for a one-year mission that is continuously in science mode. This PSD is then compared to Eqs. (2) and (5), which determines constraints for the coefficients S_{ij}, C_{ij}, and α_{KT}. Afterward, these constraints can be converted to constraints on the SME parameters with straightforward algebra.

For these estimates, we neglect terms which are already constrained below our noise level. Hence, only those which improve the current best estimates by up to 2 orders of magnitude, see Ref. [39], are shown here, cf. Footnote 1. The instrument requirements derived from this science requirement are discussed in the next section.

[2]In Ref. [36], this is called the XVV mode.

III. PAYLOAD OVERVIEW

To measure the small deviation in the photon and electron propagation, the scientific payload consists of two optical frequency references: an optical resonator and an iodine spectroscopy unit. Both frequency references shall operate with a relative stability of 10^{-15} at orbit time, i.e., approximately 90 min. A sketch of the measurement principle can be seen in Fig. 1.

In this section, an overview of the flight hardware, including the thermal and redundancy concept as well as the budgets, will be given. The following section, Sec. IV, then describes the payload subsystems including the possible error sources and the respective mitigation strategies in more detail.

A. Thermal and redundancy concept

A schematic of the payload is given in Fig. 2. Along this scheme, we will explain the thermal and redundancy concept.

The *thermal stability* of the payload is a major factor in the performance of the instrument subsystems. While the mass and power budgets could be reduced using one large compartment, housing the entire payload, the easiness of implementation into the satellite bus and the mitigation of potential thermal noises induced by one of the other systems favor individual thermal stabilization of the subsystems.

As can be seen in Fig. 2, five thermally stabilized compartments are chosen as a baseline for the payload's design with individual compartments for the optical resonator, two iodine spectroscopy units, the laser system, and the control electronics, respectively. To avoid the impact of thermal fluctuations, the beam preparation and detection stages are implemented into the same housing as the payload subsystem, i.e., the optical resonator and the iodine spectroscopy unit.

For *redundancy*, the two frequency references are doubled. The redundancy concept is sketched in Fig. 2. In the case of the optical resonator, a spacer with two crossed light paths is chosen, implementing the redundancy of the optics in one ultralow expansion glass (ULE) block. Both accessible optical paths are equipped with a beam preparation and detection stage. They are housed in one thermally stabilized box, and they are used to stabilize two individual lasers. In contrast, two complete iodine spectroscopy units in separate boxes are included in the payload. Each system is associated with one dedicated laser. All four lasers are connected to the beat unit. This allows one to compare each of the iodine spectroscopy units to each of the optical paths of the resonator. Nonetheless, to reduce the power and ease the requirements on the batteries

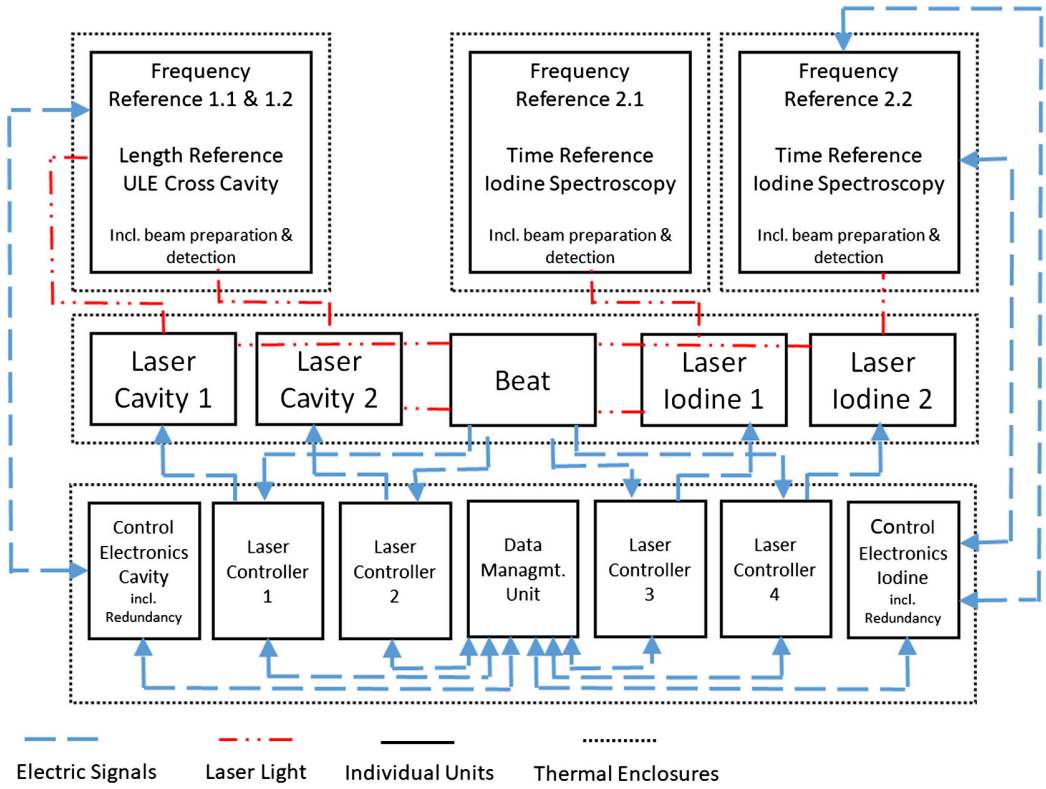

FIG. 2. Schematic overview of the payload. The beat unit as well as the data management unit are internally redundant.

TABLE III. The payload budgets including the 20% component-level margin and an additional 20% system-level margin on the total budget.

Item	# of units	Mass	Power
Optical resonator	1	57 kg	11 W
Iodine spectroscopy	2	14 kg	12 W
Laser and beat	1	15 kg	15 W
Electronics	1	44 kg	186 W
Harness	1	26 kg	0 W
Total including 20% margin		**204 kg**	**269 W**

during eclipse times, cold redundancy is chosen as a baseline for the payload.

B. Mass and power budgets

The resulting overall budgets for the payload are summarized in Table III. All of the values given in this table include a 20% component-level margin. An additional 20% system-level margin is added to the total budget of the payload. The mass and the power reflect the cold redundancy concept described above.

IV. PAYLOAD SUBSYSTEMS

A. Optical resonator unit

Optical resonators are employed to stabilize lasers using the Pound-Drever-Hall scheme [40]. Within BOOST, a cubic optical resonator based on the National Physical Laboratory (NPL) design [41] is chosen, cf. Fig. 1. The spacer of the optical resonator will be made out of ULE, and the mirrors will be made out of fused silica to reduce the thermal noise and the sensitivity to external thermal fluctuation. The spacer is mounted at four points with tetrahedral symmetry as in Ref. [41] to reduce the vibration sensitivity. We will choose the curvature radii of the mirrors to be 1 m and ∞, respectively. We deviate from the NPL design by choosing a longer path length of 8.7 cm in order to reduce the thermal noise floor. The mass and volume limitations of a space mission constrain the length, although a longer baseline would reduce the thermal noise floor further. Additionally, for the specific length and curvature radii of the mirrors, the higher transverse electromagnetic modes (TEM) modes are sufficiently separated from another to ensure that the modulation frequency of the Pound-Drever-Hall sidebands can be chosen such that they do not overlap with those modes. The cube is designed in such a way that two optical paths can be operated at any given time.

Current state-of-the-art optical resonators achieve a frequency stability in the order of several parts in 10^{-17} on timescales from one-tenth of a second up to several seconds [42]. However, optical cavities that have been designed specifically for space applications and high robustness demonstrate a frequency stability of 10^{-15} at 1 s [43,44]. For BOOST, we require, on the other hand, stabilities of 10^{-15} at 90 min, which requires additional developments. Subsequently, the major limitations and mitigation strategies to achieve this frequency stability are discussed.

External thermal fluctuations have a high impact on the long-term stability of the resonator if they are not attenuated since any length variation due to thermal expansion translates directly into a frequency variation. To counteract the occurring thermal fluctuations, two measures are taken. First, the spacer is made from ULE, which has generally a low coefficient of thermal expansion (CTE) and in particular a zero crossing of the CTE. The optical resonator is then operated near this zero-crossing temperature of the CTE. Second, a five-fold thermal shield is mounted around the resonator for a passive attenuation of external temperature fluctuations. Five aluminum shields with a thickness of 3 mm each are calculated to attenuate the temperature fluctuations by a factor of 10^5 at 90 min; see Ref. [19]. Additionally, the outer shields' temperature is actively stabilized to ± 1 mK at a temperature that is in the 10 mK range of the CTE zero crossing. The thermal shields are separated by Ti spacers, and the holes for the optical access are covered with BK7 glass to reduce the temperature fluctuations to a minimum. The materials are chosen based on their thermal conductivity and transparency to the chosen wavelength. A detailed description of the chosen materials including the impact of the properties and design can be found in Ref. [19]. A linear frequency drift due to isothermal relaxation of the ULE will be removed from the signal.

Each of the optical resonators' components contribute to the *thermal Brownian noise limit*. Taking the size and the materials of the mirror substrate and coatings as well as of the ULE spacer into account, the resulting thermal noise floor is estimated to 3.9×10^{-16}, cf. Refs. [45,46]. Indeed, this is the highest contribution to the total noise.

Additionally, frequency fluctuations are introduced via *intensity fluctuations* of the in-coupled light onto the mirror substrate. These fluctuations are typically in the order of 100–200 Hz/μW; see Ref. [47]. Assuming laser intensity fluctuations in the order of 0.5 nW, the frequency fluctuations in the optical resonator are no higher than 3.5×10^{-16} at orbit time.

The *residual amplitude modulation* (RAM) is another source for frequency fluctuations on the long timescale required by the experiment. The RAM is therefore stabilized actively. Considering a finesse of 4×10^5 for the optical resonator and a RAM stabilization of 2×10^{-5} at 90 min, the limit to the achievable frequency stability is 3×10^{-16}; see Ref. [48].

Furthermore, the refractive index and thereby the optical path length is influenced by *pressure density fluctuations* along the optical paths. To avoid these, the resonator is placed inside a vacuum chamber. The frequency fluctuation caused by pressure fluctuations of 10^{-9} mbar at a base pressure of 10^{-8} mbar is below 2.7×10^{-16}, cf. Ref. [49].

TABLE IV. Error budgets for the optical resonator.

Noise sources	$\frac{\delta\nu}{\nu} \cdot 10^{16}$	Reference
Thermal fluctuations	1	[19]
Thermal Brownian noise	3.9	[45]
Intensity fluctuations	3.5	[47]
Residual amplitude modulation	3	[48]
Pressure fluctuations	2.7	[49]
Gravity gradient	0.1	[50]
Demodulator phase instability	2	[51,52]
Vibrations	0.25	[41]
Total	**7.0**	

Other error sources for the optical resonator are *gravity-induced distortions* in the optical resonator, *residual accelerations* caused by vibrations, rotation of the satellite and orbital drag, *demodulator phase instabilities*, and *electronic noises*. All of these effects contribute in the range of 10^{-17} or below to the frequency noise of the optical resonator.

The error budgets for the optical resonator are combined in Table IV, assuming that the individual contributions are independent of one another. The aforementioned frequency noises limit the performance of the optical resonator below the required relative frequency stability of $\delta\nu/\nu$ of 10^{-15} at orbit time. In the worst case, if all noise sources except the Brownian noise would couple fully, say, via temperature fluctuations, they would sum up to 2×10^{-15}.

B. Iodine spectroscopy unit

In the iodine spectroscopy unit, a hyperfine transition of diatomic iodine at 532 nm is used to stabilize the laser via Doppler-free saturation spectroscopy [53]. For these frequency references, a performance at 10^{-15} stability level on long timescales has been established [11,21]. In further efforts, compact units for space-based applications have been developed [21,22]. The molecular iodine will be held in a compact multipass gas cell with an interaction length of approximately 90 cm. The spectroscopy setup is realized using a glass baseplate where the optical components are integrated by adhesive bonding. Subsequently, we discuss the major limitations to the stability at orbit time.

Among other factors, the achievable frequency stability of the iodine spectroscopy depends on the *line width* of the transition at 532 nm, which is in the order of 200–300 kHz; see Ref. [54]. Given the accessibility of this wavelength using lasers at 1064 nm, operating the iodine spectroscopy at 532 nm is the practical choice. The hyperfine transition at 508 nm has a natural line width of 50–100 kHz; see Ref. [54]. Thus, the performance of the spectroscopy could be enhanced by addressing this narrower line of the hyperfine spectrum. However, the currently available laser modules have a better performance at 532 nm, which is thus chosen as the baseline.

The performance of the iodine frequency reference is limited by the *gas pressure* inside the gas cell to -2.2 kHz/Pa; see Ref. [21]. Since the gas pressure is regulated via a cold finger, this translates to a fluctuation in its temperature of -300 Hz/K; see Ref. [21]. With the required stability of the cold finger of 1 mK, this results in a stability of 5×10^{-16} at orbit time.

Variations in the *laser power* induce a shift in the molecular resonance frequency. Typically, this results in a frequency fluctuation of 300 Hz/mW; see Refs. [51,52]. Assuming 10 mW of laser power, cf. Ref. [21], and fractional intensity fluctuations of 1×10^{-4}, the impact of the resulting frequency calculations can be estimated as 3.5×10^{-16} at orbit time.

The *modulation transfer spectroscopy* signal slope was measured in the laboratory setup at Humboldt University Berlin. The corresponding coefficient is in the range of 200 Hz/mV. Following the requirement that the electronic offset fluctuations shall not be higher than 1 μV, the resulting frequency fluctuation is 3.5×10^{-16}.

Residual amplitude modulation is another source of frequency fluctuations in iodine systems [55]. If the RAM contribution can be limited to 1×10^{-7} at orbit time, the resulting frequency fluctuations will be limited to 4.2×10^{-16} at orbit time; see Refs. [56,57]. This is a rather stringent requirement, but it may be close to realization considering recent performance levels of iodine frequency standards reaching below the 3×10^{-15} level, cf. Ref. [21].

The stability of the *angle between the pump and probe beam* introduces frequency fluctuations. With a decoupling of 25 mrad and a frequency shift of 2 kHz/mrad, a frequency fluctuation of 3.5×10^{-16} can be expected using adhesive bonding; see Ref. [58].

Other effects, such as *phase modulation index fluctuations*, demodulator phase instabilities, and *external magnetic field fluctuations* further contribute to the limitation of the performance of the iodine spectroscopy. The contributions for the most important error sources are displayed in Table V.

TABLE V. Error budgets for the iodine frequency reference.

Noise sources	$\frac{\delta\nu}{\nu} \cdot 10^{16}$	Reference
Pressure fluctuations	5	[21]
Light power fluctuations	3.5	[51,52]
Servoelectronic offsets	3.5	[a]
Residual amplitude modulation	4.2	[56,57]
Beam pointing instability	3.5	[58]
Phase modulation fluctuations	3	[59]
Demodulator phase instability	2	[51,52]
Magnetic field fluctuations	1	[60,61]
Total	9.7	

[a]As measured with the engineering model setup [21] at Humboldt University Berlin.

C. Laser and beat unit

The laser sources for BOOST are based on a micro-integrated diode laser technology platform developed at the Ferdinand-Braun Institute (FBH) in a joint laboratory activity with Humboldt University Berlin. This platform provides compact, robust, and energy-efficient semiconductor laser modules with the advantage of broad wavelength accessibility [62]. Other wavelengths (e.g., 508 nm) might be of interest for addressing hyperfine spectra near the B-state dissociation limit of molecular iodine. These diode laser modules operate in experiments at the Bremen drop tower to study ultracold atomic gases [63] and have been used in several sounding rocket missions to realize optical frequency Refs. [64,65] as well as the first Bose-Einstein condensate in space [23,66]. On the 13th of May 2018, a compact iodine frequency reference was launched aboard the TEXUS 54 sounding rocket as an important qualification step toward space application [21].

A part of the laser output, which is stabilized with the optical resonator or the iodine spectroscopy unit, is then routed to the beat unit. By observing the beat note, differences between the frequencies can be observed. Depending on the analysis, the observed deviation is then linked to the respective parameters in the above-discussed test theories. The quality of the beat measurement thus impacts the generated science signal.

The stability of the beat measurement is governed by the stability of the implemented radio frequency (RF) source. With the targeted relative frequency stability of 10^{-15} at orbit time and a free spectral range of the optical resonator of about 2 GHz, a stability of 1×10^{-11} at orbit time for the RF source is required. This includes already margin. This can be established by employing the Chip Scale Atomic Clock as a RF source. In consequence, an addition to the achievable frequency stability of 10^{-16} caused by the accuracy of the beat has to be taken into account.

Another reduction of the frequency stability is due to the individual housing of the payload subsystems. In this design, the lasers are housed in an enclosure separated from the optical resonator and the iodine frequency references, respectively. Thus, the fibers, connecting the laser system to the frequency references, are exposed to thermal fluctuations. The satellite bus shall be stabilized to ± 5 K. With a fiber length of 0.5 m, this introduces a frequency instability of 10^{-16} at orbit time [67,68].

V. SUMMARY

We discussed the satellite mission BOOST, which will test the Lorentz invariance in space. It is a candidate mission in the Large Mission framework of the DLR. We showed that this mission would improve our current best measurements of the parameters of the SME, in particular, in the electron sector, by 1 to 2 orders of magnitude. Moreover, we demonstrated the feasibility of such an experiment in terms of performance of the individual frequency references, their beat, and the availability of components. The details of the experiment as well as mission parameters like the satellite platform and the possible launch options will be discussed elsewhere.

ACKNOWLEDGMENTS

This work is supported by the German Space Agency (DLR) with funds provided by the Federal Ministry for Economic Affairs and Energy under Grants No. 50 OO 1604, No. 50 OO 1605, No. 50 QT 1401, No. 50 QT 1201, and No. 50 QT 1102.

APPENDIX: SCIENCE SIGNAL

The science signal (5) contains 33 fitting parameters S_{ij} and C_{ij}. We give two examples here for illustration purposes:

$$C_{10} = \frac{R_S \sin(\zeta)}{32\nu_0\pi}\left[\left(\Delta\frac{p_z^2}{2m_e}(6\omega_S - \Omega_\oplus\cos(\zeta)) + \Delta\frac{p_x^2}{2m_e}(14\omega_S + \Omega_\oplus\cos(\zeta))\right)(c_{30}^{\mathrm{SCF}} + c_{03}^{\mathrm{SCF}}) - 16\pi(2\omega_S + \Omega_\oplus\cos(\zeta))\kappa_{o+,\mathrm{SCF}}^{12}\right]$$
$$C_{32} = \frac{R_S\Omega_\oplus}{64\nu_0}(5\sin(\zeta) + 4\sin(2\zeta) + \sin(3\zeta))\kappa_{o-,\mathrm{SCF}}^{12}. \quad \text{(A1)}$$

The appearing constants have the following meaning, cf. Ref. [36]: ζ is the angle between the Earth's rotation axis, i.e., the X^3 axis in the SCF, cf. Sec. II A 2, and the normal of the satellite's orbit. For the considered orbit, this is 97°. $R_S \approx 3.5 \times 10^{13}$ eV^{-1} is the radius of the satellite's circular orbit. Here, as with the rest of the Appendix, natural units are employed as is common in the SME. The angle α is the azimuthal angle between the satellite plane and the orbital plane of the Earth measured from the X^1 axis of the SCF frame. For a Sun-synchronous orbit like we consider here, it behaves like $\alpha = \alpha_0 + \Omega_\oplus t$. This was already employed to derive Eq. (5). α_0 is a constant that is determined by the choice of the origin of the time coordinate and the launch date of the satellite and is chosen to vanish here for convenience. Not that we also assume here an optical resonator, in which one optical axis is parallel to the relative velocity of the satellite with respect to the Earth and the other is nadir pointing.

$\Delta\frac{p_x^2}{2m_e} \approx -1 \times 10^1$ eV and $\Delta\frac{p_z^2}{2m_e} \approx 3 \times 10^1$ eV are abbreviations for rough estimates[3] of the difference of the expectation values of the operators of the kinetic energy in the respective directions for the two states $X^1\Sigma_g^+$ and

[3]Note that the precision of the final results in Table II is limited by these estimates to one significant digit.

$B^3\Pi_{0+u}$ involved in the absorption. These estimates correspond to the molecule's rest frame, which is oriented such that the x^3 axis is along the molecules axis. $\nu_0 = 18.56$ eV is the frequency of the unperturbed laser.

The $\kappa^{ij}_{o-,\mathrm{SCF}}$ are linear combinations of $(k_F)^{\mathrm{SCF}}_{\mu_1\mu_2\mu_3\mu_4}$; see, e.g., Ref. [35]. They are already well constrained by astrophysical tests, cf. Ref. [39], so they appear in the fitting parameters S_{ij} and C_{ij} only below our noise limit, which is the reason why we omitted them in Table II for brevity, cf. Footnote 1. Under this assumption, C_{10} yields the second constraint in Table II. Interestingly, C_{32} is just affected by the SME modifications of the photon sector.

[1] C. J. Isham, *General Relativity and Gravitation*, edited by M. Francaviglia, G. Longhi, L. Lusanna, and E. Sorace (World Scientific, Singapore, 1997), p. 167.
[2] C. Rovelli, arXiv:gr-qc/9803024v3.
[3] C. Rovelli, Living Rev. Relativity **11**, 5 (2008).
[4] D. Colladay and V. A. Kostelecký, Phys. Rev. D **55**, 6760 (1997).
[5] D. Colladay and V. A. Kostelecký, Phys. Rev. D **58**, 116002 (1998).
[6] V. A. Kostelecký, Phys. Rev. D **69**, 105009 (2004).
[7] H. P. Robertson, Rev. Mod. Phys. **21**, 378 (1949).
[8] R. Mansouri and R. U. Sexl, Gen. Relativ. Gravit. **8**, 497 (1977).
[9] R. Mansouri and R. U. Sexl, Gen. Relativ. Gravit. **8**, 515 (1977).
[10] R. Mansouri and R. U. Sexl, Gen. Relativ. Gravit. **8**, 809 (1977).
[11] K. Döringshoff, T. Schuldt, E. V. Kovalchuk, J. Stühler, C. Braxmaier, and A. Peters, Appl. Phys. B **123**, 183 (2017).
[12] B. Sheard, G. Heinzel, K. Danzmann, D. A. Shaddock, W. M. Klipstein, and W. M. Folkner, J. Geodes. **86**, 1083 (2012).
[13] R. Thompson *et al.*, A flight-like optical reference cavity for grace follow-on laser frequency stabilization, in *Joint Conference of the IEEE International Frequency Control Symposium (IFCS 2011) and European Frequency and Time Forum (EFTF 2011)* (IEEE, New York, 2011).
[14] LISA: A proposal in response to the ESA call for L3 mission concepts, https://www.elisascience.org/files/publications/LISA_L3_20170120.pdf.
[15] Statement of work for the ESA ITT "Development of an acceleration insensitive, thermal noise mitigated, Optical Stabilising Reference Cavity (OSRC) Engineering Model. Appendix 1 to AO/1-8657/16/NL/BJ" in the GSP-6 program.
[16] K. Nicklaus *et al.*, in *Proceedings of the 10th International Conference on Space Optics—ICSO 2014, Tenerife*, edited by Z. Sodnik, B. Cugny, N. Karafolas (SPIE, Washington, 2017), Vol. 10563, DOI: 10.1117/12.2304161.
[17] B. Argence, E. Prevost, T. Lévèque, R. Le Goff, S. Bize, P. Lemonde, and G. Santarelli, Opt. Express **20**, 25409 (2012).
[18] B. Bachman *et al.*, J. Phys. Conf. Ser. **840**, 012011 (2017).
[19] J. Sanjuan, N. Gürlebeck, and C. Braxmaier, Opt. Express **23**, 17892 (2015).
[20] T. Schuldt, K. Döringshoff, A. Milke, J. Sanjuan, M. Gohlke, E. V. Kovalchuk, N. Gürlebeck, A. Peters, and C. Braxmaier, J. Phys. Conf. Ser. **723**, 012047 (2016).
[21] T. Schuldt, K. Döringshoff, E. V. Kovalchuk, A. Keetman, J. Pahl, A. Peters, and C. Braxmaier *et al.*, Appl. Opt. **56**, 1101 (2017).
[22] V. Schkolnik *et al.*, EPJ Quantum Techno. **4**, 9 (2017).
[23] V. Schkolnik *et al.*, Appl. Phys. B **122**, 217 (2016).
[24] J. A. Lipa *et al.*, arXiv:gr-qc/1203.3914.
[25] A. Milke *et al.*, in *2013 Joint European Frequency and Time Forum & International Frequency Control Symposium (EFTF/IFC)* (IEEE, New York, 2013), p. 912.
[26] N. Gürlebeck *et al.*, in *2015 Gravitation: 100 Years after GR*, edited by E. Augé, J. Dumarchez, and J. T. T. Vân (ARISF, Paris, 2015), p. 367.
[27] T. Schuldt *et al.*, in *2015 Joint Conference of the IEEE International Frequency Control Symposium the European Frequency and Time Forum* (Curran Associates, Inc., New York, 2015), p. 47.
[28] A. Michelson and E. Morley, Am. J. Sci. **s3-34**, 333 (1887).
[29] R. J. Kennedy and E. M. Thorndike, Phys. Rev. **42**, 400 (1932).
[30] H. E. Ives and G. R. Stilwell, J. Opt. Soc. Am. **28**, 215 (1938).
[31] M. E. Tobar, P. Wolf, S. Bize, G. Santarelli, and V. Flambaum, Phys. Rev. D **81**, 022003 (2010).
[32] S. Herrmann, A. Senger, K. Möhle, M. Nagel, E. V. Kovalchuk, and A. Peters, Phys. Rev. D **80**, 105011 (2009).
[33] P. Delva *et al.*, Phys. Rev. Lett. **118**, 221102 (2017).
[34] M. Nagel, S. R. Parker, E. V. Kovalchuk, P. L. Stanwix, J. G. Hartnett, E. N. Ivanov, A. Peters, and M. E. Tobar, Nat. Commun. **6**, 8174 (2015).
[35] V. A. Kostelecký and M. Mewes, Phys. Rev. D **66**, 056005 (2002).
[36] R. Bluhm, V. A. Kostelecký, C. D. Lane, and N. Russell, Phys. Rev. D **68**, 125008 (2003).
[37] H. Müller, C. Braxmaier, S. Herrmann, A. Peters, and C. Lämmerzahl, Phys. Rev. D **67**, 056006 (2003).
[38] V. A. Kostelecký and C. D. Lane, Phys. Rev. D **60**, 116010 (1999).
[39] V. A. Kostelecký and N. Russell, Rev. Mod. Phys. **83**, 11 (2011); see arXiv:0801.0287v10 for the most recent version.
[40] R. W. P. Drever, J. L. Hall, F. V. Kowalski, J. Hough, G. M. Ford, A. J. Munley, and H. Ward, Appl. Phys. B **31**, 97 (1983).
[41] S. Webster and P. Gill, Opt. Lett. **36**, 3572 (2011).
[42] D. G. Matei *et al.*, Phys. Rev. Lett. **118**, 263202 (2017).
[43] D. Świerad *et al.*, Sci. Rep. **6**, 33973 (2016).
[44] M. Abgrall *et al.*, C.R. Phys. **16**, 461 (2015).
[45] T. Kessler, T. Legero, and U. Sterr, J. Opt. Soc. Am. B **29**, 178 (2012).

[46] T. Kessler, C. Hagemann, C. Grebing, T. Legero, U. Sterr, F. Riehle, M. J. Martin, L. Chen, and J. Ye, Nat. Photonics **6**, 687 (2012).
[47] S. Häfner, S. Falke, C. Grebing, S. Vogt, T. Legero, M. Merimaa, C. Lisdat, and U. Sterr, Opt. Lett. **40**, 2112 (2015).
[48] W. Zhang *et al.*, Opt. Lett. **39**, 1980 (2014).
[49] K. P. Birch and M. J. Downs, Metrologia **31**, 315 (1994).
[50] C. Lämmerzahl, I. Ciufolini, H. Dittus, L. Iorio, H. Müller, A. Peters, E. Samain, S. Scheithauer, and S. Schiller, Gen. Relativ. Gravit. **36**, 2373 (2004).
[51] A. Y. Nevsky *et al.*, Opt. Commun. **192**, 263 (2001).
[52] F.-L. Hong, J. Ishikawa, Y. Zhang, R. Guo, A. Onae, and H. Matsumoto, Opt. Commun. **235**, 377 (2004).
[53] J. H. Shirley, Opt. Lett. **7**, 537 (1982).
[54] W.-Y. Cheng, L. Chen, T. H. Yoon, J. L. Hall, and J. Ye, Opt. Lett. **27**, 571 (2002).
[55] F. du Burck, G. Tetchewo, A. N. Goncharov, and O. Lopez, Metrologia **46**, 599 (2009).
[56] E. Jaatinen and J.-M. Chartier, Metrologia **35**, 75 (1998).
[57] E. Jaatinen, D. J. Hopper, and J. Back, Meas. Sci. Technol. **20**, 025302 (2009).
[58] S. Ressel, M. Gohlke, D. Rauen, T. Schuldt, W. Kronast, U. Mescheder, U. Johann, D. Weise, and C. Braxmaier, Appl. Opt. **49**, 4296 (2010).
[59] P. Cordiale, G. Galzerano, and H. Schnatz, Metrologia **37**, 177 (2000).
[60] A. N. Goncharov, A. Y. Nevsky, and M. N. Skvortsov, Appl. Phys. B **60**, 43 (1995).
[61] A. N. Goncharov, A. Y. Nevsky, and M. N. Skvortsov, Appl. Phys. B **62**, 427 (1996).
[62] A. Wicht *et al.*, Narrow linewidth diode laser modules for quantum optical sensor applications in the field and in space, in *Society of Photo-Optical Instrumentation Engineers (SPIE) Conference Series*, edited by A. L. Glebov and P. O. Leisher (SPIE, Washington, 2017), Vol. 10085, p. 100850F.
[63] M. Schiemangk *et al.*, Appl. Opt. **54**, 5332 (2015).
[64] M. Lezius *et al.*, Optica **3**, 1381 (2016).
[65] A. N. Dinkelaker *et al.*, Appl. Opt. **56**, 1388 (2017).
[66] http://www.dlr.de/dlr/en/desktopdefault.aspx/tabid-10081/151_read-20337/#/gallery/25194.
[67] T. Musha, J. Kamimura, and M. Nakazawa, Appl. Opt. **21**, 694 (1982).
[68] T. Toyoda and M. Yabe, J. Phys. D **16**, L251 (1983).

G Bibliography

[1] D. J. Griffiths, *Introduction to elementary particles*, 2nd Ed., Physics textbook (Wiley-VCH, New York, NY, 2008).

[2] M. D. Schwartz, *Quantum Field Theory and the Standard Model* (Cambridge University Press, 2014).

[3] H. Poincaré, "L'état actuel et l'avenir de la physique mathématique", Bull. des Sci. Math. **28**, 302 (1904).

[4] A. Einstein, "Zur Elektrodynamik bewegter Körper", Ann. d. Phys. **17**, 891 (1905).

[5] R. Berger and J. Stohner, "Parity violation", Wiley Interdiscip. Rev.-Comput. Mol. Sci. **9**, e1396 (2019).

[6] P. Higgs, "Broken symmetries, massless particles and gauge fields", Phys. Lett. **12**, 132 (1964).

[7] P. W. Higgs, "Broken symmetries and the masses of gauge bosons", Phys. Rev. Lett. **13**, 508 (1964).

[8] F. Englert and R. Brout, "Broken symmetry and the mass of gauge vector mesons", Phys. Rev. Lett. **13**, 321 (1964).

[9] G. S. Guralnik, C. R. Hagen, and T. W. B. Kibble, "Global conservation laws and massless particles", Phys. Rev. Lett. **13**, 585 (1964).

[10] CERN, *CERN experiments observe particle consistent with long-sought Higgs boson*, [accessed on January 20 2020 2:46 pm], (2012) `https://home.cern/news/press-release/cern/cern-experiments-observe-particle-consistent-long-sought-higgs-boson`.

[11] CERN, *New results indicate that particle discovered at CERN is a Higgs boson*, [accessed on January 20 2020 2:46 pm], (2013) `https://home.cern/news/press-release/cern/new-results-indicate-particle-discovered-cern-higgs-boson`.

[12] S. L. Glashow, "Partial-symmetries of weak interactions", Nucl. Phys. **22**, 579 (1961).

[13] S. Weinberg, "A model of leptons", Phys. Rev. Lett. **19**, 1264 (1967).

[14] A. Salam, "Weak and electromagnetic interactions", in Proceedings of the Eighth Nobel Symposium, Vol. 680519, edited by N. Svartholm (1968), pp. 367–377.

[15] A. López de Recalde, *The Standard Electro-Weak Theory (from the very basics)* (2014).

[16] O. Klein, "Quantentheorie und fünfdimensionale Relativitätstheorie", Z. Phys. **37**, 895 (1926).

[17] W. Gordon, "Der Comptoneffekt nach der Schrödingerischen Theorie", Z. Phys. **40**, 117 (1926).

[18] P. A. M. Dirac, "The quantum theory of the electron", Proc. Roy. Soc. Lond. A **117**, 610 (1928).

[19] P. A. M. Dirac, "The quantum theory of the electron Part II", Proc. Roy. Soc. Lond. A **118**, 351 (1928).

[20] G. Breit, "The effect of retardation on the interaction of two electrons", Phys. Rev. **34**, 553 (1929).

[21] M. C. Gonzalez-Garcia and Y. Nir, "Neutrino masses and mixing: evidence and implications", Rev. Mod. Phys. **75**, 345 (2003).

[22] T. Aoyama, M. Hayakawa, T. Kinoshita, and M. Nio, "Tenth-Order QED Contribution to the Electron $g-2$ and an Improved Value of the Fine Structure Constant", Phys. Rev. Lett. **109**, 111807 (2012).

[23] D. Hanneke, S. Fogwell Hoogerheide, and G. Gabrielse, "Cavity control of a single-electron quantum cyclotron: measuring the electron magnetic moment", Phys. Rev. A **83**, 052122 (2011).

[24] D. N. Spergel, "The dark side of cosmology: dark matter and dark energy", Science **347**, 1100 (2015).

[25] A. Einstein, "Die Feldgleichungen der Gravitation", Sitzungsber. Kgl. Preuss. Akad. Wiss. **48**, 844 (1915).

[26] A. Einstein, "Kosmologische Betrachtung zur allgemeinen Relativititätstheorie", Sitzungsber. Kgl. Preuss. Akad. Wiss. **6**, 142 (1917).

[27] J. A. Frieman, M. S. Turner, and D. Huterer, "Dark energy and the accelerating universe", Annu. Rev. Astron. Astrophys. **46**, 385 (2008).

[28] Planck Collaboration, P. A. R. Ade, N. Aghanim, M. Arnaud, M. Ashdown, J. Aumont, C. Baccigalupi, A. J. Banday, R. B. Barreiro, J. G. Bartlett, N. Bartolo, E. Battaner, R. Battye, K. Benabed, A. Benoît, A. Benoit-Lévy, J.-P. Bernard, M. Bersanelli, P. Bielewicz, J. J. Bock, A. Bonaldi, L. Bonavera, J. R. Bond, J. Borrill, F. R. Bouchet, F. Boulanger, M. Bucher, C. Burigana, R. C. Butler, E. Calabrese, J.-F. Cardoso, A. Catalano, A. Challinor, A. Chamballu, R.-R. Chary, H. C. Chiang, J. Chluba, P. R. Christensen, S. Church, D. L. Clements, S. Colombi, L. P. L. Colombo, C. Combet, A. Coulais, B. P. Crill, A. Curto, F. Cuttaia, L. Danese, R. D. Davies, R. J. Davis, P. de Bernardis, A. de Rosa, G. de Zotti, J. Delabrouille, F.-X. Désert, E. Di Valentino, C. Dickinson, J. M. Diego, K. Dolag, H. Dole, S. Donzelli, O. Doré, M. Douspis, A. Ducout, J. Dunkley, X. Dupac, G. Efstathiou, F. Elsner, T. A. Enßlin, H. K. Eriksen, M. Farhang, J. Fergusson, F. Finelli, O. Forni, M. Frailis, A. A. Fraisse, E. Franceschi, A. Frejsel, S. Galeotta, S. Galli, K. Ganga, C. Gauthier, M. Gerbino, T. Ghosh, M. Giard, Y. Giraud-Héraud, E. Giusarma, E. Gjerløw, J. González-Nuevo, K. M. Górski, S. Gratton, A. Gregorio, A. Gruppuso, J. E. Gudmundsson, J. Hamann, F. K. Hansen, D. Hanson, D. L. Harrison, G. Helou, S. Henrot-Versillé, C. Hernández-Monteagudo, D. Herranz, S. R. Hildebrandt, E. Hivon, M. Hobson, W. A. Holmes, A. Hornstrup, W. Hovest, Z. Huang, K. M. Huffenberger, G. Hurier, A. H. Jaffe, T. R. Jaffe, W. C. Jones, M. Juvela, E. Keihänen, R. Keskitalo, T. S. Kisner, R. Kneissl, J. Knoche, L. Knox, M. Kunz, H. Kurki-Suonio, G. Lagache, A. Lähteenmäki, J.-M. Lamarre, A. Lasenby, M. Lattanzi, C. R. Lawrence, J. P. Leahy, R. Leonardi, J. Lesgourgues, F. Levrier, A. Lewis, M. Liguori, P. B. Lilje, M. Linden-Vørnle, M. López-Caniego, P. M. Lubin, J. F. Macías-Pérez, G. Maggio, D. Maino, N. Mandolesi, A. Mangilli, A. Marchini, M. Maris, P. G. Martin, M. Martinelli, E. Martínez-González, S. Masi, S. Matarrese, P. McGehee, P. R. Meinhold, A. Melchiorri, J.-B. Melin, L. Mendes, A. Mennella, M. Migliaccio, M. Millea, S. Mitra, M.-A. Miville-Deschênes, A. Moneti, L. Montier, G. Morgante, D. Mortlock, A. Moss, D. Munshi, J. A. Murphy, P. Naselsky, F. Nati, P. Natoli, C. B. Netterfield, H. U. Nørgaard-Nielsen, F. Noviello, D. Novikov, I. Novikov, C. A. Oxborrow, F. Paci, L. Pagano, F. Pajot, R. Paladini, D. Paoletti, B. Partridge, F. Pasian, G. Patanchon, T. J. Pearson, O. Perdereau, L. Perotto, F. Perrotta, V.

Pettorino, F. Piacentini, M. Piat, E. Pierpaoli, D. Pietrobon, S. Plaszczynski, E. Pointecouteau, G. Polenta, L. Popa, G. W. Pratt, G. Prézeau, S. Prunet, J.-L. Puget, J. P. Rachen, W. T. Reach, R. Rebolo, M. Reinecke, M. Remazeilles, C. Renault, A. Renzi, I. Ristorcelli, G. Rocha, C. Rosset, M. Rossetti, G. Roudier, B. Rouillé dÓrfeuil, M. Rowan-Robinson, J. A. Rubiño-Martín, B. Rusholme, N. Said, V. Salvatelli, L. Salvati, M. Sandri, D. Santos, M. Savelainen, G. Savini, D. Scott, M. D. Seiffert, P. Serra, E. P. S. Shellard, L. D. Spencer, M. Spinelli, V. Stolyarov, R. Stompor, R. Sudiwala, R. Sunyaev, D. Sutton, A.-S. Suur-Uski, J.-F. Sygnet, J. A. Tauber, L. Terenzi, L. Toffolatti, M. Tomasi, M. Tristram, T. Trombetti, M. Tucci, J. Tuovinen, M. Türler, G. Umana, L. Valenziano, J. Valiviita, F. Van Tent, P. Vielva, F. Villa, L. A. Wade, B. D. Wandelt, I. K. Wehus, M. White, S. D. M. White, A. Wilkinson, D. Yvon, A. Zacchei, and A. Zonca, "Planck 2015 results - xiii. cosmological parameters", Astron. Astrophys. **594**, A13 (2016).

[29] P. Kroupa, B. Famaey, K. S. de Boer, J. Dabringhausen, M. S. Pawlowski, C. M. Boily, H. Jerjen, D. Forbes, G. Hensler, and M. Metz, "Local-group tests of dark-matter concordance cosmology - towards a new paradigm for structure formation", Astron. Astrophys. **523**, A32 (2010).

[30] D. J. Gross, "The role of symmetry in fundamental physics", Proc. Natl. Acad. Sci. USA **93**, 14256 (1996).

[31] E. Noether, "Invariante Variationsprobleme", Nachr. Ges. Wiss. Göttingen, Math. Phys. Kl., 235 (1918).

[32] E. Noether, "Invarianten beliebiger Differentialausdrücke", Nachr. Ges. Wiss. Göttingen, Math. Phys. Kl., 37 (1918).

[33] J. C. Ward, "An identity in quantum electrodynamics", Phys. Rev. **78**, 182 (1950).

[34] Y. Takahashi, "On the generalized ward identity", Il Nuovo Cimento **6**, 371 (1957).

[35] T. D. Lee, *Particle physics and introduction to field theory* (Harwood Academic Publishers, Chur, Switzerland, 1981).

[36] J. Schwinger, "The Theory of Quantized Fields. I", Phys. Rev. **82**, 914 (1951).

[37] G. Lüders, "On the equivalence of invariance under time reversal and under particle-antiparticle conjugation for relativistic field theories", Dan. Mat. Fys. Medd. **28**, 1 (1954).

[38] W. Pauli, V. Weisskopf, and L. Rosenfeld, eds., *Niels Bohr and the Development of Physics* (McGraw-Hill, 1955).

[39] J. Díaz-Cruz and A. Rosado, "Symmetry Priniciples And Conservation Laws", in *Fundam. Phys. – Vol. I*, edited by J. Díaz-Cruz and A. Rosado (Eolss Publishers Co, Ltd., Oxford, United Kingdom, 2009), p. 230.

[40] H. A. Lorentz, "Simplified Theory of Electrical and Optical Phenomena in Moving Systems", Proc. Acad. Sci. Ams. **1**, 427 (1898).

[41] H. A. Lorentz, "Electromagnetic phenomena in a system moving with any velocity smaller than that of light", Proc. Acad. Sci. Ams. **6**, 809 (1904).

[42] A. N. Katti, *The Mathematical Theory of Special and General Relativity* (CreateSpace Independent Publishing Platform, 2013).

[43] H. Poincaré, "La théorie de Lorentz et le principe de réaction", Arch. néerland. d. sci. exac. et natur. **5**, 252 (1900).

[44] H. Poincaré, "Sur les principes de la mécanique", Bib. Congrès int. phil., 457 (1900).

[45] H. Poincaré, "Sur la dynamique de l'électron", Com. Ren. **140**, 1504 (1905).

[46] A. Einstein, "Ist die Trägheit eines Körpers von seinem Energieinhalt abhängig?", Ann. d. Phys. **323**, 639 (1905).

[47] P. R. Bunker and P. Jensen, *Molecular symmetry and spectroscopy*, 2nd ed. (NRC Research Press, Ottawa, Ontaria, Canada, 2006).

[48] M. K. Gaillard, P. D. Grannis, and F. J. Sciulli, "The standard model of particle physics", Rev. Mod. Phys. **71**, S96 (1999).

[49] J. Erler, "Electroweak tests of the standard model", AIP Conf. Proc. **1560**, 95 (2013).

[50] G. Altarelli and M. W. Grünewald, "Precision electroweak tests of the Standard Model", Phys. Rep. **403-404**, 189 (2004).

[51] R. N. Cahn, "The eighteen arbitrary parameters of the standard model in your everyday life", Rev. Mod. Phys. **68**, 951 (1996).

[52] L. M. Krauss, "The standard model, dark matter, and dark energy: from the sublime to the ridiculous", in 14th Canar. Islands Winter Sch. Astrophys. Dark Matter Dark Energy Universe (2004).

[53] G. Ross, *Grand Unified Theories* (Westview Press, 2003).

[54] P. Langacker, "Grand unified theories and proton decay", Phys. Rep. **72**, 185 (1981).

[55] G. L. Kane, *Supersymmetry: Unveiling the Ultimate Laws of Nature* (Perseus, Cambridge, 2000).

[56] S. P. Martin, "A Supersymmetry Primer", in *Perspect. Supersymmetry II*, Vol. Volume 21, Advanced Series on Directions in High Energy Physics (World Scientific, 2010), pp. 1–153.

[57] M. Dine, *Supersymmetry and string theory: beyond the standard model*, 2nd ed. (Cambridge University Press, 2015).

[58] C. Rovelli, "Loop quantum gravity", Living Rev. Relativ. **1**, 1 (1998).

[59] C. Rovelli, "Loop Quantum Gravity", Living Rev. Relativ. **11**, 5 (2008).

[60] V. A. Kostelecký and S. Samuel, "Spontaneous breaking of Lorentz symmetry in string theory", Phys. Rev. D **39**, 683 (1989).

[61] V. A. Kostelecký and R. Potting, "Expectation values, lorentz invariance, and cpt in the open bosonic string", Phys. Lett. B **381**, 89 (1996).

[62] E. C. G. Stückelberg, "Die Wechselwirkungskräfte in der Elektrodynamik und in der Feldtheorie der Kernkräfte. Teil II und III.", Helv. Phys. Acta **5**, 369 (1932).

[63] C. D. Anderson, "The positive electron", Phys. Rev. **43**, 491 (1933).

[64] L. Canetti, M. Drewes, and M. Shaposhnikov, "Matter and antimatter in the universe", New J. Phys. **14**, 095012 (2012).

[65] J. Alcaraz, D. Alvisi, B. Alpat, G. Ambrosi, H. Anderhub, L. Ao, A. Arefiev, P. Azzarello, E. Babucci, L. Baldini, M. Basile, D. Barancourt, F. Barao, G. Barbier, G. Barreira, R. Battiston, R. Becker, U. Becker, L. Bellagamba, P. Béné, J. Berdugo, P. Berges, B. Bertucci, A. Biland, S. Bizzaglia, S. Blasko, G. Boella, M. Bourquin, G. Bruni, M. Buenerd, J. Burger, W. Burger, X. Cai, R. Cavalletti, C. Camps, P. Cannarsa, M. Capell, D. Casadei, J. Casaus, G. Castellini, Y. Chang, H. Chen, Z. Chen, N. Chernoplekov, A. Chiarini, T. Chiueh, Y. Chuang, F. Cindolo, V. Commichau, A. Contin, A. Cotta-Ramusino, P. Crespo, M. Cristinziani, J. daCunha, T. Dai, J. Deus, L. Ding, N. Dinu, L. Djambazov, I. D'Antone, Z. Dong, P. Emonet, F. Eppling, T. Eronen, G. Esposito, P. Extermann, J. Favier, C. Feng,

E. Fiandrini, F. Finelli, P. Fisher, R. Flaminio, G. Fluegge, N. Fouque, Y. Galaktionov, M. Gervasi, P. Giusti, W. Gu, T. Guzik, K. Hangarter, A. Hasan, V. Hermel, H. Hofer, M. Huang, W. Hungerford, M. Ionica, R. Ionica, J. Isbert, M. Jongmanns, W. Karpinski, G. Kenney, J. Kenny, W. Kim, A. Klimentov, J. Krieger, R. Kossakowski, V. Koutsenko, G. Laborie, T. Laitinen, G. Lamanna, G. Laurenti, A. Lebedev, S. Lee, G. Levi, P. Levtchenko, T. Li, C. Liu, H. Liu, M. Lolli, I. Lopes, G. Lu, Y. Lu, K. Lübelsmeyer, D. Luckey, W. Lustermann, G. Maehlum, C. Maña, A. Margotti, F. Massera, F. Mayet, R. McNeil, B. Meillon, M. Menichelli, F. Mezzanotte, R. Mezzenga, A. Mihul, G. Molinari, A. Mourao, A. Mujunen, F. Palmonari, G. Pancaldi, A. Papi, I. Park, M. Pauluzzi, F. Pauss, E. Perrin, A. Pesci, A. Pevsner, R. Pilastrini, M. Pimenta, V. Plyaskin, V. Pojidaev, H. Postema, E. Prati, N. Produit, P. Rancoita, D. Rapin, F. Raupach, S. Recupero, D. Ren, Z. Ren, M. Ribordy, J. Richeux, E. Riihonen, J. Ritakari, U. Roeser, C. Roissin, R. Sagdeev, D. Santos, G. Sartorelli, A. S. von Dratzig, G. Schwering, V. Shoutko, E. Shoumilov, R. Siedling, D. Son, T. Song, M. Steuer, G. Sun, H. Suter, X. Tang, S. C. Ting, S. Ting, F. Tenbusch, G. Torromeo, J. Torsti, J. Trümper, J. Ulbricht, S. Urpo, I. Usoskin, E. Valtonen, J. Vandenhirtz, E. Velikhov, B. Verlaat, I. Vetlitsky, F. Vezzu, J. Vialle, G. Viertel, D. Vité, H. VonGunten, S. WaldmeierWicki, W. Wallraff, B. Wang, J. Wang, Y. Wang, J. Wefel, E. Werner, C. Williams, S. Wu, P. Xia, J. Yan, L. Yan, C. Yang, M. Yang, P. Yeh, H. Zhang, D. Zhao, G. Zhu, W. Zhu, H. Zhuang, and A. Zichichi, "Search for antihelium in cosmic rays", Phys. Lett. B **461**, 387 (1999).

[66] G. Steigman, "When clusters collide: constraints on antimatter on the largest scales", J. Cosmol. Astropart. Phys. **2008**, 001 (2008).

[67] A. G. Cohen, A. D. Rújula, and S. L. Glashow, "A matter-antimatter universe?", Astrophys. J. **495**, 539 (1998).

[68] A. D. Sakharov, "Violation of CP invariance, C asymmetry, and baryon asymmetry of the universe", JETP Lett. **5**, 24 (1967).

[69] A. D. Sakharov, "Violation of CP invariance, C asymmetry, and baryon asymmetry of the universe", Sov. Phys. Usp. **34**, 392 (1991).

[70] C. Callan, R. Dashen, and D. Gross, "The structure of the gauge theory vacuum", Phys. Lett. B **63**, 334 (1976).

[71] F. W. Bessel, "On the variations of the proper motions of Procyon and Sirius", Mon. Not. R. Astron. Soc. **6**, 136 (1844).

[72] W. Thomson (Lord Kelvin), *Baltimore lectures on molecular dynamics and the wave theory of light* (CJ Clay & Sons, London, 1904).

[73] H. Poincaré, "The Milky Way and the Theory of Gases", Popular Astronomy **14**, 475 (1906).

[74] J. H. Oort, "The force exerted by the stellar system in the direction perpendicular to the galactic plane and some related problems", Bull. Astron. Inst. Neth. **6**, 249 (1932).

[75] F. Zwicky, "Die Rotverschiebung von extragalaktischen Nebeln", Helv. Phys. Acta **6**, 110 (1933).

[76] G. Bertone and D. Hooper, "History of dark matter", Rev. Mod. Phys. **90**, 045002 (2018).

[77] G. Bertone, D. Hooper, and J. Silk, "Particle dark matter: evidence, candidates and constraints", Physics Reports **405**, 279 (2005).

[78] R. H. Cyburt, B. D. Fields, K. A. Olive, and T.-H. Yeh, "Big bang nucleosynthesis: present status", Rev. Mod. Phys. **88**, 015004 (2016).

[79] C. Pitrou, A. Coc, J.-P. Uzan, and E. Vangioni, "Precision big bang nucleosynthesis with improved helium-4 predictions", Phys. Rep. **754**, 1 (2018).

[80] H. Niikura, M. Takada, N. Yasuda, R. H. Lupton, T. Sumi, S. More, T. Kurita, S. Sugiyama, A. More, M. Oguri, and M. Chiba, "Microlensing constraints on primordial black holes with Subaru/HSC Andromeda observations", Nat. Astr. **3**, 524 (2019).

[81] T. Lin, "Tasi lectures on dark matter models and direct detection", ArXiv e-prints **1904.07915**, hep (2019).

[82] L. Roszkowski, E. M. Sessolo, and S. Trojanowski, "WIMP dark matter candidates and searches—current status and future prospects", Rep. Prog. Phys. **81**, 066201 (2018).

[83] R. D. Peccei and H. R. Quinn, "CP Conservation in the Presence of Pseudoparticles", Phys. Rev. Lett. **38**, 1440 (1977).

[84] F. Wilczek, "Problem of Strong P and T Invariance in the Presence of Instantons", Phys. Rev. Lett. **40**, 279 (1978).

[85] S. Weinberg, "A new light boson?", Phys. Rev. Lett. **40**, 223 (1978).

[86] G. 't Hooft, "Symmetry Breaking through Bell-Jackiw Anomalies", Phys. Rev. Lett. **37**, 8 (1976).

[87] C. Abel, S. Afach, N. J. Ayres, C. A. Baker, G. Ban, G. Bison, K. Bodek, V. Bondar, M. Burghoff, E. Chanel, Z. Chowdhuri, P.-J. Chiu, B. Clement, C. B. Crawford, M. Daum, S. Emmenegger, L. Ferraris-Bouchez, M. Fertl, P. Flaux, B. Franke, A. Fratangelo, P. Geltenbort, K. Green, W. C. Griffith, M. van der Grinten, Z. D. Grujić, P. G. Harris, L. Hayen, W. Heil, R. Henneck, V. Hélaine, N. Hild, Z. Hodge, M. Horras, P. Iaydjiev, S. N. Ivanov, M. Kasprzak, Y. Kermaidic, K. Kirch, A. Knecht, P. Knowles, H.-C. Koch, P. A. Koss, S. Komposch, A. Kozela, A. Kraft, J. Krempel, M. Kuźniak, B. Lauss, T. Lefort, Y. Lemière, A. Leredde, P. Mohanmurthy, A. Mtchedlishvili, M. Musgrave, O. Naviliat-Cuncic, D. Pais, F. M. Piegsa, E. Pierre, G. Pignol, C. Plonka-Spehr, P. N. Prashanth, G. Quéméner, M. Rawlik, D. Rebreyend, I. Rienäcker, D. Ries, S. Roccia, G. Rogel, D. Rozpedzik, A. Schnabel, P. Schmidt-Wellenburg, N. Severijns, D. Shiers, R. Tavakoli Dinani, J. A. Thorne, R. Virot, J. Voigt, A. Weis, E. Wursten, G. Wyszynski, J. Zejma, J. Zenner, and G. Zsigmond, "Measurement of the permanent electric dipole moment of the neutron", Phys. Rev. Lett. **124**, 081803 (2020).

[88] P. W. Graham and S. Rajendran, "Axion dark matter detection with cold molecules", Phys. Rev. D **84**, 055013 (2011).

[89] P. W. Graham and S. Rajendran, "New observables for direct detection of axion dark matter", Phys. Rev. D **88**, 035023 (2013).

[90] B. M. Roberts, Y. V. Stadnik, V. A. Dzuba, V. V. Flambaum, N. Leefer, and D. Budker, "Parity-violating interactions of cosmic fields with atoms, molecules, and nuclei: concepts and calculations for laboratory searches and extracting limits", Phys. Rev. D **90**, 096005 (2014).

[91] J. E. Kim, "Weak-Interaction Singlet and Strong CP Invariance", Phys. Rev. Lett. **43**, 103 (1979).

[92] M. Shifman, A. Vainshtein, and V. Zakharov, "Can confinement ensure natural cp invariance of strong interactions?", Nucl. Phys. B **166**, 493 (1980).

[93] M. Dine, W. Fischler, and M. Srednicki, "A simple solution to the strong cp problem with a harmless axion", Phys. Lett. B **104**, 199 (1981).

[94] A. R. Zhitnitsky, "On possible suppression of the axion-hadron interactions", Sov. J. Nucl. Phys. **31**, 497 (1980).

[95] G. G. Raffelt, "Astrophysical axion bounds", in *Axions: theory, cosmology, and experimental searches*, edited by M. Kuster, G. Raffelt, and B. Beltrán (Springer Berlin Heidelberg, Berlin, Heidelberg, 2008), pp. 51–71.

[96] H. An, M. Pospelov, J. Pradler, and A. Ritz, "Direct detection constraints on dark photon dark matter", Phys. Lett. B **747**, 331 (2015).

[97] M. Pospelov, A. Ritz, and M. Voloshin, "Bosonic super-wimps as kev-scale dark matter", Phys. Rev. D **78**, 115012 (2008).

[98] P. W. Graham, D. E. Kaplan, J. Mardon, S. Rajendran, and W. A. Terrano, "Dark matter direct detection with accelerometers", Phys. Rev. D **93**, 075029 (2016).

[99] G. Gentile, P. Salucci, U. Klein, D. Vergani, and P. Kalberla, "The cored distribution of dark matter in spiral galaxies", Mon. Not. R. Astron. Soc. **351**, 903 (2004).

[100] A. Klypin, A. V. Kravtsov, O. Valenzuela, and F. Prada, "Where are the missing galactic satellites?", Astrophys. J. **522**, 82 (1999).

[101] M. S. Pawlowski, B. Famaey, H. Jerjen, D. Merritt, P. Kroupa, J. Dabringhausen, F. Lüghausen, D. A. Forbes, G. Hensler, F. Hammer, M. Puech, S. Fouquet, H. Flores, and Y. Yang, "Co-orbiting satellite galaxy structures are still in conflict with the distribution of primordial dwarf galaxies", Mon. Not. R. Astron. Soc. **442**, 2362 (2014).

[102] J. Kormendy, N. Drory, R. Bender, and M. E. Cornell, "Bulgeless giant galaxies challenge our picture of galaxy formation by hierarchical clustering", Astrophys. J. **723**, 54 (2010).

[103] S. Sachdeva and K. Saha, "Survival of pure disk galaxies over the last 8 billion years", Astrophys. J. **820**, L4 (2016).

[104] W. Hu, R. Barkana, and A. Gruzinov, "Fuzzy cold dark matter: the wave properties of ultralight particles", Phys. Rev. Lett. **85**, 1158 (2000).

[105] J.-W. Lee, "Brief history of ultra-light scalar dark matter models", EPJ Web Conf. **168**, 06005 (2018).

[106] M. Milgrom, "A modification of the Newtonian dynamics as a possible alternative to the hidden mass hypothesis.", Astrophys. J. **270**, 365 (1983).

[107] M. Milgrom, "A modification of the Newtonian dynamics - Implications for galaxies.", Astrophys. J. **270**, 371 (1983).

[108] J. D. Bekenstein, "Relativistic gravitation theory for the modified newtonian dynamics paradigm", Phys. Rev. D **70**, 083509 (2004).

[109] L. Pasteur, C. R. Hebd. Seances Acad. Sci. **26**, 535 (1848).

[110] T. D. Lee and C. N. Yang, "Question of parity conservation in weak interactions", Phys. Rev. **104**, 254 (1956).

[111] C. S. Wu, E. Ambler, R. W. Hayward, D. D. Hoppes, and R. P. Hudson, "Experimental test of parity conservation in beta decay", Phys. Rev. **105**, 1413 (1957).

[112] L. D. Barron, "True and false chirality and parity violation", Chem. Phys. Lett. **123**, 423 (1986).

[113] L. D. Barron, "Symmetry and molecular chirality", Chem. Soc. Rev. **15**, 189 (1986).

[114] L. Barron, "Cp violation and molecular physics", Chem. Phys. Lett. **221**, 311 (1994).

[115] J. H. Christenson, J. W. Cronin, V. L. Fitch, and R. Turlay, "Evidence for the 2π decay of the K_2^0 meson", Phys. Rev. Lett. **13**, 138 (1964).

[116] M. Kobayashi and T. Maskawa, "CP-violation in renormalizable theory of weak interaction", Prog. Theor. Phys. **49**, 652 (1973).

[117] H. P. Robertson, "Postulate versus observation in the special theory of relativity", Rev. Mod. Phys. **21**, 378 (1949).

[118] R. Mansouri and R. U. Sexl, "A test theory of special relativity: I. Simultaneity and clock synchronization", Gen. Relativ. Gravit. **8**, 497 (1977).

[119] D. Colladay and V. A. Kostelecký, "CPT violation and the standard model", Phys. Rev. D **55**, 6760 (1997).

[120] D. Colladay and V. A. Kostelecký, "Lorentz-violating extension of the standard model", Phys. Rev. D **58**, 116002 (1998).

[121] V. A. Kostelecký and N. Russell, "Data tables for lorentz and CPT violation", Rev. Mod. Phys. **83**, 11 (2011).

[122] A. A. Michelson, "The relative motion of the Earth and of the luminiferous ether", Am. J. Sci. **22**, 120 (1881).

[123] A. A. Michelson and E. W. Morley, "On the relative motion of the Earth and the luminiferous ether", Am. J. Sci. **34**, 333 (1887).

[124] G. F. FitzGerald, "The ether and the earth's atmosphere", Science **ns-13**, 390 (1889).

[125] H. A. Lorentz, "De relatieve beweging van de aarde en den aether", Zittingsverlag Akad. v. Wet. **1**, 74 (1892).

[126] R. J. Kennedy and E. M. Thorndike, "Experimental establishment of the relativity of time", Phys. Rev. **42**, 400 (1932).

[127] B. P. Abbott et al., "Observation of gravitational waves from a binary black hole merger", Phys. Rev. Lett. **116**, 061102 (2016).

[128] B. Y. Zel'dovich, "Parity nonconservation in the first order in the weak-interaction constant in electron scattering and other effects", Sov. Phys. JETP **9**, 682 (1959).

[129] Y. Yamagata, "A hypothesis for the asymmetric appearance of biomolecules on earth", J. Theor. Biol. **11**, 495 (1966).

[130] R. Berger, "Parity-violation effects in molecules", in Relativistic electronic structure theory, part: 2, applications, edited by P. Schwerdtfeger (2004) Chap. 4, pp. 188–288.

[131] M. S. Safronova, D. Budker, D. DeMille, D. F. J. Kimball, A. Derevianko, and C. W. Clark, "Search for new physics with atoms and molecules", Rev. Mod. Phys. **90**, 025008 (2018).

[132] I. B. Zel'dovich, "Electromagnetic interaction with parity violation", Sov. Phys. JETP **6**, 1184 (1958).

[133] C. Bouchiat and M. A. Bouchiat, "Parity violation induced by weak neutral currents in atomic physics. Part II", J. Phys. (Paris) **36**, 493 (1975).

[134] L. M. Barkov and M. S. Zolotarev, "Observation of parity nonconservation in atomic transitions", JETP Lett. **27**, 357 (1978).

[135] M. J. D. Macpherson, K. P. Zetie, R. B. Warrington, D. N. Stacey, and J. P. Hoare, "Precise measurement of parity nonconserving optical rotation at 876 nm in atomic bismuth", Phys. Rev. Lett. **67**, 2784 (1991).

[136] D. M. Meekhof, P. A. Vetter, P. K. Majumder, S. K. Lamoreaux, and E. N. Fortson, "Optical-rotation technique used for a high-precision measurement of parity nonconservation in atomic lead", Phys. Rev. A **52**, 1895 (1995).

[137] P. A. Vetter, D. M. Meekhof, P. K. Majumder, S. K. Lamoreaux, and E. N. Fortson, "Precise test of electroweak theory from a new measurement of parity nonconservation in atomic thallium", Phys. Rev. Lett. **74**, 2658 (1995).

[138] C. S. Wood, S. C. Bennett, D. Cho, B. P. Masterson, J. L. Roberts, C. E. Tanner, and C. E. Wieman, "Measurement of parity nonconservation and an anapole moment in cesium", Science **275**, 1759 (1997).

[139] K. Tsigutkin, D. Dounas-Frazer, A. Family, J. E. Stalnaker, V. V. Yashchuk, and D. Budker, "Observation of a large atomic parity violation effect in ytterbium", Phys. Rev. Lett. **103**, 071601 (2009).

[140] A. T. Nguyen, D. Budker, D. DeMille, and M. Zolotorev, "Search for parity nonconservation in atomic dysprosium", Phys. Rev. A **56**, 3453 (1997).

[141] N. Leefer, L. Bougas, D. Antypas, and D. Budker, "Towards a new measurement of parity violation in dysprosium", (2014).

[142] L. N. Labzowsky, "Λ-doubling and parity-nonconservation effects in spectra of diatomic molecules", Sov. Phys. JETP **48**, 434 (1978).

[143] O. P. Sushkov and V. V. Flambaum, "Parity breaking effects in diatomic molecules", Sov. Phys. JETP **48**, 608 (1978).

[144] M. G. Kozlov and L. N. Labzowsky, "Parity violation effects in diatomics", J. Phys. B **28**, 1933 (1995).

[145] I. B. Khriplovich, "Fundamental symmetries and atomic physics", Phys. Scr. **T112**, 52 (2004).

[146] A. V. Titov, N. S. Mosyagin, A. N. Petrov, T. A. Isaev, and D. P. DeMille, "Study of P,T-parity violation effects in polar heavy-atom molecules", Prog. Theor. Chem. Phys. **B 15**, 253 (2006).

[147] B. M. Roberts, V. A. Dzuba, and V. V. Flambaum, "Parity and time-reversal violation in atomic systems", Annu. Rev. Nucl. Part. Sci. **65**, 63 (2015).

[148] D. DeMille, S. B. Cahn, D. Murphree, D. A. Rahmlow, and M. G. Kozlov, "Using molecules to measure nuclear spin-dependent parity violation", Phys. Rev. Lett. **100**, 023003 (2008).

[149] T. A. Isaev, S. Hoekstra, and R. Berger, "Laser-cooled RaF as a promising candidate to measure molecular parity violation", Phys. Rev. A **82**, 052521 (2010).

[150] T. A. Isaev and R. Berger, "Electron correlation and nuclear charge dependence of parity-violating properties in open-shell diatomic molecules", Phys. Rev. A **86**, 062515 (2012).

[151] E. Altuntaş, J. Ammon, S. B. Cahn, and D. DeMille, "Demonstration of a sensitive method to measure nuclear-spin-dependent parity violation", Phys. Rev. Lett. **120**, 142501 (2018).

[152] D. W. Rein, "Some remarks on parity violating effects of intramolecular interactions", J. Mol. Evol. **4**, 15 (1974).

[153] G. Marx, "Weak interactions outside the laboratory", Acta Phys. Austr. Suppl. **XIII**, 569 (1974).

[154] É. Gajzágó and G. Marx, "Energy difference of mirror molecules", Atomki Közl. Suppl. **16**, 177 (1974).

[155] V. S. Letokhov, "On difference of energy levels of left and right molecules due to weak interactions", Phys. Lett. A **53**, 275 (1975).

[156] B. Y. Zel'dovich, D. B. Saakyan, and I. I. Sobel'man, "Energy difference between right-hand and left-hand molecules, due to parity nonconservation in weak interactions of electrons with nuclei", JETP Lett. **25**, 94 (1977).

[157] R. A. Harris and L. Stodolski, "Quantum beats in optical activity and weak interactions", Phys. Lett. B **78**, 313 (1978).

[158] T. Udem, R. Holzwarth, and T. W. Hänsch, "Optical frequency metrology", Nature **416**, 233 (2002).

[159] M. A. Bouchiat and C. Bouchiat, "An atomic linear Stark shift violating P but not T arising from the electroweak nuclear anapole moment", Eur. Phys. J. D **15**, 5 (2001).

[160] M.-A. Bouchiat, "Linear stark shift in dressed atoms as a signal to measure a nuclear anapole moment with a cold-atom fountain or interferometer", Phys. Rev. Lett. **98**, 043003 (2007).

[161] O. N. Kompanets, A. R. Kukudzhanov, V. S. Letokhov, and L. L. Gervits, "Narrow resonances of saturated absorption of the asymmetrical molecule CHFClBr and the possibility of weak current detection in molecular physics", Opt. Commun. **19**, 414 (1976).

[162] E. Arimondo, P. Glorieux, and T. Oka, "Observation of inverted infrared lamb dips in separated optical isomers", Opt. Commun. **23**, 369 (1977).

[163] A. Bauder, A. Beil, D. Luckhaus, F. Müller, and M. Quack, "Combined high resolution infrared and microwave study of bromochlorofluoromethane", J. Chem. Phys. **106**, 7558 (1997).

[164] C. Daussy, T. Marrel, A. Amy-Klein, C. T. Nguyen, C. J. Bordé, and C. Chardonnet, "Limit on the parity nonconserving energy difference between the enantiomers of a chiral molecule by laser spectroscopy", Phys. Rev. Lett. **83**, 1554 (1999).

[165] M. Quack and J. Stohner, "Influence of parity violating weak nuclear potentials on vibrational and rotational frequencies in chiral molecules", Phys. Rev. Lett. **84**, 3807 (2000).

[166] M. Quack and J. Stohner, "How do parity violating weak nuclear interactions influence rovibrational frequencies in chiral molecules?", Z. Phys. Chem. **214**, 675 (2000).

[167] J. K. Laerdahl and P. Schwerdtfeger and H. M. Quiney, "Theoretical analysis of parity-violating energy differences between the enantiomers of chiral molecules", Phys. Rev. Lett **84**, 3811 (2000).

[168] R. G. Viglione, R. Zanasi, P. Lazzeretti, and A. Ligabue, "Theoretical determination of parity-violating vibrational frequency differences between the enantiomers of the CHFClBr molecule", Phys. Rev. A **62**, 052516 (2000).

[169] T. Marrel, M. Ziskind, C. Daussy, and C. Chardonnet, "High precision rovibrational and hyperfine analysis of the $\nu_4 = 1$ level of bromochlorofluoromethane", J. Mol. Struct. **599**, 195 (2001).

[170] M. Quack and J. Stohner, "Molecular chirality and the fundamental symmetries of physics: Influence of parity violation on rovibrational frequencies and thermodynamic properties", Chirality **13**, 745 (2001).

[171] M. Ziskind, C. Daussy, T. Marrel, and C. Chardonnet, "Improved sensitivity in the search for a parity-violating energy difference in the vibrational spectrum of the enantiomers of CHFClBr", Eur. Phys. J. D **20**, 219 (2002).

[172] P. Schwerdtfeger, J. K. Laerdahl, and C. Chardonnet, "Calculation of parity-violating effects for the C-F stretching mode of chiral methyl fluorides", Phys. Rev. A **65**, 042508 (2002).

[173] P. Schwerdtfeger, T. Saue, J. N. P. van Stralen, and L. Visscher, "Relativistic second-order many-body and density-functional theory for the parity-violation contribution to the C-F stretching mode in CHFClBr", Phys. Rev. A **71**, 012103 (2005).

[174] R. Berger and J. L. Stuber, "Electroweak interactions in chiral molecules: two-component density functional theory study of vibrational frequency shifts in polyhalomethanes", Mol. Phys. **105**, 41 (2007).

[175] C. Thierfelder, G. Rauhut, and P. Schwerdtfeger, "Relativistic coupled-cluster study of the parity-violation energy shift of chfclbr", Phys. Rev. A **81**, 032513 (2010).

[176] A. Cournol, M. Manceau, M. Pierens, L. Lecordier, D. B. A. Tran, R. Santagata, B. Argence, A. Goncharov, O. Lopez, M. Abgrall, Y. L. Coq, R. L. Targat, H. A. Martinez, W. K. Lee, D. Xu, P. E. Pottie, R. J. Hendricks, T. E. Wall, J. M. Bieniewska, B. E. Sauer, M. R. Tarbutt, A. Amy-Klein, S. K. Tokunaga, and B. Darquié, "A new experiment to test parity symmetry in cold chiral molecules using vibrational spectroscopy", Quantum Electron. **49**, 288 (2019).

[177] M. Quack, "On the measurement of the parity violating energy difference between enantiomers", Chem. Phys. Lett. **132**, 147 (1986).

[178] M. Quack, "On the measurement of CP-violating energy differences in matter-antimatter enantiomers", Chem. Phys. Lett. **231**, 421 (1994).

[179] R. Berger, "Molecular parity violation in electronically excited states", Phys. Chem. Chem. Phys. **5**, 12 (2003).

[180] A. L. Barra, J. B. Robert, and L. Wiesenfeld, "Parity non-conservation and NMR observables. Calculation of Tl resonance frequency differences in enantiomers", Phys. Lett. A **115**, 443 (1986).

[181] A. L. Barra, J. B. Robert, and L. Wiesenfeld, "Possible observation of parity nonconservation by high-resolution NMR", Europhys. Lett. **5**, 217 (1988).

[182] A. L. Barra and J. B. Robert, "Parity non-conservation and NMR parameters", Mol. Phys. **88**, 875 (1996).

[183] J. B. Robert and A. L. Barra, "NMR and parity nonconservation. Experimental requirements to observe a difference between enantiomer signals", Chirality **13**, 699 (2001).

[184] G. Laubender and R. Berger, "*Ab initio* calculation of parity violating chemical shifts in nuclear magnetic resonance spectra of chiral molecules", ChemPhysChem **4**, 395 (2003).

[185] A. Soncini, F. Faglioni, and P. Lazzeretti, "Parity-violating contributions to nuclear magnetic shielding", Phys. Rev. A **68**, 033402 (2003).

[186] V. Weijo, P. Manninen, and J. Vaara, "Perturbational calculations of parity-violating effects in nuclear-magnetic-resonance parameters", J. Chem. Phys. **123**, 054501 (2005).

[187] G. Laubender and R. Berger, "Electroweak quantum chemistry for nuclear-magnetic-resonance-shielding constants: impact of electron correlation", Phys. Rev. A **74**, 032105 (2006).

[188] R. Bast, P. Schwerdtfeger, and T. Saue, "Parity nonconservation contribution to the nuclear magnetic resonance shielding constants of chiral molecules: a four-component relativistic study", J. Chem. Phys. **125**, 064504 (2006).

[189] V. Weijo, R. Bast, P. Manninen, T. Saue, and J. Vaara, "Methodological aspects in the calculation of parity-violating effects in nuclear magnetic resonance parameters", J. Chem. Phys. **126**, 074107 (2007).

[190] V. Weijo, M. B. Hansen, O. Christiansen, and P. Manninen, "Vibrational effects in the parity-violating contributions to the isotropic nuclear magnetic resonance chemical shift", Chem. Phys. Lett. **470**, 166 (2009).

[191] S. Nahrwold and R. Berger, "Zeroth order regular approximation approach to parity violating nuclear magnetic resonance shielding tensors", J. Chem. Phys. **130**, 214101 (2009).

[192] S. Nahrwold, R. Berger, and P. Schwerdtfeger, "Parity violation in nuclear magnetic resonance frequencies of chiral tetrahedral tungsten complexes NWXYZ (X, Y, Z = H, F, Cl, Br or I)", J. Chem. Phys. **140**, 024305, 024305 (2014).

[193] J. Eills, J. W. Blanchard, L. Bougas, M. G. Kozlov, A. Pines, and D. Budker, "Measuring molecular parity nonconservation using nuclear-magnetic-resonance spectroscopy", Phys. Rev. A **96**, 042119 (2017).

[194] P. Schwerdtfeger, "The search for parity violation in chiral molecules", in *Computational spectroscopy: methods, experiments and applications*, edited by J. Grunenberg (Wiley, Netherlands, 2010) Chap. 7, pp. 201–221.

[195] B. Darquie, C. Stoeffler, A. Shelkovnikov, C. Daussy, A. Amy-Klein, C. Chardonnet, S. Zrig, L. Guy, J. Crassous, P. Soulard, P. Asselin, T. R. Huet, P. Schwerdtfeger, R. Bast, and T. Saue, "Progress Toward the First Observation of Parity Violation in Chiral Molecules by High-Resolution Laser Spectroscopy", Chirality **22**, 870 (2010).

[196] M. Quack and M. Willeke, "Theory of Stereomutation Dynamics and Parity Violation in Hydrogen Thioperoxide Isotopomers ^{1,2,3}HSO^{1,2,3}H", Helv. Chim. Acta **86**, 1641 (2003).

[197] A. Beil, D. Luckhaus, and M. Quack, "Fermi resonance structure and femtosecond quantum dynamics of a chiral molecule from the analysis of vibrational overtone spectra of chbrclf", Ber. Bunsenges. Phys. Chem. **100**, 1853 (1996).

[198] A. Beil, D. Luckhaus, M. Quack, and J. Stohner, "Intramolecular vibrational redistribution and unimolecular reaction: Concepts and new results on the femtosecond dynamics and statistics in chbrclf", Ber. Bunsenges. Phys. Chem. **101**, 311 (1997).

[199] E. Salpeter, "Some atomic effects of an electronic electric dipole moment", Phys. Rev. **112**, 1642 (1958).

[200] F. E. Obenshain and L. A. Page, "Detection of a σ Energy Shift in Positronium Formed from Polarized Positrons", Phys. Rev. **112**, 179 (1958).

[201] W. Bernreuther and M. Suzuki, "The electric dipole moment of the electron", Rev. Mod. Phys. **63**, 313 (1991).

[202] Y. Nir, "CP Violation In and Beyond the Standard Model", in Particle physics: proceedings of the 1999 summer school, Vol. 16, edited by G. Senjanović and A. Y. Smirnov (2000), p. 165.

[203] T. Fukuyama, "Searching for new physics beyond the standard model in electric dipole moment", Int. J. Mod. Phys. A **27**, 1230015 (2012).

[204] W. Fischler, S. Paban, and S. Thomas, "Bounds on microscopic physics from P and T violation in atoms and molecules", Phys. Lett. B **289**, 373 (1992).

[205] M. Pospelov and A. Ritz, "Electric dipole moments as probes of new physics", Ann. Phys. (N. Y.) **318**, 119 (2005).

[206] T. E. Chupp, P. Fierlinger, M. J. Ramsey-Musolf, and J. T. Singh, "Electric dipole moments of atoms, molecules, nuclei, and particles", Rev. Mod. Phys. **91**, 015001 (2019).

[207] W. B. Cairncross and J. Ye, "Atoms and molecules in the search for time-reversal symmetry violation", Nat. Rev. Phys. **1**, 510 (2019).

[208] I. B. Khriplovich and S. K. Lamoreaux, CP *violation without strangeness* (Springer, Berlin, 1997).

[209] J. S. M. Ginges and V. V. Flambaum, "Violations of fundamental symmetries in atoms and tests of unification theories of elementary particles", Phys. Rep. **397**, 63 (2004).

[210] L. I. Schiff, "Measurability of nuclear electric dipole moments", Phys. Rev. **132**, 2194 (1963).

[211] N. F. Ramsey, "A molecular beam resonance method with separated oscillating fields", Phys. Rev. **78**, 695 (1950).

[212] E. S. Ensberg, "Experimental upper limit for the permanent electric dipole moment of Rb^{85} by optical-pumping techniques", Phys. Rev. **153**, 36 (1967).

[213] P. G. H. Sandars and E. Lipworth, "Electric dipole moment of the cesium atom. a new upper limit to the electric dipole moment of the free electron", Phys. Rev. Lett. **13**, 718 (1964).

[214] M. A. Player and P. G. H. Sandars, "An experiment to search for an electric dipole moment in the $^3P_2$ metastable state of xenon", J. Phys. B **3**, 1620 (1970).

[215] M. C. Weisskopf, J. P. Carrico, H Gould, E Lipworth, and T. S. Stein, "Electric Dipole Moment of the Cesium Atom. A New Upper Limit to the Electric Dipole Moment of the Electron", Phys. Rev. Lett. **21**, 1645 (1968).

[216] H. Gould, "Search for an electric dipole moment in thallium", Phys. Rev. Lett. **24**, 1091 (1970).

[217] E. K. B.V. Vasil'ev, "Measurement of the electric dipole moment of the electron with a quantum interferometer", Sov. Phys. JETP **47**, 243 (1978).

[218] S. A. Murthy, D. Krause, Z. L. Li, and L. R. Hunter, "New limits on the electron electric dipole moment from cesium", Phys. Rev. Lett. **63**, 965 (1989).

[219] K. Abdullah, C. Carlberg, E. D. Commins, H. Gould, and S. B. Ross, "New experimental limit on the electron electric dipole moment", Phys. Rev. Lett. **65**, 2347 (1990).

[220] E. D. Commins, S. B. Ross, D. DeMille, and B. C. Regan, "Improved experimental limit on the electric dipole moment of the electron", Phys. Rev. A **50**, 2960 (1994).

[221] B. C. Regan, E. D. Commins, C. J. Schmidt, and D. DeMille, "New Limit on the Electron Electric Dipole Moment", Phys. Rev. Lett. **88**, 71805 (2002).

[222] T. G. Vold, F. J. Raab, B. Heckel, and E. N. Fortson, "Search for a Permanent Electric Dipole Moment on the ^{129}Xe Atom", Phys. Rev. Lett. **52**, 2229 (1984).

[223] S. K. Lamoreaux, J. P. Jacobs, B. R. Heckel, F. J. Raab, and N. Fortson, "New constraints on time-reversal asymmetry from a search for a permanent electric dipole moment of ^{199}Hg", Phys. Rev. Lett. **59**, 2275 (1987).

[224] M. A. Rosenberry and T. E. Chupp, "Atomic Electric Dipole Moment Measurement Using Spin Exchange Pumped Masers of ^{129}Xe and ^{3}He", Phys. Rev. Lett. **86**, 22 (2001).

[225] R. H. Parker, M. R. Dietrich, M. R. Kalita, N. D. Lemke, K. G. Bailey, M. Bishof, J. P. Greene, R. J. Holt, W. Korsch, Z.-T. Lu, P. Mueller, T. P. O'Connor, and J. T. Singh, "First measurement of the atomic electric dipole moment of ^{225}Ra", Phys. Rev. Lett. **114**, 233002 (2015).

[226] B. Graner, Y. Chen, E. G. Lindahl, and B. R. Heckel, "Reduced limit on the permanent electric dipole moment of ^{199}Hg", Phys. Rev. Lett. **116**, 161601 (2016).

[227] T. A. Isaev and R. Berger, "Towards ultracold chiral molecules", Chimia **72**, 375 (2018).

[228] M. R. Tarbutt, "Laser cooling of molecules", Contemp. Phys. **59**, 356 (2018).

[229] D. Cho, K. Sangster, and E. A. Hinds, "Search for time-reversal-symmetry violation in thallium fluoride using a jet source", Phys. Rev. A **44**, 2783 (1991).

[230] J. J. Hudson, B. E. Sauer, M. R. Tarbutt, and E. A. Hinds, "Measurement of the Electron Electric Dipole Moment Using YbF Molecules", Phys. Rev. Lett. **89**, 23003 (2002).

[231] J. J. Hudson, D. M. Kara, I. J. Smallman, B. E. Sauer, M. R. Tarbutt, and E. A. Hinds, "Improved measurement of the shape of the electron", Nature **473**, 493 (2011).

[232] S. Eckel, P. Hamilton, E. Kirilov, H. W. Smith, and D. DeMille, "Search for the electron electric dipole moment using Ω-doublet levels in PbO", Phys. Rev. A **87**, 052130 (2013).

[233] J. Baron, W. C. Campbell, D. DeMille, J. M. Doyle, G. Gabrielse, Y. V. Gurevich, P. W. Hess, N. R. Hutzler, E. Kirilov, I. Kozyryev, B. R. O'Leary, C. D. Panda, M. F. Parsons, E. S. Petrik, B. Spaun, A. C. Vutha, and A. D. West, "Order of magnitude smaller limit on the electric dipole moment of the electron.", Science **343**, 269 (2014).

[234] W. B. Cairncross, D. N. Gresh, M. Grau, K. C. Cossel, T. S. Roussy, Y. Ni, Y. Zhou, J. Ye, and E. A. Cornell, "Precision measurement of the electron's electric dipole moment using trapped molecular ions", Phys. Rev. Lett. **119**, 153001 (2017).

[235] V. Andreev, D. G. Ang, D. DeMille, J. M. Doyle, G. Gabrielse, J. Haefner, N. R. Hutzler, Z. Lasner, C. Meisenhelder, B. R. O'Leary, C. D. Panda, A. D. West, E. P. West, X. Wu, and Collaboration, ACME, "Improved limit on the electric dipole moment of the electron", Nature **562**, 355 (2018).

[236] J. Lee, J. Chen, L. V. Skripnikov, A. N. Petrov, A. V. Titov, N. S. Mosyagin, and A. E. Leanhardt, "Optical spectroscopy of tungsten carbide for uncertainty analysis in electron electric-dipole-moment search", Phys. Rev. A **87**, 022516 (2013).

[237] A. C. Vutha, M. Horbatsch, and E. A. Hessels, "Orientation-dependent hyperfine structure of polar molecules in a rare-gas matrix: a scheme for measuring the electron electric dipole moment", Phys. Rev. A **98**, 032513 (2018).

[238] P. Aggarwal, H. L. Bethlem, A. Borschevsky, M. Denis, K. Esajas, P. A. B. Haase, Y. Hao, S. Hoekstra, K. Jungmann, T. B. Meijknecht, M. C. Mooij, R. G. E. Timmermans, W. Ubachs, L. Willmann, A. Zapara, and T. N.-e. collaboration, "Measuring the electric dipole moment of the electron in BaF", Eur. Phys. J. D **72**, 197 (2018).

[239] T. A. Isaev and R. Berger, "Lasercooled radium monofluoride: a molecular all-in-one probe for new physics", ArXiv e-prints **1302.5682**, physics.chem (2013).

[240] R. F. Garcia Ruiz, R. Berger, J. Billowes, C. L. Binnersley, M. L. Bissell, A. A. Breier, A. J. Brinson, K. Chrysalidis, T. E. Cocolios, B. S. Cooper, K. T. Flanagan, T. F. Giesen, R. P. de Groote, S. Franchoo, F. P. Gustafsson, T. A. Isaev, Á. Koszorús, G. Neyens, H. A. Perrett, C. M. Ricketts, S. Rothe, L. Schweikhard, A. R. Vernon, K. D. A. Wendt, F. Wienholtz, S. G. Wilkins, and X. F. Yang, "Spectroscopy of short-lived radioactive molecules", Nature **581**, 396 (2020).

[241] T. A. Isaev and R. Berger, "Polyatomic candidates for cooling of molecules with lasers from simple theoretical concepts", Phys. Rev. Lett. **116**, 063006 (2016).

[242] I. Kozyryev, L. Baum, K. Matsuda, and J. M. Doyle, "Proposal for laser cooling of complex polyatomic molecules", ChemPhysChem **17**, 3641 (2016).

[243] I. Kozyryev, L. Baum, K. Matsuda, B. L. Augenbraun, L. Anderegg, A. P. Sedlack, and J. M. Doyle, "Sisyphus laser cooling of a polyatomic molecule", Phys. Rev. Lett. **118**, 173201 (2017).

[244] M. Jung, "A robust limit for the electric dipole moment of the electron", J. High Energy Phys. **2013**, 168 (2013).

[245] P. Sandars, "The electric dipole moment of an atom", Phys. Lett. **14**, 194 (1965).

[246] P. G. H. Sandars, "Enhancement factor for the electric dipole moment of the valence electron in an alkali atom", Phys. Lett. **22**, 290 (1966).

[247] P. G. H. Sandars, "The electric-dipole moments of an atom II. The contribution from an electric-dipole moment on the electron with particular reference to the hydrogen atom", J. Phys. B **1**, 511 (1968).

[248] P. G. H. Sandars, "The electric-dipole moments of an atom I. Some general considerations", J. Phys. B **1**, 499 (1968).

[249] V. K. Ignatovich, "Amplification of the Electron Electric Dipole Moment in Atoms", Sov. Phys. JETP **29**, 1084 (1969).

[250] V. V Flambaum, "On Enhancement of the electron Electric Dipole Moment in Heavy Atoms", Yad. Fiz. **24**, 383 (1976).

[251] P. G. H. Sandars, "Measurability of the proton electric dipole moment", Phys. Rev. Lett. **19**, 1396 (1967).

[252] E. A. Hinds and P. G. H. Sandars, "Electric dipole hyperfine structure of TlF", Phys. Rev. A **21**, 471 (1980).

[253] V. G. Gorshkov, L. N. Labzowsky, and A. N. Moskalev, "Effects of nonconservation of spatial and temporal parities in spectra of diatomic molecules", Sov. Phys. JETP **49**, 209 (1979).

[254] O. P. Sushkov, V. V. Flambaum, and I. B. Khriplovich, "Possibility of investigating P- and T-odd nuclear forces in atomic and molecular experiments", Sov. Phys. JETP **60**, 873 (1984).

[255] V. V. Flambaum and I. B. Khriplovich, "On the enhancement of parity nonconserving effects in diatomic molecules", Phys. Lett. A **110**, 121 (1985).

[256] M. G. Kozlov, "Semiempirical calculations of P- and P,T-odd effects in diatomic molecules-radicals", Sov. Phys. JETP **62**, 1114 (1985).

[257] M. G. Kozlov, V. I. Fomichev, Y. Y. Dmitriev, L. N. Labzowsky, and A. V. Titov, "Calculations of the P- and T-odd spin-rotational Hamiltonian of the PbF molecule", J. Phys. B **20**, 4939 (1987).

[258] M. G. Kozlov, "Calculations of the degree of parity nonconservation in the spin-rotational spectrum of the PbF molecule", Sov. J. Quantum Electron. **18**, 713 (1988).

[259] Y. Y. Dmitriev, Y. G. Khait, M. G. Kozlov, L. N. Labzowsky, A. O. Mitrushenkov, A. V. Shtoff, and A. V. Titov, "Calculation of the spin-rotational Hamiltonian including P- and P,T-odd weak interaction terms for HgF and PbF molecules", Phys. Lett. A **167**, 280 (1992).

[260] M. G. Kozlov and V. F. Ezhov, "Enhancement of the electric dipole moment of the electron in the YbF molecule", Phys. Rev. A **49**, 4502 (1994).

[261] M. G. Kozlov and V. V. Yashchuk, "Estimate of P- and P,T-odd effects in diatomic van der waals molecules", JETP Lett. **64**, 709 (1996).

[262] M. G. Kozlov, A. V. Titov, N. S. Mosyagin, and P. V. Souchko, "Enhancement of the electric dipole moment of the electron in the BaF molecule", Phys. Rev. A **56**, R3326 (1997).

[263] N. S. Mosyagin, M. G. Kozlov, and A. V. Titov, "Electric dipole moment of the electron in the YbF molecule", J. Phys. B **31**, L763 (1998).

[264] M. G. Kozlov and A. Derevianko, "Proposal for a sensitive search for the electric dipole moment of the electron with matrix-isolated radicals", Phys. Rev. Lett. **97**, 063001 (2006).

[265] T. Fleig and M. K. Nayak, "Electron electric-dipole-moment interaction constant for HfF^+ from relativistic correlated all-electron theory", Phys. Rev. A **88**, 032514 (2013).

[266] T. Fleig and M. K. Nayak, "Electron electric dipole moment and hyperfine interaction constants for ThO", J. Mol. Spectrosc. **300**, 16 (2014).

[267] L. V. Skripnikov and A. V. Titov, "Theoretical study of ThF+ in the search for T,P-violation effects: Effective state of a Th atom in ThF+ and ThO compounds", Phys. Rev. A **91**, 042504 (2015).

[268] V. S. Prasannaa, A. C. Vutha, M. Abe, and B. P. Das, "Mercury Monohalides: Suitability for Electron Electric Dipole Moment Searches", Phys. Rev. Lett. **114**, 183001 (2015).

[269] M. Denis, M. S. Norby, H. J. A. Jensen, A. S. P. Gomes, M. K. Nayak, S. Knecht, and T. Fleig, "Theoretical study on ThF+, a prospective system in search of time-reversal violation", New J. Phys. **17**, 043005 (2015).

[270] T. Fleig, M. K. Nayak, and M. G. Kozlov, "TaN, a molecular system for probing P,T-violating hadron physics", Phys. Rev. A **93**, 012505 (2016).

[271] S. Sasmal, H. Pathak, M. K. Nayak, N. Vaval, and S. Pal, "Search for parity and time reversal violating effects in HgH: Relativistic coupled-cluster study", J. Chem. Phys. **144**, 124307 (2016).

[272] S. Sasmal, H. Pathak, M. K. Nayak, N. Vaval, and S. Pal, "Relativistic coupled-cluster study of RaF as a candidate for the parity- and time-reversal-violating interaction", Phys. Rev. A **93**, 062506 (2016).

[273] A. Sunaga, M. Abe, M. Hada, and B. P. Das, "Relativistic coupled-cluster calculation of the electron-nucleus scalar-pseudoscalar interaction constant W_s in YbF", Phys. Rev. A **93**, 042507 (2016).

[274] T. Fleig, "$\mathcal{P},\mathcal{T}$-odd and magnetic hyperfine-interaction constants and excited-state lifetime for HfF^+", Phys. Rev. A **96**, 040502 (2017).

[275] K. Gaul and R. Berger, "Zeroth order regular approximation approach to electric dipole moment interactions of the electron", J. Chem. Phys. **147**, 014109 (2017).

[276] A. Sunaga, M. Abe, M. Hada, and B. P. Das, "Analysis of large effective electric fields of weakly polar molecules for electron electric-dipole-moment searches", Phys. Rev. A **95**, 012502 (2017).

[277] T. A. Isaev, A. V. Zaitsevskii, and E. Eliav, "Laser-coolable polyatomic molecules with heavy nuclei", J. Phys. B **50**, 225101 (2017).

[278] L. V. Skripnikov, "Communication: Theoretical study of HfF+ cation to search for the T,P-odd interactions", J. Chem. Phys **147**, 021101 (2017).

[279] S. Sasmal, K. Talukdar, M. K. Nayak, N. Vaval, and S. Pal, "Electron-nucleus scalar-pseudoscalar interaction in PbF: Z-vector study in the relativistic coupled-cluster framework", Mol. Phys. **115**, 2807 (2017).

[280] B. P. Das, M. K. Nayak, M. Abe, and V. S. Prasannaa, "Relativistic many-body aspects of the electron electric dipole moment searches using molecules", in *Handbook of relativistic quantum chemistry*, edited by W. Liu (Springer Berlin Heidelberg, Berlin, Heidelberg, 2017), pp. 581–609.

[281] A. J. Geddes, L. V. Skripnikov, A. Borschevsky, J. C. Berengut, V. V. Flambaum, and T. P. Rakitzis, "Enhanced nuclear-spin-dependent parity-violation effects using the ^{199}HgH molecule", Phys. Rev. A **98**, 022508 (2018).

[282] A. Sunaga, V. S. Prasannaa, M. Abe, M. Hada, and B. P. Das, "Enhancement factors of parity- and time-reversal-violating effects for monofluorides", Phys. Rev. A **98**, 042511 (2018).

[283] A. N. Petrov, L. V. Skripnikov, A. V. Titov, and V. V. Flambaum, "Evaluation of CP violation in HfF^+", Phys. Rev. A **98**, 042502 (2018).

[284] M. Denis, P. A. B. Haase, R. G. E. Timmermans, E. Eliav, N. R. Hutzler, and A. Borschevsky, "Enhancement factor for the electric dipole moment of the electron in the BaOH and YbOH molecules", Phys. Rev. A **99**, 042512 (2019).

[285] D. V. Chubukov, L. V. Skripnikov, and L. N. Labzowsky, "On the Search for the Electric Dipole Moment of the Electron: P-, T-Odd Faraday Effect on a PbF Molecular Beam", JETP Lett. **110**, 382 (2019).

[286] A. Kudrin, A. Zaitsevskii, T. Isaev, D. Maison, and L. Skripnikov, "Towards the search for thallium nuclear schiff moment in polyatomic molecules: molecular properties of thallium monocyanide (TlCN)", Atoms **7**, 62 (2019).

[287] D. E. Maison, L. V. Skripnikov, and V. V. Flambaum, "Theoretical study of ^{173}YbOH to search for the nuclear magnetic quadrupole moment", Phys. Rev. A **100**, 032514 (2019).

[288] N. M. Fazil, V. S. Prasannaa, K. V. P. Latha, M. Abe, and B. P. Das, "RaH as a potential candidate for electron electric-dipole-moment searches", Phys. Rev. A **99**, 052502 (2019).

[289] A. Sunaga, V. S. Prasannaa, M. Abe, M. Hada, and B. P. Das, "Ultracold mercury–alkali-metal molecules for electron-electric-dipole-moment searches", Phys. Rev. A **99**, 040501 (2019).

[290] A. Sunaga, M. Abe, M. Hada, and B. P. Das, "Merits of heavy-heavy diatomic molecules for electron electric-dipole-moment searches", Phys. Rev. A **99**, 062506 (2019).

[291] A Sunaga, M Abe, V. S. Prasannaa, T Aoki, and M Hada, "Relativistic coupled-cluster study of diatomic metal-alkali-metal molecules for electron electric dipole moment searches", J. Phys. B **53**, 015102 (2019).

[292] K. Talukdar, M. K. Nayak, N. Vaval, and S. Pal, "Relativistic coupled-cluster investigation of parity (P) and time-reversal (T) symmetry violations in HgF", J. Chem. Phys **150**, 084304 (2019).

[293] K. Talukdar, M. K. Nayak, N. Vaval, and S. Pal, "Nuclear parity- and time-reversal-symmetry violation in the ^{201}HgH molecule", Phys. Rev. A **99**, 032503 (2019).

[294] V. S. Prasannaa, A. Sunaga, M. Abe, M. Hada, N. Shitara, A. Sakurai, and B. P. Das, "The role of relativistic many-body theory in electron electric dipole moment searches using cold molecules", Atoms **7**, 58 (2019).

[295] M. Denis, Y. Hao, E. Eliav, N. R. Hutzler, M. K. Nayak, R. G. E. Timmermans, and A. Borschesvky, "Enhanced P,T-violating nuclear magnetic quadrupole moment effects in laser-coolable molecules", J. Chem. Phys. **152**, 084303 (2020).

[296] K. Talukdar, M. K. Nayak, N. Vaval, and S. Pal, "Role of electron correlation in the $\mathcal{P}, \mathcal{T}$-odd effects of CdH: A relativistic coupled-cluster investigation", Phys. Rev. A **101**, 032505 (2020).

[297] R. Bala, H. S. Nataraj, and M. K. Nayak, "Calculations of $\mathcal{P}$ and $\mathcal{T}$-odd interaction constants of alkaline-earth monofluorides using KRCI method", J. Phys. B **53**, 135101 (2020).

[298] K. Talukdar, M. K. Nayak, N. Vaval, and S. Pal, "Relativistic coupled-cluster study of BaF in search of $\boldsymbol{\mathcal{CP}}$ violation", J. Phys. B **53**, 135102 (2020).

[299] T. Chupp and M. Ramsey-Musolf, "Electric dipole moments: a global analysis", Phys. Rev. C **91**, 035502 (2015).

[300] T. Fleig and M. Jung, "Model-independent determinations of the electron edm and the role of diamagnetic atoms", J. High Energy Phys. **2018**, 12 (2018).

[301] V. V. Flambaum, M. Pospelov, A. Ritz, and Y. V. Stadnik, "Sensitivity of EDM experiments in paramagnetic atoms and molecules to hadronic CP violation", Phys. Rev. D **102**, 035001 (2020).

[302] A. Mårtensson-Pendrill and P Öster, "Calculations of Atomic Electric Dipole Moments", Phys. Scr. **36**, 444 (1987).

[303] E. Lindroth, B. W. Lynn, and P. G. H. Sandars, "Order α^2 theory of the atomic electric dipole moment due to an electric dipole moment of the electron", J. Phys. B **22**, 559 (1989).

[304] A. Vutha, W. C. Campbell, Y. Gurevich, N. Hutzler, M. Parsons, D. Patterson, E. Petrik, B. Spaun, J. M. Doyle, G. Gabrielse, and D. DeMille, "Search for the electric dipole moment of the electron with thorium monoxide", J. Phys. B At. Mol. Opt. Phys. **43**, 074007 (2010).

[305] E. D. Commins and D. P. DeMille, "The Electric Dipole Moment of the Electron", in *Lept. dipole moments*, edited by B. L. Roberts and W. J. Marciano (World Scientific Publishing Company Pte Limited, 2010), p. 519.

[306] Y. V. Stadnik and V. V. Flambaum, "Searching for dark matter and variation of fundamental constants with laser and maser interferometry", Phys. Rev. Lett. **114**, 161301 (2015).

[307] J.-P. Uzan, "The fundamental constants and their variation: observational and theoretical status", Rev. Mod. Phys. **75**, 403 (2003).

[308] V. V. Flambaum, "Variation of the fundamental constants: theory and observations", Int. J. Mod. Phys. A **22**, 4937 (2007).

[309] M. Duff, "How fundamental are fundamental constants?", Contemp. Phys. **56**, 35 (2015).

[310] P. Bargueño and I. Gonzalo, "Effect of cosmological neutrinos on discrimination between the two enantiomers of a chiral molecule", Orig. Life Evol. Biosph. **36**, 171 (2006).

[311] P. Bargueño and R. Pérez de Tudela, "The role of supernova neutrinos on molecular homochirality", Orig. Life Evol. Biosph. **37**, 253 (2007).

[312] P. Bargueño, A. Dobado, and I. Gonzalo, "Could dark matter or neutrinos discriminate between the enantiomers of a chiral molecule?", Europhys. Lett. **82**, 13002 (2008).

[313] B. M. Roberts, Y. V. Stadnik, V. A. Dzuba, V. V. Flambaum, N. Leefer, and D. Budker, "Limiting P-Odd Interactions of Cosmic Fields with Electrons, Protons, and Neutrons", Phys. Rev. Lett. **113**, 081601 (2014).

[314] Y. V. Stadnik and V. V. Flambaum, "Axion-induced effects in atoms, molecules, and nuclei: Parity nonconservation, anapole moments, electric dipole moments, and spin-gravity and spin-axion momentum couplings", Phys. Rev. D **89**, 43522 (2014).

[315] V. A. Dzuba, V. V. Flambaum, I. B. Samsonov, and Y. V. Stadnik, "New constraints on axion-mediated P,T-violating interaction from electric dipole moments of diamagnetic atoms", Phys. Rev. D **98**, 035048 (2018).

[316] Z. Ahmed, D. S. Akerib, S. Arrenberg, C. N. Bailey, D. Balakishiyeva, L. Baudis, D. A. Bauer, J. Beaty, P. L. Brink, T. Bruch, R. Bunker, B. Cabrera, D. O. Caldwell, J. Cooley, P. Cushman, F. DeJongh, M. R. Dragowsky, L. Duong, E. Figueroa-Feliciano, J. Filippini, M. Fritts, S. R. Golwala, D. R. Grant, J. Hall, R. Hennings-Yeomans, S. Hertel, D. Holmgren, L. Hsu, M. E. Huber, O. Kamaev, M. Kiveni, M. Kos, S. W. Leman, R. Mahapatra, V. Mandic, D. Moore, K. A. McCarthy, N. Mirabolfathi, H. Nelson, R. W. Ogburn, M. Pyle, X. Qiu, E. Ramberg, W. Rau, A. Reisetter, T. Saab, B. Sadoulet, J. Sander, R. W. Schnee, D. N. Seitz, B. Serfass, K. M. Sundqvist, M. Tarka, G. Wang, S. Yellin, J. Yoo, and B. A. Young, "Search for axions with the cdms experiment", Phys. Rev. Lett. **103**, 141802 (2009).

[317] D. Budker, P. W. Graham, M. Ledbetter, S. Rajendran, and A. O. Sushkov, "Proposal for a Cosmic Axion Spin Precession Experiment (CASPEr)", Phys. Rev. X **4**, 021030 (2014).

[318] P. Sikivie, "Axion dark matter detection using atomic transitions", Phys. Rev. Lett. **113**, 201301 (2014).

[319] C. Abel, N. J. Ayres, G. Ban, G. Bison, K. Bodek, V. Bondar, M. Daum, M. Fairbairn, V. V. Flambaum, P. Geltenbort, K. Green, W. C. Griffith, M. van der Grinten, Z. D. Grujić, P. G. Harris, N. Hild, P. Iaydjiev, S. N. Ivanov, M. Kasprzak, Y. Kermaidic, K. Kirch, H.-C. Koch, S. Komposch, P. A. Koss, A. Kozela, J. Krempel, B. Lauss, T. Lefort, Y. Lemière, D. J. E. Marsh, P. Mohanmurthy, A. Mtchedlishvili, M. Musgrave, F. M. Piegsa, G. Pignol, M. Rawlik, D. Rebreyend, D. Ries, S. Roccia, D. Rozpędzik, P. Schmidt-Wellenburg, N. Severijns, D. Shiers, Y. V. Stadnik, A. Weis, E. Wursten, J. Zejma, and G. Zsigmond, "Search for axionlike dark matter through nuclear spin precession in electric and magnetic fields", Phys. Rev. X **7**, 041034 (2017).

[320] P. W. Graham, D. E. Kaplan, J. Mardon, S. Rajendran, W. A. Terrano, L. Trahms, and T. Wilkason, "Spin precession experiments for light axionic dark matter", Phys. Rev. D **97**, 055006 (2018).

[321] B. R. Heckel, E. G. Adelberger, C. E. Cramer, T. S. Cook, S. Schlamminger, and U. Schmidt, "Preferred-frame and CP-violation tests with polarized electrons", Phys. Rev. D **78**, 092006 (2008).

[322] I. M. Bloch, Y. Hochberg, E. Kuflik, and T. Volansky, "Axion-like relics: new constraints from old comagnetometer data", J. High Energy Phys. **2020**, 167 (2020).

[323] A. J. Vargas, "Overview of the phenomenology of lorentz and cpt violation in atomic systems", Symmetry **11**, 1433 (2019).

[324] V. A. Kostelecký and M. Mewes, "Cosmological constraints on lorentz violation in electrodynamics", Phys. Rev. Lett. **87**, 251304 (2001).

[325] V. A. Kostelecký and M. Mewes, "Signals for lorentz violation in electrodynamics", Phys. Rev. D **66**, 056005 (2002).

[326] V. A. Kostelecký, "Gravity, Lorentz violation, and the standard model", Phys. Rev. D **69**, 105009 (2004).

[327] N. Russell, "Tests of Lorentz violation in atomic and optical physics", Phys. Scr. **72**, C38 (2005).

[328] V. A. Kostelecký and C. D. Lane, "Nonrelativistic quantum Hamiltonian for Lorentz violation", J. Math. Phys. **40**, 6245 (1999).

[329] B. Altschul, "Testing electron boost invariance with $2S-1S$ hydrogen spectroscopy", Phys. Rev. D **81**, 041701 (2010).

[330] T. Pruttivarasin, M. Ramm, S. G. Porsev, I. I. Tupitsyn, M. S. Safronova, M. A. Hohensee, and H. Häffner, "Michelson-morley analogue for electrons using trapped ions to test lorentz symmetry", Nature **517**, 592 (2015).

[331] E. Megidish, J. Broz, N. Greene, and H. Häffner, "Improved test of local Lorentz invariance from a deterministic preparation of entangled states", Phys. Rev. Lett. **122**, 123605 (2019).

[332] C. Sanner, N. Huntemann, R. Lange, C. Tamm, E. Peik, M. S. Safronova, and S. G. Porsev, "Optical clock for comparison for Lorentz symmetry testing", Nature **567**, 204 (2019).

[333] M. A. Hohensee, N. Leefer, D. Budker, C. Harabati, V. A. Dzuba, and V. V. Flambaum, "Limits on violations of lorentz symmetry and the einstein equivalence principle using radio-frequency spectroscopy of atomic dysprosium", Phys. Rev. Lett. **111**, 050401 (2013).

[334] V. A. Dzuba and V. V. Flambaum, "Limits on gravitational einstein equivalence principle violation from monitoring atomic clock frequencies during a year", Phys. Rev. D **95**, 015019 (2017).

[335] C. J. Berglund, L. R. Hunter, D. Krause Jr., E. O. Prigge, M. S. Ronfeldt, and S. K. Lamoreaux, "New limits on local lorentz invariance from Hg and Cs magnetometers", Phys. Rev. Lett. **75**, 1879 (1995).

[336] B. Botermann, D. Bing, C. Geppert, G. Gwinner, T. W. Hänsch, G. Huber, S. Karpuk, A. Krieger, T. Kühl, W. Nörtershäuser, C. Novotny, S. Reinhardt, R. Sánchez, D. Schwalm, T. Stöhlker, A. Wolf, and G. Saathoff, "Test of Time Dilation Using Stored Li^+ Ions as Clocks at Relativistic Speed", Phys. Rev. Lett. **113**, 120405 (2014).

[337] M. A. Hohensee, S. Chu, A. Peters, and H. Müller, "Equivalence principle and gravitational redshift", Phys. Rev. Lett. **106**, 151102 (2011).

[338] H. Müller, S. Herrmann, A. Saenz, A. Peters, and C. Lämmerzahl, "Optical cavity tests of Lorentz invariance for the electron", Phys. Rev. D **68**, 116006 (2003).

[339] H. Müller, "Testing Lorentz invariance by the use of vacuum and matter filled cavity resonators", Phys. Rev. D **71**, 045004 (2005).

[340] B. Altschul, "Synchrotron and inverse compton constraints on lorentz violations for electrons", Phys. Rev. D **74**, 083003 (2006).

[341] H. Müller, S. Herrmann, A. Saenz, A. Peters, and C. Lämmerzahl, "Tests of lorentz invariance using hydrogen molecules", Phys. Rev. D **70**, 076004 (2004).

[342] A. Szabo and N. S. Ostlund, *Modern Quantum Chemistry: Introduction to Advanced Electronic Structure Theory* (Dover Publications, INC., Mineola, New York, 1996).

[343] T. Helgaker, P. Jørgensen, and J. Olsen, *Molecular Electronic-Structure Theory* (John Wiley & Sons, Ltd, 2000).

[344] K. G. Dyall, "Interfacing relativistic and nonrelativistic methods. I. Normalized elimination of the small component in the modified Dirac equation", J. Chem. Phys. **106**, 9618 (1997).

[345] P. Schwerdtfeger, ed., *Relativistic Electronic Structure Theory, Part: 1, Fundamentals* (Elsevier, Netherlands, 2002).

[346] P. Schwerdtfeger, ed., *Relativistic Electronic Structure Theory, Part: 2, Applications* (Elsevier, Netherlands, 2004).

[347] D. R. Hartree, "The wave mechanics of an atom with a non-Coulomb central field. Part II. Some results and discussion", Math. Proc. Camb. Phil. Soc. **24**, 111–132 (1928).

[348] V. Fock, "Näherungsmethode zur Lösung des quantenmechanischen Mehrkörperproblems", Z. Phys. **61**, 126 (1930).

[349] K. G. Dyall and K. Fægri, Jr., *Introduction to Relativistic Quantum Chemistry* (Oxford University Press, 2007).

[350] J. Čížek and J. Paldus, "Stability Conditions for the Solutions of the Hartree-Fock Equations for Atomic and Molecular Systems. Application to the Pi-Electron Model of Cyclic Polyenes", J. Chem. Phys **47**, 3976 (1967).

[351] J. Paldus and J. Čížek, "Stability conditions for the solutions of the Hartree-Fock equations for the simple open-shell case", Chem. Phys. Lett. **3**, 1 (1969).

[352] J. Čížek and J. Paldus, "Stability conditions for the solutions of the Hartree–Fock equations for atomic and molecular systems. III. Rules for the singlet stability of Hartree–Fock solutions of π-electronic systems", J. Chem. Phys. **53**, 821 (1970).

[353] J. Paldus and J. Čížek, "Stability conditions for the solutions of the Hartree-Fock equations for atomic and molecular systems. IV. A study of doublet stability for odd linear polyenic radicals", J. Chem. Phys **54**, 2293 (1971).

[354] J. Čížek and J. Paldus, "Stability conditions for the solutions of the Hartree-Fock equations for atomic and molecular systems. V. The nonanalytic behavior of the broken-symmetry solutions at the branching point", Phys. Rev. A **3**, 525 (1971).

[355] H. Fukutome, "Theory of the unrestricted Hartree-Fock equation and its solutions. I", Progr. Theor. Phys. **45**, 1382 (1971).

[356] H. Fukutome, "The unrestricted Hartree-Fock theory of chemical reactions. I: The electronic instabilities in the chemical reactions and the solutions of the unrestricted SCF LCAO MO equation for the homopolar two-center two-electron system", Progr. Theor. Phys. **47**, 1156 (1972).

[357] H. Fukutome, "The unrestricted Hartree-Fock theory of chemical reactions. II: Dissociation reaction of asymmetric two-center two-electron system", Progr. Theor. Phys. **49**, 22 (1973).

[358] H. Fukutome, "The unrestricted Hartree-Fock theory of chemical reactions. III: Instability conditions for paramagnetic and spin density wave states and application to internal rotation of ethylene", Progr. Theor. Phys. **50**, 1433 (1973).

[359] H. Fukutome, "Theory of the unrestricted Hartree-Fock equation and its solutions. II: Classification and characterization of UHF solutions by their behavior for spin rotation and time reversal", Progr. Theor. Phys. **52**, 115 (1974).

[360] H. Fukutome, "Theory of the unrestricted Hartree-Fock equation and its solutions. III: Classification of instabilities and interconnection relation between the eight classes of UHF solutions", Progr. Theor. Phys. **52**, 1766 (1974).

[361] H. Fukutome, "Theory of the unrestricted Hartree-Fock equation and its solutions. IV: Behavior of UHF solutions in the vicinity of interconnecting instability threshold", Progr. Theor. Phys. **53**, 1320 (1975).

[362] H. Fukutome, M. Takahashi, and T. Takabe, "The unrestricted Hartree-Fock theory of chemical reactions. IV: Singlet radical states with 'antiferromagnetic' spin orderings in four-center exchange reaction of hydrogen molecules", Progr. Theor. Phys. **53**, 1580 (1975).

[363] H. Fukutome, "Unrestricted Hartree-Fock theory and its applications to molecules and chemical reactions", Int. J. Quantum Chem. **20**, 955 (1981).

[364] J. Stuber, "Broken symmetry Hartree-Fock solutions and the many-electron correlation problem", PhD thesis (University of Waterloo, Ontario, Canada, 2002).

[365] P. Hohenberg and W. Kohn, "Inhomogenous electron gas", Phys. Rev. B **136**, 864 (1964).

[366] A. K. Rajagopal and J. Callaway, "Inhomogeneous electron gas", Phys. Rev. B **7**, 1912 (1973).

[367] W. Kohn and L. J. Sham, "Self-consistent equations including exchange and correlation effects", Phys. Rev. **140**, 1133 (1965).

[368] R. G. Parr and W. Yang, *Density-functional theory of atoms and molecules*, English (Oxford University Press; Clarendon Press, New York; Oxford [England], 1989).

[369] E. Engel and R. M. Dreizler, *Density Functional Theory: An Advanced Course* (Springer, 2011).

[370] W. Koch and M. C. Holthausen, *A chemist's guide to density functional theory* (John Wiley & Sons, Ltd, 2001).

[371] I. P. Grant and H. M. Quiney, "Relativistic self-consistent fields", in Relativistic Electronic Structure Theory, Part: 1, Fundamentals, edited by P. Schwerdtfeger (2002) Chap. 3, pp. 107–202.

[372] L. N. Labzowsky and I. Goidenko, "QED theory of atoms", in Relativistic Electronic Structure Theory, Part: 1, Fundamentals, edited by P. Schwerdtfeger (2002) Chap. 8, pp. 403–470.

[373] J. L. Heully, I. Lindgren, E. Lindroth, S. Lundqvist, and A. M. Mårtensson-Pendrill, "Diagonalisation of the Dirac Hamiltonian as a basis for a relativistic many-body procedure", J. Phys. B **19**, 2799 (1986).

[374] C. Chang, M. Pelissier, and P. Durand, "Regular two-component Pauli-like effective Hamiltonians in Dirac theory", Phys. Scr. **34**, 394 (1986).

[375] E. van Lenthe, E.-J. Baerends, and J. G. Snijders, "Relativistic total energy using regular approximations", J. Chem. Phys. **101**, 9783 (1994).

[376] C. van Wüllen, "Molecular density functional calculations in the regular relativistic approximation: Method, application to coinage metal diatomics, hydrides, fluorides and chlorides, and comparison with first-order relativistic calculations", J. Chem. Phys. **109**, 392 (1998).

[377] T. A. Isaev and R. Berger, "Periodic trends in parity-violating hyperfine coupling constants of open-shell diatomic molecules", J. Mol. Spectrosc. **300**, 26 (2014).

[378] K. J. Gaul, "Development of methods and models for simultaneous parity- and time-reversal violations in molecules", MSc. Thesis (Philipps-Universität Marburg, 2016).

[379] I. Kozyryev and N. R. Hutzler, "Precision measurement of time-reversal symmetry violation with laser-cooled polyatomic molecules", Phys. Rev. Lett. **119**, 133002 (2017).

[380] I. B. Khriplovich, *Parity nonconservation in atomic phenomena* (Gordon and Breach Science Publ., Philadelphia, 1991).

[381] V. A. Dzuba, V. V. Flambaum, and C. Harabati, "Relations between matrix elements of different weak interactions and interpretation of the parity-nonconserving and electron electric-dipole-moment measurements in atoms and molecules", Phys. Rev. A **84**, 052108 (2011).

[382] Wolfram Research, Inc., *Mathematica 11.0*, Champaign, Illinois, 2016.

[383] DIRAC, a relativistic ab initio electronic structure program, Release DIRAC15 (2015), written by R. Bast, T. Saue, L. Visscher, and H. J. Aa. Jensen, with contributions from V. Bakken, K. G. Dyall, S. Dubillard, U. Ekstroem, E. Eliav, T. Enevoldsen, E. Fasshauer, T. Fleig, O. Fossgaard, A. S. P. Gomes, T. Helgaker, J. Henriksson, M. Ilias, Ch. R. Jacob, S. Knecht, S. Komorovsky, O. Kullie, J. K. Laerdahl, C. V. Larsen, Y. S. Lee, H. S. Nataraj, M. K. Nayak, P. Norman, G. Olejniczak, J. Olsen, Y. C. Park, J. K. Pedersen, M. Pernpointner, R. Di Remigio, K. Ruud, P. Salek, B. Schimmelpfennig, J. Sikkema, A. J. Thorvaldsen, J. Thyssen, J. van Stralen, S. Villaume, O. Visser, T. Winther, and S. Yamamoto (see http://www.diracprogram.org).

[384] K. G. Dyall, "Relativistic and nonrelativistic finite nucleus optimized triple-zeta basis sets for the 4p, 5p and 6p elements", Theor. Chem. Acc. **108**, 335 (2002).

[385] K. G. Dyall, "Relativistic quadruple-zeta and revised triple-zeta and double-zeta basis sets for the 4p, 5p, and 6p elements", Theor. Chem. Acc. **115**, 441 (2006).

[386] L. Visscher, "Approximate molecular relativistic Dirac–Coulomb calculations using a simple Coulombic correction", Theor. Chem. Acc. **98**, 68 (1997).

[387] O. Visser, L. Visscher, P. J. C. Aerts, and W. C. Nieuwpoort, "Molecular open shell configuration interaction calculations using the Dirac-Coulomb Hamiltonian: The f 6-manifold of an embedded euo9-6 cluster", J. Chem. Phys **96**, 2910 (1992).

[388] W. A. de Jong, L. Visscher, and W. C. Nieuwpoort, "Relativistic and correlated calculations on the ground, excited, and ionized states of iodine", J. Chem. Phys **107**, 9046 (1997).

[389] R. Rydberg, "Graphische Darstellung einiger bandenspektroskopischer Ergebnisse", Z. Phys. **73**, 376 (1932).

[390] O. Klein, "Zur Berechnung von Potentialkurven für zweiatomige Moleküle mit Hilfe von Spektraltermen", Z. Phys. **76**, 226 (1932).

[391] A. L. G. Rees, "The calculation of potential-energy curves from band-spectroscopic data", Proc. Phys. Soc. **59**, 998 (1947).

[392] P. Senn, "The computation of RKR potential energy curves of diatomic molecules using mathematica", Comput. Chem. **19**, 437 (1995).

[393] R. Meyer, "Trigonometric interpolation method for one-dimensional quantum-mechanical problems", J. Chem. Phys. **52**, 2053 (1970).

[394] H. M. Quiney, J. K. Laerdahl, K. Fægri, and T. Saue, "Ab initio Dirac-Hartree-Fock calculations of chemical properties and PT-odd effects in thallium fluoride", Phys. Rev. A **57**, 920 (1998).

[395] E. R. Cohen, T. Cvitas, J. G. Frey, B. Holmström, K. Kuchitsu, R. Marquardt, I. Mills, F. Pavese, M. Quack, J. Stohner, H. L. Strauss, M. Takami, and A. J. Thor, *Quantities, units and symbols in physical chemistry, IUPAC green book*, 3rd Ed., 2nd Printing (IUPAC & RSC Publishing, Cambridge, 2008).

[396] H. M. Quiney, H. Skaane, and I. P. Grant, "Hyperfine and PT-odd effects in YbF $^2\Sigma$", J. Phys. B **31**, L85 (1998).

[397] S. A. Brück, "Analytical gradients for the investigation of parity violation in molecular spectra", Diploma Thesis (Johann Wolfgang Goethe-Universität Frankfurt am Main, 2013).

[398] K. Huber and G. Herzberg, "Constants of diatomic molecules", in *NIST Chemistry WebBook, NIST Standard Reference Database Number 69*, edited by P. J. Linstrom and W. G. Mallard (National Institute of Standards and Technology, Gaithersburg MD, 20899, 20017).

[399] R. F. Barrow and K. K. Yee, "B3Π0-X1Σ system of $^{127}I_2$: rotational analysis and long-range potential in the B3Π0 state", J. Chem. Soc., Faraday Trans. II **69**, 684 (1973).

[400] J. Wei and J. Tellinghuisen, "Parameterizing diatomic spectra: 'Best' spectroscopic constants for the I_2 B 3 X transition", J. Mol. Spectrosc. **50**, 317 (1974).

[401] R. Holzwarth, A. Nevsky, M. Zimmermann, T. Udem, T. Hänsch, J. von Zanthier, H. Walther, J. Knight, W. Wadsworth, P. Russell, M. Skvortsov, and S. Bagayev, "Absolute frequency measurement of iodine lines with a femtosecond optical synthesizer", Appl. Phys. B **73**, 269 (2001).

H

Acronyms

ΛCDM	Λ Cold Dark Matter.
ALP	Axion Like Particle.
BO	Born–Oppenheimer.
BSM	Beyond the Standard Models.
CDM	Cold Dark Matter.
cGHF	complex GHF.
CI	Configuration Interaction.
CKM	Cabibbo-Kobayashi-Maskawa.
COSCI	Complete Open-shell Configuration Interaction.
cRHF	complex RHF.
cUHF	complex UHF.
DE	Dark Energy.
DFSZ	Dine–Fischler–Srednicki–Zhitnitsky.
DFT	Density Functional Theory.
DHF	Dirac–Hartree–Fock.
DM	Dark Matter.
DVR	Discrete Variable Representation.
EDM	Electric Dipole Moment.
eEDM	Electric Dipole Moment of the electron.
FCDM	Fuzzy Cold Dark Matter.
GHF	Generalized HF.
GKS	Generalized KS.
GR	the General theory of Relativity.
GUT	Grand Unifying Theory.
HF	Hartree–Fock.
IMC	Iodine Molecular Clock.
KS	Kohn-Sham.
KSVZ	Kim–Shifman–Vainshtein–Zakharov.
LCAO	Linear Combination of Atomic Orbitals.
LHC	Large Hadron Collider.
LLIV	Local Lorentz Invariance Violation.
MACHO	Massive Astrophysical Compact Halo Objects.

MDM Magnetic Dipole Moment.
MOND MOdified Newtonian Dynamics.

NEDM Nuclear Electric Dipole Moment.
nEDM Electric Dipole Moment of the neutron.
NEOM Nuclear Electric Octupole Moment.
NIST National Institute of Standards and Technology.
NMQM Nuclear Magnetic Quadrupole Moment.
NMR Nuclear Magnetic Resonance.

pEDM Electric Dipole Moment of the proton.
pGHF paired GHF.
PSNEC Pseudoscalar-Scalar Nucleon-Electron Current.
pUHF paired UHF.

QCD Quantum Chromodynamics.
QED Quantum Electrodynamics.
QFT Quantum Field Theory.

rGHF real GHF.
RHF Restricted HF.
RKR Rydberg–Klein–Rees.
RMS Robertson–Mansouri–Sexl framework.
rRHF real RHF.
rUHF real UHF.

SCF Self-Consistent Field.
SD Slater-Determinant.
SEWT Standard Electro Weak Theory.
SM Standard Model of particle physics.
SME Standard Model Extension.
SPNEC Scalar-Pseudoscalar Nucleon-Electron Current.
SQUID Superconducting QUantum Interference Device.
SR the Special theory of Relativity.
SUSY SUperSYmmetry.

ToE Theory of Everything.
TPNEC Tensor-Pseudotensor Nucleon-Electron Current.

UHF Unrestricted HF.

WIMP Weakly Interacting Massive Particle.

ZORA Zeroth Order Regular Approximation.

I Quantities and Symbols

This thesis closely follows the suggestions of the IUPAC as summarized in the Green Book for quantities, symbols and units: E. R. Cohen et al., *Quantities, units and symbols in physical chemistry, IUPAC green book*, 3rd Ed., 2nd Printing (IUPAC & RSC Publishing, Cambridge, 2008). In the following a list of symbols frequently used in this thesis is provided.

Natural Constants

$\imath = \sqrt{-1}$	imaginary unit
c	speed of light in vacuum
e	elementary electric charge
α	fine-structure constant
g_s	strong coupling constant
G_F	Fermi/weak coupling constant
G	gravitational constant
$\hbar = \frac{h}{2\pi}$	reduced Planck constant
m_e	mass of the electron
m_p	mass of the proton
μ_0	magnetic constant
ϵ_0	electric constant
θ_W	Weinberg/weak mixing angle

Index Notation

μ, ν, ρ, σ	indices running from 0 to 3
i, j, k, l	indices running from 1 to 3
a, b, c	indices running over all representations of a gauge group
$a_\mu a^\mu = a^\mu a_\mu = \sum_{\mu=0}^{3} a^\mu a_\mu$	Einstein's sum convention

Space-time quantities

t	time coordinate
$\vec{r} = (x, y, z)^\mathsf{T}$	position coordinate in three-dimensional Euclidean space
x^μ	four-vector of spacetime coordinates
∂_μ	covariant derivative with respect to the four-vector

$\hat{\vec{p}} = -\imath\hbar\vec{\nabla}$	linear momentum in position space representation
$\gamma = \sqrt{1 - \frac{v^2}{c^2}}$	Lorentz factor for an object traveling with speed v

Energy quantities

H	Hamiltonian
$\hat{H}$	Hamiltonian operator
L	Lagrangian
$\mathcal{L}$	Lagrangian density
T	kinetic energy
V	potential energy

Molecular parameters

Z	nuclear charge number
N	number of neutrons in the nucleus
A	nuclear mass number
Q_W	weak nuclear charge
$\vec{F}$	total angular momentum
$\vec{R}$	rotational angular momentum
$\vec{L}$	electronic orbital angular momentum
$\vec{S}$	total electronic spin
$\vec{S}'$	effective electron spin
$\vec{J}_\mathrm{e}$	total electronic angular momentum
$\vec{I}$	total nuclear spin
$\vec{\lambda}$	unit vector pointing from the heavy to the light nucleus in a diatomic molecule
Λ	projection of the orbital angular momentum on the molecular axis
Σ	projection of the total electronic spin on the molecular axis
Ω	projection of the total electronic angular momentum on the molecular axis
$\vec{\mu}$	magnetic dipole moment
$\vec{d}$	electric dipole moment

Fields and functions

ϕ	(pseudo-)scalar bosonic field/wave function

A^μ	photon field
$F^{\mu\nu}$	vector field strength tensor
$\vec{\mathcal{E}}$	electric field
$\vec{\mathcal{B}}$	magnetic field
ψ	fermionic field/wave function (bispinor)
ψ^{L}	upper/large component of fermionic field/wave function (spinor)
ψ^{S}	lower/small component of fermionic field/wave function (spinor)
Ψ	many-body fermionic wave function
Φ	Slater-Determinant/configuration of a fermionic many-body system
χ	basis function
ρ	density function
$\vec{j}$	current density function

Unitary matrices

$\boldsymbol{\sigma}^\mu$	Pauli spin matrices including identity ($\mu = 0$) (basis of $SU(2)$)
$\boldsymbol{\Gamma}^{\mu\nu} = \boldsymbol{\sigma}^\mu \otimes \boldsymbol{\sigma}^\nu$	Dirac matrices (basis of $SU(2) \otimes SU(2)$)
$\boldsymbol{\gamma}^0, \boldsymbol{\beta}, \boldsymbol{\gamma}^5, \vec{\boldsymbol{\alpha}}, \vec{\boldsymbol{\Sigma}}, \boldsymbol{\gamma}^\mu$	commonly employed symbols for Dirac matrices (see eq. (1.17))

Curriculum vitae

Publikationen

Im Folgenden findet sich eine vollständige Liste meiner Artikel in wissenschaftlichen Fachzeitschriften und Präsentationen, die ich auf Konferenzen, in externen Seminaren oder auf Sommerschulen gehalten habe. Die Liste wurde zuletzt am 5. September 2020 aktualisiert. Artikel, die Teil dieser Dissertation sind, sind mit einem Stern markiert.

Artikel

12.* Konstantin Gaul, and Robert Berger,
Complementary molecules for an experimental disentanglement of sources of $\mathcal{P}$, $\mathcal{T}$-violation from simple models,
manuscript in preparation.

11.* Konstantin Gaul, Norman Gürlebeck, and Robert Berger,
Enhancement of Lorentz invariance violation in iodine molecular clock transitions,
manuscript in preparation.

10.* Konstantin Gaul, Mikhail G. Kozlov, Timur A. Isaev, and Robert Berger,
Parity nonconserving interactions of electrons in chiral molecules with cosmic fields,
Phys. Rev. A *accepted* **Aug. 2020**.

9.* Konstantin Gaul, Mikhail G. Kozlov, Timur A. Isaev, and Robert Berger,
Chiral molecules as sensitive probes for direct detection of $\mathcal{P}$-odd cosmic fields,
Phys. Rev. Lett. *accepted* **Aug. 2020**.

8. Konstantin Gaul, and Robert Berger,
Quasi-relativistic study of nuclear electric quadrupole coupling constants in chiral molecules containing heavy elements,
Mol. Phys. e1797199, **Aug. 2020**; doi:10.1080/00268976.2020.1797199.

7.* Konstantin Gaul, and Robert Berger,
Toolbox approach for quasi-relativistic calculation of molecular properties for precision tests of fundamental physics,
J. Chem. Phys 152, 044101, **Jan. 2020**; doi:10.1063/1.5121483.

6.* Konstantin Gaul, and Robert Berger,
Ab initio study of parity and time-reversal violation in laser-coolable triatomic molecules,
Phys. Rev. A 101, 012508, **Jan. 2020**; doi:10.1103/PhysRevA.101.012508.

5.* Konstantin Gaul, Sebastian Marquardt, Timur Isaev, and Robert Berger,
Systematic study of relativistic and chemical enhancements of $\mathcal{P},\mathcal{T}$-odd effects in polar diatomic radicals,
Phys. Rev. A 99, 032509, **Mar. 2019**; doi:10.1103/PhysRevA.99.032509.

4. Sergei I. Ivlev, Konstantin Gaul, Mengyi Chen, Antti J. Karttunen, Robert Berger, and Florian Kraus,
Synthesis and characterization of $[Br_3][MF_6]$ (M = Sb, Ir), as well as quantum chemical study of $[Br_3]^+$ structure, chemical bonding, and relativistic effects compared with $[XBr_2]^+$ (X = Br, I, At, Ts) and $[TsZ_2]^+$ (Z = F, Cl, Br, I, At, Ts),
Chem. Eur. J. 25, 5793, **Apr. 2019**; doi:10.1002/chem.201900442.

3.* Norman Gürlebeck, Lisa Wörner, Thilo Schuldt, Klaus Döringshoff, Konstantin Gaul, Domenico Gerardi, Arne Grenzebach, Nandan Jha, Evgeny Kovalchuk, Andreas Resch, Thijs Wendrich, Robert Berger, Sven Herrmann, Ulrich Johann, Markus Krutzik, Achim Peters, Ernst M. Rasel, and Claus Braxmaier,
BOOST: A satellite mission to test Lorentz invariance using high-performance optical frequency references,
Phys. Rev. D 97, 124051, **Jun. 2018**; doi:10.1103/PhysRevD.97.124051.

2. Konstantin Gaul, and Robert Berger,
Zeroth order regular approximation approach to electric dipole interactions of the electron,
J. Chem. Phys. 147, 014109, **Jul. 2017**; doi:10.1063/1.4985567.

1. Mewlude Imam, Konstantin Gaul, Andreas Stegmüller, Carina Höglund, Jens Jensen, Lars Hultman, Jens Birch, Ralf Tonner, and Henrik Pedersen,
Gas phase chemical vapor deposition chemistry of triethylboron probed by boron-carbon thin film deposition and quantum chemical calculations,
J. Mat. Chem. C, 3, 10898, **Sep. 2015**; doi:10.1039/C5TC02293B.

Präsentationen

Vorträge

7. Konstantin Gaul and Robert Berger,
Towards detection of dark matter and Lorentz invariance violation with chiral molecules,
Seminar des SFB 1319 (ELCH), Kassel (virtuell aufgrund der Covid-19-Pandemie), **13.07.2020**.

6. Konstantin Gaul and Robert Berger,
Signatures of discrete symmetry violation from physics beyond the standard model in molecular systems,
Symmetry in Science XVIII, Bregenz, Österreich, **08.08.2019**.

5. Konstantin Gaul and Steffen Giesen,
Computation of molecular chirality signatures in the electron cloud: Electroweak quantum chemistry and parity violation,
Workshop des SFB 1319 (ELCH), Marburg, Deutschland, **24.06.2019**.

4. Konstantin Gaul and Robert Berger,
Electronic structure theory for molecular precision tests of new physics,
DPG Frühjahrstagung, Rostock, Germany, **13.03.2019**.

3. Konstantin Gaul and Robert Berger,
Periodic trends of P,T-violation in linear molecules,
Workshop: Searching for New Physics with Cold and Controlled Molecules, Mainz, Deutschland, **26.11.2018**.

2. Konstantin Gaul and Robert Berger,
Molecules on board satellites as probes of Einstein's most famous theory,
Karrieremesse Arbeit und Zukunft, Marburg, Deutschland, **08.11.2018**.

1. Konstantin Gaul and Robert Berger,
Quasi-relativistic studies of enhancements of P,T-violating effects in heavy elemental molecules,
12th International Conference on Relativistic Effects in Heavy-Element Chemistry and Physics, Marburg, Deutschland, **04.09.2017**.

Poster Präsentationen

10. Konstantin Gaul and Robert Berger,
Contribution of sources of P,T-violation to permanent electric dipole moments of molecules,
ISOLDE Workshop and User Meeting, Meyrin (CERN), Schweiz, **05.12.2019**

9. Konstantin Gaul and Robert Berger,
Calculation of signatures of physics beyond the Standard Model with a flexible property toolbox for two-component densities,
55th Symposium on Theoretical Chemistry, Rostock, Deutschland, **23.09.2019**.

8. Konstantin Gaul and Robert Berger,
Toolbox for calculations of symmetry violating properties in chiral molecules,
Sommerschule des SFB 1319 (ELCH), Bad Arolsen, Deutschland, **18.09.2019**.

7. Konstantin Gaul and Robert Berger,
   Flexible toolbox for calculation of relativistic properties with two-component densities,
   10th Triennial Congress of the International Society for Theoretical Chemical Physics, Tromsø, Norwegen, **15.07.2019**.

6. Konstantin Gaul and Robert Berger,
   Automated property calculation for fundamental physics tests with molecules,
   54th Symposium on Theoretical Chemistry, Halle, Deutschland, **18.09.2018**.

5. Konstantin Gaul, Robert Kretschmer and Robert Berger,
   Towards a measurement of fundamental symmetry violations in chiral molecules,
   Retreat des SFB 1319 (ELCH), Königstein (Taunus), Deutschland, **14.08.2018**.

4. Konstantin Gaul and Robert Berger,
   Evaluation of customized relativistic one-electron properties via generic quasi-relativistic density functions,
   16th International Congress of Quantum Chemistry, Menton, Frankreich, **19.06.2018**.

3. Konstantin Gaul and Robert Berger,
   Purely relativistic electric dipole moment interactions of the electron from quasi-relativistic calculations,
   11th Triennial Congress of the World Association of Theoretical and Computational Chemists, München, Deutschland, **28.08.2017**.

2. Konstantin Gaul and Robert Berger,
   P,T-violating properties in molecules: Methods, models and periodic trends,
   Sommerschule: Search for new physics with low-energy precision tests, Ameland, Niederlande, **13.06.2017**.

1. Konstantin Gaul and Robert Berger,
   Periodic trends of P,T-odd properties: eEDM interactions in molecules,
   Herbstschule des LOEWE ELCH-Projekts, Mainz, Deutschland, **10.10.2016**.

Erklärung

Ich erkläre hiermit, dass eine Promotion noch zu keinem früheren Zeitpunkt versucht wurde. Weiter versichere ich, dass die vorgelegte Dissertation selbst und ohne fremde Hilfe verfasst, keine anderen als die in ihr angegebenen Quellen oder Hilfsmittel benutzt, alle vollständig oder sinngemäß übernommenen Zitate als solche gekennzeichnet, sowie die Dissertation in der vorliegenden oder einer ähnlichen Form noch bei keiner anderen in- oder ausländischen Hochschule anlässlich eines Promotionsgesuchs oder zu anderen Prüfungszwecken eingereicht wurde.

_____

Konstantin Joachim Gaul